Development of an Antisense Oligonucleotide-Based Method to Manipulate RNA Editing of AMPAR Subunits

Helena Anne Chaytow

School of Biological Sciences

Royal Holloway, University of London

Research thesis submitted for the degree of Doctor of Philosophy

Declaration of Authorship

I, Helena Anne Chaytow, hereby declare that this thesis and the work presented in it is entirely my own. Where I have consulted the work of others, this is always clearly stated.

Signed: _____

Date: _____

ABSTRACT

AMPA receptors (AMPARs) are a subset of ionotropic glutamate receptor composed of one or more of four subunits (GluA1-4) and are essential for normal synaptic function. The GluA2 subunit undergoes RNA editing at a specific base, converting the amino acid from glutamine to arginine, which is critical for regulating calcium permeability. RNA editing is performed by Adenosine Deaminases Acting on RNAs (ADARs). ADAR2 exists as multiple alternatively-spliced variants within mammalian cells and some have been shown to reduce their editing efficiency. RNA editing in AMPARs is inefficient in patients with Amyotrophic Lateral Sclerosis and manipulating this process could be therapeutic against AMPAR-triggered neuronal cell death. Antisense oligonucleotides (ASOs) are bases with chemically altered backbones used to manipulate DNA or RNA processing through complementary base pairing. ASOs were used to alter the GluA2 RNA editing event, either by disrupting the GluA2 double-stranded RNA structure essential for editing or by affecting the alternative splicing of ADAR2.

The effects of specific ASOs on RNA editing were assessed by transfection into cell lines. Editing was quantified by an RT-PCR-based assay on RNA extracts then densitometric analysis of *BbvI* digestion products. ASOs targeting the secondary structure of the GluA2 subunit disrupted editing at this site to 50% of control in HeLa cells, and further disrupted editing to less than 10% in SH-SY5Y cells endogenously expressing the GluA2 subunit. ASOs targeting the ADAR2 transcript successfully inhibited the expression of a less efficient isoform, which led to increased editing of 30% compared to control HeLa cells. Further work will include building on attempts to introduce the antisense transcripts into primary cortical cultures to analyse downstream effects of reduced editing. This is the first example of increasing RNA editing using ASOs and provides a number of potential tools to investigate associated cellular processes and implications of RNA editing.

ACKNOWLEDGEMENTS

This thesis would not have been possible without the help of several important people. Firstly, I would like to thank my supervisor Philip Chen for his endless patience and guidance throughout the past four years. I am extremely grateful for all of the support he has given me which has allowed me to grow and develop as a scientist. Thank you also to my second supervisor George Dickson, whose depth of knowledge and constructive feedback has led to some very enjoyable meetings. It was a pleasure working under the supervision of both of them.

Thanks also go to Linda Popplewell for her wisdom in all things antisense, and for her most excellent advice during chapter revisions. Many thanks go to Sharifah for her instruction on techniques during the first two years of my PhD, and to Simona Ursu for being the most knowledgeable, hardworking and reliable lab technician a student could wish for.

I am also incredibly grateful to the Motor Neuron Disease Association for funding this project, and so allowing me to complete this PhD.

Thank you to everyone in Lab 302A, Office 404 and the Dickson lab for the company through the hours of lab work, the sarcasm, the lab-based humour and the endless cups of tea. In particular, thank you to Versha, Eva, Kate and Jade for being ever-present through the highs and lows of PhD life, I am not sure I would have finished without you there. Thank you to Annemari, Em and Bex, to Jo, Rob and Ali, for reminding me that there is life outside of science and for always being there with a glass of wine.

Finally, and most importantly, I would like to thank my family for being behind me all the way through this PhD. My mother, Marysia, and sisters Alice and Susie have always had complete faith in my abilities, and it is with their love and support in mind that I submit this thesis.

ABBREVIATIONS LIST

25mer	PMO 25 bases long
2'-F	2'-deoxy-2'-fluoro
2'-MOE	2’-O-methyoxyethyl
30mer	PMO 30 bases long
5-HT	5-hydroxytryptamine; serotonin
AAV	adeno-associated virus
ADAR	adenosine deaminase acting on RNA
ALS	amyotrophic lateral sclerosis
AMPA	α-amino-3-hydroxy-5-methyl-4-isoxazole propionic acid
APOBEC	apolipoprotein B mRNA editing catalytic polypeptide-like enzyme family
ASO	antisense oligonucleotide
BBP	branch point binding protein
bcDNA	bicyclo-DNA
CNS	central nervous system
CSF	cerebrospinal fluid
DIV	days in vitro
DMD	Duchenne muscular dystrophy
DPRs	dipeptide repeats
dsRBM	double-stranded RNA binding motif
E15	embryonic day 15
ECS	exon complementary sequence
ESEs	exon splice enhancers
ESSs	exon splice silencers
fALS	familial amyotrophic lateral sclerosis
FACS	fluorescence-activated cell sorting
F-PMO	fluorescent PMO with a 5' carboxyfluorescein modification
FTLD	frontotemporal lobe dementia
FUS	fused in sarcoma protein
GABA	gamma-aminobutyric acid
hnRNPs	heterogeneous nuclear ribonucleoproteins
HSF	Human Splice Finder
IDLV	integration-deficient lentiviral vector
iPSC-MNs	induced pluripotent stem cell motor neurons
ISEs	intron splice enhancers
ISSs	intron splice silencers
LBD	ligand binding domain

LG-E4 plasmid	lentiguide-puro plasmid containing the E4 sequence
LNA	locked nucleic acid
L-PMO	leashed PMO
LTD	long-term depression
LTP	long-term potentiation
MaxExpect	maximum expected accuracy
miRNA	microRNA
MOI	multiplicity of infection
NMDA	N-methyl-D-aspartate
OMe-PS	2'-O-methylphosphorothioate
P7	postnatal day 7
PBS	phosphate-buffered saline
PCR	polymerase chain reaction
PEI	polyethyleneimine
PESE	putative exon splice enhancer
PESS	putative exon splice silencer
PMO	phosphorodiamidate morpholino oligonucleotide
PNA	peptide nucleic acid
pri-miRNA	primary microRNA
Q	glutamine
R	arginine
RNA	ribonucleic acid
RNA-seq	whole-transcriptome sequencing
RT-PCR	reverse transcriptase-polymerase chain reaction
sALS	sporadic amyotrophic lateral sclerosis
SMA	spinal muscular atrophy
snoRNA	small nucleolar RNA
snRNPs	small nuclear ribonucleoproteins
SOD1	superoxide dismutase 1
SR proteins	serine-arginine proteins
TARPs	transmembrane AMPA receptor regulatory proteins
tcDNA	tricyclo-DNA
TDP-43	TAR DNA-binding protein-43
TMD	transmembrane domain
UTR	untranslated region

TABLE OF CONTENTS

TABLE OF FIGURES

1 LITERATURE REVIEW

1.1 AMPA RECEPTORS

1.1.1 AMPA Receptor Structure

The glutamate system comprises three families of ionotropic glutamate receptors: AMPA (α-amino-3-hydroxy-5-methyl-4-isoxazole propionic acid) receptors, NMDA (N-methyl-D-aspartate) receptors and kainate receptors, named after their high-affinity agonists. These receptors are formed from subunits which assemble as tetramers, where dimers pair up in the endoplasmic reticulum before being shuttled to the membrane (Traynelis *et al.*, 2010). The subunits each have four domains: the extracellular amino-terminal domain, the extracellular ligand-binding domain (LBD), the transmembrane domain (TMD) and an intracellular carboxyl-terminal domain. Agonist binding to the ligand-binding domain leads to a conformational change in angle of the transmembrane domain (Willard & Koochekpour, 2013). This opens the pore running through the centre of the receptor, allowing for Na^+, K^+ and Ca^{2+} ions to flow through. The influx of Ca^{2+} ions is tightly controlled by the presence of the subunit GluA2 in AMPA receptors, which renders the receptor impermeable to calcium, whereas in contrast NMDA receptors are uniformly calcium-permeable.

Glutamate receptor subunits fall into distinct classes, based upon their structure, homology and pharmacology, with each class comprising subunits that can form one of the three families of receptor (other classes reviewed in Traynelis *et al.*, 2010). AMPA receptors function as ligand-activated cation channels and are formed from the subunits GluA1 to GluA4 (also known as GluR1-4 or GluRA-D, transcribed from human genes *GRIA1-4*), which are assembled as either homo- or heteromers. Determining the subunit composition of AMPA receptors *in vivo* is a challenge due to the presence of subunits within the cytoplasm, rather than at the membrane, and their dynamic regulation. Using single-cell genetic analysis, it was found that neurons in the CA1 region of the hippocampus predominantly contain GluA1/2 heteromers (around 80% of synaptic AMPA receptors) while the rest are GluA2/3 heteromers (Lu *et al.*, 2009). A study looking into co-immunoprecipitation between subunits in different brain regions found the majority of GluA1 associating with GluA2, with some GluA1 not associating with any other subunit and so apparently remaining homomeric (Reimers *et al.*, 2011). This study found that around 50% of AMPA receptors in the CA1 region were GluA2/3 heteromers, contradicting Lu *et al*., a discrepancy proposed to be due to partially assembled GluA2 subunits in particular (Reimers *et al.*, 2011). In general, it is believed that the majority of AMPA receptors in the brain are either of GluA1/2 or GluA2/3 composition, and are

therefore impermeable to calcium due to the presence of the GluA2 subunit. Less is understood about the GluA4 subunit, although it is known to be expressed in the thalamus (Mineff & Weinberg, 2000) and cerebellum (Saab *et al.*, 2012). The subunits are also differentially expressed during development, with expression of subunits generally increasing during synaptogenesis (Arai *et al.*, 1997).

1.1.2 AMPA Receptor Function

Glutamate is the major fast excitatory neurotransmitter of the mammalian central nervous system (CNS), with diverse functions in fast synaptic transmission, long-term potentiation (LTP), long-term depression (LTD) and synaptic plasticity. Glutamate is involved with most areas of the nervous system, from corticospinal tracts controlling motion to nociceptive pathways to learning and memory (Kandel *et al.*, 2000). Glutamate has also been found to play a role in disease states such as ischaemia, traumatic brain injury and hypoxia, as well as various cancers (Willard & Koochekpour, 2013). AMPA receptor gating, the binding of a ligand such as glutamate and the opening of the ion channel, involves three processes: activation, desensitisation and deactivation. Activation occurs when an agonist binding to the LBD of the AMPA receptor leads to a change in its conformation, with the clamshell-like structure of the LBD closing (Jin *et al.*, 2003). This change in conformation opens the ion pore formed of the TMDs, allowing ionic movement through the channel (Armstrong & Gouaux, 2000). Multiple possible conformations of the LBD in response to a variety of ligands allow different activation states of the AMPA receptor (reviewed in Sobolevsky, 2015). Desensitisation occurs when the pore closes, preventing movement of ions through the channel, while the agonist is still bound to the LBD thereby preventing over-stimulation. It is theorised that desensitisation causes further rearrangement of the LBD and reversal of the conformation change that occurred during activation (Sun *et al.*, 2002). The receptor is deactivated when the agonist is unbound from the LBD.

LTP, the strengthening of a synapse through repetitive usage, and LTD, the weakening of a synapse through usage, have been suggested as a molecular basis for at least some forms of learning. Indeed, LTP and LTD, particularly in the hippocampus, have been associated with different learning behaviours (Gruart *et al.*, 2015). During LTP, calcium influx at the synapse in response to NMDA receptor activation leads to AMPA receptor insertion in the post-synaptic density. GluA1-containing AMPA receptors are recruited to the synapse either as a GluA1/2 heteromers (Adesnik & Nicoll, 2007) or initially as GluA1 homomers, with GluA1/2 heteromers replacing these receptors shortly afterwards (Plant *et al.*, 2006). Once these new AMPA receptors are in place, GluA2/3 heteromers replace the subunits to limit calcium influx (Shi *et al.*, 2001). AMPA receptor trafficking to the post-synaptic density is therefore considered essential for synaptic plasticity (reviewed

in Bassani *et al.*, 2013). The process of trafficking AMPA receptors is dependent upon several elements, including the phosphorylation of the subunits themselves, the function of AMPA-receptor interacting proteins and transmembrane AMPA receptor regulatory proteins (TARPs), either in the case of movement to the post-synaptic density for LTP or endocytosing AMPA receptors for LTD (reviewed in Derkach *et al.*, 2007).

The influence of each AMPA receptor subunit can be examined in knockout mice of their respective genes. *Gria1* knockout mice show learning deficits (Reisel *et al.*, 2002) and synaptic dysfunction (Wiedholz *et al.*, 2008), as well as changes in those genes regulating calcium dynamics and processing (Zhou *et al.*, 2009). Knockout of the *Gria2* gene reduces the spine density in the dentate gyrus and alters the structure of the postsynaptic density (Medvedev *et al.*, 2008). *Gria2* knockout mice also show abnormal learning behaviour both in response to a stimulus and place preference conditioning (Mead & Stephens, 2003; Mead *et al.*, 2005). Mice lacking the *Gria3* gene show disturbed sleeping patterns and increased seizure generation (Steenland *et al.*, 2008) as well as changes in behaviour such as increased aggression (Adamczyk *et al.*, 2012). Mice lacking in both *Gria2* and *Gria3* show increased LTP in the hippocampus, possibly due to increased calcium currents (Meng *et al.*, 2003). Low expression or knockout of *Gria4* was associated with a phenotype that models absence seizures in mice (Beyer *et al.*, 2008) and neurons showed reduced spontaneous excitation in thalamic circuitry (Paz *et al.*, 2011). Knockout of both the *Gria3* and *Gria4* genes resulted in a loss of AMPA receptor response in the thalamic region (Wang *et al.*, 2011). It therefore appears that AMPA receptors play a major role in learning and behaviour by influencing synaptic function.

1.1.3 AMPA Receptor Regulation

AMPA receptor subunits are expressed in both glial and neuronal cells but their expression is much higher in neuronal cells. *Gria1* expression is regulated by acid sphingomyelinase and NFKB sites in the promoter region, while little is known about the transcriptional regulation of *Gria3* and *Gria4*. On the other hand, the transcriptional regulation of *Gria2* is well studied due to its importance in calcium intake at the synapse. The *Gria2* promoter was found to be thirty times more active in neuronal cells than in glial cells due to the RE1/NRSE promoter silencer element and the control of Sp1 and NRF-1 transcription factors (Myers *et al.*, 1998). NRF-1 appears to specifically control the GluA2 promoter region but not the other AMPA receptor subunits (Dhar *et al.*, 2009). Once transcribed, there are also controls over translation of the subunit mRNA. mRNA transcripts of AMPA receptor subunits can be transported along dendrites, suggesting that local translation can take place away from the cell soma (Grooms *et al.*, 2006). As well as regulation through changes in subunit translation, AMPA receptors are regulated

through altered shuttling to and from the membrane from intracellular reserve pools, which acts as the predominant form of AMPA receptor regulation (Petrini *et al.*, 2009).

1.1.4 Post-transcriptional Modifications

AMPA receptor subunits undergo various degrees of co-transcriptional, post-transcriptional and post-translational modifications. The RNA transcripts of subunits have been shown to be altered in different processes such as alternative splicing or the deamination of adenosines. All AMPA receptor subunits undergo alternative splicing at the ligand binding domain, forming either the “flip” or “flop” isoform with the inclusion of either exon 14 or exon 15 respectively (Sommer *et al.*, 1990). This process was found to influence desensitisation (Mosbacher *et al.*, 1994). In *Xenopus laevis* oocyte preparations, it was found that homomers with flip variants of each of the subunits have an increased time constant for desensitisation, and conversely flop variants are more readily desensitised (Koike *et al.*, 2000). While expression of the flip isoform appears to remain constant, the flop isoforms increase in expression during post-natal development, which suggests a role for them in more mature neurons (Monyer *et al.*, 1991).

Flip and flop isoforms are also differentially expressed and localised across the brain regions. The flop isoform, for example, is found uniformly across the neocortex of mice, whereas the flip isoforms are expressed in laminar patterns with higher expression in layers II, III and VI (Sommer *et al.*, 1990). Within neurons, the flip isoform has been shown to be predominantly trafficked along dendrites, whereas the flop isoform remains in the soma (Coleman *et al.*, 2006). The splicing pattern of subunits also appears to be dynamically regulated. For example, there was increased expression of the GluA2 flip isoform in the hippocampus of rats after seizures (Gitaí *et al.*, 2010), while in cultured neurons there was an increase in expression of the flip isoforms for GluA2, GluA3 and GluA4 subunits following depolarisation (Orlandi *et al.*, 2011).

Alternative splicing of subunits GluA2, 3 and 4 is governed by the so-called “R/G” editing site located on exon 13 between transmembrane domains 3 and 4, as shown in Figure 1.1A (Lomeli *et al.*, 1994). RNA editing in the GluA2 subunit describes the deamination of adenosines in its mRNA transcript, and is discussed later. A positive correlation was found between the edited form of transcripts and the flip isoform, possibly due to the editing site residing near the splice site for exon 13 and therefore influencing the splicing machinery (Schoft *et al.*, 2007). Other RNA editing sites, such as the Q/R site and hotspots within introns, are found within the GluA2 subunits and play important roles in the correct function of the AMPA receptors. Two hotspots are found within intron 11 of GluA2, hotspot 1 and hotspot 2 (Higuchi *et al.*, 1993), and editing is required for efficient removal of intron 11 (Schoft *et al.*, 2007). The Q/R editing site of the GluA2 subunit is critical for the subunit’s permeability to calcium and is discussed later. Although subunits

GluA2, 3 and 4 are all edited at the R/G site, only the GluA2 subunit of AMPA receptors is edited at the Q/R site.

Once translated, phosphorylation of the AMPA receptor subunits influences a number of intracellular events such as localisation and interactions with other proteins (Traynelis *et al.*, 2010). Other post-translational modifications include palmitoylation and ubiquitination (reviewed in Lu & Roche, 2012). Palmitoylation, along with subsequent depalmitoylation, of all four AMPA receptor subunits has been implicated in correct trafficking and also serves as protection against degradation of the proteins (Hayashi *et al.*, 2005). Ubiquitination of subunits has been linked to internalisation and occurs either before endocytosis with GluA1 (Schwarz *et al.*, 2010) or after endocytosis with GluA2 (Lussier *et al.*, 2011).

1.1.5 The GluA2 Subunit

An AMPA receptor's permeability to calcium is determined by the presence of the GluA2 subunit, which makes the receptor impermeable to divalent ions such as calcium but still permeable to monovalent ions, and can therefore regulate calcium intake of the neuron (Burnashev *et al.*, 1992). GluA2 subunits restrict calcium ion flow via a single amino acid (arginine) within the second transmembrane sequence (Figure 1.1C). The size and positive charge of arginine both contribute to the impermeability (Burnashev *et al.*, 1992). Sequencing of the *GRIA2* gene revealed that codon 586 was CAG, coding for arginine, whereas residue 607 in the amino acid sequence of GluA2, deduced by sequencing of the cDNA, was glutamine (Sommer *et al.*, 1991; Higuchi *et al.*, 1993). This change in base occurs in the RNA transcript and is the result of RNA editing at what has been termed the "Q/R site" due to the change in codon from glutamine (Q) to arginine (R). The Q/R site's location in the second transmembrane domain is next to the pore, so can influence ion flow (Figure 1.1D). Homomers of edited GluA2 subunits show lower single channel conductance than unedited homomers (Swanson *et al.*, 1997) and editing also appears to regulate tetramerisation of subunits, as edited GluA2 subunits remain in the endoplasmic reticulum while unedited subunits form tetramers before being trafficked to the cell membrane (Greger *et al.*, 2003). This localisation to the endoplasmic reticulum may regulate the number of GluA2 subunits that are included in the dimer and therefore tetramer formation of the whole AMPA receptor (Greger *et al.*, 2003). The GluA2 subunit therefore regulates ion conductance through AMPA channels at two levels: by regulating the assembly of the receptor and by changing the permeability to divalent ions.

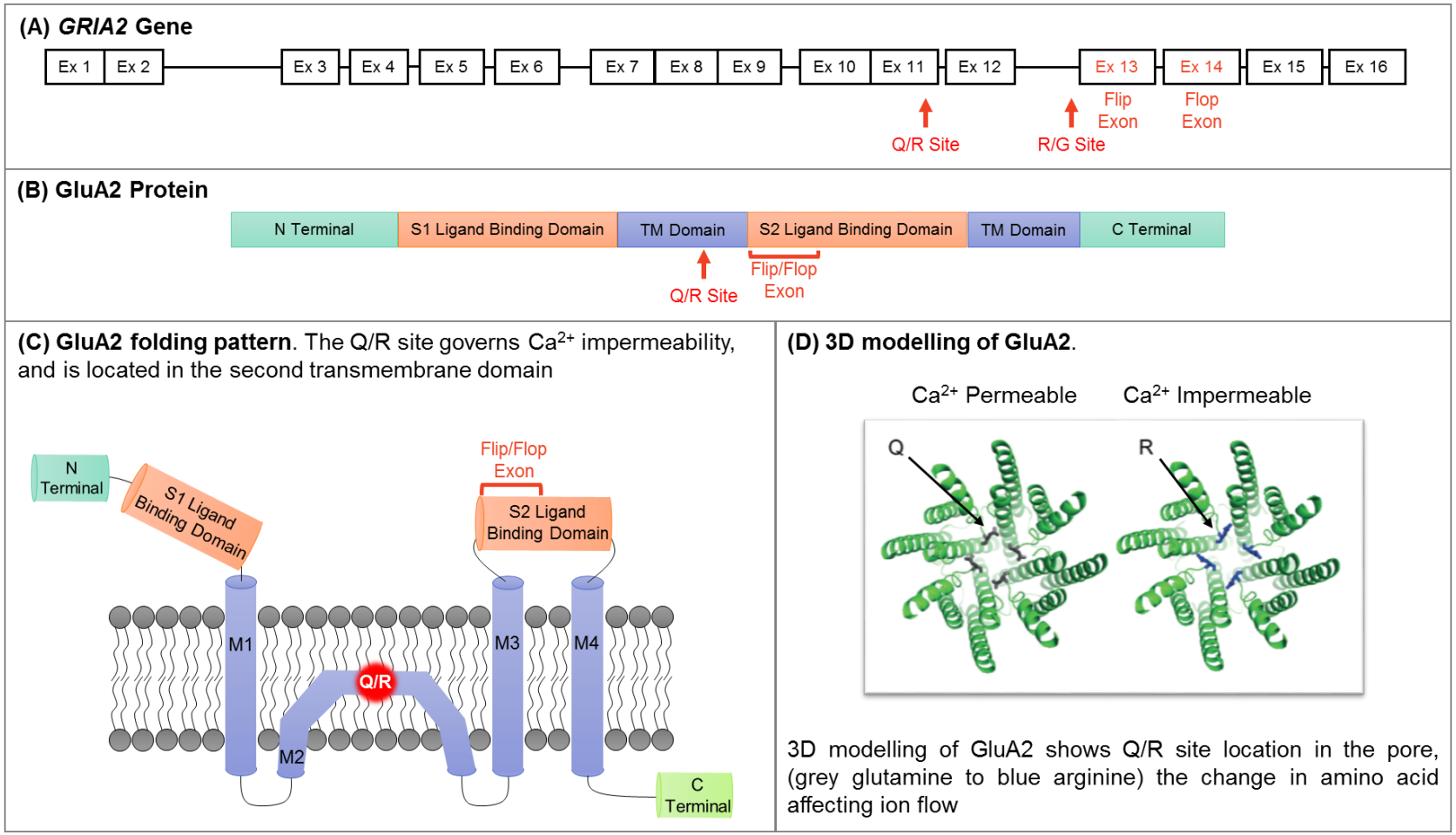

Figure 1.1 - Schematics of the GluA2 subunit in AMPA receptors. The presence of the GluA2 subunit in the AMPA receptor complex prevents calcium entry due to the arginine at the Q/R site. The Q/R site is located in the second transmembrane domain of the subunit, situating the amino acid directly next to the ion flow (modelling from Wright & Vissel, 2012). The R/G editing site is located between the third and fourth transmembrane domains and governs alternative splicing of the flip/flop exon.

Calcium entry into a neuron can be controlled by dynamically altering expression of the GluA2 subunit compared to subunits GluA1, 3 and 4. Relative expression of the AMPA subunits are known to vary throughout development, with the expression of GluA2 increasing postnatally in mouse along with other synaptic markers as synapses develop (Pandey *et al.*, 2015). AMPA receptors are predominantly expressed by neuronal cells rather than glial cells in the CNS (Orlandi *et al.*, 2011). Cultured rat cortical neurons show increasing expression of all four subunits as they undergo maturation *in vitro* (Orlandi *et al.*, 2011). Orlandi *et al.* also showed that glutamate stimulation alters the relative expression of subunits, leading to downregulation of the GluA1 subunit and upregulation of the GluA2 subunit. The opposite change was shown in response to inhibited neuron stimulation by treatment with tetrodotoxin and APV (blocking sodium channels and NMDA channels respectively). This dynamic variation in subunit expression is still an area of investigation, particularly due to the regulatory elements for this system still being unknown. However, the importance of regulating GluA2 expression is becoming apparent, as switches between AMPA receptors containing GluA2 and lacking in GluA2 have been found in the process of both long term potentiation and long term depression (Liu & Savtchouk, 2012). It also appears that expression of GluA2 is altered under pathological conditions. For example, sustained downregulation of the GluA2 subunit in the hippocampus was found following ischaemic insults in rats prior to the associated cell death (Noh *et al.*, 2005).

1.2 RNA EDITING

1.2.1 Forms of RNA Editing

RNA editing describes the modification of RNA transcripts so that the sequence differs from the original DNA. It was originally described in protozoans where uridylate residues are inserted into RNA sequences and is now thought to occur in most eukaryotes (Gray, 2012). There are two major forms of RNA editing found in mammalian transcriptomes, caused by the deamination of a base thus changing the coding sequence. The first and most prevalent is A-to-I editing, where an adenosine is deaminated by the enzyme family adenosine deaminases acting on RNA (ADARs) to form the base inosine. In the deamination process, the amine group in adenosine is hydrolysed and released as ammonia, leaving a ketone group in the inosine molecule (Figure 1.2A). Inosine is read by the translational machinery as guanosine, thereby changing the coding sequence. This is due to the inosine molecule forming a stable base pair with cytosine (Figure 1.2B), whereas bonding with a thymine base forms a less stable base pair (Figure 1.2C), and so polymerases will preferentially pair inosines with cytosines (Yasui *et al.*, 2008).

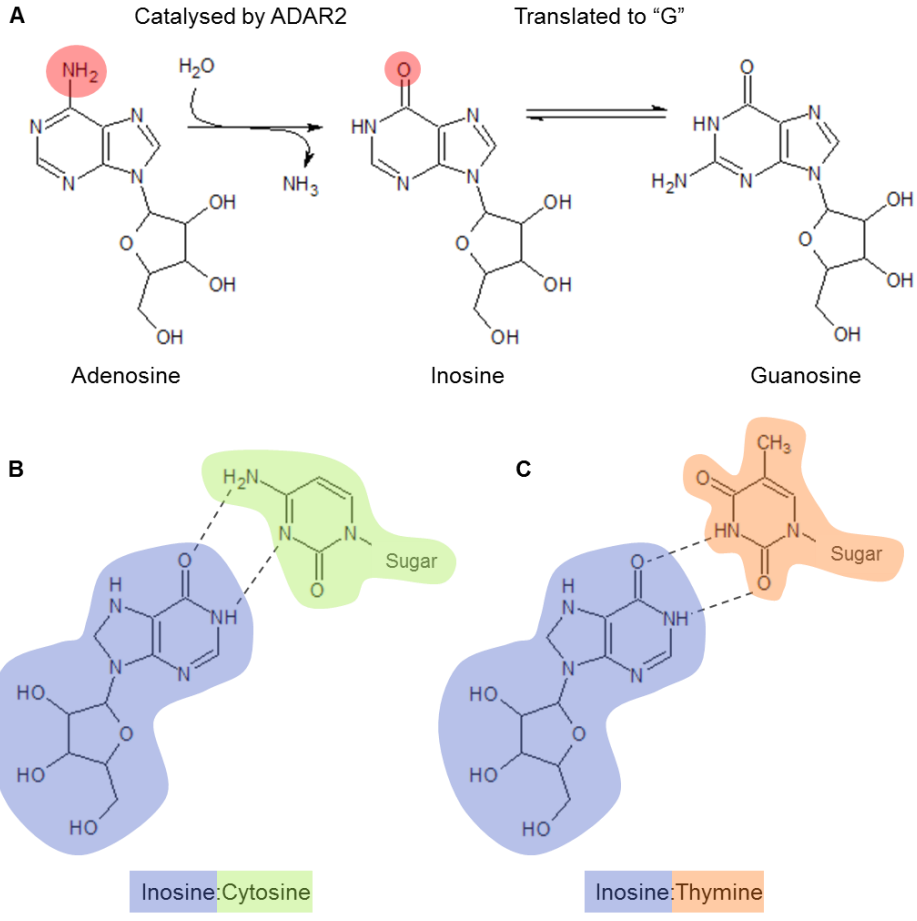

Figure 1.2 – A) Chemical structures of adenosine and inosine. The site of hydrolytic deamination is shaded red in the adenosine and inosine structures. The similarity between inosine and guanosine leads to any inosine residues being mistaken for guanosine by the translation machinery (Kono & Akiyama, 2013). *Watson-Crick base pairing between inosine and cytosine (B) is more stable than between inosine and thymine (C).*

The second form of RNA editing found in mammalian transcriptomes is C-to-U editing, where cytosine residues are deaminated to uracil bases. The most common and well-studied example of this form of editing is in the apolipoprotein B transcript, where RNA editing changes a codon from CAA in the genomic sequence to UAA in the RNA transcript and therefore introducing a stop codon (Chen *et al.*, 1990). This form of RNA editing is catalysed by the apolipoprotein B mRNA editing catalytic polypeptide-like (APOBEC) enzyme family, a diverse group of at least 10 enzymes that can recognise both DNA and RNA and therefore lead to many different modifications (reviewed in Salter *et al.*, 2016). More than 50 mRNA transcripts in the mouse transcriptome have been shown to be a target for APOBEC1 (Rosenberg *et al.*, 2011) whereas APOBEC3A has several hundred targets including roles in anti-viral and anti-retrotransposon defences (Sharma *et al.*, 2015). There are also other, rarer, forms of RNA editing. For example, APOBEC3A has been associated with G-to-A editing in the Wilm's tumour susceptibility gene through an unknown mechanism (Niavarani *et al.*, 2015). Mitochondrial tRNAs in *Physarum* species have been shown to require RNA editing in the form of insertion of a base in their precursor transcript before maturation can take place (Gott *et al.*, 2010) and U-to-C editing in tRNAs of marsupials have been shown to change their codon recognition sequences (Borner *et al.*, 1996). RNA editing in rRNA transcripts is rarer still, but insertions of bases in rRNA transcripts has been observed in *Physarum* species (Mahendran *et al.*, 1994).

1.2.1.1 Mechanism of deamination

In the context of AMPA receptor subunits, RNA editing describes the hydrolytic deamination of an adenosine to an inosine residue (Gray, 2012), or "A-to-I editing", shown in Figure 1.2 and henceforth referred to simply as "RNA editing". Deamination is catalysed by the enzyme family adenosine deaminases acting on RNA (ADARs) which recognise the double-stranded structure of RNA transcripts, rather than displaying sequence recognition. Unusually for RNA binding proteins, ADARs approach the RNA from the minor groove at the editing site, requiring a conformational change in the RNA to widen the major groove opposite the editing site (Matthews *et al.*, 2016). Once the ADAR is bound to the duplex RNA structure, the targeted adenosine "flips" out of alignment of the duplex and into the hydrophobic active site of the catalytic domain of the ADAR (Yi-Brunozzi *et al.*, 2001). In this state, the amine group can be hydrolysed and the adenosine is deaminated to form inosine, catalysed by a zinc ion found within the ADAR structure (Macbeth *et al.*, 2005). Genes coding for ADAR enzymes are found in genomes throughout the animal kingdom (Jepson & Reenan, 2008), and comparative genetic analysis has suggested that the first ADAR-like gene originated just after the split of protozoa and metazoa (Jin *et al.*, 2009). Three ADARs are coded for in the mammalian genome, although ADAR3 appears to be non-functional and may compete

for binding sites with ADAR1 and ADAR2, possibly acting as a form of negative regulation (Hogg *et al.*, 2011). ADAR1 is prevalent in the CNS and elsewhere in the body, whereas ADAR2 and ADAR3 appear to be more localised to the CNS (Gray, 2012).

1.2.1.2 Function of RNA editing

Initially, the concept of altering bases after transcription could be considered at best unnecessarily laborious and at worst detrimental to the genes being expressed. Indeed, there are some sites in the human coding sequence at which A-to-I editing occurs at a high frequency and are deleterious to the protein, although *in silico* analysis of protein reactions indicate little change at the system level (Solomon *et al.*, 2014). However, there are several advantages to the editing process. The majority of editing sites show variable levels of editing, with many showing an editing level of less than 50% (Ramaswami *et al.*, 2013). Although there are instances where the edited base has been permanently changed to a guanosine in the genome across different species (Li *et al.*, 2009), indicating that a mutation at the DNA level is a viable alternative in these cases, the flexibility of the editing process allows a single cell to transcribe both sequences, possibly safeguarding against deleterious mutations (Rieder & Reenan, 2012). In a study analysing 28 editing sites across four different developmental time points, two embryonic and two post-natal, it was found that almost all editing sites began with low levels of editing that increased through development, with the exception of the Q/R site in the GluA2 subunit which was edited at 100% at all time points (Wahlstedt *et al.*, 2009). This regulation is apparently separate from expression levels of either ADAR1 or ADAR2, indicating other regulatory elements in the editing system that have yet to be identified. This flexibility in RNA editing levels therefore allows the embryonic cell to express a different isoform to the adult cell. Although RNA editing is prevalent across species, it has been suggested that the editing process has played a role in the evolution of higher organisms, as they show increased RNA editing activity (Gommans *et al.*, 2010). In fact, the high levels of editing in the human transcriptome compared to other non-human primates, and their predominance in the CNS, suggests that this may be a factor in the development of higher brain function in humans (Paz-Yaacov *et al.*, 2010). As well as the benefits in transcriptome diversity, RNA editing plays a role in the immune response. ADAR1 has an isoform that is inducible by interferon, and can edit the double-stranded RNA of invading viruses, preventing pathogenicity (Samuel, 2012), although some viruses such as HIV have evolved to take advantage of the RNA editing system in their propagation (Doria *et al.*, 2009).

The importance of editing is highlighted by *Adar1*$^{-/-}$ knockout mice, which have a phenotype that is lethal at embryonic day 11 due to defects in liver structure (Hartner *et*

al., 2004). These mice also show that ADAR1 is essential for maintenance of haematopoietic stem cells, where it suppresses interferon signalling pathways (Hartner *et al.*, 2009). *Adar2*$^{-/-}$ knockout mice survive until around post-natal day 21 after developing early-onset epilepsy (Brusa *et al.*, 1995). This lethality is specifically due to the editing at the Q/R site of the GluA2 subunit, as crossing these knockout mice with a line containing the "edited" codon rescued the phenotype (Horsch *et al.*, 2011). Therefore, although the editing process has been shown to be beneficial, both in terms of development and evolution, as well as normal functioning of organisms, the RNA editing of the Q/R site remains something of an enigma. The usual advantage of RNA editing, its flexibility, is lethal at the GluA2 Q/R site. In fact, in some fish species a mutation has changed the base to a guanosine in the genomic sequence so that the codon codes for an arginine without the need for RNA editing, thus removing the potential for error (Kung *et al.*, 1996). Why the GluA2 Q/R site has remained dependent on the RNA editing process in the majority of species, despite the possibility of a lethal phenotype if the process is inefficient, remains unclear.

1.2.2 ADAR Structure

All ADARs in the mammalian genome have a similar modular structure, with a catalytic domain at their C-terminus and double-stranded RNA binding domains (dsRBMs), and Z-DNA binding domains in the case of ADAR1, at their N-terminus (Figure 1.3). The Z-DNA binding domains of ADAR1 make this ADAR unique across the adenosine deaminase enzyme family, although the function of this interaction is still unknown (Herbert *et al.*, 1997). ADAR1p150 (1226 amino acids) is the interferon-inducible isoform of the enzyme, and contains the active Z-DNA binding domain (Patterson & Samuel, 1995). ADAR1p110 is constitutively expressed and begins at exon 2 of the enzyme, making it a shorter protein of 931 amino acids in humans (George *et al.*, 2011). ADAR2 is a shorter enzyme still, with 701 amino acids and just two dsRBMs compared to ADAR1's three (Figure 1.3). The catalytic domain is conserved across fish and mammals, whilst the dsRBMs vary (Slavov *et al.*, 2000), although dsRBM1 appears to be better conserved than dsRBM2 (Slavov & Gardiner, 2002). The dsRBM is a 65-70 amino acid domain that is conserved across eukaryotic proteins with a conserved αββββα structure (Masliah *et al.*, 2013). It is common across RNA-binding proteins such as Dicer and Drosha, processing miRNAs, and TRBP in the RNAi pathway. Deletion or mutations introduced into either of the two dsRBMs in ADAR2 found that dsRBM1 appears to be more important for localisation of the enzyme, as the deletion of dsRBM1 led to diffuse fluorescence throughout the cell compared to localisation in the nucleolus, while dsRBM2 is more involved in the editing process as deletion reduced editing activity to 50% of wild-type ADAR2 (Xu *et al.*, 2006). Inositol hexakisphosphate bound to ADAR2

stabilises the enzyme and is thought to contribute to its catalytic activity by slightly modifying the structure (Macbeth *et al.*, 2005).

Figure 1.3 - Structural features of mammalian ADARs. Both transcripts of ADAR1 contain three double-stranded RNA binding motifs (dsRBMs), with ADAR1p150 containing two Z-DNA binding domains while ADAR1p110 only contains one. ADAR2 is shorter than the ADAR1 transcripts and only contains two dsRBMs. ADAR3 also contains two dsRBMs and an arginine-rich domain (noted as R). All four transcripts have the catalytic domain at their C-terminal.

Both ADAR1 and ADAR2 form homodimers at certain editing sites around the RNA molecule, a process dependent upon the presence of RNA, and this quaternary structure is necessary for efficient editing (Jaikaran *et al.*, 2002; Cho *et al.*, 2003). There was no evidence of heterodimer formation between ADARs. ADAR3 on the other hand does not dimerise, which may explain why it is non-functional (Chen *et al.*, 2000). ADAR3 is also shown to inhibit the actions of ADAR1 and ADAR2 on RNA, indicating a possible role as a negative regulator of RNA editing (Chen *et al.*, 2000).

Efficient deamination of adenosines is dependent upon the formation of double-stranded regions of RNA. There are two forms of A-to-I editing found in the genome: site-specific and promiscuous editing. Site-specific deamination is found amongst imperfect RNA duplexes. Complementary sequences in the RNA substrate that form the double-stranded regions can be interspersed by large sections of single-stranded RNA, forming bulges and loops in the molecule's secondary structure (Dawson *et al.*, 2004). The imperfect duplex is important for RNA editing, as mutating the sequence so that base pairing was complete, apart from the binding partner of the edited adenosine, halved the editing efficiency (Ohman *et al.*, 2000). This indicates that the bulges and loops formed from imperfect double-stranded RNA are a requirement for efficient editing, possibly reducing the number of ways that the ADAR can bind to the double-stranded RNA. Apart from loops within a duplex of RNA, editing is not dependent upon other secondary structure features and is not found to be particularly focussed in disordered regions of secondary structure (Solomon *et al.*, 2014).

It is difficult to determine the structure of the ADAR-RNA complex due to the lack of specific recognition sites, and so ADAR may bind in multiple conformations to the same double-stranded RNA transcript with equal affinities. Different groups have concluded

that site selectivity is controlled by either the catalytic deaminase domain (Wong *et al.*, 2001) or by the dsRBMs (Stephens *et al.*, 2004). More recently, it has been suggested through binding analysis that ADAR-RNA binding is controlled through the catalytic domain, but binding is dependent upon the presence of double-stranded RNA 5' to the editing site dsRBMs (Phelps *et al.*, 2015). Indeed, there are specific amino acids within the catalytic domain that have been shown to be involved in ADAR2 binding but are different from the ADAR1 sequence, possibly contributing to the differences in the two enzymes' binding substrates (Matthews *et al.*, 2016).

An adenosine on its own is not enough to be recognised by an ADAR, its position on the duplex and the surrounding bases also play a role (Dawson *et al.*, 2004). For example, at the R/G site of the GluA2 subunit, there are other adenosines within the duplex which are not deaminated (Stephens *et al.*, 2000). ADAR1 and ADAR2 have distinct but overlapping rules when it comes to selection of an adenosine to be deaminated. ADAR1 shows a preference for adenosine or uracil over cytidine or guanosine as the 5' neighbouring base of the edited adenosine, but does not appear to have a similar rule for the 3' neighbour (Polson & Bass, 1994). Similarly, ADAR2 shows a preference for adenosine and uracil for the 5' neighbouring base, but it also shows a preference for the 3' base of guanosine or uracil over cytidine and adenosine (Lehmann & Bass, 2000). The base opposite the edited adenosine in the duplex cannot be uracil, as the adenosine must remain unpaired, and there is also a preference for cytidine over guanosine at this position (Wong *et al.*, 2001). It appears that these preferences over neighbouring bases are not caused by the sequence itself, but are rather due to the effect of the neighbouring bases on the base flipping of adenosine (Kuttan & Bass, 2012). The point at which the targeted adenosine falls in the duplex structure also appears to be important, as ADAR1 will not edit a base within three nucleotides of the 5' end of the helix or 8 nucleotides from the 3' end of the helix, and ADAR2 has a limit of two nucleotides from either end (Lehmann & Bass, 2000). However, these rules cannot fully describe why ADAR1 edits some sites and not others, likewise for ADAR2, nor can it explain why some adenosines fulfilling these preferences remain unedited.

1.2.3 RNA Editing of Non-coding RNAs

Promiscuous editing, or non-site specific editing, is found throughout intronic sequences of the genome and particularly in Alu sequences. In a perfect double-stranded section of RNA, up to 50% of adenosines may be edited (Savva *et al.*, 2012). Alu sequences are short, interspersed elements; retrotransposons which duplicate themselves through reverse transcription of an RNA intermediate and spread through germline transmission. At present, Alu sequences are thought to make up 11% of the human genome (Ade *et al.*, 2013). As long as the Alu element has another in the reverse orientation nearby to

form the double-stranded structure, which is virtually always the case, it can be edited (Bazak *et al.*, 2014). It was found that almost all adenosine bases within Alu sequences of non-coding regions had the capacity to be edited, although most showed very low levels of editing at less than 1% (Bazak *et al.*, 2014). Despite this low level of editing at individual sites, the cumulative editing across the non-coding regions of the transcriptome dwarfs editing within coding regions, and so cannot be discounted (Bazak *et al.*, 2014). Having large quantities of double-stranded RNA is detrimental to the cell, often activating anti-viral defences, however Alu elements appear to be the exception to this rule (Levanon & Eisenberg, 2015). Editing within Alu elements destabilises the double-stranded structures formed, and so may be a compensatory mechanism against the increase in double-stranded elements in the primate genome. It is also interesting to note that, as Alu elements invaded the primate genome, the editing rate at functional sites did not change, despite the increasing number of target sites for ADAR enzymes. This may be due to a division of labour as, whilst ADAR2 edits many of the functional editing sites such as the Q/R site in the GluA2 subunit, ADAR1 has been found to mainly edit the non-coding editing sites, although there is a great degree of overlap (Riedmann *et al.*, 2008). One theory suggests that the editing of Alu sequences is used to promote sequence-specific editing sites, possibly through recruitment of ADARs, as site-specific editing is found closer to Alu sequences than would simply be predicted by chance (Daniel *et al.*, 2014). Alu sequences are also commonly found as alternatively spliced exons, and editing of Alu elements can change the splicing patterns by removing stop codons (reviewed in Levanon & Eisenberg, 2015).

Alu elements are known to contain microRNA (miRNA) target sites, and so editing Alu sequences may play a role in regulating the miRNA system (Liang & Landweber, 2007). As well as editing their target sites, miRNA sequences are also known to undergo editing themselves. Around 6% of primary miRNAs (pri-miRNAs) are edited at one or more bases, destabilising the hairpin structure essential for correct pri-miRNA processing (Gommans, 2012). By disrupting the cleavage of pri-miRNA into miRNAs, there will be fewer miRNAs available to perform their regulatory function. This editing may therefore lead to drastic changes in gene expression. Editing of non-coding RNAs has also been implicated in the RNA interference system, with roles both supporting and inhibiting the RISC complex (Nishikura, 2006). A decrease in editing is associated with several forms of cancer (Paz *et al.*, 2007). For example, under-edited miRNA-376a* contributes to increased migration and invasiveness of human glioma cells (Choudhury *et al.*, 2012), whereas under-editing of miRNA-455-5p has been linked to severity of melanomas, possibly through inhibited expression of tumour-suppressant genes (Shoshan *et al.*, 2015). When analysing RNA-seq samples from a variety of cancer patients, a positive correlation was found between dysregulation of RNA editing in the 3’ UTR of mRNAs,

often containing miRNA target sites, and the progression of tumours (Zhang *et al.*, 2016). On the other hand, increased levels of RNA editing of antizyme inhibitor 1 were found in samples of hepatocellular carcinoma (Chen *et al.*, 2013).

1.2.4 Identification of RNA Editing Sites

A variety of methods have been used to determine RNA editing sites in the transcriptome. When RNA editing was first discovered, it was through identified mismatches between sequencing of DNA and RNA. It was therefore difficult to distinguish true RNA editing sites from mistakes in sequencing, with individual sites being characterised through laborious cloning and RNA isolation techniques (Sommer *et al.*, 1991; Burns *et al.*, 1997). The complete sequencing of various genomes allowed comparisons between known editing sites and the surrounding sequences across species. This led to proposed “signatures” at RNA editing sites that could be used to search for novel edited adenosines (Hoopengardner *et al.*, 2003). However, these approaches overly constrained the search for editing sites, and novel adenosines were mostly located in coding sequences. The editing sites in coding sequences could be experimentally verified, and groups published results identifying handfuls of editing sites at a time (Hoopengardner *et al.*, 2003; Levanon *et al.*, 2005). The development of whole-transcriptome sequencing (RNA-seq) technology revealed the complexity of the transcriptome (reviewed in Wang *et al.*, 2009). Comparisons between DNA and RNA sequences showed that RNA editing was not just found in coding sequences, but was also prevalent in non-coding regions. Initial comparisons estimated 10,000 editing sites in human cell lines (Bahn *et al.*, 2012), which has since expanded to predicting millions of A-to-I editing sites in the human transcriptome (Bazak *et al.*, 2014). With such a large number of editing sites, there are now databases cataloguing editing sites and average editing levels at each site. Databases include RADAR (Ramaswami & Li, 2014), DARNED (Kiran & Baranov, 2010), RCARE (Lee *et al.*, 2015) and RED (Sun *et al.*, 2016). However, these databases are only as strong as the data that support them, leading to discrepancies. For example, the number of editing sites found in coding sequences is dependent upon the detection method. The RADAR database identifies 2411 editing sites in the human coding sequence, whereas the DARNED database records a more conservative 710 sites. When comparing these editing sites with the RefSeq gene sequences, Solomon *et al*. calculated a total of 708 non-synonomous editing sites in the human coding sequence (Solomon *et al.*, 2014). Databases now also include tissue-specific editing frequencies at individual sites, and are constantly improving techniques to correct for detection errors, such as including “hyper edited” RNAs which are often missed in RNA-seq analysis (Porath *et al.*, 2014; Picardi *et al.*, 2015).

1.2.5 ADAR2

ADAR2, first distinguished from ADAR1 in the 1990s, was the second enzyme in the mammalian ADAR family to be discovered, and has also been known as ADARB1, RED1 or DRADA2 (Melcher *et al.*, 1996; O'Connell *et al.*, 1997). In the developing mouse at embryonic day 15 (E15), ADAR2 expression is not detected (Jacobs *et al.*, 2009). In early development, expression of ADAR2 is limited to the thalamic nuclei of mice, but by postnatal day 7 (P7) is to be found in areas such as the hippocampus and cerebellum, while there is very low expression in the neocortex even at P21 (Paupard *et al.*, 2000). In adult mice, ADAR2 has a relatively low expression in the cortex compared to other brain regions, with the highest expression in the thalamus. This coincides with high levels of editing in thalamic neurons compared to other neuronal populations (Jacobs *et al.*, 2009). The regulation of ADAR2 expression remains an area of active investigation. It is known that CREB can act as a transcription factor to activate ADAR2 expression (Peng *et al.*, 2006), and that ADAR2 can regulate its own expression through a negative feedback loop which requires self-editing (Rueter *et al.*, 1999). This self-editing alters the alternative splicing pattern of ADAR2, introducing a 47 nucleotide cassette (shown in Figure 1.4) which shifts the reading frame, forming a truncated protein which is non-functional. ADAR2 is also regulated by tight control of localisation, specifically to the nucleolus (Sansam *et al.*, 2003), as opposed to ADAR1 which is also found throughout the cytoplasm (Desterro *et al.*, 2003). ADAR2 is shuttled into and out of the nucleolus from the nucleoplasm dynamically, which may be governed by the presence of editing substrates or small nucleolar RNAs (snoRNAs) (Desterro *et al.*, 2003). Pin1 aids in the nuclear localisation of ADAR2, with WWP2 acting as a negative regulator (Marcucci *et al.*, 2011) alongside the nuclear localisation signal found within ADAR2 itself (Maas & Gommans, 2009a). Another *trans*-factor implicated in ADAR2 regulation is a snoRNA, MBII-52. This snoRNA is brain-specific and has been shown to inhibit editing of the 5-HT_{2C} serotonin receptor through binding to the pre-mRNA itself thus preventing editing (Vitali *et al.*, 2005). It is therefore possible that snoRNAs contribute to ADAR2 regulation by acting as site-specific inhibitors. Interestingly, there have been recent reports of altered editing events in response to neuronal activity in the hippocampus (Balik *et al.*, 2013), further supporting the idea that RNA editing is a mechanism for the fine-tuning of the nervous system. However, overstimulation of neurons by long-term exposure to glutamate at high concentrations (100 μM for an hour) leads to cleavage of ADAR2 and therefore a loss of editing (Mahajan *et al.*, 2011).

1.2.6 Alternative Splicing of ADAR2

Alternative splicing refers to the inclusion or exclusion of sections of RNA in the final mRNA transcript, allowing the expression of different isoforms of the same protein. Intronic sections or whole exons, sometimes called cassette exons, can be introduced

or removed from the transcript depending on the splicing machinery. ADAR2 has long been known to undergo alternative splicing (Lai *et al.*, 1997; Rueter *et al.*, 1999). Splicing events include an 'AluJ cassette' insertion after exon 5, early termination at the C-terminus, a 47 nucleotide insertion in exon 2, and the inclusions of intron 9 and exons 7a, 0 and 1a as summarised in Figure 1.4. Splicing of ADAR2 at any given site appears to be independent of the other splicing events, leading to a large number of splice variants in the human transcriptome (Kawahara *et al.*, 2005). The splice variants also seem to be able to edit RNA substrates with different efficiencies, and the rates of splicing are variable between species. For example, the insertion of the 47 nucleotide cassette shows low inclusion in humans (15%) compared to mice (80%) (Slavov & Gardiner, 2002). The 47 nucleotide insertion causes a shift in the reading frame creating an editing site that forms an early stop sequence. This truncated protein is not functional, and is thought to be part of the regulation of ADAR2 expression, as mentioned above (Slavov & Gardiner, 2002).

The inclusion of the 120 nucleotide AluJ cassette after exon 5 reduces the editing efficiency of the human ADAR2 enzyme by 50%, whereas the equivalent inclusion of a 30 nucleotide AluJ cassette in the murine version improved its editing efficiency (Slavov & Gardiner, 2002). The C-terminus of ADAR2 can be spliced in a variety of ways. Splice variant "L-1" is the most prevalent in the human brain and contains the insertion of intron 9. The second most prevalent isoform is the "S" variant in which exon 9 and intron 9 are not included and this splice variant shows no catalytic activity. It is debatable whether this variant is even translated into a protein (Kawahara *et al.*, 2005). Variants "L-2" and "L-3" are relatively rare and contain longer or shorter versions of exon 9 respectively, without intron 9 (Kawahara *et al.*, 2005). "Exon 0" is an insertion upstream of exon 1 and is thought to be controlled by a different promoter. ADAR2 transcripts containing exon 0 have been found in both human and mouse brains although there is apparently no difference in catalytic activity (Maas & Gommans, 2009b). "Exon 7a" has been described as showing high levels of inclusion in ADAR2 transcripts in other tissues such as the heart and testes but low inclusion in the brain (around 3%), although its inclusion does appear to reduce ADAR2 catalytic activity significantly (Agranat *et al.*, 2011). Although there are multiple possible alternatively spliced transcripts of ADAR2, the insertion of the AluJ cassette after exon 5 merits attention. The AluJ cassette is expressed in the mammalian nervous system and its inclusion decreases the efficiency of the ADAR2 enzyme. Therefore manipulation of splicing to inhibit expression of this less efficient isoform could be a potential therapeutic target.

A

Exon	Description	Expression Pattern	Impact on Editing Activity	Reference
-2	Non-coding exon in 5' UTR			Villard et al., 1997
-1	Non-coding exon in 5' UTR			Villard et al., 1997
0	Coding exon using a separate translational start site and initiation codon	Found in around 10% of transcripts from CNS, lower expression in other tissues	Not reported	Maas and Gommans, 2009
1a	Alternatively spliced exon altering N terminal properties	Included in around 40% of all tissues examined	Not reported	Slavov and Gardiner, 2002
1	Constitutive exon			Villard et al., 1997
2	47 nucleotide insertion leading to premature stop codon	Found in around around 15% of transcripts	Forms a non-functional, truncated protein	Slavov and Gardiner, 2002
	Alternatively spliced exon, exclusion leads to premature stop codon in exon 3	Exclusion found in around 20% of CNS transcripts	Exclusion leads to truncated protein	Kawahara et al., 2005
3	Constitutive exon			Villard et al., 1997
4	Constitutive exon			Villard et al., 1997
5	Constitutive exon			Villard et al., 1997
5a	Alternatively spliced exon, the "AluJ Cassette"	Higher inclusion in brain tissues than peripheral tissues	Inclusion reduces editing by around 50%	Lai et al., 1997, Gerber et al., 1997
6	Constitutive exon			Villard et al., 1997
7	Constitutive exon			Villard et al., 1997
7a	Alternatively spliced exon	High levels (~ 50%) found in skeletal muscle, heart and testes, low levels (3%) in the CNS	Some evidence of an inverse correlation between exon 7a inclusion and editing activity	Agranat et al,. 2010
8	Constitutive exon			Villard et al., 1997
C Terminal Variations				
L-1	Inclusion of Exon 9, Intron 9 and Exon 10	Most common variant (67-91% of transcripts across tissues and developmental time points)	Each may be synthesised from the L-1 termini and play a role in regulation of expression	Kawahara et al., 2005
L-2	Includes Exon 9 and Exon 10	Uncommon in transcripts		Kawahara et al., 2005
L-3	Includes a large portion of Exon 9 and Exon 10	Least common in transcripts		Kawahara et al., 2005
S	Includes a small portion of Exon 9 and Exon 10	Second most common C terminal		Kawahara et al., 2005

B

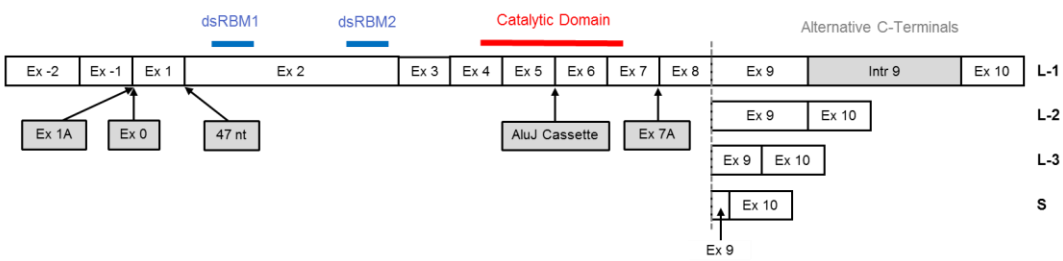

Figure 1.4 – (A) Table describing each constitutive or alternatively spliced exon, their expression and impact on ADAR2 editing activity. "UTR" denotes untranslated region. (B) Schematic to represent possible alternative splicing events in the ADAR2 transcript. Adapted from Kawahara et al., 2005. "Ex" denotes an exon. "Intr" denotes an intron. Boxes shaded in grey indicate insertions from the intronic sequence. Two insertions can be made between exon -1 and exon 1, and these have been entitled exons 1a and 0. The 47 nucleotide cassette is inserted at the start of exon 2. The AluJ sequence is inserted between exon 5 and exon 6, and there can be another insertion after exon 7. There are four variations of the C-terminal of ADAR2. "L-1" is the most common C-terminal which includes intron 9 between the full length exon 9 and exon 10. "S" is the second most common variant, with a splice site within exon 9 truncating this exon and splicing prematurely onto exon 10. "L-2" and "L-3" are both fairly rare.

1.2.7 RNA Editing in the Central Nervous System

Within the millions of RNA editing events in the human transcriptome, a disproportionate number of site-specific editing sites are restricted to nervous tissue and associated with neuronal excitability (Holmgren & Rosenthal, 2013). Most site-specific editing events have been found in mRNA transcripts encoding receptor subunits, including $GABA_A$ α3; AMPA subunits GluA2, 3 and 4; kainate receptor subunits GluK1 and 2; and the 5-HT_{2C} subunit, as summarised in Table 1.1.

Gene	Protein	Editing site	ADAR	Function	Reference
GRIA2	GluA2	Q/R	ADAR2	Calcium impermeability	Higuchi *et al.*, 1993
		R/G	ADAR1, ADAR2	Enhanced rate of desensitisation/modulation of alternative splicing	Lomeli *et al.*, 1994
GRIA3	GluA3	R/G	ADAR1, ADAR2	Enhanced rate of desensitisation/modulation of alternative splicing	Lomeli *et al.*, 1994
GRIA4	GluA4	R/G	ADAR1, ADAR2	Enhanced rate of desensitisation/modulation of alternative splicing	Lomeli *et al.*, 1994
GRIK1	GluK1	Q/R	ADAR1, ADAR2	Reduced conductance	Swanson *et al.*, 1996
GRIK2	GluK2	Q/R	ADAR1, ADAR2	Reduced conductance; calcium impermeability	Swanson *et al.*, 1996
		Y/C	ADAR2	Calcium impermeability	Köhler *et al.*, 1993
		I/V	ADAR1, ADAR2	Calcium impermeability	Köhler *et al.*, 1993
HTR2C	5-HT_{2C}	I/M, V	ADAR1	Effectiveness of coupling to G proteins	Burns *et al.*, 1997
		N/S, G, D	ADAR1, ADAR2	Effectiveness of coupling to G proteins	Burns *et al.*, 1997
		I/V	ADAR2	Effectiveness of coupling to G proteins	Burns *et al.*, 1997
GABRA3	$GABA_A$ α3	I/M	ADAR1, ADAR2	Enhanced rate of deactivation	Ohlson *et al.*, 2007
KCNA1	Voltage-gated K^+ channel (Kv1.1)	I/V	ADAR2	Potassium permeability	Bhalla *et al.*, 2004
CACNA1D	$Ca_v1.3$ channel	I/M	ADAR2	Reduced inactivation	Huang *et al.*, 2013
		Q/R	ADAR2	Reduced inactivation	Huang *et al.*, 2013
		Y/C	ADAR2	Reduced inactivation	Huang *et al.*, 2013

Table 1.1 - Summary of selected editing sites in coding sequences of genes in the central nervous system.

ɣ-aminobutyric acid (GABA) receptors are the major inhibitory class of receptors in the mammalian CNS. It was found that the *Gabra-3* transcript, which codes for the α3 subunit of $GABA_A$ receptors, is edited in exon 9 by both ADAR1 and ADAR2, leading to a change in amino acid sequence from isoleucine to methionine (Ohlson *et al.*, 2007). This I/M editing site was found to be developmentally regulated in mice, with around 15% of transcripts edited at E15 increasing to more than 90% of transcripts being edited in the adult nervous system (Rula *et al.*, 2008). This increase in editing has been shown to occur at the same time as reduced overall expression of the *Gabra-3* transcript, as well as changing trafficking of the α3 subunit so that less was found at the cell surface (Daniel *et al.*, 2011). This suggests that the increased editing at the I/M site is associated with the change in subunit composition of $GABA_A$ subunits, from predominantly α3 during development, to predominantly α1 in the adult CNS (Daniel *et al.*, 2011).

Serotonin (5-hydroxytryptamine, or 5-HT) is one of the neurotransmitters involved in reward pathways, food intake and the regulation of mood (Kandel *et al.*, 2000). There are multiple 5-HT receptor subtypes with associated subunits. One of which, the 5-HT_{2C} subunit, has been shown to undergo RNA editing (Burns *et al.*, 1997). This group found four A-to-I sites (A, B, C and D) within five consecutive codons, each resulting in a change in amino acid, and so multiple transcript variations were possible. The various transcripts were found to be expressed at different levels in different areas of the mouse CNS, with the most common transcript in whole brain RNA edited at sites A, B and D (Burns *et al.*, 1997). Interestingly, they found the choroid plexus to have a distinct editing pattern, which was the first indication of a biological role for these editing sites. They also showed that 5-HT_{2C} subunits edited at all four sites were 10-15 fold less responsive to agonists than subunits which remained unedited, possibly due to ineffective coupling to G proteins (Burns *et al.*, 1997).

Since this original research, the 5-HT_{2C} subunit has become one of the most studied RNA editing sites in the mammalian genome, and as such is one of the best characterised. The fact that editing reduces responsiveness to agonists, and that the editing is differentially regulated temporally and spatially, has led to RNA editing being linked to multiple conditions associated with serotonin. Reduced RNA editing at the 5-HT_{2C} subunit has been associated with mood disorders such as schizophrenia (Sodhi *et al.*, 2001), depression (Gurevich *et al.*, 2002) and bipolar disorder (Dracheva *et al.*, 2008), as well as other serotonin pathways such as neuropathic pain (Nakae *et al.*, 2008). In a mouse model with genetically determined lower serotonin levels in the forebrain (BALB/c mice) leading to increased spontaneous anxiety responses, stress led to increased editing at the 5-HT_{2C} subunit and therefore decreasing the responsiveness to serotonin, while treatment with the anti-depressant fluoxetine abolished this change in editing (Englander *et al.*, 2005). In a mouse model expressing a transgene of the fully edited 5-HT_{2C} transcript, mice developed a phenotype similar to Prader-Willi syndrome, including hyperphagia and neonatal muscular hypotonia (Morabito *et al.*, 2010).

RNA transcripts encoding voltage-gated ion channel subunits have also been shown to undergo RNA editing. Potassium channels have been found to contain multiple editing sites across three different K^+ channel genes (Hoopengardner *et al.*, 2003). K_V1.1 is particularly well characterised. As the editing site falls within the permeation pathway of the channel, changing an isoleucine to a valine, this change in amino acid alters the channel's kinetics (Bhalla *et al.*, 2004). The same study also found the site to be edited predominantly by ADAR2. The editing at this I/V site was shown to be variable spatially across the CNS, with highest editing levels in the spinal cord, thalamus and medulla (Hoopengardner *et al.*, 2003). In the same comparative genomics study, several editing

sites were found in calcium channels. These editing sites have been characterised less comprehensively, although several have been localised to the calmodulin binding site of the $Ca_V1.3$ channel (Huang *et al.*, 2012). ADAR2 knockout mice, crossed with mice expressing the fully edited version of the GluA2 subunit, show reduced editing in the $Ca_V1.3$ channel, particularly in neurons in the suprachiasmatic nucleus, which lead to reduced calcium channel inhibition and so increased firing (Huang *et al.*, 2012). This, Huang *et al.* argue, implies an effect of RNA editing on the modulation of the rhythmicity of the suprachiasmatic nucleus and so may have broader implications in circadian rhythms.

These studies into editing of receptors and channels have led to the hypothesis that editing may have evolved to fine-tune components of the nervous system, due to the differential regulation of editing throughout development and altered neuronal function (Penn *et al.*, 2013). RNA editing would therefore have the same effect as alternative splicing, in which one gene can give multiple products with different activity profiles, and in some cases these two processes work in conjunction with each other.

1.2.8 RNA Editing in Glutamate Receptors

Within kainate receptors, subunits GluK1 and GluK2 both have an equivalent Q/R site in the same codon as the GluA2 subunit, and RNA editing reduces the kainate receptor's conductance here (Swanson *et al.*, 1996). Both GluK1 and GluK2 transcripts have also been shown to have sequences in the intron following the Q/R site that are complementary to the bases surrounding the edited adenosine, allowing the formation of double-stranded RNA for ADAR recognition (Herb *et al.*, 1996). The Q/R site of GluK2 is edited at a higher level than GluK1 in the brain, and is developmentally regulated with very low editing during embryogenesis that increases to around 80% efficiency in the adult CNS (Bernard *et al.*, 1999). It appears that editing at the Q/R site of the GluK2 subunit affects its trafficking from the endoplasmic reticulum to the membrane, and may also impact subunit assembly (Ball *et al.*, 2010). As well as the Q/R site, GluK2 is edited at two other non-synonymous sites in its first transmembrane domain which can also affect the subunit's permeability to calcium (Köhler *et al.*, 1993).

The deamination associated with AMPA receptors' permeability to calcium takes place in codon 586 of the *GRIA2* gene within exon 11 and is catalysed by ADAR2. The resulting inosine is read by translation machinery as a guanosine base, so the codon changes from CAG (glutamine) to CGG (arginine); hence this is called the Q/R site as shown in Figure 1.5 (Higuchi *et al.*, 1993). This editing reaction produces the changes in calcium permeability previously mentioned. Other sites in the GluA2 subunit undergo RNA editing, including "hotspots" around exon 11 thought to aid splicing, and the "R/G site", found in exon 13, which affects desensitisation of the AMPA receptor (Tariq & Jantsch,

2012). The R/G site is found at codon 764 and changes an arginine to a glycine in the extracellular loop between transmembrane domains 3 and 4 in subunits GluA2, 3 and 4 but not GluA1 (Lomeli *et al.*, 1994). Editing at this site has implications on the alternative splicing of the AMPA subunits as previously mentioned, and editing can be carried out by either ADAR1 or ADAR2 (Liu & Samuel, 1999). The R/G site also seems to have a wider range of editing levels when compared with the strict high editing efficiency of the Q/R site. R/G site editing ranges from around 10% in immature neurons to more than 60% in mature neurons *in vitro*, which then decreased to around 30% editing after depolarisation with KCl (Orlandi *et al.*, 2011). This correlates with findings that, following acute spinal cord injury, there is a reduction in R/G site editing in AMPA receptors in the spinal cord (Barbon *et al.*, 2010).

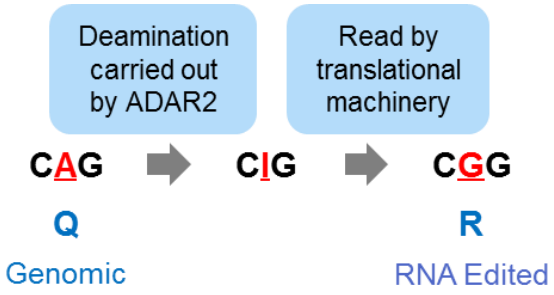

Figure 1.5 – Schematic of RNA editing reaction at the Q/R site of the GluA2 subunit. The Q/R site falls in codon 586 of the GluA2 transcript, part of exon 11. ADAR2 deaminates the adenosine within codon 586 forming an inosine, which is read by the cell's translation machinery as guanosine. This changes the coded amino acid from glutamine (Q) to arginine (R).

1.3 RNA EDITING AT THE Q/R SITE OF GLUA2

1.3.1 Discovery of the Exon Complementary Sequence and Imperfect Repeat

Much of our knowledge on RNA editing at the Q/R site of the GluA2 subunit stems from work carried out by a German group in the early 1990's (Higuchi *et al.*, 1993). Transgene expression of a section of murine *GluRB* (previous nomenclature for *Gria2*) in PC12 cells was analysed using cDNA copies of RNA extracts. It was found that editing at the endogenous Q/R site was close to 100%. However, when plasmids containing small sections of *GluRB* were transfected into PC12 cells they showed lower editing of around 43%. This was interpreted as evidence for additional elements needed for complete editing further up- or downstream of the Q/R site (Higuchi *et al.*, 1993). Different plasmids were examined, each containing *GluRB* fragments with varying portions of exon 11 and the following intron. Through changing the length of the intron following the Q/R site, they discovered sequences within the non-coding bases that are essential for efficient editing, as summarised in Figure 1.6A. Using sequential deletions it was shown that there is a sequence of bases in intron 11 that are complementary to those surrounding the editing

site, and which were necessary for editing (Higuchi *et al.*, 1993). This was termed the exon complementary sequence (ECS).

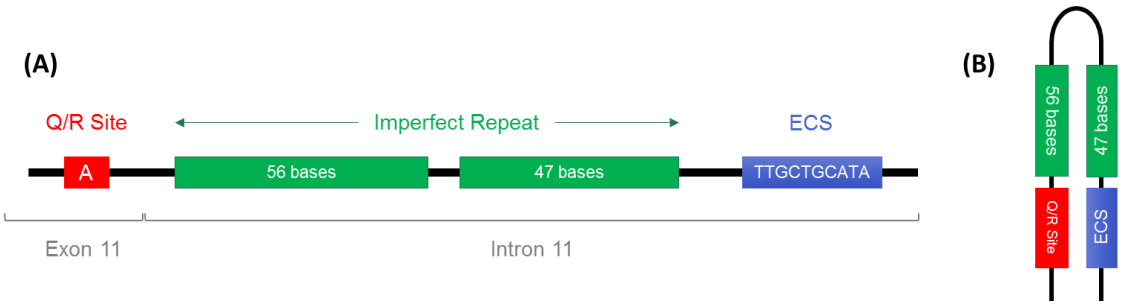

Figure 1.6 – (A) Schematic showing the arrangement of the Q/R site, imperfect repeat and exon complementary sequence (ECS) on the GRIA2 gene as found by Higuchi et al. 1993. (B) Inverted complementarity of base sequences allow the formation of a double-stranded RNA structure.

By substituting bases along this section of the gene, it was also shown that between the Q/R site and the ECS there were a series of bases that formed a so-called imperfect repeat, a series of inverted complementary bases that were able to form a predicted double-stranded section of RNA (Figure 1.6B). If the bases in the imperfect repeat were substituted but the complementary pairing (and therefore double-stranded structure) remained, then the Q/R site was still edited. This implied a reliance on secondary structure of the RNA molecule for the editing process. One of the plasmids used by this group contained a section of exon 11 and intron 11 including both the ECS and imperfect repeat from the murine sequence of *GluRB*. This they dubbed as the "B13 minigene" and is the transgene available in a plasmid for this project.

1.3.2 Q/R Site Editing and Disease

Editing at the Q/R site is unusual compared to most RNA editing events in that it is carried out to 100% efficiency in most mature neurons (Sommer *et al.*, 1991). However, dysregulation of RNA editing has been studied in several degenerative diseases. Downregulation of the enzyme ADAR2 itself has been associated with the cell death of retinal ganglia cells in glaucoma (Wang *et al.,* 2014). Lower ADAR2 expression was found in a mouse model of glaucoma and knockdown of ADAR2 using siRNA in retinal ganglion cells caused increased calcium currents and cell death *in vitro* (Wang *et al.*, 2014). Downregulation of ADAR2 was also found in a rat model of ischemia, in which it lead to reduced Q/R site editing (Peng *et al.*, 2006). If ADAR2 expression was enhanced via transfection with the ADAR2 gene or through treatment with CREB, then Q/R site editing was restored and improved cell survival (Peng *et al.*, 2006). A decrease in Q/R site editing has also been found in cells from human glioblastomas, which was associated with a change in ADAR2's self-editing but no change in overall ADAR2 expression (Maas *et al.*, 2001).

Dysregulation of Q/R site editing has also previously been associated with neurodegenerative disorders. Through post-mortem analysis of neurons from the prefrontal cortex, patients with Alzheimer's disease were shown to have a statistically significant decrease in Q/R site editing from more than 99.9% in control groups to 99% (Akbarian *et al.*, 1995). The same study found 5% of GluA2 RNA was unedited at the Q/R site in neurons from the striatum of Huntington's disease patients, again compared to the control group's striatal neurons with 0.5% of RNA unedited (Akbarian *et al.*, 1995). Another group looked at neurons from Alzheimer's Disease patients and found that hippocampal neurons showed reduced Q/R site editing (down to 95% from more than 99%) in those patients who carried the apolipoprotein E4 allele with no apparent change in ADAR2 expression (Gaisler-Salomon *et al.*, 2014). RNA editing has also been shown to be inefficient in the lower motor neurons of patients with Amyotrophic Lateral Sclerosis (Kawahara *et al.*, 2004). This group found that patients' motor neurons had extremely variable editing efficiencies at the Q/R site (discussed later; Figure 1.9). It therefore appears that a decrease in Q/R site editing is common across a number of disease states where neuronal cell death is a factor.

1.3.3 Transgenic Models Changing the Q/R Site

Transgenic animal models have emphasised the importance of RNA editing in the GluA2 subunit. A mouse model was created with the ECS from intron 11 removed, abolishing Q/R site editing (Brusa *et al.*, 1995). Heterozygous mice of this model therefore had fewer edited subunits available, leading to higher calcium intake in neurons. By postnatal day 13, all carriers of the transgene developed seizures and had died by postnatal day 20 (Brusa *et al.*, 1995). On the other hand, when the genomic sequence is altered so that the "edited" form is coded in the DNA (i.e. the exon is originally transcribed as CGG rather than CAG), there appear to be no side effects (Kask *et al.*, 1998). Mice expressing a transgenic inactive form of ADAR2 showed a similar phenotype to those without the ECS in intron 11 (Higuchi *et al.*, 2000), which was rescued when the line was crossed with transgenic mice possessing a *GRIA2* gene that was already the "edited" form (Horsch *et al.*, 2011). This phenotypic rescue showed the importance of this particular editing event, and that although there were other lesser phenotypes such as reduced white blood cell count and altered lung function, they were not severe and the transgenic line was viable (Horsch *et al.*, 2011).

A conditional transgenic model was produced where ADAR2 is specifically targeted by the Cre/lox system in motor neurons under the VAChT promoter, titled AR2 mice (Hideyama *et al.*, 2010). Exons 7 to 9 of the ADAR2 gene were flanked by loxP sites, targeted as they contain the majority of the catalytic domain, and then crossed with the VAChT-Cre.Fast line, which express Cre recombinase in cholinergic neurons including

motor neurons under the VAChT promoter (Misawa *et al.*, 2003). Both homozygous and heterozygous mice for Cre recombinase displayed around 50% expression, and so AR2 mice (ADAR2$^{flox/flox}$/VAChT-Cre.fast) lack ADAR2 in roughly half of their motor neurons (Hideyama *et al.*, 2010). When RNA from anterior horn neurons was obtained by laser-dissection, it was found that editing at the Q/R site of GluA2 was variable, with less than half of the neurons showing 100% editing, and that those neurons that had less efficient editing also had evidence of removal of ADAR2. These mice were hypokinetic and had an abnormal posture, although there was no evidence of paralysis, and they showed lower rotarod performance and grip strength from 5 weeks onwards, correlating with the Cre expression profile (Hideyama *et al.*, 2010). The mice also showed lower survival compared to controls of 81.5 ± 16.4 weeks compared to 105.1 ± weeks of control. The changes in motor behaviour corresponded with an observed reduction in anterior horn neurons from 2 months onwards, and AR2 mice's muscles showed evidence of denervation. Again, rescue of the degenerative phenotype was possible when crossed with the transgenic line expressing the "edited" form of GluA2, producing the line AR2res (AR2/GluR-B$^{R/R}$). These mice were phenotypically normal, with full motor function until 6 months of age and the same number of anterior horn neurons as control at all time points (Hideyama *et al.*, 2010). AR2 mice were shown to mislocalise the nuclear protein TDP-43, mimicking a symptom of amyotrophic lateral sclerosis, and showed calpain-induced cleavage of TDP-43 which was not found in the AR2res line (Yamashita *et al.*, 2012a). AR2 mice also show nuclear vacuoles in anterior horn neurons (Sasaki *et al.*, 2014) and increased autophagy markers (Sasaki *et al.*, 2015). These characteristics appear to be directly correlated with the decrease in functional ADAR2 expression, which is something that may occur naturally in aged mice (Hideyama *et al.*, 2012a) and has also been found to a greater extent in motor neurons of ALS patients (Hideyama *et al.*, 2012b).

The same research group has created an AAV9 vector containing wild type ADAR2 under a SYN1 promoter. This vector was injected into the tail vein of AR2 mice at 9 to 13 weeks, the presymptomatic stage, or at 15 weeks after the mice start showing behavioural changes (Yamashita *et al.*, 2013). Treatment at the presymptomatic stage showed a dramatic improvement, with little decline evident on the rotarod test, although less of an improvement was seen after treatment in the symptomatic stage. There was no improvement seen in grip strength, although there were an increased number of anterior horn neurons compared to AR2 mice injected with saline (Yamashita *et al.*, 2013). AAV9-ADAR2 injections lead to a 1.5 times increase in ADAR2 expression in spinal cord and brain homogenates, and Q/R site editing of the GluA2 subunit in laser-captured anterior horn neurons showed an increase in editing to over 90%.

The importance of editing at the Q/R site in the GluA2 subunit is therefore clear, and has led to the proposed hypothesis for the aetiology of amyotrophic lateral sclerosis (ALS), whereby there is progressively lower ADAR2 activity in motor neurons, leading to higher incidence of unedited GluA2 subunits. When a majority of neurons contain the unedited form of GluA2, this causes the appearance of the clinical signs of ALS (Hideyama & Kwak, 2011).

1.4 AMYOTROPHIC LATERAL SCLEROSIS

1.4.1 Incidence and Symptoms

Amyotrophic Lateral Sclerosis (ALS) is a progressive neurodegenerative disease with characteristic death of motor neurons. ALS is the third most common adult neurodegenerative disease after Alzheimer's Disease and Parkinson's Disease, with an incidence of 2 in every 100,000 (Chiò *et al.*, 2013). Sometimes referred to as Lou Gehrig's Disease after the famous American baseball player who suffered from ALS, this disease appears to be more prevalent in people who have a lower body mass index and who often take part in physical activity (Huisman *et al.*, 2013). However, in a population-based study there was no correlation found between ALS and physical activity (Veldink *et al.*, 2005). There might still be the possibility of traits that lend towards an active lifestyle being significant in ALS development, but what these traits are and how they are linked to ALS have not been confirmed. A recent study looking at a population of American patients with ALS found no association with increased physical exercise, nor with other previously suggested environmental factors such as smoking or exposure to metal, dust or radiation (Yu *et al.*, 2014). They did find an association with exposure to fertiliser. However, this study had a small sample size of n=66 and exposure levels were based on surveys, so associations need to be further investigated in a larger study. Several other environmental factors, such as smoking, vitamin E or antioxidants or exposure to metals or pesticides have also been suggested to be risk factors with varying degrees of association (reviewed in Ingre *et al.*, 2015).

The median survival for ALS patients is 2 years after confirmed diagnosis, or 3 years after symptom onset (Talbot, 2014). However, ALS can present in a variety of clinical manifestations, and 10% of patients will survive 10 years after diagnosis (Chiò *et al.*, 2013). The variation in clinical symptoms of ALS is not limited to life expectancy. In 30% of cases, onset of muscle weakness begins in an upper limb, whereas 35% of cases begin in a lower limb. 30% of cases begin with weakness in the muscles associated with speech or swallowing while the remainder of patients first show weakness in respiratory or axial muscles (Talbot, 2014). Muscle weakness then progresses through the voluntary neuromuscular system, although rate of progression can vary depending on genetic

background and possibly environmental factors. ALS is fatal through respiratory failure caused by paralysis of the diaphragm or intercostal muscles (Rothstein, 2009).

1.4.2 Genetic Mutations in ALS

5-10% of ALS cases are familial (fALS) while the remaining 90% of cases appear to be sporadic (sALS). Within cases of fALS, mutations have been found in a variety of genes, as summarised in Figure 1.7. A database maintained by King's College London, ALS Online Database or ALSoD, which tracks all known mutations found in ALS patients currently shows 659 mutations across 58 genes (Abel *et al.*, 2012).

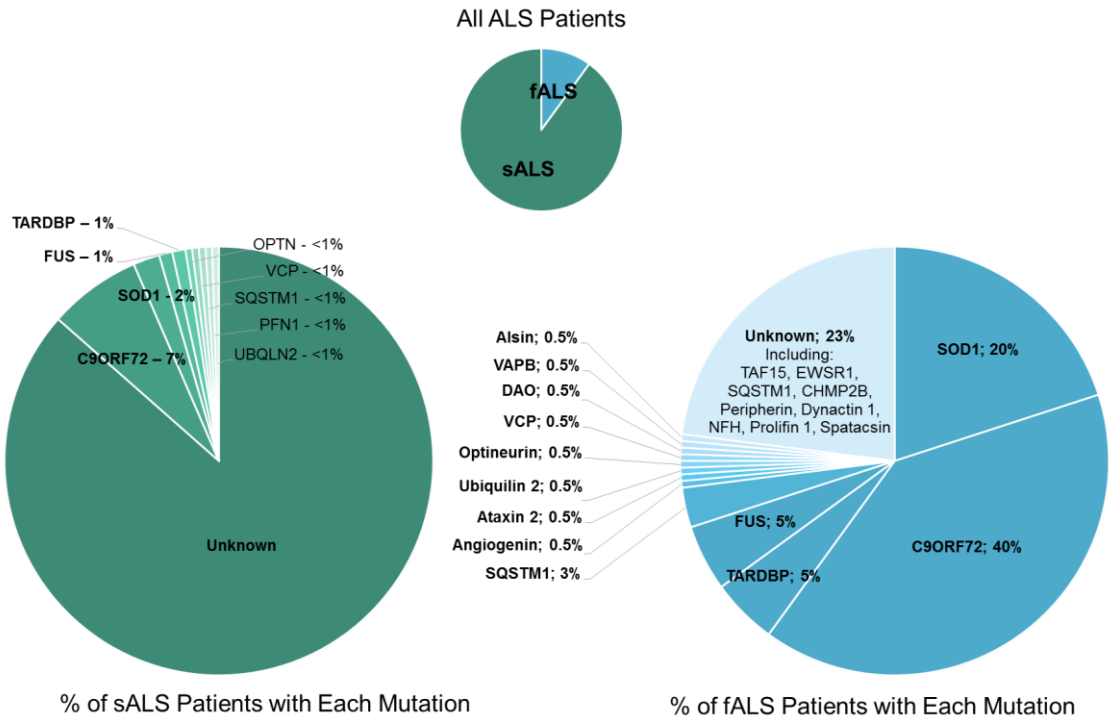

Figure 1.7 - Pie charts indicating the proportion of familial ALS (fALS) to sporadic ALS (sALS) patients and the genes in which mutations are found. Data taken from (Robberecht & Philips, 2013; Lattante *et al.*, 2015).

The first identified mutation associated with fALS was in the superoxide dismutase 1 (*SOD1*) gene (Rosen *et al.*, 1993), and since then over 180 mutations in this gene have been identified. Mutations in SOD1 are found in around 20% of cases of fALS and around 1% of sALS, with different mutations being associated with different presentations of ALS. For example, the A4V mutation is extremely aggressive leading to death within a year of symptom onset whereas the D90A mutation leads to much slower progression, with patients developing respiratory failure up to 10 years after onset (Renton *et al.*, 2014).

Since the 1990s, improved sequencing techniques led to the discovery of mutations in genes such as *TARDBP*, *FUS*, *VCP* and *ANG* in fALS patients. Together with *SOD1*, these mutations can account for around 30% of those with familial ALS, as well as occurring in some cases previously designated sporadic (Ticozzi *et al.*, 2011). For example, in a large cohort of more than 500 patients with ALS, mutations in the *TARDBP* gene were found in 5% of familial ALS cases and in 0.4% of sporadic ALS cases (Kirby

et al., 2010). Likewise, a study found *FUS* mutations in 5% of their cohort of fALS patients although only in a single sALS patient (Hewitt *et al.*, 2010). Recently, linkage analysis of some familial ALS cases to chromosome 9 was shown to be due to a GGGGCC hexanucleotide repeat expansion within intron 1 of the C9ORF72 gene (Dejesus-hernandez *et al.*, 2011; Renton *et al.*, 2011). It has been reported that this expanded repeat may account for around 40% of cases with familial ALS (Cooper-Knock *et al.*, 2012). Many of the less frequent genes are only found in specific populations of ALS patients. For example, mutations coding for *OPTN* (optineurin) were initially found in a Japanese family but are rarely found in European patients (Chiò *et al.*, 2012). Despite these advances in understanding the genetics of ALS, how they relate to the specific death of motor neurons in the disease remain unknown. However, the genes affected and the proteins they code for are presumably involved in the pathological pathway. It is likely that several pathways may lead to the same outcome of motor neuron death and the symptoms of ALS.

1.4.3 ALS and FTLD

Frontotemporal lobe dementia (FTLD) is characterised by changes in behaviour, language and personality, with degeneration of neuronal populations in the frontal or temporal lobes detectable by MRI scans (Rosen *et al.*, 2002). The discovery that TDP-43 was a major component of the intracellular inclusions in both ALS and FTLD (Neumann *et al.*, 2006) gave the first molecular evidence for the relationship between these two diseases. It is now a widely held view that ALS and FTLD are part of a continuum, with pure cases of each disease at either end but many patients showing aspects of both. For example, a large-scale study found 15% of ALS patients had signs of cognitive impairment (Ringholz *et al.*, 2005), and those patients without dementia still showed a range of deficits in executive function (Massman *et al.*, 1996). At a molecular level, FTLD is characterised by ubiquitin-positive plaques co-localising with either TDP-43 or FUS (Neumann *et al.*, 2009). Around 40% of patients with FTLD were found to be familial, with mutations in *MAPT* and *GRN* found specifically in FTLD cases (Rohrer *et al.*, 2009), while patients with *SOD1* mutations are unlikely to show cognitive impairment (Wicks *et al.*, 2009). Mutations in *C9ORF72* on the other hand are found in patients throughout the FTLD-ALS spectrum (Benussi *et al.*, 2014).

1.4.4 Molecular Pathology of ALS

Decades of research has discovered several intracellular processes that are dysregulated in ALS, although it is still unclear which, if any, of these events are the initial cause of disease. These mechanisms include aggregation of several different proteins including SOD1 and TDP-43, dysfunctional RNA processing, mitochondrial dysfunction and glutamate excitotoxicity (summarised in Figure 1.8).

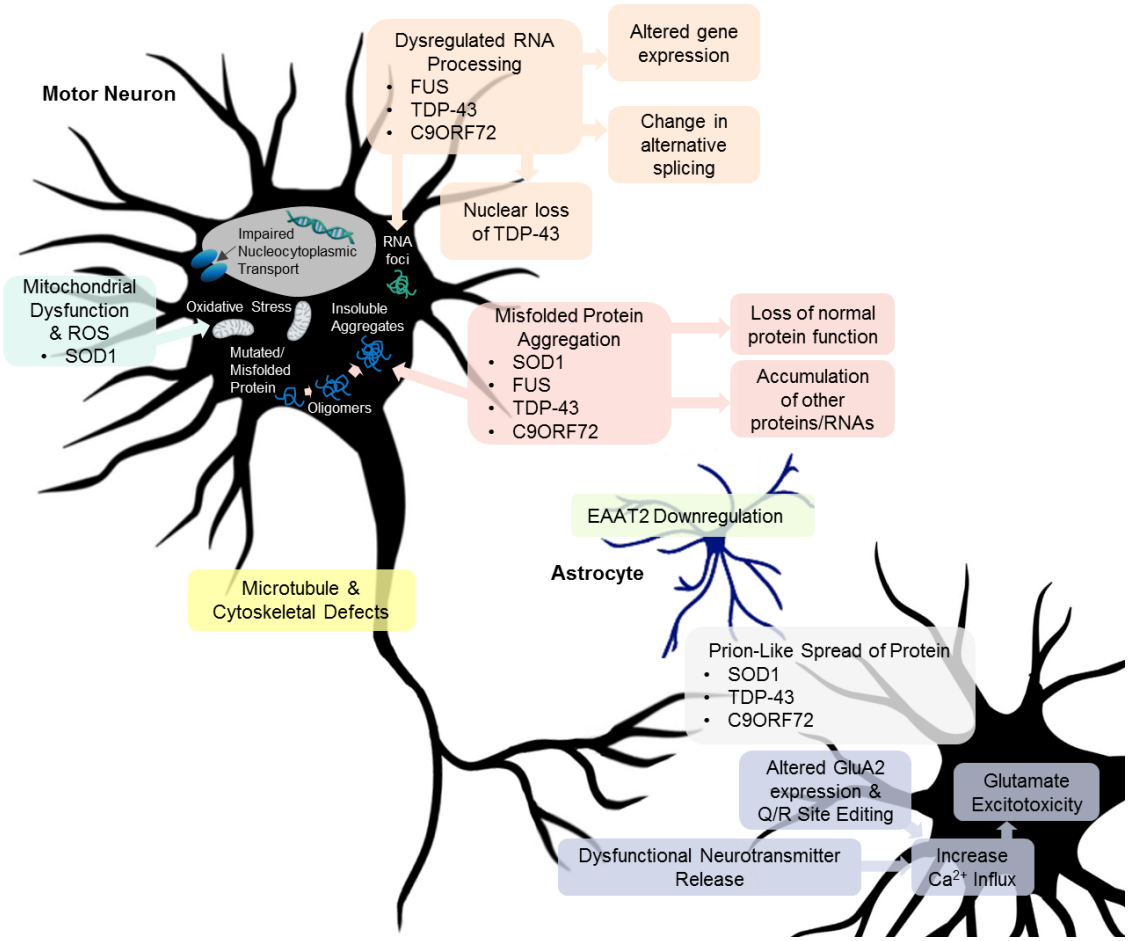

Figure 1.8 - Summary of intracellular dysfunction found in ALS. Insoluble protein aggregates and RNA foci are characteristic markers of ALS patients. Cells also show impaired nucleocytoplasmic transport, mitochondrial dysfunction and increased oxidative stress, with changes in glutamate receptor composition also shown in both motor neurons and astrocytes.

1.4.4.1 Motor Neuron Susceptibility

As the progression of both familial and sporadic ALS is similar, it is reasonable to assume a common pathway in the degeneration of motor neurons. Why motor neurons are specifically targeted in ALS remains unclear, although it is true that they appear to be particularly vulnerable to cellular stresses associated with ALS, such as endoplasmic reticulum stress (Jara *et al.*, 2015). They may also be more susceptible to excitotoxicity, as oculomotor neurons, which are spared in ALS, show a reduced inward calcium current after AMPA receptor stimulation compared to corticospinal neurons (Brockington *et al.*, 2013). Motor neurons also stretch a remarkably long distance with massive cytoskeletal networks, and microtubule defects are known to be part of ALS pathology (Bilsland *et al.*, 2010). Neurons in general are particularly at risk of damage through misfolded proteins, as they are large and post-mitotic, so they cannot dilute any toxic waste through division and high rates of metabolism are needed to process the proteins produced over

their large surface area (Parakh & Atkin, 2016). It is possible that the small differences that set the motor neuron population apart sum up to the susceptibility seen in ALS.

1.4.4.2 SOD1

Superoxide dismutase 1, SOD1, is an important antioxidant enzyme converting superoxide (O_2^-) to H_2O_2 and O_2. SOD1 is a homomeric Cu/Zn-binding enzyme (Rosen *et al.*, 1993) found throughout motor neurons, associated with their mitochondria (Pardo *et al.*, 1995). A large number of ALS-linked mutations are associated with this gene, and such mutations have been linked to a variety of downstream effects such as altered gene expression, dysfunctional mitochondria and activation of caspases (Liu *et al.*, 2004). Mutations in SOD1 tend to be split into two groups, those that affect the β-barrel structure and those that affect the metal binding sites, both of which can affect the oligomerisation and formation of SOD1 aggregates (Kaur *et al.*, 2016). Collection of mutant SOD1 into insoluble aggregates causes a build-up of reactive oxygen species in the cell, damaging other cellular components, due to a decrease in SOD1 activity (Graffmo *et al.*, 2013). Mutated SOD1 has also been linked to dysfunction of the endoplasmic reticulum and Golgi apparatus (Soo *et al.*, 2015).

ALS is often considered a prion-like disease, due to its characteristic progression from an initial focal starting point then spread to neighbouring neuroanatomical structures, rather than from multiple but diverse locations (Ravits *et al.*, 2013). In order for a protein to be classified as prion-like, it must have a prion-like binding domain and have the capacity to act as a “seed” protein, inducing other proteins to misfold. Although SOD1 does not contain a prion-like domain, there is some evidence that it has prion-like properties. For example, spinal cord tissue homogenate from $SOD1^{G93A}$ mice can cause aggregates to form from wild-type SOD1 *in vitro* (Chia *et al.*, 2010). In order for SOD1 to behave like a prion in the progression of ALS, it must be able to leave the motor neurons to travel to the neighbouring cells. Mutant SOD1 has been found in the media of primary neurons grown in culture from $SOD1^{G93A}$ mice, with evidence that the SOD1 has been secreted in exosomes (Basso *et al.*, 2013). Spinal cord homogenates from $SOD1^{G93A}$ mice injected into another transgenic model ($SOD1^{G85R}$ mice) with low levels of aggregates induced motor neuron disease (Ayers *et al.*, 2014). The second passage homogenates, taken from the induced strain into a second generation, also showed faster disease onset, as in prion disease. However, similar effects could be seen in a small proportion of mice who were injected with wild type SOD1, and seeding with two other mutant SOD1 strains failed to accelerate the disease (Ayers *et al.*, 2016). Astrocytes have also been implicated in SOD1 pathology, as co-cultures with astrocytes expressing mutant SOD1 reduces the viability of motor neurons but not interneurons, GABAergic neurons or sensory neurons (Nagai *et al.*, 2007). This could be due to

increase excitability of the motor neurons with increased sodium channel permeability (Fritz *et al.*, 2013).

Some now consider ALS with *SOD1* mutations a separate pathology to the rest of ALS cases due to these patients often not presenting with the classic ALS hallmarks of ubiquitin-positive, TDP-43-positive cellular inclusions (Mackenzie *et al.*, 2007; Arai *et al.*, 2006). Aggregates found in SOD1 fALS are SOD1 and ubiquitin positive, but in general do not recruit TDP-43 (Farrawell *et al.*, 2015). Even though the mutated SOD1 protein has been shown to interact with endogenous TDP-43 in co-immunoprecipitation studies (Higashi *et al.*, 2010), it has proven difficult to incorporate mutated *SOD1* with the pathology associated with TDP-43 and C9ORF72.

1.4.4.3 TDP-43

TAR DNA-binding protein-43 (TDP-43) is generally localised to the nucleus but can be shuttled to and from the cytoplasm under normal conditions (Ayala *et al.*, 2008). TDP-43 has been associated with many roles, including acting as a transcription factor (Acharya *et al.*, 2006), regulating splicing of exons (Mercado *et al.*, 2005; Buratti *et al.*, 2001) and stabilisation of mRNA transcripts (Strong *et al.*, 2007). Knockdown of TDP-43 expression in the adult mouse brain led to changes in expression levels of over 600 genes and more than 900 changes in splicing (Polymenidou *et al.*, 2011). TDP-43 binds to single stranded sequences, mainly to intronic repeat motifs (Xiao *et al.*, 2011). It is therefore clear that TDP-43 plays a role in RNA processing.

There are around 44 ALS-linked mutations in *TARDBP* (the gene coding for TDP-43), and the protein itself is abnormally cleaved and phosphorylated in ALS (Neumann *et al.*, 2006). Mutations in *TARDBP* appear to cause both loss of normal function of the protein TDP-43 and toxic gain-of-function (Kabashi *et al.*, 2010). Altered splicing patterns are seen in mice carrying TDP-43 mutations, accompanied by increasing loss of motor neurons in the spinal cord, due to the loss of normal TDP-43 function (Arnold *et al.*, 2013; Tsuiji *et al.*, 2013). Gain of toxic function can be seen in the aggregates found in the cells of almost all ALS patients, both with sALS and fALS (Mackenzie *et al.*, 2007), and increasing burden of deposits correlates with progression of ALS which can be tracked using diffusion tensor imaging (Kassubek *et al.*, 2014). Unlike SOD1, TDP-43 fulfils both requirements for a prion-like protein, as it contains a predicted prion-like binding domain which is essential for its aggregation (Udan-Johns *et al.*, 2014) and mutations in TDP-43 at this domain can enhance aggregation properties (Lim *et al.*, 2016). Extracts from diseased brains can also induce misfolding of TDP-43 in cell culture, showing the TDP-43 aggregates have seeding properties (Nonaka *et al.*, 2013). Misfolded TDP-43 has even been shown to act as a seed for incorrect folding of wild-type SOD1 in cell culture

(Pokrishevsky *et al.*, 2016), hinting at a link between the tertiary structure of these two proteins and their influence on each other.

1.4.4.4 FUS

FUS (fused in sarcoma) protein shares both structural and functional similarities with TDP-43. FUS has been shown to bind to RNA polymerase II as well as RNAs from over 5,000 genes, affecting both transcription and splicing patterns (Lagier-Tourenne *et al.*, 2012), particularly in cortical and motor neurons (Fujioka *et al.*, 2013). FUS-positive inclusions are found in almost all ALS patients apart from those with SOD1-linked ALS (Deng *et al.*, 2010). Those patients with mutations in the *FUS* gene show different forms of inclusions according to their mutation (Mackenzie *et al.*, 2011), which then cause mislocalisation of the protein and the formation of stress granules (Gal *et al.*, 2011). The original reports of FUS mutations in ALS also showed the change in localisation of the protein from the nucleus to the cytoplasm, indicating a loss of normal function (Kwiatkowski *et al.*, 2009). The involvement of FUS supports the idea that the pathology of ALS at least involves dysregulated RNA processing.

1.4.4.5 C9ORF72

The major focus of the last few years of research into ALS pathology has been on the G_4C_2 repeat in *C9ORF72*. Before the expanded repeat mutation was linked to this gene, it was not known what the C9ORF72 protein did within the cell. Since the original discovery of the expanded repeat (Dejesus-hernandez *et al.*, 2011; Renton *et al.*, 2011), the normal function of the C9ORF72 protein has been linked to endosomal trafficking as it associates with Rab proteins (Farg *et al.*, 2014), and high expression of the gene can be seen in the central nervous system (Rizzu *et al.*, 2016). Normal function of C9ORF72 may also aid stress granule formation, and so loss of expression could be linked to the increased number of stress granules seen in ALS neurons (Maharjan *et al.*, 2016). How the expanded repeat could lead to neurodegeneration is still unclear, although there are three competing theories which are not necessarily mutually exclusive. The neurodegeneration may be through loss-of-function, where the expanded repeat causes reduced transcription of *C9ORF72*. There is conflicting evidence of this, as some groups have shown reduced expression of *C9ORF72* in a zebrafish model, leading to changes in motor neuron pathology and reduced motion (Ciura *et al.*, 2013), and there is evidence of reduced protein expression in the brains of ALS patients (Waite *et al.*, 2014), possibly due to increased methylation of the *C9orf72* gene itself (Belzil *et al.*, 2013) although the methylation may also be a protective mechanism (Bauer, 2016). On the other hand, no change in expression was seen in ALS patient-derived induced pluripotent stem cell motor neurons (iPSC-MNs) (Sareen *et al.*, 2013) and there are no identified loss-of-function mutations found in this gene (Harms *et al.*, 2013).

There are two possible mechanisms for toxic gain-of-function following the expanded repeat. Firstly, evidence that the repeat is transcribed into RNA and forms RNA foci in the cytoplasm of affected cells indicates that the RNA itself may be toxic (Dejesus-hernandez *et al.*, 2011). iPSC-MNs derived from patients with the *C9ORF72* mutation maintain the expanded repeat, making them a useful model for analysis. These neurons show collection of RNA transcripts of the repeat into discrete RNA foci, which then allow the association of various RNA binding proteins (Cooper-Knock *et al.*, 2014), and the toxic pathology associated with these foci can be diminished by treatment of antisense oligonucleotides with complementary sequences to C9ORF72 reducing RNA expression (Donnelly *et al.*, 2013). One RNA-binding protein found to co-localise with the C9ORF72 RNA foci was ADAR2, and when ADAR2 expression was knocked down with siRNA the RNA foci load was reduced by nearly 50% (Donnelly *et al.*, 2013). Although this study did not find an association between C9ORF72 RNA foci and other ALS-linked RNA binding proteins, other groups have found co-localisation with Purα (Xu *et al.*, 2013) and TDP-43 (Cooper-Knock *et al.*, 2015). The repeat expansion appears to be transcribed without the means of a traditional promoter, with expression of sequences either up or downstream of the promoter not being detected in the RNA foci (Donnelly *et al.*, 2013). This leads to both the sense and antisense sequence of the repeat being transcribed and forming foci (Mizielinska *et al.*, 2013), and it appears that the antisense rather than the sense transcripts are associated with a nuclear loss of TDP-43 (Cooper-Knock *et al.*, 2015).

As well as the RNA transcripts disrupting intracellular mechanisms, the RNA is translated into peptides which are the third proposed mechanism of pathology. Due to the sequence of the G_4C_2 repeat, translation from both the sense and antisense RNA strands form sections of di-peptide repeats (DPRs), either containing glycine-alanine (GA), glycine-proline (GP), glycine-arginine (GR), alanine-proline (AP) or arginine-proline (RP). These DPRs form intracellular aggregates that are TDP-43-negative but ubiquitin- and p62-positive (Mackenzie *et al.*, 2014). It appears that DPR load does not correlate with degree of neurodegeneration in ALS patients (Mackenzie *et al.*, 2013) as opposed to RNA foci (Mizielinska *et al.*, 2013). It has recently been discovered that a major effect of the DPRs is on the nucleocytoplasmic transport of the cell. The DPRs of C9ORF72 interact with RanGAP, a major protein in nucleocytoplasmic transport, and *Drosophila* and iPSC-MNs expressing the repeat expansion show nuclear pore pathology (Zhang *et al.*, 2015) and altered expression of over a dozen genes associated with nucleocytoplasmic transport (Freibaum *et al.*, 2015).

1.4.4.6 Glutamate and Excitotoxicity

Excitotoxicity describes over-stimulation from glutamate, which causes an increased influx in calcium leading to other downstream events such as oxidative stress (Sun *et al.*, 2010). Glutamate is a fundamental neurotransmitter in the CNS, and it is known to be abnormally regulated in ALS. Focus was originally targeted on the glutamate transmission system after there were significantly decreased levels of glutamate found in the spinal cord and brain homogenates of ALS patients (Plaitakis *et al.*, 1988), although there were increased levels of glutamate found in the cerebrospinal fluid (CSF) in one study (Shaw *et al.*, 1995) but reduced levels found in the CSF of ALS patients in a more recent study (Wuolikainen *et al.*, 2011). Although in the spinal cord there was no reported change in overall AMPA or kainate receptor expression, NMDA receptors were expressed at lower levels in ALS patients (Allaoua *et al.*, 1992) and a reduced expression of the GluA2 subunit has been seen (Takuma *et al.*, 1999). Motor neurons were found to be particularly sensitive to AMPA or kainate receptor activation as opposed to NMDA receptor activity (Rothstein *et al.*, 1993), and there was death specifically of motor neurons following injection with kainic acid, an agonist of both AMPA and kainate receptors, into the subarachnoid space of the spinal cord in rats (Sun *et al.*, 2006). Motor neurons appear to be a particularly vulnerable neuronal population when it comes to excitotoxicity, possibly because of their low expression of the GluA2 subunit in their AMPA receptors leading to increased calcium currents (Van Damme *et al.*, 2002). In organotypic spinal cord slices, it was found that non-NMDA receptor antagonists or blockade of glutamate synthesis and release prevented motor neuron death when exposed to high levels of glutamate (Rothstein *et al.*, 1993).

An important glutamate transporter expressed in astrocytes, EAAT2, was found to be downregulated in ALS patients compared to matched controls (Fray *et al.*, 1998), possibly due to abnormally processed RNA transcripts as aberrant mRNAs were found in ALS patients (Lin *et al.*, 1998). EAAT2 downregulation was found early in the pathology of rats carrying the $SOD1^{G93A}$ mutation (Howland *et al.*, 2002), although not until late in the disease in mice carrying the same transgene (Warita *et al.*, 2002). Additionally, synaptosomes from $SOD1^{G93A}$ mice showed an increase in glutamate release in response to depolarisation due to an increase in number of vesicles, indicating that it is not just the astrocytes that display dysregulation of glutamate (Milanese *et al.*, 2011). Double transgenic mice carrying the $SOD1^{G93A}$ mutation along with overexpression of EAAT2 delayed the degeneration of motor function, although there was no effect on the lifespan of the mice (Guo *et al.*, 2003). It appears that mutant SOD1 and dysregulation of glutamate can work synergistically to promote motor neuron death (Yin & Weiss, 2012) which corresponds with a more significant reduction in glutamate levels in the CSF of ALS patients with the familial disease compared to those with

sporadic ALS (Wuolikainen *et al.*, 2011). There is also evidence that other neurotransmitter systems are dysfunctional in ALS, for example inhibitory currents are decreased in ALS patients (Zanette *et al.*, 2002) correlating with a loss of interneurons in the spinal cord (Stephens *et al.*, 2006), which could exaggerate the glutamate excitotoxicity. iPSC-MNs derived from ALS patients with SOD1, FUS and C9ORF72 mutations also appear to be hyperexcitable (Wainger *et al.*, 2014). Taken together, these studies suggest that dysregulation of glutamate transmission in motor neurons may at least be a contributing factor in ALS pathogenesis.

Currently, the only therapy for ALS is the drug riluzole (Rattray & Bendotti, 2006). Riluzole, an inhibitor of glutamate release, showed great promise in extending the lifespan of the $SOD1^{G93A}$ mouse (Gurney, 1997), and was taken to clinical trials with results showing an increased life span of patients between 2 and 3 months (Bensimon *et al.*, 1994; Lacomblez *et al.*, 1996). Despite this reduced translation in effect between mouse model and human patient, riluzole remains the only treatment currently available for ALS as no other treatment has so far progressed beyond clinical trials. Riluzole's effects, depending on dose, range from inhibition of Na^+ currents and potentiation of calcium-dependent K^+ currents to promotion of growth factors and modulation of ligand-gated receptors (reviewed in Bellingham, 2011). More recently, Riluzole has been used in the treatment of other disorders associated with glutamate dysregulation such as spinal cord injury (Vasconcelos *et al.*, 2016), glaucoma (Pirhan *et al.*, 2016), major depressive disorder (Salardini *et al.*, 2016) and even Alzheimer's Disease (Pereira *et al.*, 2016).

1.4.5 Mouse Models of ALS

A great deal of effort has been put into creating a mouse model that properly recreates the clinical phenotype of ALS as well as the genetic component, with the models described here summarised in Table 1.2. The first transgenic mouse, and subsequently the most studied, is the $SOD1^{G93A}$ mouse with inserted transgenic copies of the G93A mutation in the mutant *SOD1* gene. This mutation causes paralysis starting generally in one hind limb and ascends, caused by motor neuron death, and a higher copy number of the transgene causes a more severe phenotype (Gurney *et al.*, 1994). Transferring the mutation onto a C57BL6/SLJ background reduced the mean survival by a month, indicating the presence of as yet unidentified genetic modifiers (Gurney, 1997; Heiman-Patterson *et al.*, 2011), and changing the genetic background has allowed slow and quick progressive models to be established (Marino *et al.*, 2015). Over the past 20 years, the $SOD1^{G93A}$ mouse has shown a varied length of survival from 102 to 151 days (Benatar, 2007), which in some ways reflects the variability seen in ALS patients. Those patients who carry the G93A mutation in *SOD1* have also shown varied survival spanning

from 62 to 243 months (Régal *et al.*, 2006). Up to 20 different *SOD1* mutations have now been modelled in mice with varying phenotypes, for example the G85R mutation gives a rapidly progressive paralysis with SOD1 inclusions (Bruijn *et al.*, 1997). Knockout of the *Sod1* gene in mice does not induce motor neuron cell death, and so mutations in *SOD1* appear to be more than simply loss-of-function (Reaume *et al.*, 1996). Indeed, overexpression of wild-type human SOD1 in mice can also induce motor neuron degeneration (Graffmo *et al.*, 2013).

After the discovery of TDP-43 inclusions and mutations in *TARDBP*, several groups attempted to produce mouse models replicating these mutations. However, no mouse model with expression of mutated TDP-43 shows the ascending paralysis seen in ALS, although several lines show abnormal motor behaviour (reviewed in Philips & Rothstein, 2015). Overexpression of wild type human TDP-43 does not appear to cause the formation of insoluble aggregates at lower expression levels (Arnold *et al.*, 2013) although at higher expression levels human wild type TDP-43 induces similar pathology to mutated TDP-43^{A315T} (Stallings *et al.*, 2010). This group found that the TDP-43^{A315T} mutation could cause an extremely aggressive set of symptoms, with formation of aggregates and later onset of paralysis (Stallings *et al.*, 2010). Compared to the plethora of attempts at a mutant TDP-43 mouse model, only a handful of transgenic FUS models have been created. Overexpression of wild-type human FUS led to progressive hind-limb paralysis and FUS-positive inclusions in motor neurons (Mitchell *et al.*, 2013), while expression of FUS containing ALS-linked mutations led to a more aggressive pathology, with a higher number of aggregates in motor neurons (Verbeeck *et al.*, 2012).

Although the repeat expansion in *C9ORF72* is known to be important in ALS due to its prevalence in fALS cases, it has proven difficult to model in mice. Knockout of the *C9ORF72* gene did not induce motor neuron degeneration or a decrease in survival in mice (Koppers *et al.*, 2015), despite motor deficits being observed in a *C9ORF72* knockdown model in zebrafish (Ciura *et al.*, 2013). However, expression of the repeated sequence, G_4C_2, alone in an AAV vector in mice leads to motor deficits, although not actual paralysis, as well as a behavioural deficits, TDP-43-positive inclusions and loss of motor neurons (Chew *et al.*, 2015). These mice only had 66 repeats of G_4C_2 due to size limitations in AAV vectors, which is not a pathological repeat size in humans. Another study introduced the entire human *C9ORF72* gene including the expansion repeated up to 1,000 times in a bacterial artificial chromosome. Despite the presence of RNA foci and dipeptide repeats, these mice showed no neurodegeneration or changes in behaviour (O'Rourke *et al.*, 2015). Comparison of these mouse models, summarised in Table 1.2, shows that there is still no mouse model that encapsulates the ALS phenotype completely. The SOD1^{G93A} mouse model is still in use due to its phenotype of ascending

paralysis, but does not incorporate the molecular features of TDP-43 and C9ORF72 dysfunction. On the other hand, those that do model these characteristics do not show the ascending paralysis that is the main clinical feature of ALS.

Protein$^{(Mutation)}$ Overexpressed	Reference	Disease Onset (months)	Survival (months)	Paralysis	Motor Neuron Loss	Protein Aggregation
$SOD1^{G93A}$	Gurney *et al.*, 1994	3	4	Yes	Yes	-
$SOD1^{G85R}$	Bruijn *et al.*, 1997	8	8.5	Yes	Yes	SOD1
WT TDP-43	Arnold *et al.*, 2013	-	>17	No	No	None
$TDP\text{-}43^{Q331K}$	Arnold *et al.*, 2013	-	>17	No	Yes	None
WT TDP-43	Stallings *et al.*, 2010	-	>11	No	No	None
$TDP\text{-}43^{A315T}$	Stallings *et al.*, 2010	1	2	Yes	Yes	TDP-43 and Ubiquitin
WT FUS	Mitchell *et al.*, 2013	1	3	Yes	Yes	FUS
FUS^{R521C}	Verbeeck *et al.*, 2012	-	-	-	-	FUS and Ubiquitin
C9ORF72 KO	Koppers *et al.*, 2015	-	>24	No	No	None
C9ORF72 $(G_4C_2)_{66}$	Chew *et al.*, 2015	-	-	No	Yes	DPRs
C9ORF72 $(G_4C_2)_{1000}$	O'Rourke *et al.*, 2015	-	>20	No	No	DPRs

Table 1.2 - Comparison of described mouse models of ALS. WT = wild type; $(G_4C_2)_N$ = number of hexanucleotide repeats in transgene; "-" = not reported; DPRs = dipeptide repeats

The disheartening lack of correlation to the clinical phenotype of ALS, as well as recent technological advances, has led to the focus being shifted more onto cell models, in particular iPSC-MNs. Fibroblasts can be taken from patients and "reprogrammed" into first stem cells and then motor neurons, forming neuronal cultures with any genetic mutation, as well as any undetected genetic modifiers, intact. This has been performed with *TARDBP* mutations as well as the *C9ORF72* repeat expansion, which are both maintained after iPSC-MN induction (Devlin *et al.*, 2015).

1.4.6 ALS and the GluA2 Subunit

In culture, motor neurons showed significantly more cell death in response to excitotoxicity induced by either kainate or an AMPA-specific agonist compared to dorsal horn neurons prepared in a similar manner (Van Den Bosch *et al.*, 2000). This experiment was in the presence of inhibitors of NMDA receptors, and so the cell death appears to be mediated through the AMPA receptors themselves. By staining for Ca^{2+}-permeable AMPA receptors, it was shown that a significantly higher percentage of receptors were permeable to calcium in the motor neurons compared to the dorsal horn neurons (Van Den Bosch *et al.*, 2000). It is possible that the increased selective cell death of motor neurons is due to decreased expression of the GluA2 subunit. However, Kawahara *et al*. investigated the distribution of GluA2 expression in neurons in the human CNS and found that, although there is a relatively low abundance of GluA2

subunits in spinal motor neurons, there was no difference in expression between ALS patients versus controls (Kawahara *et al.*, 2003).

Editing at the Q/R site of GluA2 was shown to be decreased in patients suffering from ALS (Kawahara *et al.*, 2004). Laser dissection of spinal cords from patients with ALS versus control subjects after autopsy allowed editing efficiencies to be measured in individual motor neurons. In all control subjects' neurons, editing was at 100% (see Figure 1.9) whereas in patients with ALS, editing efficiency varied between 0 and 100% (Kawahara *et al.*, 2004). It has previously been found that editing at the Q/R site was complete in the motor cortex of patients with ALS (Takuma *et al.*, 1999) and so it is possible that this editing deficiency is specific to spinal motor neurons. Associated with the decrease in editing efficiency, the same group analysed the expression of ADAR2. It was found that in ALS patients, some motor neurons do not express ADAR2 (Hideyama *et al.*, 2012b). These neurons also showed TDP-43 pathology. When compared to expression of the GluA2 subunit, expression of ADAR2 was reduced by up to a third in ALS patients whereas there was normal ADAR1 and ADAR3 expression. Conversely, it has also been shown that editing is at 100% in transgenic rats expressing mutant human SOD1 (Kawahara *et al.*, 2006). There are two possible conclusions from this, firstly SOD1 transgenic animals are only a model for ALS and so may not show all of the pathology associated with the disease. Alternatively, under-editing may only occur in the sporadic form of ALS rather than in the familial disease, or simply not in the SOD1-linked version of ALS. This may also support the theory that SOD1-associated ALS follows a different pathway to TDP-43-associated ALS. Downregulation of ADAR2 occurs naturally in ageing C57BL/6J mice, and was found to coincide with the mislocalisation of TDP-43 (Hideyama *et al.*, 2012a). Manipulation of TDP-43 in cell culture did not alter ADAR2 expression (Yamashita *et al.*, 2012b), and so it is possible that cytoplasmic TDP-43 inclusions in ALS are a downstream event of altered ADAR2 expression and/or under-editing of GluA2.

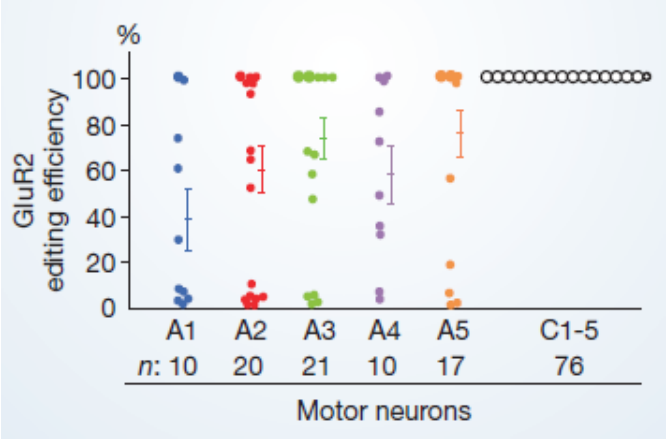

Figure 1.9 – Results from Kawahara et al. 2004, showing the range of editing efficiency from ALS patients in lower motor neurons compared to control subjects. A1-5 indicates successive patients with ALS. C1-5 are control subjects. N = number of motor neurons analysed per patient. The y-axis indicates editing efficiency. Each coloured circle represents a single neurons whose editing of the Q/R site of the GluA2 subunit was calculated.

1.5 Antisense Oligonucleotides

For the past three decades, antisense oligonucleotides have been a promising area of research for a variety of diseases. The term “antisense oligonucleotide” (ASO) refers to complementary sequences of RNA or DNA, with or without modified backbones, that are directly targeted to a gene or RNA transcript. ASO technology was first published in 1978, with an unmodified ASO targeting the 35S RNA of the *Rous sarcoma virus* (Stephenson & Zamecnik, 1978). This effectively inhibited translation of the virus’ RNA in chick embryo fibroblasts when the ASO bound to the RNA transcript via Watson-Crick base pairing (Zamecnik & Stephenson, 1978). Over the past four decades, this approach has been improved through altering the chemistry of the DNA or RNA backbone. There are multiple reasons for altering the backbone of the oligonucleotide, such as improving binding affinity, increasing resistance to degradation of the ASO by nucleases or increasing cellular penetration.

1.5.1 Mechanisms of Action

1.5.1.1 RNase H Degradation

Antisense oligonucleotides can be used to knock down expression of genes through recruitment of RNase H, which cleaves the RNA strand of RNA/DNA hybrids. These ASOs are called gapmers, where flanking sequences complementary to the target RNA surround a central sequence that recruits endogenous RNase H to the complex, degrading the RNA. One example of this design of ASO is mipomersen, which targets apolipoprotein B100 in hypercholesterolemia. Mouse models showed a reduction in LDL cholesterol which was both dose-dependent and time-dependent (Crooke *et al.*, 2005). These results were replicated in human trials with only mild reactions at the injection

sites (Kastelein *et al.*, 2006; Raal *et al.*, 2010) and this drug now has FDA approval for use in cases of hypercholesterolemia. Another example is the drug custirsen, targeting clusterin which is upregulated in some cancers. Clinical trials showed improved survival in patients with prostate cancer (Chi *et al.*, 2010) although only a slight effect was seen in patients with metastatic breast cancer (Chia *et al.*, 2009). Custirsen is currently in phase III clinical trials for prostate cancer and non-small cell lung cancer (OncoGeneX, 2016).

1.5.1.2 Disruption through Steric Hindrance

Another approach to using antisense technology is through interfering with RNA processes through steric hindrance rather than recruiting enzymatic degradation. This was the approach used by Zamecnik and Stephenson (1978), and has been improved on over the years. Due to the dependence of many RNA processes on recognition sites or secondary structure of the RNA molecules, the simple addition of the short complementary sequences of modified nucleotides ought to be sufficient for disruption. The specificity of ASOs allow them to be directed to discrete regions of the RNA transcript, covering binding sequences and so preventing RNA binding proteins from carrying out their actions, or disrupting the secondary structure of transcripts and so preventing actions of the RNA transcript. By covering sequences associated with either splice enhancers or splice silencers, ASOs can promote exon skipping or exon inclusion respectively.

This approach has successfully altered splicing in multiple models including those for Duchenne Muscular Dystrophy (DMD) and Spinal Muscular Atrophy (reviewed in Kole *et al.*, 2012). Through targeting ASOs to sequences recruiting the spliceosome and preventing its action, therefore skipping exons containing mutations associated with DMD, a functional albeit shortened protein can be expressed and alleviate the DMD phenotype (Popplewell *et al.*, 2009). Exon skipping using ASOs in DMD has reached the clinical trial phase, although drisapersen, an ASO that targets exon 51 of the *DMD* gene, did not show enough of a benefit over placebo in phase III trials for GSK to continue (Echigoya & Yokota, 2014). There are many possible reasons why the clinical trials failed. For example, exon 51 has been shown to contain mutations in 13% of DMD patients (Echigoya & Yokota, 2014), which is a relatively high percentage but clearly not broadly applicable. This highlights one downfall of ASO technology which needs consideration. When targeting diseases that have been associated with multiple genetic mutations, the specificity of an ASO means that one treatment will only be applicable to a small percentage of patients. One possible way to get around this would be to combine a cocktail of ASOs that target multiple exons, leading to a treatment that can be aimed at more patients (Echigoya & Yokota, 2014). Eteplirsen is another ASO targeting exon

skipping of exon 51 on the dystrophin gene with a different chemistry to drisapersen and produced by Sarepta, with good outcomes in clinical trials (Mendell *et al.*, 2013) although it has recently been declined FDA approval. Exon skipping has also been used to improve specificity of ASO approaches, for example targeting exon 27 of apolipoprotein B reduces LDL cholesterol without influencing levels of the APOB48 transcript, unlike mipomersen (Disterer *et al*., 2013).

1.5.2 Chemistries of Antisense Oligonucleotides

Synthetic ASOs can have varied chemistries of phosphate backbone, the choice of which is important when considering stability, administration and biodistribution. Applying unmodified DNA bases to a cell would lead to nuclease degradation, and so altering the structure is important for the efficacy of any therapy. Chemical modifications of ASOs fall into two broad classes: altering the phosphate of the oligonucleotide to either a phosphorodiamidate or phosphorothioate backbone (blue in Figure 1.10) or modifying the ribose ring (green in Figure 1.10). All of these modifications maintain the oligonucleotide's ability to form Watson-Crick base pairs with RNA transcripts, but stabilise the ASO as a single strand. Both the phosphorothioate backbone, with a sulphur atom instead of the non-bridging oxygen, and the phosphorodiamidate backbone are resistant to nuclease degradation (Hudziak *et al.*, 1996; Noy *et al.*, 2008).

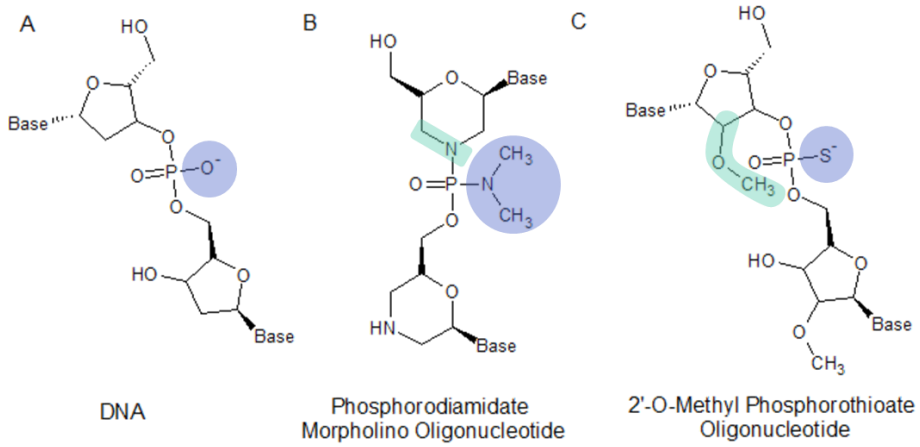

Figure 1.10 - Structures of DNA (A) compared to phosphorodiamidate morpholino oligonucleotides (B) and 2'-O-methyl phosphorothioate oligonucleotides. Green indicates modifications to the ribose sugar; blue indicates modifications to the phosphate backbone.

1.5.2.1 Ribose Ring Modifications

The most common ASO with a 2'-O-methyl modification is 2'-O-methylphosphorothioate (OMe-PS), which has been used in several applications including familial hypercholesterolemia (Disterer *et al.*, 2013) and Duchenne muscular dystrophy (Verhaart *et al.*, 2014) where they have been shown to have a long half-life of around 35 days in skeletal muscle and even longer in the heart. Drisaspersen is an OMe-PS currently in clinical trials for exon 51 skipping in DMD, apparently showing a good safetly

profile (Goemans *et al.*, 2011). Another 2' modified antisense chemistry is the 2'-O-methyoxyethyl (2'-MOE) group of ASOs, which have been shown to be effective in exon skipping in spinal muscular atrophy (Hua *et al.*, 2007) and have reached clinical trial stage with Nusinersen (Chiriboga *et al.*, 2016). For use in Duchenne muscular dystrophy, it was determined that 2'-MOEs induced a higher percentage of exon skipping at exon 23 of the *DMD* gene compared to 2'-OMe-PSs (Yang *et al.*, 2013). RNase H degradation can also be induced using this chemistry through the use of gapmers, ASOs with 2'-MOE modified bases at 5'- and 3'- ends and a central region of unmodified bases to activate RNase H activity. This method has been shown for example in myotonic dystrophy to knock down CUG RNA repeats in skeletal muscle (Wheeler *et al.*, 2012). Further modifying the ribose ring to a 2'-deoxy-2'-fluoro (2'-F) ASO, with the intention of improving exon skipping efficiencies, was found to recruit the interleukin enhancer-binding factor 2 and 3 complex resulting in omission of the exon from the RNA transcript (Rigo *et al.*, 2012).

Through creation of a cyclic structure where a 2'-alkyl substitute is replaced at the 4' position of the ribose ring, the sugar is "locked" into the conformation similar to RNA. These locked nucleic acids (LNAs) have greatly increased thermal stability, creating incredibly stable Watson-Crick base pairing even when mixed with other conformations within an ASO (Singh & Wengel, 1998). LNAs are capable of RNase H activation (Wahlestedt *et al.*, 2000) as well as in exon skipping, particularly in a mixmer (Shimo *et al.*, 2014). Other cyclic structures of ASOs include bicyclo-DNAs (bcDNAs) and tricyclo-DNAs (tcDNAs). TcDNAs in particular show promising efficacies in terms of exon skipping in the *DMD* gene, with good biodistribution throughout tissues including the CNS and low toxicity (Goyenvalle *et al.*, 2015).

1.5.2.2 Neutrally Charged ASOs

Charge-neutral ASOs are often used in exon-skipping studies due to their long half-life. Peptide nucleic acids (PNAs) are derivatives of 2-aminoethylglycine and positively charged lysine residues are often included to improve water solubility of the ASO (Hyrup & Nielsen, 1996). PNAs have particularly good cell-penetration when attached to DNA oligomers, for example conjugation to a nuclear localisation signal (Cutrona *et al.*, 2000), or to cell penetrating peptides (Cordier *et al.*, 2014). The other neutrally-charged chemistry that is predominant in antisense studies is the phosphorodiamidate morpholino oligomer (PMO). PMOs are synthetic oligonucleotides that have a phosphorodiamidate backbone instead of the naturally occurring phosphodiester linkage between bases and a morpholine ring instead of the ribose ring **(**Figure 1.10B). As a result of this modified backbone, PMOs are extremely stable, with resistance to endogenous nucleases allowing the PMO to remain intact for longer (Eisen & Smith,

2008). The neutral charge of PMOs also reduces the chances of toxicity (Amantana & Iversen, 2005). Effective biodistribution of ASOs remains a challenge. Due to the neutral charge of PMOs, it is particularly difficult to get them into the target cells both in cell culture and *in vivo* as they require a charged carrier molecule to cross membranes. One method is to "leash" the PMO with a charged cDNA molecule to facilitate uptake into the cell (Morcos *et al.*, 2008). Another method is to attach a charged cell-penetrating peptide to the PMO (Veltrop & Aartsma-Rus, 2014).

The pharmacodynamics of the oligonucleotide are obviously important if they are to be therapeutic. ASOs with a phosphorothioate linkage, with their negative charge, bind to plasma proteins allowing infiltration to diverse tissues, whereas a phosphorodiamidate backbone is neutrally charged and so show a more rapid clearance from the blood at low concentrations (Geary *et al.*, 2015). However, neutrally charged ASOs may be conjugated to a cell-penetrating peptide which would carry the ASO through the blood and into the cells (reviewed in Copolovici *et al.*, 2014). Subcutaneous or intravenous injection will deliver ASOs to the periphery, however most will not cross the blood-brain barrier. Cell-penetrating peptides, nanoparticles or other kinds of carrier may be able to deliver ASOs into the CNS (Falzarano *et al.*, 2014), alternatively direct administration to the CSF allows the ASO to target neurons with the potential to combat neurodegenerative diseases (Kordasiewicz *et al.*, 2012). Intrathecal administration of ASOs have also reached phase I clinical trials with only relatively mild adverse effects experienced in both test and control groups (Miller *et al.*, 2013).

1.5.3 ASOs and Disease

Diseases that are essentially monogenic are well-suited to treatment from ASOs. The specificity of the oligonucleotide reduces the potential for off-target effects, making this approach an attractive therapeutic option. Thanks to chemical modifications or differing routes of administration, ASOs can reach the CNS and so also target neurodegenerative disorders. Diseases such as Neurofibromatosis type 1 and 2, frontal-temporal dementia and Niemann-Pick Disease are all candidates for ASO therapy by targeting their associated genetic mutations (Siva *et al.*, 2014).

1.5.3.1 Exon Skipping in Duchenne Muscular Dystrophy

Duchenne Muscular Dystrophy (DMD) is an X-linked neuromuscular disorder affecting boys, characterised by progressive weakness of muscles beginning early in childhood, eventually reaching the diaphragm and respiratory muscles leading to respiratory failure. The disorder is caused by mutations in the *dystrophin* gene, coding for the protein dystrophin which is integral for correct muscle contraction. These mutations often disrupt the reading frame leading to non-functional transcripts or premature stop codons

(Aartsma-Rus *et al.*, 2003). ASOs can be targeted to the exons containing the mutation, preventing the spliceosome from reaching the RNA and so “splicing out” the affected exon (Popplewell *et al.*, 2009). This approach has been shown to produce shortened but functional dystrophin protein in mouse models for DMD (Lu *et al.*, 2003). These ASOs, having been promising in animal models, continued to clinical trials with drisapersen and eteplirsen as previously mentioned. Other approaches to DMD treatment using antisense technology include targeting multiple exons with a “cocktail” of ASOs, therefore making a more generic therapy for DMD patients with a broad range of mutations (Aartsma-Rus & van Ommen, 2007).

1.5.3.2 Exon Skipping and Spinal Muscular Atrophy

Spinal muscular atrophy (SMA) is a neurodegenerative disorder affecting motor neurons generally in infants, caused by a mutation in exon 7 of the *SMN1* gene leading to loss of expression (Ahmad *et al.*, 2016). This loss of function is partially compensated for by expression of *SMN2*, a duplication of *SMN1* but with a nucleotide change in exon 7 leading its exclusion in most transcripts. However, an ASO targeting an exon splice silencer in the preceding intron removes the inhibition and so promotes inclusion of exon 7 in the *SMN2* transcript. The function of these ASOs are therefore the opposite of those used in DMD, where the goal is promoting exon inclusion rather than exon skipping. This has been shown to ameliorate the SMA phenotype in a mouse model (Passini *et al.*, 2011). Further work has shown that so-called bi-functional ASOs can be used which both block the silencing sequence and recruit exon splice enhancers to the splice site, again showing amelioration of the SMA phenotype in mice (Osman *et al.*, 2012). Nusinersen, the ASO that targets the intronic silencer element promoting exon 7 inclusion, was shown to have good distribution amongst neurons of the spinal cord after intrathecal injection in non-human primates (Rigo *et al.*, 2014) and had good results following a phase I clinical trial (Chiriboga *et al.*, 2016)

1.5.3.3 ASOs and ALS

Some research has been carried out into the prospect of ASO therapy in ALS, in three main areas. One target is the *SOD1* gene, where targeting mutated *SOD1* led to a 50% reduction in mutant *SOD1* expression in rats, which did not delay symptom onset but did significantly delay symptom progression and increased mean survival (Smith *et al.*, 2006). In iPSC-MNs derived from patients with SOD1-linked fALS, treatment with a PMO targeting the mutant SOD1 lead to reduced cell death and lower levels of misfolded protein (Nizzardo *et al.*, 2016). This ASO was well-tolerated in a preliminary in-human trial when delivered intrathecally, and is now in Phase I/II clinical trials (Miller *et al.*, 2013).

Alternatively, the C9ORF72 expanded repeat proved to be an effective target, with several groups working in this area. The most popular approach has been to target the repeat with ASOs that recruit RNase H to degrade the RNA transcript (Sareen *et al.*, 2013; Donnelly *et al.*, 2014; Lagier-Tourenne *et al.*, 2013) although steric hindrance of the expansion preventing RNA-binding protein association has also been attempted (Donnelly *et al.*, 2013). It was found that ASOs with RNase H binding targeting the intronic region downstream of the repeat had the greatest impact on expression, with a significant reduction in the number of cells containing RNA foci (Donnelly *et al.*, 2014). A more specific ASO was designed to target the repeat expansion of C9ORF72 and therefore keep any expression of the normal length transcript, which reduced the behavioural deficits of increased anxiety and cognitive dysfunctions shown in a mouse model overexpressing 450 hexanucleotide repeats (Jiang *et al.*, 2016).

Acetylcholinesterase has also been a target for ASO therapy. Acetylcholinesterase has been shown to be increased in the serum of ALS patients and an ASO reducing acetylcholinesterase transcription in $SOD1^{G93A}$ mice showed a non-significant trend towards improved survival (Marc *et al.*, 2013).

1.6 AIMS AND OBJECTIVES

Editing at the Q/R site of the GluA2 subunit in AMPA receptor subunits is clearly crucial to the normal function of the neuron. Through its regulation of calcium permeability, dysregulation of the RNA editing process has been associated with several diseases, including ALS. However, the consequences of this dysregulation at an intracellular level remain unclear. This project will therefore have two sections:

In the first section, ASOs will be designed to disrupt the Q/R editing site of the GluA2 subunit. Specifically, PMOs will be used due to their previous success in manipulating splicing and RNA editing through steric hindrance, as well as their resistance to nuclease degradation. The following objectives will be met:

1. An assay will be established to detect changes in Q/R site editing in cell lines
2. Using this assay, the sequences of PMOs will be optimised to allow maximal disruption of the RNA editing process
3. These PMOs will then be tested in increasingly neuronal-like cell models, finally attempting to test the effects of PMOs in primary cortical neuronal cultures

Hypothesis 1:

PMOs can be used to inhibit Q/R site editing through disruption of the secondary structure of the GluA2 transcript.

Secondly, ASOs will be targeted to the ADAR2 transcript to change the alternative splicing pattern. Again, PMOs will be used. The following objectives will be met:

1. An assay will be established to determine the inclusion of the AluJ cassette
2. PMOs will be designed to prevent the AluJ cassette inclusion into the ADAR2 transcript
3. These PMOs will be tested in cell models to determine their efficiency at exon skipping and any effect that this has on Q/R site editing in the GluA2 subunit

Hypothesis 2:

PMOs can be used to "skip" the AluJ cassette in the ADAR2 transcript and therefore increase ADAR2's ability to edit the Q/R site of the GluA2 subunit.

2 MATERIALS AND METHODS

2.1 BIOINFORMATICS ANALYSIS

2.1.1 Online Resources

- Ensembl (www.ensembl.org)
  - *Genomic sequences*
- MFold (mfold.rna.albany.edu)
  - *RNA folding*
- RNAstructure (rna.urmc.rochester.edu/RNAstructure)
  - *RNA folding (software download)*
- SFold (sfold.wadsworth.org)
  - *RNA folding and thermodynamics calculations*
- Human Splice Finder (www.umd.be/HSF/)
  - *Detection of splicing elements*
- Sigma Aldrich “OligoEvaluator™” (www.oligoevaluator.com)
  - *Thermodynamics of short sequences of nucleic acids*
- Clustal MUSCLE (www.ebi.ac.uk/Tools/msa/muscle/)
  - *Sequence alignment and homology comparisons*

2.1.2 RNA Sequences

The nucleotide sequences for the transcripts analysed were taken from the Ensembl database, the details of which are shown in Table 2.1. Sequences were exported from the Ensembl website in the FASTA format for input into subsequent web servers or software, or in some cases the Ensembl transcript code could be directly inputted into the online tool, such as with the Human Splice Finder.

Gene Name	Species	Ensembl Entry Number	Transcript ID
GRIA2	*Homo sapiens*	ENSG00000120251	ENST00000296526
Gria2	*Mus musculus*	ENSMUSG00000033981	ENSMUST00000075316
Gria2	*Rattus norvegicus*	ENSRNOG00000054204	ENSRNOT00000077941
ADARB1	*Homo sapiens*	ENSG00000197381	ENST00000360697

Table 2.1 - Details of Ensembl gene entries used.

2.1.3 RNA Secondary Structure

To determine the secondary structure of the RNA molecules in both the GRIA2 and ADARB1 genes, the websites MFold, RNAstructure and SFold were used.

2.1.3.1 MFold

The MFold web server has previously been used to predict RNA structure for use in PMO design (Popplewell *et al.*, 2009). Mfold calculated the Minimum Free Energy structure for a given sequence. The RNA Folding Form was used, with the default conditions maintained. Folding temperature was at 37°C, in 1M NaCl. Maximum loop sizes were kept at 30 bases and there was no limit on the distance between base pairs. The MFold RNA folding form has a limit of 9,000 bases to keep the processing times to a minimum. Fasta sequences of *GRIA2* and *ADARB1* were inputted into the entry form and output structures were saved as pdf files for later comparison.

2.1.3.2 RNAstructure

RNAstructure software was downloaded and the *GRIA2* sequence opened in Fasta format within the RNAstructure program. First, a Partition Function file was created for the RNA sequence. From the RNA menu, the Partition Function RNA option was selected and the *GRIA2* sequence in fasta format was inputted, and the file saved. The Partition Function calculates the base pair probabilities for a sequence. The Maximum Expected Accuracy (MaxExpect) structure could then be calculated based on probabilities from the partition function file. From the RNA menu, the MaxExpect: Predict RNA MEA Structure option was selected, and the partition function file inputted. Once the MaxExpect model had been calculated, the structures were drawn in the RNAstructure program and saved as pdf files for later comparison.

2.1.3.3 SFold

The SFold web server was used for further comparison of folding for the *GRIA2* sequence based on centroid structures. In the Srna application, the fasta sequence for *GRIA2* was inputted with the default conditions kept. There was no limit for maximum distance between paired bases and folding was predicted at 37°C in 1M NaCl. Output structures were saved as pdf files for later comparison.

2.1.4 Exon Splice Enhancer/Silencer Sequences

Human Splice Finder gives information regarding consensus sequences, splice donor and acceptor sites, splice enhancer and splice silencer sequences in both the exon and the neighbouring introns. On the Human Splice Finder website, the Ensembl transcript number was inputted and the exon specified. The transcript number used for the *ADARB1* gene was ENST00000360697, which is protein coding. Exon 6 of this transcript contains the AluJ cassette. 100 bases either side of the exon were included in analysis.

2.1.5 Oligonucleotide Binding Energy

The website SFold was used to assess binding energies of potential oligonucleotide sequences. Within the SFold website, the SOligo tool was used (Ding & Lawrence, 2003; Ding *et al.*, 2005). DNA sequences were inputted into the online form and the default parameters were used, with the exception of “preferred length of antisense oligos” which was increased to either 25 or 30 bases. Once the website had calculated the data, the output version “oligo_f.out” was chosen. This produced the data in a table format showing the binding energy for every oligonucleotide of the desired length that could bind to the inputted sequence (Column 5 in Figure 2.1). The binding energies for potential oligonucleotides were noted.

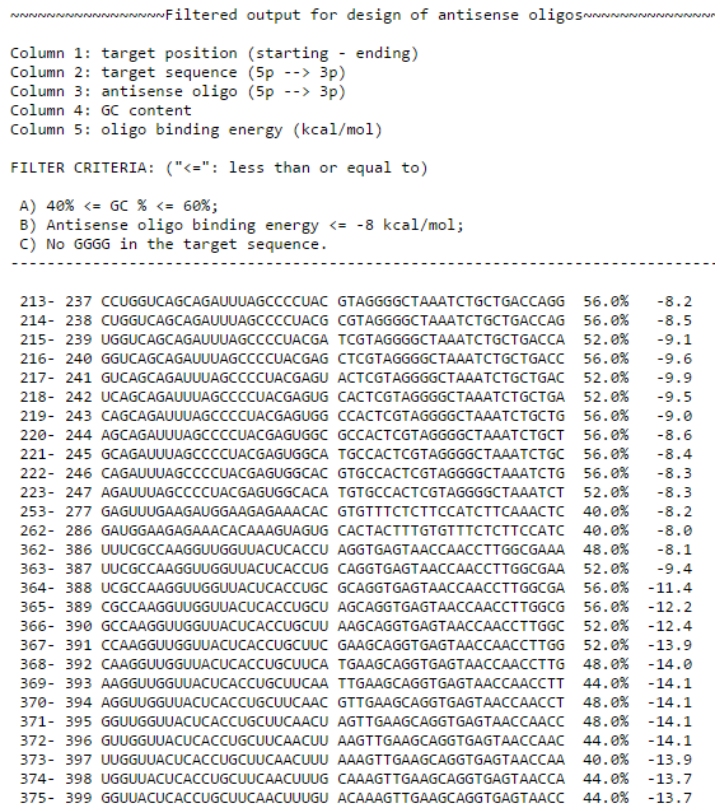

~~~~~~~~~~~~~~~~~~Filtered output for design of antisense oligos~~~~~~~~~~~~~~~~~~

Column 1: target position (starting - ending)
Column 2: target sequence (5p --> 3p)
Column 3: antisense oligo (5p --> 3p)
Column 4: GC content
Column 5: oligo binding energy (kcal/mol)

FILTER CRITERIA: ("<=": less than or equal to)

A) 40% <= GC % <= 60%;
B) Antisense oligo binding energy <= -8 kcal/mol;
C) No GGGG in the target sequence.

213-	237	CCUGGUCAGCAGAUUUAGCCCCUAC	GTAGGGGCTAAATCTGCTGACCAGG	56.0%	-8.2
214-	238	CUGGUCAGCAGAUUUAGCCCCUACG	CGTAGGGGCTAAATCTGCTGACCAG	56.0%	-8.5
215-	239	UGGUCAGCAGAUUUAGCCCCUACGA	TCGTAGGGGCTAAATCTGCTGACCA	52.0%	-9.1
216-	240	GGUCAGCAGAUUUAGCCCCUACGAG	CTCGTAGGGGCTAAATCTGCTGACC	56.0%	-9.6
217-	241	GUCAGCAGAUUUAGCCCCUACGAGU	ACTCGTAGGGGCTAAATCTGCTGAC	52.0%	-9.9
218-	242	UCAGCAGAUUUAGCCCCUACGAGUG	CACTCGTAGGGGCTAAATCTGCTGA	52.0%	-9.5
219-	243	CAGCAGAUUUAGCCCCUACGAGUGG	CCACTCGTAGGGGCTAAATCTGCTG	56.0%	-9.0
220-	244	AGCAGAUUUAGCCCCUACGAGUGGC	GCCACTCGTAGGGGCTAAATCTGCT	56.0%	-8.6
221-	245	GCAGAUUUAGCCCCUACGAGUGGCA	TGCCACTCGTAGGGGCTAAATCTGC	56.0%	-8.4
222-	246	CAGAUUUAGCCCCUACGAGUGGCAC	GTGCCACTCGTAGGGGCTAAATCTG	56.0%	-8.3
223-	247	AGAUUUAGCCCCUACGAGUGGCACA	TGTGCCACTCGTAGGGGCTAAATCT	52.0%	-8.3
253-	277	GAGUUUGAAGAUGGAAGAGAAACAC	GTGTTTCTCTTCCATCTTCAAACTC	40.0%	-8.2
262-	286	GAUGGAAGAGAAACACAAAGUAGUG	CACTACTTTGTGTTTCTCTTCCATC	40.0%	-8.0
362-	386	UUUCGCCAAGGUUGGUUACUCACCU	AGGTGAGTAACCAACCTTGGCGAAA	48.0%	-8.1
363-	387	UUCGCCAAGGUUGGUUACUCACCUG	CAGGTGAGTAACCAACCTTGGCGAA	52.0%	-9.4
364-	388	UCGCCAAGGUUGGUUACUCACCUGC	GCAGGTGAGTAACCAACCTTGGCGA	56.0%	-11.4
365-	389	CGCCAAGGUUGGUUACUCACCUGCU	AGCAGGTGAGTAACCAACCTTGGCG	56.0%	-12.2
366-	390	GCCAAGGUUGGUUACUCACCUGCUU	AAGCAGGTGAGTAACCAACCTTGGC	52.0%	-12.4
367-	391	CCAAGGUUGGUUACUCACCUGCUUC	GAAGCAGGTGAGTAACCAACCTTGG	52.0%	-13.9
368-	392	CAAGGUUGGUUACUCACCUGCUUCA	TGAAGCAGGTGAGTAACCAACCTTG	48.0%	-14.0
369-	393	AAGGUUGGUUACUCACCUGCUUCAA	TTGAAGCAGGTGAGTAACCAACCTT	44.0%	-14.1
370-	394	AGGUUGGUUACUCACCUGCUUCAAC	GTTGAAGCAGGTGAGTAACCAACCT	48.0%	-14.1
371-	395	GGUUGGUUACUCACCUGCUUCAACU	AGTTGAAGCAGGTGAGTAACCAACC	48.0%	-14.1
372-	396	GUUGGUUACUCACCUGCUUCAACUU	AAGTTGAAGCAGGTGAGTAACCAAC	44.0%	-14.1
373-	397	UUGGUUACUCACCUGCUUCAACUUU	AAAGTTGAAGCAGGTGAGTAACCAA	40.0%	-13.9
374-	398	UGGUUACUCACCUGCUUCAACUUUG	CAAAGTTGAAGCAGGTGAGTAACCA	44.0%	-13.7
375-	399	GGUUACUCACCUGCUUCAACUUUGU	ACAAAGTTGAAGCAGGTGAGTAACC	44.0%	-13.7

Figure 2.1 - Example SFold SOligo output. Column 5 shows the binding energy between the target sequence and the designed antisense oligonucleotide.

In order to calculate the internal binding energy of each oligonucleotide to itself, the Sigma Aldrich OligoEvaluator™ was used. Sequences of potential PMOs were inputted into their calculator. Default conditions were maintained and the option of “Display Primer Dimer and Hairpin Structures” was selected. For each PMO, if multiple outputs were calculated then the structure with the highest energy was selected. GC content for each morpholino was also taken using this online tool. The PMO-PMO (“primer-dimer”) and Hairpin structures with the highest energy were then subtracted from the binding energy calculated from the SOligo tool. Potential PMOs could then be ranked according to proposed binding energy to the RNA substrate.
~~~~~~~~~~~~~~~~~~

2.2 PMOs

2.2.1 Synthesis

Phosphorothiodiamidate morpholino oligonucleotides (PMOs), once designed (see Bioinformatics section), were ordered from GeneTools (http://www.gene-tools.com/). 25mer PMOs were ordered in the standard morpholino request form with no end modifications. 30mer PMOs were ordered with the first 25 bases (5' to 3') in the standard request form with the extra 5 bases requested in the Notes section. The fluorescent PMO was requested with a fluorescein modification at the 3' end of the PMO9 (AluJ+93+117) sequence). Sequences are shown in Table 2.2.

PMO Name	PMO Sequence (5'-3')
25mers:	
PMO1 (GRIA2+284+308)	AATGAGAATATGCAGCAAAAACACG
PMO2 (GRIA2-30-6)	GAAATATCGCATCCTTGCTGCATAA
PMO3 (GRIA2-14+10)	AGTGACCAACCTTGGCGAAATATCG
PMO4 (GRIA2+262+286)	ACGGTACCCCTCCAAGCAGGCATGG
PMO5 (GRIA2+19+43)	TGAGACCTAAAATGCACAAAGTTGA
PMO6 (GRIA2+50+74)	AGTGAATTCATAGACACCATGAATA
PMO8 (AluJ+1+25)	CCAGCCTGGGTGTAAGAGCGAGACC
PMO9 (AluJ+93+117)	TAGTCCCAGCTCCTTGGAAGGTTGA
PMO9A (AluJ+94+118)	GTAGTCCCAGCTCCTTGGAAGGTTG
PMO9B (AluJ+95+119)	TGTAGTCCCAGCTCCTTGGAAGGTT
PMO10 (AluJ+96+120)	CTGTAGTCCCAGCTCCTTGGAAGGT
30mers:	
PMOE1 (GRIA2+279+308)	AATGAGAATATGCAGCAAAAACACGGTACC
PMOE4 (GRIA2+261+290)	AAACACGGTACCCCTCCAAGCAGGCATGGA
PMOE4B (GRIA2+250+279)	CCCTCCAAGCAGGCATGGAATGATAGGAAC

Table 2.2 - PMO names and sequences

2.2.2 Suspension

PMOs were shipped as sterile lyophilised solids. 300 µl of DEPC-treated sterile water (Ambion #AM9915G) was added per 300 nanomoles of PMO to make a 1 mM stock solution. Stock solutions were vortexed to ensure complete suspension of the PMO.

2.2.3 Storage

Stock solutions of PMO (1 mM) are stable at room temperature in sealed containers as recommended by GeneTools.

2.3 CELL CULTURE

2.3.1 Media Recipes

2.3.1.1 Media for HeLa and SH-SY5Y cell lines

Growth media (500 ml total volume)

- 440 ml Dulbecco's Modified Eagle's Medium (Sigma #D5796)
- 50 ml foetal bovine serum (10%; Gibco #10500-064)
- 5 ml L-Glutamine (2 mM final concentration; Gibco #A2916801)
- 5 ml penicillin-streptomycin (100 units/ml penicillin final concentration; 100 µg/ml streptomycin final concentration; Gibco #15140122)

Freezing media (50 ml total volume)

- 35 ml Dulbecco's Modified Eagle's Medium (Sigma #D5796)
- 10 ml foetal bovine serum (20%; Gibco #10500-064)
- 5 ml DMSO (10%; Sigma #D8418)

2.3.1.2 Media for primary cortical neurons

Dissociation media (5 ml total volume)

- 4.5 ml Dulbecco's Modified Eagle's Medium (Sigma #D5796)
- 50 µl DNase (100 µg/ml final concentration)
- 0.5 ml Trypsin (Thermo Fisher #12604021)

Plating media (50 ml total volume)

- 50 ml Dulbecco's Modified Eagle's Medium (Sigma #D5796)
- 2.5 ml foetal bovine serum (10%; Gibco #10500-064)
- 0.5 ml penicillin-streptomycin (100 units/ml penicillin final concentration; 100 µg/ml streptomycin final concentration; Gibco #15140122)
- 0.5 ml L-Glutamine (2 mM final concentration; Gibco #A2916801)

Neurobasal media (50 ml total volume)

- 48 ml Neurobasal media (Thermo Fisher #21103049)
- 1 ml B27 supplement (Thermo Fisher #17504044)
- 0.5 ml penicillin-streptomycin (100 units/ml penicillin final concentration; 100 µg/ml streptomycin final concentration; Gibco #15140122)
- 0.5 ml Glutamax (2 mM final concentration; Thermo Fisher #35050061)

2.3.2 Cell Lines and Storage

HeLa cells and SH-SY5Y cells were kindly provided by Professor George Dickson and Professor Robin Williams respectively (both Centre of Biomedical Sciences, Royal Holloway University of London). All work was performed with sterile plasticware inside a class II laminar flow hood. For long term storage, cells were washed with 10 ml of 1x phosphate buffered saline solution (PBS; Sigma-Aldrich #P4417) per T75 flask and detached from the plate via trypsinisation involving incubation for 1 minute with TrypLE (Thermo Fisher #12604021). Trypsin was inactivated by the addition of 9 ml of growth media and cells were counted using a haemocytometer. Cells were pelleted and resuspended at 1 x 10^5 cells per ml in freezing media. Suspended cells were aliquoted into cryovials (Thermo Fisher #377267) at 1 ml per vial and cooled slowly to -80°C before long-term storage in liquid nitrogen (gaseous phase).

2.3.3 Thawing of frozen stocks and Maintenance

Frozen HeLa and SH-SY5Y cells were quickly defrosted by placing the cryovial in a water bath at 37°C. Once defrosted, suspended cells were diluted with 9 ml of growth media then spun at 3,000 rpm for 5 minutes to pellet the cells. The media was removed and the cells resuspended in 1 ml of growth media before being seeded in a T75 flask (Corning #430372) with another 15 ml of growth media. Cells were then kept at 37°C with 5% CO_2 and subcultured every 3 to 4 days or when 80% confluent. Immediately after defrosting, cells were allowed to recover for one week before being used in experiments.

2.3.4 Sub-culturing

When cells were 80% confluent, the media was aspirated and cells were washed with 1x PBS. 1 ml of TrypLE was added to the cells and incubated for 1-2 minutes at 37°C to detach the cells from the flask. 9 ml of growth media was then added to the cells to a total volume of 10 ml, which was spun at 3,000 rpm for 5 minutes to pellet the cells. The media was removed and cells were resuspended in 1 ml of fresh growth media, pre-warmed to 37°C, followed by a further 9 ml. A portion of the suspended cells (1 ml of 10 ml for HeLa and 2 ml of 10 ml for SH-SY5Y) was placed in a fresh T75 flask with an additional 15 ml of growth media and allowed to grow in the incubator.

2.3.5 Primary Cortical Neurons

2.3.5.1 Plate Preparation

6 well plates were coated with poly-D-lysine (100 µg/ml in PBS) and incubated at 37°C for 5 hours or at 4°C overnight. Plates were washed three times with sterile H_2O and left to air dry.

2.3.5.2 Dissection

Primary cortical rat neurons were prepared by Dr Ursu (Centre for Biomedical Sciences, Royal Holloway University of London) in accordance with Home Office regulations and the Animals Scientific Act 1986. A pregnant Sprague-Dawley rat at E18 was euthanised, the embryos removed and placed on ice. For each embryo, the head was severed and the top of the skull was carefully peeled off to expose the brain which was removed and placed in ice cold PBS. Under a dissection microscope, the meninges were removed and the two cortices separated and non-cortical tissue removed. Dissected cortices were cut into smaller sections before being transferred to a 15 ml tube containing 5 ml dissociation media. Sections were manually dissociated by pipetting before being incubated at 37°C for 10 minutes. Trypsin was then inactivated by the addition of 1.5 ml of FBS and incubated for 5 minutes at 37°C. Cells were spun at 1,500 rpm for 3 minutes and the media aspirated before the cells were resuspended in 1 ml of plating. Cells were counted using a haemocytometer and plated at 500,000 cells per well of a 6 well plate unless otherwise stated. Cells were incubated in plating media overnight at 37°C and 5% CO_2. After 24 hours, plating media was aspirated and 2.5 ml of primary neuron growth media was added per well. Plates were then incubated at 37°C and 5% CO_2 for 21 days, unless otherwise stated, with 500 µl of primary neuron growth media added to each well on top of existing media every 7 days.

2.3.6 Plasmids

2.3.6.1 Acquisition

Both the plasmids containing the B13 minigene and the ADAR2 gene were kindly provided by the O'Connell group (University of Edinburgh).

2.3.6.2 Transformation

In order to grow sufficient plasmid for transfections, plasmids were transformed and then grown in *E. coli* competent cells. NEB 5α competent cells (New England Biolabs #C2987I), stored at -80°C, were thawed on ice and mixed gently. 50 µl were pipetted into an microcentrifuge tube on ice with 1 µg of plasmid and mixed by flicking before being placed on ice for 30 minutes. The bacteria were then heat shocked at 42°C for 30 seconds and placed on ice for another 5 minutes. 950 µl of warm SOC media (Thermo Fisher #15544034) was added to the microcentrifuge tube which was then placed on a shaker (250 rpm) at 37°C for 60 minutes. Cells were then mixed by flicking and inverting before being streaked on an LB agar plate with 100 µg/ml of ampicillin. Plates were incubated at 37°C overnight.

2.3.6.3 Mini-Prep of Plasmid DNA

Plasmid DNA was prepared in low quantities using the QIAprep spin Miniprep kit (Qiagen #27104) to check the plasmid composition. Single colonies from the agar plates were picked and grown up in a starter culture of 5 ml of Terrific Broth (Sigma #T0918) with 100 µg/ml of ampicillin at 37°C in a shaking incubator (250 rpm) overnight. 2 ml of each starter culture was then centrifuged at 6,800 x g for 3 minutes at room temperature. The supernatant was removed and the cells resuspended in 250 µl Buffer P1 before being transferred to a microcentrifuge tube. 250 µl of Buffer P2 was added and the tube mixed thoroughly through multiple inversions. 350 µl of Buffer N3 was then added and mixed immediately through inversions followed by centrifugation for 10 minutes at 13,000 rpm. 800 µl of the supernatant was then added to a QIAprep spin column and centrifuged at 13,000 rpm for 30 seconds. The flow-through was discarded and the spin column washed by the addition of 500 µl of Buffer PB and centrifuged at 13,000 rpm for 30 seconds. 750 µl of Buffer PE was then added to the column and centrifuged at 13,000 rpm for 30 seconds. The flow-through was discarded and the column centrifuged at 13,000 rpm for 1 minute to remove residual wash buffer. The QIAprep column was then placed in a sterile microcentrifuge tube and the DNA eluted in 50 µl of Buffer EB by incubation at room temperature for 1 minute followed by centrifugation at 13,000 rpm for 1 minute. The plasmid DNA was quantified using NanoDrop (Thermo Scientific).

2.3.6.4 Restriction Enzyme Digestion

Plasmids containing the B13 minigene and ADAR2 transcript were confirmed through restriction enzyme digests according to previously published plasmid maps (O'Connell *et al.*, 1998; Higuchi *et al.*, 1993). For each digestion, 0.5 µg of plasmid DNA was mixed with 0.5 µl of enzyme, 1 µl of corresponding stock buffer solution and ddH_2O water to a total volume of 10 µl. Diagnostic digestion reactions were incubated at 37°C for 1 hour and visualised under UV trans illumination after being run on a 1% agarose gel in 1x TAE buffer.

2.3.6.5 Gel Electrophoresis

A 50x stock solution of TAE was prepared for gel electrophoresis (40mM Tris, 20mM acetic acid, 1mM EDTA). Agarose gels were prepared using 1x TAE buffer. Restriction digest products were run on a 1% agarose gel. 0.6 g of agarose (Bioline #BIO-41025) was heated in 60 ml 1x TAE buffer until fully dissolved, then 0.5% SYBR Safe DNA gel stain (v/v) was added before the solution was poured into the gel cast and cooled. Gel electrophoresis tanks (Scie-Plas) were used to cast and run the agarose gels. Digest products were run at 90 volts for 45 minutes and visualised using the Ebox VX2 imaging system (PeqLab).

2.3.6.6 Maxi-Prep of Plasmid DNA

Once the plasmid was confirmed through restriction digests, the EndoFree Plasmid Maxi Kit (Qiagen #12362) was used. From a starter culture, 250 µl of LB broth with the grown culture was placed in 250 ml of fresh, sterile LB broth and left on a shaker (250 rpm) overnight at 37°C. Bacterial cells were harvested by centrifugation at 5,000 rpm at 4°C for 15 minutes. The supernatant was discarded and the pellet resuspended in Buffer P1. 10 ml of Buffer P2 was added and mixed thoroughly through multiple inversions. The solution was then centrifuged at 5,000 rpm for 60 minutes and the supernatant transferred to a fresh 50 ml tube. 2.5 ml of Buffer ER was added to the lysate and mixed through inversions before being incubated on ice for 30 minutes. The QIAGEN-tip 500 was equilibrated by applying 10 ml of Buffer QBT and allowing the column to empty via gravity flow. The filtered lysate was added to the QIAGEN-tip 500, which was then washed with 30 ml of Buffer QC twice. DNA was eluted into 15 ml of Buffer QN in precipitated using 10.5 ml of isopropanol followed by centrifugation at 5,000 rpm for 60 minutes at 4°C. The supernatant was carefully decanted and the pellet washed with 5 ml of 70% ethanol, before another centrifugation at 5,000 rpm for 60 minutes at 4°C. The supernatant was removed and the pellet allowed to air dry for 5 to 10 minutes before being redissolved in 200 µl Buffer TE. The plasmid DNA was the quantified using NanoDrop (Thermo Scientific).

2.3.7 Transfection

2.3.7.1 Preparing Cells for Transfection

In preparation for transfection, cells were trypsinised and suspended in media before being seeded in 24 well plates at 200,000 cells per well. Cells were incubated at 37°C for 24 hours prior to transfection until at least 80% confluent.

2.3.7.2 Lipofectamine 2000

Plasmids containing the B13 minigene and ADAR2 transcript were transfected into HeLa cells using the transfection agent Lipofectamine® 2000 (Thermo Fisher #11668019). Following optimisation of transfection conditions for using these plasmids with the transfection reagent, a ratio of 1 µl Lipofectamine: 0.5 µg plasmid DNA per well in a 24 well plate was found to give the best transfection efficiency with lowest cytotoxicity. For one 24 well plate, 1 µl of Lipofectamine and 0.5 µg of plasmid DNA were first each suspended separately in 600 µl of DMEM only (without serum or antibiotics) and incubated at room temperature for five minutes per manufacturer's instructions. After incubation, the two suspensions were mixed together thoroughly through pipetting and incubated for a further 20 minutes (or up to six hours) at room temperature. 50 µl of the DMEM/Lipofectamine/DNA mix was then added to each well of the 24 well plate.

2.3.7.3 Endo-Porter

PMOs were transfected at a range of concentrations, from 0.1-10 µM, as discussed in relevant results chapters. For HeLa and SH-SY5Y cells grown in a 24 well plate, prior to transfection the media was aspirated and 0.5 ml of fresh growth media was added to each well. Appropriate volumes from the stock solution of the required PMO were added directly to cells' media followed by 3 µl of Endo-Porter (GeneTools; final concentration 6 mM) and the plates swirled to mix. Following transfection, cells were incubated at 37°C for 24 hours (unless otherwise stated) before RNA extraction.

For transfection of primary cortical neurons, media was removed, placed in a 15 ml tube and mixed, with 1 ml being returned to each well of the 6 well plate. 5 µl of PMO stock solution (final volume 5 µM) was then added to each well followed by 6 µl of aqueous Endo-Porter (GeneTools; final concentration 6 mM). Plates were swirled to mix and returned to the incubator.

2.3.7.4 Leashing of PMOs

For magnetofection to be effective, PMOs require a charged leash to be added for proper binding to the magnetic nanoparticles. Leashes were designed as the reverse-complementary sequence of the 17 most 5' bases of the PMO, with additional tail sequences of "gattg" (5' to 3') at the 5' end and "gtgat" (5' to 3') at the 3' end, ordered as DNA oligos from Sigma-Aldrich (sequences shown in Table 2.3). The leashes were suspended in DEPC-treated sterile water (Ambion #AM9915G) to form a 200 µM stock solution. 25 µl of leash stock solution was mixed with 5 µl of 1 mM PMO stock, 7.5 µl sterile H_2O and 12.5 µl sterile 10x PBS. This leash mixture was then heated in the following heat cycle: 95°C for 5 min, 85°C for 1 min, 75°C for 1 min, 65°C for 5 min, 55°C for 1 min, 45°C for 1 min, 35°C for 5 min, 25°C for 1 min, and held at 15°C. Leashed PMOs were stable at 4°C for up to 6 weeks. To confirm leashing was successful, 1 µl of leashed PMO and 1 µl of leash only was added to 2 µl of 1x PBS and 1 µl ddH_2O and incubated at 37°C for 30 minutes before being run on a 3% agarose gel in 1x TAE buffer. Successfully leashed PMOs will run at a higher molecular weight on the gel compared to leash only due to the larger size.

	PMO Sequence (5'-3')	Leash Sequence (5'-3')
General Leash Sequence	-	gattg-*[complementary 17 most-5' bases]*-gtgat
PMOE1 (GRIA2+279+308)	AATGAGAATATGCAGCAAAAACACGGTACC	gattg*TGCTGCATATTCTCATT*gtgat
PMOE4 (GRIA2+261+290)	AAACACGGTACCCCTCCAAGCAGGCATGGA	gattg*GGAGGGGTACCGTGTTT*gtgat
PMOE4B (GRIA2+250+279)	CCCTCCAAGCAGGCATGGAATGATAGGAAC	gattg*CATGCCTGCTTGGAGGG*gtgat

Table 2.3 - Leash sequences for each 30mer PMO designed against the GRIA2 sequence for magnetofection.

2.3.7.5 Magnetofection

10 µl of leashed PMO (1 µM final concentration) was added to 200 µl of DMEM only. PolyMag (Oz Biosciences #PN30100) or NeuroMag (Oz Biosciences # NM50200) were thoroughly vortexed before use, and 8 µl was added to the bottom of a 1.5 ml microcentrifuge tube (for a ratio of 1:1 unless otherwise stated). The leashed PMO in DMEM and reagent were then vigorously mixed together through pipetting and incubated at room temperature for 20 minutes. For transfection of primary cortical neurons, media was removed from each well, placed in a 15 ml tube and mixed, with 1 ml being returned to each well of the 6 well plate. 100 µl of the leashed PMO/reagent mix was then added to each well and the plate returned to the incubator on top of a magnetic plate (Oz Bioscience #MF10000). Neuronal plates were left on the magnetic plate for 1 hour unless otherwise stated before the magnetic plate was removed and neurons were kept at 37°C with 5% CO_2 for 48 hours unless otherwise stated.

2.3.8 Lentiviral Vector Transduction

Lentiviral vectors were stored at -80°C. Immediately before transduction, aliquots of vectors were placed on ice and allowed to thaw. For transduction of primary cortical neurons, media was removed, placed in a 15 ml tube and mixed, with 1 ml being returned to each well of the 6 well plate. Volumes of virus based on required MOI were calculated by multiplying number of cells per well by the desired MOI to calculate the total transducing units needed, followed by dividing the total transducing units needed by the titre of the virus. The volume of virus was then added directly to the media in the wells and swirled to mix before the plate was returned to the incubator.

2.3.9 Live Cell Imaging

Cells were imaged without fixing due to the PMOs' neutral charge not reacting with fixative reagents. PMOs would leach out of fixed cells as they would not be held by the fixative. Cells were therefore imaged whilst alive to maintain PMO localisation within the cell. Imaging was performed using an inverted Zeiss Vert.A1 microscope. Images were taken at x100 magnification with an Axiocam 503 mono camera combined with AxioVision software (Carl Zeiss, UK). For fluorescent images, the FITC channel was used in the same field for comparison between images. Images of cells transfected with F-PMO were taken at an exposure of 1500 ms, while cells transduced with the GFP-expressing lentiviral vector were taken at an exposure of 300 ms.

2.3.10 Flow Cytometry

HeLa and SH-SY5Y cells were plated at 350,000 cells per well of a 6 well plate and allowed to become 80% confluent. Cells were transfected with fluorescent PMO and EndoPorter as described (Section 2.3.7.3) for 24 hours before being trypsinised. Cells

were spun for 3 minutes at 3,000 rpm and resuspended in FACSFlow Solution (BD Biosciences #342003). The cytometer was standardised using CSPT standard beads (Thermo Scientific #C16509) in FACSFlow Solution. Cells were run through the cytometer at a medium flow rate. The FITC voltage was used to detect the green fluorescence tag of the fluorescent PMO. Samples were run until there were more than 25,000 total counts. First, forward scatter vs side scatter was plotted for the cell population and those events with low forward scatter and high side scatter were excluded so that live cells remained (P1 gate; Figure 2.2). Next, events within the P1 gate were plotted with height versus area to gate for single cells and exclude clumps of cells or cell debris (P2 gate; Figure 2.2). The events within the P2 gate were then plotted on a histogram with FITC fluorescence. Control cells without transfection were used to gate background fluorescence (P3 gate), and percentage of events exceeding the P3 gate was taken as the transfection efficiency.

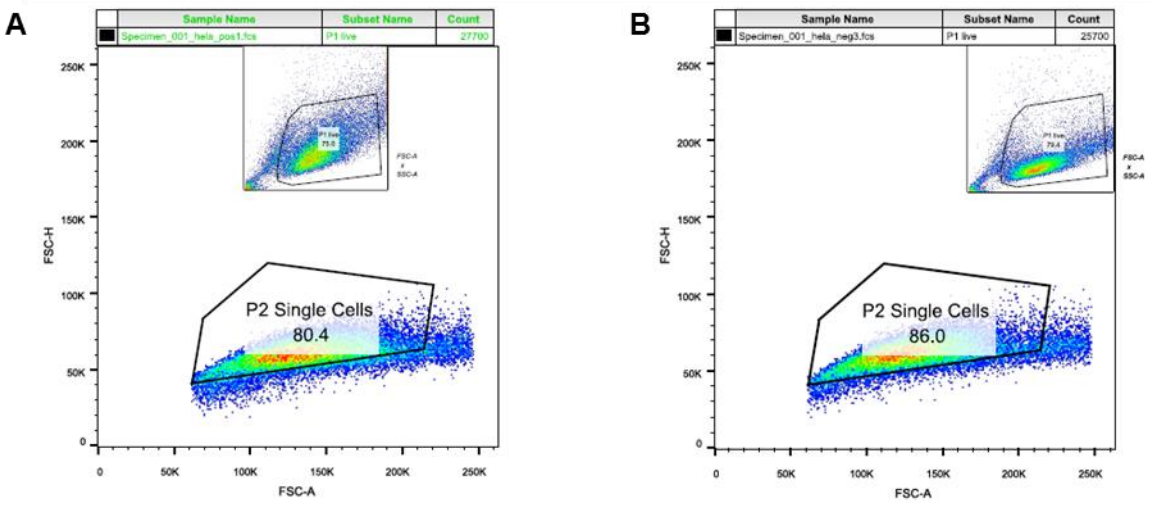

Figure 2.2 - P1 and P2 gates for FACS analysis indicating live and single cell populations. P1 gates (inserts of each graph) show the polygons excluding low forward scatter and high side scatter to gate for live cells. P2 gate (main graph) shows the exclusion of low height versus high area to gate for single cells. Gating in transfected cells (A) was consistent with gating in control cells (B), showing no bias between control and test samples.

2.3.11 Cell Toxicity Assay

The MTT assay was used to calculate cell toxicity. 250 mg of MTT powder (Sigma #M2128) was dissolved in 250 ml PBS to form a stock solution of 5 mg/ml before being filter sterilised, aliquoted and stored at -20°C in the dark. 1/10th volume of total media (i.e. 100 µl of MTT in 1 ml of media) was added per well and swirled to evenly distribute the MTT/media mixture across the bottom of each well before being incubated for 4 hours in the incubator at 37°C with 5% CO_2. Media was gently removed and the plates allowed to air dry at room temperature. 1 ml of DMSO was added per well of a 6 well plate and placed on a shaker (200 rpm) to dissolve the crystals. 75 µl from each well was added to a 96 well plate and OD was read at 570 nm using the GloMax®-Microplate

Multimode Reader (Promega, USA). Readings were normalised against blank measurements (DMSO only, no MTT) and compared to control cells with no treatment.

2.4 MOLECULAR BIOLOGY

2.4.1 RNA extraction and DNase Treatment

RNA extraction was performed using the ReliaPrep RNA Cell Miniprep System (Promega #Z6011). Cells were harvested by removal of media, washed with ice cold PBS and 250 µl of the "BL + TG" buffer was added. Wells were scraped using cell scrapers (USA Scientific #CC7600-0220) and the lysate removed and placed in 1.5 ml tubes. 85 µl of isopropanol was added per sample and the tubes vortexed for 30 seconds to shear genomic DNA. The lysate was then added to the minicolumns and centrifuged at 12,000 x g for 30 seconds at room temperature. The flow-through was discarded. 500 µl of RNA wash solution was added to the minicolumns and centrifuged at 12,000 x g for 30 seconds at room temperature. The flow-through was discarded. The DNase incubation mix was prepared in a separate tube on ice, with 24 µl of yellow core buffer, 3 µl $MnCl_2$ 0.09M and 3 µl of DNase I per sample, and mixed gently by pipetting. 30 µl of this mix was added to the membrane of each minicolumn and incubated at room temperature for 15 minutes. 200 µl of column wash solution was then added to the minicolumn and centrifuged at 12,000 x g for 15 seconds at room temperature. 500 µl of RNA wash solution was added to the column and centrifuged at 12,000 x g for 30 seconds at room temperature. The minicolumn was then placed in a fresh collection tube, 300 µl of RNA wash solution was added and centrifuged at 12,000 x g for 2 minutes at room temperature to remove all traces of ethanol. The minicolumn was then transferred to an elution tube and 30 µl of nuclease-free water added to the column. This was incubated for 1 minute at room temperature before being centrifuged at 12,000 x g for 1 minute. The minicolumn was discarded and the RNA in the elution tube quantified using the NanoDrop (Thermo Scientific) before being stored at -80°C.

2.4.2 One-step Reverse Transcription and First Round Polymerase Chain Reaction

500 ng of DNase-treated RNA was used per reverse transcriptase-polymerase chain reaction (RT-PCR) reaction. The reverse transcriptase and PCR reactions were performed within one mix using the GeneScript RT-PCR system (GeneSys Ltd. #GS003). Each 25 µl reaction contained 1x GeneScript buffer (including $MgSO_4$), 0.2 mM dNTP, 15 pM of each primer and 0.625 units of Taq polymerase made up to a final volume of 25 µl with RNase-free, DNase-free H_2O provided. Samples were then put in an MJ Research PTC-200 Thermal Cycler (GMI #8252-30-0001) using a heat cycle of 45°C for 30 minutes, 92°C for 2 minutes, 10 cycles of 92°C for 30 seconds, 62°C

for 30 seconds and 68°C for 45 cycles, then 25 cycles of 92°C for 30 seconds, 60°C for 30 seconds and 68°C for 45 seconds with an added 5 seconds per cycle, then a final anneal step at 68°C for 10 minutes. Primers are shown in Table 2.4.

Target Gene (Species)	Primer Name	Sequence (5'-3')	Product Size (bp)
ADARB1 (Human)	ADAR2 Forward Outer	ATCCATCTTTCAGAAATCAGAGC	-
	ADAR2 Reverse Outer	TTTGGTCCGTAGCTGTCCTC	
	ADAR2 Forward Inner	AGGCTGAAGGAGAATGTCCA	247
	ADAR2 Reverse Inner	TTGCTTTACGATTTGGGTGTC	
GRIA2 (Murine premRNA)	B13 Forward	ATCTGGATGTGCATTGTGTTTGCC	314
	B13 Reverse	ACAAATGGTCGGCAGCTGCTGA	
GRIA2 (Human premRNA)	GluA2 intron_exon Forward Outer	CAAAGCCCTTCATGAGCCTC	-
	GluA2 intron_exon Reverse Outer	CCATGAATGTCCACTTGAGACC	
	GluA2 intron_exon Forward Inner	GCCTCAGAAGTCCAAACCAG	322
	GluA2 intron_exon Reverse Inner	CCATGAATGTCCACTTGAGACC	
GRIA2 (Human and Murine mRNA)	GluA2 exon_exon Forward Outer	CAGCAGATTTAGCCCCTACG	-
	GluA2 exon_exon Reverse Outer	ATCCTCAGCACTTTCGATGG	
	GluA2 exon_exon Forward Inner	CAGCAGATTTAGCCCCTACG	225
	GluA2 exon_exon Reverse Inner	GCCGTGTAGGAGGAGATTATG	

Table 2.4 - List of primers, sequences and product sizes of respective PCR fragments.

2.4.3 Second Round Nested PCR

Endogenously expressed GRIA2 required a nested PCR for proper analysis due to low levels of expression. Amplification of ADAR2 transcripts required a second amplification to remove some bias inherent in PCRs towards smaller fragments. For ADAR2 products, 1 µl of product from the first round RT-PCR reaction was diluted 1:100 in ddH_2O for the second round PCR. For GRIA2 products, 1 µl of first round product was added directly to the second round PCR. The GoTaq® DNA Polymerase kit (Promega #M3001) was used. The PCR master mix contained 1x GoTaq Reaction Buffer, 1 mM additional $MgCl_2$, 0.2mM of each dNTP, 1 µM of each primer (shown in Table 2.4) and 0.125 µl of GoTaq® DNA Polymerase (5u/µl) made up to 25 µl total volume with nuclease-free water. The PCR was performed in an MJ Research PTC-200 Thermal Cycler (GMI #8252-30-0001) with the following heat cycle: 95°C for 3 minutes, 18 cycles of 94°C for 30 seconds, 60°C for 30 seconds and 72°C for 45 seconds followed by a final annealing step of 72°C for 10 minutes. Samples could then be stored at 4°C.

2.4.4 Restriction digest

RT-PCR cDNA products of the Q/R editing site were digested with the *BbvI* restriction endonuclease (New England Biolabs #R0173S). 10 µl of PCR product was incubated with 2 µl of 10x CutSmart® Buffer and 2 µl of *BbvI* (2U/µl) made up to total volume of 20 µl with ddH_2O. Digest samples were incubated at 37°C for 1 hour. The enzyme was then inactivated by the addition of 0.1% SDS to each sample before adding loading dye.

Samples were then run on a 3% agarose (w/v) gel as described at 80 V for one hour against HyperLadder® 25bp (Bioline # BIO-33057).

2.4.5 Densitometry

Images of gels were taken under ultraviolet light with 0.16 ms acquisition using the Ebox VX2 imaging system (PeqLab) and saved as Tiff files. Images could then be opened using ImageJ and the intensity of bands in each lane could be quantified (Figure 2.3; Figure 2.4). The lanes were drawn around and the “plot lanes” function used to graphically illustrate the intensity of each band. The peaks of intensity for each band were defined and the area measured (Figure 2.3B-D; Figure 2.4B-D). This area was then exported to excel for Q/R site editing or AluJ insertion analysis.

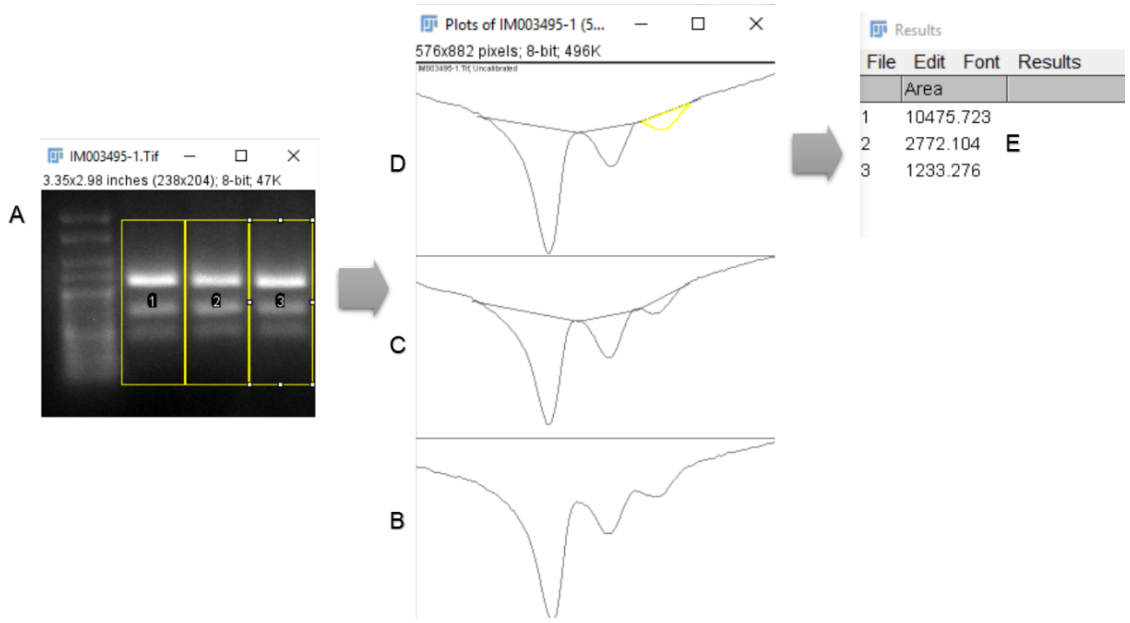

Figure 2.3 - Example analysis of Q/R site editing. Gel image (A) is opened in ImageJ and successive lanes are highlighted. The "Plot Lanes" function then charts the intensity of each band in a lane as peaks (B). These lanes are then closed to discount background (C) and the area of the peak calculated (D & E).

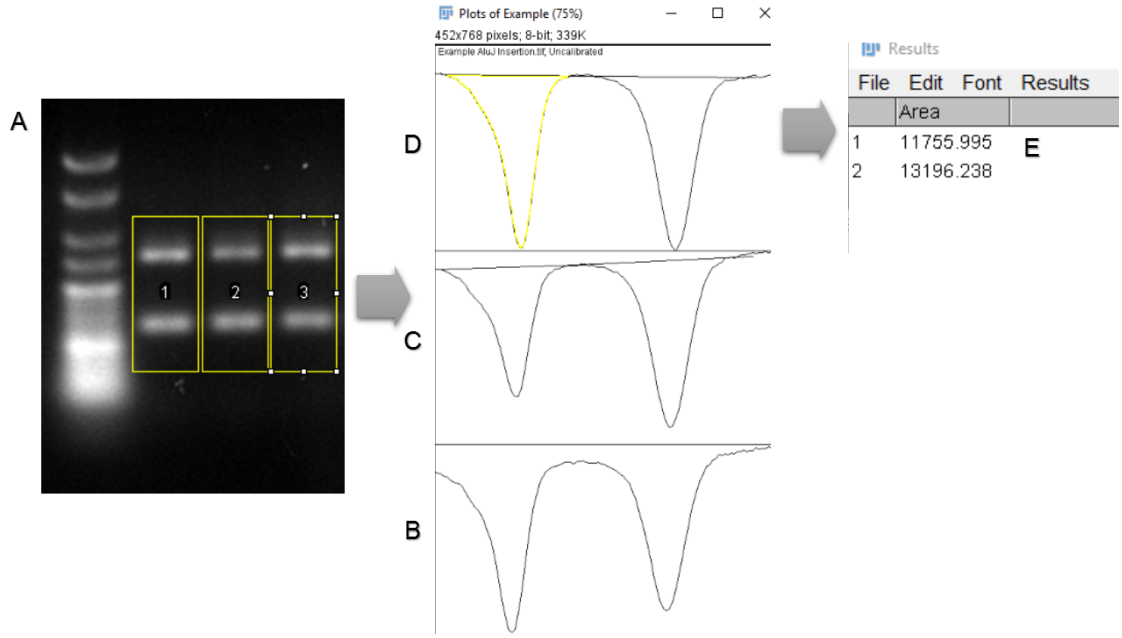

Figure 2.4 - Example analysis of AluJ Cassette insertion. Gel image (A) is opened in ImageJ and successive lanes are highlighted. The "Plot Lanes" function then charts the intensity of each band in a lane as peaks (B). These lanes are then closed to discount background (C) and the area of the peak calculated (D & E).

2.5 Q/R Site Editing Quantification

Having determined the fluorescence of each band, the relative intensity of edited to unedited DNA was then compared. The *BbvI* enzyme has a recognition sequence that covers the Q/R editing site (shown in Figure 2.5).

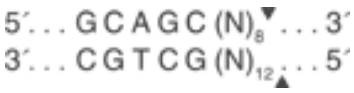

Figure 2.5 - Recognition site for BbvI enzyme taken from New England Bioloabs (neb.com)

Primers were designed to span the edited adenosine and give distinct digest fragments following *BbvI* digest. The recognition site is the unedited sequence of DNA, so cDNA copies originating from RNA that had not undergone Q/R site editing would be cleaved into two fragments. Those copies that contained the edited sequence would not have a recognition site for the *BbvI* enzyme and so the cDNA product would remain undigested. Therefore, after the *BbvI* digest, three bands are visible on the agarose gels (as seen in Figure 2.3A): one relating to the undigested (edited) fragment and two for the digested fragments (unedited sequences). Fluorescence of each band was calculated as described above. The fluorescence of the edited fragment was divided by the total fluorescence of all three bands (total DNA) to give a percentage of edited DNA fragments for each sample.

2.6 Exon Skipping of the AluJ Cassette

The same technique used for calculating editing percentages was applied to exon skipping of the AluJ cassette. Primers for both rounds of the nested PCR were targeted to exons 5 and 7, which surround the AluJ cassette. Therefore, if the AluJ cassette is included in the gene transcript the fragment will have a larger size than if the AluJ cassette has been skipped. The fluorescence of each band was calculated as previously described (Figure 2.4) and exon skipping percentages were determined by dividing the “skipped band” with total fluorescence (total DNA).

2.7 Cloning and Production of Lentiviral Vectors

2.7.1 Annealed Oligo Insert Design and Hybridisation

The lentiviral transfer plasmid containing the E4 sequence was created using the annealed oligo method. The E4 sequence was flanked by *BsmBI* overhangs (recognition site shown in Figure 2.6) according the method described by the Zhang lab, and the sequences shown in Figure 2.7 (Sanjana *et al.*, 2014).

Figure 2.6 - Recognition site for BsmBI enzyme taken from New England Biolabs (neb.com)

	Annealed Oligo Sequence with *BsmBI* overhang
Forward	5'- CACCGTTTGTGCCATGGGGAGGTTCGTCCGTACCT -3'
Complement	3'- CAAACACGGTACCCCTCCAAGCAGGCATGGACAAA -5'
Reverse complement	5' - AAACAGGTACGGACGAACCTCCCCATGGCACAAAC - 3'

Figure 2.7 - Annealed oligo sequences, forward and reverse complement with BsmBI overhangs highlighted in blue. Complement sequence shown to indicate bases that will anneal together.

Sequences were ordered as DNA oligos from Sigma Aldrich and suspended as 100 µM stock solutions. Oligos were phosphorylated and hybridised in a single reaction. 1 µl each of the forward and reverse oligos were mixed with 1 µl of 10x T4 ligation buffer (also containing ATP) and 0.5 µl of T4 polynucleotide kinase made up to a final volume of 10 µl with sterile H_2O. The mix was heated to 37°C for 30 minutes then 95°C for 5 minutes with a temperature ramp down to 25°C at 5°C per minute.

2.7.2 Production of LentiGuide Puro Plasmid

The LentiGuide Puro plasmid (Addgene Plasmid #52963) was streaked on LB agar plates with ampicillin from glycerol stocks and incubated overnight at 37°C. Single colonies were picked and grown in a 5 ml starter culture with 100 µg/ml ampicillin on a shaker (250 rpm) overnight before a mini-prep was performed as described (Section 2.3.6.3) and the DNA quantified using NanoDrop. The plasmid was checked using a restriction endonuclease digest. 500 ng of LentiGuide Puro plasmid was digested with either *BsmBI* (Thermo Scientific #FD0454) in Buffer 3.1 at 55°C or *XmaI* (New England Biolabs #R0180) and *SapI* (New England Biolabs #R0569) enzymes in CutSmart buffer at 37°C for 3 hours. Digest products were run on a 1% agarose gel as previously described (Section 2.3.6.5) to confirm product sizes. Once the LentiGuide

Puro plasmid had been confirmed, a maxi-prep was performed as previously described (Section 2.3.6.6) and quantified using the NanoDrop.

2.7.3 Digestion of LentiGuide Puro Backbone and Ligation

Digestion of the LentiGuide Puro plasmid backbone and ligation of the annealed oligos was performed together in a single step as previously reported (Cong *et al.*, 2013). The annealed oligo mix was diluted 1:250 in sterile water. 100 ng of the uncut LentiGuide Puro plasmid was added to 2 µl of the diluted annealed oligos, with 1 µl of *BsmBI* (Thermo Fisher #FD0454), 2 µl of FastDigest buffer, 0.5 µl of T4 Ligase (New England Biolabs #M0202S), 1 µl of DTT (100 mM stock; Sigma #DTT-RO), 1 µl of ATP (10 mM stock; New England Biolabs #P0756S) and sterile H_2O made up to a final volume of 20 µl. The mix was placed in a heat cycle of 37°C for 5 minutes then 23°C for 5 minutes for 6 cycles and stored at 4°C. The ligated plasmid was then transformed into competent cells as previously described (Section 2.3.6.2). Transformed cells were streaked on LB agar plates with ampicillin and incubated at 37°C for 24 hours. Single colonies were picked and grown in a 5 ml starter culture at 37°C overnight before a mini-prep was performed as previously described (Section 2.3.6.3).

2.7.4 Diagnostic Digestions to Confirm Successful Ligation

Two methods were used to check for successful ligation of the annealed oligos into the LentiGuide Puro backbone. Firstly, restriction endonuclease digests were performed as previously described with enzymes *BsmBI* (Thermo Fisher #FD0454), *NcoI*, *XmaI* and *SapI* (New England Biolabs #R0193; #R0180 and #R0569 respectively) and analysed using gel electrophoresis. Once the correct fragment sizes had been confirmed, a sample of the ligated plasmid (LG-E4) was sent for Sanger sequencing (MWG Eurofins). Chromatograms were compared and the presence of the E4 sequence following the promoter confirmed.

2.7.5 Production of Complete Lentiviral Vector

Production of lentiviral vectors was performed by Dr Ursu (Royal Holloway University of London). Briefly, HEK293T cells were seeded at 3 x 10^6 cells per 15 cm plates containing 25 ml growth media and allowed to become 80% confluent. 2 hours prior to transfection, the media was replaced with fresh growth media. Plasmids were mixed in a 1:1:1:2 molar ratio (packaging:REV:envelope:transfer) to which 125 µl of 2.5 M $CaCl_2$ was added and incubated at room temperature for 5 minutes. 1,250 µl of 2x HBS-buffered saline was added dropwise to the plasmid mix while it was being vortexed at high speed, and then this mix was added to the HEK293T media. Cells were incubated for 16 hours at 37°C with 5% CO_2 then the media replaced with 18 ml of growth media. The cells were then incubated until the media was harvested 48 hours post-transfection, when another 18 ml

of growth media was added to the cells and harvested 72 hours post-transfection. Cell debris was removed from the harvested media (containing the virus) by being centrifuged at 1000 x g for 10 minutes at room temperature then filtered using a 0.22 µm pore size filter. The virus was then concentrated by ultracentrifugation at 50,000 x g for 2 hours at 4°C. The supernatant was discarded and the virus resuspended in 50 µl of serum-free DMEM, before being spun again at 1,000 x g for 10 minutes at 4°C to further remove any debris. The virus was then incubated with 1 µl DNase at 37°C for 30 minutes to remove any residual DNA and the stored at -80°C. Lentiviral vectors were then titred using qPCR.

2.8 SOFTWARE

Densitometry was carried out using ImageJ (Schneider *et al.*, 2012). Graphs were created using Igor Pro (WaveMetrics, Inc., Lake Oswego, OR, USA). Microscope images were captured and analysed using ZEN lite (Zeiss, Germany). Plasmid maps were drawn using SnapGene® software (from GSL Biotech; available at snapgene.com).

2.9 STATISTICS

Mean and standard deviation were calculated using Excel. Statistical analyses were carried out using IBM SPSS Statistics (Version 21). One-way or two-way ANOVAs were performed as appropriate followed by Bonferroni post hoc analysis. IC50s were calculated by fitting the Hill equation using Igor Pro 6.37 (WaveMetrics, Inc., Lake Oswego, OR, USA). Graphs were plotted using Igor Pro 6.37 and all error bars show standard error. All results are reported as mean ± standard error.

3 OPTIMISATION OF A Q/R SITE EDITING ASSAY AND DESIGN OF PMOS

3.1 INTRODUCTION

It is known that ADAR enzymes require double-stranded RNA for the recognition of editing sites, and that disrupting this structure through nucleotide base substitution inhibits the editing of the Q/R site (Higuchi *et al.*, 1993). It may therefore be possible to prevent this editing reaction from taking place by interfering with the folding of the RNA transcript using PMOs to competitively bind to the target sequences via Watson-Crick base pairing. In order to investigate the effect of PMOs on Q/R site editing, an assay was needed for the reliable quantification of editing. The ideal initial model should be simple to establish and reproducible, with specific and reliable quantification of Q/R site editing which is sensitive to manipulations causing either an increase or decrease in editing. It should also be easy to introduce the designed PMOs into the model in order to assess their effects. Cultured cell lines are often initially used as models for rapid assessment, even if this means sacrificing some components of the model such as neuronal characteristics or a human origin. Cell lines are a useful model for analysis of intracellular function, and have been frequently used for analysis of Q/R site editing.

The research group who originally determined that the Q/R site was an RNA editing event used three different cell lines in their analysis, two originating from mouse (AtT20 and Neuro2A) and one from rat (PC12) (Higuchi *et al.*, 1993). AtT20 cells originated from a mouse pituitary tumour (Buonassisi *et al.*, 1962) and have been shown to display neuronal-like characteristics such as neurite projections (Tooze *et al.*, 1989). Neuro2A cells are from a mouse neuroblastoma and have also been differentiated into neuronal-like cells with dopaminergic characteristics (Tremblay *et al.*, 2010). PC12 cells originated from a rat adrenal pheochromocytoma and can differentiate into sympathetic neuron-like cells (Greene & Tischler, 1976). RNA editing in coding sequences is well conserved within mammals (Pinto *et al.*, 2014), but the different cell lines showed varying endogenous editing capacities. In the original Q/R site editing paper, the sequence spanning the Q/R site was amplified through PCR and cloned into M13 phages, then screened according to editing status (Higuchi *et al,*. 1993). Editing of small sections of the GluA2 subunit transfected into mouse cell lines was calculated at 87% (AtT20 cells) and 72% (Neuro2A cells), whereas PC12 cells were shown to endogenously express the GluA2 subunit and edited the Q/R site at 100% (Higuchi *et al*., 1993). Choice of cell line

is therefore important when studying Q/R site editing and may affect results. The group who originally discovered reduced editing efficiency in neurons of ALS patients have also examined the editing capacities of different cell lines (Yamashita *et al*., 2012c). Of the six cell lines used in this study, 3 showed an editing percentage at the Q/R site of close to 100%. This includes a HeLa cell line that stably expresses a section of the *GRIA2* gene controlled by the Tet-on system, which was used to study the interactions between TDP-43 and ADAR2 activity (Yamashita *et al*., 2012b). This HeLa cell line stably expressing the fragment of the GluA2 subunit was established when HeLa cells were found to be variable in their editing ability (Sawada *et al.*, 2009), although other groups have found consistent HeLa Q/R site editing at around 25% (Penn *et al.*, 2012). One human neuroblastoma cell line, SH-SY5Y cells, showed Q/R site editing of 50% (Yamashita *et al*., 2012c). This is contrary to another report of SH-SY5Y mRNA Q/R site editing at nearly 90% (Penn *et al.*, 2012). Q/R site editing percentages appear to positively correlate with ADAR2 endogenous expression in the different cell lines (Yamashita *et al*., 2012c) which may explain the variability in reported Q/R site editing percentages.

Cell lines have previously been used to analyse the effects of PMOs on Q/R site editing. Three cell lines were used: HeLa, SH-SY5Y and MIN-6 (Penn *et al.*, 2012). HeLa and SH-SY5Y cells are of human origin, from a cervical cancer and neuroblastoma respectively, whereas MIN-6 originate from a rat β-pancreatic cell line. The HeLa cells were used as an exogenous reporter system with similar conditions used by Higuchi *et al.* (1993), where a plasmid containing the same sequence of the GluA2 gene (Figure 3.1) was transfected into cells to analyse editing percentages. They found SH-SY5Y cells to have endogenous editing of around 85%, whereas MIN-6 cells were shown to have nearly 100% editing, similar to editing levels found in the brain (Penn *et al*., 2012).

To measure the editing efficiency of the different cell lines, Penn et al. (2012) extracted RNA from cell samples and cDNA templates were made. These cDNA samples were then digested with the restriction endonuclease *BbvI* which has a recognition site that covers the unedited sequence of the Q/R editing site (GCAGC). Unedited cDNA copies were therefore digested by the enzyme and so showed two bands when separated on a gel, whereas edited DNA remained undigested. They also used Sanger sequencing methods to determine editing by comparing relative peaks of A versus G bases at the editing site within the RT-PCR product (Penn *et al.*, 2012). These two methods for determining editing efficiency are the most commonly used throughout the literature (Pachernegg *et al.*, 2015; Venø *et al.*, 2012; Gaisler-Salomon *et al.*, 2014). Other methods have also been developed to measure RNA editing, often in the 5-HT_{2C} subunit, such as using real-time quantitative PCR, where different probes are designed to

recognise the separate isoforms (Lanfranco *et al.*, 2009) or using high-throughput sequencing techniques (Abbas *et al.*, 2010). There have also been some creative alternative editing assays developed. For example, a yeast reporter system was developed where expression of the *HIS3* gene, required for histidine auxotrophy, is linked to a shortened version of the R/G editing site on the GluA2 subunit (Garncarz *et al.*, 2013). Editing at the R/G site was required for histidine expression and therefore for growth of the yeast culture in histidine-deficient medium (unedited transcripts coded for a stop codon). Potential enhancers for RNA editing were then transfected into this system and colonies that grew were identified and the enhancer further analysed (Garncarz *et al.*, 2013). They also developed an editing assay in mammalian cells where the editing site was preceded by an RFP gene and followed by the gene for GFP. Editing was required for GFP expression, as again unedited R/G sites coded for a stop codon. Relative expression of GFP compared to RFP could then be assayed using FACS (Garncarz *et al.*, 2013). However, this method is highly specific to the R/G site, which has a short sequence and little associated secondary structure, and it would probably not be possible to translate this system to the Q/R site.

Bearing these previous studies in mind, a model was developed using HeLa cells transfected with the same plasmid originally used by Higuchi *et al.,* (1993) and also used in the Penn *et al*. paper (2012). This plasmid contains the “B13 minigene”, a short sequence of the murine *GluA2* gene, under the control of a CMV promoter (Figure 3.1). The B13 sequence contains the Q/R site, the exon complementary sequence and the imperfect repeat, features of the GluA2 transcript all known to be important in Q/R site editing (Figure 3.2). Transfection procedures were optimised to give strong B13 expression in HeLa cells. It was also important that the endogenous editing efficiency of the cell models have the capacity to demonstrate both improved and reduced editing depending on the treatment added to give maximum flexibility to future experiments. HeLa cells had previously been shown to have an endogenous editing efficiency of 25% (Penn *et al*., 2012) and were therefore ideal. The editing assay was optimised for quantification of editing levels using *BbvI* restriction enzyme digestion followed by densitometric analysis of DNA digest fragment fluorescence. Having established the editing assay, a reliable model of secondary structure of the GluA2 RNA transcript was produced and used to design PMOs targeting the Q/R site, with an aim of sterically hindering RNA editing.

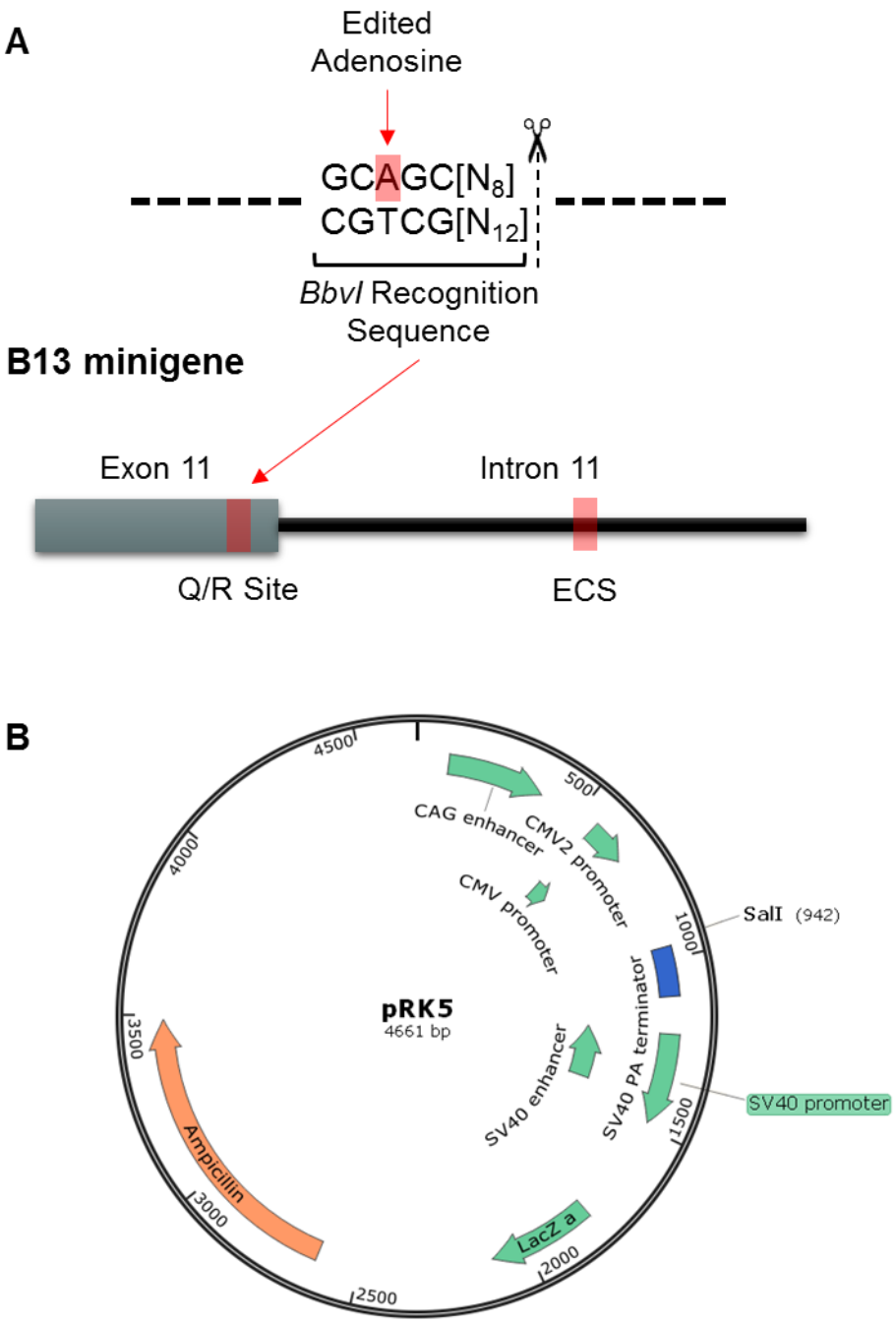

Figure 3.1 – A) Schematic of the B13 minigene, with locations of the Q/R site and exon complementary sequence (ECS), and the BbvI recognition sequence which covers the Q/R site. B) The pRK5 plasmid backbone with the SalI site indicated where the B13 minigene was inserted under the control of the CMV promoter.

AGATCTGGATGTGCATTGTGTTTGCCTACATTGGGGTCAGTGTAGTTTTAT

TCCTGGTCAGCAGATTTAGCCCCTACGAGTGGCACACTGAGGAATTTGA

AGATGGAAGAGAAACACAAAGTAGTGAATCAACTAATGAATTTGGGATTT

TTAATAGTCTCTGGTTTTCCTTGGGTGCCTTTATGCAGCAAGGATGCGATA

TTTCGCCAAGGTTGGTCACTCACCTGCTTCAACTTTGTGCATTTTAGGTCT

CAAGTGGATATTCATGGTGTCTATGAATTCACTATAAAGATGTCAGCAGCTG

CCGACCATTTGTCCAAGCAAATTTAAGATGCTTAGAAGGCAAATTTTTACCG

TCGGCGTAAGCCTGTGAAATACCTGAACAATGTTCCTTGAATGTTGATCAT

GTGTTTCCCTGGTGAAATCATATACACCATGGAGAGGCTATAAAATGCAGA

AGGTTCCTATCATTCCATGCCTGCTTGGAGGGGTACCGTGTTTTTGCTGCA

TATTCTCATTTTACAGTTATCTGTGTGTTCATCCACAGACCTGTATATGGGAA

AATGGGCGAGGTTAGATTTTTCCTACAGGGTCAACAACTTGTTAGACAACA

CTTCATTTGCACATACCTCATCTCTTTATTTCTCTAACATCAATTCATGGAAA

TGGTGTGTTTGTGAGGTTATTAAAAGTTTTAAATGTTAGGCTCCTGGAGTAA

AAAGTTGATCACACATATCTAGA

Figure 3.2 - Sequence of B13 minigene. Exon 11 is shown in bold and the remaining sequence is the beginning of intron 11. The Q/R site is underlined in red. Bases surrounding the Q/R site highlighted in blue have their complementary bases found in the "exon complementary sequence" highlighted in blue in the intron. Highlighted in green are the bases in the "imperfect repeat".

3.2 RESULTS

3.2.1 Design of PCR-*BbvI* digest assay

To quantify Q/R site editing in HeLa cells, a PCR-digest assay was designed. This was possible as the bases over the A-to-I editing site in this sequence are the recognition site of the *BbvI* restriction endonuclease in the unedited form (Figure 3.3). This means that cDNA copies of transcripts that are unedited will be cut by the enzyme whereas those that were edited will remain uncut. Due to the reliance of a complete enzymatic digest for reliable assessment of editing, high levels of *BbvI* were used (2 units per PCR reaction product) for an incubation time of 1 hour compared to the recommended 15 minutes using the Fast Digest conditions. During optimisation of the PCR-digest assay, it was discovered that SDS was needed in the loading dye of *BbvI* digest products, otherwise the enzyme interfered with the movement of DNA through the agarose gel (Figure 3.3B). Addition of 0.05% SDS denatured the enzyme sufficiently to allow the digest products to run as a distinct band. The intensity of these bands could then be quantified using densitometric analysis. Q/R site editing percentages could be calculated using the following equation:

$$\%\ Editing = \frac{Intensity\ of\ Undigested\ (Edited) Band}{(Total\ intensity\ of\ undigested\ and\ digested\ bands)} * 100$$

This assay could now be used on cDNA copies of RNA transcripts from a mammalian cell model.

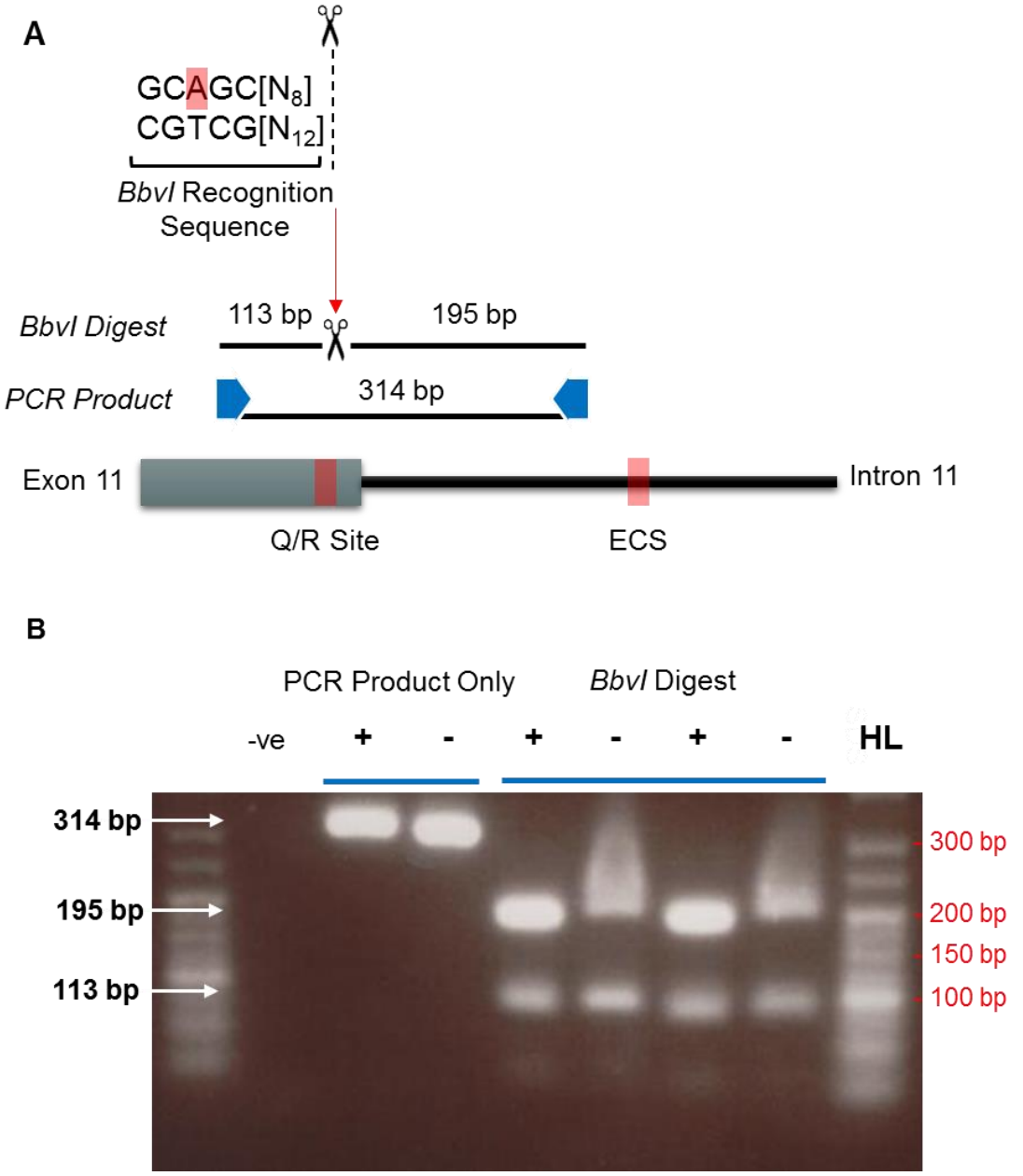

Figure 3.3 - PCR-Digest assay design. A) Schematic showing the B13 minigene and the BbvI recognition site. Forward and reverse primer placements are shown with blue arrows. If the transcript is edited then the adenosine is replaced by a guanosine and the recognition site is destroyed. B) Shows a 3% agarose gel run in 1x TAE buffer with the full PCR product only (314 base pairs) compared to the BbvI digest products (195 and 113 base pairs). Samples were either treated with 0.05% SDS (+) or not (-). Product sizes compared against HyperLadder V (HL). "-ve" indicates water control PCR reaction with no DNA present.

3.2.2 Transfection of the B13 minigene in HeLa cells

The pRK5 plasmid containing the B13 minigene was kindly donated from the O'Connell lab (Figure 3.1). HeLa cells were grown in 24 well plates at 200,000 cells per well over 24 hours until 90% confluent. The transfection reagent Lipofectamine was tested at three different ratios, 0.5:1, 1:1 and 2:1 DNA to Lipofectamine. The results are shown in Figure 3.4. Extracts from HeLa cells with no plasmid were shown to not amplify this section of the GluA2 transcript, which was expected. A plasmid containing the GFP transcript was used as a control transfection, and also showed no amplification of the GluA2 transcript. All three ratios of B13:Lipofectamine showed sufficient transfection to produce strong RT-PCR products (314 bp fragment in Figure 3.4). A ratio of 0.5 µg plasmid DNA to 1 µl of Lipofectamine per well was chosen to prevent cell toxicity.

The RT-PCR reaction amplified only the RNA transcripts extracted and not any residual DNA from the plasmid. If RNA extracts, before DNase treatment, were used in a PCR reaction using the same B13 primers, a small amount of DNA was amplified (Figure 3.5). However, following DNase treatment there was no amplification of DNA. Following the reverse transcription reaction, a strong RT-PCR product was amplified (Figure 3.5).

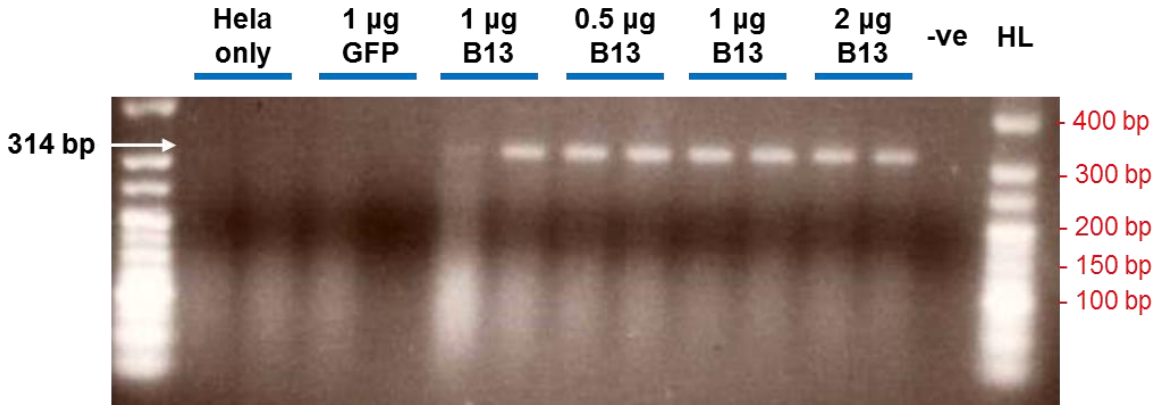

Figure 3.4 - Gel image of RT-PCR products run on a 2% agarose gel in 1x TAE buffer using HyperLadder V (HL) following different transfection conditions in HeLa cells. Extracts from HeLa cells only show no amplification of the GluA2 transcript. Control transfection of a plasmid with the GFP gene also showed no amplification. Transfections of 0.5 µg, 1 µg and 2 µg all showed good amplification of the GluA2 band at 314 base pairs. "-ve" indicates water control PCR reaction with no DNA present.

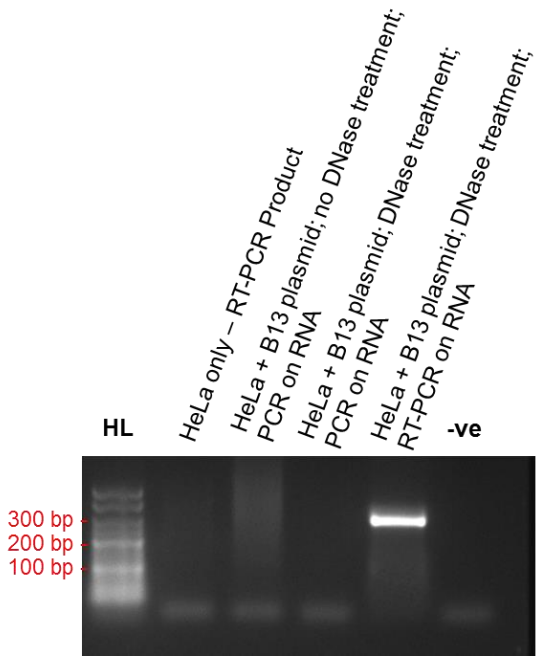

Figure 3.5 - 2% agarose gel in 1x TAE buffer using HyperLadder V (HL) to show that a PCR reaction on DNase-treated RNA does not amplify any DNA, whereas reverse transcription followed by PCR reaction produces a strong product at 314 base pairs. "-ve" indicates water control PCR reaction with no DNA or RNA present.

3.2.3 Length of *BbvI* Digest on RT-PCR Product

In order to establish the length of time the RT-PCR product needed to be incubated with the *BbvI* enzyme, the RT-PCR product was incubated for increasing lengths of time. The digest fragments were then run on a 3% agarose gel and the intensities quantified. Results, shown in figure Figure 3.6, indicate that the enzyme takes 10 minutes to complete digestion at this quantity of DNA, as indicated by the plateau in % digest (Figure 3.6B). Subsequent digests were incubated for 1 hour at 37°C to ensure complete digestion.

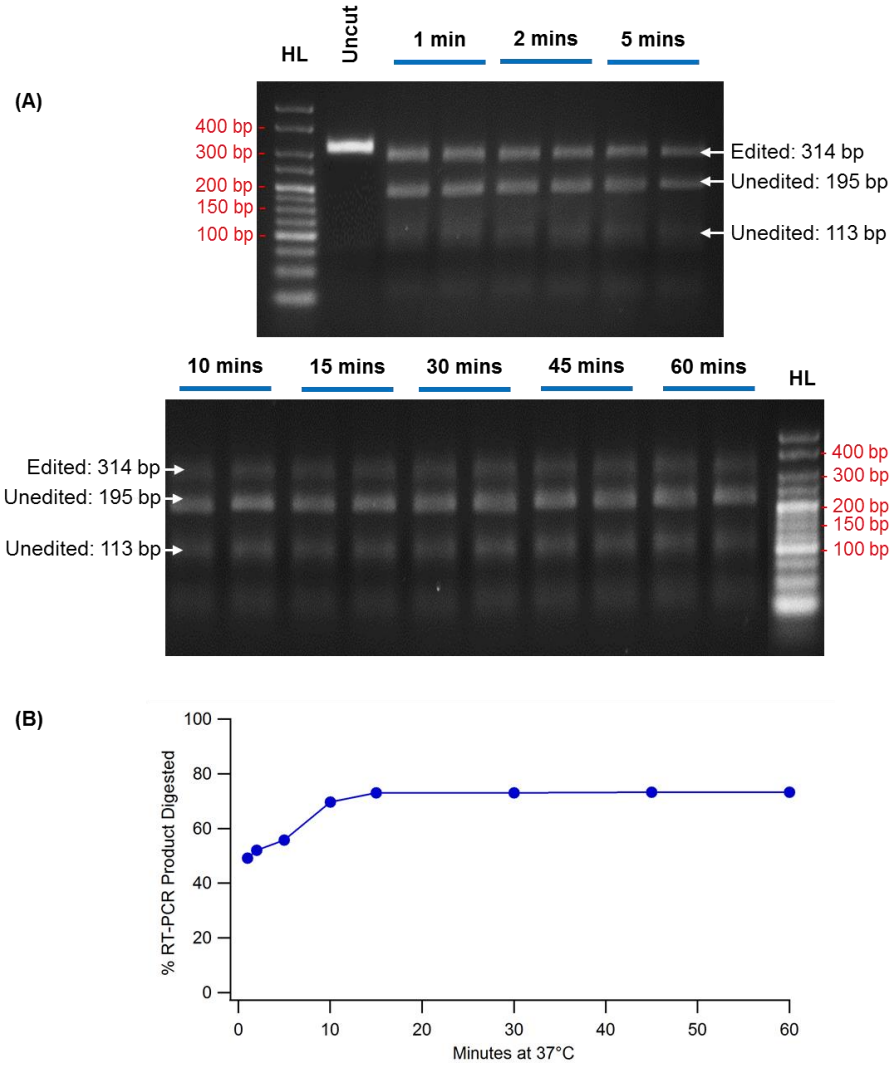

Figure 3.6 - (A) Gel images of 3% agarose gel run in 1% TAE buffer using HyperLadder V (HL) showing digest products of RT-PCR products following B13 plasmid transfection in HeLa cells. (B) Graph showing quantification of digestion at each time point. The graph plateaus after 10 minutes, indicating a complete digest.

3.2.4 Baseline Q/R site editing in the HeLa-B13 system

Once the conditions for transfection of the B13 plasmid into HeLa cells had been optimised, a baseline measurement of the editing in the HeLa-B13 system could be determined. The B13 plasmid was transfected into HeLa cells, RNA was extracted and an RT-PCR was performed followed by a *BbvI* digest as described above (Figure 3.3). Digestion products were run on a 3% agarose gel in 1x TAE buffer (Figure 3.7A) and the Q/R site editing percentage determined through comparison of the intensity of each band measured through densitometric analysis; the results are shown in Figure 3.7B. Average editing in the HeLa-B13 system was calculated at 29.4 ± 1.04% (n=8), consistent with previous studies (Penn *et al.*, 2012).

There were two features necessary for the HeLa-B13 system if it was to be used as a model: reliability and scope for manipulation. The sensitivity of the HeLa-B13 system to change was demonstrated through co-transfection of the B13 plasmid with a plasmid containing another copy of ADAR2 (kindly donated by O'Connell lab). This increased pool of enzyme ought to increase the Q/R site editing. After co-transfection of the two plasmids into HeLa cells, RNA was extracted and analysed as before leading to an increase in Q/R site editing of 86.2 ± 6.14% (Figure 3.7B). The HeLa-B13 system therefore appears to be a suitable model to test treatments that may affect Q/R site editing.

The endogenous editing at the Q/R site needed to be reliable and stable in a variety of conditions in order for any changes in Q/R site editing to be attributed to the PMO rather than B13 transfection. Editing was assessed after transfection over 24, 48 and 72 hours and remained consistent at 27.8 ± 1.06% with no significant difference between the time points (p=0.839, Figure 3.8) although there was some loss in cell viability at the 72 hour time point, likely due to over-confluency of cells and prolonged exposure to the transfection reagent. It therefore appears that the HeLa-B13 system is appropriate for testing any PMOs targeting the Q/R site, as it produces a reliable endogenous editing that is sensitive to changes made within the system.

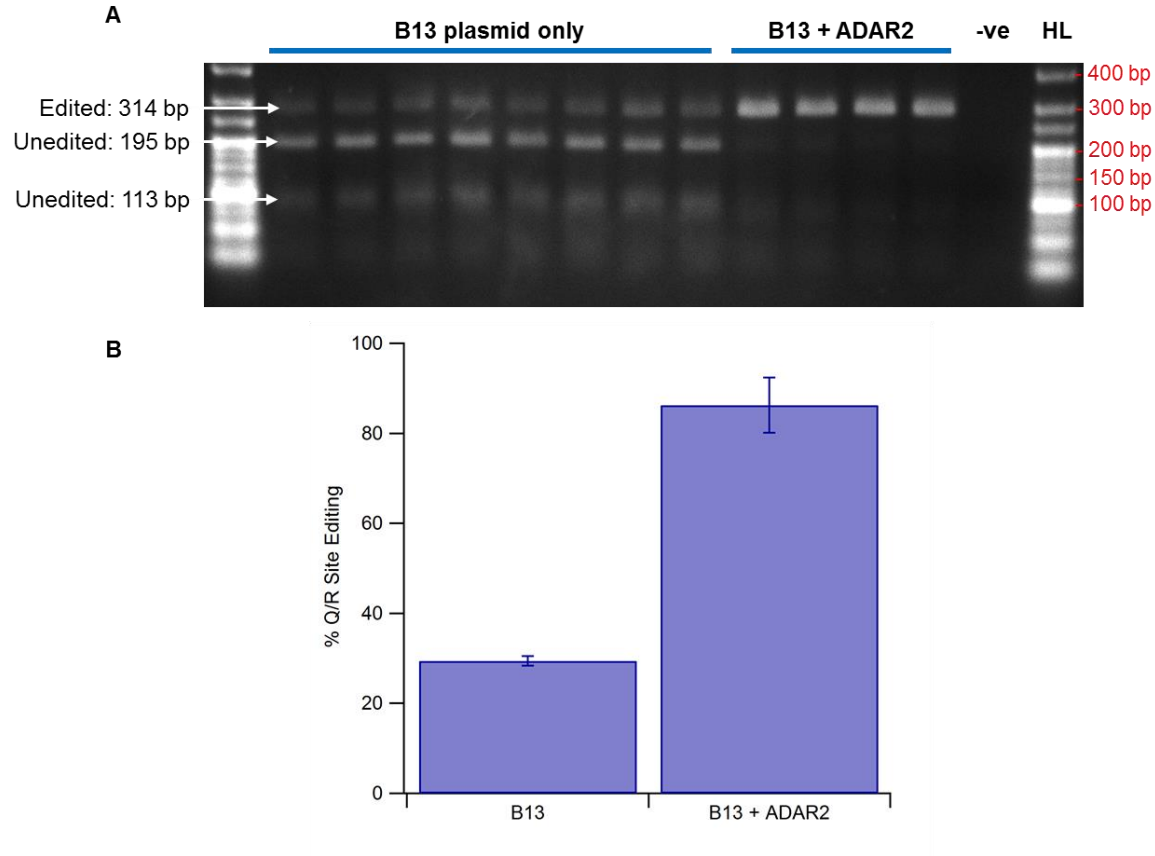

Figure 3.7 – Q/R site editing in HeLa cells. A) Shows the gel image of the BbvI digest run on a 3% agarose gel in 1x TAE buffer with the B13 minigene only, and after a co-transfection with another plasmid containing ADAR2 cDNA. Product sizes compared against HyperLadder V (HL). "-ve" indicates water control PCR reaction with no DNA present. B) Shows quantification of the editing using densitometric analysis. Average editing of the B13 minigene in HeLa cells was 29.4 ± 1.04%, whereas after co-transfection with ADAR2 this increased to 86.2 ± 6.14% ($p<0.05$, $n=8$).

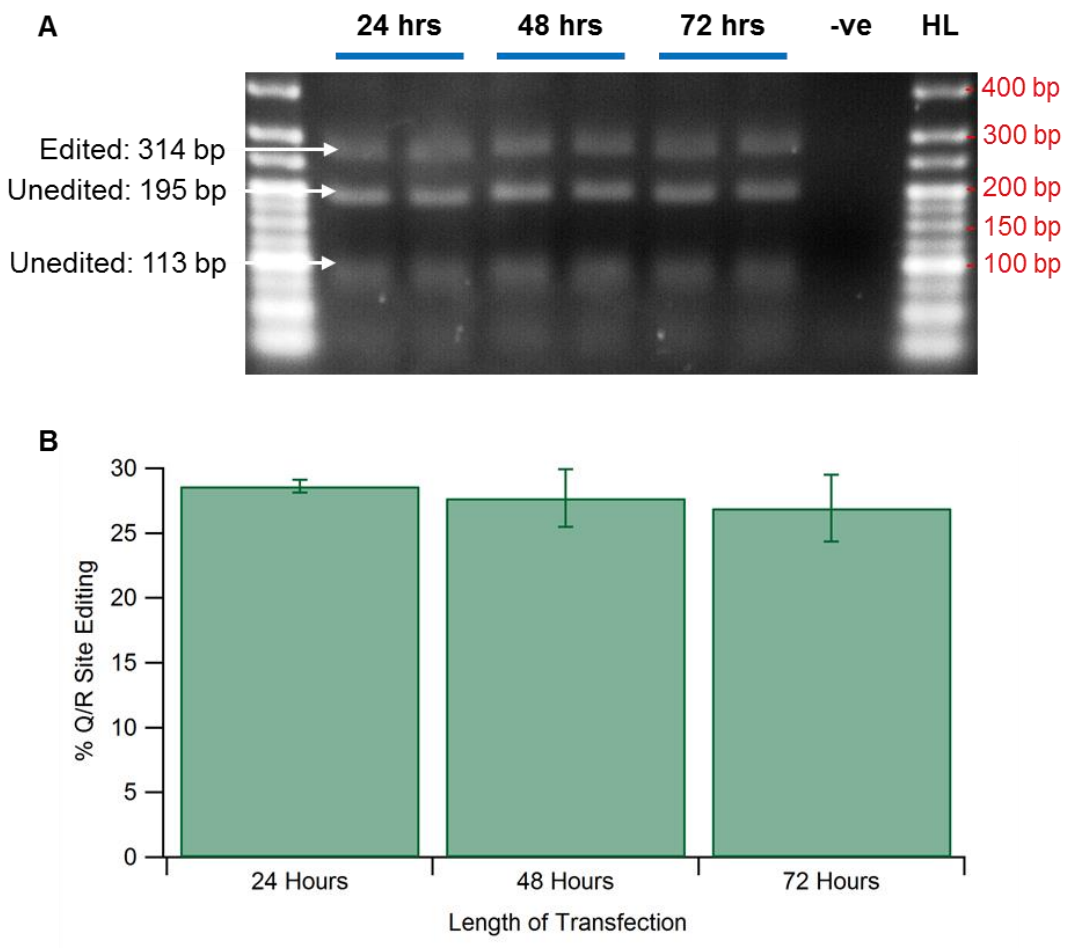

Figure 3.8 - A) Example of a 3% agarose gel of BbvI digest products from HeLa transfection with the B13 minigene for 24, 48 or 72 hours. Product sizes compared against HyperLadder V (HL). "-ve" indicates water control PCR reaction with no DNA present. B) Quantification of Q/R site editing of the B13 minigene after 24, 48 and 72 hours (28.6 ± 0.49%, 27.7 ± 2.23% and 26.9 ± 2.58% respectively) with no significant difference between groups (p=0.836; n=4).

3.2.5 Transfection of HeLa-B13 system with PMOs

It is important that PMOs can be transfected into the HeLa-B13 system effectively, with a high transfection efficiency. The neutral charge of the PMO means that a specialised transfection reagent, EndoPorter (Gene Tools) was used for transfection. To assess the transfection efficiency, a 25mer PMO (F-PMO) was produced with a fluorescent tag of carboxyfluorescein attached to the 3' end. Carboxyfluorescein emits light in the green wavelength with an excitation peak at 501.5 nm and an emission peak at 524.5 nm, and so can be viewed in the FITC channel. Two methods were used to assess transfection efficiency: cell imaging and flow cytometry, or FACS analysis. Due to the neutral charge of the F-PMO, the cells could not be fixed for staining as the F-PMO would not be immobilised, and so would leach out of the cells. Fixed cells would therefore not give an accurate transfection efficiency, and so images were taken with live cells, maintaining the compartmentalisation of the PMO (Figure 3.9A). Figure 3.9 shows HeLa cells transfected with 5 μM of F-PMO, the concentration chosen from the upper end of the range predicted to be used in the HeLa-B13 model. The first column of Figure 3.9A shows HeLa cells under phase-contrast. The third column shows the HeLa cells under the GFP channel, and the second column show these two channels merged. These merged images indicate that a high percentage of cells have taken up the F-PMO. From the images in GFP channel, it is not clear whether the fluorescence is background or a fluorescent cell due to the diffuse spread of the PMO. The two channels were therefore merged to show that the fluorescence pattern overlapped with the cells in the phase-contrast images. Figure 3.9B shows a higher magnification of the HeLa cells. The white arrow indicates a cell with diffuse fluorescence, while the blue arrow indicates a cell which is showing higher fluorescence. A cell showing very high uptake of the F-PMO is unlikely to survive the transfection. On the other hand, a diffuse pattern within each cell is the indication that an effective transfection has taken place. Although the cell images give a good overall idea of the level of transfection in the HeLa cells, it does not give an exact percentage of cells transfected.

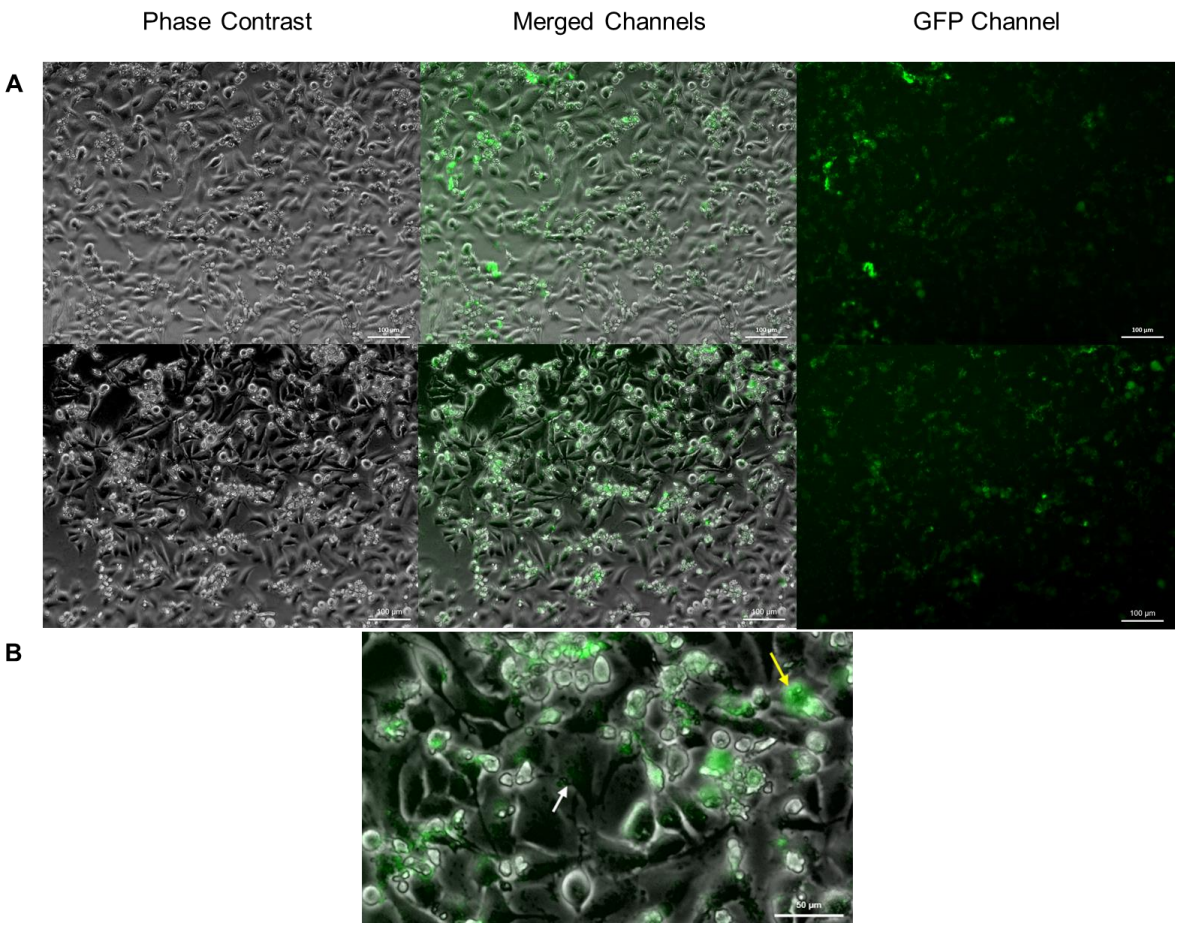

Figure 3.9 - Live microscope images of HeLa cells transfected with F-PMO. (A) scale bars indicate 100 µm. Left hand column show cells under phase-contrast, right hand column show cells in the GFP channel, centre column show the same field with merged channels. (B) shows a section at higher magnification, scale bar indicates 50 µm. White arrow indicates a cell showing diffuse fluorescence, yellow arrow indicates a cell showing intense fluorescence.

A more accurate method for quantifying transfection efficiency is FACS analysis, where transfected cells are sorted according to their fluorescence. The fluorescence of the PMO within cells will be at a higher intensity than the natural fluorescence of untransfected cells. A range of intensities were expected, correlating with the amount of PMO taken up into each cell. Here, the cells were not fixed. Instead, live cells were trypsinised and immediately placed in FACS buffer for flow cytometry in order to maintain compartmentalisation of the PMO in live cells.

The output of the FACS analysis is shown in Figure 3.10. Live cells were selected based on avoiding those with low height (FSC-H) and low fluorescence (P1 gate) and single cells were selected based on avoiding those cells with a very low or very high FSC-H and FSC-A (P2 gate). The natural fluorescence of a HeLa cell was found using control samples, (Figure 3.10 top row) and any cells with a higher fluorescence than 10^2 of FITC-A intensity were counted as transfected (P3 gate; Figure 3.10 bottom row). The number of cells found at each level of fluorescence could then be represented in a histogram (Figure 3.11). These results show that the transfected HeLa cells show a large shift in fluorescence compared to control, and that the majority of cells have been transfected.

The peaks in the histograms for the positive sample (top three rows of Figure 3.11) are low and spread over a wide range of fluorescence intensities as expected. This mirrors the results from the live images of transfected HeLa cells, where fluorescence intensity can be low and diffuse or much brighter. This may indicate that within a population of HeLa cells, for example a well of a plate, the transfection of PMO is not uniform, which in turn may account for variation in the system. Table 3.1 shows the frequency of cells per sample that were positive for the fluorescent PMO, with a mean value of 99.5%. Subtracting the error of control cells captured in the P3 gate (2.41%), this gives a transfection efficiency of 97.09%. Table 3.1 also shows the median fluorescence in the FITC-A channel for each sample, highlighting the shift in fluorescence in transfected cells. This shows that, although the transfected cells show a range of fluorescence, over 95% have taken up some of the PMO.

These results indicate that the F-PMO was readily taken up by HeLa cells using the EndoPorter transfection reagent, and so the HeLa-B13 system was considered sufficiently optimised and appropriate for analysis of PMOs.

Sample Number	Frequency in P3 Gate (positive for F-PMO fluorescence)		Median Fluorescence in FITC Channel	
	F-PMO	Control	F-PMO	Control
1	99.4	2.70	2144	910
2	99.5	2.16	2156	1086
3	99.7	2.37	2599	952
Mean	**99.5**	**2.41**	**2300**	**983**
SD	*0.15*	*0.27*	*259*	*91.9*

Table 3.1 - FACS analysis of HeLa cells transfected F-PMO. Table shows frequency of sample cells in the P3 (positive for green fluorescence) gate and the median fluorescence in the FITC-A channel per sample.

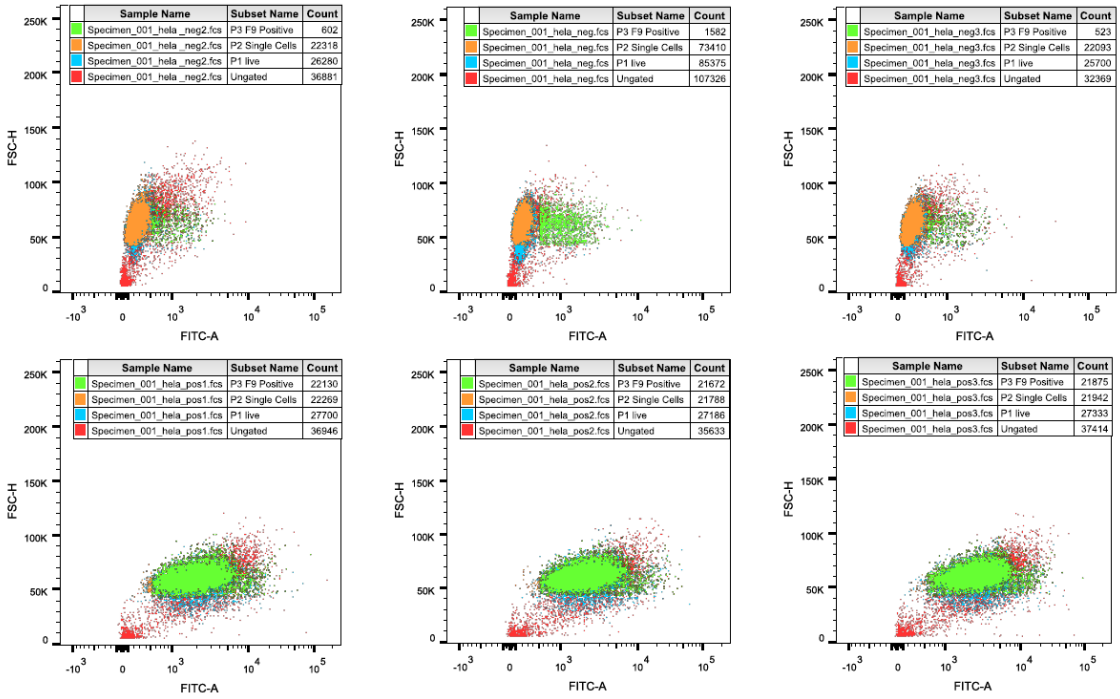

Figure 3.10 - FACS analysis showing the overlaid gates for each sample. Top row are control HeLa cells, bottom row are HeLa cells transfected with F-PMO. Overlaid colours show: P1 gate selecting live cells (blue); P2 gate selecting single cells (orange) and P3 gate selecting fluorescent cells (green). Red cells are not included in any gates.

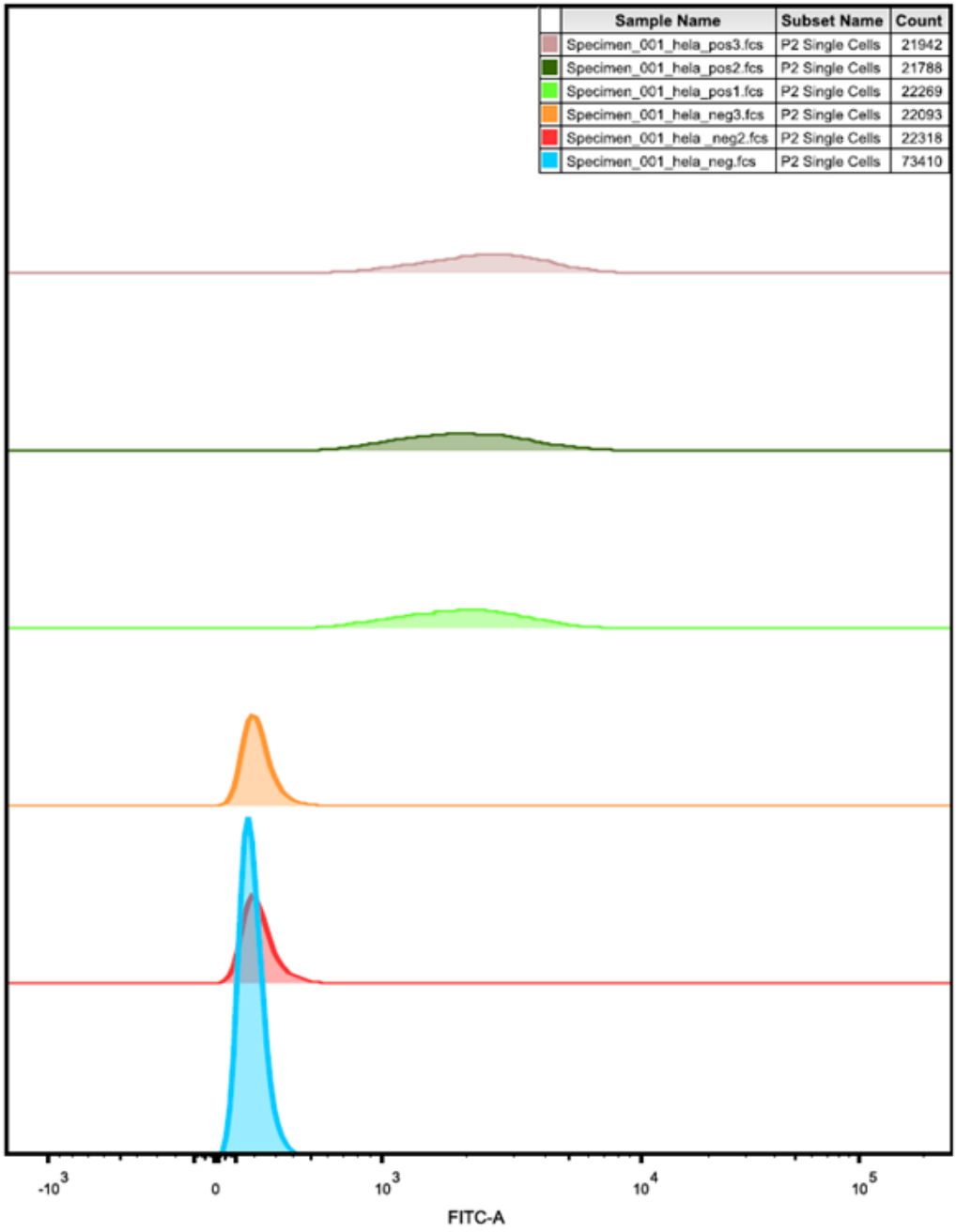

Figure 3.11 - Staggered histogram showing intensity of fluorescence for each sample. Top three rows show samples transfected with F-PMO, showing a shift to the right indicating green fluorescence compared to the bottom three rows of control HeLa cells.

3.2.6 Comparison of human *GRIA2* sequence against mouse and rat homologues

Antisense oligonucleotides are specific to their target due to their exact reverse-complement sequence. It was anticipated that multiple cell lines would be used to test the PMOs designed in this chapter, which would come from either human or murine origin. The B13 minigene (Figure 3.1) is a section of the murine *GluA2* sequence. Therefore alignments were performed comparing the human *GRIA2* sequence to the *GluA2* of rat and mouse (Figure 3.12, Appendix 1). There is a high degree of homology between all three sequences. A percentage similarity was calculated as part of the Clustal MUSCLE package, and is shown in Table 3.2. The rat sequence shows 70.96% homology to the human sequence, which is slightly lower than the mouse homology of 71.54%. The majority of the discrepancy between sequences is found in the intronic region, as shown in Table 3.3 where only exon 11 is compared between species. This is expected. It was found that homologous exons were conserved to around 85% identity overall between human and mouse, whereas in those intronic regions that could be aligned there was only 60% identity (Waterston *et al.*, 2002). Both rat and mouse *Gria2* exon 11 show a 97.04% similarity to the human sequence, which when analysed in Figure 3.12 proves to be a difference of only 13 bases. It is not always the same base that differs between the mouse and rat sequences compared to human. The region surrounding the Q/R site (highlighted in row 3 of Figure 3.12) shows complete homology across the species, indicating that it is a conserved region due to its importance to the function of the AMPA receptor. Likewise, the exon complementary sequence (ECS) is conserved across the species. The imperfect repeat, also highlighted in Figure 3.12, shows 11 bases where there are substitutions across the species, indicating that it is less important than the ECS and Q/R site itself.

% Identity Matrix Exon 11 & Intron 11	Human	Rat	Mouse
Human	100.00	70.96	71.54
Rat	70.96	100.00	87.84
Mouse	71.54	87.84	100.00

Table 3.2 - Percentage identity of human GRIA2 exon 11 and intron 11 compared to mouse and rat sequences. Comparison performed by MUSCLE.

% Identity Matrix Exon 11 only	Human	Rat	Mouse
Human	100.00	97.04	97.04
Rat	97.04	100.00	98.65
Mouse	97.04	98.65	100.00

Table 3.3 - Percentage identity of human GRIA2 exon 11 only compared to mouse and rat sequences. Comparison performed by MUSCLE.

Figure 3.12 - Alignment of Exon 11 and the beginning of Intron 11 of GRIA2 in the human sequence versus rat and mouse. Alignment was performed using MUSCLE with sequences from Ensembl. Full alignment of Exon 11 and Intron 11 is shown in Appendix 1. Exon 11 is shown in grey and the adenosine targeted by ADAR2 is highlighted by the blue box in row 3. Stars beneath the sequences indicate a perfect consensus at that base between the three species. Regions indicated as important for Q/R site editing (Higuchi et al 1993) are highlighted in blue. Imperfect repeat highlighted in intron 11, rows 4 and 5, while ECS is highlighted in row 5.

3.2.7 Prediction of the secondary structure surrounding the Q/R site

The secondary structure of the GluA2 transcript is essential for normal Q/R site editing (Higuchi *et al.*, 1993), and one aim of this project is to design antisense oligonucleotides to inhibit editing through disruption of surrounding double-stranded regions. Therefore, to accurately target these double-stranded sequences, a reliable model of the secondary structure surrounding the Q/R site was needed. Prediction of folding in RNA transcripts has progressed over the last few decades, but is still reliant on several assumptions and simplifications. Modelling secondary structures based on thermodynamic parameters (for example the MFold web serve; Zuker, 2003) is a common method and has been previously used to design antisense oligonucleotides (Penn *et al.*, 2012). Other methods include comparative analysis and prediction through cluster analysis.

To generate the most reliable structure possible, multiple models were produced initially using the MFold program to find the minimum free energy model, and the resulting structures were qualitatively compared, specifically around the Q/R site. The structure was compared across human and murine sequences for consistency across the different models used in future experiments. Variations in sequence length were tested, looking at either the complete exon 11 and intron 11 of *GRIA2* or just the short section of *GRIA2* found in the B13 minigene. Finally, three methods for RNA structure prediction, based on production of a minimum free energy model, base-pair probabilities or Boltzmann weight coefficients, were compared on the B13 minigene sequence to see if the predicted structure was influenced by the different approaches. If the predicted structure remained the same despite changing these factors, then it can be assumed that the model is as accurate as possible and can be used as the basis for antisense oligonucleotide design.

3.2.7.1 Comparison of predicted human and murine secondary structures of GRIA2

A major limitation with most structure prediction software is that the number of bases allowed in the input is limited to improve computing speed; for example MFold has a limit of 9,000 bases. This means that, in most cases, a complete premRNA transcript cannot be modelled due to the presence of large introns. However, Higuchi et al. (1993) showed the importance of intron 11 in A-to-I editing at the Q/R site as it contains the exon complementary sequence as well as the imperfect repeat (Figure 3.2). It is also possible that bases several hundred nucleotides up or downstream may influence the secondary structure of a transcript. A balance is therefore needed between using enough bases in the model for a meaningful prediction but that are still be able to be inputted into the software.

The Q/R editing site, exon complementary sequence and the imperfect repeat are all found at the end of exon 11 and at the beginning of intron 11 of the *GRIA2* gene. Therefore, the complete sequence of exon 11 and intron 11 was used, at a total of 4,887 bases in human *GRIA2*, to predict a detailed model of the GluA2 transcript. Although the human sequence was used, any antisense oligonucleotides will initially be tested in the HeLa-B13 system, and the B13 minigene was derived from mouse DNA (Higuchi et al. 1993). At later stages, if any oligonucleotides were to be tested in primary neuronal cultures, these would be of rat origin. Therefore, it was important to compare the predicted secondary structure of mouse and rat GluA2 to that of human so that any targeted secondary structure was present in all three species, especially as the intronic regions of these genes varied (Figure 3.12). The same section of mouse and rat GluA2 sequence (exon 11 and intron 11; 4,602 bases and 4,960 bases respectively) were inputted into the MFold secondary structure prediction software.

MFold is often used for designing small molecules (Zuker, 2003; Penn *et al.*, 2012). Sequences were inputted into the online form and simulations were performed under default settings. MFold calculates the secondary structure of RNA transcripts through nearest neighbour energy parameters, predicting structures with the minimum free energy (MFE structure). The MFE models for the human, rat and mouse sequences are shown in Figure 3.13 (complete output for each sequence shown in Appendix 2). Overall, the whole structures appear similar but not identical. This is unsurprising due to the variation in intronic sequences between the species. A qualitative comparison of the region surrounding the Q/R site however shows that the structure here appears to be preserved (inserts of Figure 3.13). The edited adenosine (highlighted in each insert) is consistently six bases into the beginning of a section of double-stranded RNA, just downstream from a large loop. This double-stranded region extends to a small internal loop of a couple of bases then a large loop of 16 bases on each strand, followed by another region of double-stranded structure. The exon complementary sequence is paired to the Q/R site, and is 5' to a second section of double-stranded structure. This analysis indicates that the structure of the RNA surrounding the Q/R site has been conserved across these three species, probably due to the reliance of ADAR2 on secondary structure of the RNA transcript to perform the A-to-I editing reaction. This same structure around the Q/R site is found in 38 out of 47 predicted models in the human sequence.

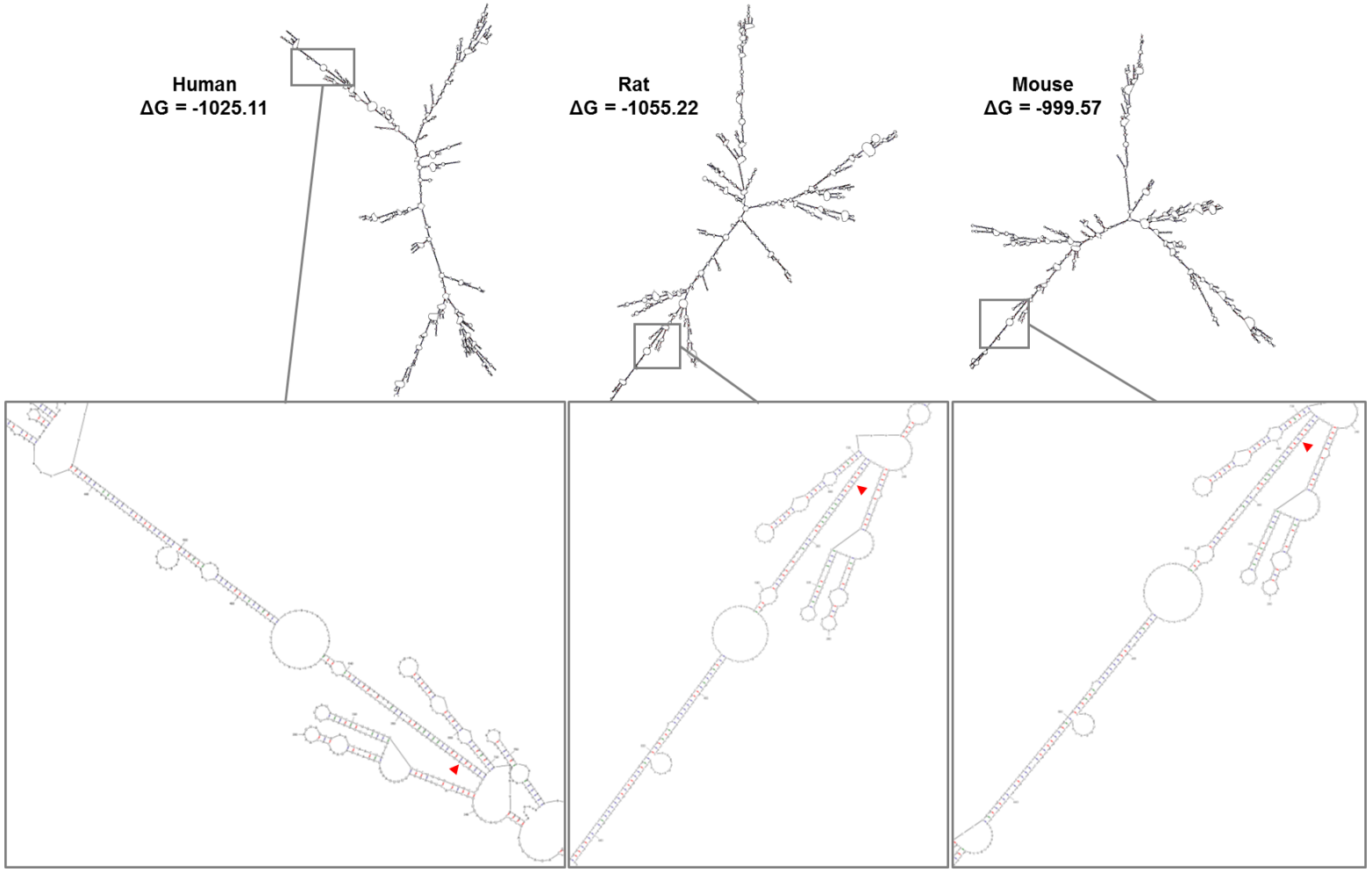

Figure 3.13 - Secondary structures of Exon 11 and Intron 11 of the GRIA2 gene in human (dG = -1025.11), rat (dG = -1055.22) and mouse (-999.57) as predicted by MFold. Each model is the predicted structure with the lowest free energy for each sequence. All predicted structures for each sequence can be found in Appendix 2. Inserts in each structure indicate the location of the Q/R site, shown by a red arrow.

3.2.7.2 Predicted secondary structure of the B13 minigene

The B13 minigene (Figure 3.1), a small section of the end of exon 11 and the beginning of intron 11 of *Gria2*, will be initially expressed within HeLa cells in order to test the antisense oligonucleotides. Therefore, the secondary structure of the B13 transcript (741 bases) itself was predicted for the PMO design. The MFE model is shown in Figure 3.14, and all predicted models from the MFold output can be found in Appendix 3. This structure shows the same pattern as was found in the complete exon 11 – intron 11 MFE model (Figure 3.13). The edited adenosine is found six bases into a double-stranded region, followed by a small and then larger internal loop which leads to a further double-stranded region. This pattern can be seen in 11 out of the 15 predicted secondary structure models for the B13 minigene given in the MFold output (Appendix 3). Repeatedly finding the same secondary structure surrounding the editing site supports its reliability as a basis for PMO design. The free energy for each model is shown on the structures in Appendix 3, and the free energy for the MFE structure is shown in Figure 3.14. The free energies for all 15 structures are within 10.3 kcal/mol, indicating that any may occur within the cell. The different predicted structures are important to consider as the RNA transcript may not remain in one conformation, and so any ASO should apply to as many structures as possible.

The MFE approach to predicting nucleotide secondary structure was the first to be used widely in molecular biology, and is based on the assumption that the structure with the MFE is the most likely to occur. However, comparing the equilibrium constants across all predicted structures for a given sequence, Mathews et al showed that the probability of the complete MFE structure of an RNA transcript existing is extremely small (Mathews *et al.*, 2010), which is supported by the fact that the difference in binding energy between the MFE and all other predicted structures is within -10.3 kcal/mol. The probability of a base pair occurring can be calculated by comparing the free energy within each predicted structure and how often that base pair occurs; base pairs with a higher probability have been shown to be more likely to be incorporated in the actual structure (Mathews, 2004). This probability can then be added to the MFE model, and the areas of secondary structure that have a higher base pair probability can be considered more reliable. Furthermore, a composite structure showing only those base pairs with the highest probabilities can be produced, giving a structure of the maximum expected accuracy (Lu *et al.*, 2009). A maximum expected accuracy model for the B13 minigene was produced using the MaxExpect function within the RNA Structure software (Reuter & Mathews, 2010). The output is shown in Figure 3.15. If compared to the MFE model (Figure 3.14), it can be seen that the structure surrounding the Q/R site is preserved. The edited adenosine is six bases from a large loop, within a section of double-stranded RNA,

followed be a small then larger internal loop then another region of double-stranded RNA. The MaxExpect program has calculated the probability of the bases surrounding the edited adenosine to be paired at 90-95%, whereas the bases leading to the small and large internal loops have a low probability of base pairing, indicating that they are more likely to remain single-stranded. The probability of the imperfect repeat forming the double-stranded structure was calculated as >99%, probably due to the complete complementary sequences.

A third approach to secondary structure prediction is the production of a centroid structure using the web server SFold (sfold.wadsworth.org/cgi-bin/index.pl; Ding *et al.*, 2005). This assumes that the base pairing of RNA follows a Boltzmann distribution (i.e. the structure is dependent on the temperature and free energy of the system). Structures can then be assigned Boltzmann probabilities and clustered according to base-pair distances. A centroid is a single structure that best represents a group of structures within the cluster, based on the lowest base-pair distance for each individual structure. SFold also determines an ensemble centroid, where the entire set of structures is included in the production of the structure. A particular sequence may therefore produce several centroid structures with one overall ensemble centroid. The ensemble centroid for the B13 minigene is shown in Figure 3.16, and shows a comparable free energy of -216.54 kcal/mol compared to the MFE structure which had -237 kcal/mol. As can be seen by comparison to the MFE model and the MaxExpect output (Figure 3.14; Figure 3.15), the structure surrounding the Q/R editing site is again conserved according to this method of prediction. The edited adenosine is still six bases into a region of double-stranded sequence, which extends further and ends at a small then larger internal loop which is followed by more double-stranded RNA. This structure is consistent across all methods of secondary structure prediction, whether the sequence is extended, between species tested here and using different prediction software.

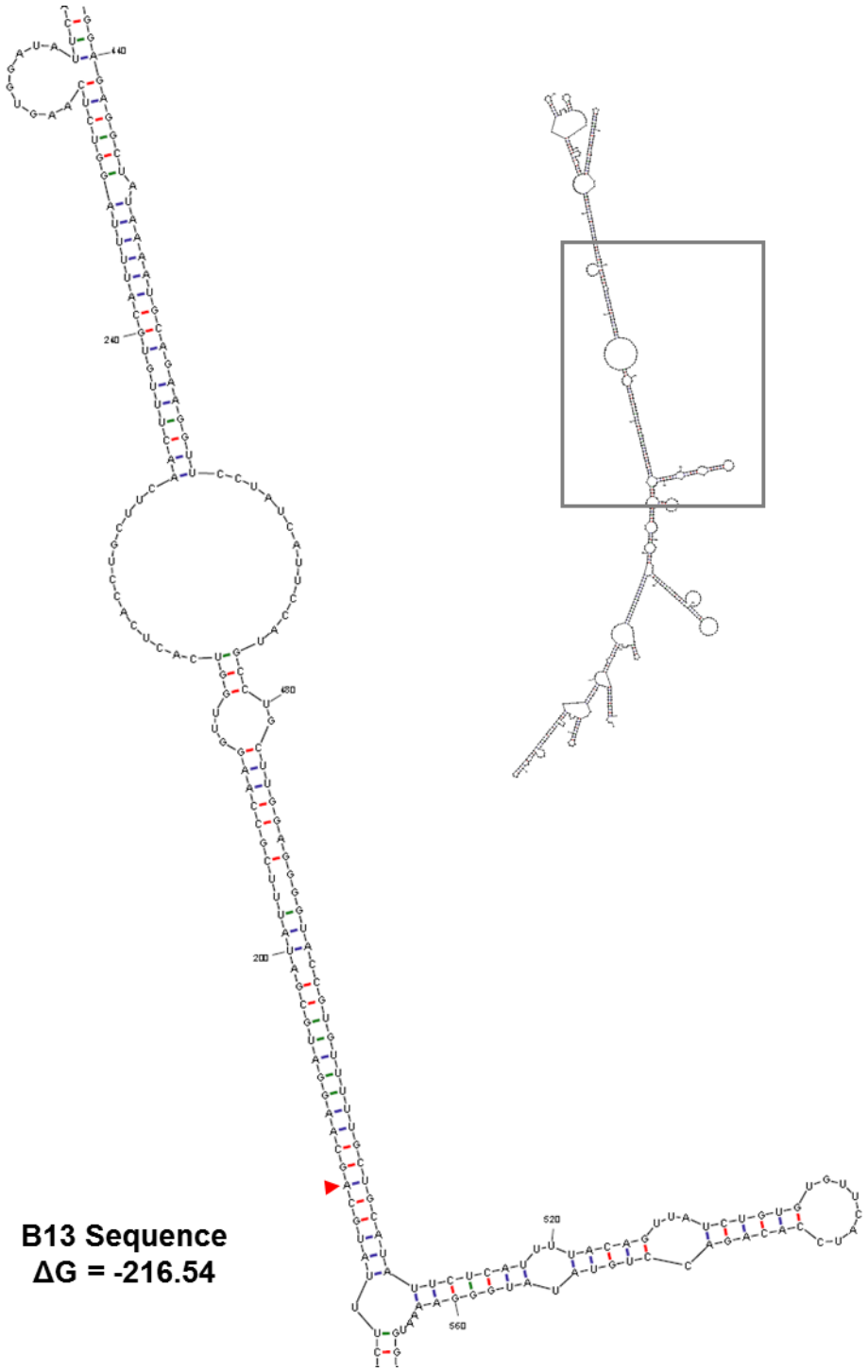

Figure 3.14 – MFE model of predicted secondary structure of B13 minigene. The total predicted RNA transcript is shown in the top right hand corner, with the areas of secondary structure surrounding the Q/R site expanded. The edited adenosine is highlighted by the red arrow and the free energy (ΔG) indicated.

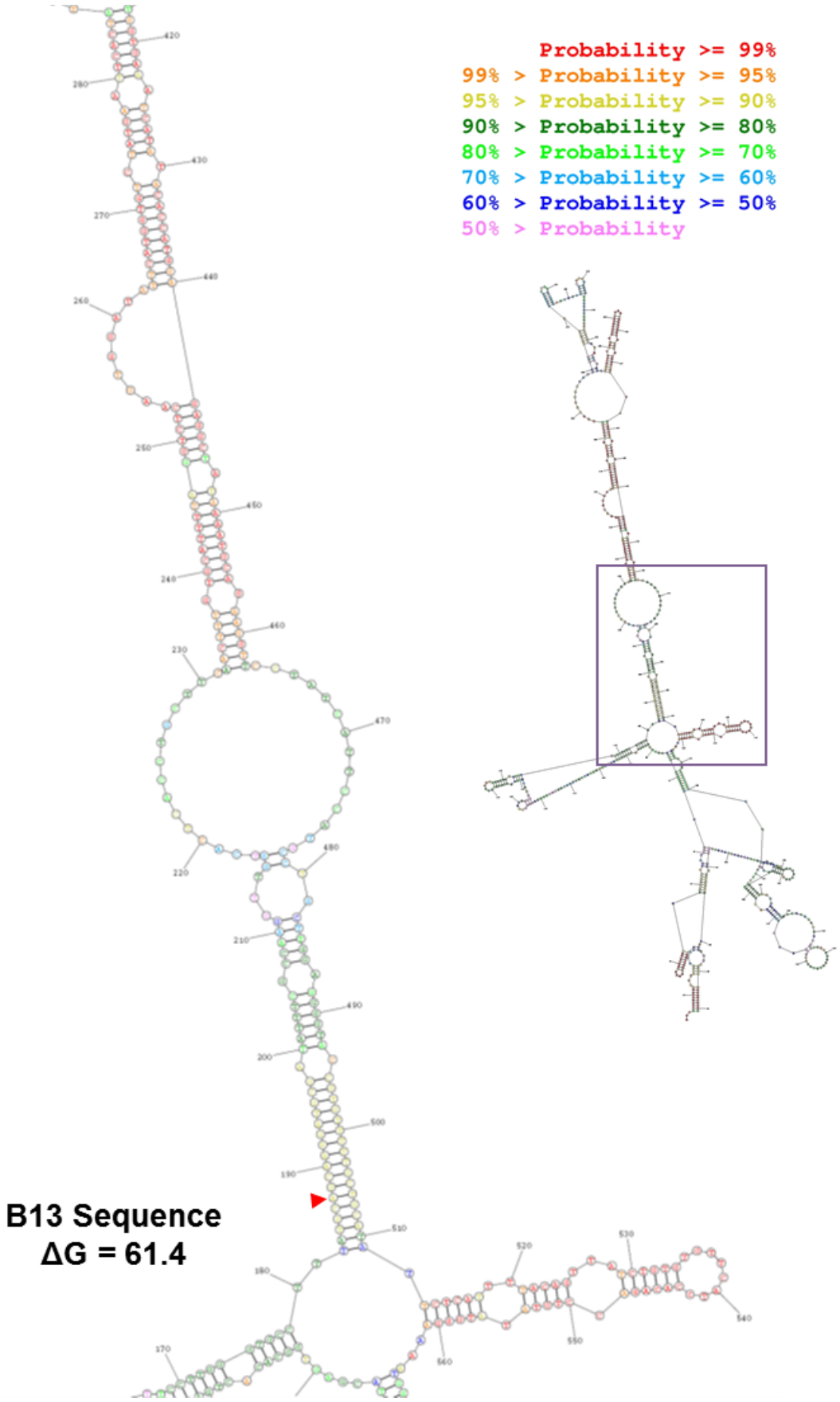

Figure 3.15 - MaxExpect output from the RNA Structure software. Probabilities of each base pair are indicated according to colour, with a key in the top left hand corner. Complete structure is shown on the left hand side, with the area surrounding the Q/R editing site enlarged. The base pairs surrounding the Q/R site have a 90-95% probability of binding. The edited adenosine is highlighted with a red arrow and the free energy (ΔG) indicated.

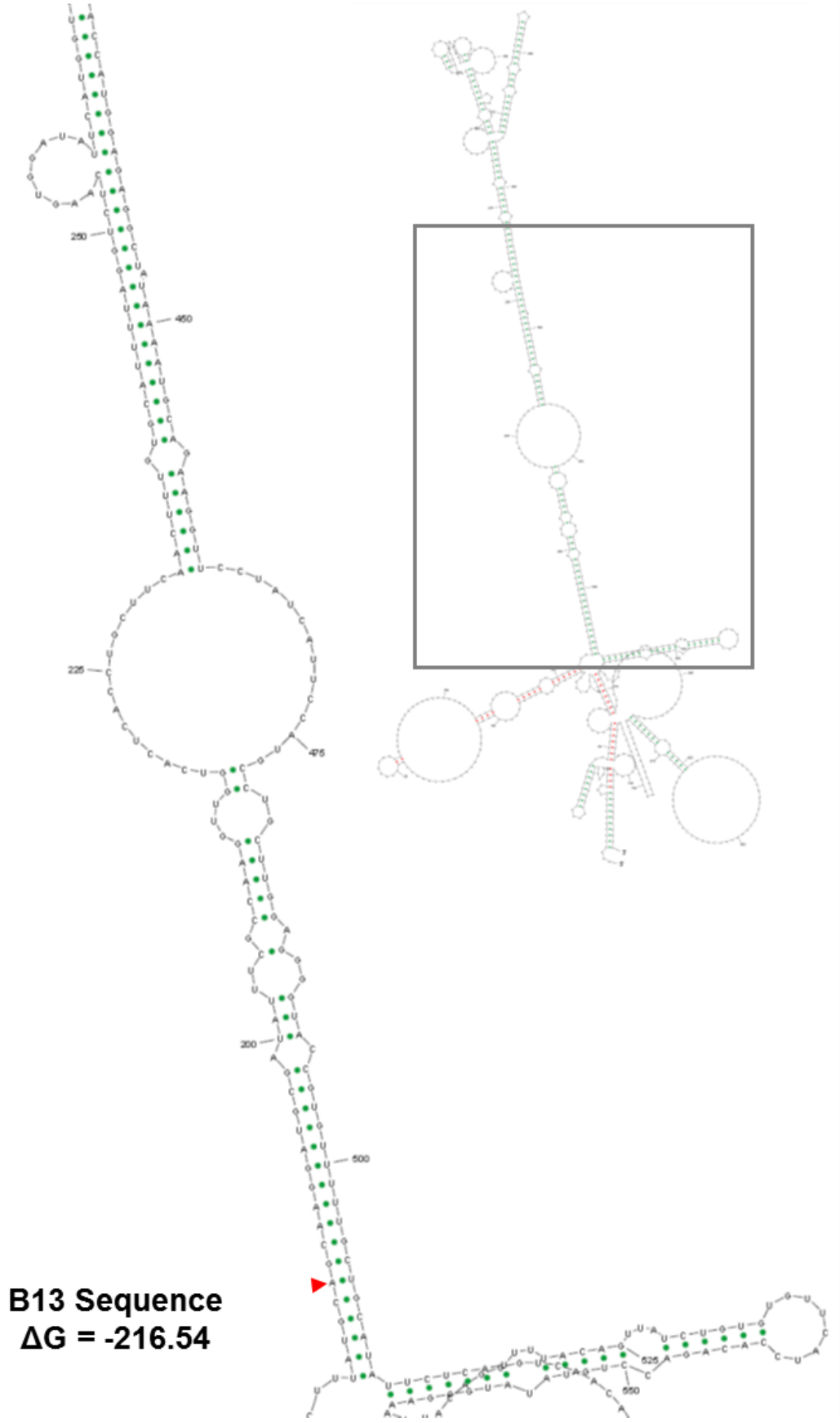

Figure 3.16 - Ensemble centroid structure for the B13 minigene as predicted by SFold. Complete structure shown in the top corner with the Q/R editing site expanded. The edited adenosine is highlighted with a red arrow and the free energy (ΔG) indicated.

3.2.8 Design of antisense oligonucleotide

Through changing the length of inputted sequence, species of origin and using different software, a consensus secondary structure has been formed that appears to be conserved in the majority of predicted models. This structure was then used for the design of PMOs to disrupt Q/R site editing. The double-stranded region of RNA surrounding the edited adenosine is essential for the editing reaction to take place, and so targeting PMOs to this region should lead to competition between the PMO and the RNA transcript itself for binding. This steric interference should disrupt the secondary structure sufficiently for ADAR2 to not bind to the Q/R editing site. A second area of secondary structure that is important for editing is the imperfect repeat, found downstream of the edited adenosine after a loop of single stranded structure. This imperfect repeat was also shown to be essential for Q/R site editing (Higuchi *et al.*, 1993) and so disruption of the double-stranded structure through PMOs binding may also inhibit the editing reaction.

The PMOs designed here were given a sequential number (PMO 1-6) as well as an indication of the target sequence. This set of PMOs were titled with the target gene, *GRIA2*, followed by numbers according to the bases that they bind to up or downstream from the exon 11/intron 11 boundary, which was designated “0” (Figure 3.17A). For example, PMO1 (GRIA2+284+308) is a previously published antisense oligonucleotide that has been shown to disrupt Q/R site editing (Penn *et al.*, 2012), and binds to bases 284 to 308 downstream of the exon 11/intron 11 boundary (Figure 3.17A). The remaining five PMOs were designed to target specific areas of secondary structure based on the model predicted to be most reliable. All six PMOs shown here (Figure 3.17) are 25 bases long, the longest standard PMO length possible from GeneTools. Increased length of PMO is thought to correlate to improved PMO binding (Popplewell *et al.*, 2009).

PMO1 (GRIA2+284+308) binds to the complementary strand of RNA to the edited adenosine, including the exon complementary sequence. PMO2 (GRIA2-30-6) was designed to bind to the same strand as the edited adenosine and so directly covers the Q/R editing site, with the most 5’ base targeting a small area of single-stranded structure for improved binding. This PMO will test whether targeting the strand containing the edited adenosine itself, rather than the exon complementary sequence, influences the potential for editing inhibition. The double-stranded structure that includes the edited adenosine extends further than the reach of PMO1 (GRIA2+284+308) and PMO2 (GRIA2-30-6). Therefore two more PMOs were designed, targeting each strand, to completely cover this section. PMO3 (GRIA2-14+10) binds downstream to PMO2 (GRIA2-30-6), not directly covering the edited adenosine but still extending into the double-stranded structure. It also has the advantage of binding to bases in the large

internal loop, and therefore might be able to better penetrate the double-stranded structure. PMO4 (GRIA2+262+286) binds to the complementary strand opposite PMO3 (GRIA2-14+10), and again has target bases in the single-stranded region. PMO5 (GRIA2+19+43) and PMO6 (GRIA2+50+74) target the imperfect repeat, which forms a region of double-stranded RNA the other side of the large internal loop from the region targeted by the other PMOs. The target bases for PMO5 (GRIA2+19+43) begin in the internal loop and extend into the imperfect repeat, ending one base into a bulge of single stranded RNA. PMO6 (GRIA2+50+74) begins in this bulge and extends further into the imperfect repeat. The newly designed PMOs are summarised in Figure 3.17, with a schematic of where the PMOs bind in relation to the exon 11/intron 11 boundary (A) as well as in terms of the secondary structure (B). PMO sequences and targets are summarised in Figure 3.17C.

A

B

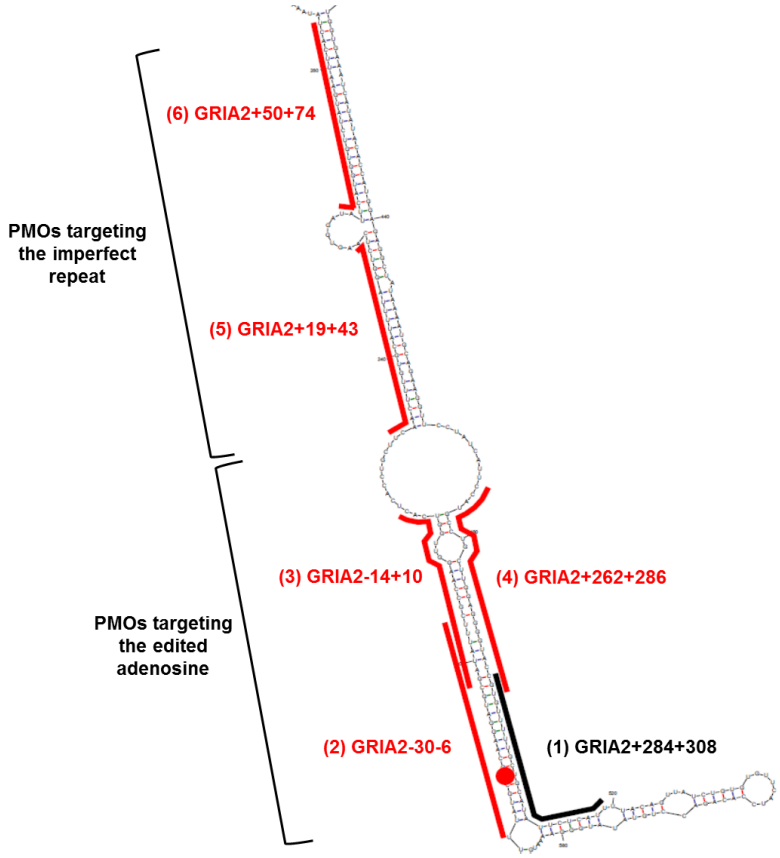

C

PMO Name		Sequence	Target Sequence
1	GRIA2+284+308	AATGAGAATATGCAGCAAAAACACG	Complementary to edited adenosine
2	GRIA2-30-6	GAAATATCGCATCCTTGCTGCATAA	Strand containing edited adenosine
3	GRIA2-14+10	AGTGACCAACCTTGGCGAAATATCG	Downstream of edited adenosine
4	GRIA2+262+286	ACGGTACCCCTCCAAGCAGGCATGG	Downstream and complementary to edited adenosine
5	GRIA2+19+43	TGAGACCTAAAATGCACAAAGTTGA	Imperfect repeat
6	GRIA2+50+74	AGTGAATTCATAGACACCATGAATA	Imperfect repeat

Figure 3.17 - PMOs designed around the secondary structure predicted by MFold. A) Placement of PMOs along the exon 11/intron 11 boundary of the mouse GRIA2 sequence. Numbers refer to bases up (-) or downstream (+) of the exon 11/intron 11 boundary (designated 0) where the PMO begins and ends. B) Placement of PMOs targeting areas of secondary structure and the edited adenosine, shown as the red circle. C) Table of PMO names and sequences and their target regions. The edited adenosine is indicated by the red circle. PMO1 (GRIA2+284+308) has been previously published (Penn et al 2012).

The main purpose of this set of PMOs was to target the desired secondary structure elements around the Q/R site. However, other components of PMO design have been shown to improve binding, such as the percentage of G or C bases in the PMO (GC content) or the energy involved in the binding of PMO to RNA transcript (Popplewell *et al.*, 2009) and these calculations are shown in Table 3.4. PMO1 (GRIA2+284+308) has been previously shown to inhibit Q/R site editing (Penn *et al.,* 2012) and so presumably binds to the RNA transcript. However, the GC content is lower than the 40-60% ideal (Aartsma-Rus *et al.*, 2009). For the 5 new PMOs designed here, three have a GC content that falls within this range, whereas PMO5 (GRIA2+19+43) and PMO6 (GRIA2+50+74) have GC contents that also fall lower than the suggested range (Table 3.4). Higher GC content should increase PMO binding as base pair bonds between G and C are stronger than between A and T, and so those three PMOs with lower GC contents may show decreased binding.

The intermolecular binding energy was calculated using the SFold webserver (sfold.wadsworth.org; Table 3.4). A more negative binding energy was shown to be correlated with effective PMOs (Aartsma-Rus *et al.*, 2009). Again, the published PMO1 (GRIA2+284+308) shows a high intermolecular dimer energy, which is in fact positive. When calculated for each newly designed PMO, there was a range of binding energies, with the lowest intermolecular dimer for PMO4 (GRIA2+262+286) at -4.9 kcal/mol and all are lower than 2.2 kcal/mol for PMO1 (GRIA2+284+308), except PMO6 (GRIA2+50+74) with a binding energy of 2.3 kcal/mol. From this energy required to form the intermolecular dimer, the energy needed to overcome secondary structure within the PMO is subtracted, both any hairpin structures and inter-PMO binding. Once these values had been taken into account, all PMOs were calculated to have a positive binding energy (Table 3.4). PMO3 (GRIA2-14+10), PMO4 (GRIA2+262+286) and PMO5 (GRIA2+19+43) all have a total binding energy of less than that for PMO1 (GRIA2+284+308), which was calculated to have a binding energy of 5.7 kcal/mol. PMO2 (GRIA2-30-6) has a total binding energy of 7.1 kcal/mol, while PMO6 (GRIA2+50+74) has an even more positive total binding energy of 13.8 kcal/mol.

	PMO Name	GC Content (%)	ΔG - InterMolecular Dimers	ΔG - Hairpin Structure	ΔG – PMO-PMO	Total Binding Energy
1	GRIA2+284+308	36	2.2	0	-3.5	**5.7**
2	GRIA2-30-6	40	1.6	-2	-3.5	**7.1**
3	GRIA2-14+10	48	-0.6	-1.8	-2.8	**4**
4	GRIA2+262+286	64	-4.9	-1.6	-6	**2.7**
5	GRIA2+19+43	36	1.4	0	-3.5	**4.9**
6	GRIA2+50+74	32	2.3	-4.1	-7.4	**13.8**

Table 3.4 - GC content and binding energies of designed PMOs. Intermolecular energies calculated using SFold (sfold.wadsworth.org). Hairpin and PMO-PMO energies calculated using OligoAnalyzer 3.1 (IDT). All ΔG are in kcal/mol.

3.3 DISCUSSION

This chapter has established the HeLa-B13 system for analysing the effect of antisense oligonucleotides on Q/R site editing. Transfection, RT-PCR and restriction digest procedures were adjusted for reliable assessment of the RNA editing reaction. The HeLa-B13 system was shown to be appropriate for Q/R site analysis as it reliably reproduced endogenous editing of 30%, which would allow treatments to both increase and decrease editing, and proved to be sensitive to manipulations in editing after co-transfection with an extra copy of ADAR2, which increased the editing percentage. HeLa cells were also shown to have a high transfection efficiency using the EndoPorter transfection reagent when tested with a fluorescent PMO. The B13 minigene, of mouse origin, was compared to human and rat sequences and shown to share a high identity, and the sequence surrounding the Q/R site and the ECS was conserved as shown by aligning the three sequences. Any antisense oligonucleotides targeted to the B13 minigene would therefore be able to be tested in cell models from any of these species in future experiments. In order to design antisense oligonucleotides that disrupted secondary structure of the transcript, a reliable model of the secondary structure was needed. It was found that the secondary structure surrounding the Q/R site remained the same regardless of changes to sequence length, species of origin or program used. This model was therefore considered sufficiently reliable for antisense oligonucleotide design. Finally, PMOs were designed to target bases covering all of the predicted double-stranded structure surrounding the edited adenosine.

The HeLa-B13 system was chosen to be the original model for testing the effect of antisense oligonucleotides on Q/R site editing as HeLa cells are easily manipulated and the overexpression of a small section of *GRIA2* simplifies the system by removing any variables associated with expression levels. The PCR-digest was based on previously reported methods, where the sequence surrounding the Q/R site is amplified and then digested with the *BbvI* restriction enzyme if unedited (Peng *et al.*, 2006; Sawada *et al.*, 2009; Penn *et al.*, 2012). The digest fragments can then be separated on an agarose gel, and any edited (undigested) fragments can be compared in intensity to the unedited (digested) fragments to achieve a Q/R site editing percentage. Once this assay was set up, transfection conditions for the plasmid containing the B13 minigene into HeLa cells were optimised. This allowed an endogenous editing capacity of 30% in HeLa cells to be calculated. This was shown to be consistent across three different time points of 24, 48 and 72 hours, indicating that this is the maximum possible editing efficiency for HeLa cells under these conditions. One limiting factor is the endogenous ADAR2 expression within the cell line, as shown by the increase in editing found after co-transfection with an additional copy of the ADAR2 gene.

An endogenous editing capacity of around 30% at the Q/R site of transfected HeLa cells is similar to previous work (Penn *et al.*, 2012). However, editing in HeLa cells has been reported to be variable by different groups. In a study into the regulation of RNA editing at the Q/R site, one group found endogenous editing of HeLa cells transfected with the B13 minigene to be 60% (Marcucci *et al.*, 2011). In this paper, the Q/R site editing was measured through PCR amplification of the sequence which was then cloned into a vector and sequenced. The relative heights of the peak at the edited adenosine between adenosine and guanosine were measured and a percentage of editing calculated. Another lab has analysed the endogenous editing capacity of a variety of cell lines (Yamashita *et al*., 2012c). This group had previously found wide variation in HeLa Q/R site editing, with some cells showing no editing and some showing 100% editing, although the average was around 25% (Sawada *et al.*, 2009). They therefore developed a HeLa cell line that stably expressed a section of GluA2, and found Q/R site editing in this cell line to be at 100% (Yamashita *et al*., 2012c). This study calculated the Q/R site editing using the *BbvI* digest method, and comparing the intensities of edited to unedited bands using a Bioanalyzer. It therefore appears that the endogenous editing capacity of HeLa cells is variable between research groups.

This variability may be attributed to the changes in method for calculated Q/R site editing. Indeed, Wong et al compared the *BbvI* restriction digest analysis to the method of clone sequencing (Wong *et al.*, 2009). Using the clone sequencing technique is labour-intensive and takes a significantly longer time than the restriction analysis, making it less appropriate for studies looking at changes in Q/R site analysis. On the other hand, Wong et al. discuss the major bias within the restriction analysis, which is dependent on the strands hybridising to form either wholly edited or wholly unedited hybrid strands. However, an edited and unedited strand may hybridise. This would then not be cut by the *BbvI* enzyme as the recognition site is not complete despite half of the DNA remaining unedited, and so the amount of undigested (edited) transcripts would be overestimated. This group suggest an alternative method for calculated Q/R site editing through qPCR analysis, where probes are targeted to the edited adenosine (Wong *et al.*, 2009). This method is dependent on the probes being sensitive enough to distinguish between transcripts with one base pair different, but would remove the bias in the hybridisation. qPCR analysis was used in detecting the presence of edited isoforms in the 5-HT_{2C}, some of which are expressed at very low levels (Lanfranco *et al.*, 2009). This approach was advantageous in the context of the serotonin subunit as the different probes could distinguish between the many possible isoforms. However, there is only one edited adenosine at the Q/R site, and so only two isoforms to account for: edited and unedited. Therefore, for this study the *BbvI* restriction analysis was chosen due to its high reproducibility and cost- and time-effectiveness. However, it may be interesting to use

the qPCR editing analysis to try and detect subtler changes in response to PMO transfection.

It was also established that PMOs were able to be transfected efficiently into the HeLa cell line. Two methods were used for this analysis, first a visual confirmation that cells were being transfected with the F-PMO by live imaging and then a quantitative analysis using flow cytometry. Both methods showed that F-PMO using the EndoPorter transfection reagent displayed a good transfection efficiency in HeLa cells, with the FACS analysis calculating a transfection efficiency of 97.04%. This efficiency is extremely high, and so supports the HeLa-B13 system as an appropriate model for this project. The FACS analysis indicates that the cells had a varied uptake of the F-PMO, and that although the majority were transfected, there were some cells that took up much more than others as shown by a shallow and broad peak in the fluorescence histogram. This difference in transfection between cells could contribute to variation in the HeLa-B13 system, as there would be mixed populations of cells with high and low concentrations of intracellular PMO within one sample. It is possible that the F-PMO has not actually entered the cell and is instead bound at the membrane, despite the cells being washed with PBS before imaging or with FACS buffer before flow cytometry analysis. However, the neutral charge of the PMO makes this explanation for fluorescence unlikely, and so the transfection efficiency for HeLa cells was considered high.

Having optimised the HeLa-B13 system, the next step was to design the PMOs to disrupt editing. A reliable model for secondary structure was needed in order to target the PMOs to regions of double-stranded RNA within the secondary structure. The most common method for finding the secondary structure of an RNA transcript is using nearest-neighbour parameters to find the structure with the minimum free energy (MFE), indicating that it would be most stable. MFold is a web server where RNA and DNA sequences can be inputted and MFE models predicted (Zuker, 2003). This program has been used for over a decade in multiple areas of molecular biology from using the CRISPR-Cas system (Hwang *et al.*, 2013) to microRNA target prediction (Rajewsky, 2006). Although this method of structure calculation determines the nearest neighbouring base a given nucleotide is likely to pair to, it is possible that sequences several hundred bases up- or downstream would influence the structure. Therefore, working within the sequence length limits in MFold, the total sequence of exon 11 and intron 11 from *Gria2* was compared to that of the short section found in the B13 minigene. It appears that the B13 minigene contains enough of the intronic and exonic sequence to maintain the secondary structure surrounding the Q/R site, as these comparisons showed a conserved structure across the models. This almost certainly contributes to

the ability of the B13 transcript to be recognised by ADAR2, which recognises editing sites through double-stranded RNA regions (Savva *et al.*, 2012).

As well as using a shorter sequence of *Gria2* in the HeLa-B13 system than would be found endogenously in neurons, the B13 minigene is of mouse origin whereas future experiments with these PMOs could be conducted in cell lines of rat or even human origin. It was therefore important that any targeted secondary structure was conserved across the three species. Through comparison of the MFE models for mouse, rat and human for exon 11 and intron 11 of *Gria2*, it was demonstrated that the double-stranded RNA regions surrounding the edited adenosine appeared to be conserved between these species. This is perhaps understandable due to the importance of the Q/R site in terms of normal neuronal function, as abolishing editing leads to severe seizures in a mouse model (Brusa *et al.*, 1995) and reduced editing specifically in motor neurons leads to progressive paralysis (Hideyama *et al.*, 2010).

Despite being used intensively in the literature, the model with the minimum free energy is not always accurate. It does not account for any tertiary interactions, and has been shown to not always be accurate in identifying the most probable structure (Ding & Lawrence, 2003). This is likely due to RNA transcripts being actively folded rather than passively folding into minimum free energy states, as well as other factors altering secondary structure such as alterations in pH, ionic composition or interactions with other RNAs or RNA-binding proteins. Attempts have been made to make the prediction more accurate. MaxExpect is part of the RNA Structure program that, while still calculating the MFE model, builds on this prediction by calculating base pairing probabilities and giving the structure with the highest overall probability. SFold is another web server that collects predicted structures into clusters based on their similarities according to their Boltzmann weights and base pairing probabilities, and uses these clusters to generate an overall prediction based on the most probable clusters (Ding *et al.*, 2005). Each of these programs was used to predict the secondary structure of the B13 minigene. Although some intronic sections varied, the region surrounding the edited adenosine is conserved. It therefore appears that the structure surrounding the Q/R editing site is predicted to be the same despite different approaches to the prediction. RNA structure prediction still has a place in molecular biology due to the time-intensive assays needed for *in vivo* (or even *in vitro*) study of RNA secondary structure, which involves targeting the RNA with different probes that cut at specific double- or single-stranded regions and then running the results on capillary electrophoresis (Wan *et al.*, 2013).

Due to the similarities across the different secondary structure predictions, the MFE model was taken as the basis for PMO design. The main aim of this set of PMOs was to target specific regions of double-stranded structure, either around the edited adenosine

itself or at the imperfect repeat. Taken as a set, these PMOs cover this whole region. When taking the calculated binding energies into account, it is perhaps surprising that PMO1 (GRIA2+284+308) has been reported to disrupt Q/R site editing (Penn *et al.,* 2012) due to its positive binding energy of 5.7 kcal/mol and low GC content of 36%. However, if this PMO is used as a benchmark, the more negative total binding energies for PMO3 (GRIA2-14+10), PMO4 (GRIA2+262+286) and PMO5 (GRIA2+19+43) at 4, 2.7 and 4.9 kcal/mol respectively indicate that these PMOs show strong potential for binding to the RNA transcript. PMO2 (GRIA2-30-6) on the other hand shows a higher total binding energy of 7.1 kcal/mol. This positive binding energy means that this PMO might not be strong enough to penetrate the RNA transcript's secondary structure. However, PMO2 (GRIA2-30-6) targets the edited adenosine itself and its surrounding sequence. Therefore, if the PMO can bind to the target RNA, this one has the potential to prevent ADAR2 editing to the greatest extent. PMO6 (GRIA2+50+74) targets the section of the imperfect repeat furthest from the edited adenosine in the model of secondary structure, and the total binding energy for this PMO was calculated as 13.8 kcal/mol, the highest in the set. Both of these aspects indicate that PMO6 (GRIA2+50+74) is least likely to have an effect on Q/R site editing.

4 USING ANTISENSE OLIGONUCLEOTIDES TO DISRUPT EDITING AT THE Q/R SITE THROUGH STERIC HINDRANCE

4.1 INTRODUCTION

The formation of RNA duplex structures and how they influence RNA secondary structure is known to be crucial for efficient RNA editing, as discussed (Higuchi *et al.,* 1993). In the previous chapter, models for the secondary structure of the GluA2 RNA transcript were produced using minimum free energy and base pair probability predictions. Using these models, PMOs were designed to target the secondary structure that surrounds the Q/R site. Through complementary base pairing, these PMOs will bind to the RNA sequence and therefore disrupt the internal secondary structure. By designing sequences that are completely complementary to the RNA molecule, binding to the PMOs should be preferable compared to the imperfect complementary sequences within the RNA sequence itself. Disruption of the RNA secondary structure, and therefore inhibition of editing at the Q/R site, would mimic the decline in Q/R site editing found in patients with ALS (Kawahara *et al.*, 2004). This could produce a model for any cellular events found downstream of Q/R site editing disruption, for example increased susceptibility to excitotoxicity from overstimulation by glutamate.

In this chapter, PMOs were tested in cell models. The first aim was to replicate the results published by Gregor's lab in 2012. This group found that a PMO designed to be complementary to the Exon Complementary Sequence (PMO1 (GRIA2+284+308) from the previous chapter) of the Q/R site could inhibit RNA editing, with an IC_{50} of 1.9 μM in the HeLa-B13 system (Penn *et al.*, 2012). This PMO, along with 5 other PMOs designed in the previous chapter, were transfected into the HeLa-B13 system and the Q/R site editing was analysed. PMOs were then redesigned and again tested in the HeLa-B13 system followed by a cell line that endogenously expresses GluA2, SH-SY5Y cells. Using these two cellular models, the efficiency of each PMO could be compared for its ability to disrupt Q/R site editing.

4.2 RESULTS

4.2.1 Transfection of 25mer PMOs into the HeLa-B13 system

The PMOs designed in the previous chapter and summarised in Figure 3.15 were transfected into HeLa-B13 system (HeLa cells transfected with a plasmid containing the B13 minigene). After 24 hours, RNA was extracted and the editing at the Q/R site was quantified using the *BbvI* assay established in the previous chapter. All editing percentages were normalised to control samples transfected with the B13 plasmid only. An initial transfection at 1 µM per PMO did not show any significant effect of the 25mers on Q/R site editing compared to control (Figure 4.1A), although there appears to be a non-significant effect with treatment of PMO1 (GRIA2+284+308) and PMO4 (GRIA2+262+286). The results may not have reached significance due to the variation seen between samples as shown by the large error bars (Figure 4.1A).

PMO concentration was then increased to 10 µM, and Q/R site editing was measured using the same method. This concentration is recommended by GeneTools as a test concentration. PMO2 (GRIA2-30-6) and PMO4 (GRIA2+262+286) significantly decreased editing (86.9 ± 6.36% and 71.1 ± 2.4% of control respectively, $p<0.05$; Figure 4.1B). Interestingly, PMO1 (GRIA2+284+308) showed no effect on Q/R site editing (103 ± 1.28% of control), despite being previously reported to inhibit editing by more than 50% at this concentration (Penn *et al.*, 2012). In fact, PMO1 (GRIA2+284+308) shows more of an effect at 1 µM, with a non-significant decrease to 69.64 ± 10.0 % of control, than at 10 µM which showed no change in editing percentage. This lack of reproducibility is a concern, and may be due to variation in individual transfected cells as seen with the fluorescently tagged PMO in the previous chapter.

When considering the targeted secondary structure for each PMO, it was hoped that PMO2 (GRIA2-30-6) would have a strong inhibitory effect on Q/R site editing as it covers the edited adenosine itself (Figure 3.15) and so when placed over the target sequence would completely prevent ADAR2 binding. However, at both 1 µM and 10 µM there was only a reduction in editing percentage to around 85% of control. There was no significant change in efficacy between the concentrations of 1 µM and 10 µM for this PMO despite a ten-fold increase in concentration ($p=0.953$), although there is less variation in the samples at 10 µM of PMO, which reaches significance when compared to control ($p<0.05$). The same can be said for PMO4 (GRIA2+262+286), where there is no significant change in editing inhibition between treatments at 1 µM and 10 µM (73.10 ± 9.57% compared to 71.18 ± 2.43; $p=0.856$), although samples treated with 10 µM of PMO4 (GRIA2+262+286) were significantly different from control samples ($p<0.05$).

PMO3 (GRIA2-14+10) targets the same strand as the Q/R site but slightly downstream from the edited adenosine, extending into the loop of RNA in an attempt to improve PMO-RNA binding. Despite the strong potential for disruption in terms of target sequence, PMO3 (GRIA2-14+10) follows a similar pattern to PMO1 (GRIA2+284+308). At 1 µM there was a non-significant reduction in Q/R site editing (82.39 ± 7.77%) while at 10 µM there was no change in editing at all (108.4 ± 4.14%). PMO5 (GRIA2+19+43) and PMO6 (GRIA2+50+74) target consecutive sections of the imperfect repeat, separated from the double-stranded structure around the Q/R site by an internal loop of RNA. These two PMOs appear to have the least impact on editing inhibition. At 1 µM, each of these PMOs led to a non-significant decrease in editing at 90.46 ± 6.79% and 85.90 ± 6.58% respectively. At 10 µM, these PMOs did not cause any decrease in Q/R site editing. In fact, they appear to increase editing to 119.55 ± 0.87% and 135.2 ± 4.24% respectively. The reason for this increase in editing is unknown.

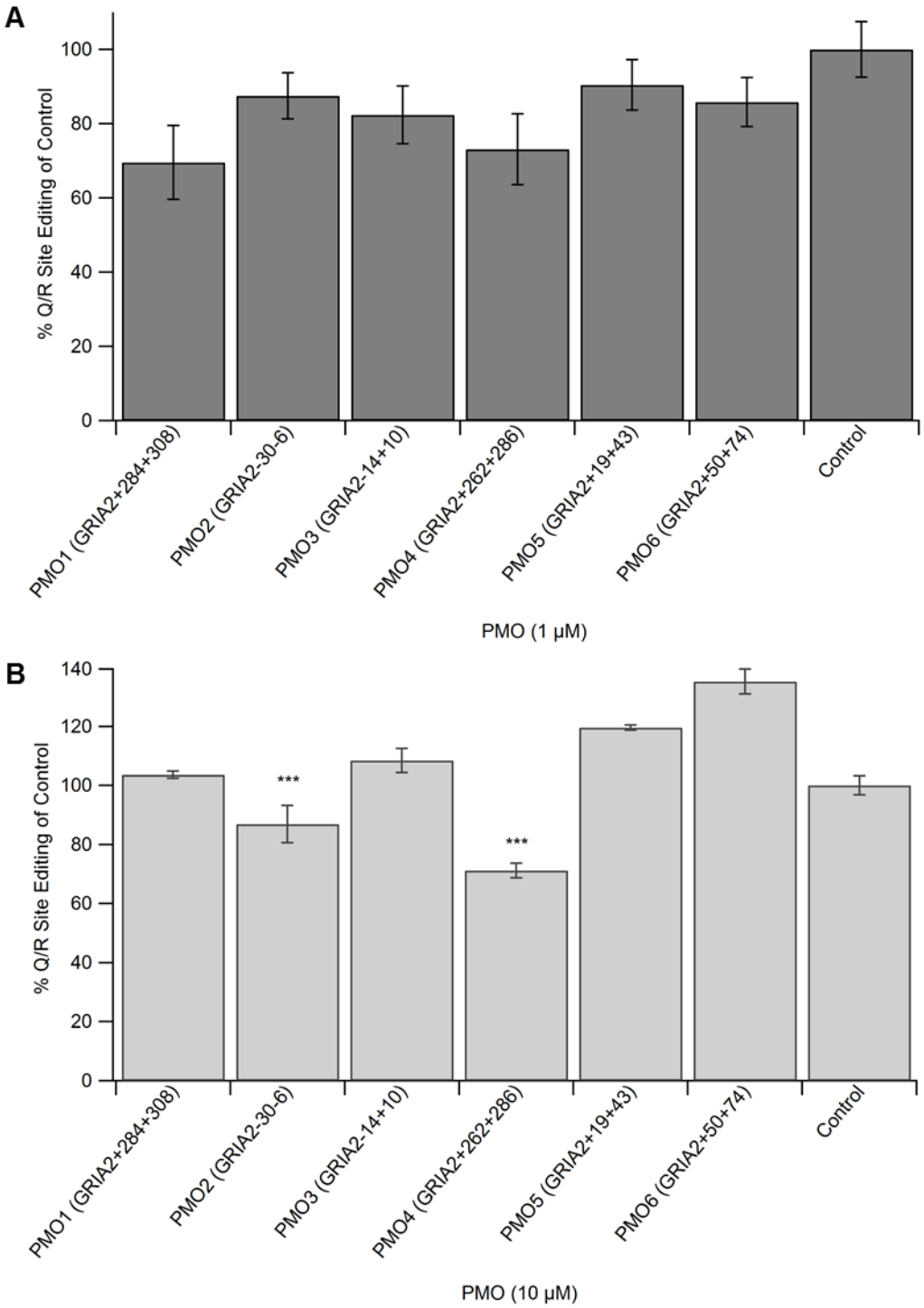

*Figure 4.1 - Changes in editing after treatment with PMOs 1-6 at 1 µM (A) or 10 µM (B). All editing percentages are normalised to levels of editing in control transfections of the B13 plasmid only. Treatment with 1 µM of each PMO did not significantly change the Q/R site editing in the HeLa-B13 system (A). Treatment with PMO2 (GRIA2-30-6) and PMO4 (GRIA2+262+286) at 10 µM significantly reduced Q/R site editing to 86.9 ± 6.36% and 71.1 ± 2.4% of control, respectively (n=3, *** = p<0.05). Interestingly, PMO1 (GRIA2+284+308) shows no effect even at high concentrations.*

4.2.2 Redesigned 30mer PMOs

Although PMO2 (GRIA2-30-6) and PMO4 (GRIA2+262+286) showed a significant reduction in editing, this effect could not be improved through adjusting the transfection conditions, either by extending the time of transfection or applying the PMO first then transfecting in the B13 plasmid and vice versa. Therefore new PMOs were redesigned based on PMO4 (GRIA2+262+286), which showed the greatest effect at 10 μM, and PMO1 (GRIA2+284+308), which has been previously published. The aim of the redesigned PMOs was to improve potential binding through analysing the binding energies of the PMOs based on predicted intermolecular and intramolecular energies, as well as using predicted secondary structure models to further improve targeted disrupt the secondary structure.

4.2.2.1 Targeting the Double-Stranded RNA with 30mer PMOs

The length of PMOs were extended to 30 bases, as longer PMO length has been reported to increase binding (Pramono *et al.*, 2012), and extending the targeted bases further into the double-stranded region should increase the disruption to the secondary structure. To assess the best placement for the extra five bases, the secondary structure of the GluA2 RNA transcript predicted in the previous chapter was used as a guide (Figure 4.2). PMOs could also be targeted to regions of single-stranded RNA, such as the open loop (Figure 4.2) for improved binding, as targeting accessible RNA has been shown to be an important factor for PMO design (Popplewell *et al.*, 2009). Using the placement of PMO1 (GRIA2+284+308) and PMO4 (GRIA2+262+286) as starting points, the best placements for 30mers could then be calculated.

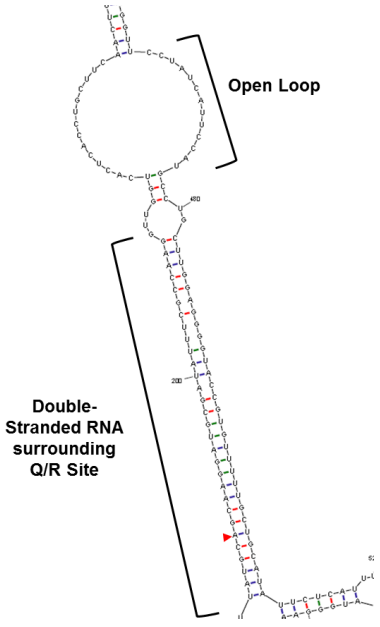

Figure 4.2 - Targeted regions of secondary structure. 30mer PMOs were extended further into the double-stranded region to disrupt the secondary structure, but also with an aim of beginning in the open loop region for enhanced binding. Edited adenosine is indicated by the red arrow.

4.2.2.2 Calculating Intermolecular Binding Energies for Prospective 30mers

Alongside the secondary structure, predicted binding energies between the RNA molecule and potential new PMOs were also used to develop the 30mers. SFold predicts the energy of every oligonucleotide of a given length along the target RNA sequence, and so regions with a more negative binding energy can be targeted (example in Figure 4.3), as a more negative binding energy should allow the PMO to bind more strongly to the RNA. The final PMOs were taken as a balance between the desired target sequence and the sequence with the most favourable binding energy.

The target sequence of the B13 minigene was used and intermolecular binding energies for 30mers were calculated. The original 25mers were found within the suggested outputs; any 30mer containing PMO4 (GRIA2+262+286) or PMO1 (GRIA2+284+308) was considered. Figure 4.3 shows the potential antisense sequences around the original PMO4 (GRIA2+262+286) sequence. Sequences shifted downstream along the target sequence (down the rows in the output) reach further into the double-stranded region of the structure (Figure 4.2). Of the 6 30mers shown that contain PMO4 (GRIA2+262+286) (highlighted in yellow), although the last sequence binds to the most bases within the double-stranded structure, there is a relatively large difference in binding energies between this sequence (-5.7 kcal/mol) and the sequence shifted one base 5' (-7.1 kcal/mol). The sequence for PMOE4 (GRIA2+261+290) was therefore chosen by including the most penetration of the double-stranded structure while also accounting for predicted binding energies (Figure 4.6; Table 4.1).

Target RNA Sequence	Antisense Sequences	GC Content	ΔG	
AUCAUUCCAUGCCUGCUUGGAGGGGUACCG	CGGTACCCCTCCAAGCAGGCATGGAATGAT	56.7%	-10.2	
UCAUUCCAUGCCUGCUUGGAGGGGUACCGU	ACGGTACCCCTCCAAGCAGGCATGGAATGA	56.7%	-9.4	
CAUUCCAUGCCUGCUUGGAGGGGUACCGUG	CACGGTACCCCTCCAAGCAGGCATGGAATG	60.0%	-8.8	
AUUCCAUGCCUGCUUGGAGGGGUACCGUGU	ACACGGTACCCCTCCAAGCAGGCATGGAAT	56.7%	-8.1	
UUCCAUGCCUGCUUGGAGGGGUACCGUGUU	AACACGGTACCCCTCCAAGCAGGCATGGAA	56.7%	-7.3	
UCCAUGCCUGCUUGGAGGGGUACCGUGUUU	AAACACGGTACCCCTCCAAGCAGGCATGGA	56.7%	-7.1	PMOE4 (GRIA2+261+290)
CCAUGCCUGCUUGGAGGGGUACCGUGUUUU	AAAACACGGTACCCCTCCAAGCAGGCATGG	56.7%	-5.7	
CAUGCCUGCUUGGAGGGGUACCGUGUUUUU	AAAAACACGGTACCCCTCCAAGCAGGCATG	53.3%	-3.6	

Figure 4.3 - Sample output from SFold webserver for the design of PMOE4 (GRIA2+261+290). Left hand RNA sequence is the target GluA2 sequence. Right hand sequence is the complementary sequence for PMO design, shifting one base along the target sequence per row. PMO4 (GRIA2+262+286) is highlighted in orange and yellow in progressive oligonucleotide designs. "GC content" gives a percentage of GC bases in the suggested antisense design. ΔG gives the intermolecular energy between target sequence and antisense sequence.

A second 30mer based on PMO4 (GRIA2+262+286) was designed using recommendations from the SFold web server (sfold.wadsworth.org) as guidance, which suggests avoiding a "GGGG" sequence, keeping the intermolecular binding energy to less than -8 kcal/mol and with a GC content of between 40 and 60%. PMOE4B (GRIA2+250+279) is the only 30mer that fulfils all of these criteria (Figure 4.4), although

this led to its target being further away from the Q/R site than the other two 30mer PMOs (Figure 4.6).

Target RNA Sequence	Antisense Sequences	GC Content	ΔG	
AGGUUCCUAUCAUUCCAUGCCUGCUUGGAG	CTCCAAGCAGGCATGGAATGATAGGAACCT	50.0%	-11.6	
GGUUCCUAUCAUUCCAUGCCUGCUUGGAGG	CCTCCAAGCAGGCATGGAATGATAGGAACC	53.3%	-11.6	PMOE4B (GRIA2+250+279)
GUUCCUAUCAUUCCAUGCCUGCUUGGAGGG	CCCTCCAAGCAGGCATGGAATGATAGGAAC	53.3%	-14.0	
UUCCUAUCAUUCCAUGCCUGCUUGGAGGGG	CCCCTCCAAGCAGGCATGGAATGATAGGAA	53.3%	-14.0	
UCCUAUCAUUCCAUGCCUGCUUGGAGGGGU	ACCCCTCCAAGCAGGCATGGAATGATAGGA	53.3%	-14.0	
CCUAUCAUUCCAUGCCUGCUUGGAGGGGUA	TACCCCTCCAAGCAGGCATGGAATGATAGG	53.3%	-13.8	
CUAUCAUUCCAUGCCUGCUUGGAGGGGUAC	GTACCCCTCCAAGCAGGCATGGAATGATAG	53.3%	-11.8	
UAUCAUUCCAUGCCUGCUUGGAGGGGUACC	GGTACCCCTCCAAGCAGGCATGGAATGATA	53.3%	-10.9	
AUCAUUCCAUGCCUGCUUGGAGGGGUACCG	CGGTACCCCTCCAAGCAGGCATGGAATGAT	56.7%	-10.3	
UCAUUCCAUGCCUGCUUGGAGGGGUACCGU	ACGGTACCCCTCCAAGCAGGCATGGAATGA	56.7%	-9.5	
CAUUCCAUGCCUGCUUGGAGGGGUACCGUG	CACGGTACCCCTCCAAGCAGGCATGGAATG	60.0%	-8.9	
AUUCCAUGCCUGCUUGGAGGGGUACCGUGU	ACACGGTACCCCTCCAAGCAGGCATGGAAT	56.7%	-8.2	
UUCCAUGCCUGCUUGGAGGGGUACCGUGUU	AACACGGTACCCCTCCAAGCAGGCATGGAA	56.7%	-7.4	
UCCAUGCCUGCUUGGAGGGGUACCGUGUUU	AAACACGGTACCCCTCCAAGCAGGCATGGA	56.7%	-7.2	
CCAUGCCUGCUUGGAGGGGUACCGUGUUUU	AAAACACGGTACCCCTCCAAGCAGGCATGG	56.7%	-5.8	
CAUGCCUGCUUGGAGGGGUACCGUGUUUUU	AAAAACACGGTACCCCTCCAAGCAGGCATG	53.3%	-3.7	

Figure 4.4 - SFold output indicating binding for PMOE4B (GRIA2+250+279). Left hand RNA sequence is the target GluA2 sequence. Right hand sequence is the complementary sequence for PMO design, shifting one base along the target sequence per row. PMO4 (GRIA2+262+286) is highlighted in orange and yellow in progressive oligonucleotide designs. "GC content" gives a percentage of GC bases in the suggested antisense design. ΔG gives the intermolecular energy between target sequence and antisense sequence.

PMO1 (GRIA2+284+308) and the 30mers binding to the surrounding bases have a positive ΔG. However, as PMO1 (GRIA2+284+308) has been previously reported to be functional even with the positive binding energy, PMOE1 (GRIA2+279+308) was designed based simply on the secondary structure (Figure 4.6).

Target RNA Sequence	Antisense Sequences	GC Content	ΔG	
GGGUACCGUGUUUUUGCUGCAUAUUCUCAU	ATGAGAATATGCAGCAAAAACACGGTACCC	43.3%	-0.2	
GGUACCGUGUUUUUGCUGCAUAUUCUCAUU	AATGAGAATATGCAGCAAAAACACGGTACC	40.0%	2.1	PMOE1 (GRIA2+279+308)
GUACCGUGUUUUUGCUGCAUAUUCUCAUUU	AAATGAGAATATGCAGCAAAAACACGGTAC	36.7%	2.0	
UACCGUGUUUUUGCUGCAUAUUCUCAUUUU	AAAATGAGAATATGCAGCAAAAACACGGTA	33.3%	2.0	
ACCGUGUUUUUGCUGCAUAUUCUCAUUUUA	TAAAATGAGAATATGCAGCAAAAACACGGT	33.3%	2.0	
CCGUGUUUUUGCUGCAUAUUCUCAUUUUAC	GTAAAATGAGAATATGCAGCAAAAACACGG	36.7%	2.0	
CGUGUUUUUGCUGCAUAUUCUCAUUUUACA	TGTAAAATGAGAATATGCAGCAAAAACACG	33.3%	2.0	
GUGUUUUUGCUGCAUAUUCUCAUUUUACAG	CTGTAAAATGAGAATATGCAGCAAAAACAC	33.3%	2.0	
UGUUUUUGCUGCAUAUUCUCAUUUUACAGU	ACTGTAAAATGAGAATATGCAGCAAAAACA	30.0%	2.0	

Figure 4.5 - SFold output indicating binding for PMOE1 (GRIA2+279+308). Left hand RNA sequence is the target GluA2 sequence. Right hand sequence is the complementary sequence for PMO design, shifting one base along the target sequence per row. PMO1 (GRIA2+284+308) is highlighted in orange and yellow shows progressive oligonucleotide designs. "GC content" gives a percentage of GC bases in the suggested antisense design. ΔG gives the intermolecular energy between target sequence and antisense sequence.

4.2.2.3 Calculating Total Binding Energy

Hairpin ΔG and ΔG of PMO-PMO interactions were calculated using Oligo Analyzer (IDT). These are possible internal structures formed with the PMO to itself or to another PMO molecule. ΔG of PMO-PMO interactions of -9.78 kcal/mol indicates a sequence of 6 bases (4 G/C and 2 A/T) that bind somewhere else in the PMO, while -7.05 kcal/mol and -6.6 kcal/mol both indicate a 4 base sequence (2 G/C and 2 A/T). The total binding energy of a PMO was then calculated by taking the energy of intermolecular bonds and subtracting the internal binding energies (PMO-PMO interactions or hairpin structures).

Total binding energies are shown in Table 4.1. Theoretically, only a negative binding energy is energetically favourable for a PMO to bind to an RNA molecule. However, PMO4 (GRIA2+262+286) has already shown to have an effect on Q/R site editing, presumably through binding to the RNA molecule itself, and has a calculated binding energy of 5.24 kcal/mol. This probably indicates that the modelled calculations used in the binding energy calculations are not taking all factors into account. Of the 30mer PMOs, PMOE1 (GRIA2+279+308) and PMOE4 (GRIA2+261+290) have the highest potential for PMO-PMO interactions, with a ΔG of -9.78 kcal/mol, indicating that they may be less effective as they form dimers with themselves rather than binding to RNA. PMOE4B (GRIA2+250+279) is the only 30mer here with a negative total binding energy, and so in this context shows the strongest potential for binding.

	PMO Name	% GC Content	ΔG - InterMolecular Dimers	ΔG - Hairpin Structure	ΔG – PMO-PMO	**Total Binding energy**
1	GRIA2+284+308	36	2.2	0.31	-7.05	8.94
E1	GRIA2+279+308	40	2.1	0.31	-9.78	11.57
4	GRIA2+262+286	64	-4.9	-0.36	-9.78	5.24
E4	GRIA2+261+290	56	-7.1	-1.16	-9.78	3.84
E4B	GRIA2+250+279	53.3	-13.9	-1.12	-6.6	-6.18

Table 4.1 - Binding energies of 30mer PMOs. Intermolecular energies calculated using SFold (sfold.wadsworth.org). Hairpin and PMO-PMO interaction energies calculated using OligoAnalyzer 3.1 (IDT). All ΔG are in kcal/mol.

4.2.2.4 Final 30mer PMO Design

Newly designed PMOs are shown in Figure 4.6 as well as their overlap with the original 25mer on which they were based. PMOE1 (GRIA2+279+308) has 5 bases extended 5' to cover more of the double-stranded region around the Q/R site (Figure 4.6). PMOE4 (GRIA2+261+290) has 4 bases further 3', reaching into the double-stranded region, with one more base 5' extending into the internal loop which would improve initial binding between the PMO and the RNA. PMOE4B (GRIA2+250+279) fulfils SFold's suggested criteria and as a result is shifted further away from the Q/R site. Based on the energy calculations, PMOE4B (GRIA2+250+279) is predicted to bind most effectively to the RNA whereas based on the secondary structure model and previous work with the 25mers, PMOE4 (GRIA2+261+290) is predicted to be the most effective.

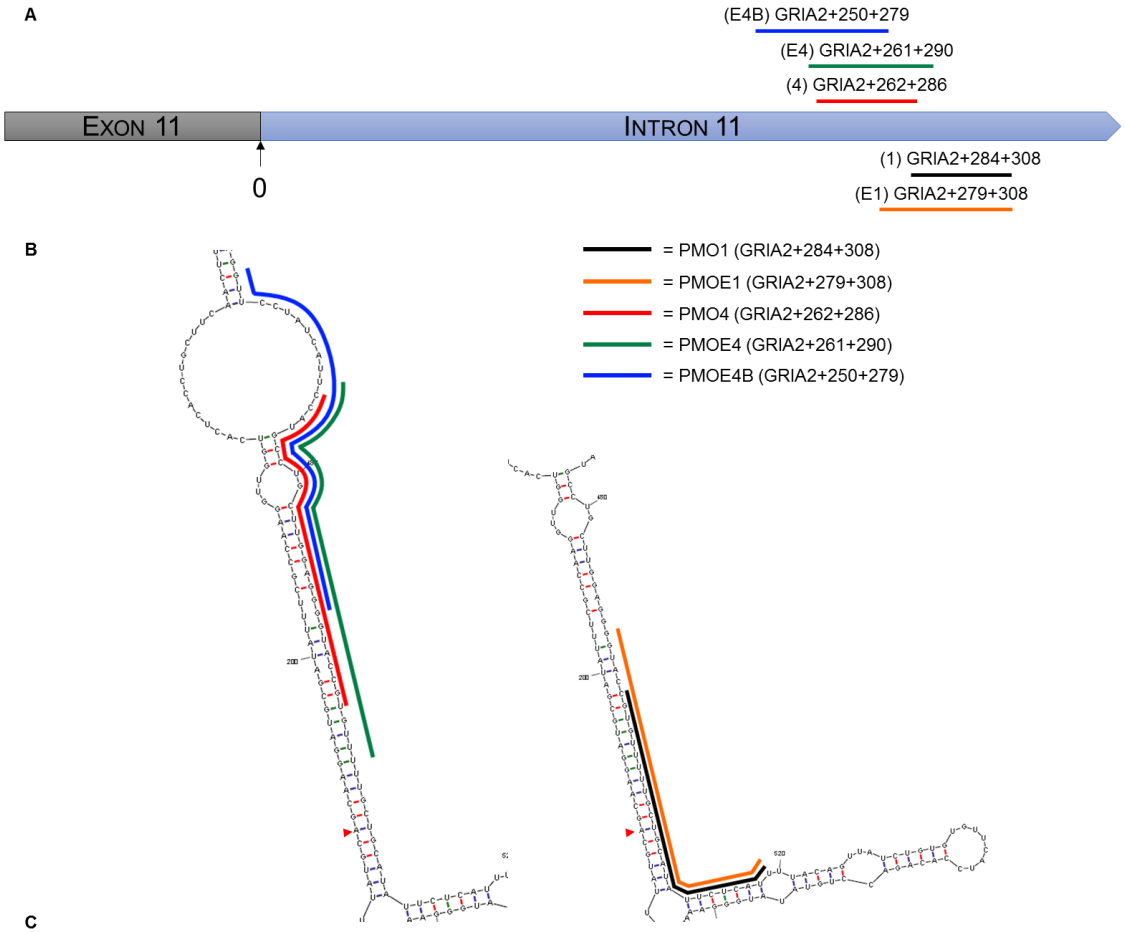

C

	PMO Name	PMO Sequence	Target Sequence
1	GRIA2+284+308	AATGAGAATATGCAGCAAAAACACG	Complementary to edited adenosine
E1	GRIA2+279+308	AATGAGAATATGCAGCAAAAACACGGTACC	5 bases upstream from PMO1 (GRIA2+284+308), further into double-stranded region
4	GRIA2+262+286	ACGGTACCCCTCCAAGCAGGCATGG	Downstream and complementary to edited adenosine
E4	GRIA2+261+290	AAACACGGTACCCCTCCAAGCAGGCATGGA	1 base upstream and four bases downstream of PMO4 (GRIA2+262+286), further into double-stranded region
E4B	GRIA2+250+279	CCCTCCAAGCAGGCATGGAATGATAGGAAC	12 bases upstream of PMO4 (GRIA2+262+286), beginning in the loop of single-stranded RNA

Figure 4.6 – A) Placement of 30mer PMOs in relation to the original 25mers and the exon 11/intron 11 boundary. B) Regions of binding for new 30mer PMOs extending further into the double-stranded region. Overlap with the original 25mers indicated on the MFE model of the B13 minigene. PMOE1 (GRIA2+279+308) is extended 5 bases further 5' than PMO1 (GRIA2+284+308). PMOE4 (GRIA2+261+290) is extended 4 bases 3' and one base 5' to PMO4 (GRIA2+262+286). PMOE4B (GRIA2+250+279) is shifted and extended 12 bases 5' to PMO4 (GRIA2+262+286), avoiding the GGGG sequence and targeting the open loop region, as recommended by SFold. C) Table of 30mer PMOs, their sequence and their target.

4.2.3 Transfection of 30mer PMOs

The newly designed 30mer PMOs were transfected into the HeLa-B13 system at 10 µM as previously described. Q/R site editing was quantified as before; the results are shown in Figure 4.7. PMO1 (GRIA2+284+308) achieved a small effect that reached significance (78.0 ± 5.39% of control, $p<0.01$), which was a similar inhibition to that found in the previous transfection at 1 µM and is a larger effect than the transfection at 10 µM under the same conditions (Figure 4.1). However, the 30mer PMOE1 (GRIA2+279+308), which is an extension of PMO1 (GRIA2+284+308), was significantly more effective than PMO1 (54.3 ± 3.66%, $p<0.01$). PMO4 (GRIA2+262+286) showed a strong ability to inhibit Q/R site editing, which was measured as 26.4 ± 3.57% of control ($p<0.01$) and is significantly greater than the inhibition shown under the same conditions previously (Figure 4.1). PMOE4 (GRIA2+261+290), which is PMO4 (GRIA2+262+286) but extended into the double-stranded structure, also showed a strong effect at Q/R site editing inhibition (40.0 ± 4.72%, $p<0.01$) which was not significantly different to the effect of PMO4 (GRIA2+262+286). PMOE4B (GRIA2+250+279), which was shifted away from the "GGGG" sequence and into the open loop region, showed significantly less inhibition compared to PMOE4 (GRIA2+261+290) (52.4 ± 2.88%, $p<0.05$) which was similar in effect to PMOE1 (GRIA2+279+308).

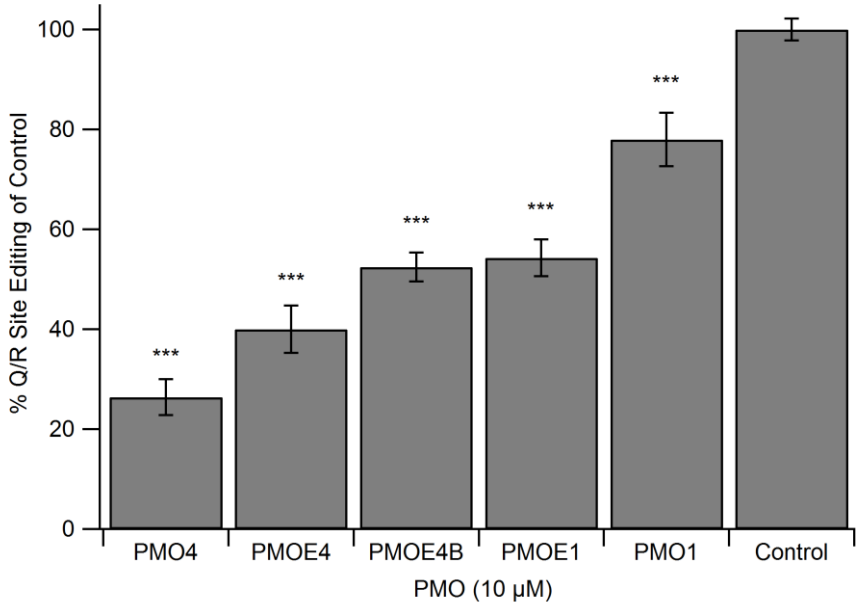

*Figure 4.7 - Q/R site editing with 30mer PMOs. N=3 per group, *** = p<0.01 compared to control. The strongest inhibition of Q/R site editing is seen with PMO4 (GRIA2+262+286) and PMOE4 (GRIA2+261+290) (26.4 ± 3.57% and 40.0 ± 4.72%). PMOE4B (GRIA2+250+279) and PMOE1 (GRIA2+279+308) showed similar effects (52.4 ± 2.88% and 54.3 ± 3.66%) while PMO1 (GRIA2+284+308) showed a small effect (78.0 ± 5.39%).*

4.2.4 Concentration-inhibition curves for RNA editing elicited by the 30mer PMOs

For a better comparison of efficacy of the different PMOs, a range of concentrations for each 30mer was tested in the HeLa-B13 system. Due to the variability seen across transfections of the same conditions, each concentration was repeated in six biological repeats. The concentration-inhibition curves are shown in Figure 4.8. These results show that all three 30mer PMOs are effective at inhibiting Q/R site editing at lower doses, with IC_{50}s of 1.78 ± 0.11 μM, 1.93 ± 0.13 μM and 2.42 ± 0.42 μM for PMOE4 (GRIA2+261+290), PMOE4B (GRIA2+250+279) and PMOE1 (GRIA2+279+308) respectively. Based on these data, PMOE4 (GRIA2+261+290) is the most effective at Q/R site inhibition. This correlates with the initial transfection at 10 μM where PMOE4 (GRIA2+261+290) was most effective of the 30mer PMOs (Figure 4.7). Compared to the published IC_{50} for PMO1 (GRIA2+284+308), PMOE4 (GRIA2+261+290), PMOE4B (GRIA2+250+279) and the published PMO have similar effects while PMOE1 (GRIA2+279+308) is slightly less effective (Table 4.2).

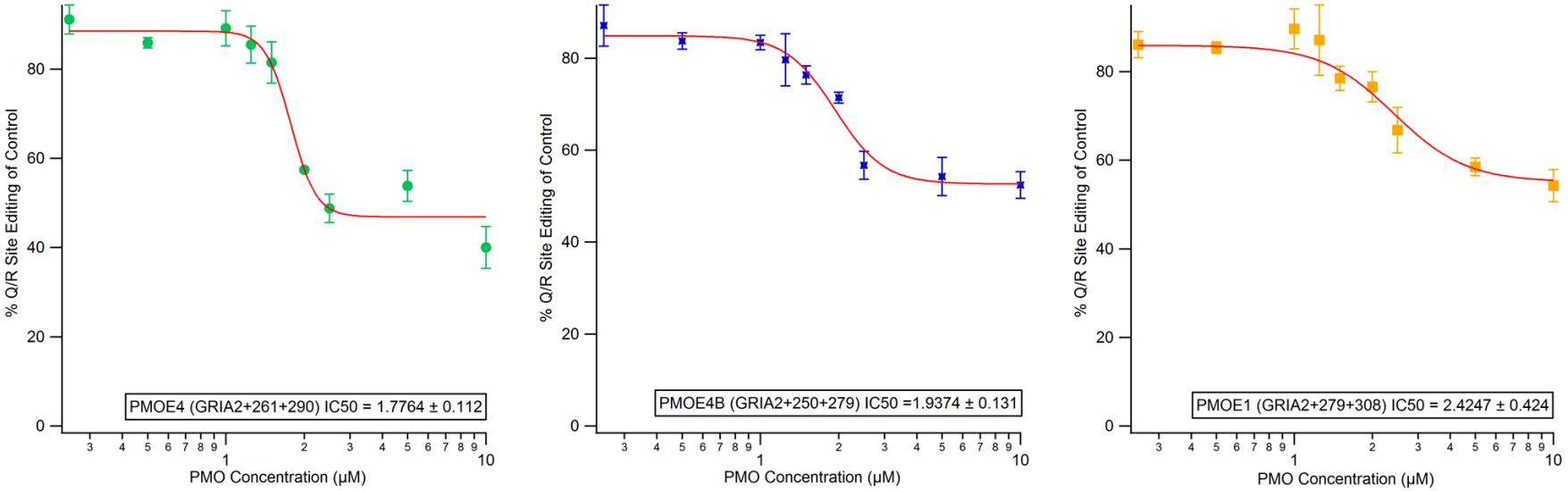

Figure 4.8 – Concentration curves for PMOE4 (GRIA2+261+290), PMOE4B (GRIA2+250+279) and PMOE1 (GRIA2+279+308). N=6 per concentration. IC_{50} values were calculated using the Hill equation.

PMO	IC_{50} (μM)	Residual Q/R Site Editing (% of Control)
PMOE4 (GRIA2+261+290)	1.78 ± 0.11	40.00 ± 4.72
PMOE4B (GRIA2+250+279)	1.93 ± 0.13	52.44 ± 2.88
PMOE1 (GRIA2+279+308)	2.42 ± 0.42	54.31 ± 3.66
PMO1 (GRIA2+284+308) (Penn et al. 2012)	1.9	Not reported

Table 4.2 - Comparison of IC50s for each 30mer PMO in the HeLa-B13 system and their maximum inhibition percentages of control.

4.2.5 Testing PMOs in a Cell Line Endogenously Expressing GluA2

Although the HeLa-B13 system was useful as a primary test due to its easy manipulation, a system which endogenously expresses the GluA2 subunit would be a better model to test the PMOs. The SH-SY5Y cell line, derived from a human neuroblastoma, is often used as a neuronal model (Lopes *et al.*, 2010; Agholme *et al.*, 2010), and has previously been shown to express AMPA receptor subunits (Sun *et al.*, 2010), including GluA2 (Kritis *et al.*, 2015). SH-SY5Y cells are from a human origin (Biedler *et al.*, 1978). Of the three 30mer PMOs designed in this chapter, only PMOE1 (GRIA2+279+308) is completely complementary to the human sequence of *GRIA2*, and so this was tested in SH-SY5Y cells.

One advantage of an endogenously expressing cell line is that both mRNA and premRNA can be analysed through alternative primer design. Figure 4.9 describes the primers designed for this system. Both forward primers are placed in exon 11. The reverse primer for premRNA transcripts is placed in intron 11 to target RNA transcripts before splicing has occurred. The reverse primer for detecting mRNA transcripts is placed in exon 12, so that premRNA transcripts will not be amplified as the intron is too large for the polymerase enzyme. Both of these primer sets cover the Q/R site and therefore contain the *BbvI* recognition site, and so the restriction digest analysis could be used to determine the Q/R editing state of SH-SY5Y cells with and without PMOE1 (GRIA2+279+308).

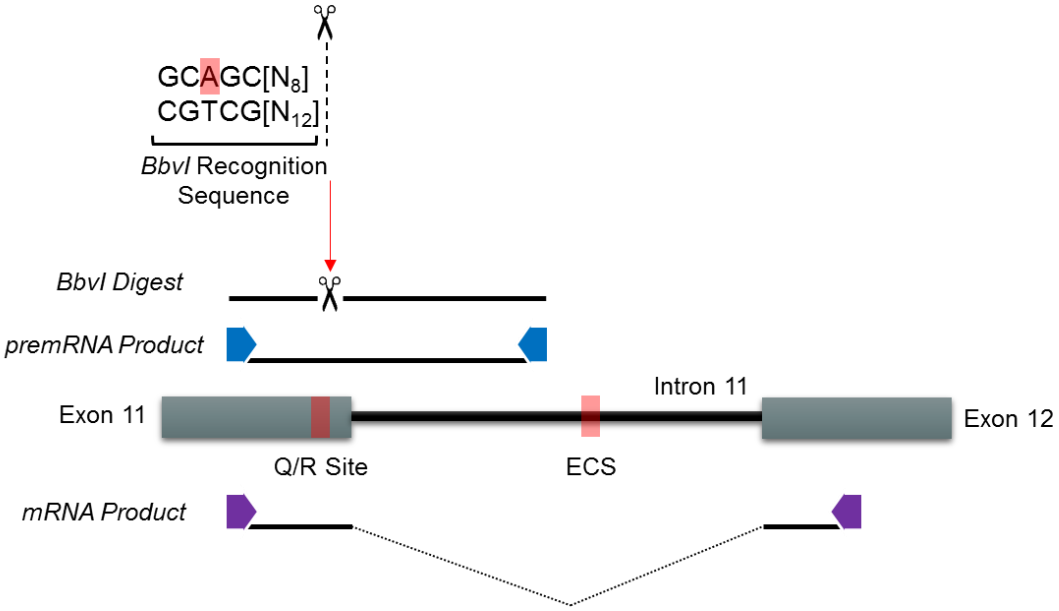

Figure 4.9 - Primer design for premRNA and mRNA transcripts targeting the area of GRIA2 surrounding the edited adenosine. Exon 11 contains the edited adenosine. Primers for premRNA transcripts are indicated with blue arrows, targeting intron 11, while primers for mRNA transcripts are indicated in purple targeting exon 12, both sets covering the Q/R site and therefore the BbvI recognition site, allowing editing percentage quantification.

4.2.6 Transfecting SH-SY5Y cells with PMOE1 (GRIA2+279+308) and the effect on GluA2 Q/R site RNA editing

SH-SY5Y cells showed endogenous editing at the Q/R site in mRNA of 90.89 ± 1.10% in control samples at 24 hours and 97.20 ± 1.72% at 48 hours (Figure 4.10). Editing in premRNA transcripts appears to be more variable, with samples measured after 48 hours showing high levels of editing (88.6 ± 1.41%) while samples measured at 24 hours showed a large variation with editing at 58.5 ± 14.0% (Figure 4.11). SH-SY5Y cells were transfected with 10 μM of PMOE1 (GRIA2+279+308) for 24 or 48 hours. The effects of transfection and length of time of transfection were compared using a two-way ANOVA. PMOE1 (GRIA2+279+308) showed a strong inhibition of Q/R site editing in premRNA transcripts after only 24 hours (9.63 ± 3.67% editing) compared to control at this time point (58.5 ± 14.0%; $p<0.05$) and editing remained inhibited at the 48 hour time point (8.25 ± 1.5%; $p<0.05$ compared to control). Transcripts of mRNA from cells transfected with PMOE1 (GRIA2+279+308) showed a significant decrease in Q/R site editing after 24 hours (Figure 4.10: 46.6 ± 1.84%, $p<0.01$), although at 48 hours following transfection the Q/R site editing was almost completely inhibited (15.4 ± 1.22%, $p<0.01$ compared to both 24 hour transfection and control). The two-way ANOVA showed a statistically significant interaction between transfection and length of time of transfection in mRNA transcripts ($p<0.025$), highlighting the fact that longer transfection times improved the inhibitory effect of PMOE1 (GRIA2+279+308).

Editing in mRNA was used to analyse the effect of PMOE1 (GRIA2+279+308) transfection. GluA2 premRNA appears to have variable editing as shown by the large error bars in control samples (Figure 4.11), and so calculating editing of the mRNA transcript was considered to be a more reliable method. Transcripts were analysed after 24 hours or 48 hours of transfection with a range of concentrations (Figure 4.12). After 24 hours of transfection, low concentrations of PMOE1 (GRIA2+279+308) had little effect on Q/R site editing, shown in blue in Figure 4.12. PMOE1 (GRIA2+279+308) sharply increases in effectiveness between 0.5 and 2.5 μM then reaches steady state inhibition at the higher concentrations with around 60% inhibition of editing compared to control levels. When the curve was fit with the Hill Function, an IC_{50} of 0.92 ± 0.11 μM was calculated, indicating that 920 nM of PMOE1 (GRIA2+279+308) is sufficient to cause half of the total inhibition possible under these conditions. When incubated for 48 hours, lower concentrations of PMOE1 (GRIA2+279+308) have a greater effect on Q/R site editing. For example 250 nM of PMOE1 (GRIA2+279+308) will only reduce editing to 97.6 ± 0.51% after 24 hours whereas after a 48 hour incubation the same concentration reduces Q/R site editing to 89.7 ± 2.02% of control. As the lower concentrations have a larger effect on Q/R site editing at 48 hours, the slope of the Hill Function fit is less steep,

with an IC_{50} of 1.48 ± 0.17 µM. Overall there is the potential for greater steady state inhibition with 48 hour incubation periods, with a maximum inhibition leading to just 15.4 ± 1.22% editing (Table 4.3). These IC_{50} values show that PMOE1 (GRIA2+279+308) is more effective than data previously published on PMO1 (GRIA2+284+308) (Penn *et al.*, 2012), which had an IC50 value of 2.8 µM in SH-SY5Y cells after 24 hours of transfection (Table 4.3) and which did not show any effect on Q/R site editing at 10 µM in this work (Figure 4.1).

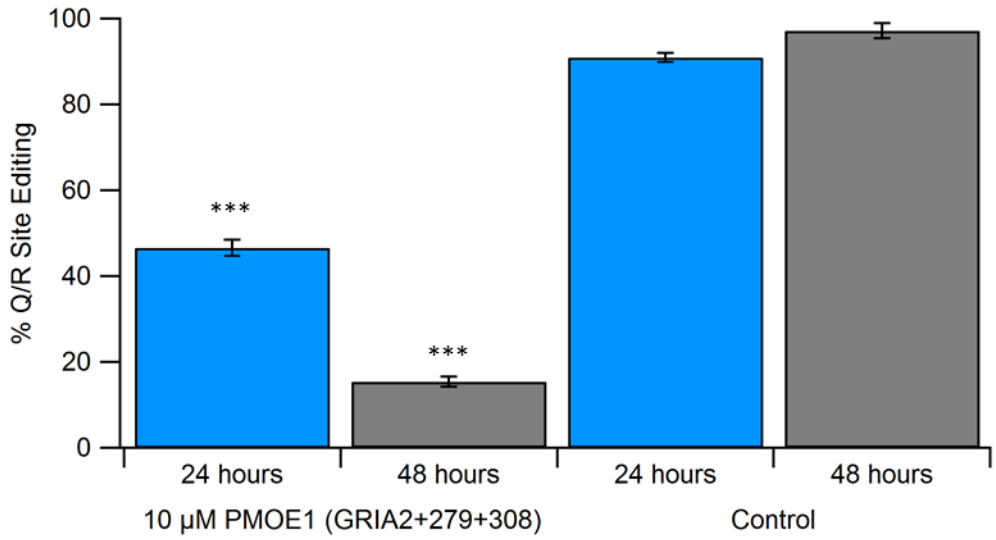

*Figure 4.10 - Q/R site editing in mRNA of SH-SY5Y cells after treatment with 10 µM PMOE1 (GRIA2+279+308) compared to control cells of EndoPorter only; n=3 per condition. Q/R site editing was measured after either 24 or 48 hours. Two-way ANOVA was used to determine significance between length of time and transfection conditions on Q/R site editing, *** = p<0.05 compared to control at 48 hours.*

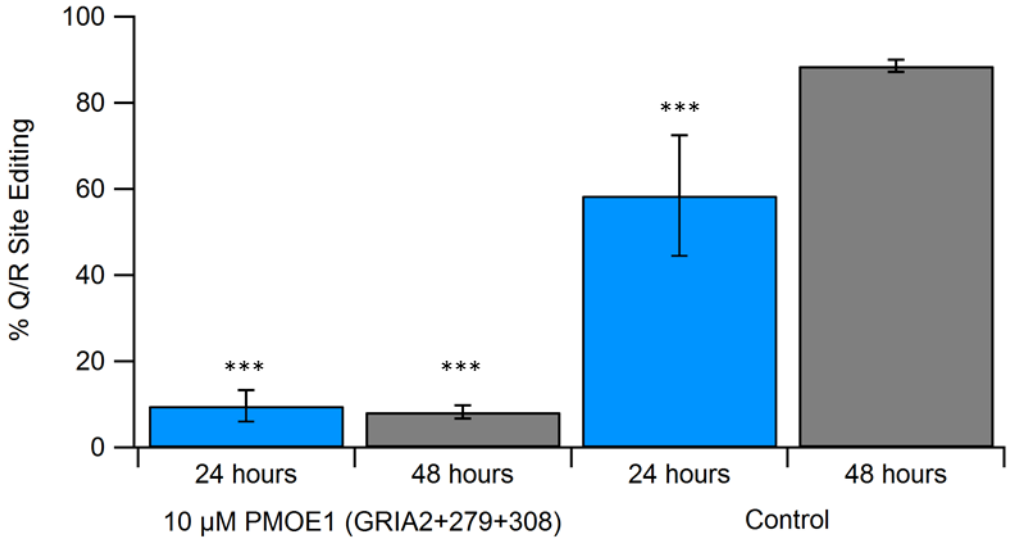

*Figure 4.11 - Q/R site editing in premRNA of SH-SY5Y cells after treatment with 10 µM PMOE1 (GRIA2+279+308) compared to control cells of EndoPorter only; n=3 per condition. Q/R site editing was measured after either 24 or 48 hours. Two-way ANOVA was used to determine significance between length of time and transfection conditions on Q/R site editing, *** = p<0.05 compared to control at 48 hours.*

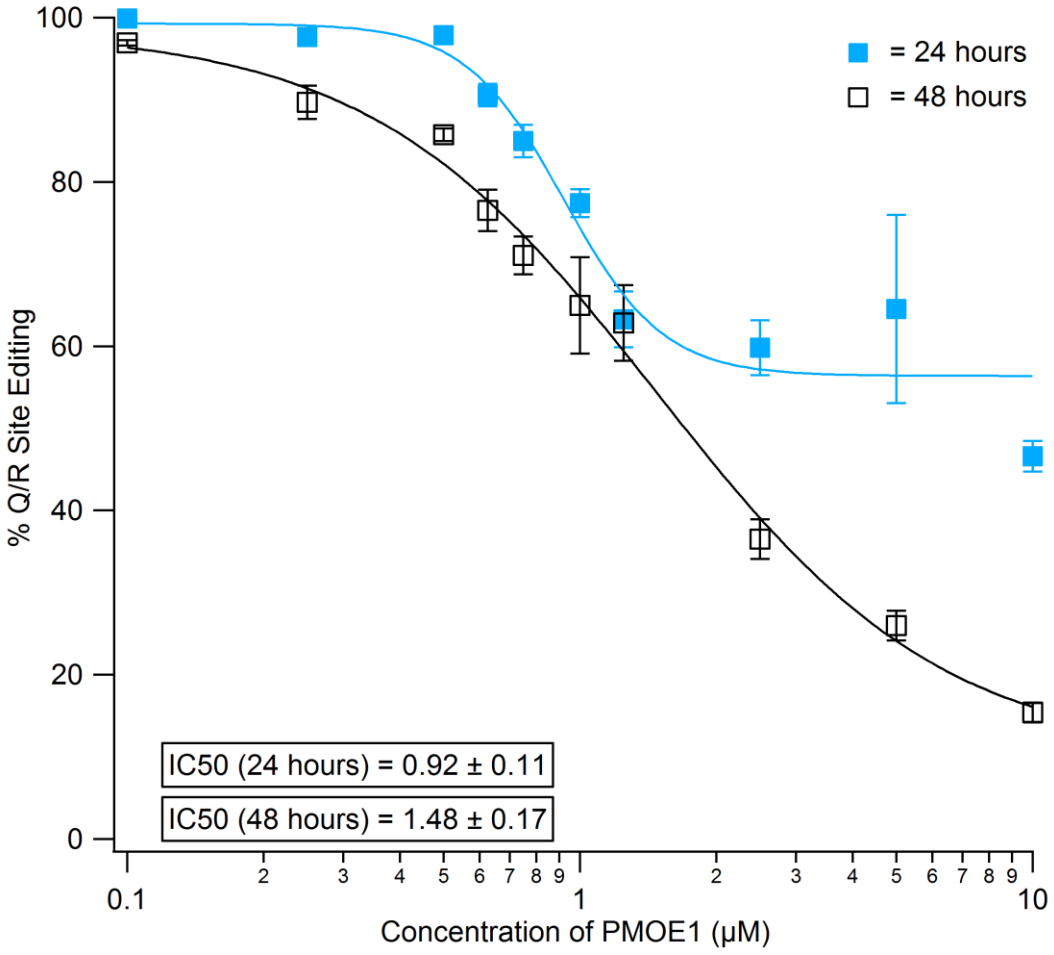

Figure 4.12 - SH-SY5Y mRNA after transfection with PMOE1 (GRIA2+279+308) for 24 vs 48 hours at increasing concentrations. N=6 per concentration. IC50 of PMOE1 (GRIA2+279+308) in SH-SY5Y cells for 24 hours and 48 hours shown in the bottom left hand corner, calculated using the Hill Function.

Transfection Conditions	IC50 (μM)	Maximum Inhibition
PMOE1 (GRIA2+279+308) – 24 hours	0.92 ± 0.11	46.61 ± 1.83%
PMOE1 (GRIA2+279+308) – 48 hours	1.48 ± 0.17	15.4 ± 1.22%
PMO1 (GRIA2+284+308) (Penn et al. 2012)	2.8	Not Reported

Table 4.3 - IC50 for PMOE1 (GRIA2+279+308) after 24 or 48 hours transfection compared to PMO1 (GRIA2+284+308) IC50 previously reported in SH-SY5Y cells, and the maximum inhibition found at these time points.

4.3 DISCUSSION

This chapter looks at the effect of 25mer and 30mer PMOs on the disruption of Q/R site RNA editing in both the HeLa-B13 system and an endogenously expressing GluA2 system, SH-SY5Y cells. In the previous chapter, 25mer PMOs were designed to span the region of double-stranded structure surrounding the Q/R site. These 25mers were transfected into the HeLa-B13 system and the Q/R site editing analysed using the *BbvI* assay. Two PMOs, PMO2 (GRIA2-30-6) and PMO4 (GRIA2+262+286), show a moderate effect at disrupting Q/R site editing at 10 μM, although there was no significant effect at 1 μM for any PMO. PMO1 (GRIA2+284+308) was previously reported to disrupt editing to 60% of control samples (Penn *et al.*, 2012). However in this analysis under the same conditions, PMO1 (GRIA2+284+308) only showed a limited effect in the HeLa-B13 system. The same plasmid backbone with the B13 minigene was used to transfect the HeLa cells, and PMOs were transfected with EndoPorter in both the previous study and this assay. Various other transfection conditions were tested to try and improve the efficiency of PMO1 (GRIA2+284+308) as well as the other 25mers such as adjusting transfection conditions of the B13 plasmid or transfecting plasmid before the PMO. None of these adjustments improved the impact of the 25mers on Q/R site editing. There are several variables that may affect the impact of PMOs in the HeLa-B13 system, including transfection reagents, efficiency of expression of the B13 plasmid as well as how functional the PMO is itself.

Due to the limited effect of the 25mers in the HeLa-B13 system, new PMOs were designed in an effort to improve their impact on Q/R site editing. It has previously been suggested that longer PMOs are more effective due to their increased binding energies, and so are more likely to bind to the target bases and have an effect (Pramono *et al.*, 2012). Therefore, the length of the PMO was extended from 25 bases to 30. For these 30mers, binding energies were predicted using online tools to calculate the inter- and intramolecular energies. Total binding energy was calculated by taking the energy needed to overcome any internal structure of the PMO (hairpin structures and PMO-PMO interactions) and subtracting this from the energy given by the PMO binding to the RNA molecule. A more negative overall binding energy should mean that the most favourable condition would be for the PMO to bind to the GluA2 RNA transcript, disrupting the secondary structure through steric hindrance. Total binding energies have previously been suggested to be one of the factors considered for ideal PMO design (Pramono *et al.*, 2012). The only PMO to be predicted to have a negative total binding energy was PMOE4B (GRIA2+250+279) with -6.18 kcal/mol; the total binding energies of the other extended PMOs and the 25mers PMO1 (GRIA2+284+308) and PMO4 (GRIA2+262+286) were all positive. Considering these energy calculations, PMOE4B

(GRIA2+250+279) should bind more effectively than PMOE4 (GRIA2+261+290) and PMO4 (GRIA2+262+286). Indeed, PMOE4B (GRIA2+250+279) could be the only PMO to have an effect as a positive total binding energy would mean that it would take an input of energy for the PMO to bind to RNA, which is unlikely to happen under normal cellular conditions. However, when transfected into the HeLa-B13 system, all 30mers showed a strong ability to disrupt Q/R site editing despite their predicted energies. Although there is no evidence that these PMOs are directly binding to the RNA transcript, this is the simplest explanation for the change in Q/R site editing. It therefore appears that this method of calculating binding energies is too simplistic for the complex conditions of the cell nucleus, and cannot accurately predict how well a PMO will bind to RNA.

The most accurate method for determining effectiveness of a PMO is still *in vitro* testing. The HeLa-B13 system was used to study each of the 30mer PMOs at decreasing concentrations. The results from these experiments produced a graph with a plateau at the lower concentrations where the PMO did not have any effect, and a plateau at the higher concentrations where the maximum effect had been reached. These graphs could then be treated as dose-response curves for each PMO. These dose responses were then fit with the Hill Function allowing an IC_{50} to be calculated. IC50s for PMOE4 (GRIA2+261+290), PMOE4B (GRIA2+250+279) and PMOE1 (GRIA2+279+308) were 1.78 ± 0.11 μM, 1.93 ± 0.13 μM and 2.42 ± 0.42 μM respectively. These are similar to the IC_{50} calculated by Penn et al. for PMO1 (GRIA2+284+308), which they found to be 1.9 μM when fit with a sigmoidal curve (Penn *et al.*, 2012). An IC_{50} in this context represents the concentration of PMO needed to produce half of the maximum inhibition under these conditions. However, the value is dependent on the model, and the concentrations needed for an inhibition of 50% of Q/R site editing may vary in any other system. There are multiple variables that might affect this outcome, for example the transfection efficiency of EndoPorter and so concentration of PMO per cell, expression of ADAR2 in HeLa cells and therefore efficiency of Q/R site editing itself, as well as the ability of the PMO to prevent Q/R site editing. The plateau at the higher concentrations of PMO shows where the inhibition of Q/R site editing is limited by another variable in the system. This is likely to be the high expression of the B13 minigene in the plasmid and therefore increased production of GluA2 RNA, meaning that there is not sufficient PMO within the cell to interfere with every transcript.

Due to these limitations of the system, the IC_{50}s do not give biologically relevant concentrations of the PMO's inhibitory effect. However, they are a useful means for comparison across the PMO designs. It is evident that the 30mers based on PMO4 (GRIA2+262+286) are more efficient at Q/R site editing disruption than the 30mer based

on PMO1 (GRIA2+284+308). PMOE4 (GRIA2+261+290) also appears to be slightly more effective than PMOE4B (GRIA2+250+279) as their maximum effect is significantly different. Comparing the IC_{50}s shows that PMOE4 (GRIA2+261+290) is fairly similar to PMOE4B (GRIA2+250+279), with an IC_{50} of 1.78 ± 0.11 µM versus 1.93 ± 0.13 µM. PMOE4B (GRIA2+250+279) accommodates the suggestions for antisense oligonucleotide design from the SFold website, namely to avoid "GGGG" sequences, to keep the GC content between 40 and 60% and to keep the intermolecular binding energy below -8 kcal/mol. Both PMOE4 (GRIA2+261+290) and PMOE4B (GRIA2+250+279) have a GC content within these boundaries, however avoidance of the "GGGG" sequence does not appear to have been necessary. Of the three 30mers tested in the HeLa-B13 editing system, PMOE4 (GRIA2+261+290) appears to be the most effective.

Having compared the 30mers in the HeLa-B13 system, the next step was to test the PMOs in a cell line that endogenously expressed the GluA2 subunit, and so co-transfection with the B13 plasmid was not necessary. As the B13 minigene was comprised of the sequence from the murine *Gria2* gene, the ideal cell line would be derived from a mouse neuronal lineage. Neuro2A cells are derived from a mouse neuroblastoma and can be differentiated to develop neuronal-like features (Klebe & Ruddle, 1969). However, in the proliferative form these cells do not appear to express the GluA2 subunit. SH-SY5Y cells are derived from a human neuroblastoma patient (Biedler *et al.*, 1973). These cells show expression of the GluA2 subunit in both their proliferating and differentiated forms (Yamashita *et al.*, 2012; Voss *et al.*, 2007), and Q/R site editing was shown to be up to 100% in mRNA transcripts. Due to the differences in sequence between the human *GRIA2* and mouse *Gria2* genes, only PMOE1 (GRIA2+279+308) is completely complementary to the human sequence. Therefore, although this model is not ideal, it provides a useful proof-of-principle that these PMOs work in an endogenous cellular system for GluA2 Q/R site editing, and so PMOE1 (GRIA2+279+308) was tested in SH-SY5Y cells.

With an initial high concentration of 10 µM, it was clear that PMOE1 (GRIA2+279+308) would have a strong effect on this endogenous cell line, as it was able to inhibit Q/R site editing to around 10% in premRNA samples after just 24 hours, and similar inhibition in mRNA after 48 hours. A-to-I editing occurs in the nucleus, probably at the same time as splicing events (Bentley, 2014). PMOE1 (GRIA2+279+308) therefore needs to interfere with the secondary structure of the transcript within the nucleus at the time of transcription. PMOs have been shown to localise to both the cytoplasm and the nucleus (Summerton, 2005), and should therefore be able to disrupt Q/R site editing efficiently, as shown in Figure 4.10. After 24 hours, mRNA samples only showed a 50% inhibition in editing. This could be accounted for by transportation of RNA transcripts from the

nucleus. At the time of transfection there will already be some GluA2 transcripts present in the cytoplasm with complete Q/R site editing. 24 hours post-transfection, the mRNA transcript population will be mixed between those influenced by PMOE1 (GRIA2+279+308) and those transcripts that were already in the cytoplasm, whereas after 48 hours the turnover of transcripts could mean that they have all been affected by PMOE1 (GRIA2+279+308), accounting for the improved inhibition after longer transfection time.

Lower concentrations of PMOE1 (GRIA2+279+308) were then tested to compare dose response curves to those found in the HeLa-B13 assay. The IC_{50} for PMOE1 (GRIA2+279+308) was 0.92 ± 0.11 µM after 24 hours and 1.48 ± 0.17 µM after 48 hours. Although the concentration of PMOE1 (GRIA2+279+308) needed for half of the inhibitory effect was less after 24 hours, the maximum inhibition possible is much greater after 48 hours. At every concentration of PMOE1 (GRIA2+279+308) the effect is equal or greater after 48 hours of incubation compared to 24 hours, indicating that the PMO is remaining in the nucleus and continuing to affect RNA editing throughout this incubation time. Penn et al. also investigated the effect of PMO1 (GRIA2+284+308) in SH-SY5Y mRNA after 24 hours, where they found an IC_{50} of 2.8 µM using a logarithmic regression. Direct comparison of these IC_{50}s indicate that PMOE1 (GRIA2+279+308) is around three times more potent, although the IC_{50} for PMOE1 (GRIA2+279+308) was calculated using the Hill Function. When comparing between the two systems studied in this chapter, the IC_{50} for PMOE1 (GRIA2+279+308) falls from 2.42 ± 0.42 µM in the HeLa-B13 system to 0.92 ± 0.11 µM in SH-SY5Y cells. This shows the beneficial effect of removing variables from a model system. The major variable of the B13 plasmid, and therefore the unknown efficiency of both its transfection and expression, is not part of the SH-SY5Y model and so the IC_{50} is closer to a value representing the efficiency of the PMO at steric hindrance of Q/R site editing alone.

5 THE DELIVERY OF ANTISENSE OLIGONUCLEOTIDES INTO PRIMARY NEURONAL CULTURES

5.1 INTRODUCTION

Neurons taken from the neocortex of embryonic or early postnatal mice or rats can be used in primary cultures to study neuronal development and function *in vitro*. The cortex is dissected and the meninges removed to reduce contamination with other cell types before the neurons are dissociated by trypsinisation and plated (Hilgenberg & Smith, 2007). Neurons are then kept generally for three to four weeks *in vitro*, although they can be kept longer (Lesuisse & Martin, 2002). Culturing the neurons in neurobasal (low-serum) media supplemented with B27 selects against dividing cells, such as glial cells contaminating the cultures, and selects for the post-mitotic neurons. Neurons cultured in neurobasal media showed staining for astrocytic markers can be as low as less than 1% of the total cell count (Brewer *et al.*, 1993). Cortical neurons cultured in this manner develop large, pyramidal-like cell bodies and begin extending neurite-like projections after a few days *in vitro*, with synaptic markers such as GAP-43 showing expression after just 4 days *in vitro* (DIV). After 5 DIV, neurons show low level expression of synaptic markers such as synaptophysin and α- and β-synuclein, with expression increasing over successive weeks in culture both for excitatory and inhibitory synapses (Harrill *et al.*, 2015). These cultures can be depolarised with potassium chloride which leads to an influx of Ca^{2+} into the neurons, an effect also seen through stimulation by glutamate, kainate or AMPA (Glaum *et al.*, 1990). After 14 DIV, neurons exposed to 500 nM of glutamate for 5 minutes showed around 80% cell death after 24 hours (Choi, 1988). More dense neuronal cultures showed a higher sensitivity to glutamate excitotoxicity, largely mediated by NMDA receptors (Ha *et al.*, 2009). Mature synapses have been observed in neuronal cultures from 10 DIV, with synaptogenesis increasing throughout the second and third week *in vitro* (Grabrucker *et al.*, 2009).

AMPA receptor subunits GluA1, 2 and 3 are all found at both the RNA and protein level in primary cortical cultures after 6-10 DIV, with GluA4 only showing low expression (Janssens & Lesage, 2001). GluA1 and GluA2 are more highly expressed than GluA3, showing relatively stable expression from 12 DIV onwards (Orlandi *et al.*, 2011). Q/R site editing of the GluA2 subunit is efficient to 100%, and is not affected by activity unlike the R/G editing site which shows reduced editing levels after depolarisation (Sanjana *et al.*, 2012). Although the editing at the Q/R site remains constant, ADAR2 expression is shown to decrease after acute or chronic glutamate stimulation (Bonini *et al.*, 2015). The

endogenous expression of AMPA receptor subunits and high endogenous editing of the Q/R site, as well as other neuronal characteristics, make primary cortical neurons a more realistic model than the HeLa-B13 system and SH-SY5Y cells used in the previous chapter. This chapter therefore focuses on examining methods for introducing our PMOs into primary cortical neurons. These PMOs could then reduce the RNA editing as seen in models in previous chapters, and the effect of inhibited RNA editing on neuronal viability as well as other downstream processes could be assessed.

Primary neuronal cultures are notoriously challenging to transfect due to their sensitivity to changes in pH and temperature as well as being post-mitotic, and so all transfection techniques have costs and benefits that need to be taken into account (reviewed in Karra & Dahm, 2010). Nucleofection, for example, has shown high efficiency in transfection of primary neurons but can only be performed on cells on the day of isolation, and therefore before the extension of neurites or synaptogenesis (Zeitelhofer *et al.*, 2007). Calcium-phosphate transfection is a classic technique with high efficiency in other cell types, but only around 1-5% transfection efficiency in primary neuronal cultures (Watanabe *et al.*, 1999). Although this may be sufficient for single-cell techniques such as microscopy or electrophysiology, a higher transfection efficiency would be needed to demonstrate any effects of inhibited RNA editing. Electroporation or biolistic delivery again show relatively low efficiency of between 5 and 20% as well as only being possible before the neurons have differentiated *in vitro* (Dib-Hajj *et al.*, 2009). Lipid-based transfection reagents such as Lipofectamine 2000 traditionally show a very low transfection efficiency of between 1-5% in primary neurons with high levels of toxicity, although transfection can be as high as 20% in some reports (Ohki *et al.*, 2001).

Considering the low transfection efficiencies of these classic techniques, alternative methods were investigated. The 30mer PMOs from the previous chapter showed the highest efficacy in the HeLa-B13 system (Figure 4.4), and so these PMOs were tested in primary cortical neurons. Three methods were used in this chapter with varying levels of success: transfection with Endo-Porter; magnetofection and transduction using a lentiviral vector (summarised in Figure 5.1). Endo-Porter is the transfection reagent developed specifically for use with the neutrally-charged PMOs by GeneTools, and is reported by the manufacturer to be successful in primary neuronal culture (Summerton, 2005). Magnetofection involves binding the molecule that needs to be carried to a magnetic nanoparticle, and has been shown to be effective with DNA and shRNA sequences in primary neuronal cultures to a transfection efficiency of more than 20% (Buerli *et al.*, 2007). However, in order to carry the neutrally-charged PMO into the neurons, the PMO must first be bound to a negatively charged “leash”, a short section of DNA which is partly complementary to the PMO leaving a charged overhang to bind to

the magnetic nanoparticle (Popplewell *et al.*, 2012). Finally, lentiviral vectors are known to transduce primary neuronal cultures with as high as 90% efficiency (Ding & Kilpatrick, 2013). Although the virus cannot produce the PMO chemistry backbone, lentiviral vectors have previously been used to express small nuclear RNA for steric hindrance purposes such as exon skipping (Goyenvalle *et al.*, 2009) as well as to produce guide RNAs for the CRISPR-Cas9 system (Vidigal & Ventura, 2015). Therefore the sequence of the PMO can be cloned into the lentiviral system with the appropriate promoter, leading to overexpression of the RNA which can then target the GluA2 transcript. These three techniques were optimised in order to enhance RNA editing inhibition in primary neuronal cultures.

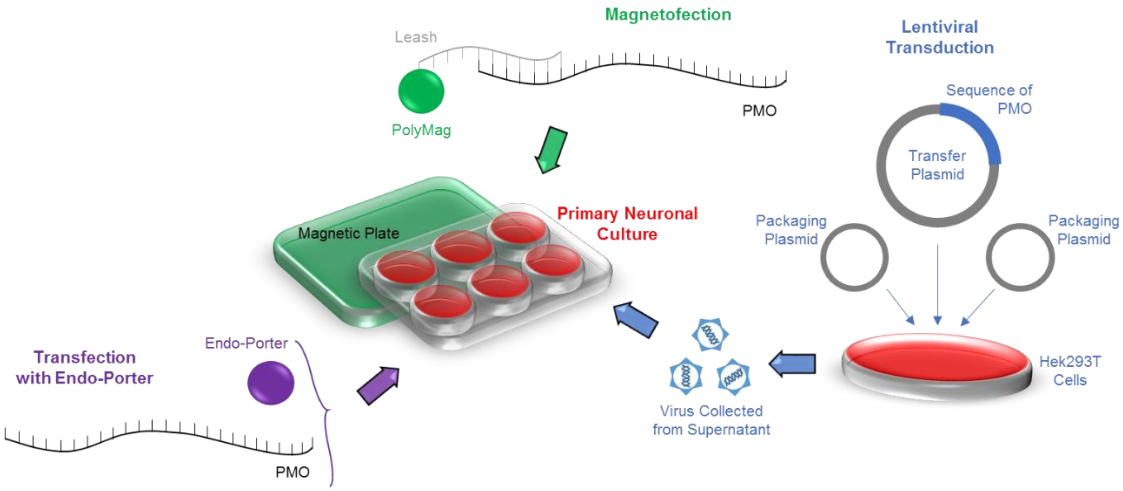

Figure 5.1 - Schematic of transfection and transduction techniques tested in this chapter. Three methods were tested: transfection of the PMO with Endo-Porter (purple); magnetofection of the PMO (green) and transduction of the PMO sequence with a lentiviral vector (blue).

5.2 RESULTS

5.2.1 Transfections using Endo-Porter

Endo-Porter is the transfection reagent produced specifically for the neutral charge of PMOs, and successfully transfected PMOs into the HeLa-B13 system and SH-SY5Y cells in the previous chapter. This was therefore the first transfection method tested in primary cortical neurons.

5.2.1.1 Cell Viability Assay

The standard Endo-Porter reagent is in DMSO solution. However, even very low concentrations of DMSO have been shown to be toxic to primary neuronal cultures (Hanslick *et al.*, 2009). GeneTools also produces a version of Endo-Porter that is instead in aqueous solution, and would therefore be less toxic to sensitive cell cultures. This Endo-Porter variant was compared to Endo-Porter in DMSO in terms of viability of the primary neurons at 21 DIV. Both the standard concentration of Endo-Porter (6 mM) and half of that concentration were tested, and cell viability was measured using the MTT assay after 24 hours compared to the viability shown in untreated neurons (control). Endo-Porter in DMSO was shown to decrease cell viability to 48.8 ± 1.8% and 52.5 ± 2.28% of control at 6 mM and 3 mM respectively ($p<0.05$), whereas Endo-Porter in aqueous solution showed no effect on cell viability at either concentration (6 mM, $p=1.00$; 3 mM, $p = 0.610$; Figure 5.2).

Aqueous Endo-Porter was then tested over 24, 48 and 72 hours for any effect on viability after prolonged exposure. At 24 and 48 hours there was no difference in cell viability compared to control, although after 72 hours of exposure there was a slight decrease in cell viability at both concentrations tested, to 86.8 ± 2.38% ($p<0.01$) and 82.3 ± 4.62% ($p<0.05$) for 6 mM and 3 mM respectively (Figure 5.3). Aqueous Endo-Porter could therefore be used for short-term experiments in primary cortical neurons.

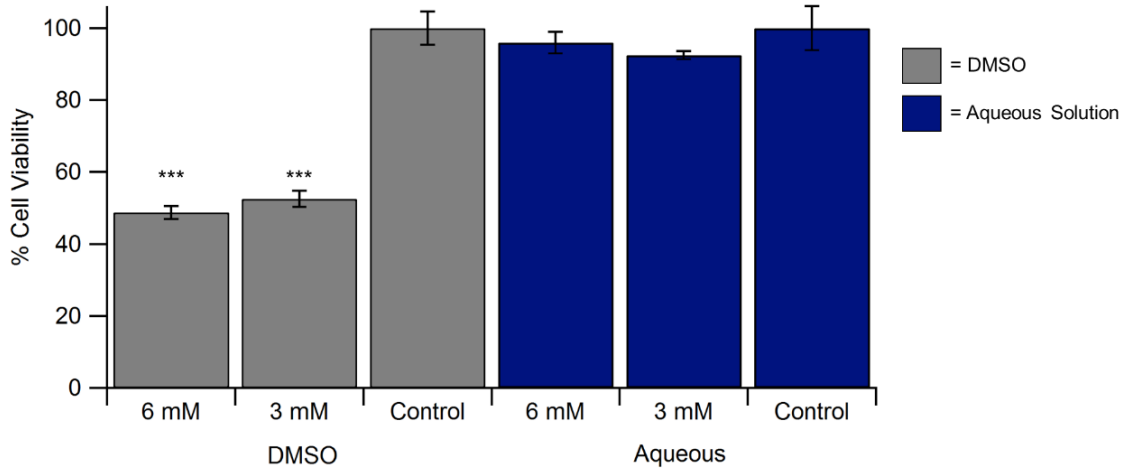

*Figure 5.2 - Cell viability assay testing for toxicity of different concentrations of Endo-Porter in DMSO compared to aqueous solution in primary neurons at 21 DIV (n=6). Endo-Porter in DMSO showed a significant decrease in cell viability after 24 hours (*** = p<0.05) whereas there was no toxicity after incubation with Endo-Porter in aqueous solution. Treatments compared to control neurons with no EndoPorter added.*

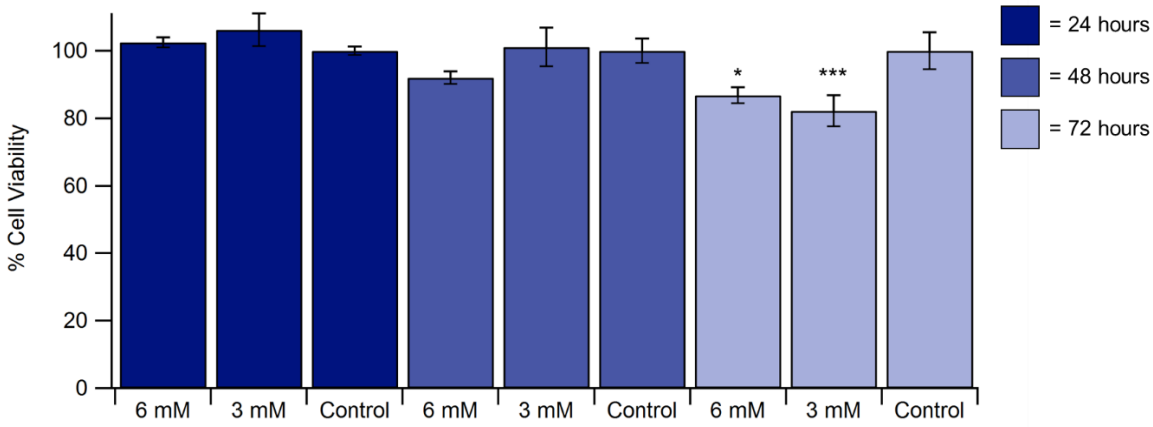

*Figure 5.3 - Cell viability assay testing the toxicity of Endo-Porter in aqueous solution over 24, 48 and 72 hours at 6 mM and 3 mM concentrations in primary neurons at 21 DIV (n=6). Aqueous Endo-Porter showed no change in cell viability until 72 hours. * = p<0.1; *** = p<0.05. Treatments compared to control neurons with no EndoPorter added.*

5.2.1.2 F-PMO Transfection

The PMO tagged with a carboxyfluorescein 5' modification (F-PMO) used in a previous chapter to test transfection efficiency could also be used to test the transfection of primary cortical neurons. Primary cultures were transfected with 5 µM of F-PMO with 6 µM of aqueous Endo-Porter and fluorescence was visualised after 24, 48 and 72 hours. Media was changed to clear (without phenol red), PMO-free media immediately before visualisation to remove background fluorescence. After 24 hours, there was a strong fluorescent signature in the FITC channel (Figure 5.4A) with F-PMO collecting in discrete areas rather than the general background fluorescence of F-PMO in the media. When viewed in bright field, the cell bodies of the neurons remained intact and there was good neurite extension without any obvious cell debris in the media (Figure 5.4B). The collections of F-PMO seen in the FITC channel coincided with the cell bodies of the neurons when the two channels were merged (Figure 5.4C). This pattern is still seen after 48 hours, where images from the FITC channel show a strong fluorescent signature of the F-PMO (Figure 5.4D), the cells appeared healthy when viewed in bright field (Figure 5.4E) and the merged channels images show that most if not all cell bodies show some uptake of the F-PMO (Figure 5.4F). The transfection then appears to remain stable after 72 hours (Figure 5.4G-I).

When qualitatively comparing the fluorescence in the FITC channel over the different time points, there was a general trend of increasing levels of F-PMO fluorescence, and the strongest fluorescence was judged to be at the 72 hour time point (Figure 5.4G). It was not possible to perform FACS analysis with neurons at this stage *in vitro*, as detachment from the plate would destroy the neurite projections and not give an accurate transfection efficiency. As before with the live cell imaging of the F-PMO, staining for other markers was not possible as the PMO would leach out of a fixed cell and not maintain its normal localisation, therefore qualitative image analysis was relied upon. Images from each of these time points show a strong co-localisation of the F-PMO to the cell bodies of the neuron when compared to the bright field image (yellow arrows), but the F-PMO does not appear to localise to the whole neuron, particularly the neurite projections seen in the bright field images (red arrows). This is clearer under the FITC channel (Figure 5.4A, D, G) which shows the collection of the F-PMO into puncta rather than diffusely spreading throughout the cytoplasm. Although the Q/R site editing is thought to occur in the nucleus, and so localisation to the cell body is ideal, these puncta indicate that the PMO may be collected in endosomes and so may prove detrimental to the PMOs' ability to disrupt Q/R site editing.

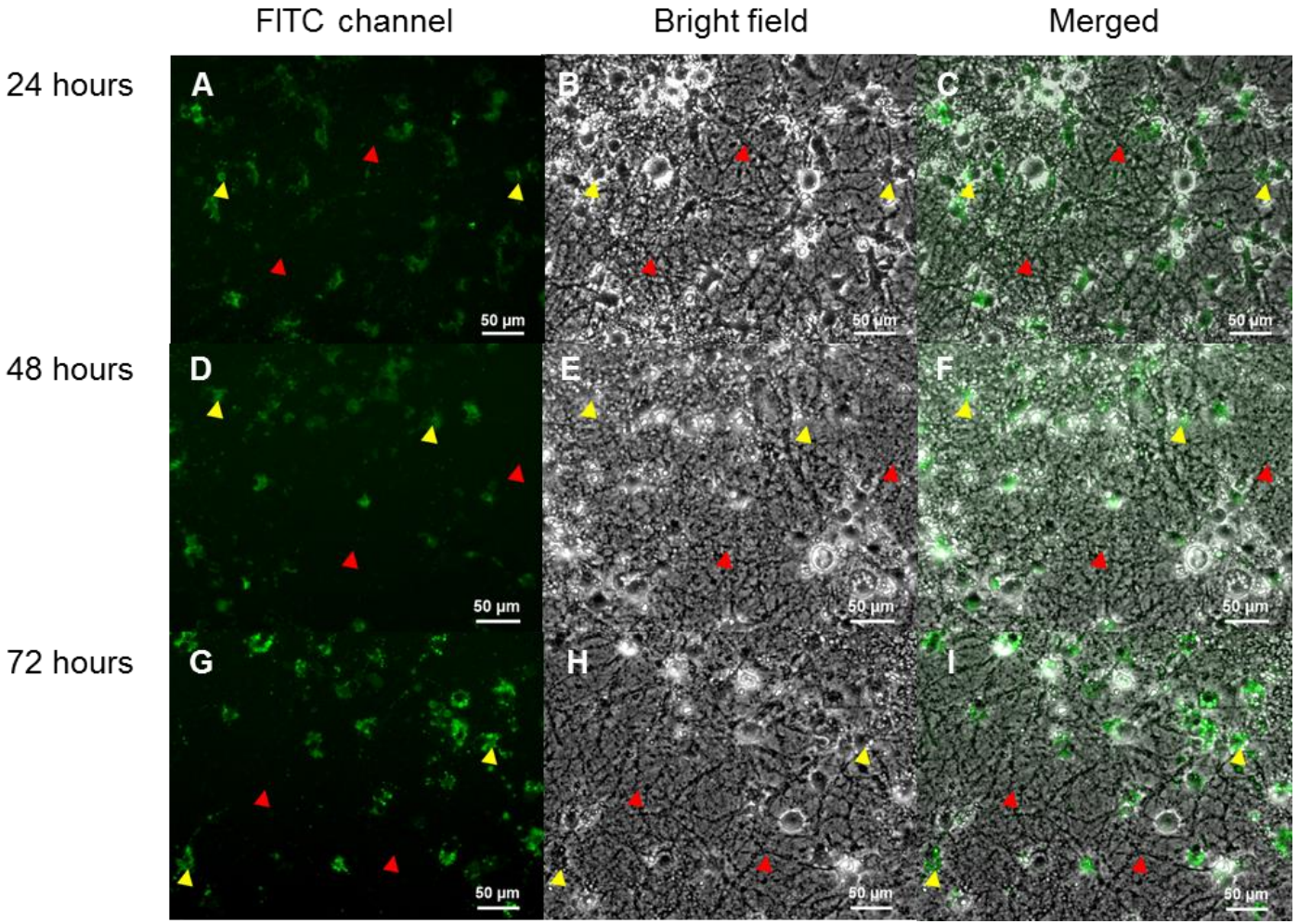
FITC channel
Bright field
Merged
24 hours
48 hours
72 hours
A
B
C
D
E
F
G
H
I
50 µm

Figure 5.4 - Transfection of primary cortical neurons with fluorescent PMO and aqueous Endo-Porter after 24 hours (A-C), 48 hours (D-F) and 72 hours (G-I). Images taken under the FITC channel (A, D, G) and bright field (B, E, H) were merged (C, F, I). Yellow arrows show F-PMO in puncta, coinciding with cell bodies of neurons in the bright field image. Red arrows show neurite projections with no coinciding fluorescence.

5.2.1.3 Changes in Q/R Site Editing

Experiments with the fluorescent PMO suggest that aqueous Endo-Porter can localise the PMO to the primary neurons (Figure 5.4), and so the 30mer PMOs targeting the Q/R site designed in the previous chapter (Figure 4.4) were tested in this model. PMOE4 (GRIA2+261+290), PMOE4B (GRIA2+250+279) and PMOE1 (GRIA2+279+308) were transfected at 5 µM into primary cortical neurons for 24, 48 or 72 hours. The F-PMO was used as a scrambled PMO control, as well as cells treated with Endo-Porter only and cells left without treatment. At each time point, RNA was extracted from which cDNA created and digested with the *BbvI* enzyme. The results of the digest are shown in Figure 5.5, where the edited (uncut) DNA was compared to unedited (digested) DNA.

cDNA run on an agarose gel showed that there is no change in editing in any of the samples treated with a PMO (Figure 5.5A, B or C at each time point) compared to the 100% editing efficiency of control samples (Figure 5.5D, E and F at each time point). This experiment was repeated twice with the same results. It therefore appears that, although the fluorescent PMO seemed to show localisation to the neuronal cell bodies, the transfection did not cause the PMOs to interfere with RNA editing. Due to the success of the PMOs in previous cell models, this is likely due to inefficient transfection into the neurons themselves or into the nucleus, or collection of the PMO into endosomes within the cell. Alternative transfection methods were therefore considered.

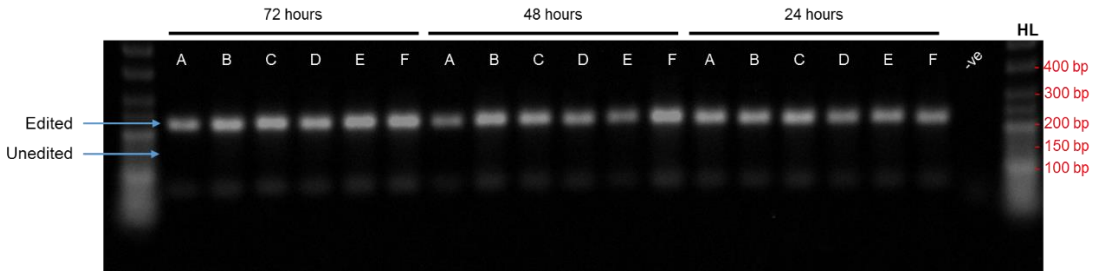

Figure 5.5 - A sample gel image of a 3% agarose gel run in 1X TAE buffer, with 5 µl of Hyperladder V ("HL"; 25 bp, Bioline) visualised using the Ebox VX2 imaging system and quantified using ImageJ analysis."-ve" indicates negative (water) control. Results are of PMO transfections into primary cortical neurons at 21 DIV with Endo-Porter in aqueous solution. Primary cortical neurons were transfected for 72, 48 or 24 hours with 5 µM PMOE4 (GRIA2+261+290) (A), 5 µM PMOE4B (GRIA2+250+279) (B), 5 µM PMOE1 (GRIA2+279+308) (C), 5 µM F-PMO (D), Endo-Porter only (E) or left as cells only (F). DNA bands show that all samples have remained completely edited.

5.2.2 Transfections using Magnetofection

5.2.2.1 Initial Magnetofection

An alternative method for transfection of primary neuronal cultures that has previously been shown to be successful is magnetofection (Oz Biosciences; Buerli *et al.*, 2007). Magnetofection relies on the binding of DNA, in this case the PMOs, to magnetic nanoparticles which are then concentrated onto the surfaces of cell membranes by a magnet underneath the cell's plate. As PMOs have a neutral charge, in order for the PMOs to bind to the magnetic nanoparticles they first have to be leashed to a short sequence of charged DNA (Amantana & Iversen, 2005). The leashed PMOs (L-PMO) PMOE4 (GRIA2+261+290) and PMOE4B (GRIA2+250+279) were incubated with the standard magnetofection reagent, PolyMag; added to the neuron media and placed on the magnetic plate for half an hour. Media was changed after either 20 minutes (lanes "A" in Figure 5.6) as previously described (Buerli *et al.*, 2007) or 24 hours (lanes "B" in Figure 5.6) according to manufacturer's instructions. PMOE4 (GRIA2+261+290) showed a slight inhibition with 7.4% of the sample remaining unedited, while PMOE4B (GRIA2+250+279) did not show any impact on editing. This is a small effect compared to that seen in the HeLa-B13 system, and so the magnetofection conditions were adjusted in an attempt to optimise editing inhibition.

The PMOE4 (GRIA2+261+290) samples showing a slight inhibition in editing did not show any difference at the cDNA level between the media change 20 minutes or 24 hours after magnetofection (lanes A versus B in Figure 5.6). However, visual inspection of the neurons confirmed that the toxicity of the PolyMag reagent was reduced after the shorter exposure to the magnetofection reagent (A), whereas there was pronounced cell death after leaving the reagents on the neurons for 24 hours (B). This media change was therefore incorporated into the magnetofection protocol.

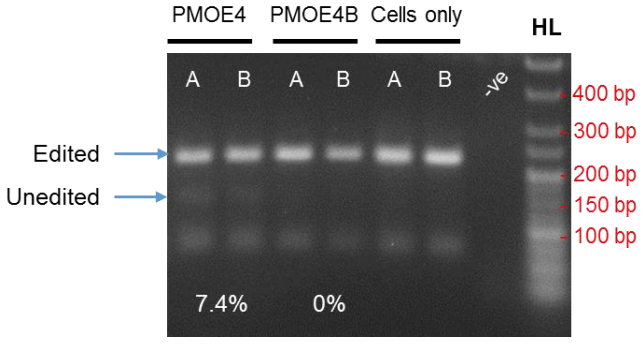

Figure 5.6 - A sample gel image of a 3% agarose gel run in 1X TAE buffer, with 5 µl of Hyperladder V ("HL"; 25 bp, Bioline) visualised using the Ebox VX2 imaging system and quantified using ImageJ analysis."-ve" indicates negative (water) control. Gel shows the initial magnetofection conditions of a 1:1 ratio of PolyMag:L-PMO, changing the media after either 20 minutes (A) or 24 hours (B). Cells were incubated for 48 hours post-magnetofection. Percentages show average Q/R site editing inhibition in each condition, n=2. PMOE4 (GRIA2+261+290) shows 7.4% reduction in Q/R site editing compared to controls.

5.2.2.2 PolyMag versus NeuroMag

As well as the generic magnetofection reagent, other versions are available that have been optimised for specific cell culture systems. PolyMag, although moderately effective, caused a considerable amount of cell death, as seen when the neurons were observed under a microscope. Alternatively, NeuroMag has been developed specifically for primary neuronal cultures, shows low toxicity in primary neuronal cultures and has been shown to transfect primary neurons with an efficiency of around 30% (Wang *et al.*, 2014a). NeuroMag was therefore compared to PolyMag with leashed PMOE4 (GRIA2+261+290) under the same transfection conditions (Figure 5.7). A 1:1 ratio was used for both transfection reagents, and neurons were left for 48 hours post-magnetofection. PolyMag again caused 10% of the sample to remain unedited, whereas there was no effect seen in the samples treated with NeuroMag. Without knowing the exact difference between the two magnetofection reagents, it is difficult to determine the reason for this loss in transfection efficiency. It is possible that, in order to reduce the toxicity in the sensitive primary culture, NeuroMag was made to be a weaker reagent than PolyMag, which would explain the reduced efficacy. We therefore focused on the slight inhibition found using PolyMag with PMOE4 (GRIA2+261+290) and adjusted these conditions, both attempting to improve the inhibition and reduce the cell death. Once the magnetofection conditions had been improved using PMOE4 (GRIA2+261+290), they could then be applied to the other 30mer PMOs.

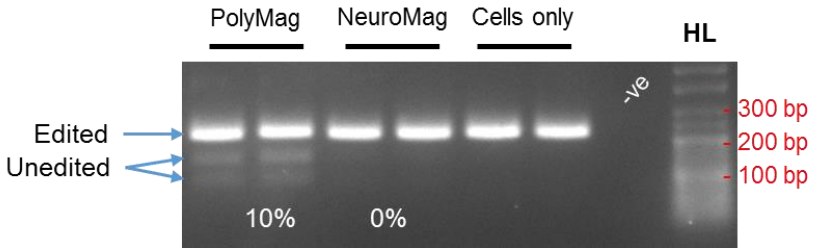

Figure 5.7 - A sample gel image of a 3% agarose gel run in 1X TAE buffer, with 5 µl of Hyperladder V ("HL"; 25 bp, Bioline) visualised using the Ebox VX2 imaging system and quantified using ImageJ analysis."-ve" indicates negative (water) control. Comparison between PolyMag and the primary neuron-specific NeuroMag transfection of PMOE4 (GRIA2+261+290), each at a 1:1 ratio. RNA was extracted after 48 hours and editing quantified. Percentages show average Q/R site editing inhibition in each condition, n=2.

5.2.2.3 *Increasing PMO Concentration and Length of Magnetofection*

One condition that could be optimised is the ratio of PolyMag reagent to L-PMO. Initial conditions used a 1:1 ratio, which had a final concentration of 1 µM of PMO. This is a low concentration which achieved only a 10% reduction in editing in the HeLa-B13 system. However, keeping a 1:1 ratio of PolyMag to L-PMO at higher PMO concentrations leads to large volumes of PolyMag being added to the primary neuronal cultures which would certainly cause cell death. The concentration of L-PMO was therefore increased to 2 µM while keeping the same volume of PolyMag, using a ratio of 1:2. Figure 5.8A shows the results of primary cortical cultures magnetofected at a 1:1 or 1:2 ratio.

As well as increasing the concentration of L-PMO, in an attempt to improve the inhibitory effect of PMOE4 (GRIA2+261+290), the incubation time post-magnetofection was increased from 48 hours to 96 hours (Figure 5.8B). It was hoped that a prolonged exposure of the neurons to the PMOs would lead to more interactions with the GluA2 transcripts and so an increase in RNA editing inhibition. However, as can be seen in Figure 5.8B, the editing inhibition remained marginal. In fact, the samples with a 1:2 ratio of PolyMag to L-PMO after 96 hours show no change in editing at all compared to control samples. Samples with a 1:1 ratio of PolyMag to L-PMO show an improvement compared to those incubated for 48 hours, but inhibition remains marginal at 5%.

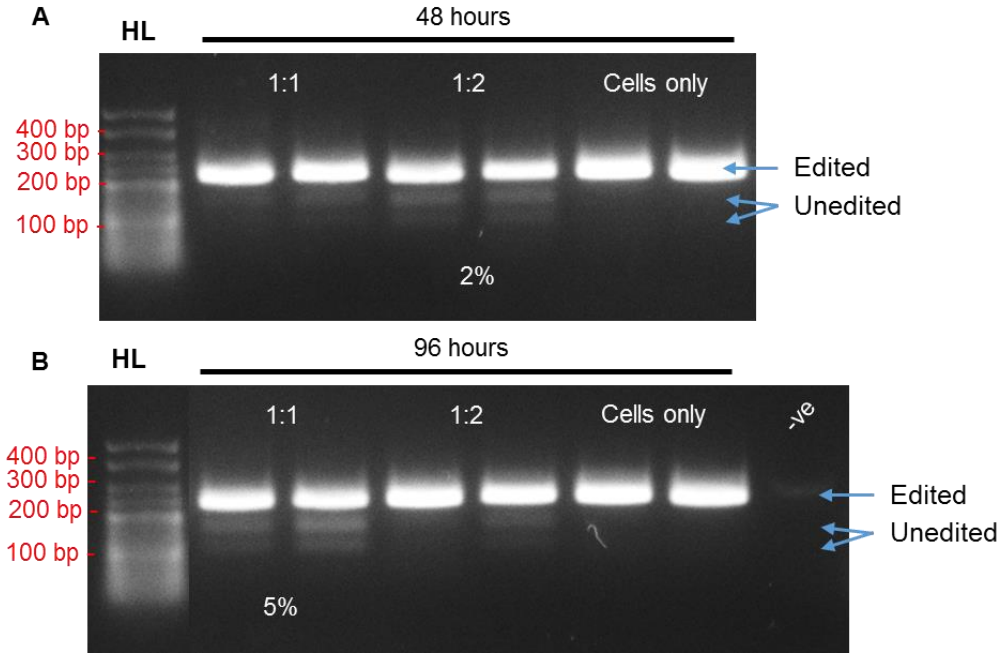

Figure 5.8 - A sample gel image of a 3% agarose gel run in 1X TAE buffer, with 5 µl of Hyperladder V ("HL"; 25 bp, Bioline) visualised using the Ebox VX2 imaging system and quantified using ImageJ analysis."-ve" indicates negative (water) control. Transfection of primary cortical neurons using magnetofection changing the ratio of PolyMag:L-PMO of PMOE4 (GRIA2+261+290) from 1:1 to 1:2 with incubation of either 48 or 96 hours. Percentages show average Q/R site editing inhibition in each condition, n=2.

5.2.2.4 Reducing Concentration of PolyMag and Length of Magnetofection

One possible reason for the low levels of inhibition could be due to the cell death in the cultures following magnetofection. If a large majority of the cells are dying, then any of these neurons where the editing has been affected by the PMO will not be included in the Q/R site editing analysis. Conditions were therefore tested in an attempt to improve cell viability, either by reducing the concentration of PolyMag by half (leading to a 0.5:1 ratio of PolyMag to L-PMO; lanes A in Figure 5.9) or reducing the incubation time post-magnetofection (Figure 5.9). Reducing the time post-magnetofection to 24 hours eliminated any RNA editing inhibition from PMOE4 (GRIA2+261+290), either at 0.5:1 (24 hours lane A; Figure 5.9) or 1:1 ratios (24 hours lane B; Figure 5.9). However, by reducing the ratio of PolyMag to L-PMO to 0.5:1, there was a large increase in editing inhibition after 48 hours with 60% of cDNA remaining unedited (48 hours lane A; Figure 5.9), whereas no change in editing was seen at the 1:1 ratio (48 hours lane B; Figure 5.9). This was accompanied by an increase in cell viability, which appears to be a crucial limiting factor in this model.

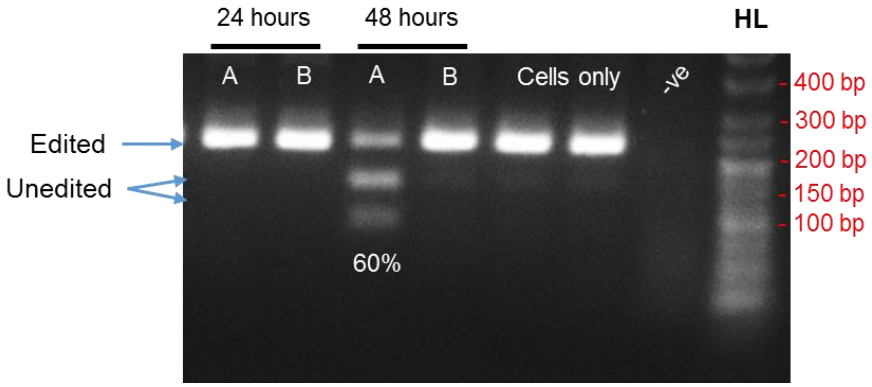

Figure 5.9 – A sample gel image of a 3% agarose gel run in 1X TAE buffer, with 5 µl of Hyperladder V ("HL"; 25 bp, Bioline) visualised using the Ebox VX2 imaging system and quantified using ImageJ analysis."-ve" indicates negative (water) control. Transfection of primary cortical neurons using magnetofection changing the ratio of PolyMag:L-PMO of PMOE4 (GRIA2+261+290) from 0.5:1 (A) to 1:1 (B) with incubation of either 24 or 48 hours. Percentages show average Q/R site editing inhibition in each condition.

5.2.2.5 Increasing Cell Density

In a further attempt to increase cell viability after magnetofection, the density of primary cortical neurons in the plate was increased. Cultures used up to this point had a seeding density of 500,000 cells per well. An increase to 1 million cells per well could improve cell viability as more dense neuronal cultures tend to be more tolerant to harmful reagents. The previously effective conditions of a 0.5:1 ratio of PolyMag to L-PMO, with media changed 20 minutes post-magnetofection and incubated for 48 hours, were used. The results, shown in Figure 5.10, indicate that increasing the neuronal density to 1 million cells per well does improve the editing inhibition, calculated at 14%, compared to 500,000 cells per well with an inhibition of 10% (n=2 per condition). However, these results show a smaller effect on RNA editing compared to the previous magnetofection (Figure 5.9) which showed a 60% reduction in editing, despite using the same conditions here.

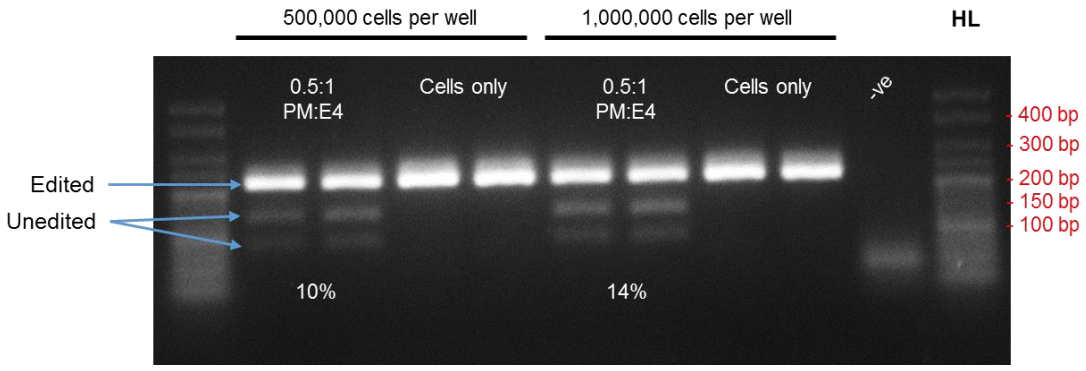

Figure 5.10 – A sample gel image of a 3% agarose gel run in 1X TAE buffer, with 5 µl of Hyperladder V ("HL"; 25 bp, Bioline) visualised using the Ebox VX2 imaging system and quantified using ImageJ analysis."-ve" indicates negative (water) control. Transfection of primary cortical neurons using magnetofection comparing seeding densities between 500,000 and 1,000,000 neurons per well of a 6 well plate (n=2 per condition). Ratio of PolyMag:L-PMO of PMOE4 (GRIA2+261+290) was 0.5:1 with incubation of 48 hours, after which RNA was extracted and editing quantified. Percentages show average Q/R site editing inhibition in each condition.

5.2.2.6 Changing the Magnetofection Time Point

Previous magnetofections were performed on primary cortical neurons that had been in culture for 21 DIV. This is a standard time point for experiments involving receptors, as after three weeks neuronal cultures show robust expression of synaptic markers (Harrill *et al.*, 2015) and respond to stimulation indicating mature synapse formation (Glaum *et al.*, 1990). However, neurons at 21 DIV are also known to be less responsive to transfection than neurons at early time points in culture, and the efficiency of magnetofection decreases by 50% at this time point compared to 7 DIV (Buerli *et al.*, 2007). However, neurons can be transfected at an earlier time point and then allowed to mature further (Wang *et al.*, 2014a). As primary cortical neurons have been shown to be responsive to glutamate after 14 DIV, this time point was also tested in an attempt to improve transfection efficiency. Results in Figure 5.11 show that none of the conditions tested had any effect on editing. Comparisons were made between 500,000 (A) and 1 million (B) cells per well at 14 DIV and 21 DIV, with a 0.5:1 ratio of PolyMag to L-PMO and an incubation of 48 hours. These conditions, which had previously shown transfection leading to an inhibition of Q/R site editing (Figure 5.9; Figure 5.10), now showed no change in editing despite using the same conditions and reagents.

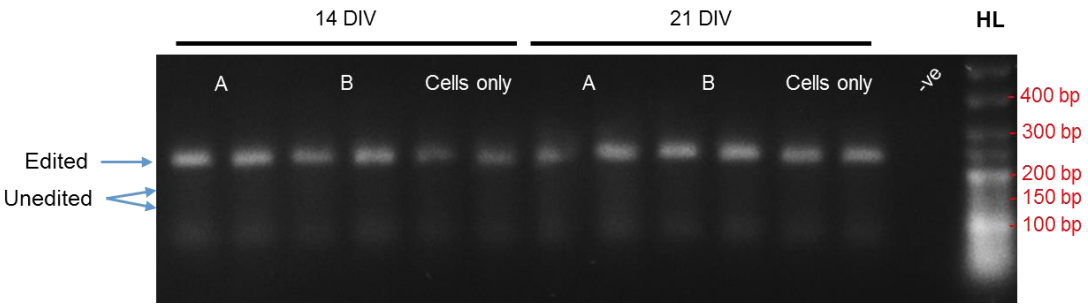

Figure 5.11 – A sample gel image of a 3% agarose gel run in 1X TAE buffer, with 5 µl of Hyperladder V ("HL"; 25 bp, Bioline) visualised using the Ebox VX2 imaging system and quantified using ImageJ analysis."-ve" indicates negative (water) control. Transfection of primary cortical neurons using magnetofection comparing seeding densities between 500,000 (A) and 1,000,000 (B) neurons per well of a 6 well plate (n=2 per condition) at 14 DIV or 21 DIV. Ratio of PolyMag:L-PMO of PMOE4 (GRIA2+261+290) was 0.5:1 with incubation of 48 hours, after which RNA was extracted and editing quantified. Percentages show average Q/R site editing inhibition in each condition.

5.2.2.7 Summary of Magnetofection Conditions

Magnetofection appears to have a better transfection efficiency than Endo-Porter, the transfection reagent produced specifically for PMOs, which didn't show any effect in primary neuronal cultures (Figure 5.6). Several conditions were varied in an attempt to optimise a robust and reliable magnetofection protocol including the ratio of magnetofection reagent to leashed PMO, the length of transfection, the time point of transfection for the neurons *in vitro* and number of seeded neurons. These conditions and the resulting percentage inhibition of Q/R site editing are summarised in Table 5.1.

Although the magnetofection technique did at one point reduce editing by 60%, this result was not reproducible, and often repetition of identical conditions did not result in a change of editing at all. The conditions resulting in an inhibition of editing to 60% were a 0.5:1 ratio of PolyMag to leashed PMOE4 (GRIA2+261+290) magnetofected into neurons seeded at 1,000,000 cells per well at 21 DIV and incubated for 48 hours (Figure 5.9). However, when these conditions were repeated in successive magnetofections, Q/R site editing was inhibited by 14% (Figure 5.10) and <1% (Figure 5.11). Several conditions showed a decrease in editing by around 10%, but were not replicable in successive biological repeats. Magnetofection therefore appears to have the potential to introduce PMOs into neurons, but this system for delivery is not reliable enough to allow for the analysis of downstream intracellular effects of reduced Q/R site editing.

Figure Number	Magnetofection Reagent	Leashed PMO	Ratio (Mag. Reagent: Leashed PMO)	Length of Transfection (hours)	Time Point of Magnetofection (DIV)	Seeded Neurons per Well	Average Q/R Site Editing Inhibition (%)
5.7	PolyMag	PMOE4 (GRIA2+261+290)	1:1	48	21	1,000,000	7.4
	PolyMag	PMOE4B (GRIA2+250+279)	1:1	48	21	1,000,000	<1
5.8	PolyMag	PMOE4 (GRIA2+261+290)	1:1	48	21	1,000,000	10
	NeuroMag	PMOE4 (GRIA2+261+290)	1:1	48	21	1,000,000	<1
5.9	PolyMag	PMOE4 (GRIA2+261+290)	1:1	48	21	1,000,000	<1
	PolyMag	PMOE4 (GRIA2+261+290)	1:2	48	21	1,000,000	2
	PolyMag	PMOE4 (GRIA2+261+290)	1:1	96	21	1,000,000	5
	PolyMag	PMOE4 (GRIA2+261+290)	1:2	96	21	1,000,000	<1
5.10	PolyMag	PMOE4 (GRIA2+261+290)	0.5:1	24	21	1,000,000	<1
	PolyMag	PMOE4 (GRIA2+261+290)	1:1	24	21	1,000,000	<1
	PolyMag	PMOE4 (GRIA2+261+290)	0.5:1	48	21	1,000,000	60
	PolyMag	PMOE4 (GRIA2+261+290)	1:1	48	21	1,000,000	<1
5.11	PolyMag	PMOE4 (GRIA2+261+290)	0.5:1	48	21	500,000	10
	PolyMag	PMOE4 (GRIA2+261+290)	0.5:1	48	21	1,000,000	14
5.12	PolyMag	PMOE4 (GRIA2+261+290)	0.5:1	48	14	500,000	<1
	PolyMag	PMOE4 (GRIA2+261+290)	0.5:1	48	14	1,000,000	<1
	PolyMag	PMOE4 (GRIA2+261+290)	0.5:1	48	21	500,000	<1
	PolyMag	PMOE4 (GRIA2+261+290)	0.5:1	48	21	1,000,000	<1

Table 5.1 - Summary of magnetofection conditions tested and calculated inhibition of Q/R site editing in primary cortical neuron cultures.

5.2.3 Transductions using Lentiviral Vectors

Lentiviral vectors are an efficient transduction system that harness the properties of the HIV-1 virus to transfer genetic material into cells, and have been shown to efficiently transfer genes into post-mitotic neurons with low cytotoxicity and high efficiency (reviewed in Hutson *et al.*, 2014). Lentiviral vectors can also be adapted with mutations in their integrase enzyme, forming integration-deficient vectors able to stably transduce neurons *in vitro* and *in vivo* without introducing genetic material into the host's genome (Yáñez-Muñoz *et al.*, 2006). Here, a third generation integration-deficient lentiviral vector system was used, with the HIV-derived genome split into three vectors to improve safety (Dull *et al.*, 1998). The sequence of PMOE4 (GRIA2+261+290) was taken and inserted into a transfer plasmid under a U6 promoter, which when co-transfected with the packaging and envelope vectors in HEK293T cells combined and produced a lentivirus containing the PMOE4 (GRIA2+261+290) sequence to be expressed under a U6 promoter.

5.2.3.1 Cloning Strategy

The LentiGuide-Puro plasmid was purchased from AddGene (Plasmid #52963) and was originally designed to produce guide RNAs for the CRISPR-Cas9 system (Sanjana *et al.*, 2014). The plasmid contains a filler region flanked by *BsmBI* cut sites which can be removed and replaced with the desired oligo sequence. Figure 5.12A shows the plasmid map for LentiGuide-Puro plasmid. The plasmid backbone was checked using restriction endonucleases with a known number of cut sites within the sequence (Figure 5.12B). Digestion using the *BsmBI* restriction endonuclease removed the filler sequence, leaving the two digest fragments of the backbone with 8,309 base pairs and the filler sequence of 1,873 base pairs. The *XmaI* endonuclease only has one cut site within the plasmid and so digestion with this enzyme linearised the plasmid. The *SapI* enzyme has three cut sites on the plasmid creating digest fragments of 6,183, 2,828 and 1,171 base pairs (Figure 5.12B).

Once the plasmid backbone had been confirmed, the PMOE4 (GRIA2+261+290) sequence could be cloned into the plasmid using the annealed oligo cloning technique, summarised in Figure 5.13. PMOE4 (GRIA2+261+290) was chosen for this stage as it gave the highest inhibition in primary neurons using the magnetofection technique and in the HeLa-B13 system. The base sequence from PMOE4 (GRIA2+261+290) and its complementary sequence were taken and the overhangs from a *BsmBI* digest were added. These oligos could then be hybridised. The plasmid backbone was digested with *BsmBI* and run on an agarose gel. The plasmid backbone without the filler sequence was extracted and the DNA ligated with the annealed oligos. The complete plasmid could

be checked for complete insertion using specific restriction endonucleases. By removing the filler sequence from the plasmid, both of the *BsmBI* sites and one *SapI* site were destroyed. Correct ligation of the E4 (GRIA2+261+290) sequence introduced one *NcoI* recognition site, along with one already found in the plasmid backbone. An *NcoI* digest would therefore give digest fragments of 4,938 and 3,388 base pairs. These digest checks were performed on the ligated plasmid and the resulting gel image is shown in Figure 5.14.

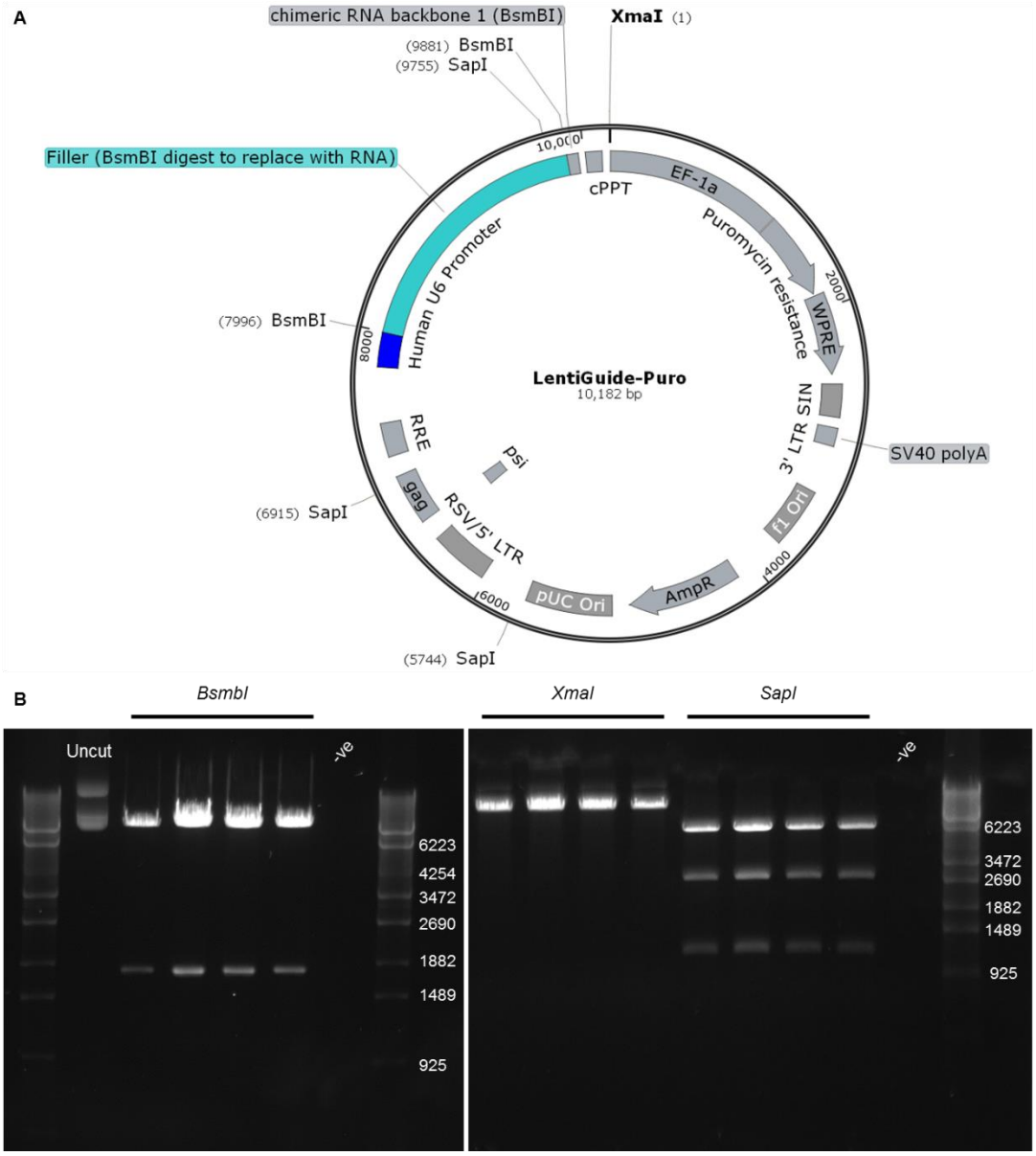

Figure 5.12 – (A) Plasmid map for lentiGuide-Puro plasmid. Filler sequence flanked by BsmBI cut sites shown in light blue. Sequences inserted between BsmBI cut sites are preceded by a human U6 promoter. (B) A sample gel image of a 1% agarose gel run in 1X TAE buffer visualised using the Ebox VX2 imaging system. The gel shows the results of a restriction digest of LentiGuide-Puro confirming that the BsmbI cut sites are intact (two cut sites, predicted bands of 8,309 + 1,873 bp) and that the plasmid backbone is as expected with XmaI (one cut site, plasmid is linearised) and SapI (three cut sites, predicted bands of 6,183 + 2,828 + 1,171 bp). Phage Lambda DNA StyI size markers shown on the right of each gel.

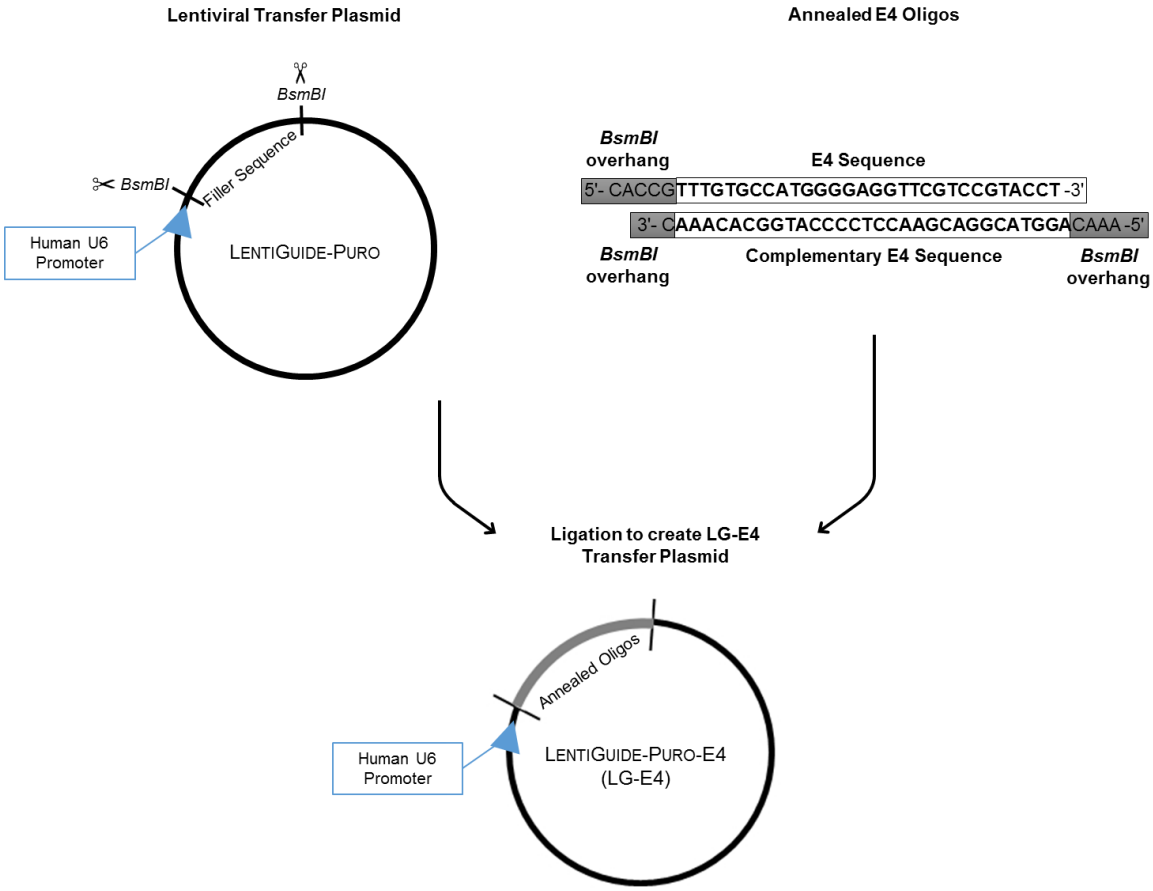

Figure 5.13 - Cloning strategy for the development of a vector containing the PMOE4 (GRIA2+261+290) sequence. Sequence from PMOE4 (GRIA2+261+290) was synthesised as an oligo, along with its complementary sequence, BsmBI overhangs were added and the two oligos hybridised. LentiGuide-Puro plasmid was digested using the BsmBI enzyme, and the linearised plasmid was ligated to the annealed oligos.

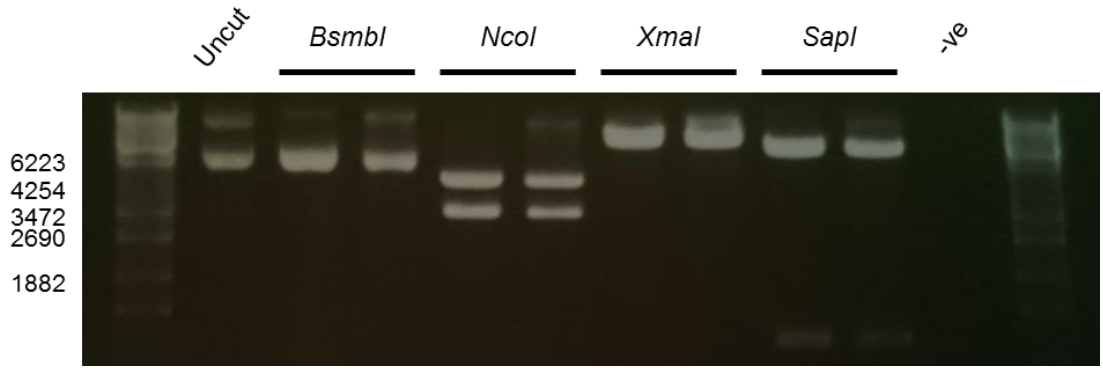

Figure 5.14 – A sample gel image of a 1% agarose gel run in 1X TAE buffer visualised using the Ebox VX2 imaging system. Diagnostic digest of two plasmid vectors obtained from two mini prep cultures. BsmBI sites and one SapI have been destroyed. One NcoI site introduced in the PMOE4 (GRIA2+261+290) sequence, with one in the backbone, gives two digest fragments (4,938 + 3,388 bp) indicating that both plasmids contain the correct inserts. Phage Lambda DNA StyI size markers shown on the left.

Following the positive checks on the plasmid using restriction endonuclease digests, the transfer plasmid was sequenced to confirm the insertion of the PMOE4 (GRIA2+261+290) sequence in the correct site. Figure 5.15 shows the sequencing results, confirming that the LG-E4 plasmid contains the E4 (GRIA2+261+290) oligo. Once the ligation was confirmed to be successful, the integration-deficient lentiviral vector was synthesised by co-transfecting feeder cells with all plasmids and harvesting the virus from the supernatant. The virus was then purified and titred. An integration-deficient lentiviral vector was used as integration of the E4 sequence was not necessary, and instead the sequence could be transcribed into short sequences of RNA.

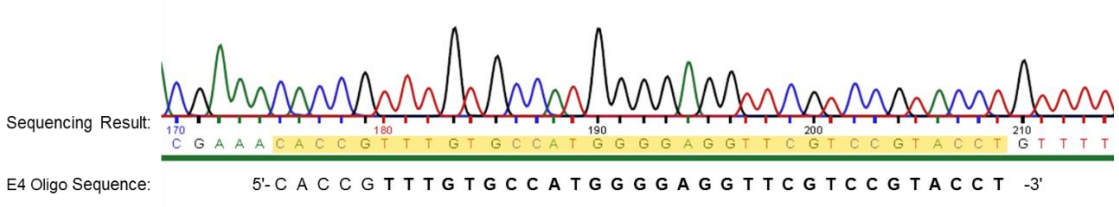

Figure 5.15 - Sequencing chromatograms from LG-E4 ligation using forward primers in the U6 promoter sequence. E4 (GRIA2+261+290) sequence was confirmed to be within the plasmid, following the U6 promoter.

5.2.3.2 GFP Transductions

To test for the appropriate multiplicity of infection (MOI) for efficient transduction of primary cortical neurons, a range of MOIs were tested in primary cortical neurons at 21 DIV. Transduction of lentiviral vectors into primary neuronal cultures are usually performed either at the time of plating or at 1 DIV (Bender *et al.*, 2007; Cisterni *et al.*, 2000). However, at this stage the neurons are undifferentiated, and expression of the GluA2 subunit is not stable until 12 DIV (Orlandi *et al.*, 2011). Therefore at 21 DIV, relatively high MOIs were tested using a lentiviral vector expressing the green fluorescent protein (GFP). GFP is often used as a reporter gene for expression (Kain *et al.*, 1995) due to its easy visual readout of transfection efficiency, as successfully transduced neurons will overexpress GFP and the fluorescence can be detected under the microscope in the 488 nm channel. The plasmid map for the GFP-expressing transfer vector is shown in Figure 5.16. The GFP gene is under the CMV promoter, which has been previously reported to show moderate expression in primary neuronal cultures (Boulos *et al.*, 2006).

Primary cortical neurons at 21 DIV were transduced using the GFP-expressing lentiviral vector and incubated for 48 hours. A range of MOIs from 5 to 25 were tested to determine the optimum conditions for this system. At an MOI of 5, neurons showed a low level of transduction (Figure 5.17A-C). Qualitative comparison of the merge of GFP and bright field and images indicate a transduction efficiency of roughly 50% in the 10 and 25 MOI conditions (Figure 5.17F, I), whereas there was a much lower transduction efficiency at 5 MOI (Figure 5.17C).

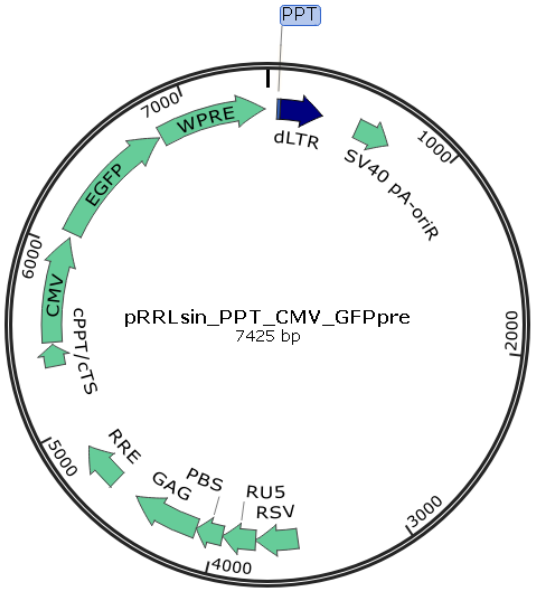

Figure 5.16 - Plasmid map for the GFP-expressing transfer vector. The GFP gene is under the CMV promoter.

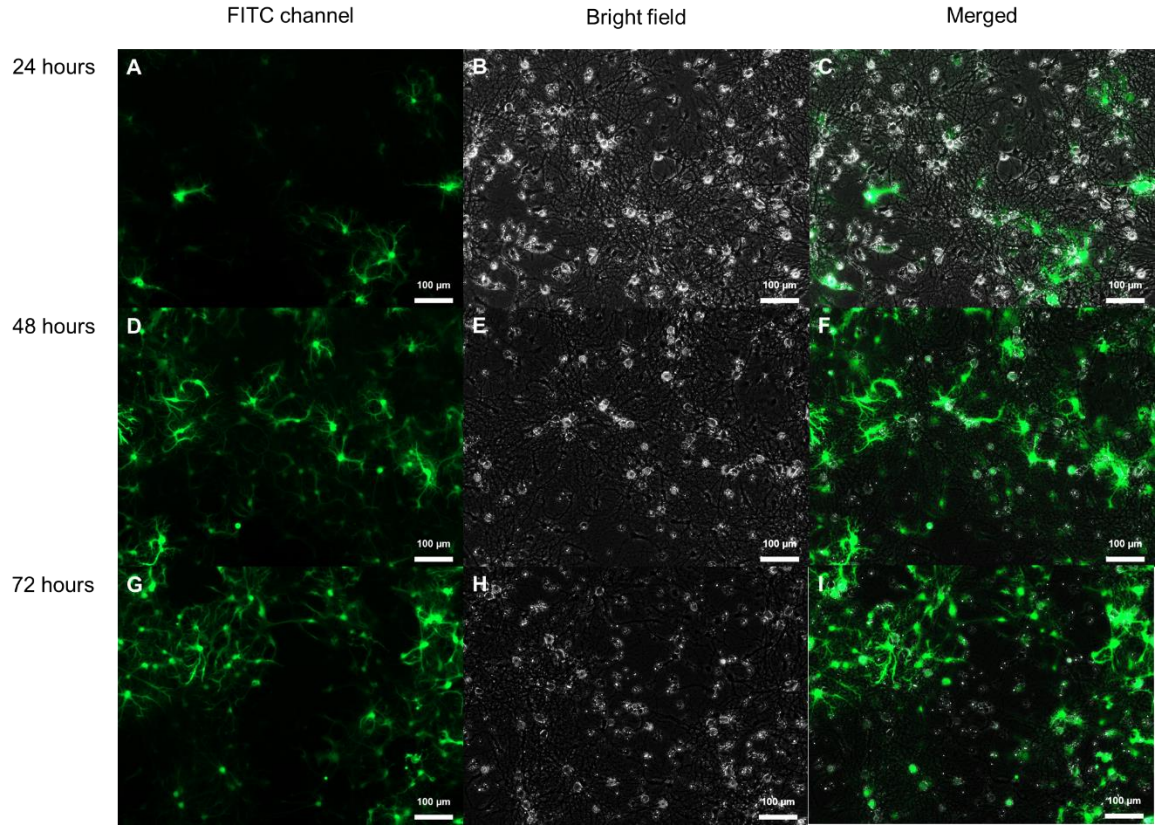

Figure 5.17 - Comparing MOIs of lentiviral vector expressing GFP in primary neuronal culture. Primary neurons were transduced with 5 MOI (A, B, C), 10 MOI (D, E, F) and 25 MOI (G, H, I). Images taken in FITC channel (A, D, G) and bright field (B, E, H) were merged to compare transduced neurons to those that have not taken up the GFP-expressing viral vector.

5.2.3.3 LG-E4 and Q/R Site Editing

Based on the GFP expression from the neurons transduced with a GFP-expressing lentiviral vector, neurons were transduced at 21 DIV across the same range of MOIs. Neurons transduced with the LG-E4 vector were compared to those transduced with the GFP vector as a control and neurons only. RNA was extracted and Q/R site editing was measured as before. Figure 5.18 shows the results of the Q/R site editing analysis. There was apparently no change in Q/R site editing after transduction with the LG-E4 vector at any of the MOI ranges, as seen by the absence of bands at the unedited position. This was repeated twice with the same results found.

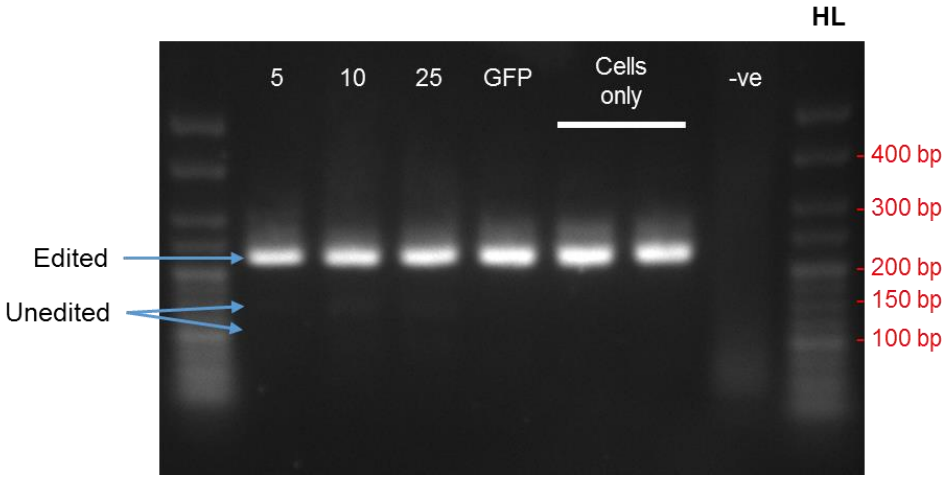

Figure 5.18 - A sample gel image of a 3% agarose gel run in 1X TAE buffer, with 5 µl of Hyperladder V ("HL"; 25 bp, Bioline) visualised using the Ebox VX2 imaging system and quantified using ImageJ analysis."-ve" indicates negative (water) control. Transduction of primary cortical neurons at 21 DIV using MOIs of 5, 10 and 25 of the LG-E4 lentiviral vector. RNA was extracted after 48 hours and Q/R site editing quantified, with no observed change in editing status.

5.3 DISCUSSION

In this chapter, attempts were made to introduce the PMOs, or the equivalent sequence in to be transcribed in RNA form, into primary neuronal cultures. Three methods were tested: using the Endo-Porter transfection reagent which had success in previous cell models, an alternative transfection method called magnetofection and designing a lentiviral vector to overexpress the sequence as RNA. Test transfections using Endo-Porter with the fluorescent PMO appeared to successfully localise the PMO to the neurons, in particular to the cell body. However, subsequent transfections using this method with the PMOs targeting the double-stranded region of the GluA2 transcript had no effect on editing at the Q/R site. The alternative transfection method, magnetofection, showed some change to Q/R site editing, but this was unreliable as transfections using identical conditions gave variable resulting inhibition of Q/R site editing. The final strategy was to create a lentiviral vector containing the antisense sequence of PMOE4 (GRIA2+261+290) under the human U6 promoter. This would then be overexpressed as RNA transcripts which would perform the same function as the PMOs. However, despite the neurons showing good transduction of a vector expressing GFP, again there was no change in Q/R site editing after transduction with the LG-E4 vector.

These results are disappointing but perhaps not unexpected. As previously mentioned, primary neuronal cultures are notoriously difficult to transfect, despite multiple methods being available (Karra & Dahm, 2010). Although Endo-Porter was specifically designed for use with PMOs, these results show it is not effective in primary neuronal cultures. Endo-Porter was developed based on a number of peptides previously shown to cross animal cell membranes due to basic and amphiphilic sections of amino acids such as the HIV protein tat (Mann & Frankel, 1991). Synthetic versions of these peptides were made containing a lipophilic face of leucines and lysines, which were even more efficient at penetrating cell membranes (Summerton, 2005). However, these peptides showed high cell toxicity, possibly due to alterations to the permeability of the cell membrane. Focus then changed to indirect delivery into the cell through endosomes, thereby not compromising the permeability of the cell membrane. The PMO would be leashed to a complementary section of anionic DNA, which would then form a stable complex with polyethyleneimine (PEI). PEI could then bind to the plasma membrane and be endocytosed, along with the bound PMO, after which the PEI would be ionised causing permeabilisation of the endosome membrane and movement of the PMO from the endosome into the cytosol (Morcos, 2001). However, PEI has reduced activity in the presence of serum and shows some cell toxicity. Therefore Endo-Porter was developed, with the aim to make a transfection reagent with high efficiency in the presence of serum, simplifying cell culture practice, and with reduced cell toxicity. Endo-Porter is a short

peptide based on the indirect, endocytosis-based delivery system with a lipophilic face and a weak-base face with a lysines in the sequence to improve solubility, and was shown to permeabilise membranes at the lower pH associated with endosomes but showed no permeabilisation at the neutral pH found at the cell membrane therefore reducing cell toxicity (Summerton, 2005). However, it is unclear how Endo-Porter recruits the neutrally-charged PMOs to the membrane, as most transfection reagents rely on the charged nature of the DNA particles. It is possible that the transfection is reliant on the increased endocytosis caused by Endo-Porter and the PMO being in a high enough concentration in the media to have collected near the cell membrane. Images taken after transfection with the fluorescently-tagged PMO showed the PMO collecting near the cell body of the neurons (Figure 5.4). However, there is no evidence that the PMO has actually entered the neuron, as similar images would be seen if the PMO were simply bound to the membrane. If the PMO were collecting at the membrane rather than being endocytosed, this could account for the lack of inhibition of Q/R site editing. Equally, assuming the PMO has entered the cell, it is unclear from the images whether it reaches the nucleus of the neuron. The PMO may be collected in endosomes rather than being free in the cytosol. Ideally, counter-staining for nuclear markers would give more indication as to the location of the PMO. However, the neutral charge of the PMO means that it is not held by fixing agents and so fixed cells will not retain the PMO in the correct cellular compartment for analysis.

A different version of Endo-Porter, suspended in aqueous solution rather than DMSO, was used compared to previous chapters in an attempt to reduce cell toxicity. This change in transfection reagent may have had an effect on the efficiency of the reagent itself. There are very few reported studies using Endo-Porter in aqueous solution as opposed to in DMSO, mainly *in vivo* experiments in sheep (Wang *et al.*, 2014b). This may be due to the low toxicity of Endo-Porter in DMSO for most cell types, so researchers do not need to use a less-toxic version. However, this means that it is difficult to determine whether aqueous Endo-Porter is equally effective at the same concentrations. Here, the same concentration was used as previously in the HeLa-B13 system and in SH-SY5Y cells. However, the lack of effect may have been due to reduced efficiency, and so higher concentrations of aqueous Endo-Porter could be explored.

Magnetofection of the PMOs was partially successful, in that a reduction in editing was achieved under some conditions. The method of magnetofection has previously been reported by two separate groups to successfully transfect DNA and shRNAs into neurons. The first group transfected primary hippocampal neurons (Buerli *et al.*, 2007) while the second used primary motor neurons from the spinal cord (Fallini *et al.*, 2010). Although both are using the same magnetofection technique, their protocols vary

significantly. Buerli et al. use the CombiMag reagent with additional Lipofectamine 2000 while Fallini et al. use NeuroMag, the magnetofection reagent specifically designed for use with primary neurons. In the experiments conducted in this chapter, magnetofection using NeuroMag was not found to have any effect on the RNA editing while Lipofectamine in combination with magnetofection was not tested due to the known toxicity of Lipofectamine and its low transfection efficiency (Ohki *et al.*, 2001). These two papers also varied in age of neurons transfected, with the hippocampal neurons being transfected between 10 and 21 DIV and the motor neurons being transfected at 2 DIV. Buerli et al. used a ratio of 1 µg plasmid DNA to 2 µl of 1:10 diluted CombiMag to 2 µl Lipofectamine, while Fallini et al. used a ratio of 0.5 µg DNA to 1.75 µl NeuroMag. Results in this chapter show varied results in response to changing the L-PMO to PolyMag ratio, with a 0.5:1 ratio giving the largest change in RNA editing (Figure 5.9). Buerli et al. left the neurons on the magnet for 25 minutes following no change in media while Fallini et al. left the neurons on the magnet for only 15 minutes with a change of media after one hour. The results in this chapter also support a change of media after incubation on the magnet, as this reduced cell toxicity. The largest change in Q/R site editing seen in this chapter was under the conditions of 21 DIV, a 0.5:1 ratio of L-PMO to PolyMag, with a media change 20 minutes post-transfection and then incubation of 48 hours (Figure 5.9). These conditions are within the range set by the two previous studies on magnetofection. The differences between methods from these two papers and those reported in this chapter may be due to the different populations of neurons, as this chapter looks at the transfection of cortical neurons rather than hippocampal or motor neurons. However, the results from this chapter found that the method of magnetofection does not produce reliable results. The same conditions on successive experiments would alternatively show a change in editing and then show no change at all. This unreliability indicates that this method would not be useful to study the downstream effects of inhibited Q/R site editing, as it is not reproducible over successive biological repeats.

One limitation in the magnetofection protocol is that the PMOs need to be leashed to charged DNA fragments so that they can properly interact with the magnetic nanoparticles. Once the magnetic nanoparticles have bound to the leashed PMO, they are then pulled onto the neuron and endocytosed. However, although this is an additional step compared to transfection using Endo-Porter, leashing of PMOs has previously been reported to transfect muscle cells using Lipofectamine (Gebski *et al.*, 2003). Another factor in this magnetofection reaction is that there is no additional transfection reagent increasing the permeability of the neuronal membrane, instead the method is reliant on the collection of the L-PMO-magnetic nanoparticle complex on the cell membrane in the cell's natural endocytosis mechanisms. This is the reason for the combination approach of magnetofection reagent CombiMag with Lipofectamine 2000, as seen in Buerli et al.

However, as mentioned previously, transfection reagents such as Lipofectamine 2000 are known to be toxic to primary neurons, and so although they can be used in combination with PolyMag for increased transfection efficiency, they could not be used in this context. Due to the lack of additional transfection reagent, this then leads to the question of how the leashed PMO enters the cell at all, as the magnetic nanoparticles will only concentrate them onto the membrane. Clearly some PMOs have entered the primary neurons, as a small change in Q/R site editing was achieved. However, the variability seen in the results may be a reflection on this reliance of endogenous endocytosis mechanisms.

It was hoped that lentiviral vectors would solve the issue of introducing the antisense sequence into the primary neuronal cultures. Lentiviral vectors are an excellent tool for the transfer of genetic material and have been shown to transduce post-mitotic primary cortical neurons at high efficiency (Zhang *et al.*, 2006), with promising use as therapies for neurodegenerative diseases (reviewed in Hutson *et al.*, 2014). The vectors used in this chapter were third generation lentiviral vectors, with the necessary genes for production of the virus split over three plasmids: the packaging plasmid, envelope plasmid and the transfer plasmid containing the desired sequence. Lentiviral vectors have previously been used to express shRNAs under the same human U6 promoter for the purposes of knockdown of gene expression (Van den Haute *et al.*, 2003). The vector backbone used in this chapter was previously created for use in the CRISPR-Cas9 system to express guide RNAs in target cells, and has since been used effectively (Sanjana *et al.*, 2014). The major change in this strategy was that the sequence is no longer in the form of a PMO, but would now be single-stranded RNA transcripts binding to the GluA2 transcript. The positive control for successful transduction used a lentiviral vector that expressed GFP, which showed good expression at 10 and 25 MOI at 21 DIV. GFP expression was driven by the CMV promoter, which has previously been reported to give transduction efficiencies of more than 50% (Bender *et al.*, 2007). However, the LG-E4 RNA was under the human U6 promoter, which is commonly used for siRNA expression in lentiviral systems and has shown high expression in neurons (Mäkinen *et al.*, 2006). This change in promoter between the two vectors may mean that the good transduction seen with GFP was not replicated with the human U6 promoter in the LG-E4 vector. An alternative positive control would be to tag the E4 (GRIA2+261+290) sequence itself with the GFP construct. However, this would inhibit binding of the RNA to the GluA2 subunit, so a vector without the GFP insert would still need to be used. Due to these limitations in a GFP-tagged RNA sequence, the output of a positively transduced sample was a change in Q/R site editing.

From the conditions used here, there was no impact on Q/R site editing following LG-E4 transduction. It may be possible to induce inhibition of RNA editing through changing the transduction conditions. Polybrene is often used to improve lentiviral transduction, but is known to be toxic to neurons so cannot be used in this case (Peluffo *et al.*, 2012). To improve transduction, higher MOIs may be used. The highest MOI used in this study was 25. As no cell death was seen at this MOI, this range could be increased first in a toxicity assay to check that the neurons can tolerate this high MOI followed by the Q/R site editing assay. Ultimately, following this pilot study, a log range of MOIs will be tested to ascertain the efficient transduction conditions for primary cortical neurons. Caffeine may also be used during production of the lentiviral vector, which has been reported to increase the titre of viral production up to 8 fold (Ellis *et al.*, 2011). Through increasing the titre, higher MOIs may be used in transduction allowing an increased expression of the E4 sequence.

Alternatively, transductions at different time points could be investigated. The neurons in this study were transduced at 21 DIV, whereas transductions at much earlier time points such as 4 DIV have been reported (Zhang *et al.*, 2006). Earlier transductions with the LG-E4 vector could be investigated, although at this stage the neuronal cultures are more vulnerable as they have not yet formed networks. A range of MOIs would again need to be investigated at this early time point to assess the correct level for minimal toxicity. Once the lentiviral vector is within the neurons, the cultures could be maintained for several weeks to observe changes in Q/R site editing at a later stage. Alternatively, it may be that the human U6 promoter is not working in this system and there is no expression of E4 (GRIA2+261+290) RNA. The human U6 promoter has been found to be more effective at expressing shRNA than the murine equivalent, even in murine cells, and so changing species of the U6 promoter would be unlikely to change the outcome (Roelz *et al.*, 2010). Other promoters that are used to express short RNA sequences such as siRNAs and shRNAs in lentiviral vectors include the U1 promoter (Denti *et al.*, 2004) or the U7 promoter (Goyenvalle *et al.*, 2009). Use of either of these promoters may increase the effect of E4 (GRIA2+261+290) RNA in the neurons, although there are some reports that these promoters have similar expression patterns (ter Brake *et al.*, 2008).

Attempts at transfection and transduction of primary neurons in this chapter were made once the neurons had already been plated and networks had begun to be established. This was so that the PMO could interact with the GluA2 subunit once it had been expressed stably at around 12 DIV (Orlandi *et al.*, 2011). Methods such as nucleofection, which must be carried out before the neurons are plated, were discounted for this reason. However, the backbone chemistry of the PMO renders it resistant to nuclease activity,

and as such can remain in cells for long periods of time without being degraded. Additionally, neurons are post-mitotic, and so any transfection performed on the day of plating should not be diluted by successive cell divisions. Considering these points, nucleofection of primary neurons with a leashed PMO at 0 DIV, then plating them and allowing them to mature, may be an alternative method worthy of investigation.

6 EXON SKIPPING OF THE ALUJ CASSETTE

6.1 INTRODUCTION

Splicing of the introns in an RNA transcript is a process carried out by the spliceosome, a ribonucleoprotein megaparticle formed from multiple small nuclear ribonucleoproteins (snRNPs) and associated splicing factors that bind to the RNA and carry out the intron excision (reviewed in Lee & Rio, 2015). The way that the spliceosome recognises the difference between exons and introns is still not completely understood. There are two possibilities: the spliceosome either recognises the introns to be spliced out ("intron definition") or the exons to be ligated together ("exon definition"). If the splicing factors recognise the intron, and the basal machinery is placed across the intronic regions, then this would put a limit on the length of introns. Evidence suggests that intron definition is the more ancient mechanism, as single-celled organisms such as yeast have introns in general no longer than 350 nucleotides (Ram & Ast, 2007). In exon definition, the basal splice machinery is placed over the exon. This limits the length of exons and frees introns to extend for several kilobases as is seen in multicellular organisms (Ram & Ast, 2007). It may be that the extension of introns through evolution forced the spliceosome to instead recognise the exon, shifting the definition away from intronic definition (Robberson *et al.*, 1990). The average length of the vertebrate exon is 170 bases, and if the exon is extended beyond 300 bases then cryptic splice sites may be activated within the exon or the exon may be skipped altogether as the splice machinery cannot span the exon, further supporting the idea of exon definition (Robberson *et al.*, 1990).

The splicing reaction begins with the assembly of the spliceosome around the premRNA transcript. U1 snRNP is initially recruited to the 5' splice site due to its recognition of the consensus sequence. Other splice factors become involved, such as BBP (Branch point Binding Protein) interacting with the branch point within the intron and U2AF65/U2AF35 interacting with the 3' splice site, forming the E complex (Figure 6.1 part 2). The U2 snRNP then stably interacts with the branch point, displacing the BBP/U2AF splice factors and forming the A complex (Figure 6.1 part 3). The U4.U5.U6 tri-snRNPs recognise and bind to the 5' splice site, forming the pre-catalytic B complex (Figure 6.1 part 4), before U1 and U4 snRNPs destabilise and the activated B complex is formed (Figure 6.1 part 5) which catalyses the first transesterification reaction. Complex C is then reached (Figure 6.1 part 6) which completes the final esterification reaction of splicing.

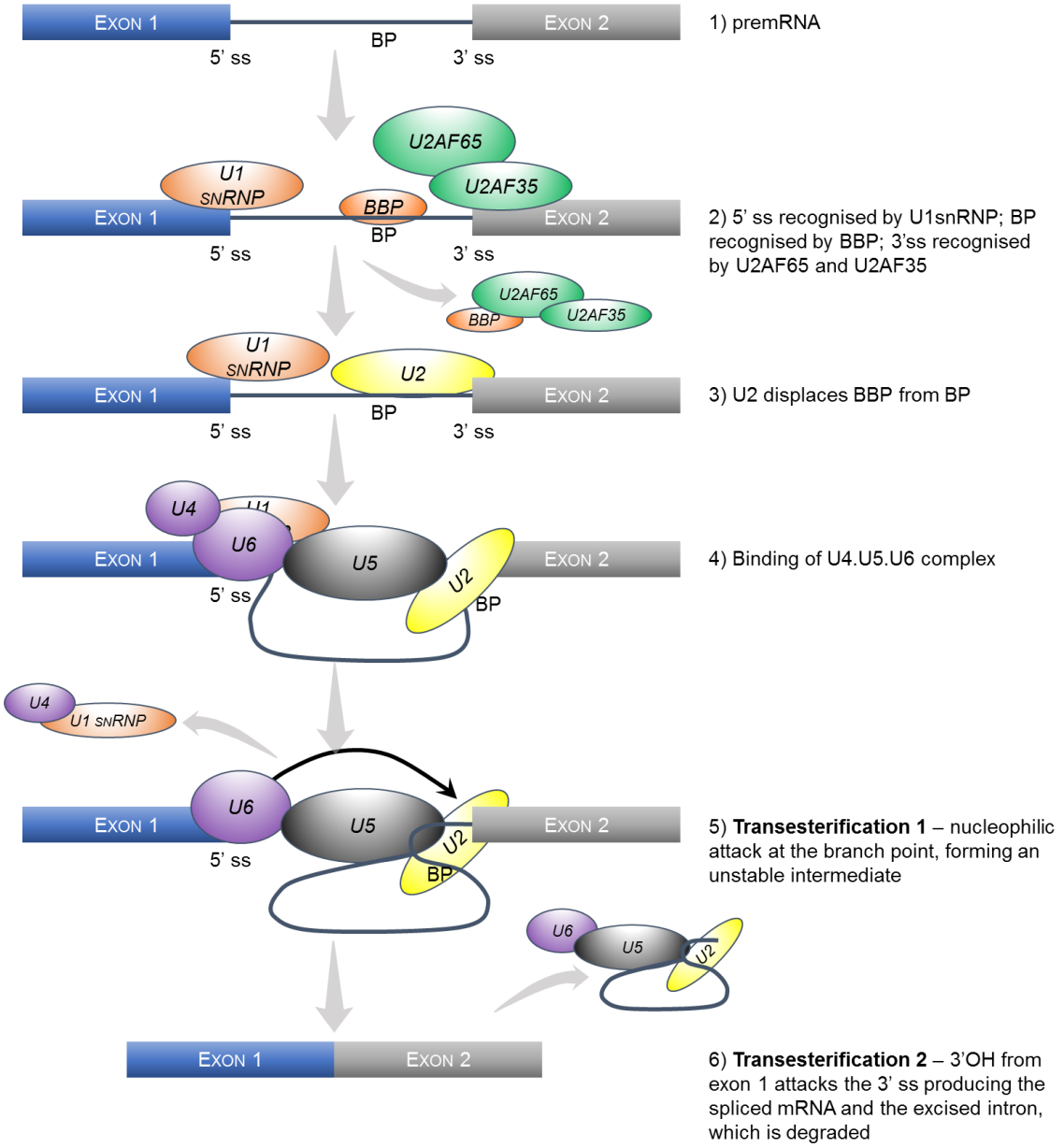

Figure 6.1 - Summary of the recruitment and action of the spliceosome. 5' ss = 5' splice site. 3' ss = 3' splice site. BP = branch point. BBP = Branch point Binding Protein. Small nuclear ribonucleoproteins (snRNPs) U1, U2, U4, U5 and U6 as well as auxiliary factors U2AF64 and U2AF35 form the spliceosome. Diagram adapted from (Kornblihtt *et al.*, 2013; De Conti *et al.*, 2013).

The spliceosome itself, containing the necessary snRNPs and associated splicing factors, has been isolated from mammalian cells with other splice regulatory elements in a huge complex called the supraspliceosome which also contains other RNA processing components such as those for 3'-end processing (Raitskin *et al.*, 2002) and RNA editing (Raitskin *et al.*, 2001). Structural analysis shows four active spliceosomes within the supraspliceosome connected to the same premRNA transcript and therefore able to process four introns simultaneously (Azubel *et al.*, 2006), and may play a part in regulation of alternative splicing by recruiting the appropriate splice regulatory elements (Sebbag-Sznajder *et al.*, 2012).

Splicing at a given junction may be constitutive, i.e. present in all transcripts, or alternative, i.e. only present in some transcripts, allowing different RNA sequences and therefore variation in proteins (Siva *et al.*, 2014). There are several events that can be classified as alternative splicing: an exon may be "skipped" or an intron retained in the mRNA sequence; there may be mutually exclusive exons of which only one or the other is found within a transcript; there may be alternative 3' splice sites, 5' splice sites or 3' untranslated regions as well as alternative first and last exons.

Splice sites can be defined as either "strong" or "weak", depending on their similarity to the consensus sequence, which is a sequence of 9 bases at the 5' splice site and 15 bases at the 3' splice site that are sufficient to ensure splicing takes place (Roca *et al.*, 2005). The consensus sequence for the 5' splice site is the exact complementary sequence for the U1 snRNP, which is required for the assembly of the splicing machinery (Figure 6.1), while the 3' splice site and branch point consensus sequences are more loosely defined (De Conti *et al.*, 2013). Each splice site can be ranked according to its similarity to the consensus sequence, and the more similar the sequence is, the more likely the site is to be spliced. However, a splice site does not necessarily need to completely match the consensus sequence to be functional. Indeed, out of 5,000 constitutively expressed exons examined, less than 5% matched the consensus perfectly (Chasin, 2007). The presence of pseudo-splice sites (sequences that are similar to or match the consensus but are not spliced) or cryptic splice sites (sequences that become spliced when the natural splice site is inactivated) further support the idea that there are factors governing the use of a splice site other than its similarity to the consensus sequence. For example, an exon in the human genome is more likely to be included in the mRNA transcript if it is flanked by shorter introns (Fox-Walsh *et al.*, 2005).

Other factors that can help determine whether a splice site is used or not are called splice regulatory elements and can take the form of either *cis*-acting or *trans*-acting. *Cis*-acting elements are regulatory sequences in the RNA that recruit RNA-binding factors to either aid or repress splicing. These include hexamer recognition sites that act as Exon Splice Enhancers (ESEs) or Exon Splice Silencers (ESSs), or Intronic Splice Enhancers (ISEs) and Intronic Splice Silencers (ISSs), depending on their location and the factors they recruit (Gamazon & Stranger, 2014). ESEs tend to be found close to splice sites and can compensate if the splice site is "weak", promoting exon inclusion in the mRNA transcript. If the splice site is mutated to be closer to the consensus sequence then the reliance on the ESE for exon inclusion is removed (Graveley, 2000). A study of human gene sequences found hexamer recognition sites at both 5' and 3' splice sites that could be grouped to form five 5' ESE hexamer motifs and eight 3' ESE motifs (Fairbrother *et al.*, 2002). ESS sites are abundant and highly conserved, and in general fall into two classes:

those than resemble the hnRNPA1 recognition site and those that recruit other silencing factors (Wang *et al.*, 2006). ISEs cluster into 6 motifs according to sequence, with similar patterns to ESSs, and each group likely recruits specific *trans*-acting factors leading to intron splicing (Wang *et al.*, 2012).

Trans-acting factors are the RNA-binding elements that bind to the *cis*-regulatory sequences and include several heterogeneous ribonucleoprotein families (Kornblihtt *et al.*, 2013). There are two large families of *trans*-acting regulators that can determine splicing. Serine-arginine (SR) proteins in general enhance splicing, binding to ESEs and ISEs as well as recruiting the U1 snRNP, while heterogeneous nuclear ribonucleoproteins (hnRNPs) appear to be antagonistic to SR proteins and in general are negative regulators of splicing (reviewed in Fu & Ares, 2014). Although several *cis*-acting elements resemble the recognition sites for individual *trans*-acting elements, there is not always a one-to-one relationship between a *cis*-acting splice factor and an RNA binding protein. For example, the action of some regulatory elements may depend upon the proximity of the element to the splice site itself or whether or not it is located in the exon (Goren *et al.*, 2006). The balance between the splice enhancer and splice silencer regulatory elements, both in *cis* and *trans*, help determine whether or not a splice site is used.

More than 90% of human genes are capable of undergoing alternative splicing, and most have alternative isoforms present in more than 15% of their transcripts (Wang *et al.*, 2008). Alternative splicing has an important role in both normal physiology and disease. Genes that are alternatively spliced are found to be differentially regulated throughout the nervous system, governing various processes such as development, pre-synaptic function and post-synaptic responses (as reviewed in Li *et al.*, 2007). Defects in alternative splicing, such as mutations disrupting splice sites, have been linked to several disorders including cystic fibrosis and schizophrenia (Gamazon & Stranger, 2014). The most common method of endogenous alternative splicing in the human transcriptome is “exon skipping” or “cassette exon inclusion” (Wang *et al.*, 2008). An exon that is not present in one or more transcripts of a gene, either due to a “weak” splice site or silencer elements, can be defined as a cassette exon and the method of alternatively splicing this exon is termed exon skipping. This is the method of alternative splicing that can include the AluJ cassette within the ADAR2 transcript (Gerber *et al.*, 1997). The AluJ cassette is so called due to its similarity to Alu transposon sequences. It was found that its inclusion in the ADAR2 transcript led to a reduced editing efficiency *in vitro* (Gerber *et al.*, 1997). In this study, synthetic double-stranded RNA was used to assess the editing of ADAR2 containing the AluJ cassette or without the AluJ cassette at the Q/R site, hotspot 1 and R/G editing sites of the GluA2 transcript. In all cases, purified ADAR2 without the AluJ

cassette exon was around twice as efficient at editing as purified ADAR2 containing the AluJ cassette (Gerber *et al.*, 1997).

ASO technologies have been used to alter natural splicing patterns in several areas. These previous studies have utilised bioinformatic design tools to predict the optimal sequence to manipulate splicing. By targeting the ASO to sequences around the splice site, the ASOs can compete with the splice machinery and so interfere with the splicing process. This method can be used to promote either exon inclusion or exon skipping depending on the sequence targeted. In spinal muscular atrophy, ASOs have been used to include exon 7 in the *SMN2* gene, thereby increasing SMN protein production, by targeting the ASO to an ISS in intron 7 (Zhou *et al.*, 2013). The ASO blocks the silencer site, therefore promoting exon inclusion in the mRNA transcript. Alternatively, ASOs can block enhancer sites where the same principle is applied and the removal of the enhancer reduces exon inclusion, for example to restore the reading frame in mutated genes (Aartsma-Rus *et al.*, 2003).

In order to design effective ASOs, guidelines have been suggested which identify important parameters to consider, and these parameters have been compared to observed efficacy of the designed ASOs (Aartsma-Rus *et al.*, 2009; Popplewell *et al.*, 2009). Both of these studies looked at the application of ASOs in exon skipping. It appears that targeting exonic sequences show improved results compared to targeting intronic sequences, possibly due to greater GC content and so stronger binding. A strong determinant was reported to be the difference in free energy between the oligonucleotide sequence and the exonic sequence (Aartsma-Rus *et al.*, 2009). The number of predicted ESE sites, either by the RESCUE-ESE database (Fairbrother *et al.*, 2002) or by the Human Splice Finder database (Desmet *et al.*, 2009) covered by the ASO also correlated with efficacy, particularly the strength of binding for SC35 and Tra2β splice factors (Aartsma-Rus *et al.*, 2009). The length of the ASO, the folding of the premRNA transcript and so the accessibility of the target site, as well as the proximity of the target sequence to the exon acceptor site are also factors to be considered (Popplewell *et al.*, 2009). ASO-induced exon skipping has been applied to several degenerative disorders, including Duchenne muscular dystrophy (Popplewell *et al.*, 2009) which has progressed to clinical trials (Sarepta, 2015) and spinal muscular atrophy (Porensky *et al.*, 2012), also in Phase III clinical trials with IONIS Pharmaceuticals.

The aim of this chapter was to use ASOs to promote exclusion of the AluJ cassette from the ADAR2 mRNA transcript, which has the potential to improve the enzyme's editing efficiency. The PMO chemistry was again used due to the success of this ASO backbone in exon skipping in other contexts such as the *DMD* gene (Wu *et al.*, 2014). Bioinformatic resources were used analyse the sequence of the AluJ cassette as well as its flanking

intronic regions. Entropies of the AluJ cassette splice sites were calculated and compared to neighbouring splice sites in order to assess their strength. Secondary structure models of ADAR2 pre-mRNA were generated to analyse target sequence accessibility and the AluJ cassette sequence was scanned for *cis*-acting splice regulatory elements. Binding energies for potential ASO sequences were calculated to maximise binding to the premRNA transcript. PMOs were then designed that fulfilled each of these requirements: they covered regions containing enhancer sequences and avoided silencer elements, targeted open loop regions of secondary structure and had a negative binding energy. Once the PMOs were designed, they could then be tested for their ability to exclude the AluJ cassette by transfection into HeLa cells. HeLa cells co-transfected with the B13 minigene were used to detect any changes in A-to-I editing at the Q/R site of the GluA2 transcript. The HeLa-B13 system edits the Q/R site at around 30% and so any increase in editing efficiency could be detected. Increasing the Q/R site editing in the GluA2 transcript has the potential to be a therapeutic target for ALS, as editing has been shown to be variable in ALS patients compared to 100% efficiency in healthy controls (Kawahara *et al.*, 2004). The PMOs designed in this chapter were therefore developed to exclude the AluJ cassette from the ADAR2 transcript with an aim to increase its editing efficiency, and therefore indirectly increase Q/R site editing.

6.2 RESULTS

6.2.1 Targeting PMOs against Inclusion of the AluJ Cassette

6.2.1.1 Targeting Splice Sites

There are several factors to consider in the process of designing a PMO for exon skipping. The first areas to target are the splice sites themselves, as a PMO binding to these sequences may prevent the spliceosome from incorporating the exon into the final transcript. MaxEntScan is a web server that calculates the maximum entropy for each splice site (Yeo & Burge, 2004), and the higher the entropy score the more likely a splice site will be used (Ye *et al.*, 2014). Figure 6.2 shows the consensus sequence for U2-dependent introns, the most common form of intron and the form that surrounds the AluJ cassette. Below are the corresponding sequences for the AluJ cassette and its surrounding introns, with the MaxEntScan scores for each splice site. The splice sites at either end of the AluJ cassette are much weaker (4.19 and 2.05 for 3' splice site and 5' splice site respectively) than the splice sites up- and downstream with which they are in competition (9.83 and 9.11 for the 3' splice site and 5' splice site respectively). Mismatched bases are shown in red in Figure 6.2. As can be seen, although the AluJ 3' splice site matches the consensus sequence, there are mismatches in the 5' splice site and in the branch point. This indicates that the spliceosome will not be efficiently recruited and may explain why this exon is alternatively spliced, supported by the lower MaxEntScan entropy scores at each splice site. As this is considered a "weak" splice site, the AluJ cassette may be more reliant on splice enhancers (De Conti *et al.*, 2013). It may also mean that ASOs targeted at the splice sites have a good chance of preventing inclusion of the AluJ cassette.

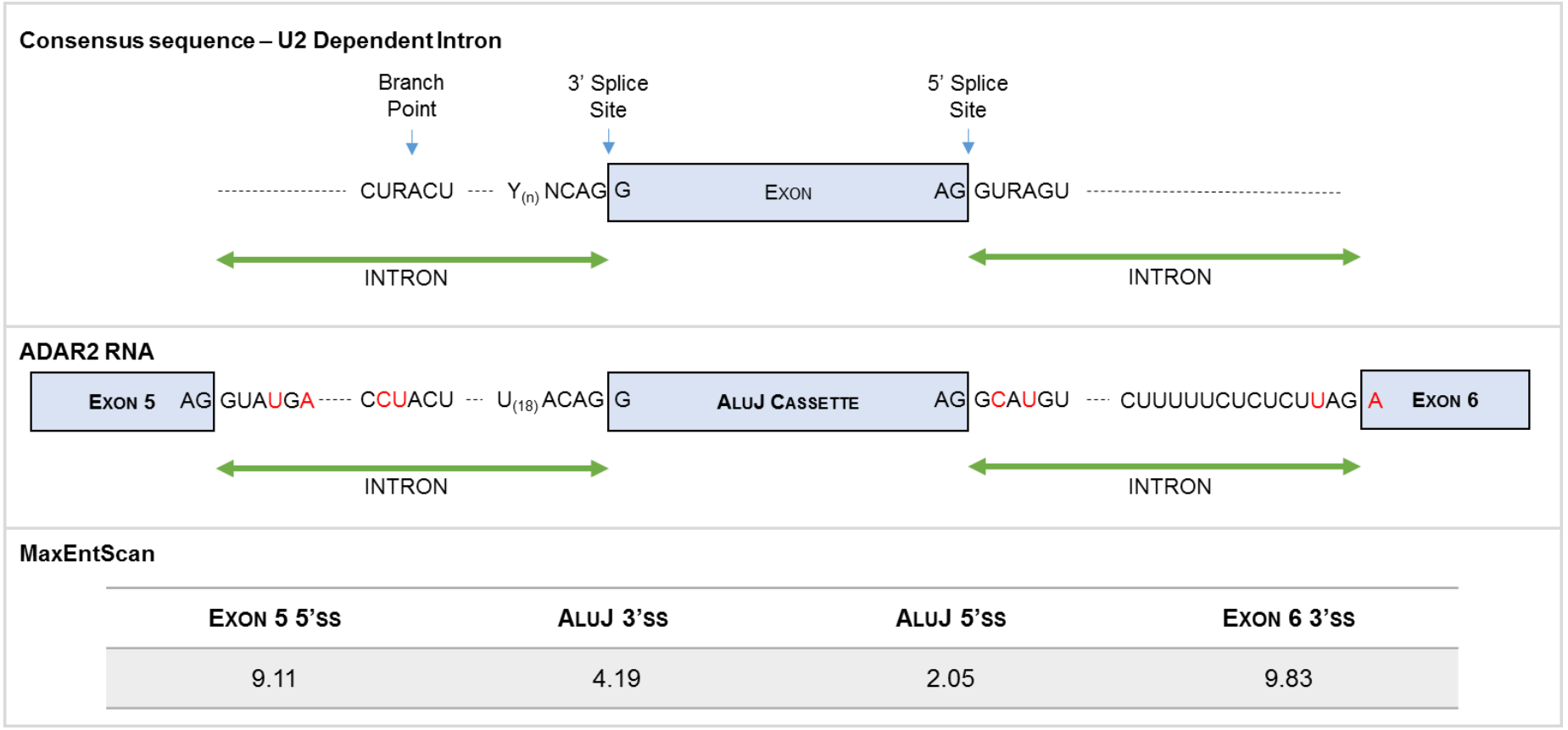

EXON 5 5'SS	ALUJ 3'SS	ALUJ 5'SS	EXON 6 3'SS
9.11	4.19	2.05	9.83

Figure 6.2 - Schematic of consensus splice sites at either end of an exon and the branch point within the intron, compared to the AluJ sequence and its upstream and downstream exon. Bases in red indicate a mismatch with the consensus sequence. Below shows the MaxEntScan scores for each splice site (arbitrary units), with a higher maximum entropy score indicating a stronger splice site. Splice sites are labelled 5' or 3' in relation to the intron being excised.

6.2.1.2 Exon Splice Enhancers and Silencers

Other sequences to target in ASO design would be the exon splice enhancers, which facilitate the inclusion of an exon, while sequences to avoid would be the exon splice silencers as they encourage the exclusion of an exon, which is our aim. Online resources were therefore utilised to determine where the enhancers and silencers were in the AluJ cassette itself and surrounding intronic sequences. The website Human Splicing Finder (HSF) was preferred for this task as this tool incorporates a number of sources of motifs including ESE Finder (Cartegni *et al.*, 2003) and RESCUE-ESE (Fairbrother *et al.*, 2002) databases, and as the title suggests this is specifically for human sequences. In the input form, "Analyse sequence" was selected and the sequence was chosen by the Ensembl transcript number – ENST00000360697 – and exon 6 (the AluJ cassette). HSF automatically analyses the 100 bases of intronic sequence either side of the chosen exon as well as the exonic sequence itself.

The graphical output of splice enhancer and silencer motifs is shown in Figure 6.3. Along the x-axis runs the RNA sequence (5'-3') and the grey box represents the AluJ cassette. Coloured lines represent predicted *cis*-regulatory elements for different factors: above the x-axis indicates ESE motifs in shades of red and pink and below indicates ESS motifs in shades of blue and green. This graph shows that there are multiple predicted binding sites throughout the AluJ sequence for both ESE and ESS elements. ESS motifs should be avoided in ASO design for exon skipping, as they help to exclude the exon. However, this analysis shows that the ESS binding sites (blue) are evenly spaced throughout the sequence and so there is not an obvious area to avoid. On the other hand, there is a cluster of binding sites for ESEs at the 3' end of the sequence, indicating a potential target for PMO design as covering the enhancer sequences may prevent exon inclusion. Specifically targeting SC35 hexamers has previously been reported to be beneficial in ASO design for exon skipping (Aartsma-Rus *et al.*, 2009) although elsewhere it did not show an effect on ASO design (Echigoya *et al.*, 2015). SC35 hexamers (shown in bright red; Figure 6.3) appear to be spaced fairly evenly throughout the sequence, although there are three spaced within 30 bases in the centre of the exon, as well as two at the 3' end.

The Human Splice Finder analysis also searches for putative exon splice enhancer (PESE) and putative exon splice silencer (PESS) octamers (Zhang & Chasin, 2004). These octamers were determined through a different set of criteria, where sequences overrepresented in noncoding exons were classed as PESEs whereas octamers underrepresented in noncoding exons were classed as PESSs when compared to their prevalence in intronic sequences (Zhang & Chasin, 2004). Octamers were chosen to include potential binding sites that exceeded six bases. PESSs are shown in green

(Figure 6.3), and indicate that intronic regions immediately flanking the AluJ cassette are rich in silencer elements, and so ought to be avoided. PESEs are indicated in pink, and show a small cluster of enhancer elements in the centre of the AluJ cassette and a larger cluster of enhancer elements at the 3’ end of the exon. 0

Targeting the 3’ end of the exon would also cover the splice consensus sequence, which should also prevent exon inclusion. The yellow line running through the graph indicates overall balance of the ESEs to ESSs, and so peaks in the yellow line indicate an overall enhanced area while a trough below the x axis indicates an overall silenced area. This again supports the idea of covering the 3’ end of the AluJ cassette as there is a “peak” of ESE strength in this region.

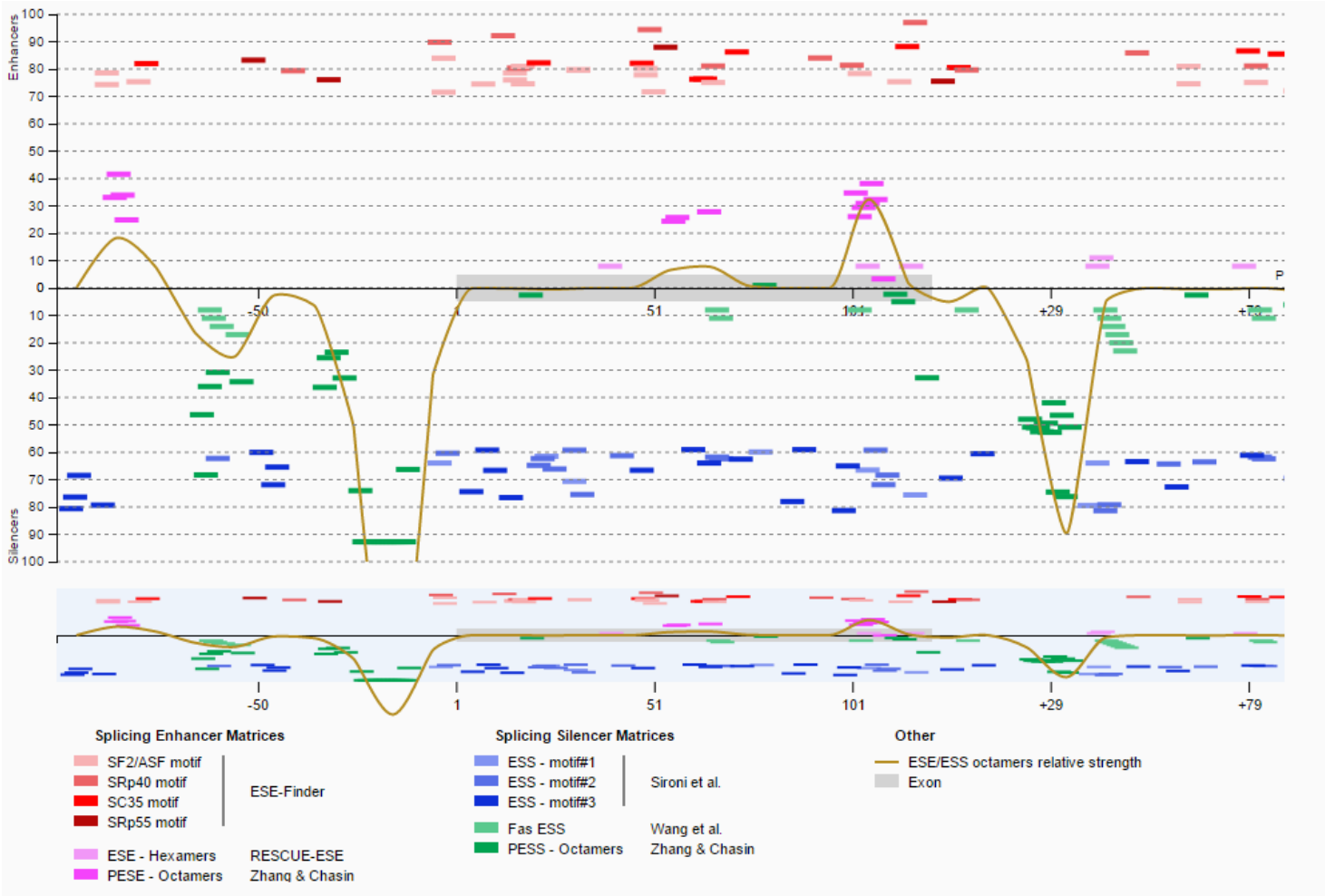

Figure 6.3 - Results from Human Splicing Finder analysing exon splice enhancers and silencers surrounding the AluJ cassette. Sequence runs 5' to 3' along the x axis with the grey box indicating the 120 bases of the AluJ cassette. Boxes above the x axis (in red and pink) indicate sequences associated with splice enhancers while boxes below (in blue and green) represent motifs for exon silencers.

6.2.1.3 Secondary Structure of the AluJ Cassette

In order to bind to RNA, an ASO must be able to access its complementary target bases. The secondary structure of the RNA transcript can be complex, and RNA naturally folds due to Watson-Crick base pairing to form double-stranded regions within the transcript interspersed with loops and bulges of single-stranded regions. If the target sequence for an ASO is within a region of double-stranded RNA, the ASO will need to compete for binding with the RNA transcript and so may have less of an effect. It would therefore be ideal to target the PMO to bases found in single-stranded regions of RNA so that it can access the complementary bases. Targeting ASOs to open regions of RNA secondary structure as predicted by MFold has previously been shown to correlate with efficacy of the ASO (Aartsma-Rus *et al.*, 2009; Popplewell *et al.*, 2009).

The AluJ cassette and its surrounding upstream and downstream intronic sequence was submitted to the RNA folding form of the MFold website, a total of 1,412 bases. This produced 23 predicted secondary structures within the default constraints and the structure with the lowest free energy is shown in Figure 6.4. Using this diagram it was possible to target potential ASO sequences towards single-stranded regions, which theoretically would allow the ASO to bind more easily to the RNA. At the 3' end of the exon (3'ss in Figure 6.4), the splice site is within a double-stranded region. However, there is an open region starting four bases in from the splice site, and so this is a potential target for ASO design. At the 5' end of the exon, the predicted structure shows a mixture of double-stranded regions and bulges of single-stranded RNA, therefore this is also a good target for ASO design, especially if the ASO begins within one of the single-stranded sections (Figure 6.4).

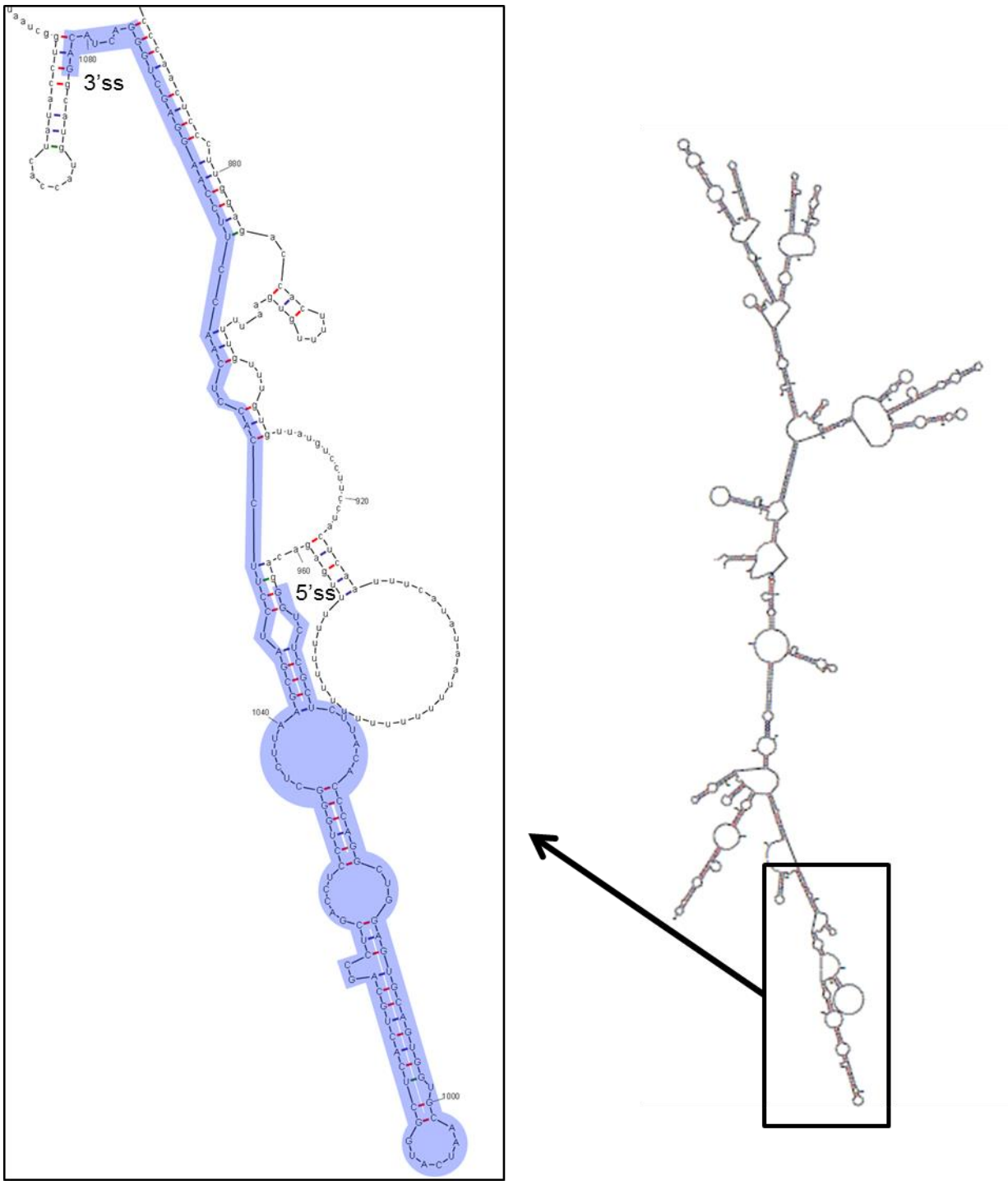

Figure 6.4 - Secondary structure of the AluJ cassette and surrounding intronic region. On the right is the complete secondary structure, with the AluJ cassette itself highlighted in blue (and with capital letters) and shown in the left hand image. Also indicated are the 5' and 3' splice sites (5'ss and 3'ss respectively).

6.2.1.4 Binding Energies

The information from predicted RNA secondary structure and splice regulatory element location narrowed down the area for ASO design to the 5' and 3' end of the AluJ exon, while avoiding the flanking intronic sequences due to their ESS sequences. The next step for ASO design was to calculate the binding energies of different possible sequences, and therefore choose the ASO that will have the highest binding efficiency to the RNA transcript. To do this, the sequence of the AluJ cassette was assessed using the RNA dimer prediction tools available on the SFold website. This website analyses every possible complementary oligonucleotide of a pre-chosen length (in this case 25 bases) along the selected gene sequence and calculates the intermolecular dimer energy between the RNA sequence provided and its exact complementary sequence. The output for SFold oligo is shown in Figure 6.5. At the 5' and 3' end of the exon, oligonucleotides 25 bases long complementary to the very end of the exon had intermolecular dimer energies of -3.4 kcal/mol and -11.6 kcal/mol respectively. If the binding energy is more negative then the ASO is more likely to bind to the RNA. Therefore, the 25 bases at either end of the AluJ exon make promising candidates for ASOs. Shifting the sequences slightly along the exon did not improve the potential binding energy, as they did not become more negative. Choosing the sequence needs to be based on a balance between covering the splice sites and enhancer sequences of the exon and finding the most efficient binding, and these two considerations appear to be fulfilled with the 25-base sequences at either end of the AluJ exon.

~~~~~~~~~~~~~~~~~~~~Output for design of antisense oligos~~~~~~~~~~~~~~~~~~~~

Column 1: target position (starting - ending)
Column 2: target sequence (5p --> 3p)
Column 3: antisense oligo (5p --> 3p)
Column 4: GC content
Column 5: oligo binding energy (kcal/mol)
Column 6: GGGG indicator

NOTES:

GGGG indicator=1 for at least one GGGG in the target
sequence; indicator=0 otherwise.

1-	25	GGUCUCGCUCUUACACCCAGGCUGG	CCAGCCTGGGTGTAAGAGCGAGACC	64.0%	-3.4	0
2-	26	GUCUCGCUCUUACACCCAGGCUGGA	TCCAGCCTGGGTGTAAGAGCGAGAC	60.0%	-3.4	0
3-	27	UCUCGCUCUUACACCCAGGCUGGAG	CTCCAGCCTGGGTGTAAGAGCGAGA	60.0%	-3.5	0
4-	28	CUCGCUCUUACACCCAGGCUGGAGU	ACTCCAGCCTGGGTGTAAGAGCGAG	60.0%	-3.3	0
5-	29	UCGCUCUUACACCCAGGCUGGAGUG	CACTCCAGCCTGGGTGTAAGAGCGA	60.0%	-3.3	0
6-	30	CGCUCUUACACCCAGGCUGGAGUGC	GCACTCCAGCCTGGGTGTAAGAGCG	64.0%	-3.3	0
7-	31	GCUCUUACACCCAGGCUGGAGUGCA	TGCACTCCAGCCTGGGTGTAAGAGC	60.0%	-3.3	0
8-	32	CUCUUACACCCAGGCUGGAGUGCAG	CTGCACTCCAGCCTGGGTGTAAGAG	60.0%	-3.3	0
9-	33	UCUUACACCCAGGCUGGAGUGCAGU	ACTGCACTCCAGCCTGGGTGTAAGA	56.0%	-3.3	0
10-	34	CUUACACCCAGGCUGGAGUGCAGUG	CACTGCACTCCAGCCTGGGTGTAAG	60.0%	-3.3	0
11-	35	UUACACCCAGGCUGGAGUGCAGUGG	CCACTGCACTCCAGCCTGGGTGTAA	60.0%	-3.2	0
12-	36	UACACCCAGGCUGGAGUGCAGUGGU	ACCACTGCACTCCAGCCTGGGTGTA	60.0%	-3.2	0
13-	37	ACACCCAGGCUGGAGUGCAGUGGUG	CACCACTGCACTCCAGCCTGGGTGT	64.0%	-3.0	0
14-	38	CACCCAGGCUGGAGUGCAGUGGUGC	GCACCACTGCACTCCAGCCTGGGTG	68.0%	-1.2	0
15-	39	ACCCAGGCUGGAGUGCAGUGGUGCA	TGCACCACTGCACTCCAGCCTGGGT	64.0%	-0.8	0
16-	40	CCCAGGCUGGAGUGCAGUGGUGCAA	TTGCACCACTGCACTCCAGCCTGGG	64.0%	-0.6	0
17-	41	CCAGGCUGGAGUGCAGUGGUGCAAU	ATTGCACCACTGCACTCCAGCCTGG	60.0%	-0.7	0
18-	42	CAGGCUGGAGUGCAGUGGUGCAAUC	GATTGCACCACTGCACTCCAGCCTG	60.0%	-0.8	0
19-	43	AGGCUGGAGUGCAGUGGUGCAAUCA	TGATTGCACCACTGCACTCCAGCCT	56.0%	-1.1	0
20-	44	GGCUGGAGUGCAGUGGUGCAAUCAU	ATGATTGCACCACTGCACTCCAGCC	56.0%	-1.5	0
21-	45	GCUGGAGUGCAGUGGUGCAAUCAUG	CATGATTGCACCACTGCACTCCAGC	56.0%	-2.1	0
22-	46	CUGGAGUGCAGUGGUGCAAUCAUGG	CCATGATTGCACCACTGCACTCCAG	56.0%	-2.2	0
23-	47	UGGAGUGCAGUGGUGCAAUCAUGGC	GCCATGATTGCACCACTGCACTCCA	56.0%	-2.1	0
24-	48	GGAGUGCAGUGGUGCAAUCAUGGCU	AGCCATGATTGCACCACTGCACTCC	56.0%	-2.0	0
25-	49	GAGUGCAGUGGUGCAAUCAUGGCUC	GAGCCATGATTGCACCACTGCACTC	56.0%	-2.0	0
26-	50	AGUGCAGUGGUGCAAUCAUGGCUCA	TGAGCCATGATTGCACCACTGCACT	52.0%	-1.9	0
27-	51	GUGCAGUGGUGCAAUCAUGGCUCAC	GTGAGCCATGATTGCACCACTGCAC	56.0%	-1.9	0
28-	52	UGCAGUGGUGCAAUCAUGGCUCACU	AGTGAGCCATGATTGCACCACTGCA	52.0%	-1.9	0
29-	53	GCAGUGGUGCAAUCAUGGCUCACUG	CAGTGAGCCATGATTGCACCACTGC	56.0%	-1.9	0
30-	54	CAGUGGUGCAAUCAUGGCUCACUGC	GCAGTGAGCCATGATTGCACCACTG	56.0%	-1.9	0
31-	55	AGUGGUGCAAUCAUGGCUCACUGCA	TGCAGTGAGCCATGATTGCACCACT	52.0%	-1.9	0
32-	56	GUGGUGCAAUCAUGGCUCACUGCAG	CTGCAGTGAGCCATGATTGCACCAC	56.0%	-1.9	0
33-	57	UGGUGCAAUCAUGGCUCACUGCAGC	GCTGCAGTGAGCCATGATTGCACCA	56.0%	-2.8	0
34-	58	GGUGCAAUCAUGGCUCACUGCAGCC	GGCTGCAGTGAGCCATGATTGCACC	60.0%	-2.8	0
35-	59	GUGCAAUCAUGGCUCACUGCAGCCU	AGGCTGCAGTGAGCCATGATTGCAC	56.0%	-2.9	0
36-	60	UGCAAUCAUGGCUCACUGCAGCCUC	GAGGCTGCAGTGAGCCATGATTGCA	56.0%	-3.1	0
37-	61	GCAAUCAUGGCUCACUGCAGCCUCG	CGAGGCTGCAGTGAGCCATGATTGC	60.0%	-3.4	0
38-	62	CAAUCAUGGCUCACUGCAGCCUCGA	TCGAGGCTGCAGTGAGCCATGATTG	56.0%	-3.6	0
39-	63	AAUCAUGGCUCACUGCAGCCUCGAC	GTCGAGGCTGCAGTGAGCCATGATT	56.0%	-4.2	0
40-	64	AUCAUGGCUCACUGCAGCCUCGACC	GGTCGAGGCTGCAGTGAGCCATGAT	60.0%	-5.1	0
41-	65	UCAUGGCUCACUGCAGCCUCGACCU	AGGTCGAGGCTGCAGTGAGCCATGA	60.0%	-5.1	0
42-	66	CAUGGCUCACUGCAGCCUCGACCUC	GAGGTCGAGGCTGCAGTGAGCCATG	64.0%	-5.1	0
43-	67	AUGGCUCACUGCAGCCUCGACCUCC	GGAGGTCGAGGCTGCAGTGAGCCAT	64.0%	-5.9	0
44-	68	UGGCUCACUGCAGCCUCGACCUCCU	AGGAGGTCGAGGCTGCAGTGAGCCA	64.0%	-5.9	0
45-	69	GGCUCACUGCAGCCUCGACCUCCUG	CAGGAGGTCGAGGCTGCAGTGAGCC	68.0%	-5.4	0
46-	70	GCUCACUGCAGCCUCGACCUCCUGG	CCAGGAGGTCGAGGCTGCAGTGAGC	68.0%	-5.4	0
47-	71	CUCACUGCAGCCUCGACCUCCUGGG	CCCAGGAGGTCGAGGCTGCAGTGAG	68.0%	-5.4	0
48-	72	UCACUGCAGCCUCGACCUCCUGGGC	GCCCAGGAGGTCGAGGCTGCAGTGA	68.0%	-5.4	0
49-	73	CACUGCAGCCUCGACCUCCUGGGCU	AGCCCAGGAGGTCGAGGCTGCAGTG	68.0%	-5.9	0
50-	74	ACUGCAGCCUCGACCUCCUGGGCUC	GAGCCCAGGAGGTCGAGGCTGCAGT	68.0%	-6.8	0
51-	75	CUGCAGCCUCGACCUCCUGGGCUCU	AGAGCCCAGGAGGTCGAGGCTGCAG	68.0%	-7.5	0
52-	76	UGCAGCCUCGACCUCCUGGGCUCUU	AAGAGCCCAGGAGGTCGAGGCTGCA	64.0%	-7.7	0
53-	77	GCAGCCUCGACCUCCUGGGCUCUUA	TAAGAGCCCAGGAGGTCGAGGCTGC	64.0%	-8.2	0
54-	78	CAGCCUCGACCUCCUGGGCUCUUAA	TTAAGAGCCCAGGAGGTCGAGGCTG	60.0%	-9.0	0
55-	79	AGCCUCGACCUCCUGGGCUCUUAAG	CTTAAGAGCCCAGGAGGTCGAGGCT	60.0%	-9.9	0
56-	80	GCCUCGACCUCCUGGGCUCUUAAGC	GCTTAAGAGCCCAGGAGGTCGAGGC	64.0%	-11.3	0
57-	81	CCUCGACCUCCUGGGCUCUUAAGCG	CGCTTAAGAGCCCAGGAGGTCGAGG	64.0%	-10.8	0
58-	82	CUCGACCUCCUGGGCUCUUAAGCGA	TCGCTTAAGAGCCCAGGAGGTCGAG	60.0%	-11.2	0
59-	83	UCGACCUCCUGGGCUCUUAAGCGAU	ATCGCTTAAGAGCCCAGGAGGTCGA	56.0%	-11.5	0
60-	84	CGACCUCCUGGGCUCUUAAGCGAUC	GATCGCTTAAGAGCCCAGGAGGTCG	60.0%	-12.2	0
61-	85	GACCUCCUGGGCUCUUAAGCGAUCC	GGATCGCTTAAGAGCCCAGGAGGTC	60.0%	-13.1	0
62-	86	ACCUCCUGGGCUCUUAAGCGAUCCU	AGGATCGCTTAAGAGCCCAGGAGGT	56.0%	-13.2	0
63-	87	CCUCCUGGGCUCUUAAGCGAUCCUU	AAGGATCGCTTAAGAGCCCAGGAGG	56.0%	-12.1	0
64-	88	CUCCUGGGCUCUUAAGCGAUCCUUC	GAAGGATCGCTTAAGAGCCCAGGAG	56.0%	-11.0	0
65-	89	UCCUGGGCUCUUAAGCGAUCCUUCC	GGAAGGATCGCTTAAGAGCCCAGGA	56.0%	-11.3	0
66-	90	CCUGGGCUCUUAAGCGAUCCUUCCA	TGGAAGGATCGCTTAAGAGCCCAGG	56.0%	-11.0	0
67-	91	CUGGGCUCUUAAGCGAUCCUUCCAC	GTGGAAGGATCGCTTAAGAGCCCAG	56.0%	-11.4	0
68-	92	UGGGCUCUUAAGCGAUCCUUCCACC	GGTGGAAGGATCGCTTAAGAGCCCA	56.0%	-12.8	0
69-	93	GGGCUCUUAAGCGAUCCUUCCACCU	AGGTGGAAGGATCGCTTAAGAGCCC	56.0%	-13.3	0
70-	94	GGCUCUUAAGCGAUCCUUCCACCUC	GAGGTGGAAGGATCGCTTAAGAGCC	56.0%	-14.2	0
71-	95	GCUCUUAAGCGAUCCUUCCACCUCA	TGAGGTGGAAGGATCGCTTAAGAGC	52.0%	-14.9	0
72-	96	CUCUUAAGCGAUCCUUCCACCUCAA	TTGAGGTGGAAGGATCGCTTAAGAG	48.0%	-15.8	0
73-	97	UCUUAAGCGAUCCUUCCACCUCAAC	GTTGAGGTGGAAGGATCGCTTAAGA	48.0%	-17.3	0
74-	98	CUUAAGCGAUCCUUCCACCUCAACC	GGTTGAGGTGGAAGGATCGCTTAAG	52.0%	-18.3	0
75-	99	UUAAGCGAUCCUUCCACCUCAACCU	AGGTTGAGGTGGAAGGATCGCTTAA	48.0%	-18.5	0
76-	100	UAAGCGAUCCUUCCACCUCAACCUU	AAGGTTGAGGTGGAAGGATCGCTTA	48.0%	-18.5	0
77-	101	AAGCGAUCCUUCCACCUCAACCUUC	GAAGGTTGAGGTGGAAGGATCGCTT	52.0%	-19.3	0
78-	102	AGCGAUCCUUCCACCUCAACCUUCC	GGAAGGTTGAGGTGGAAGGATCGCT	56.0%	-20.5	0
79-	103	GCGAUCCUUCCACCUCAACCUUCCA	TGGAAGGTTGAGGTGGAAGGATCGC	56.0%	-20.4	0
80-	104	CGAUCCUUCCACCUCAACCUUCCAA	TTGGAAGGTTGAGGTGGAAGGATCG	52.0%	-19.2	0
81-	105	GAUCCUUCCACCUCAACCUUCCAAG	CTTGGAAGGTTGAGGTGGAAGGATC	52.0%	-19.1	0
82-	106	AUCCUUCCACCUCAACCUUCCAAGG	CCTTGGAAGGTTGAGGTGGAAGGAT	52.0%	-18.7	0
83-	107	UCCUUCCACCUCAACCUUCCAAGGA	TCCTTGGAAGGTTGAGGTGGAAGGA	52.0%	-18.3	0
84-	108	CCUUCCACCUCAACCUUCCAAGGAG	CTCCTTGGAAGGTTGAGGTGGAAGG	56.0%	-17.4	0
85-	109	CUUCCACCUCAACCUUCCAAGGAGC	GCTCCTTGGAAGGTTGAGGTGGAAG	56.0%	-16.2	0
86-	110	UUCCACCUCAACCUUCCAAGGAGCU	AGCTCCTTGGAAGGTTGAGGTGGAA	52.0%	-15.7	0
87-	111	UCCACCUCAACCUUCCAAGGAGCUG	CAGCTCCTTGGAAGGTTGAGGTGGA	56.0%	-15.6	0
88-	112	CCACCUCAACCUUCCAAGGAGCUGG	CCAGCTCCTTGGAAGGTTGAGGTGG	60.0%	-14.8	0
89-	113	CACCUCAACCUUCCAAGGAGCUGGG	CCCAGCTCCTTGGAAGGTTGAGGTG	60.0%	-13.7	0
90-	114	ACCUCAACCUUCCAAGGAGCUGGGA	TCCCAGCTCCTTGGAAGGTTGAGGT	56.0%	-13.2	0
91-	115	CCUCAACCUUCCAAGGAGCUGGGAC	GTCCCAGCTCCTTGGAAGGTTGAGG	60.0%	-11.7	0
92-	116	CUCAACCUUCCAAGGAGCUGGGACU	AGTCCCAGCTCCTTGGAAGGTTGAG	56.0%	-10.1	0
93-	117	UCAACCUUCCAAGGAGCUGGGACUA	TAGTCCCAGCTCCTTGGAAGGTTGA	52.0%	-9.5	0
94-	118	CAACCUUCCAAGGAGCUGGGACUAC	GTAGTCCCAGCTCCTTGGAAGGTTG	56.0%	-10.6	0
95-	119	AACCUUCCAAGGAGCUGGGACUACA	TGTAGTCCCAGCTCCTTGGAAGGTT	52.0%	-10.8	0
96-	120	ACCUUCCAAGGAGCUGGGACUACAG	CTGTAGTCCCAGCTCCTTGGAAGGT	56.0%	-11.6	0

Figure 6.5 - SFold oligo output for the AluJ cassette. Highlighted columns indicate the binding energy between an antisense oligonucleotide and the RNA transcript at that location.
~~~~~~~~~~~~~~~~~~~~

Taking the two sequences at each end of the exon, it was then possible to calculate the energy needed for these two ASOs to overcome any internal secondary structure. This was done using the OligoEvaluator program, which gives the PMO-PMO interaction and hairpin binding energies for a given sequence. For the sequence at the 5' splice site, the energy needed to overcome PMO-PMO interactions and hairpins structures were -3.2 and -1.6 kcal/mol respectively. For the sequence at the 3' splice site, the energy needed to overcome PMO-PMO interactions and hairpins structures were -3.1 and -1.6 kcal/mol respectively. These energies were then subtracted from the intermolecular binding energy given by the SFold website to produce a total binding energy for the ASO. This correction provides a more accurate prediction for the energy involved in binding between ASO and RNA transcript (Popplewell et al., 2009). The more negative the binding energy, the stronger the bonds between ASO and RNA molecule, and each of these sequences had total binding energies of 1.4 and -6.9 kcal/mol respectively. These results are summarised in Table 6.1. Although the PMO at the 5' splice site has been calculated to have a positive binding energy of 1.4 kcal/mol, previous studies on the effective design of ASOs for exon skipping purposes have indicated that targeting the acceptor splice site, i.e. at the 5' end of an exon, will improve the potential for exon skipping (Aartsma-Rus et al., 2009). Therefore this sequence was included despite the positive predicted binding energy.

Drawing on the information from both the predicted secondary sequences and the predicted splice enhancer elements, a third ASO was designed. The 3' splice site has the most ESE binding sites as predicted by HSF (Figure 6.3), and so could be considered the prime target. However, secondary structure analysis of the sequence indicates that the splice site is within a region of double-stranded structure (Figure 6.4). Therefore, a third sequence was designed which targets the open loop structure found 3 bases upstream of the 3' splice site, hopefully improving binding to the target RNA. The same binding energy analysis was performed with this sequence. The results from the SFold website calculated an intermolecular binding energy of -9.5 kcal/mol, while OligoEvaluator calculated energies for hairpin structures and PMO-PMO interactions to be -1.6 and -3.1 kcal/mol respectively, giving a total binding energy of -4.8 kcal/mol (Table 6.1).

The GC content of each PMO was also calculated as a higher GC content improves binding due to the strength of a GC bond. Each sequence showed a GC content of more than 50% (Table 6.1). The SFold oligo output also show that all sequences avoid runs of four or more G bases, as the presence of this motif has been associated with weaker ASO activity (Chan et al., 2006).

Target sequence	ΔG InterMolecular Dimers (kcal/mol)	ΔG Hairpin Structure (kcal/mol)	ΔG PMO-PMO interaction (kcal/mol)	**Total Binding energy**	GC Content (%)
5' splice site	-3.4	-1.6	-3.2	1.4	64
3 bases upstream of 3' splice site	-9.5	-1.6	-3.1	-4.8	52
3' splice site	-11.6	-1.6	-3.1	-6.9	56

Table 6.1 - Binding energies for potential PMO sequences

6.2.1.5 Final PMO Designs

The final PMOs are shown in Figure 6.6, and are based on the combination of predicted ESEs and ESSs, the predicted secondary structure of the AluJ cassette and surrounding introns and the predicted binding energies of each of the sequences. At the 5' end, PMO8 (AluJ+1+25) targets the first 25 nucleotides in the AluJ cassette. At the 3' end, PMO10 (AluJ+96+120) targets the 25 nucleotides at the 3' splice site. PMO9 (AluJ+93+117) is shifted 3 bases upstream of PMO10 (AluJ+96+120), targeting the predicted single-stranded region. The binding sites of each PMO on the secondary structure model are shown in Figure 6.6A and summarised in the schematic in Figure 6.6B. Figure 6.6C shows a table with the sequences of each PMO. These three PMOs were produced by GeneTools and tested for their ability to skip the AluJ cassette in HeLa cells.

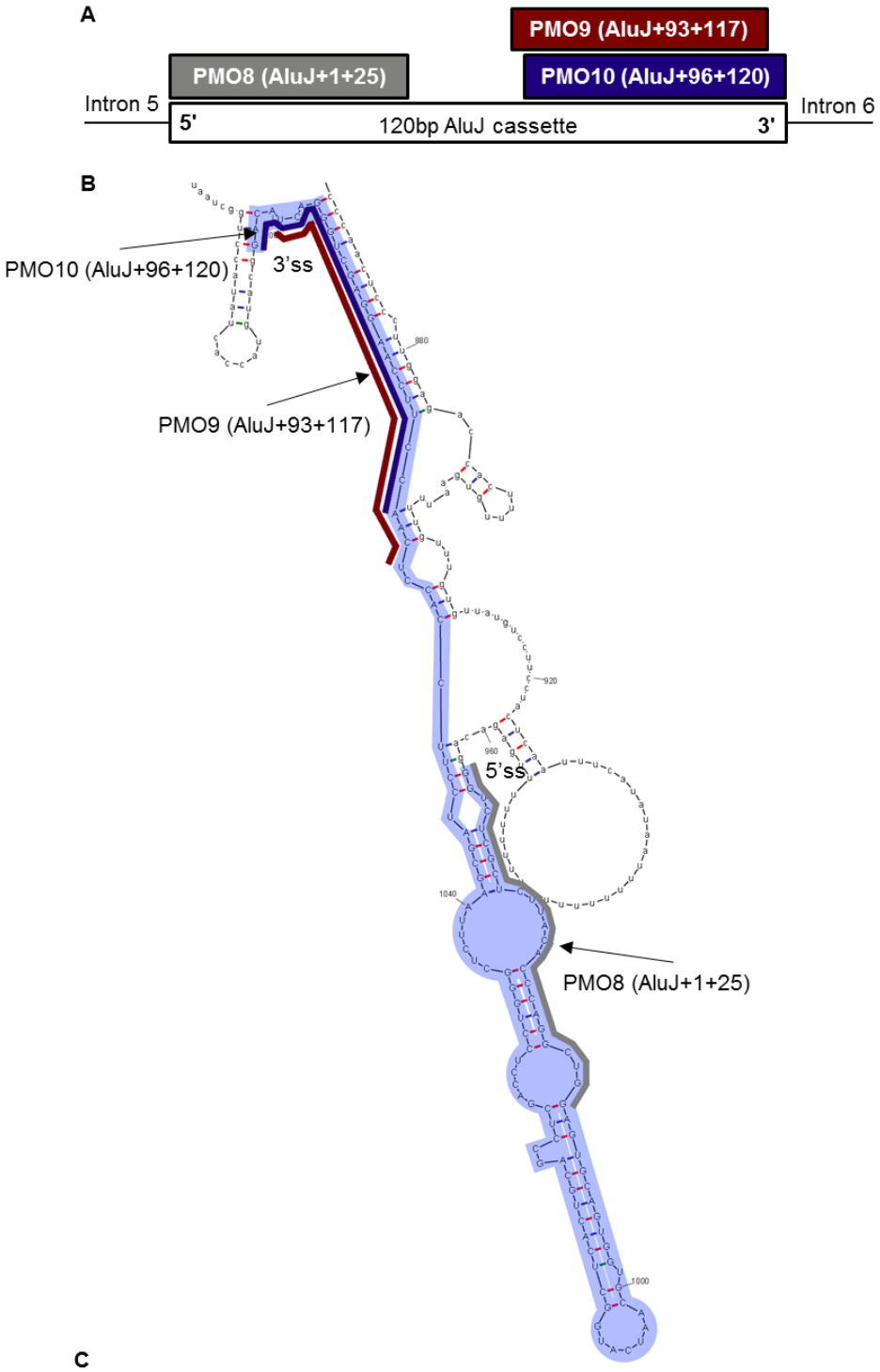

C

PMO Name	Sequence
PMO8 (AluJ+1+25)	CCAGCCTGGGTGTAAGAGCGAGACC
PMO9 (AluJ+93+117)	TAGTCCCAGCTCCTTGGAAGGTTGA
PMO10 (AluJ+96+120)	CTGTAGTCCCAGCTCCTTGGAAGGT

Figure 6.6 – A) Schematic diagram showing complementary binding sites of each ASO to the AluJ cassette. B) Secondary structure of AluJ cassette and surrounding intronic sequence. AluJ cassette is highlighted in blue, and each ASO's binding site is indicated. C) Table of sequences of each ASO.

6.2.2 Exclusion of the AluJ Cassette

Once the PMOs were designed (Figure 6.6) they were transfected into HeLa cells using EndoPorter and the inclusion of the AluJ cassette was quantified by comparing intensities of PCR fragments including the AluJ cassette to those that did not. HeLa cells endogenously express the ADAR2 enzyme, and there was found to be an endogenous inclusion of the AluJ cassette of 62.7 ± 0.97% in transcripts (Figure 6.7). The PMO designed to target the 5' splice site, PMO8 (AluJ+1+25), was compared to those PMOs targeting the 3' end of the AluJ cassette, PMO9 (AluJ+93+117) and PMO10 (AluJ+96+120). Figure 6.7 shows the effect on exon skipping of all three of these PMOs at 2 µM. PMO8 (AluJ+1+25) shows a moderate effect on exon skipping, reducing the inclusion of AluJ to 44.1 ± 0.96% compared to control HeLa cells. However, PMO9 (AluJ+93+117) appears to have a much stronger exon skipping effect, with 2 µM inducing near-complete exon skipping (0.62 ± 0.41% AluJ inclusion; Figure 6.7). Interestingly, PMO10 (AluJ+96+120) does not have any significant effect on inclusion of the AluJ cassette (58.6 ± 1.45%), even though it is simply shifted three bases from PMO9 (AluJ+93+117).

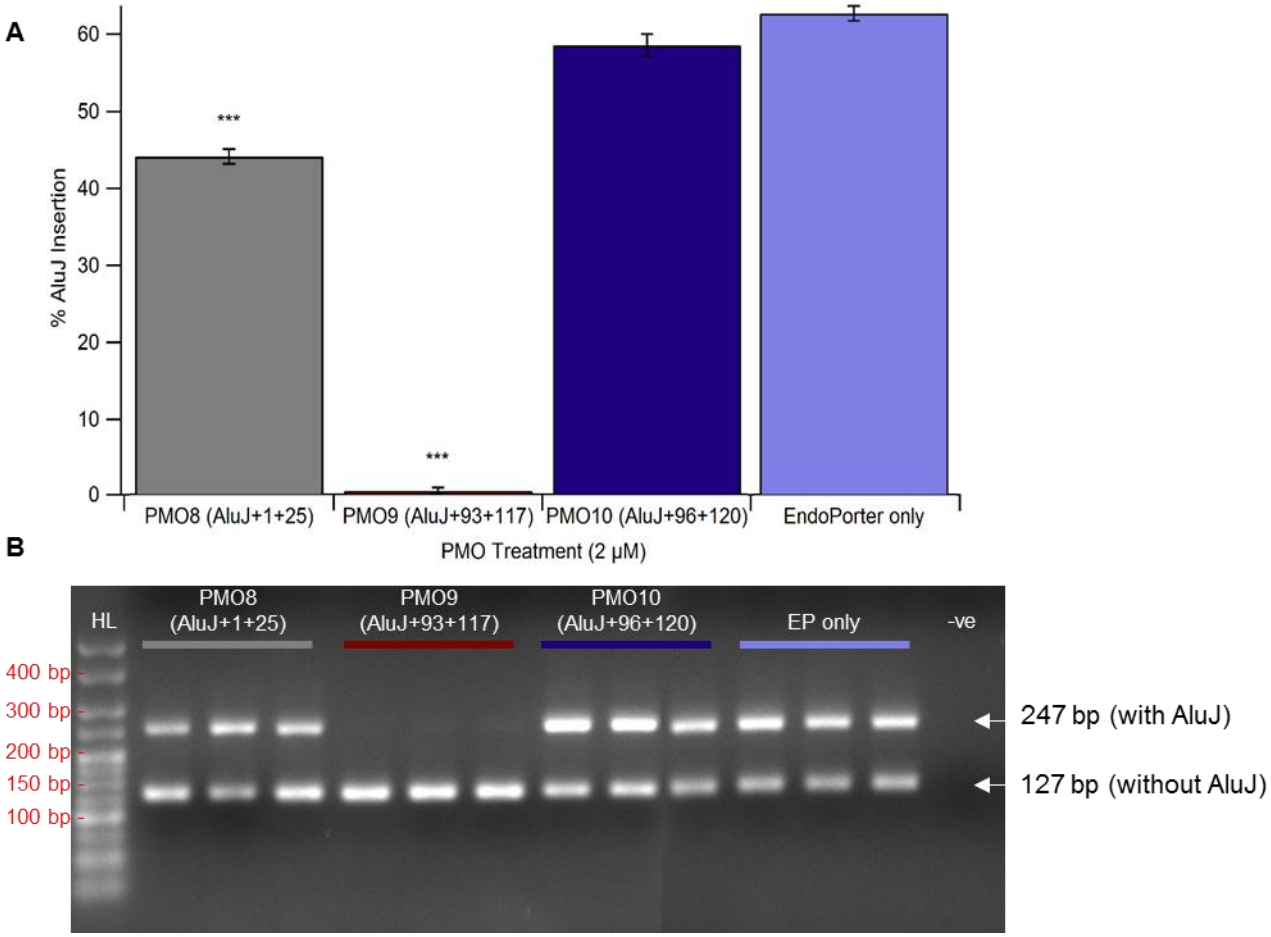

*Figure 6.7 – The effect of 2 µM of each PMO on AluJ insertion in HeLa cells 24 hours after transfection. A) PMO9 (AluJ+93+117) shows the strongest exon skipping ability with AluJ cassette insertion reduced to 0.63 ± 0.41%. PMO8 (AluJ+1+25) shows a moderate ability to exclude the AluJ cassette (44.1 ± 0.96%) whereas PMO10 (AluJ+96+120) shows no significant change in editing (58.6 ± 1.45%) compared to endogenous HeLa AluJ inclusion (62.7 ± 0.97%). N=3, *** = p<0.05 compared to control. B) A sample gel image of a 3% agarose gel run in TAE buffer, with 5 µl of Hyperladder V (25 bp, Bioline) visualised using the Ebox VX2 imaging system and quantified using ImageJ analysis."-ve" indicates negative (water) control. Gel shows the change in AluJ inclusion after different PMO treatments at 2 µM. The larger band (247 base pairs) includes the AluJ cassette. Inclusion is almost completely inhibited with 2 µM of PMO9 (AluJ+93+117).*

To further compare the effect of each PMO, a range of concentrations were transfected into HeLa cells; the results are shown in Figure 6.8. These results support the initial comparison performed at 2 µM. A dose-response curve shifted to the left indicates increased potency against AluJ cassette inclusion, and is supported by a lower IC_{50}. PMO10 (AluJ+96+120) shows little effect on AluJ inclusion, and only shows a significant reduction in percent inclusion at the highest concentration of 5 µM (50.9 ± 1.25%, $p<0.05$). Due to this marginal effect on AluJ inclusion, it was not possible to calculate an IC_{50} for this PMO from this concentration range. The dose-response curve of PMO8 (AluJ+1+25) is to the left of PMO10 (AluJ+96+120), and shows a moderate potency, while PMO9 (AluJ+93+117) in comparison shows a stronger effect on AluJ inclusion and so the curve is shifted even further to the left.

PMO8 (AluJ+1+25) showed a maximum effect at 2 µM (15.87 ± 5.22% AluJ inclusion) and at 500 nM of PMO8 (AluJ+1+25) there was no significant difference to control (52.94 ± 1.95% AluJ inclusion; $p=0.292$). PMO9 (AluJ+93+117) on the other hand showed excellent exon skipping of the AluJ cassette. This is evident by the lower IC_{50} of PMO9 (AluJ+93+117) (0.18 ± 0.015 µM) compared to PMO8 (AluJ+1+25) (IC_{50} = 1.19 ± 0.24 µM). PMO9 (AluJ+93+117) has a greater maximum inhibition of AluJ inclusion compared to PMO8 (AluJ+1+25), with higher concentrations (>3 µM) showing less than 5% inclusion of the AluJ cassette. These data show that PMO9 (AluJ+93+117) is the most efficient PMO at preventing inclusion of the AluJ cassette in the ADAR2 transcript of these original three PMOs. Interestingly, PMO10 (AluJ+96+120) has no effect on exon skipping compared to PMO9 (AluJ+93+117) which has a very strong effect, even though there are only 3 bases difference between them.

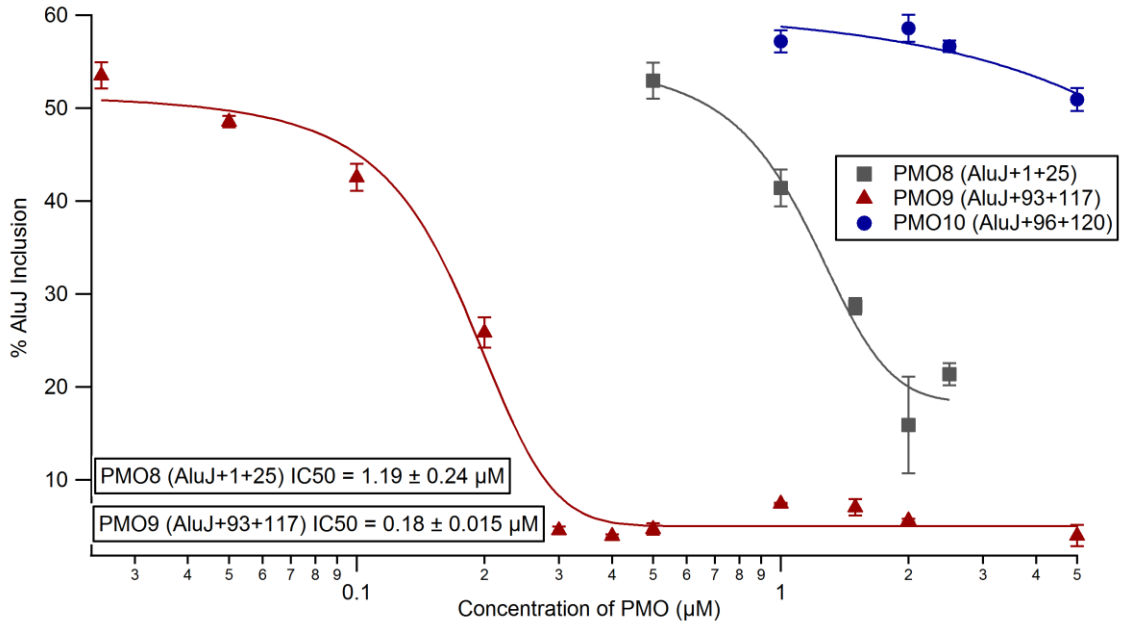

Figure 6.8 - Dose response curves showing exon skipping abilities of PMOs 8 and 9. N=3 per concentration. PMO9 (AluJ+93+117) is more effective at excluding the AluJ cassette as can be seen by the shift of the dose-response curve to the left and the lower IC_{50} (0.18 ± 0.015 µM) compared to PMO8 (AluJ+1+25) (IC_{50} = 1.19 ± 0.24 µM).

6.2.3 Targeting the 3' end of the AluJ Cassette

The difference between PMO9 (AluJ+93+117) and PMO10 (AluJ+96+120) in their ability to prevent AluJ cassette inclusion is striking despite having a difference in nucleotide sequence of only 3 bases. A possible reason for this change in efficacy is an inability for PMO10 (AluJ+96+120) to bind to the RNA transcript. The 5' end of the PMO will bind to the 3' end of the target sequence, and in this instance the 3' end of PMO10 (AluJ+96+120)'s target sequence is within a predicted region of double-stranded secondary structure (Figure 6.9A). This could be preventing the PMO from accessing the bases. If this were the case, then PMOs designed to bind successively further into the double-stranded region would become less effective. Therefore, two more PMOs (PMO9A (AluJ+94+118) and PMO9B (AluJ+95+119)) were designed to shift one base in the 3' direction between PMO9 (AluJ+93+117) and PMO10 (AluJ+96+120), shifting one base at a time (Figure 6.9B). These four PMOs now cover the 3' end of the AluJ cassette moving along the sequence towards the 3' end.

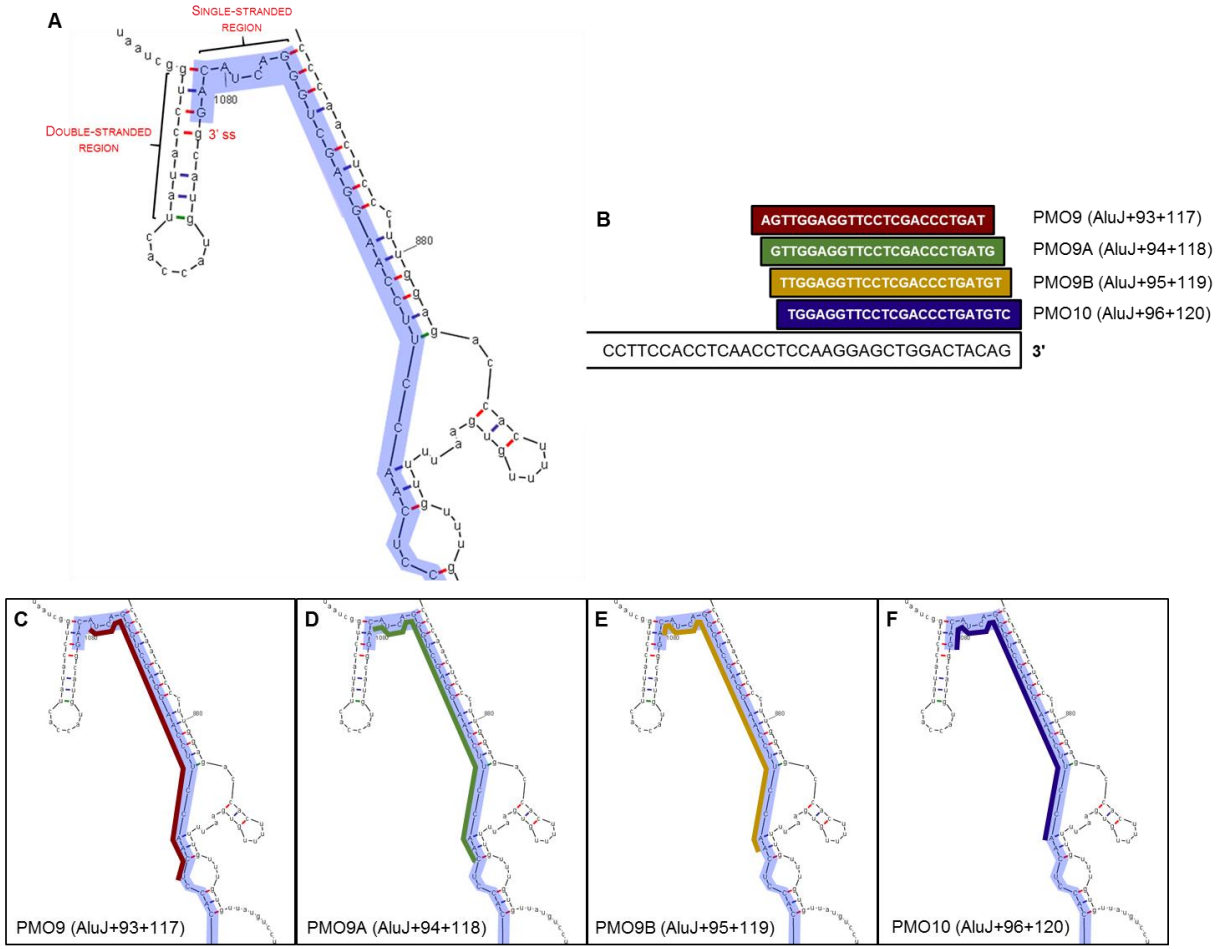

Figure 6.9 – Schematic to show the newly designed PMO9A (AluJ+94+118) and PMO9B (AluJ+95+119) on the 3' end of the AluJ cassette. A) 3' splice site of the AluJ exon and associated secondary structure. Double-stranded and single-stranded regions of RNA are also indicated B) Sequences of each PMO targeting the 3' splice site C) target site for PMO9 (AluJ+93+117) D) target site for PMO9A (AluJ+94+118) E) target site for PMO9B (AluJ+95+119) F) target site for PMO10 (AluJ+96+120)

HeLa cells were transfected with the new PMOs and the AluJ inclusion was determined. The resultant dose-response graphs are shown in Figure 6.10. At 2 µM, PMO9 (AluJ+93+117), PMO9A (AluJ+94+118) and PMO9B (AluJ+95+119) all show excellent skipping of the AluJ cassette, with less than 5% inclusion after treatment with each PMO. At 100 nM none of the PMOs showed any effect on AluJ inclusion. However, PMO9 (AluJ+93+117) is more effective at the lower concentrations, as shown by the lower IC_{50} of 0.18 ± 0.02 µM, compared to PMO9A (AluJ+94+118) which had an IC_{50} of 0.36 ± 0.03 µM. PMO9B (AluJ+95+119) had a slightly increased IC_{50} compared to PMO9A (AluJ+94+118) at 0.47 ± 0.03 µM, although this may be difficult to assess accurately given the poor curve fits to the data. It does appear that these PMOs do follow the trend of becoming less effective as they move further towards the 3' splice site, as predicted. However, the difference between each PMO is only seen at lower concentrations, and the differences between PMO9A (AluJ+94+118) and PMO9B (AluJ+95+119) are marginal. At 2 µM they produce near-complete AluJ exclusion whereas PMO10 (AluJ+96+120), targeting one base downstream, is completely ineffective.

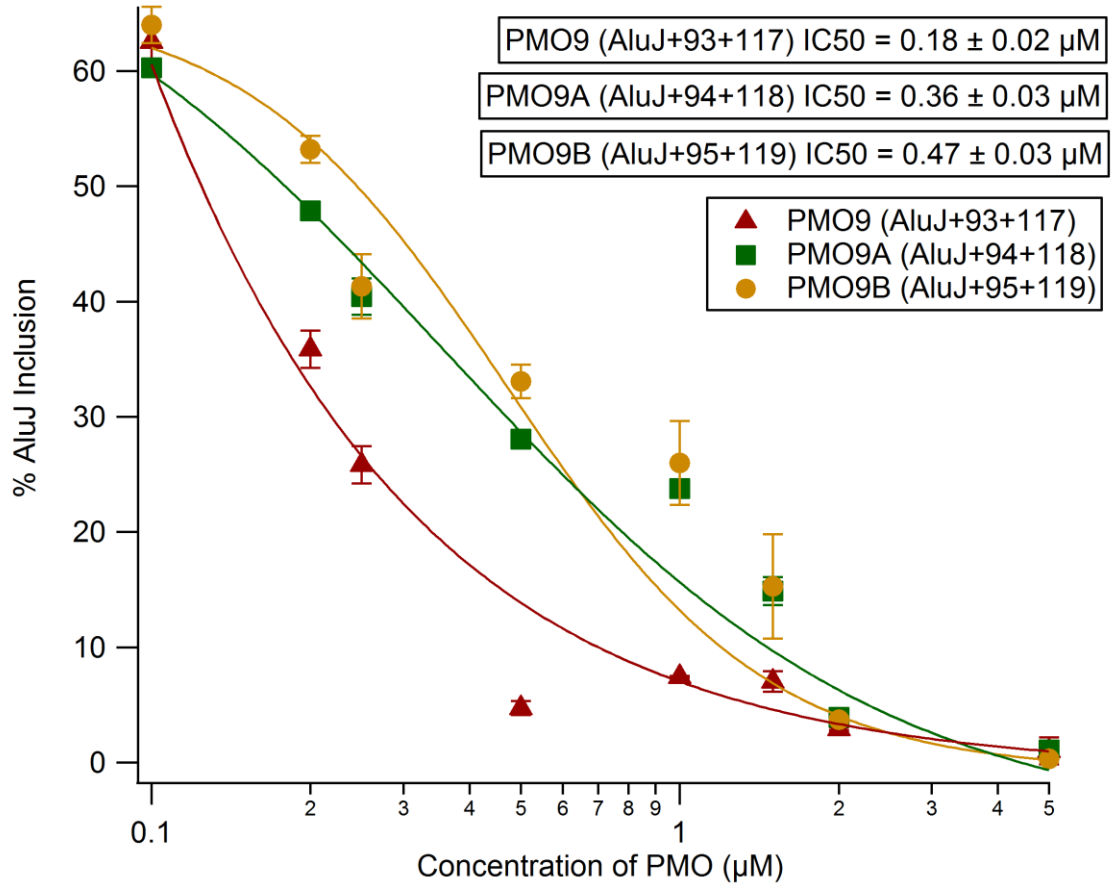

Figure 6.10 – Comparison of newly designed PMOs targeting the 3' splice site and their efficacy on AluJ cassette exclusion (n=3). IC_{50}s of each PMO shown in the top right hand corner.

6.2.4 Effect of Exon Skipping on Q/R Site Editing

ADAR2 transcripts without the AluJ cassette have previously been reported to exhibit a higher rate of RNA editing at the Q/R site (Gerber *et al.*, 1997). Therefore, removal of the AluJ cassette from the transcript using the PMOs designed in this chapter could affect the Q/R site editing of the GluA2 transcript. This was tested in the HeLa-B13 system used previously, where HeLa cells were co-transfected with a plasmid containing a short section of the GluA2 subunit, covering the Q/R editing site, as well as a PMO. 2 µM of each PMO was transfected into the HeLa-B13 system and the Q/R site editing was quantified. 2 µM was chosen as an initial concentration as this produced near-complete AluJ exclusion for PMO9 (AluJ+93+117), PMO9A (AluJ+94+118) and PMO9B (AluJ+95+119) (Figure 6.10). Q/R site editing percentages were calculated as in previous experiments and normalised to control, the results of which are shown in Figure 6.11. PMO9 (AluJ+93+117) was the only PMO to have a significant effect on Q/R site editing ($p<0.05$), with an increase to 124 ± 1.62% of control. PMO9A (AluJ+94+118) and PMO9B (AluJ+95+119), although they do cause the AluJ cassette to be excluded, do not appear to have any significant effect on Q/R site editing (105 ± 0.79% and 110 ± 2.5% respectively), nor do PMO8 (AluJ+1+25) with a moderate effect on AluJ exclusion (107 ± 1.00% of control) or PMO10 (AluJ+96+120) with no effect on AluJ exclusion (113 ± 3.93%).

As PMO9 (AluJ+93+117) showed an ability to alter Q/R site editing, transfection conditions were manipulated in an attempt to increase the Q/R site editing percentage further. PMO9 (AluJ+93+117) concentrations were increased from 2 µM to 5 µM, ensuring high levels of exon skipping, and the transfection was carried out across 24 hours and 48 hours. A longer transfection time would allow for more of the transcripts without the AluJ cassette to be translated into functional protein, and so within the pool of ADAR2 enzyme available for RNA editing, successively more would be without the AluJ cassette. It could therefore be hypothesised that an increase in transfection time would increase the change in Q/R site editing.

Results from this experiment are shown in Figure 6.12. Under the original transfection conditions (2 µM for 24 hours), PMO9 (AluJ+93+117) increased Q/R site editing to 127.72 ± 4.25% of control. If the concentration of PMO9 (AluJ+93+117) was increased to 5 µM, Q/R site editing was not further increased to a significant extent (134.04 ± 1.02%). An increase in concentration of PMO9 (AluJ+93+117) may not have had an effect as 2 µM was likely already sufficient for almost complete exclusion of the AluJ cassette. Prolonging the time of transfection from 24 hours to 48 hours also did not significantly change the increase in Q/R site editing (136.31 ± 1.71% at 2 µM and 128.67

± 2.47% at 5 µM). It therefore appears that this increase of roughly 30% compared to control is the highest increase in Q/R site editing possible within the HeLa-B13 system.

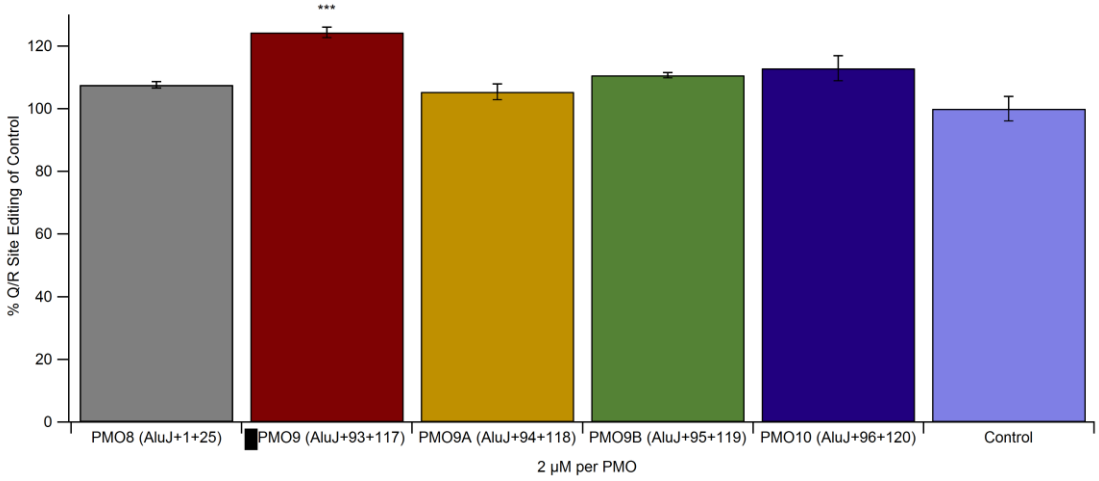

*Figure 6.11 - Changes in Q/R site editing after transfection with 2 µM of each PMO. N=3 per condition, *** = p<0.05 compared to control. All Q/R site editing percentages are normalised to control HeLa-B13 system samples.*

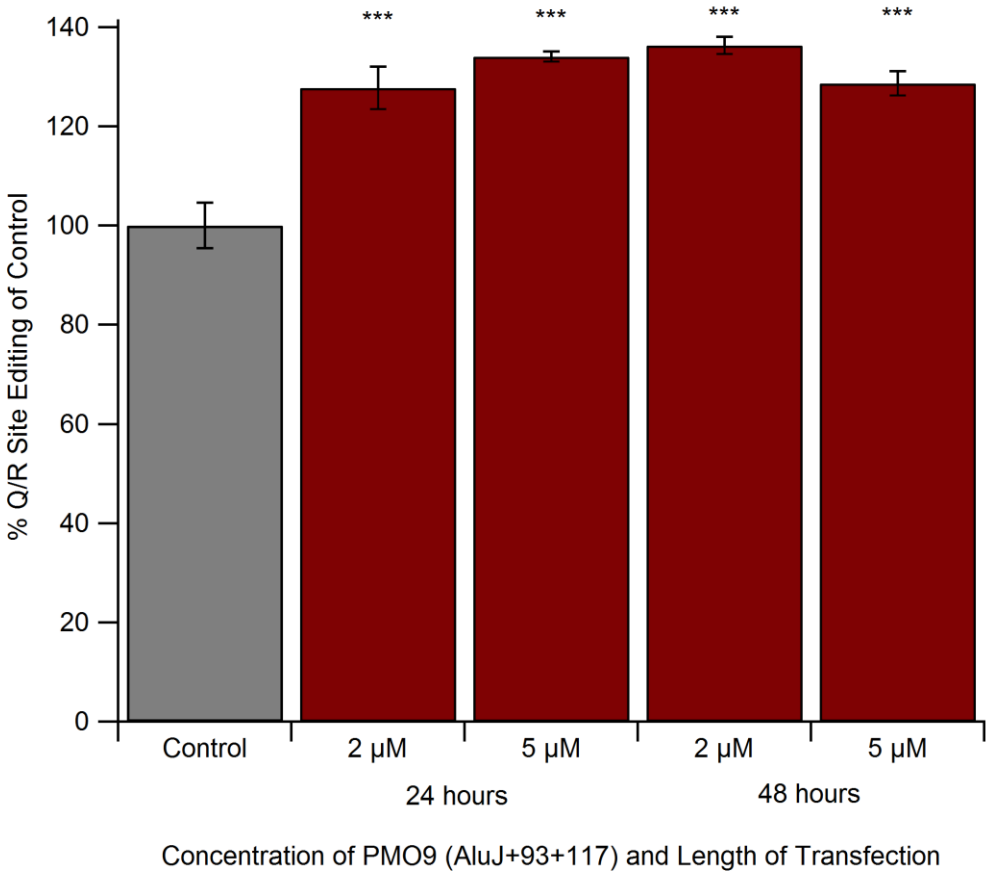

*Figure 6.12 - Changes in Q/R site editing after increasing concentrations of PMO9 (AluJ+93+117) and after increased transfection time as % change of control. N=3 per condition, *** = p<0.05 compared to control. All Q/R site editing percentages are normalised to control HeLa-B13 system samples.*

6.3 DISCUSSION

This chapter has looked at the design of antisense oligonucleotides to force the exclusion of the AluJ cassette from the ADAR2 transcript through a technique commonly referred to as exon skipping and the subsequent impact on Q/R site editing. The success of the majority of these PMOs for inducing exon skipping supports the idea of relying on bioinformatic resources for antisense oligonucleotide design. A major guidance in the design of the PMOs was the prediction of binding sites for exon splice enhancers (ESEs) and exon splice silencers (ESSs). These were predicted using the Human Splice Finder web server, the results of which showed a high abundance of ESEs at the 3' splice site. Although there was a cluster of ESE sites near the 5' splice site of the AluJ cassette, these appeared to be balanced out by a cluster of ESS sites, and so the output of this analysis favoured targeting the 3' splice site, which is unusual as ESEs are generally found at the 5' end of an exon (Wang *et al.*, 2006). The bioinformatic analysis was then supported by the *in vitro* testing of the PMOs in the HeLa cell line, as PMO9 (AluJ+93+117) (targeting the 3' splice site) showed an improved efficiency over PMO8 (AluJ+1+25) (targeting the 5' splice site).

Another guide to PMO design was the prediction of the binding energy of each PMO. To calculate the binding energy for each sequence, the intermolecular energy between the PMO and the RNA transcript was calculated using the SFold web server, and the energy needed to overcome any internal structure of hairpins or PMO-PMO interactions was subtracted. These calculations showed that PMO9 (AluJ+93+117) had a negative total binding energy of -4.8 kcal/mol. PMO8 (AluJ+1+25) has a calculated total binding energy of 1.4 kcal/mol. This could be considered detrimental to the ability of PMO8 (AluJ+1+25) to promote exon skipping, as energy would have to be put into the system to enable binding between PMO8 (AluJ+1+25) and the ADAR2 transcript. PMO10 (AluJ+96+120) on the other hand had a calculated binding energy of -6.9 kcal/mol and so, based purely on these parameters, ought to bind most effectively and so induce the greatest exon skipping, with PMO9 (AluJ+93+117) being slightly less effective (with a total binding energy of -4.8 kcal/mol) and PMO8 (AluJ+1+25) not having any effect at all. This was not the case when tested *in vitro*, as PMO10 (AluJ+96+120) turned out to be ineffective at inducing exon skipping whereas PMO8 (AluJ+1+25) had a moderate effect despite having a positive calculated binding energy. This could indicate that the prediction of binding energies is not accurate enough to properly determine the required energy for PMO binding. There are clearly other parameters not included in these calculations that affect whether or not the PMOs bind to the RNA. It has previously been reported that a PMO with a more negative binding energy correlates with improved exon skipping (Popplewell *et al.*, 2009). However, in this paper the total binding energies for the PMOs

were more negative than those tested here, with binding energies in the region of -30 kcal/mol to -40 kcal/mol, and also the PMOs ranged in length up to 30 bases. It could therefore be the case that binding energies may influence the PMO design process but only when the binding energy is calculated to be within this range, and that longer PMOs have the potential for a more negative binding energy. Nevertheless, if the binding energy is calculated to be higher, it does not necessarily mean that the PMO will not bind.

The secondary structure of the ADAR2 transcript surrounding the AluJ cassette was also predicted using the MFold web server, and used to guide PMO design towards single-stranded regions of RNA. Based on this prediction, PMO9 (AluJ+93+117) was designed to target an open region of RNA found 3 bases upstream of the 3' splice site compared to PMO10 (AluJ+96+120) which targeted a region of double-stranded RNA at the 3' splice site itself. This proved to be an important adjustment, as PMO9 (AluJ+93+117) showed excellent exon skipping efficiency while PMO10 (AluJ+96+120) did not have any effect. This large difference in efficacy when there was just a 3 base shift in the sequence was unexpected, and so PMO9A (AluJ+94+118) and PMO9B (AluJ+95+119) were designed to be intermediate steps, moving a single base towards the 3' splice site each time. PMO9A (AluJ+94+118), one base shifted to downstream of PMO9 (AluJ+93+117), proved to be marginally more effective than PMO9B (AluJ+95+119) *in vitro* at lower concentrations as shown by changes in the IC_{50} for each PMO. PMO9 (AluJ+93+117) was the most effective at AluJ cassette exclusion, with an IC_{50} of 0.18 ± 0.02 µM, then PMO9A (AluJ+94+118) with an IC_{50} of 0.36 ± 0.03 µM followed by PMO9B (AluJ+95+119) with an IC_{50} of 0.47 ± 0.03 µM. The IC_{50}s for PMO9A (AluJ+94+118) and PMO9B (AluJ+95+119) are very similar, and analysis of the dose-response curves indicate PMO9B (AluJ+95+119) in particular does not produce a good fit. PMO9A (AluJ+94+118) and PMO9B (AluJ+95+119) could therefore be considered to have the same effect on AluJ exclusion. PMO10 (AluJ+96+120) only showed a minimal effect on exon skipping within the concentration range tested here. When comparing the sequences to the secondary structure of the RNA target, it can be seen that PMO9A (AluJ+94+118), PMO9B (AluJ+95+119) and PMO10 (AluJ+96+120) are entering progressively further into the double-stranded region around the 3' splice site. The PMOs may therefore be prevented from accessing these bases and so are unable to form strong enough bonds with the RNA, leading to inefficient exon skipping. These IC_{50} values follow the predicted trend of decreasing efficacy as the PMO moves further into the double-stranded structure. However, PMO9A (AluJ+94+118) and PMO9B (AluJ+95+118) were still effective at exon skipping at the higher concentrations, whereas PMO10 (AluJ+96+120) only showed a slight effect at 5 µM. This large difference in potency between PMO9B (AluJ+95+119) and PMO10 (AluJ+96+120) is still

unexplained. To further investigate the reasons for PMO10 (AluJ+96+120) not showing any effect, it might be interesting to design PMOs that target bases further into the double-stranded region, beyond the splice site, to assess whether they too are prevented from binding. Alternatively, other splice sites located within double-stranded regions of RNA could be targeted to see whether these aspects of secondary structure should be avoided in all designs for exon skipping ASOs.

Looking at which PMOs of the five designed were successful at preventing the inclusion of the AluJ cassette, it could be considered that targeting the predicted ESE binding sites and single-stranded RNA, while avoiding ESS binding sites and double-stranded RNA regions, are the more important considerations in antisense oligonucleotide design, while prediction of intermolecular binding energies is not accurate enough to be an effective guide. While this was true of the five PMOs tested in this chapter, splice sites in other transcripts would need to be tested in order to rule out using binding energies to predict PMO targets and instead focus on secondary structure and ESE binding sites. Aartsma-Rus et al. have performed analyses on previously published ASOs using exon skipping in the dystrophin gene, both effectively and ineffectively, to determine whether guidelines can be extrapolated from these studies (Aartsma-Rus *et al.*, 2009). The conclusions from their work are partly contradictory to those reported in this experiment, as they concluded that of the 156 ASOs analysed (104 that showed good exon skipping, 52 that were ineffective) the best parameters for guiding design were the GC content of the sequence and its predicted binding energy, which were found to not be of significance to these five PMOs. To truly determine whether these parameters aid ASO design, much higher numbers of PMOs would need to be tested, ideally across a large number of exons spliced at different rates, although this scale of analysis is prohibitively expensive. Aartsma-Rus et al. also determined that the majority of effective PMOs covered ESE binding sites, which supports the findings from this chapter (Aartsma-Rus *et al.*, 2009). It appears that the most reliable parameter for PMO design in exon skipping from those evaluated here would be targeting the predicted binding sites of ESEs. Predicted secondary structure, and therefore targeting accessible bases in the RNA transcript, was an important aspect of the *in silico* PMO design. However, previous work has shown that a more accurate and reliable method for finding accessible bases is to use hybridisation array analysis (Popplewell *et al.*, 2009). Here, the target RNA sequence is amplified and exposed to all possible hexamers. Binding, detected through biotinylated bases and fluorescent labelling, indicates an accessible sequence of hexamers and so could be targets for ASOs. This technique could aid further ASO design to the AluJ cassette sequence, as the results are experimentally verified rather than relying on the assumptions that are part of predictive software.

PMO9 (AluJ+93+117) was not only extremely efficient at excluding the AluJ cassette, but this also led to an indirect increase in RNA editing at the Q/R site of the GluA2 subunit. When the ADAR2 transcript does not include the AluJ cassette, it is more efficient at A-to-I editing (Gerber *et al.*, 1997), and so PMO9 (AluJ+93+117), through exon skipping technology, can influence the efficiency of the ADAR2 enzyme. What is curious is that PMO9A (AluJ+94+118) and PMO9B (AluJ+95+119) also prevented the inclusion of the AluJ cassette, but did not show any change in Q/R site editing in the HeLa-B13 system. It is possible that these PMOs did have an effect on RNA editing but it was not large enough to achieve significance, although the reasons why they would have a smaller effect than PMO9 (AluJ+93+117) are unclear. In order to have an impact on RNA editing at the Q/R site, the PMO needs to bind efficiently to the ADAR2 RNA transcript in the nucleus to prevent AluJ cassette inclusion. This process must be carried out on the majority of transcripts, so that the translated ADAR2 protein does not include this sequence. Once the majority of ADAR2 does not contain the AluJ cassette sequence then the enzyme's editing efficiency has the potential to be affected. Since PMO9 (AluJ+93+117) was shown to be more efficient at exon skipping than PMO9A (AluJ+94+118) and PMO9B (AluJ+95+119) at lower concentrations, it is possible that this difference in exon skipping ability was magnified across the pathway. There are several steps between the exon skipping effect of the PMO and the Q/R site editing efficiency, with multiple opportunities for other variables to influence the result. These external variables could be related to the PMOs themselves, for example PMO9A (AluJ+94+118) and PMO9B (AluJ+95+119) may not enter the nucleus as efficiently or may not bind to the RNA transcript as strongly, or it could be related to how the ADAR2 transcript is processed or transported after splicing takes place. Furthermore we have not examined the protein levels of ADAR2 in our HeLa cell lines and we do not know whether the PMOs used in this study have significantly altered the expression levels of ADAR2 protein within the cell.

PMO9 (AluJ+93+117) increased Q/R site editing to 130% of control at 2 μM after 24 hours of transfection, although this percentage increase could not be improved by increasing the concentration of PMO9 (AluJ+93+117) nor increasing the transfection time. It therefore appears that this 30% increase in RNA editing is limited by some factor other than the efficiency of ADAR2. This is likely to be an inherent limitation within the HeLa-B13 system. One possible constraint could be ADAR2 expression levels within HeLa cells, particularly as it was shown in a previous chapter that Q/R site editing could be increased through simply overexpressing ADAR2. It has also been previously shown that increasing ADAR2 mRNA concentrations can increase the extent of Q/R site editing in HeLa cells modified to stably express the GluA2 transcript (Sawada *et al*., 2009, Yamashita *et al.,* 2012c). It is therefore possible that manipulation of endogenous levels

of ADAR2 can only increase editing by 30%, particularly as the B13 minigene is under the control of a CMV promoter and is expected to be expressed at very high levels and so possibly overwhelming the ADAR2 enzyme available. Due to the transfection conditions of the HeLa-B13 system, the cells cannot be incubated for longer than 48 hours without significant cell death. It is therefore possible that even at this longer incubation time there remains a pool of ADAR2 enzyme that include the AluJ cassette as they were translated before PMO treatment and so were not subject to exon skipping.

In the original paper describing the difference in editing between the two ADAR2 isoforms, with and without the AluJ cassette, ADAR2 containing AluJ was 50% more active than the transcript without AluJ on synthetic double-stranded DNA (Gerber *et al.*, 1997). However, at higher concentrations of ADAR2, both isoforms performed equally well. This indicates that the difference in editing efficiency between the two isoforms of ADAR2 is subtle, and so perhaps the editing assay used in our study is not sensitive enough to detect any smaller differences in editing. The previous study was also performed over one hour, whereas this study looked at Q/R site editing after 24 or 48 hours. It is therefore possible that any difference in editing was evident at a shorter time period and had been corrected by the time the analysis took place.

On the other hand, an increase of 30% could be sufficient protection against excitotoxicity for motor neurons. The Q/R site editing in motor neurons of ALS patients was extremely variable, with some motor neurons showing no editing at the Q/R site at all (Kawahara *et al.*, 2004). This lack of Q/R site editing has been attributed to low expression of ADAR2 in motor neurons of ALS patients (Hideyama *et al.*, 2012). Therefore, in cells with this low expression level, the subtle difference between transcripts containing the AluJ cassette and those without could make a large impact on the editing efficiency. However, it is difficult to find a model in which to test this hypothesis. The AluJ cassette is only found in human (and possibly other primate) ADAR2 transcripts, and so basic primary neuronal models from mouse or rat cortices could not be used. A possibility would be to use human induced pluripotent stem cell-derived motor neurons. The expression levels of alternatively spliced ADAR2 transcripts in these cells have not yet been determined, and it is not known whether Q/R site editing is variable in motor neurons derived from stem cells of ALS patients as was seen in the original study with laser-captured motor neurons from the spinal cord. However, using the PMOs designed here to manipulate Q/R site editing in motor neurons would allow for functional assessments to be performed. The Ca^{2+} influx through AMPA receptors following treatment with the PMOs could be determined, and the effect of overstimulation by glutamate on cell viability could be analysed.

7 DISCUSSION

In this work, antisense oligonucleotide technology was utilised to both disrupt and enhance RNA editing at the Q/R site of the GluA2 subunit in AMPA receptors. Editing at the Q/R site, with its known importance in normal neurological function (Brusa *et al.*, 1995; Hideyama *et al.*, 2010), was targeted due to the variability in editing levels seen in patients with ALS (Kawahara *et al.*, 2004). Antisense oligonucleotides are a useful tool in molecular biology due to their specificity, limited off-target effects, and their resistance to degradation allowing for prolonged interactions. Antisense technology is commonly used in exon skipping, where the oligonucleotide influences splicing machinery to alter patterns of exons (Osman & Miller, 2014; Wu *et al.*, 2014). This work aimed to use antisense technology to manipulate another intracellular process, RNA editing, through disruption of RNA secondary structure as well as to use exon skipping to change alternative splicing patterns of the ADAR2 enzyme and increase its efficiency. Manipulating Q/R site editing could have consequences for ALS research, both providing a model for disrupted editing in cells and a potential therapy by increasing the editing efficiency.

7.1 USING PMOS TO INHIBIT Q/R SITE EDITING

In the first part of this thesis, PMOs were designed to inhibit Q/R site editing. Building on the design published by Penn *et al* (2012), 30mer PMOs were designed to target the double-stranded structure around the Q/R editing site of the GluA2 transcript. These PMOs were shown to inhibit editing in the HeLa-B13 system, and the effect of PMOE1 (GRIA2+279+313) was shown to successfully translate to the SH-SY5Y cell line which endogenously express the GluA2 subunit. Q/R site editing in the mRNA of SH-SY5Y cells was inhibited from 100% edited transcripts to less than 20% after 48 hours of treatment. For the first time, PMOs were shown to inhibit Q/R site editing in primary cortical neurons, although the method for transfection was unreliable and continues to require further optimisation before the downstream consequences of inhibited Q/R site editing can be fully analysed. Lentiviral vectors have the potential to introduce the antisense sequence easily into primary cortical neurons, and this avenue also continues to be explored. Integration-deficient lentiviral vectors (IDLVs), with mutations in the integrase enzyme preventing insertion of the transgene into the genome, have been shown to efficiently transduce neurons both *in vivo* and *in vitro* (Yáñez-Muñoz *et al.*, 2006). Following an intracortical injection, IDLVs have been shown to effectively transduce corticospinal neurons *in vivo* (Hutson *et al.*, 2012), and so are a promising potential vector to introduce antisense sequences into neurons both in culture

and in future *in vivo* models. Lentiviral vectors containing the human U6 small nuclear promoter (U6) have been show to express shRNA sequences in mouse models (Mäkinen *et al.*, 2006) and are now commonly used to express guide RNA sequences in the CRIPSR/Cas9 system (Koike-Yusa *et al.*, 2014). Expression of the equivalent RNA sequences used in the PMOs for this chapter by IDLVs could therefore provide a system to test the effect of Q/R site editing inhibition in a variety of models.

This model of disrupted Q/R site editing *in vitro* would contribute to the knowledge gained from AR2 mice, which have a conditional knockdown of ADAR2 in motor neurons (Hideyama *et al.*, 2010). In these mice, reduced Q/R site editing was associated with behavioural phenotypes of loss of motor function and a reduced life expectancy. Application of the GRIA2 PMOs to primary cortical neurons could elucidate intracellular events downstream of a loss of editing that may contribute to these behavioural changes. Here we show the first evidence for antisense technology targeting the Q/R site editing in primary neurons, with slight, albeit unreliable, inhibition of editing. PMO-mediated inhibition of Q/R site editing could be improved through conjugation of the PMOs to a cell-penetrating peptide, which have the ability to both cross the blood-brain barrier and enter neuronal populations (Stalmans *et al.*, 2015). This modification would also allow the PMOs to be used in mouse models of ALS as well as in primary cell cultures.

With strong disruption of Q/R site editing in cell lines, it is hoped that further adjustment of the methods for introducing the PMOs into primary cortical neurons would establish a consistent neuronal model to investigate these proposed molecular events, which could be key in understanding the molecular pathogenesis of ALS. Disruption of Q/R site editing is not only found in ALS patients, but in other neurological pathologies such as Alzheimer's disease (Gaisler-Salomon *et al.*, 2014) and ischaemia (Peng *et al.*, 2006). It is possible that disruption of Q/R site editing, with or without downregulation of ADAR2, is part of a general pathway for neuronal damage and so this model could have more far-reaching applications.

A model has been proposed by Yamashita and Kwak explaining the role of disrupted RNA editing at the Q/R site in the pathology of ALS (Yamashita & Kwak, 2014). TDP-43 aggregation is a hallmark of ALS (Neumann *et al.*, 2006) and in laser-captured motor neurons from sporadic ALS patients, all those that showed downregulation of ADAR2 also showed TDP-43 pathology (Aizawa *et al.*, 2010). However, overexpression of full length or fragments of TDP-43 and knockdown of *TARDBP* expression failed to induce downregulation of ADAR2 in cell lines, indicating that TDP-43 pathology is not upstream of ADAR2 dysregulation (Yamashita *et al.*, 2012b). Loss of ADAR2 expression may therefore be upstream of TDP-43 pathology, as loss of the RNA binding protein is only found in neurons with downregulated editing enzyme. This hypothesised cascade is

shown in Figure 7.1A. PMOs designed to disrupt the secondary structure of GluA2 have the same effect on Q/R site editing as downregulation of ADAR2. The model developed here could therefore mimic the hypothesised cascade from this stage (shown in red in Figure 7.1B), and it would be interesting to determine whether loss of Q/R site editing was sufficient to cause mislocalisation and aggregation of TDP-43. If so, this would be further evidence that TDP-43 pathology is a downstream event from ADAR2 dysregulation, supporting the hypothesised cascade.

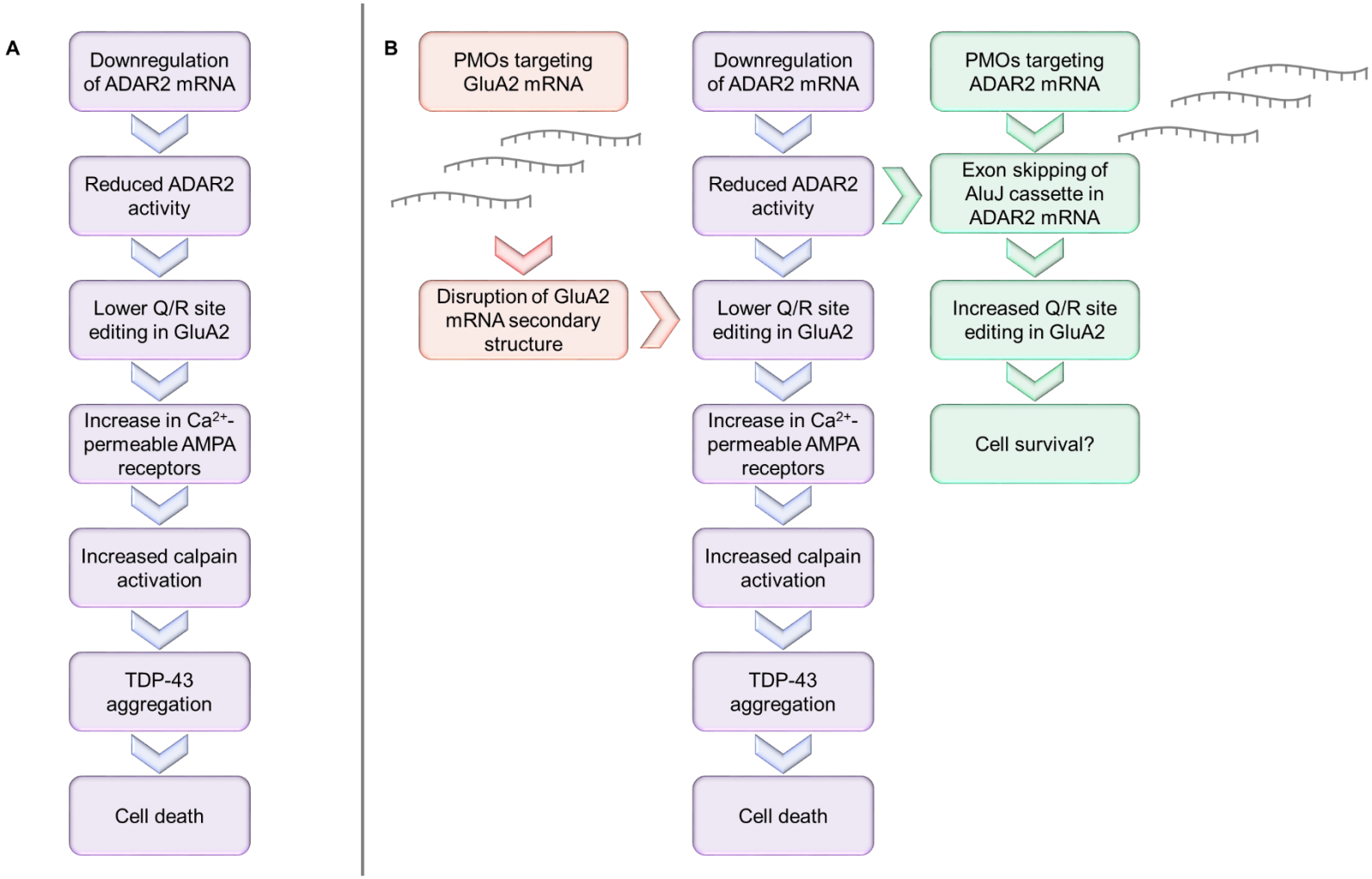

Figure 7.1 - A) proposed ALS cascade hypothesis by Yamashita and Kwak (2014) where inhibited Q/R site editing in motor neurons leads to TDP-43 aggregation and cell death. B) Incorporating the PMOs designed in this thesis into the cascade.

7.2 USING PMOS TO CHANGE THE ALTERNATIVE SPLICING PATTERN OF ADAR2

This work also shows the first time that antisense technology has targeted the ADAR2 enzyme in order to change its alternative splicing patterns. PMOs were designed based on information from a variety of bioinformatic resources such as prediction of splice regulatory elements, secondary structure of the RNA transcript and binding energies. Using these data, a total of 5 PMOs were designed targeting the AluJ cassette with varying degrees of exon skipping ability. PMO9 (AluJ+93+117) was then also shown to indirectly promote the RNA editing reaction at the Q/R site through increasing the availability of the more active form of ADAR2, the transcript without the AluJ cassette. This is the first preliminary evidence that changing the alternative splicing pattern of ADAR2 can change the percentage of editing at the Q/R site. This could have important implications. As previously discussed, variability of Q/R site editing percentage is found in motor neurons of ALS patients (Kawahara *et al.*, 2004). Therefore if improving ADAR2's editing efficiency could increase Q/R site editing in those neurons with underedited sites, associated increases in calcium influx and neuronal cell death could be prevented. It would be interesting to investigate whether ADAR2 expression or Q/R site editing of the GluA2 transcript is impacted in any other model for ALS, such as the $SOD1^{G93A}$ mouse model, and if so whether our PMO can have an effect on these processes.

Work with AR2 mouse model of ALS showed that increasing ADAR2 expression could rescue their degenerative phenotype by preventing the loss of motor function, reducing motor neuron cell death and increasing Q/R site editing to over 95% (Yamashita *et al.*, 2013). In this study, the ADAR2 sequence was inserted into AAV9 vectors which could then be injected intravenously in the mouse tail vein. The ADAR2 sequence was taken from the cDNA amplicons of "ADAR2a", without the AluJ cassette. The ADAR2 gene, under the SYN1 promoter, was specifically expressed in neurons with no observable expression in the periphery. Total ADAR2 mRNA expression increased by 1.5-fold, with no change in expression of endogenous mouse ADAR2 (Yamashita *et al.*, 2013). This paper focussed on the effect of ADAR2 overexpression on the Q/R editing site, but did not discuss any side effects of this treatment. It would be interesting to determine whether expression of the "ADAR2b" isoform in an AAV vector, including the AluJ cassette, would have the same effect on Q/R site editing.

ADAR2 edits adenosines at thousands of sites across the genome, and so a 1.5-fold increase in expression could have broader consequences. Mice with a knockout of ADAR2, when crossed with the mouse line expressing the "edited" version of *Gria2*,

show changes in expression across a range of genes, many of which are expressed in neurons, as well as specific phenotypic changes such as altered startle reflexes which may be associated with a loss of editing in the 5-HT_{2C} gene (Horsch *et al.*, 2011). Therefore, although the overexpression of ADAR2 using the AAV9 vector was limited to neuronal cells, general overexpression of the ADAR2 enzyme may cause nonspecific effects. In this thesis, we have described a more subtle approach to increase endogenous ADAR2 activity, which if applied successfully *in vivo* could potentially limit the side-effects seen with ADAR2 overexpression.

Overexpressing ADAR2 is an efficient treatment in the AR2 mouse model for ALS, but currently this method would not be a viable therapeutic approach for humans. Although gene therapy has reached clinical trials for many applications including cancers, immune disorders and neurological disorders (summarised in Figure 7.2), only two therapies have so far received European approval: Glybera (uniQure), which uses an AAV vector to deliver additional lipoprotein lipase in patients with pancreatitis (Ylä-Herttuala, 2012), and Strimvelis, an *ex vivo* therapy correcting expression of adenosine deaminase in SCID patients (Schimmer & Breazzano, 2016). Fears over patients developing leukaemia due to random insertion of transgenes into the genome, which has occurred in several clinical trials, form a large part of the argument against approval for gene therapies (Ginn *et al.*, 2013).

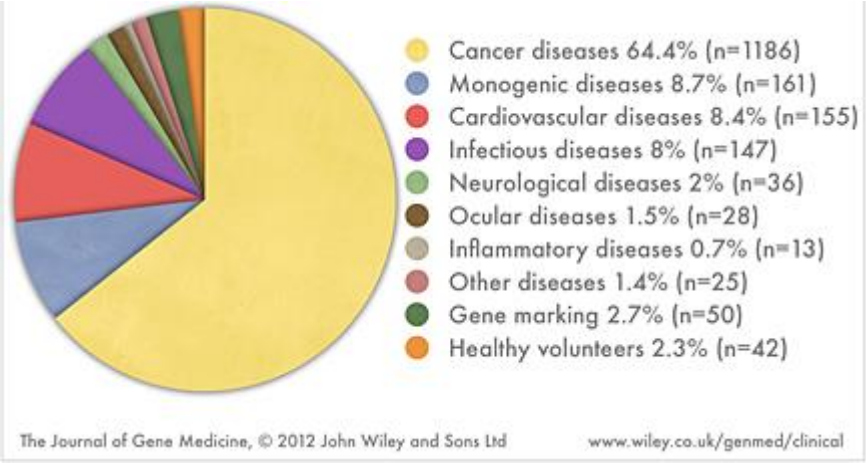

Figure 7.2 - Indications addressed by gene therapy clinical trials, figure taken from (Ginn *et al.*, 2013)

Use of antisense technology, on the other hand, does not carry the same risk for oncogenesis. Mipomersen, targeting apolipoprotein B expression in patients with familial hypercholesterolaemia (Raal *et al.*, 2010), was approved by the FDA for use in 2013 (Toth, 2013). Alicaforsen is an antisense oligonucleotide targeting ICAM-1 in cases of ulcerative colitis and inflammatory bowel disease (van Deventer *et al.*, 2004; Greuter *et al.*, 2016) and has been given orphan drug status by both the US and the EU, allowing its fast track through the regulatory processes. For patients with Duchenne Muscular

Dystrophy, the battle to get Eteplirsen approved by the FDA continues. Eteplirsen targets the *DMD* gene, employing exon skipping technology to skip exon 51 and produce a functional truncated dystrophin protein which delays the progression of Duchenne Muscular Dystrophy symptoms (Mendell *et al.*, 2016). If approved, these successful antisense therapies could pave the way for the dozens of other drug candidates showing success in clinical trials, such as Nusinersen in the treatment of spinal muscular atrophy (Haché *et al.*, 2016). Antisense oligonucleotides have a good safety profile in clinical trials, in general showing only mild adverse effects such as flu-like symptoms or reactions around the site of administration such as post-lumbar puncture syndrome or back pain (Miller *et al.*, 2013). Elevated transaminases, a possible indication of liver damage, have also been reported in some clinical trials with mipomersen (Raal *et al.*, 2010) but not in other cases (Haché *et al.*, 2016). Therefore, while gene therapy to increase expression of the ADAR2 enzyme might show good results in mouse models, the safety profile of this kind of therapy is prohibitive. On the other hand, antisense therapies have been shown to be well-tolerated by humans, and so increasing the efficacy of the ADAR2 enzyme through PMO-mediated exon skipping as a therapy for ALS could be more likely to pass regulatory standards in a potentially rapid line of clinical development.

7.3 STUDY LIMITATIONS

There are, of course, limitations to any scientific experiment which will affect the quality of results given and the ability to comprehensively answer a given hypothesis. If broader conclusions are to be drawn then these limitations must be acknowledged and addressed. Firstly, this work was limited by the restriction to cell culture models. Secondly, the method for quantification of Q/R site editing, using quantification of restriction endonuclease digest products, may have impacted the quality of results found. Also, a limit on the number of PMOs available to test in this body of work prevented broader conclusions from being drawn on ideal PMO target sequences. Finally, the method of delivery of PMOs prevented the assessment of the effects of Q/R site editing inhibition in primary neuronal cultures.

Use of cell culture models in this work was necessary, but limiting. There is no replacement for working with cell lines in molecular biology that is comparable in terms of ease of manipulation, cost and replicability. The main limitation of working with cell lines is the basic nature of the model. Only one cell type exists in the system, which is not neuronal, and the cells do not necessarily behave in the same way as *in vivo*. For example, SH-SY5Y cells were used to test the effect of PMOs on endogenously expressed GluA2 transcripts. However, there is little evidence that these transcripts develop into a mature AMPA receptor, and so this model may be more closely related to

an immature neuron (Kovalevich & Langford, 2013). Despite these drawbacks, cell culture work will likely remain the preliminary model for many areas of molecular biology. However, alternative options will continue to develop into more physiologically comparable models. For example, the ease with which fibroblasts form induced pluripotent stem cells, which can then differentiate into a multitude of cell types including motor neurons, opens new possibilities for physiologically comparable *in vitro* work. Use of these models could overcome the limiting basic nature of working with cell lines, and possibly make the results more predictive of *in vivo* effects.

The method chosen for measurement of percentage editing at the Q/R site was based on previous reports (Sawada *et al.*, 2009; Yamashita *et al.*, 2012a; Whitney *et al.*, 2008) and ease of replication. However, densitometric analysis of restriction endonuclease products contains some inherent bias. This method relies on detection of DNA bands on visualisation of agarose gels, and so may not be accurate enough to pick up small changes in editing. For this work, this limitation was accepted as unavoidable but as a point which may affect the quality of results. For example, the effect of PMO9A (AluJ+94+118) or PMO9B (AluJ+95+119) on Q/R site editing may have been too small for detection using this method despite these PMOs showing strong exon skipping of the AluJ cassette. Therefore in future work, alternative methods of quantification of editing may be compared.

In this project, a number of PMOs targeted at specific sites were examined. This required the usage of a number of bioinformatic prediction tools to assess the target sequence before PMO production and involved an important part of this thesis. However, it also meant that the ideal scenario of “walking” the PMOs along the gene, shifting the target sequence by a few bases each time, was not possible. Therefore, conclusions made on the success of the PMOs *in vitro* compared to the predicted success *in silico* cannot be definitively made without analysis of further sequences. Despite this restriction, the *in silico* predictions were sufficiently successful to produce PMO sequences that both inhibited Q/R site editing when targeting GluA2 secondary structure and increasing Q/R site editing when targeting skipping of the AluJ cassette in the ADAR2 transcript.

The main limitation in this project was the method of delivery of the PMOs. Use of peptide-based transfection reagents are common practice in cell lines, but have limited efficiencies in more complex systems as shown with the primary cortical neurons here. Transfection reagents also do not allow the PMOs to be taken into *in vivo* models. In order to further the work done here, a more efficient method of delivery ought to be utilised such as peptide conjugation.

7.4 FURTHER WORK

Following the work discussed in this thesis, work in the immediate future would be characterising the effects of both of these sets of PMOs in more relevant cell models, either inhibiting the Q/R site editing in primary cortical neurons or testing PMOs targeting either the GluA2 subunit or the ADAR2 transcript in induced pluripotent stem cell-derived motor neurons. This would be the most accurate cell culture model possible and, as fibroblasts could be sourced from ALS patients, may test the PMOs in an ALS model of motor neurons. The results shown in this thesis confirm that the PMOs can target the first steps of the cascade proposed in Figure 7.1A, however the effect of PMOs on later steps would need to be characterised. Therefore, analysis of PMOs in neuronal models could assess the effect of inhibited Q/R site editing on TDP-43 aggregation, and whether altering ADAR2 splicing patterns can improve cell viability (Figure 7.1B). Ultimately, with appropriate peptide conjugations for administration, these PMOs would need to be tested *in vivo* to assess the true effect of altered editing on cell viability.

Beyond validating these PMOs in a more applicable model, an interesting avenue for exploration would be whether other editing sites in the genome could be disrupted using PMOs. This thesis has shown that PMOs targeting regions of double-stranded secondary structure can effectively disrupt Q/R site editing. Other editing sites in coding regions are known to have important physiological functions, for example editing of the 5-HT_{2C} transcript occurs within a predicted double-stranded loop, with reduced editing being associated with schizophrenia (Sodhi *et al.*, 2001), depression (Gurevich *et al.*, 2002) and neuropathic pain (Nakae *et al.*, 2008). Using PMOs to disrupt the secondary structure of this editing site could therefore give indications towards molecular mechanisms affected in these disorders. This thesis has also shown that skipping of the AluJ cassette exon in the ADAR2 transcript leads to an increase in Q/R site editing. Further work should determine whether any other editing sites, both in coding and noncoding sequences, are affected by this shift in ADAR2 isoform. Additionally, there are several other ADAR2 isoforms expressed in mammalian tissue (Kawahara *et al.*, 2005). Directing exon skipping to these other alternatively spliced exons may also impact RNA editing either at the Q/R site of the GluA2 transcript or others throughout the genome

8 BIBLIOGRAPHY

AARTSMA-RUS, A., JANSON, A.A.M., KAMAN, W.E., BREMMER-BOUT, M., DEN DUNNEN, J.T., BAAS, F., VAN OMMEN, G.-J.B. & VAN DEUTEKOM, J.C.T. (2003) Therapeutic antisense-induced exon skipping in cultured muscle cells from six different DMD patients. *Human molecular genetics*. 12 (8), 907–914.

AARTSMA-RUS, A. & VAN OMMEN, G.-J.B. (2007) Antisense-mediated exon skipping: a versatile tool with therapeutic and research applications. *RNA*. 13 (10), 1609–1624.

AARTSMA-RUS, A., VAN VLIET, L., HIRSCHI, M., JANSON, A. A M., HEEMSKERK, H., DE WINTER, C.L., DE KIMPE, S., VAN DEUTEKOM, J.C.T., 'T HOEN, P. A C. & VAN OMMEN, G.-J.B. (2009) Guidelines for antisense oligonucleotide design and insight into splice-modulating mechanisms. *Molecular Therapy.* 17 (3), 548–553.

ABBAS, A.I., URBAN, D.J., JENSEN, N.H., FARRELL, M.S., KROEZE, W.K., MIECZKOWSKI, P., WANG, Z. & ROTH, B.L. (2010) Assessing serotonin receptor mRNA editing frequency by a novel ultra high-throughput sequencing method. *Nucleic acids research.* 38 (10), e118

ABEL, O., POWELL, J.F., ANDERSEN, P.M. & AL-CHALABI, A. (2012) ALSoD: A user-friendly online bioinformatics tool for amyotrophic lateral sclerosis genetics. *Human mutation*. 33 (9), 1345–1351.

ACHARYA, K.K., GOVIND, C.K., SHORE, A.N., STOLER, M.H. & REDDI, P.P. (2006) cis-requirement for the maintenance of round spermatid-specific transcription. *Developmental biology*. 295 (2), 781–790.

ADAMCZYK, A., MEJIAS, R., TAKAMIYA, K., YOCUM, J., KRASNOVA, I., CALDERON, J., CADET, J.L., HUGANIR, R., PLETNIKOV, M. & WANG, T. (2012) GluA3-deficiency in Mice is Associated with Increased Social and Aggressive Behaviour and Elevated Dopamine in Striatum. *Behavioral Brain Research*. 229 (1), 265–272.

ADE, C., ROY-ENGEL, A.M. & DEININGER, P.L. (2013) Alu elements: an intrinsic source of human genome instability. *Current opinion in virology*. 3 (6), 639–645.

ADESNIK, H. & NICOLL, R.A. (2007) Conservation of Glutamate Receptor 2-Containing AMPA Receptors during Long-Term Potentiation. *Journal of Neuroscience.* 27 (17), 4598–4602.

AGHOLME, L., LINDSTRÖM, T., KÅGEDAL, K., MARCUSSON, J. & HALLBECK, M. (2010) An in vitro model for neuroscience: differentiation of SH-SY5Y cells into cells with morphological and biochemical characteristics of mature neurons. *Journal of Alzheimer's disease.* 20 (4), 1069–1082.

AGRANAT, L., SPERLING, J. & SPERLING, R. (2011) A novel tissue-specific alternatively spliced form of the A-to-I RNA editing enzyme ADAR2. *RNA biology*. 7 (2), 253–262.

AHMAD, S., BHATIA, K., KANNAN, A. & GANGWANI, L. (2016) Molecular Mechanisms of Neurodegeneration in Spinal Muscular Atrophy. *Journal of experimental neuroscience.* 10, 39–49.

AIZAWA, H., SAWADA, J., HIDEYAMA, T., YAMASHITA, T., KATAYAMA, T., HASEBE, N., KIMURA, T., YAHARA, O. & KWAK, S. (2010) TDP-43 pathology in sporadic ALS occurs in motor neurons lacking the RNA editing enzyme ADAR2. *Acta neuropathologica*. 120 (1), 75–84.

AKBARIAN, S., SMITH, M.A. & JONES, E.G. (1995) Editing for an AMPA receptor subunit RNA in prefrontal cortex and striatum in Alzheimer's disease, Huntington's disease and schizophrenia. *Brain research*. 699 (2), 297–304.

ALLAOUA, H., CHAUDIEU, I., KRIEGER, C., BOKSA, P., PRIVAT, A. & QUIRION, R. (1992) Alterations in spinal cord excitatory amino acid receptors in amyotrophic lateral sclerosis patients. *Brain Research.* 579 (1), 169–172.

AMANTANA, A. & IVERSEN, P.L. (2005) Pharmacokinetics and biodistribution of phosphorodiamidate morpholino antisense oligomers*. Current opinion in pharmacology.* 5 (5), 550–555.

ARAI, T., HASEGAWA, M., AKIYAMA, H., IKEDA, K., NONAKA, T., MORI, H., MANN, D., TSUCHIYA, K., YOSHIDA, M., HASHIZUME, Y. & ODA, T. (2006) TDP-43 is a component of ubiquitin-positive tau-negative inclusions in frontotemporal lobar degeneration and amyotrophic lateral sclerosis. *Biochemical and biophysical research communications.* 351 (3), 602–611.

ARAI, Y., MIZUGUCHI, M. & TAKASHIMA, S. (1997) Developmental changes of glutamate receptors in the rat cerebral cortex and hippocampus. *Anatomy and embryology.* 195 (1), 65–70.

ARMSTRONG, N. & GOUAUX, E. (2000) Mechanisms for activation and antagonism of an AMPA-sensitive glutamate receptor: crystal structures of the GluR2 ligand binding core*. Neuron*. 28 (1), 165–181.

ARNOLD, E.S., LING, S.-C., HUELGA, S.C., LAGIER-TOURENNE, C., POLYMENIDOU, M., DITSWORTH, D., KORDASIEWICZ, H.B., MCALONIS-DOWNES, M., PLATOSHYN, O., PARONE, P.A., DA CRUZ, S., CLUTARIO, K.M., SWING, D., TESSAROLLO, L., MARSALA, M., SHAW, C.E., YEO, G.W. & CLEVELAND, D.W. (2013) ALS-linked TDP-43 mutations produce aberrant RNA splicing and adult-onset motor neuron disease without aggregation or loss of nuclear TDP-43. *PNAS* 110 (8), E736–E745.

AYALA, Y.M., ZAGO, P., D'AMBROGIO, A., XU, Y.-F., PETRUCELLI, L., BURATTI, E. & BARALLE, F.E. (2008) Structural determinants of the cellular localization and shuttling of TDP-43. *Journal of cell science*. 121 (Pt 22), 3778–3785.

AYERS, J.I., FROMHOLT, S., KOCH, M., DEBOSIER, A., MCMAHON, B., XU, G. & BORCHELT, D.R. (2014) Experimental transmissibility of mutant SOD1 motor neuron disease. *Acta neuropathologica.* 128 (6), 791–803.

AYERS, J.I., FROMHOLT, S.E., O'NEAL, V.M., DIAMOND, J.H. & BORCHELT, D.R. (2016) Prion-like propagation of mutant SOD1 misfolding and motor neuron disease spread along neuroanatomical pathways. *Acta Neuropathologica*. 131 (1), 103–114

AZUBEL, M., HABIB, N., SPERLING, R. & SPERLING, J. (2006) Native spliceosomes assemble with pre-mRNA to form supraspliceosomes. *Journal of Molecular Biology.* 356 (4), 955–966.

BAHN, J.H., LEE, J.-H., LI, G., GREER, C., PENG, G. & XIAO, X. (2012) Accurate identification of A-to-I RNA editing in human by transcriptome sequencing. *Genome research.* 22 (1), 142–150.

BALIK, A., PENN, A.C., NEMODA, Z. & GREGER, I.H. (2013) Activity-regulated RNA editing in select neuronal subfields in hippocampus. *Nucleic acids research*. 41 (2), 1124–1134.

BALL, S.M., ATLASON, P.T., SHITTU-BALOGUN, O.O. & MOLNÁR, E. (2010) Assembly and intracellular distribution of kainate receptors is determined by RNA editing and subunit composition. *Journal of neurochemistry*. 114 (6), 1805–1818.

BARBON, A., FUMAGALLI, F., CARACCIOLO, L., MADASCHI, L., LESMA, E., MORA, C., CARELLI, S., SLOTKIN, T.A., RACAGNI, G., DI GIULIO, A.M., GORIO, A. & BARLATI, S. (2010) Acute spinal cord injury persistently reduces R/G RNA editing of AMPA receptors. *Journal of neurochemistry*. 114 (2), 397–407.

BASSANI, S., FOLCI, A., ZAPATA, J. & PASSAFARO, M. (2013) AMPAR trafficking in synapse maturation and plasticity. *Cellular and Molecular Life Sciences*. 70 (23), 4411–4430

BASSO, M., POZZI, S., TORTAROLO, M., FIORDALISO, F., BISIGHINI, C., PASETTO, L., SPALTRO, G., LIDONNICI, D., GENSANO, F., BATTAGLIA, E., BENDOTTI, C. & BONETTO, V. (2013) Mutant copper-zinc superoxide dismutase (SOD1) induces protein secretion pathway alterations and exosome release in astrocytes: implications for disease spreading and motor neuron pathology in amyotrophic lateral sclerosis. *The Journal of biological chemistry*. 288 (22), 15699–15711.

BAUER, P.O. (2016) Methylation of C9orf72 expansion reduces RNA foci formation and dipeptide-repeat proteins expression in cells. *Neuroscience letters*. 612, 204–209.

BAZAK, L., HAVIV, A., BARAK, M., JACOB-HIRSCH, J., DENG, P., ZHANG, R., ISAACS, F.J., RECHAVI, G., LI, J.B., EISENBERG, E. & LEVANON, E.Y. (2014) A-to-I RNA editing occurs at over a hundred million genomic sites, located in a majority of human genes. *Genome research*. 24 (3), 365–376.

BELLINGHAM, M.C. (2011) A Review of the Neural Mechanisms of Action and Clinical Efficiency of Riluzole in Treating Amyotrophic Lateral Sclerosis: What have we Learned in the Last Decade? *CNS Neuroscience and Therapeutics*. 17 (1), 4–31.

BELZIL, V. V., BAUER, P.O., PRUDENCIO, M., GENDRON, T.F., STETLER, C.T., YAN, I.K., PREGENT, L., DAUGHRITY, L., BAKER, M.C., RADEMAKERS, R., BOYLAN, K., PATEL, T.C., DICKSON, D.W. & PETRUCELLI, L. (2013) Reduced C9orf72 gene expression in c9FTD/ALS is caused by histone trimethylation, an epigenetic event detectable in blood. *Acta Neuropathologica*. 126 (6), 895–905.

BENATAR, M. (2007) Lost in translation: treatment trials in the SOD1 mouse and in human ALS. *Neurobiology of disease*. 26 (1), 1–13.

BENDER, F.L.P., FISCHER, M., FUNK, N., OREL, N., RETHWILM, A. & SENDTNER, M. (2007) High-efficiency gene transfer into cultured embryonic motoneurons using recombinant lentiviruses. *Histochemistry and Cell Biology*. 127 (4), 439–448.

BENSIMON, G., LACOMBLEZ, L. & MEININGER, V. (1994) A controlled trial of riluzole in amyotrophic lateral sclerosis. ALS/Riluzole Study Group. *The New England journal of medicine.* 330 (9), 585–591.

BENTLEY, D.L. (2014) Coupling mRNA processing with transcription in time and space. *Nature Reviews Genetics*. 15 (3), 163–175.

BENUSSI, L., ROSSI, G., GLIONNA, M., TONOLI, E., PICCOLI, E., FOSTINELLI, S., PATERLINI, A., FLOCCO, R., ALBANI, D., PANTIERI, R., CEREDA, C., FORLONI, G., TAGLIAVINI, F., BINETTI, G. & GHIDONI, R. (2014) C9ORF72 hexanucleotide repeat number in frontotemporal lobar degeneration: a genotype-phenotype correlation study. *Journal of Alzheimer's disease* 38 (4), 799–808.

BERNARD, A., FERHAT, L., DESSI, F., CHARTON, G., REPRESA, A., BEN-ARI, Y. & KHRESTCHATISKY, M. (1999) Q/R editing of the rat GluR5 and GluR6 kainate receptors in vivo and in vitro: evidence for independent developmental, pathological and cellular regulation. *The European Journal of Neuroscience*. 11 (2), 604–616.

BETTS, C., SALEH, A.F., ARZUMANOV, A. A, HAMMOND, S.M., GODFREY, C., COURSINDEL, T., GAIT, M.J. & WOOD, M.J. (2012) Pip6-PMO, A New Generation of Peptide-oligonucleotide Conjugates With Improved Cardiac Exon Skipping Activity for DMD Treatment. *Molecular Therapy — Nucleic Acids*. 1 (8), e38.

BEYER, B., DELEUZE, C., LETTS, V.A., MAHAFFEY, C.L., BOUMIL, R.M., LEW, T.A., HUGUENARD, J.R. & FRANKEL, W.N. (2008) Absence seizures in C3H/HeJ and knockout mice caused by mutation of the AMPA receptor subunit Gria4. *Human Molecular Genetics*. 17 (12), 1738–1749.

BHALLA, T., ROSENTHAL, J.J.C., HOLMGREN, M. & REENAN, R. (2004) Control of human potassium channel inactivation by editing of a small mRNA hairpin. *Nature structural & molecular biology*. 11 (10), 950–956.

BIEDLER, J.L., HELSON, L. & SPENGLER, B.A. (1973) Morphology and Growth , Tumorigenicity , and Cytogenetics of Human Neuroblastoma Cells in Continuous Culture Morphology and Growth , Tumorigenicity , and Cytogenetics of Human Neuroblastoma Cells in Continuous Culture. *Cancer Research*. 33, 2643–2652.

BIEDLER, J.L., ROFFLER-TARLOV, S., SCHACHNER, M. & FREEDMAN, L.S. (1978) Multiple Neurotransmitter Synthesis by Human Neuroblastoma Cell Lines and Clones Multiple Neurotransmitter Synthesis by Human Neuroblastoma Cell Lines and Clones. *Cancer Research*. 38, 3751–3757.

BILSLAND, L.G., SAHAI, E., KELLY, G., GOLDING, M., GREENSMITH, L. & SCHIAVO, G. (2010) Deficits in axonal transport precede ALS symptoms in vivo. *PNAS*. 107 (47), 20523–20528.

BONINI, D., FILIPPINI, A., VIA, L. LA, FIORENTINI, C., FUMAGALLI, F., COLOMBI, M. & BARBON, A. (2015) Chronic glutamate treatment selectively modulates AMPA RNA editing and ADAR expression and activity in primary cortical neurons. *RNA Biology*. 12 (1), 1–11.

BORNER, G.V., MORL, M., JANKE, A. & PAABO, S. (1996) RNA editing changes the identity of a mitochondrial tRNA in marsupials. *EMBO Journal*. 15 (21), 5949–5957.

BOULOS, S., MELONI, B.P., ARTHUR, P.G., BOJARSKI, C. & KNUCKEY, N.W. (2006) Assessment of CMV, RSV and SYN1 promoters and the woodchuck post-transcriptional regulatory element in adenovirus vectors for transgene expression in cortical neuronal cultures. *Brain research*. 1102 (1), 27–38.

BREWER, G.J., TORRICELLI, J.R., EVEGE, E.K. & PRICE, P.J. (1993) Optimized survival of hippocampal neurons in B27-supplemented Neurobasal, a new serum-free medium combination. *Journal of neuroscience research*. 35 (5), 567–576.

BROCKINGTON, A., NING, K., HEATH, P.R., WOOD, E., KIRBY, J., FUSI, N., LAWRENCE, N., WHARTON, S.B., INCE, P.G. & SHAW, P.J. (2013) Unravelling the enigma of selective vulnerability in neurodegeneration: motor neurons resistant to degeneration in ALS show distinct gene expression characteristics and decreased susceptibility to excitotoxicity. *Acta neuropathologica*. 125 (1), 95–109.

BRUIJN, L.I., BECHER, M.W., LEE, M.K., ANDERSON, K.L., JENKINS, N.A., COPELAND, N.G., SISODIA, S.S., ROTHSTEIN, J.D., BORCHELT, D.R., PRICE, D.L. & CLEVELAND, D.W. (1997) ALS-linked SOD1 mutant G85R mediates damage to astrocytes and promotes rapidly progressive disease with SOD1-containing inclusions. *Neuron*. 18 (2), 327–338.

BRUSA, R., ZIMMERMANN, F., KOH, D., FELDMEYER, D., GASS, P., SEEBURG, P.H. & SPRENGEL, R. (1995) Early-Onset Epilepsy and Postnatal Lethality Associated with an Editing-Deficient GluR-B Allele in Mice. *Science*. 270, 1677–1680.

BUERLI, T., PELLEGRINO, C., BAER, K., LARDI-STUDLER, B., CHUDOTVOROVA, I., FRITSCHY, J.-M., MEDINA, I. & FUHRER, C. (2007) Efficient transfection of DNA or shRNA vectors into neurons using magnetofection. *Nature protocols*. 2 (12), 3090–3101.

BUONASSISI, V., SATO, G. & COHEN, A. (1962) Hormone-producing cultures of adrenal and pituitary tumor origin. *PNAS*. 1184–1190.

BURATTI, E., DÖRK, T., ZUCCATO, E., PAGANI, F., ROMANO, M. & BARALLE, F.E. (2001) Nuclear factor TDP-43 and SR proteins promote in vitro and in vivo CFTR exon 9 skipping. *The EMBO journal*. 20 (7), 1774–1784.

BURNASHEV, N., MONYER, H., SEEBURG, P.H. & SAKMANN, B. (1992) Divalent ion permeability of AMPA receptor channels is dominated by the edited form of a single subunit. *Neuron*. 8 (1), 189–198.

BURNS, C.M., CHU, H., RUETER, S.M., HUTCHINSON, L.K., CANTON, H., SANDERS-BUSH, E. & EMESON, R.B. (1997) Regulation of serotonin-2C receptor G-protein coupling in RNA editing. *Nature*. 387303–308.

CAO, G., PEI, W., GE, H., LIANG, Q., LUO, Y., SHARP, F.R., LU, A., RAN, R., GRAHAM, S.H. & CHEN, J. (2002) In Vivo Delivery of a Bcl-xL Fusion Protein Containing the TAT Protein Transduction Domain Protects against Ischemic Brain Injury and Neuronal Apoptosis. *The Journal of neuroscience* 22 (13), 5423–5431.

CARTEGNI, L., WANG, J., ZHU, Z., ZHANG, M.Q. & KRAINER, A.R. (2003) ESEfinder: A web resource to identify exonic splicing enhancers. *Nucleic acids research.* 31 (13), 3568–3571.

CHAN, J.H.P., LIM, S. & WONG, W.S.F. (2006) Antisense Oligonucleotides: From Design to Therapeutic Application. *Clinical and Experimental Pharmacology and Physiology*. 33 (February), 533–540.

CHASIN, L.A. (2007) Searching for splicing motifs. *Advances in experimental medicine and biology*. 623, 85–106.

CHEN, C.X., CHO, D.S., WANG, Q., LAI, F., CARTER, K.C. & NISHIKURA, K. (2000) A third member of the RNA-specific adenosine deaminase gene family, ADAR3, contains both single- and double-stranded RNA binding domains. *RNA*. 6 (5), 755–767.

CHEN, L., LI, Y., LIN, C.H., CHAN, T.H.M., CHOW, R.K.K., SONG, Y., LIU, M., YUAN, Y.-F., FU, L., KONG, K.L., QI, L., ZHANG, N., TONG, A.H.Y., KWONG, D.L., MAN, K., LO, C.M., LOK, S., TENEN, D.G. & GUAN, X.-Y. (2013) Recoding RNA editing antizyme inhibitor 1 predisposes to hepatocellular carcinoma*. Nature*. 19 (2), 209–216.

CHEN, S.H., LI, X.L., LIAO, W.S.L., WU, J.H. & CHAN, L. (1990) RNA editing of apoliopoprotein B mRNA. J. Biol. Chem. 265 (12), 6811–6816.

CHEW, J., GENDRON, T.F., PRUDENCIO, M., SASAGURI, H., ZHANG, Y.-J., CASTANEDES-CASEY, M., LEE, C.W., JANSEN-WEST, K., KURTI, A., MURRAY, M.E., BIENIEK, K.F., BAUER, P.O., WHITELAW, E.C., ROUSSEAU, L., STANKOWSKI, J.N., STETLER, C., DAUGHRITY, L.M., PERKERSON, E.A., DESARO, P., ET AL. (2015) C9ORF72 repeat expansions in mice cause TDP-43 pathology, neuronal loss, and behavioral deficits. *Science*. 348 (6239), 1151–1154.

CHI, K.N., HOTTE, S.J., YU, E.Y., TU, D., EIGL, B.J., TANNOCK, I., SAAD, F., NORTH, S., POWERS, J., GLEAVE, M.E. & EISENHAUER, E.A. (2010) Randomized phase II study of docetaxel and prednisone with or without OGX-011 in patients with metastatic castration-resistant prostate cancer. *Journal of clinical oncology*. 28 (27), 4247–4254.

CHIA, R., TATTUM, M.H., JONES, S., COLLINGE, J., FISHER, E.M.C. & JACKSON, G.S. (2010) Superoxide dismutase 1 and tgSOD1 mouse spinal cord seed fibrils, suggesting a propagative cell death mechanism in amyotrophic lateral sclerosis*. PloS one*. 5 (5), e10627.

CHIA, S., DENT, S., ELLARD, S., ELLIS, P.M., VANDENBERG, T., GELMON, K., POWERS, J., WALSH, W., SEYMOUR, L. & EISENHAUER, E.A. (2009) Phase II trial of OGX-011 in combination with docetaxel in metastatic breast cancer. *Clinical cancer research* 15 (2), 708–713.

CHIÒ, A., CALVO, A., MAZZINI, L., CANTELLO, R., MORA, G., MOGLIA, C., CORRADO, L., D'ALFONSO, S., MAJOUNIE, E., RENTON, A., PISANO, F., OSSOLA, I., BRUNETTI, M., TRAYNOR, B.J. & RESTAGNO, G. (2012) Extensive genetics of ALS: a population-based study in Italy. *Neurology*. 79 (19), 1983–1989.

CHIÒ, A., LOGROSCINO, G., TRAYNOR, B., COLLINS, J., SIMEONE, J., GOLDSTEIN, L. & WHITE, L. (2013) Global Epidemiology of Amyotrophic Lateral Sclerosis: a Systematic Review of the Published Literature. *Neuroepidemiology*. 41 (2), 118–130.

CHIRIBOGA, C.A., SWOBODA, K.J., DARRAS, B.T., IANNACCONE, S.T., MONTES, J., DE VIVO, D.C., NORRIS, D.A., BENNETT, C.F. & BISHOP, K.M. (2016) Results from a phase 1 study of nusinersen (ISIS-SMNRx) in children with spinal muscular atrophy. *Neurology*. 86 (10), 890–897.

CHO, D.S.C., YANG, W., LEE, J.T., SHIEKHATTAR, R., MURRAY, J.M. & NISHIKURA, K. (2003) Requirement of dimerization for RNA editing activity of adenosine deaminases acting on RNA. *Journal of Biological Chemistry*. 278 (19), 17093–17102.

CHOI, D.W. (1988) Glutamate neurotoxicity and diseases of the nervous system. *Neuron.* 1 (8), 623–634.

CHOUDHURY, Y., TAY, F.C., LAM, D.H., SANDANARAJ, E., TANG, C., ANG, B.-T. & WANG, S. (2012) Attenuated adenosine-to-inosine editing of microRNA-376a * promotes invasiveness of glioblastoma cells. *Journal of Clinical Investigation.* 122 (11), 4059–4076.

CISTERNI, C., HENDERSON, C.E., AEBISCHER, P., PETTMANN, B. & DEGLON, N. (2000) Efficient gene transfer and expression of biologically active glial cell line-derived neurotrophic factor in rat motoneurons transduced wit lentiviral vectors. J *Neurochem*. 74 (5), 1820–1828.

CIURA, S., LATTANTE, S., LE BER, I., LATOUCHE, M., TOSTIVINT, H., BRICE, A. & KABASHI, E. (2013) Loss of function of C9orf72 causes motor deficits in a zebrafish model of Amyotrophic Lateral Sclerosis. *Annals of neurology* 74 (2), 180-7

COLEMAN, S.K., MÖYKKYNEN, T., CAI, C., VON OSSOWSKI, L., KUISMANEN, E., KORPI, E.R. & KEINÄNEN, K. (2006) Isoform-specific early trafficking of AMPA receptor flip and flop variants. *The Journal of neuroscience* 26 (43), 11220–11229.

CONG, L., RAN, F.A., COX, D., LIN, S., BARRETTO, R., HABIB, N., HSU, P.D., WU, X., JIANG, W., MARRAFFINI, L.A. & ZHANG, F. (2013) Multiplex genome engineering using CRISPR/Cas systems. *Science*. 339 (6121), 819–823

COOPER-KNOCK, J., HEWITT, C., HIGHLEY, J.R., BROCKINGTON, A., MILANO, A., MAN, S., MARTINDALE, J., HARTLEY, J., WALSH, T., GELSTHORPE, C., BAXTER, L., FORSTER, G., FOX, M., BURY, J., MOK, K., MCDERMOTT, C.J., TRAYNOR, B.J., KIRBY, J., WHARTON, S.B., ET AL. (2012) Clinico-pathological features in amyotrophic lateral sclerosis with expansions in C9ORF72. *Brain.* 135 (Pt 3), 751–764.

COOPER-KNOCK, J., WALSH, M.J., HIGGINBOTTOM, A., HIGHLEY, J.R., DICKMAN, M.J., EDBAUER, D., INCE, P.G., WHARTON, S.B., WILSON, S. A., KIRBY, J., HAUTBERGUE, G.M. & SHAW, P.J. (2014) Sequestration of multiple RNA recognition motif-containing proteins by C9orf72 repeat expansions. *Brain*. 137 (7), 2040–2051.

COOPER-KNOCK, J., HIGGINBOTTOM, A., STOPFORD, M.J., HIGHLEY, J.R., INCE, P.G., WHARTON, S.B., PICKERING-BROWN, S., KIRBY, J., HAUTBERGUE, G.M. & SHAW, P.J. (2015) Antisense RNA foci in the motor neurons of C9ORF72-ALS patients are associated with TDP-43 proteinopathy. *Acta Neuropathologica* 130 (7), 63-75

COPOLOVICI, D.M., LANGEL, K., ERISTE, E. & LANGEL, Ü. (2014) Cell-penetrating peptides: design, synthesis, and applications. *ACS nano*. 8 (3), 1972–1994

CORDIER, C., BOUTIMAH, F., BOURDELOUX, M., DUPUY, F., MET, E., ALBERTI, P., LOLL, F., CHASSAING, G., BURLINA, F. & SAISON-BEHMOARAS, T.E. (2014) Delivery of Antisense Peptide Nucleic Acids to Cells by Conjugation with Small Arginine-Rich Cell-Penetrating Peptide (R/W)9. *PLoS ONE*. 9 (8), e104999.

CROOKE, R.M., GRAHAM, M.J., LEMONIDIS, K.M., WHIPPLE, C.P., KOO, S. & PERERA, R.J. (2005) An apolipoprotein B antisense oligonucleotide lowers LDL cholesterol in hyperlipidemic mice without causing hepatic steatosis. *Journal of lipid research.* 46 (5), 872–884.

CUTRONA, G., CARPANETO, E.M., ULIVI, M., RONCELLA, S., LANDT, O., FERRARINI, M. & BOFFA, L.C. (2000) Effects in live cells of a c-myc anti-gene PNA linked to a nuclear localization signal. *Nature biotechnology*. 18 (3), 300–303

DANIEL, C., WAHLSTEDT, H., OHLSON, J., BJÖRK, P. & OHMAN, M. (2011) Adenosine-to-inosine RNA editing affects trafficking of the gamma-aminobutyric acid type A (GABA(A)) receptor. *The Journal of biological chemistry.* 286 (3), 2031–2040.

DANIEL, C., SILBERBERG, G., BEHM, M., OHMAN, M. & ÖHMAN, M. (2014) Alu elements shape the primate transcriptome by cis-regulation of RNA editing. *Genome Biology*. 15 (2), R28.

DAWSON, T.R., SANSAM, C.L. & EMESON, R.B. (2004) Structure and sequence determinants required for the RNA editing of ADAR2 substrates. *The Journal of biological chemistry.* 279 (6), 4941–4951.

DE CONTI, L., BARALLE, M. & BURATTI, E. (2013) Exon and intron definition in pre-mRNA splicing. *RNA*. 4 (1), 49–60.

DEJESUS-HERNANDEZ, M., MACKENZIE, I.R., BOEVE, B.F., BOXER, A.L., BAKER, M., RUTHERFORD, N.J., NICHOLSON, A.M., FINCH, N.A., GILMER, F., ADAMSON, J., KOURI, N., WOJTAS, A., SENGDY, P., HSIUNG, G.R., KARYDAS, A., SEELEY, W.W., JOSEPHS, K.A., GESCHWIND, D.H., WSZOLEK, Z.K., ET AL. (2011) Expanded GGGGCC hexanucleotide repeat in non-coding region of C9ORF72 causes chromosome 9p-linked frontotemporal dementia and amyotrophic lateral sclerosis. *Neuron.* 72 (2), 245–256.

DENG, H.-X., ZHAI, H., BIGIO, E.H., YAN, J., FECTO, F., AJROUD, K., MISHRA, M., AJROUD-DRISS, S., HELLER, S., SUFIT, R., SIDDIQUE, N., MUGNAINI, E. & SIDDIQUE, T. (2010) FUS-immunoreactive inclusions are a common feature in sporadic and non-SOD1 familial amyotrophic lateral sclerosis. *Annals of neurology.* 67 (6), 739–748.

DENTI, M.A., ROSA, A., STHANDIER, O., DE ANGELIS, F.G. & BOZZONI, I. (2004) A new vector, based on the PolII promoter of the U1 snRNA gene, for the expression of siRNAs in mammalian cells. *Molecular therapy* 10 (1), 191–199.

DERKACH, V. A, OH, M.C., GUIRE, E.S. & SODERLING, T.R. (2007) Regulatory mechanisms of AMPA receptors in synaptic plasticity. *Nature reviews. Neuroscience.* 8 (2), 101–113.

DESMET, F.-O., HAMROUN, D., LALANDE, M., COLLOD-BÉROUD, G., CLAUSTRES, M. & BÉROUD, C. (2009) Human Splicing Finder: an online bioinformatics tool to predict splicing signals. *Nucleic acids research*. 37 (9), e67.

DESTERRO, J.M.P., KEEGAN, L.P., LAFARGA, M., BERCIANO, M.T., O'CONNELL, M.A. & CARMO-FONSECA, M. (2003) Dynamic association of RNA-editing enzymes with the nucleolus. *Journal of Cell Science.* 116 (9), 1805–1818.

DEVLIN, A., BURR, K., BOROOAH, S., FOSTER, J.D., CLEARY, E.M., GETI, I., VALLIER, L., SHAW, C.E., CHANDRAN, S. & MILES, G.B. (2015) Human iPSC-derived motoneurons harbouring TARDBP or C9ORF72 ALS mutations are dysfunctional despite maintaining viability. *Nature Communications.* 12 (6), 5999

DHAR, S.S., LIANG, H.L. & WONG-RILEY, M.T.T. (2009) Nuclear respiratory factor 1 co-regulates AMPA glutamate receptor subunit 2 and cytochrome c oxidase: tight coupling of glutamatergic transmission and energy metabolism in neurons*. Journal of neurochemistry*. 108 (6), 1595–1606.

DIB-HAJJ, S.D., CHOI, J.S., MACALA, L.J., TYRRELL, L., BLACK, J.A., CUMMINS, T.R. & WAXMAN, S.G. (2009) Transfection of rat or mouse neurons by biolistics or electroporation. *Nature protocols*. 4 (8), 1118–1126.

DING, B. & KILPATRICK, D.L. (2013) Lentiviral vector production, titration, and transduction of primary neurons. *Methods in molecular biology* 1018, 119–131.

DING, Y. & LAWRENCE, C.E. (2003) A statistical sampling algorithm for RNA secondary structure prediction. *Nucleic Acids Research.* 31 (24), 7280–7301.

DING, Y.E., CHAN, C.H.I.Y.U. & LAWRENCE, C.E. (2005) RNA secondary structure prediction by centroids in a Boltzmann weighted ensemble. *RNA*. 11, 1157–1166.

DISTERER, P., AL-SHAWI, R., ELLMERICH, S., WADDINGTON, S.N., OWEN, J.S., SIMONS, J.P. & KHOO, B. (2013) Exon skipping of hepatic APOB pre-mRNA with splice-switching oligonucleotides reduces LDL cholesterol in vivo. *Molecular therapy* 21 (3), 602–609

DONNELLY, C.J., ZHANG, P.-W., PHAM, J.T., HEUSLER, A.R., MISTRY, N. A, VIDENSKY, S., DALEY, E.L., POTH, E.M., HOOVER, B., FINES, D.M., MARAGAKIS, N., TIENARI, P.J., PETRUCELLI, L., TRAYNOR, B.J., WANG, J., RIGO, F., BENNETT, C.F., BLACKSHAW, S., SATTLER, R., ET AL. (2013) RNA toxicity from the ALS/FTD C9ORF72 expansion is mitigated by antisense intervention. *Neuron*. 80 (2), 415–428.

DONNELLY, C.J., ZHANG, P., PHAM, J.T., HEUSLER, A.R., MISTRY, N.A., VIDENSKY, S., DALEY, E.L., POTH, E.M., FINES, D.M., MARAGAKIS, N., TIENARI, P.J., PETRUCELLI, L., TRAYNOR, B.J., WANG, J., RIGO, F., BENNETT, C.F. & BLACKSHAW, S. (2014) RNA Toxicity from the ALS/FTD C9ORF72 Expansion Is Mitigated by Antisense Intervention. *Neuron*. 80 (2), 415–428.

DORIA, M., NERI, F., GALLO, A., FARACE, M.G. & MICHIENZI, A. (2009) Editing of HIV-1 RNA by the double-stranded RNA deaminase ADAR1 stimulates viral infection. *Nucleic acids research.* 37 (17), 5848–5858.

DRACHEVA, S., PATEL, N., WOO, D. A, MARCUS, S.M., SIEVER, L.J. & HAROUTUNIAN, V. (2008) Increased serotonin 2C receptor mRNA editing: a possible risk factor for suicide. *Molecular psychiatry*. 13 (11), 1001–1010.

DULL, T., ZUFFEREY, R., KELLY, M., MANDEL, R.J., NGUYEN, M., TRONO, D. & NALDINI, L. (1998) A third-generation lentivirus vector with a conditional packaging system. *Journal of virology*. 72 (11), 8463–8471.

ECHIGOYA, Y. & YOKOTA, T. (2014) Skipping multiple exons of dystrophin transcripts using cocktail antisense oligonucleotides*. Nucleic acid therapeutics*. 24 (1), 57–68..

ECHIGOYA, Y., MOULY, V., GARCIA, L., YOKOTA, T. & DUDDY, W. (2015) In Silico Screening Based on Predictive Algorithms as a Design Tool for Exon Skipping Oligonucleotides in Duchenne Muscular Dystrophy. *Plos One.* 10 (3), e0120058.

EISEN, J.S. & SMITH, J.C. (2008) Controlling morpholino experiments: don't stop making antisense. *Development* 135 (10), 1735–1743.

ELLIS, B.L., POTTS, P.R. & PORTEUS, M.H. (2011) Creating higher titer lentivirus with caffeine. *Human gene therapy.* 22 (1), 93–100.

ENGLANDER, M.T., DULAWA, S.C., BHANSALI, P. & SCHMAUSS, C. (2005) How stress and fluoxetine modulate serotonin 2C receptor pre-mRNA editing. *The Journal of neuroscience* 25 (3), 648–651.

FAIRBROTHER, W.G., YEH, R.-F., SHARP, P.A. & BURGE, C.B. (2002) Predictive identification of exonic splicing enhancers in human genes. *Science*. 297 (5583), 1007–1013.

FALLINI, C., BASSELL, G.J. & ROSSOLL, W. (2010) High-efficiency transfection of cultured primary motor neurons to study protein localization, trafficking, and function. *Molecular neurodegeneration*. 21 (5), 17.

FALZARANO, M.S., PASSARELLI, C. & FERLINI, A. (2014) Nanoparticle delivery of antisense oligonucleotides and their application in the exon skipping strategy for duchenne muscular dystrophy. *Nucleic acid therapeutics*. 24 (1), 87–100.

FARG, M.A., SUNDARAMOORTHY, V., SULTANA, J.M., YANG, S., ATKINSON, R.A.K., LEVINA, V., HALLORAN, M.A., GLEESON, P.A., BLAIR, I.P., SOO, K.Y., KING, A.E. & ATKIN, J.D. (2014) C9ORF72, implicated in amytrophic lateral sclerosis and frontotemporal dementia, regulates endosomal trafficking. *Human Molecular Genetics.* 23 (13), 3579–3595

FARRAWELL, N.E., LAMBERT-SMITH, I.A., WARRAICH, S.T., BLAIR, I.P., SAUNDERS, D.N., HATTERS, D.M. & YERBURY, J.J. (2015) Distinct partitioning of ALS associated TDP-43, FUS and SOD1 mutants into cellular inclusions. *Scientific reports.* 5, 13416.

FOX-WALSH, K.L., DOU, Y., LAM, B.J., HUNG, S.-P., BALDI, P.F. & HERTEL, K.J. (2005) The architecture of pre-mRNAs affects mechanisms of splice-site pairing. *PNAS* 102 (45), 16176–16181.

FRAY, A.E., INCE, P.G., BANNER, S.J., MILTON, I.D., USHER, P.A., COOKSON, M.R. & SHAW, P.J. (1998) The expression of the glial glutamate transporter protein EAAT2 in motor neuron disease: an immunohistochemical study. *European Journal of Neuroscience.* 10 (8), 2481–2489.

FREIBAUM, B.D., LU, Y., LOPEZ-GONZALEZ, R., KIM, N.C., ALMEIDA, S., LEE, K., BADDERS, N., VALENTINE, M., MILLER, B.L., WONG, P.C., PETRUCELLI, L., KIM, H.J., GAO, F. & TAYLOR, J.P. (2015) GGGGCC Repeat Expansion in C9ORF72 Compromises Nucleocytoplasmic Transport. *Nature*. 525129–133. FRITZ, E., IZAURIETA, P., WEISS, A., MIR, F.R., ROJAS, P., GONZALEZ, D., ROJAS, F., BROWN, R.H., MADRID, R. & VAN ZUNDERT, B. (2013) Mutant SOD1-expressing astrocytes release toxic factors that trigger motoneuron death by inducing hyperexcitability*. Journal of neurophysiology*. 109 (11), 2803–2814.

FU, X.-D. & ARES, M. (2014) Context-dependent control of alternative splicing by RNA-binding proteins. *Nature Reviews Genetics*. 15 (10), 689–701.

FUJIOKA, Y., ISHIGAKI, S., MASUDA, A., IGUCHI, Y., UDAGAWA, T., WATANABE, H., KATSUNO, M., OHNO, K. & SOBUE, G. (2013) FUS-regulated region- and cell-type-specific transcriptome is associated with cell selectivity in ALS/FTLD. *Scientific reports*. 3, 2388.

GAISLER-SALOMON, I., KRAVITZ, E., FEILER, Y., SAFRAN, M., BIEGON, A., AMARIGLIO, N. & RECHAVI, G. (2014) Hippocampus-specific deficiency in RNA editing of GluA2 in Alzheimer's disease. *Neurobiology of aging*. 35 (8), 1785-91

GAL, J., ZHANG, J., KWINTER, D.M., ZHAI, J., JIA, H., JIA, J. & ZHU, H. (2011) Nuclear localization sequence of FUS and induction of stress granules by ALS mutants. *Neurobiology of aging.* 32 (12), 2323.e27–e40.

GAMAZON, E.R. & STRANGER, B.E. (2014) Genomics of alternative splicing: evolution, development and pathophysiology. *Human genetics.* 133 (6), 679–687.

GARNCARZ, W., TARIQ, A., HANDL, C., PUSCH, O. & JANTSCH, M.F. (2013) A high-throughput screen to identify enhancers of ADAR-mediated RNA-editing. *RNA biology*. 10 (2), 192–204

GEARY, R.S., NORRIS, D., YU, R. & BENNETT, C.F. (2015) Pharmacokinetics, biodistribution and cell uptake of antisense oligonucleotides. *Advanced Drug Delivery Reviews*. 87, 46-51

GEBSKI, B.L., MANN, C.J., FLETCHER, S. & WILTON, S.D. (2003) Morpholino antisense oligonucleotide induced dystrophin exon 23 skipping in mdx mouse muscle. *Human Molecular Genetics*. 12 (15), 1801–1811.

GEORGE, C.X., GAN, Z., LIU, Y. & SAMUEL, C.E. (2011) Adenosine deaminases acting on RNA, RNA editing, and interferon action. *Journal of interferon & cytokine research* 31 (1), 99–117.

GERBER, A., O'CONNELL, M. A & KELLER, W. (1997) Two forms of human double-stranded RNA-specific editase 1 (hRED1) generated by the insertion of an Alu cassette. *RNA*. 3453–463.

GINN, S.L., ALEXANDER, I.E., EDELSTIEN, M.L., ABEDI, M.R. & WIXON, J. (2013) Gene therapy clinical trials worldwide to 2012 - an update. *The journal of gene medicine.* 15(2):65-77.

GITAÍ, D.L.G., MARTINELLI, H.N., VALENTE, V., PEREIRA, M.G.A.G., OLIVEIRA, J.A.C., ELIAS, C.F., BITTENCOURT, J.C., LEITE, J.P., COSTA-NETO, C.M., GARCIA-CAIRASCO, N. & PACÓ-LARSON, M.L. (2010) Increased expression of GluR2-flip in the hippocampus of the wistar audiogenic rat strain after acute and kindled seizures. *Hippocampus*. 20 (1), 125–133.

GLAUM, S.R., SCHOLZ, W.K. & MILLER, R.J. (1990) Acute- and long-term glutamate-mediated regulation of [Ca++]i in rat hippocampal pyramidal neurons in vitro. *J Pharmacol Exp Ther.* 253 (3), 1293–1302.

GOEMANS, N.M., TULINIUS, M., VAN DEN AKKER, J.T., BURM, B.E., EKHART, P.F., HEUVELMANS, N., HOLLING, T., JANSON, A.A., PLATENBURG, G.J., SIPKENS, J.A., SITSEN, J.M.A., AARTSMA-RUS, A., VAN OMMEN, G.-J.B., BUYSE, G., DARIN, N., VERSCHUUREN, J.J., CAMPION, G. V, DE KIMPE, S.J. & VAN DEUTEKOM, J.C. (2011) Systemic administration of PRO051 in Duchenne's muscular dystrophy. *The New England journal of medicine*. 364 (16), 1513–1522

GOMMANS, W.M., MULLEN, S.P. & MAAS, S. (2010) RNA editing: a driving force for adaptive evolution? *Bioessays* 31 (10), 1137–1145.

GOMMANS, W.M. (2012) A-to-I editing of microRNAs: regulating the regulators? *Seminars in cell & developmental biology.* 23 (3), 251–257.

GOREN, A., RAM, O., AMIT, M., KEREN, H., LEV-MAOR, G., VIG, I., PUPKO, T. & AST, G. (2006) Comparative Analysis Identifies Exonic Splicing Regulatory Sequences-The Complex Definition of Enhancers and Silencers. *Molecular Cell.* 22 (6), 769–781.

GOTT, J.M., SOMERLOT, B.H. & GRAY, M.W. (2010) Two forms of RNA editing are required for tRNA maturation in Physarum mitochondria. *Rna*. 16 (3), 482–488.

GOYENVALLE, A., BABBS, A., VAN OMMEN, G.-J.B., GARCIA, L. & DAVIES, K.E. (2009) Enhanced exon-skipping induced by U7 snRNA carrying a splicing silencer sequence: Promising tool for DMD therapy. *Molecular therapy* 17 (7), 1234–1240.

GOYENVALLE, A., GRIFFITH, G., BABBS, A., ANDALOUSSI, S. EL, EZZAT, K., AVRIL, A., DUGOVIC, B., CHAUSSENOT, R., FERRY, A., VOIT, T., AMTHOR, H., BÜHR, C., SCHÜRCH, S., WOOD, M.J. A, DAVIES, K.E., VAILLEND, C., LEUMANN, C. & GARCIA, L. (2015) Functional correction in mouse models of muscular dystrophy using exon-skipping tricyclo-DNA oligomers. *Nature Medicine*. (October 2014).

GRABRUCKER, A., VAIDA, B., BOCKMANN, J. & BOECKERS, T.M. (2009) Synaptogenesis of hippocampal neurons in primary cell culture. *Cell and Tissue Research.* 338 (3), 333–341

GRAFFMO, K.S., FORSBERG, K., BERGH, J., BIRVE, A., ZETTERSTRÖM, P., ANDERSEN, P.M., MARKLUND, S.L. & BRÄNNSTRÖM, T. (2013) Expression of wild-type human superoxide dismutase-1 in mice causes amyotrophic lateral sclerosis. *Human molecular genetics*. 22 (1), 51–60.

GRAVELEY, B.R. (2000) Sorting out the complexity of SR protein functions. *RNA*. 6 (9), 1197–1211.

GRAY, M.W. (2012) Evolutionary origin of RNA editing. *Biochemistry*. 51 (26), 5235–5242.

GREENE, L. A & TISCHLER, A S. (1976) Establishment of a noradrenergic clonal line of rat adrenal pheochromocytoma cells which respond to nerve growth factor. *PNAS* 73 (7), 2424–2428.

GREGER, I.H., KHATRI, L., KONG, X. & ZIFF, E.B. (2003) AMPA Receptor Tetramerization is Mediated by Q/R Editing. *Neuron*. 40, 763–774.

GREUTER, T., BIEDERMANN, L., ROGLER, G., SAUTER, B. & SEIBOLD, F. (2016) Alicaforsen, an antisense inhibitor of ICAM-1, as treatment for chronic refractory pouchitis after proctocolectomy: A case series. *United European gastroenterology journal.* 4 (1), 97–104.

GROOMS, S.Y., NOH, K.-M., REGIS, R., BASSELL, G.J., BRYAN, M.K., CARROLL, R.C. & ZUKIN, R.S. (2006) Activity bidirectionally regulates AMPA receptor mRNA abundance in dendrites of hippocampal neurons. *The Journal of neuroscience* 26 (32), 8339–8351.

GRUART, A., LEAL-CAMPANARIO, R., LÓPEZ-RAMOS, J.C. & DELGADO-GARCÍA, J.M. (2015) Functional basis of associative learning and their relationships with long-term potentiation evoked in the involved neural circuits: Lessons from studies in behaving mammals. *Neurobiology of Learning and Memory.* 124, 3–18.

GUO, H., LAI, L., BUTCHBACH, M.E.R., STOCKINGER, M.P., SHAN, X., BISHOP, G.A. & LIN, C.G. (2003) Increased expression of the glial glutamate transporter EAAT2 modulates excitotoxicity and delays the onset but not the outcome of ALS in mice. *Human molecular genetics*. 12 (19), 2519–2532.

GUREVICH, I., TAMIR, H., ARANGO, V., DWORK, A.J., MANN, J.J. & SCHMAUSS, C. (2002) Altered editing of serotonin 2C receptor pre-mRNA in the prefrontal cortex of depressed suicide victims. *Neuron*. 34 (3), 349–356.

GURNEY, M.E. (1997) The use of transgenic mouse models of amyotrophic lateral sclerosis in preclinical drug studies. *Journal of the neurological sciences*. 152 Suppl S67–S73.

GURNEY, M.E., PU, H., CHIU, A.Y., DAL CANTO, M.C., POLCHOW, C.Y., ALEXANDER, D.D., CALIENDO, J., HENTATI, A., KWON, Y.W. & DENG, H.X. (1994) Motor neuron degeneration in mice that express a human Cu,Zn superoxide dismutase mutation. *Science*. 264 (5166), 1772–1775.

HA, J.S., LEE, C.S., MAENG, J.S., KWON, K.S. & PARK, S.S. (2009) Chronic glutamate toxicity in mouse cortical neuron culture. *Brain Research*. 1273, 138–143

HACHÉ, M., SWOBODA, K.J., SETHNA, N., FARROW-GILLESPIE, A., KHANDJI, A., XIA, S. & BISHOP, K.M. (2016) Intrathecal Injections in Children With Spinal Muscular Atrophy: Nusinersen Clinical Trial Experience. *Journal of child neurology.* 31 (7), 899–906.

HANSLICK, J.L., LAU, K., NOGUCHI, K.K., OLNEY, J.W., ZORUMSKI, C.F., MENNERICK, S. & FARBER, N.B. (2009) Dimethyl sulfoxide (DMSO) produces widespread apoptosis in the developing central nervous system. *Neurobiology of disease.* 34 (1), 1–10.

HARMS, M.B., CADY, J., ZAIDMAN, C., COOPER, P., BALI, T., ALLRED, P., CRUCHAGA, C., BAUGHN, M., LIBBY, R.T., PESTRONK, A., GOATE, A., RAVITS, J. & BALOH, R.H. (2013) Lack of C9ORF72 coding mutations supports a gain of function for repeat expansions in amyotrophic lateral sclerosis. *Neurobiology of aging.* 34 (9), 2234.e13–e19.

HARRILL, J.A., CHEN, H., STREIFEL, K.M., YANG, D., MUNDY, W.R. & LEIN, P.J. (2015) Ontogeny of biochemical, morphological and functional parameters of synaptogenesis in primary cultures of rat hippocampal and cortical neurons. *Molecular brain*. 8, 1–15.

HARTNER, J.C., SCHMITTWOLF, C., KISPERT, A., MÜLLER, A.M., HIGUCHI, M. & SEEBURG, P.H. (2004) Liver disintegration in the mouse embryo caused by deficiency in the RNA-editing enzyme ADAR1. *The Journal of biological chemistry.* 279 (6), 4894–4902.

HARTNER, J.C., WALKLEY, C.R., LU, J. & ORKIN, S.H. (2009) ADAR1 is essential for maintenance of hematopoiesis and suppression of interferon signaling. *Nature Immunology.* 10 (1), 109–115.

HAYASHI, T., RUMBAUGH, G. & HUGANIR, R.L. (2005) Differential regulation of AMPA receptor subunit trafficking by palmitoylation of two distinct sites. *Neuron*. 47 (5), 709–723.

HEIMAN-PATTERSON, T.D., SHER, R.B., BLANKENHORN, E.A., ALEXANDER, G., DEITCH, J.S., KUNST, C.B., MARAGAKIS, N. & COX, G. (2011) Effect of genetic background on phenotype variability in transgenic mouse models of amyotrophic lateral sclerosis: a window of opportunity in the search for genetic modifiers. *Amyotrophic lateral sclerosis* 12 (2), 79–86.

HERB, A., HIGUCHI, M., SPRENGEL, R. & SEEBURG, P.H. (1996) Q/R site editing in kainate receptor GluR5 and GluR6 pre-mRNAs requires distant intronic sequences *PNAS*. 93 (March), 1875–1880.

HERBERT, A., ALFKEN, J., KIM, Y.G., MIAN, I.S., NISHIKURA, K. & RICH, A. (1997) A Z-DNA binding domain present in the human editing enzyme, double-stranded RNA adenosine deaminase. *PNAS*. 94 (16), 8421–8426.

HEWITT, C., KIRBY, J., HIGHLEY, J.R., HARTLEY, J.A., HIBBERD, R., HOLLINGER, H.C., WILLIAMS, T.L., INCE, P.G., MCDERMOTT, C.J. & SHAW, P.J. (2010) Novel FUS/TLS Mutations and Pathology in Familial and Sporadic Amyotrophic Lateral Sclerosis. *Arch Neurol*. 67 (4), 455–461.

HIDEYAMA, T., YAMASHITA, T., SUZUKI, T., TSUJI, S., HIGUCHI, M., SEEBURG, P.H., TAKAHASHI, R., MISAWA, H. & KWAK, S. (2010) Induced loss of ADAR2 engenders slow death of motor neurons from Q/R site-unedited GluR2. *The Journal of Neuroscience*. 30 (36), 11917–11925.

HIDEYAMA, T. & KWAK, S. (2011) When Does ALS Start? ADAR2-GluA2 Hypothesis for the Etiology of Sporadic ALS. *Frontiers in molecular neuroscience.* 4 (November), 33.

HIDEYAMA, T., TERAMOTO, S., HACHIGA, K., YAMASHITA, T. & KWAK, S. (2012a) Co-occurrence of TDP-43 mislocalization with reduced activity of an RNA editing enzyme, ADAR2, in aged mouse motor neurons. *PloS one*. 7 (8), e43469.

HIDEYAMA, T., YAMASHITA, T., AIZAWA, H., TSUJI, S., KAKITA, A., TAKAHASHI, H. & KWAK, S. (2012b) Profound downregulation of the RNA editing enzyme ADAR2 in ALS spinal motor neurons. *Neurobiology of disease*. 45 (3), 1121–1128.

HIGASHI, S., TSUCHIYA, Y., ARAKI, T., WADA, K. & KABUTA, T. (2010) TDP-43 physically interacts with amyotrophic lateral sclerosis-linked mutant CuZn superoxide dismutase. *Neurochemistry*. 57 (8), 906–913.

HIGUCHI, M., SINGLE, F.N., KÖHLER, M., SOMMER, B., SPRENGEL, R. & SEEBURG, P.H. (1993) RNA editing of AMPA receptor subunit GluR-B: a base-paired intron-exon structure determines position and efficiency. *Cell*. 75 (7), 1361–1370.

HIGUCHI, M., MAAS, S., SINGLE, F.N., HARTNER, J., ROZOV, A., BURNASHEV, N., FELDMEYER, D., SPRENGEL, R. & SEEBURG, P.H. (2000) Point mutation in an AMPA receptor gene rescues lethality in mice deficient in the RNA-editing enzyme ADAR2. *Nature*. 406 (July), 1998–2001.

HILGENBERG, L.G.W. & SMITH, M.A. (2007) Preparation of dissociated mouse cortical neuron cultures. *Journal of visualized experiments : JoVE*. (10), 562.

HOGG, M., PARO, S., KEEGAN, L.P. & O'CONNELL, M. A (2011) RNA editing by mammalian ADARs. 1st edition. Elsevier Inc.

HOLMGREN, M. & ROSENTHAL, J.J.C. (2013) Regulation of Ion Channel and Transporter Function Through RNA Editing. In: Stefan Maas (ed.). *RNA Editing*. Norfolk, Caister Academic Press. pp. 1–16.

HOOPENGARDNER, B., BHALLA, T., STABER, C. & REENAN, R. (2003) Nervous system targets of RNA editing identified by comparative genomics. *Science*. 301 (5634), 832–836.

HORSCH, M., SEEBURG, P.H., ADLER, T., AGUILAR-PIMENTEL, J.A., BECKER, L., CALZADA-WACK, J., GARRETT, L., GÖTZ, A., HANS, W., HIGUCHI, M., HÖLTER, S.M., NATON, B., PREHN, C., PUK, O., RÁCZ, I., RATHKOLB, B., ROZMAN, J., SCHREWE, A., ADAMSKI, J., ET AL. (2011) Requirement of the RNA-editing enzyme ADAR2 for normal physiology in mice. *The Journal of biological chemistry.* 286 (21), 18614–18622.

HOWLAND, D.S., LIU, J., SHE, Y., GOAD, B., MARAGAKIS, N.J., KIM, B., ERICKSON, J., KULIK, J., DEVITO, L., PSALTIS, G., DEGENNARO, L.J., CLEVELAND, D.W. & ROTHSTEIN, J.D. (2002) Focal loss of the glutamate transporter EAAT2 in a transgenic rat model of SOD1 mutant-mediated amyotrophic lateral sclerosis (ALS). *PNAS* 99 (3), 1604–1609.

HUA, Y., VICKERS, T.A., BAKER, B.F., BENNETT, C.F. & KRAINER, A.R. (2007) Enhancement of SMN2 exon 7 inclusion by antisense oligonucleotides targeting the exon. *PLoS biology*. 5 (4), e73.

HUANG, H., TAN, B.Z., SHEN, Y., TAO, J., JIANG, F., SUNG, Y.Y., NG, C.K., RAIDA, M., KÖHR, G., HIGUCHI, M., FATEMI-SHARIATPANAHI, H., HARDEN, B., YUE, D.T. & SOONG, T.W. (2012) RNA editing of the IQ domain in Ca(v)1.3 channels modulates their Ca2+-dependent inactivation. *Neuron*. 73 (2), 304–316.

HUDZIAK, R.M., BAROFSKY, E., BAROFSKY, D.F., WELLER, D.L., HUANG, S.B. & WELLER, D.D. (1996) Resistance of morpholino phosphorodiamidate oligomers to enzymatic degradation. *Antisense & nucleic acid drug development.* 6 (4), 267–272

HUISMAN, M.H.B., SEELEN, M., DE JONG, S.W., DORRESTEIJN, K.R.I.S., VAN DOORMAAL, P.T.C., VAN DER KOOI, A.J., DE VISSER, M., SCHELHAAS, H.J., VAN DEN BERG, L.H. & VELDINK, J.H. (2013) Lifetime physical activity and the risk of amyotrophic lateral sclerosis. J*ournal of neurology, neurosurgery, and psychiatry.* 84 (9), 976–981.

HUTSON, T.H., VERHAAGEN, J., YANEZ-MUNOZ, R.J. & MOON, L.D. (2012) Corticospinal tract transduction: a comparison of seven adeno-associated viral vector serotypes and a non-integrating lentiviral vector. *Gene Ther.* 19 (1), 49–60.

HUTSON, T.H., FOSTER, E., MOON, L.D.F. & YÁÑEZ-MUÑOZ, R.J. (2014) Lentiviral vector-mediated RNA silencing in the central nervous system. *Human gene therapy methods*. 25 (1), 14–32.

HWANG, W.Y., FU, Y., REYON, D., MAEDER, M.L., TSAI, S.Q., SANDER, J.D., PETERSON, R.T., YEH, J.-R.J. & JOUNG, J.K. (2013) Efficient genome editing in zebrafish using a CRISPR-Cas system. *Nature biotechnology.* 31 (3), 227–229.

HYRUP, B. & NIELSEN, P.E. (1996) Peptide Nucleic Acids (PNA): Synthesis, Properties and Potential Applications. *Bioorganic and Medicinal Chemistry*. 4 (1), 5–23

INGRE, C., ROOS, P.M., PIEHL, F., KAMEL, F. & FANG, F. (2015) Risk factors for amyotrophic lateral sclerosis. *Clinical epidemiology.* 7, 181–193.

JACOBS, M.M., FOGG, R.L., EMESON, R.B. & STANWOOD, G.D. (2009) ADAR1 and ADAR2 expression and editing activity during forebrain development. *Developmental Neuroscience*. 31 (3), 223–237.

JAIKARAN, D.C.J., COLLINS, C.H. & MACMILLAN, A.M. (2002) Adenosine to inosine editing by ADAR2 requires formation of a ternary complex on the GluR-B R/G site. *The Journal of biological chemistry.* 277 (40), 37624–37629.

JANSSENS, N. & LESAGE, A.S.J. (2001) Glutamate receptor subunit expression in primary neuronal and secondary glial cultures*. Journal of Neurochemistry*. 77, 1457–1474.

JARA, J.H., GENÇ, B., COX, G.A., BOHN, M.C., ROOS, R.P., MACKLIS, J.D., ULUPINAR, E. & ÖZDINLER, P.H. (2015) Corticospinal Motor Neurons Are Susceptible to Increased ER Stress and Display Profound Degeneration in the Absence of UCHL1 Function. *Cerebral cortex.* 25 (11), 4259–4272

JEPSON, J.E.C. & REENAN, R. A (2008) RNA editing in regulating gene expression in the brain*. Biochimica et biophysica acta*. 1779 (8), 459–470.

JIANG, J., ZHU, Q., GENDRON, T.F., RIGO, F., CLEVELAND, D.W., JIANG, J., ZHU, Q., GENDRON, T.F., SABERI, S., MCALONIS-DOWNES, M., SEELMAN, A. & CLEVELAND, D.W. (2016) Gain of Toxicity from

ALS/FTD-Linked Repeat Expansions in C9ORF72 Is Alleviated by Antisense Oligonucleotides Targeting GGGGCC-Containing RNAs. *Neuron*. 1–16.

JIN, R., BANKE, T.G., MAYER, M.L., TRAYNELIS, S.F. & GOUAUX, E. (2003) Structural basis for partial agonist action at ionotropic glutamate receptors. *Nat. Neurosci*. 6 (8), 803–810.

JIN, Y., ZHANG, W. & LI, Q. (2009) Origins and evolution of ADAR-mediated RNA editing. *IUBMB life.* 61 (6), 572–578.

KABASHI, E., LIN, L., TRADEWELL, M.L., DION, P. A, BERCIER, V., BOURGOUIN, P., ROCHEFORT, D., BEL HADJ, S., DURHAM, H.D., VANDE VELDE, C., ROULEAU, G. A & DRAPEAU, P. (2010) Gain and loss of function of ALS-related mutations of TARDBP (TDP-43) cause motor deficits in vivo. *Human molecular genetics.* 19 (4), 671–683.

KAIN, S.R., ADAMS, M., KONDEPUDI, A., YANG, T.T., WARD, W.W. & KITTS, P. (1995) Green fluorescent protein as a reporter of gene expression and protein localization. *BioTechniques.* 19 (4), 650–655.

KANDEL, E.R., SCHWARTZ, J.H. & JESSELL, T.M. (2000) *Principles of Neural Science*. Fourth. Eric R. Kandel, James H. Schwartz, & Thomas M. Jessell (eds.). New York, McGraw-Hill, Health and Professions Division.

KARRA, D. & DAHM, R. (2010) Transfection techniques for neuronal cells. *The Journal of Neuroscience*. 30 (18), 6171–6177.

KASK, K., ZAMANILLO, D., ROZOV, A, BURNASHEV, N., SPRENGEL, R. & SEEBURG, P.H. (1998) The AMPA receptor subunit GluR-B in its Q/R site-unedited form is not essential for brain development and function. *PNAS* 95 (23), 13777–13782.

KASSUBEK, J., MÜLLER, H.-P., DEL TREDICI, K., BRETTSCHNEIDER, J., PINKHARDT, E.H., LULÉ, D., BÖHM, S., BRAAK, H. & LUDOLPH, A.C. (2014) Diffusion tensor imaging analysis of sequential spreading of disease in amyotrophic lateral sclerosis confirms patterns of TDP-43 pathology. *Brain* 137 (Pt 6), 1733–1740.

KASTELEIN, J.J.P., WEDEL, M.K., BAKER, B.F., SU, J., BRADLEY, J.D., YU, R.Z., CHUANG, E., GRAHAM, M.J. & CROOKE, R.M. (2006) Potent reduction of apolipoprotein B and low-density lipoprotein cholesterol by short-term administration of an antisense inhibitor of apolipoprotein B. *Circulation*. 114 (16), 1729–1735.

KAUR, S.J., MCKEOWN, S.R. & RASHID, S. (2016) Mutant SOD1 mediated pathogenesis of Amyotrophic Lateral Sclerosis. *Gene*. 577 (2), 109–118.

KAWAHARA, Y., KWAK, S., SUN, H., ITO, K., HASHIDA, H., AIZAWA, H., JEONG, S.-Y. & KANAZAWA, I. (2003) Human spinal motoneurons express low relative abundance of GluR2 mRNA: an implication for excitotoxicity in ALS. *Journal of Neurochemistry.* 85 (3), 680–689.

KAWAHARA, Y., ITO, K., SUN, H., AIZAWA, H., KANAZAWA, I. & KWAK, S. (2004) RNA editing and death of motor neurons. *Nature*. 427 (February), 801.

KAWAHARA, Y., ITO, K., ITO, M., TSUJI, S. & KWAK, S. (2005) Novel splice variants of human ADAR2 mRNA: Skipping of the exon encoding the dsRNA-binding domains, and multiple C-terminal splice sites. *Gene*. 363, 193–201.

KAWAHARA, Y., SUN, H., ITO, K., HIDEYAMA, T., AOKI, M., SOBUE, G., TSUJI, S. & KWAK, S. (2006) Underediting of GluR2 mRNA, a neuronal death inducing molecular change in sporadic ALS, does not occur in motor neurons in ALS1 or SBMA. *Neuroscience research.* 54 (1), 11–14.

KIRAN, A. & BARANOV, P. V. (2010) DARNED: A DAtabase of RNa editing in humans. *Bioinformatics*. 26 (14), 1772–1776.

KIRBY, J., GOODALL, E.F., SMITH, W., HIGHLEY, J.R., MASANZU, R., HARTLEY, J. A, HIBBERD, R., HOLLINGER, H.C., WHARTON, S.B., MORRISON, K.E., INCE, P.G., MCDERMOTT, C.J. & SHAW, P.J. (2010) Broad clinical phenotypes associated with TAR-DNA binding protein (TARDBP) mutations in amyotrophic lateral sclerosis. *Neurogenetics*. 11 (2), 217–225.

KLEBE, R. & RUDDLE, F. (1969) Neuroblastoma: Cell culture analysis of a differentiating stem cell system. *Journal of Cell Biology.* 4369A.

KÖHLER, M., BURNASHEV, N., SAKMANN, B. & SEEBURG, P.H. (1993) Determinants of Ca2+ permeability in both TM1 and TM2 of high affinity kainate receptor channels: diversity by RNA editing. *Neuron*. 10 (3), 491–500.

KOIKE, M., TSUKADA, S., TSUZUKI, K., KIJIMA, H. & OZAWA, S. (2000) Regulation of kinetic properties of GluR2 AMPA receptor channels by alternative splicing. *The Journal of neuroscience* 20 (6), 2166–2174.

KOIKE-YUSA, H., LI, Y., TAN, E.-P., VELASCO-HERRERA, M.D.C. & YUSA, K. (2014) Genome-wide recessive genetic screening in mammalian cells with a lentiviral CRISPR-guide RNA library. *Nature biotechnology.* 32 (3), 267–273.

KOLE, R., KRAINER, A.R. & ALTMAN, S. (2012) RNA therapeutics: beyond RNA interference and antisense oligonucleotides. *Nature reviews. Drug discovery*. 11 (2), 125–140.

KONO, M. & AKIYAMA, M. (2013) Dyschromatosis Symmetrica Hereditaria and RNA Editing Enzyme. *Current Genetics in Dermatology.* pp. 105–119.

KOPPERS, M., BLOKHUIS, A.M., WESTENENG, H.J., TERPSTRA, M.L., ZUNDEL, C.A.C., VIEIRA DE S??, R., SCHELLEVIS, R.D., WAITE, A.J., BLAKE, D.J., VELDINK, J.H., VAN DEN BERG, L.H. & PASTERKAMP, R.J. (2015) C9orf72 ablation in mice does not cause motor neuron degeneration or motor deficits*. Annals of Neurology*. 78 (3), 426–438.

KORDASIEWICZ, H.B., STANEK, L.M., WANCEWICZ, E. V, MAZUR, C., MCALONIS, M.M., PYTEL, K.A., ARTATES, J.W., WEISS, A., CHENG, S.H., SHIHABUDDIN, L.S., HUNG, G., BENNETT, C.F. & CLEVELAND, D.W. (2012) Sustained therapeutic reversal of Huntington's disease by transient repression of huntingtin synthesis. *Neuron*. 74 (6), 1031–1044.

KORNBLIHTT, A.R., SCHOR, I.E., ALLÓ, M., DUJARDIN, G., PETRILLO, E. & MUÑOZ, M.J. (2013) Alternative splicing: a pivotal step between eukaryotic transcription and translation. *Nature reviews. Molecular cell biology*. 14 (3), 153–165.

KOVALEVICH, J. & LANGFORD, D. (2013) *Considerations for the Use of SH-SY5Y Neuroblastoma cells in Neurobiology.* In: Shohreh Amini & Martyn K. White (eds.). Neuronal Cell Culture. Methods in Molecular Biology. Totowa, NJ, Humana Press. pp. 9–21.

KRITIS, A. A., STAMOULA, E.G., PANISKAKI, K. A. & VAVILIS, T.D. (2015) Researching glutamate - induced cytotoxicity in different cell lines: a comparative/collective analysis/study. *Frontiers in Cellular Neuroscience*. 9 (March), 1–18.

KUNG, S.S., WU, Y.M. & CHOW, W.Y. (1996) Characterization of two fish glutamate receptor cDNA molecules: absence of RNA editing at the Q/R site. *Brain research.* 35 (1-2), 119–130.

KUTTAN, A. & BASS, B.L. (2012) Mechanistic insights into editing-site specificity of ADARs. *PNAS* 109 (48), E3295–E3304.

KWIATKOWSKI, T.J., BOSCO, D.A., LECLERC, A.L., TAMRAZIAN, E., VANDERBURG, C.R., RUSS, C., DAVIS, A., GILCHRIST, J., KASARSKIS, E.J., MUNSAT, T., VALDMANIS, P., ROULEAU, G.A., HOSLER, B.A., CORTELLI, P., DE JONG, P.J., YOSHINAGA, Y., HAINES, J.L., PERICAK-VANCE, M.A., YAN, J., ET AL. (2009) Mutations in the FUS/TLS gene on chromosome 16 cause familial amyotrophic lateral sclerosis. *Science*. 323 (5918), 1205–1208.

LACOMBLEZ, L., BENSIMON, G., LEIGH, P.N., GUILLET, P. & MEININGER, V. (1996) Dose-ranging study of riluzole in amyotrophic lateral sclerosis. *Lancet*. 347 (9013), 1425–1431.

LAGIER-TOURENNE, C., POLYMENIDOU, M., HUTT, K.R., VU, A.Q., BAUGHN, M., HUELGA, S.C., CLUTARIO, K.M., LING, S.-C., LIANG, T.Y., MAZUR, C., WANCEWICZ, E., KIM, A.S., WATT, A., FREIER, S., HICKS, G.G., DONOHUE, J.P., SHIUE, L., BENNETT, C.F., RAVITS, J., ET AL. (2012) Divergent roles of ALS-linked proteins FUS/TLS and TDP-43 intersect in processing long pre-mRNAs. *Nature neuroscience*. 15 (11), 1488–1497.

LAGIER-TOURENNE, C., BAUGHN, M., RIGO, F., SUN, S., LIU, P., LI, H.-R., JIANG, J., WATT, A.T., CHUN, S., KATZ, M., QIU, J., SUN, Y., LING, S.-C., ZHU, Q., POLYMENIDOU, M., DRENNER, K., ARTATES, J.W., MCALONIS-DOWNES, M., MARKMILLER, S., ET AL. (2013) Targeted degradation of sense and antisense C9orf72 RNA foci as therapy for ALS and frontotemporal degeneration. *PNAS*. 110 (47), E4530–E4539.

LAI, F., CHEN, C.X., CARTER, K.C. & NISHIKURA, K. (1997) Editing of glutamate receptor B subunit ion channel RNAs by four alternatively spliced DRADA2 double-stranded RNA adenosine deaminases. *Molecular and cellular biology.* 17 (5), 2413–2424.

LANFRANCO, M.F., SEITZ, P.K., MORABITO, M. V., EMESON, R.B., SANDERS-BUSH, E. & CUNNINGHAM, K.A. (2009) An innovative real-time PCR method to measure changes in RNA editing of the serotonin 2C receptor (5-HT2CR) in brain. *Journal of neuroscience methods*. 179 (2), 247–257.

LATTANTE, S., CIURA, S., ROULEAU, G.A. & KABASHI, E. (2015) Defining the genetic connection linking amyotrophic lateral sclerosis (ALS) with frontotemporal dementia (FTD). *Trends in genetics*. 31 (5), 263–273.

LEBLEU, B., MOULTON, H.M., ABES, R., IVANOVA, G.D., ABES, S., STEIN, D.A., IVERSEN, P.L., ARZUMANOV, A.A. & GAIT, M.J. (2008) Cell penetrating peptide conjugates of steric block oligonucleotides. *Advanced drug delivery reviews*. 60 (4-5), 517–529.

LEE, S., JOUNG, J.-G., PARK, C., PARK, J. & KIM, J.H. (2015) RCARE: RNA Sequence Comparison and Annotation for RNA Editing. *BMC Medical Genomics.* 8 (Suppl 2), S8

LEE, Y. & RIO, D.C. (2015) Mechanisms and Regulation of Alternative Pre-mRNA Splicing. *Annual review of biochemistry.* (March), 1–33.

LEHMANN, K.A. & BASS, B.L. (2000) Double-Stranded RNA Adenosine Deaminases ADAR1 and ADAR2 Have Overlapping Specificities. *Biochemistry*. 39 (42), 12875–12884.

LESUISSE, C. & MARTIN, L.J. (2002) Long-term culture of mouse cortical neurons as a model for neuronal development, aging, and death. *Journal of Neurobiology*. 51 (1), 9–23.

LEVANON, E.Y., HALLEGGER, M., KINAR, Y., SHEMESH, R., DJINOVIC-CARUGO, K., RECHAVI, G., JANTSCH, M.F. & EISENBERG, E. (2005) Evolutionarily conserved human targets of adenosine to inosine RNA editing. *Nucleic acids research*. 33 (4), 1162–1168.

LEVANON, E.Y. & EISENBERG, E. (2015) Does RNA editing compensate for Alu invasion of the primate genome? *BioEssays*. 37, 175–181.

LI, J.B., LEVANON, E.Y., YOON, J.-K., AACH, J., XIE, B., LEPROUST, E., ZHANG, K., GAO, Y. & CHURCH, G.M. (2009) Genome-wide identification of human RNA editing sites by parallel DNA capturing and sequencing. *Science*. 324 (5931), 1210–1213.

LI, Q., LEE, J.-A. & BLACK, D.L. (2007) Neuronal regulation of alternative pre-mRNA splicing. *Nature reviews. Neuroscience*. 8 (11), 819–831.

LIANG, H. & LANDWEBER, L.F. (2007) Hypothesis: RNA editing of microRNA target sites in humans? *RNA*. 13 (4), 463–467.

LIM, L., WEI, Y., LU, Y. & SONG, J. (2016) ALS-Causing Mutations Significantly Perturb the Self-Assembly and Interaction with Nucleic Acid of the Intrinsically Disordered Prion-Like Domain of TDP-43 *PLOS Biology*. 14 (1), e1002338. LIN, C.-L.G., BRISTOL, L.A., JIN, L., DYKES-HOBERG, M., CRAWFORD, T., CLAWSON, L. & ROTHSTEIN, J.D. (1998) Aberrant RNA Processing in a Neurodegenerative Disease: the Cause for Absent EAAT2, a Glutamate Transporter, in Amyotrophic Lateral Sclerosis. *Neuron*. 20 (3), 589–602.

LIU, J., LILLO, C., JONSSON, P.A., VANDE VELDE, C., WARD, C.M., MILLER, T.M., SUBRAMANIAM, J.R., ROTHSTEIN, J.D., MARKLUND, S., ANDERSEN, P.M., BRÄNNSTRÖM, T., GREDAL, O., WONG, P.C., WILLIAMS, D.S. & CLEVELAND, D.W. (2004) Toxicity of familial ALS-linked SOD1 mutants from selective recruitment to spinal mitochondria. *Neuron*. 43 (1), 5–17.

LIU, S.J. & SAVTCHOUK, I. (2012) Ca(2+) permeable AMPA receptors switch allegiances: mechanisms and consequences. *The Journal of physiology*. 590 (Pt 1), 13–20.

LIU, Y. & SAMUEL, C.E. (1999) Editing of glutamate receptor subunit B pre-mRNA by splice-site variants of interferon-inducible double-stranded RNA-specific adenosine deaminase ADAR1. *The Journal of biological chemistry*. 274 (8), 5070–5077.

LOMELI, H., MOSBACHER, J., MELCHER, T., HÖGER, T., GEIGER, J.R., KUNER, T., MONYER, H., HIGUCHI, M., BACH, A & SEEBURG, P.H. (1994) Control of kinetic properties of AMPA receptor channels by nuclear RNA editing. *Science*. 266 (5191), 1709–1713.

LOPES, F.M., SCHRÖDER, R., DA FROTA, M.L.C., ZANOTTO-FILHO, A., MÜLLER, C.B., PIRES, A.S., MEURER, R.T., COLPO, G.D., GELAIN, D.P., KAPCZINSKI, F., MOREIRA, J.C.F., FERNANDES, M.D.C. & KLAMT, F. (2010) Comparison between proliferative and neuron-like SH-SY5Y cells as an in vitro model for Parkinson disease studies. *Brain research*. 1337, 85–94

LU, Q.L., MANN, C.J., LOU, F., BOU-GHARIOS, G., MORRIS, G.E., XUE, S., FLETCHER, S., PARTRIDGE, T.A. & WILTON, S.D. (2003) Functional amounts of dystrophin produced by skipping the mutated exon in the mdx dystrophic mouse. *Nature medicine*. 9 (8), 1009–1014.

LU, W. & ROCHE, K.W. (2012) Posttranslational regulation of AMPA receptor trafficking and function. *Current Opinion in Neurobiology*. 22 (3), 470–479.

LU, W., SHI, Y., JACKSON, A.C., BJORGAN, K., DURING, M.J., SPRENGEL, R., SEEBURG, P.H. & NICOLL, R.A. (2009) Subunit Composition of Synaptic AMPA Receptors Revealed by a Single-Cell Genetic Approach. *Neuron*. 62 (2), 254–268.

LU, Z.J., GLOOR, J.W. & MATHEWS, D.H. (2009) Improved RNA secondary structure prediction by maximizing expected pair accuracy. *RNA* 15 (10), 1805–1813.

LUSSIER, M.P., NASU-NISHIMURA, Y. & ROCHE, K.W. (2011) Activity-dependent ubiquitination of the AMPA receptor subunit GluA2. *The Journal of neuroscience* 31 (8), 3077–3081..

MAAS, S., PATT, S., SCHREY, M. & RICH, A (2001) Underediting of glutamate receptor GluR-B mRNA in malignant gliomas *PNAS* 98 (25), 14687–14692.

MAAS, S. & GOMMANS, W.M. (2009a) Identification of a selective nuclear import signal in adenosine deaminases acting on RNA. *Nucleic acids research*. 37 (17), 5822–5829.

MAAS, S. & GOMMANS, W.M. (2009b) Novel exon of mammalian ADAR2 extends open reading frame. *PloS one.* 4 (1), e4225.

MACBETH, M.R., SCHUBERT, H.L., VANDEMARK, A.P., LINGAM, A.T., HILL, C.P. & BASS, B.L. (2005) Inositol hexakisphosphate is bound in the ADAR2 core and required for RNA editing. *Science*. 309 (5740), 1534–1539.

MACKENZIE, I.R.A., BIGIO, E.H., INCE, P.G., GESER, F., NEUMANN, M., CAIRNS, N.J., KWONG, L.K., FORMAN, M.S., RAVITS, J., STEWART, H., EISEN, A., MCCLUSKY, L., KRETZSCHMAR, H.A., MONORANU, C.M., HIGHLEY, J.R., KIRBY, J., SIDDIQUE, T., SHAW, P.J., LEE, V.M.-Y., ET AL. (2007) Pathological TDP-43 distinguishes sporadic amyotrophic lateral sclerosis from amyotrophic lateral sclerosis with SOD1 mutations. *Annals of neurology*. 61 (5), 427–434.

MACKENZIE, I.R.A., ANSORGE, O., STRONG, M., BILBAO, J., ZINMAN, L., ANG, L.-C., BAKER, M., STEWART, H., EISEN, A., RADEMAKERS, R. & NEUMANN, M. (2011) Pathological heterogeneity in amyotrophic lateral sclerosis with FUS mutations: two distinct patterns correlating with disease severity and mutation. *Acta neuropathologica.* 122 (1), 87–98.

MACKENZIE, I.R., ARZBERGER, T., KREMMER, E., TROOST, D., LORENZL, S., MORI, K., WENG, S.-M., HAASS, C., KRETZSCHMAR, H.A., EDBAUER, D. & NEUMANN, M. (2013) Dipeptide repeat protein pathology in C9ORF72 mutation cases: clinico-pathological correlations. *Acta neuropathologica*. 126 (6), 859–879.

MACKENZIE, I.R. A, FRICK, P. & NEUMANN, M. (2014) The neuropathology associated with repeat expansions in the C9ORF72 gene. *Acta Neuropathologica*. 127 (3), 347–357.

MAHAJAN, S.S., THAI, K.H., CHEN, K. & ZIFF, E. (2011) Exposure of neurons to excitotoxic levels of glutamate induces cleavage of the RNA editing enzyme, adenosine deaminase acting on RNA 2, and loss of GLUR2 editing. *Neuroscience*. 189, 305–315.

MAHARJAN, N., KÜNZLI, C., BUTHEY, K. & SAXENA, S. (2016) C9ORF72 Regulates Stress Granule Formation and Its Deficiency Impairs Stress Granule Assembly, Hypersensitizing Cells to Stress. *Molecular neurobiology* [Epub ahead of print]

MAHENDRAN, R., SPOTTSWOOD, M.S., GHATE, A., LING, M.L., JENG, K. & MILLER, D.L. (1994) Editing of the mitochondrial small subunit rRNA in Physarum polycephalum.

MÄKINEN, P.I., KOPONEN, J.K., KÄRKKÄINEN, A.-M., MALM, T.M., PULKKINEN, K.H., KOISTINAHO, J., TURUNEN, M.P. & YLÄ-HERTTUALA, S. (2006) Stable RNA interference: comparison of U6 and H1 promoters in endothelial cells and in mouse brain. *The journal of gene medicine*. 8 (4), 433–441.

MANN, D.A. & FRANKEL, A.D. (1991) Endocytosis and targeting of exogenous HIV-1 Tat protein. *The EMBO journal.* 10 (7), 1733–1739.

MARC, G., LEAH, R., OFIRA, E., ODED, A., ZOHAR, A. & HANNA, R. (2013) Presymptomatic Treatment with Acetylcholinesterase Antisense Oligonucleotides Prolongs Survival in ALS (G93A-SOD1) Mice. *BioMed research international*. 2013, 845345

MARCUCCI, R., BRINDLE, J., PARO, S., CASADIO, A., HEMPEL, S., MORRICE, N., BISSO, A., KEEGAN, L.P., DEL SAL, G. & O'CONNELL, M.A. (2011) Pin1 and WWP2 regulate GluR2 Q/R site RNA editing by ADAR2 with opposing effects. *The EMBO journal*. 30 (20), 4211–4222.

MARINO, M., PAPA, S., CRIPPA, V., NARDO, G., PEVIANI, M., CHERONI, C., TROLESE, M.C., LAURANZANO, E., BONETTO, V., POLETTI, A., DEBIASI, S., FERRAIUOLO, L., SHAW, P.J. & BENDOTTI, C. (2015) Differences in protein quality control correlate with phenotype variability in 2 mouse models of familial amyotrophic lateral sclerosis. *Neurobiology of aging*. 36 (1), 492–504..

MASLIAH, G., BARRAUD, P. & ALLAIN, F.H.T. (2013) RNA recognition by double-stranded RNA binding domains: A matter of shape and sequence. *Cellular and Molecular Life Sciences.* 70 (11), 1875–1895.

MASSMAN, P.J., SIMS, J., COOKE, N., HAVERKAMP, L.J., APPEL, V. & APPEL, S.H. (1996) Prevalence and correlates of neuropsychological deficits in amyotrophic lateral sclerosis. *Journal of neurology, neurosurgery, and psychiatry*. 61 (5), 450–455.

MATHEWS, D.H., MOSS, W.N. & TURNER, D.H. (2010) Folding and finding RNA secondary structure. *Cold Spring Harbor perspectives in biology*. 2 (12), 1–15.

MATHEWS, D.H. (2004) Using an RNA secondary structure partition function to determine confidence in base pairs predicted by free energy minimization. *RNA*. 10, 1178–1190.

MATTHEWS, M.M., THOMAS, J.M., ZHENG, Y., TRAN, K., PHELPS, K.J., SCOTT, A.I., HAVEL, J., FISHER, A.J. & BEAL, P.A. (2016) Structures of human ADAR2 bound to dsRNA reveal base-flipping mechanism and basis for site selectivity. *Nature Structural & Molecular Biology.* (April), 1–10.

MEAD, A.N. & STEPHENS, D.N. (2003) Involvement of AMPA receptor GluR2 subunits in stimulus-reward learning: evidence from glutamate receptor gria2 knock-out mice. *The Journal of neuroscience* 23 (29), 9500–9507.

MEAD, A.N., BROWN, G., LE MERRER, J. & STEPHENS, D.N. (2005) Effects of deletion of gria1 or gria2 genes encoding glutamatergic AMPA-receptor subunits on place preference conditioning in mice. *Psychopharmacology*. 179 (1), 164–171.

MEDVEDEV, N.I., RODRÍGUEZ-ARELLANO, J.J., POPOV, V.I., DAVIES, H.A., TIGARET, C.M., SCHOEPFER, R. & STEWART, M.G. (2008) The glutamate receptor 2 subunit controls post-synaptic density complexity and spine shape in the dentate gyrus. *European Journal of Neuroscience*. 27 (2), 315–325

MELCHER, T., MAAS, S., HERB, A., SPRENGEL, R., SEEBERG, P.H. & HIGUCHI, M. (1996) A mammalian RNA editing enzyme. *Nature*. 379 (1), 460–464.

MENDELL, J.R., GOEMANS, N., LOWES, L.P., ALFANO, L.N., BERRY, K., SHAO, J., KAYE, E.M. & MERCURI, E. (2016) Longitudinal effect of eteplirsen versus historical control on ambulation in Duchenne muscular dystrophy. *Annals of Neurology*. 79 (2), 257–271.

MENDELL, J.R., RODINO-KLAPAC, L.R., SAHENK, Z., ROUSH, K., BIRD, L., LOWES, L.P., ALFANO, L., GOMEZ, A.M., LEWIS, S., KOTA, J., MALIK, V., SHONTZ, K., WALKER, C.M., FLANIGAN, K.M., CORRIDORE, M., KEAN, J.R., ALLEN, H.D., SHILLING, C., MELIA, K.R., ET AL. (2013) Eteplirsen for the treatment of Duchenne muscular dystrophy. *Annals of neurology.* 74 (5), 637–647.

MENG, Y., ZHANG, Y. & JIA, Z. (2003) Synaptic transmission and plasticity in the absence of AMPA glutamate receptor GluR2 and GluR3. *Neuron*. 39 (1), 163–176.

MERCADO, P.A., AYALA, Y.M., ROMANO, M., BURATTI, E. & BARALLE, F.E. (2005) Depletion of TDP 43 overrides the need for exonic and intronic splicing enhancers in the human apoA-II gene. *Nucleic acids research*. 33 (18), 6000–6010.

MILANESE, M., ZAPPETTINI, S., ONOFRI, F., MUSAZZI, L., TARDITO, D., BONIFACINO, T., MESSA, M., RACAGNI, G., USAI, C., BENFENATI, F., POPOLI, M. & BONANNO, G. (2011) Abnormal exocytotic release of glutamate in a mouse model of amyotrophic lateral sclerosis. *Journal of neurochemistry*. 116 (6), 1028–1042.

MILLER, T.M., PESTRONK, A., DAVID, W., ROTHSTEIN, J., SIMPSON, E., APPEL, S.H., ANDRES, P.L., MAHONEY, K., ALLRED, P., ALEXANDER, K., OSTROW, L.W., SCHOENFELD, D., MACKLIN, E.A., NORRIS, D.A., MANOUSAKIS, G., CRISP, M., SMITH, R., BENNETT, C.F., BISHOP, K.M., ET AL. (2013) An antisense oligonucleotide against SOD1 delivered intrathecally for patients with SOD1 familial amyotrophic lateral sclerosis: a phase 1, randomised, first-in-man study. *The Lancet. Neurology*. 12 (5), 435–442.

MINEFF, E.M. & WEINBERG, R.J. (2000) Differential synaptic distribution of AMPA receptor subunits in the ventral posterior and reticular thalamic nuclei of the rat. *Neuroscience*. 101 (4), 969–982.

MISAWA, H., NAKATA, K., TODA, K., MATSUURA, J., ODA, Y., INOUE, H., TATENO, M. & TAKAHASHI, R. (2003) VAChT-Cre. Fast and VAChT-Cre.Slow: postnatal expression of Cre recombinase in somatomotor neurons with different onset. *Genesis*. 37 (1), 44–50.

MITCHELL, J.C., MCGOLDRICK, P., VANCE, C., HORTOBAGYI, T., SREEDHARAN, J., ROGELJ, B., TUDOR, E.L., SMITH, B.N., KLASEN, C., MILLER, C.C.J., COOPER, J.D., GREENSMITH, L. & SHAW, C.E. (2013) Overexpression of human wild-type FUS causes progressive motor neuron degeneration in an age- and dose-dependent fashion. *Acta Neuropathologica*. 125 (2), 273–288.

MIZIELINSKA, S., LASHLEY, T., NORONA, F.E., CLAYTON, E.L., RIDLER, C.E., FRATTA, P. & ISAACS, A.M. (2013) C9orf72 frontotemporal lobar degeneration is characterised by frequent neuronal sense and antisense RNA foci. *Acta neuropathologica*. 126 (6), 845–857

MONYER, H., SEEBURG, P.H. & WISDEN, W. (1991) Glutamate-operated channels: developmentally early and mature forms arise by alternative splicing. *Neuron*. 6 (5), 799–810.

MORABITO, M. V, ABBAS, A.I., HOOD, J.L., KESTERSON, R.A., JACOBS, M.M., KUMP, D.S., HACHEY, D.L., ROTH, B.L. & EMESON, R.B. (2010) Mice with altered serotonin 2C receptor RNA editing display characteristics of Prader-Willi syndrome. *Neurobiology of disease.* 39 (2), 169–180.

MORCOS, P.A. (2001) Achieving efficient delivery of morpholino oligos in cultured cells. *Genesis*. 30 (3), 94–102.

MORCOS, P., LI, Y. & JIANG, S. (2008) Vivo-Morpholinos: A non-peptide transporter delivers Morpholinos into a wide array of mouse tissues. *BioTechniques*. 45 (6), 613–623.

MOSBACHER, J., SCHOEPFER, R., MONYER, H., BURNASHEV, N., SEEBURG, P.H. & RUPPERSBERG, J.P. (1994) A molecular determinant for submillisecond desensitization in glutamate receptors. *Science*. 266 (5187), 1059–1062.

MYERS, S.J., PETERS, J., HUANG, Y., COMER, M.B., BARTHEL, F. & DINGLEDINE, R. (1998) Transcriptional regulation of the GluR2 gene: neural-specific expression, multiple promoters, and regulatory elements. *The Journal of neuroscience* 18 (17), 6723–6739.

NAGAI, M., RE, D.B., NAGATA, T., CHALAZONITIS, A., JESSELL, T.M., WICHTERLE, H. & PRZEDBORSKI, S. (2007) Astrocytes expressing ALS-linked mutated SOD1 release factors selectively toxic to motor neurons. *Nature neuroscience*. 10 (5), 615–622.

NAKAE, A., NAKAI, K., TANAKA, T., TAKASHINA, M., HAGIHIRA, S., SHIBATA, M., UEDA, K. & MASHIMO, T. (2008) Serotonin2C receptor mRNA editing in neuropathic pain model. *Neuroscience research*. 60 (2), 228–231.

NEUMANN, M., SAMPATHU, D.M., KWONG, L.K., TRUAX, A.C., MICSENYI, M.C., CHOU, T.T., BRUCE, J., SCHUCK, T., GROSSMAN, M., CLARK, C.M., MCCLUSKEY, L.F., MILLER, B.L., MASLIAH, E., MACKENZIE, I.R., FELDMAN, H., FEIDEN, W., KRETZSCHMAR, H.A., TROJANOWSKI, J.Q. & LEE, V.M.-Y. (2006) Ubiquitinated TDP-43 in frontotemporal lobar degeneration and amyotrophic lateral sclerosis. *Science*. 314 (5796), 130–133.

NEUMANN, M., RADEMAKERS, R., ROEBER, S., BAKER, M., KRETZSCHMAR, H.A. & MACKENZIE, I.R.A. (2009) A new subtype of frontotemporal lobar degeneration with FUS pathology. *Brain*. 132 (Pt 11), 2922–2931.

NIAVARANI, A., CURRIE, E., REYAL, Y., ANJOS-AFONSO, F., HORSWELL, S., GRIESSINGER, E., SARDINA, J.L. & BONNET, D. (2015) APOBEC3A is implicated in a novel class of G-to-A mRNA editing in WT1 transcripts. *PLoS ONE*. 10 (3), 1–17.

NISHIKURA, K. (2006) Editor meets silencer: crosstalk between RNA editing and RNA interference. *Nature reviews. Molecular cell biology*. 7 (12), 919–931

NIZZARDO, M., SIMONE, C., RIZZO, F., ULZI, G., RAMIREZ, A., RIZZUTI, M., BORDONI, A., BUCCHIA, M., GATTI, S., BRESOLIN, N., COMI, G.P. & CORTI, S. (2016) Morpholino-mediated SOD1 reduction ameliorates an amyotrophic lateral sclerosis disease phenotype. *Scientific Reports*. 6 (October 2015), 21301.

NOH, K.-M., YOKOTA, H., MASHIKO, T., CASTILLO, P.E., ZUKIN, R.S. & BENNETT, M.V.L. (2005) Blockade of calcium-permeable AMPA receptors protects hippocampal neurons against global ischemia-induced death. *PNAS*. 102 (34), 12230–12235.

NONAKA, T., MASUDA-SUZUKAKE, M., ARAI, T., HASEGAWA, Y., AKATSU, H., OBI, T., YOSHIDA, M., MURAYAMA, S., MANN, D.M.A., AKIYAMA, H. & HASEGAWA, M. (2013) Prion-like properties of pathological TDP-43 aggregates from diseased brains. *Cell reports*. 4 (1), 124–134.

NOY, A., LUQUE, F.J. & OROZCO, M. (2008) Theoretical analysis of antisense duplexes: determinants of the RNase H susceptibility. *Journal of the American Chemical Society.* 130 (11), 3486–3496.

O'CONNELL, M. A, GERBER, A. & KELLER, W. (1997) Purification of human double-stranded RNA-specific editase 1 (hRED1) involved in editing of brain glutamate receptor B pre-mRNA. *The Journal of Biological Chemistry.* 272 (1), 473–478.

O'CONNELL, M. A, GERBER, A & KEEGAN, L.P. (1998) Purification of native and recombinant double-stranded RNA-specific adenosine deaminases. *Methods* 15 (1), 51–62

O'ROURKE, J.G., BOGDANIK, L., MUHAMMAD, A.K.M.G., GENDRON, T.F., KIM, K.J., AUSTIN, A., CADY, J., LIU, E.Y., ZARROW, J., GRANT, S., HO, R., BELL, S., CARMONA, S., SIMPKINSON, M., LALL, D., WU, K., DAUGHRITY, L., DICKSON, D.W., HARMS, M.B., ET AL. (2015) C9orf72 BAC Transgenic Mice Display Typical Pathologic Features of ALS/FTD. *Neuron*. 88 (5), 892–901.

OHKI, E.C., TILKINS, M.L., CICCARONE, V.C. & PRICE, P.J. (2001) Improving the transfection efficiency of post-mitotic neurons. *Journal of Neuroscience Methods*. 112 (2), 95–99.

OHLSON, J., PEDERSEN, J.S., HAUSSLER, D. & OHMAN, M. (2007) Editing modifies the GABA(A) receptor subunit alpha3. *RNA*. 13 (5), 698–703.

OHMAN, M., KÄLLMAN, A.M. & BASS, B.L. (2000) In vitro analysis of the binding of ADAR2 to the pre-mRNA encoding the GluR-B R/G site. *RNA*. 6 (5), 687–697.

OncoGeneX (2016) ONCOGENEX. [Online]. 2016. Available from: http://oncogenex.com/physicians/custirsen-ogx-011 [Accessed: 3 May 2016].

ORLANDI, C., LA VIA, L., BONINI, D., MORA, C., RUSSO, I., BARBON, A. & BARLATI, S. (2011) AMPA receptor regulation at the mRNA and protein level in rat primary cortical cultures. *PloS one*. 6 (9), e25350.

OSMAN, E. & MILLER, M. (2014) Morpholino Antisense Oligonucleotides Targeting Intronic Repressor Element1 Improve Phenotype in SMA Mouse Models. *Human Molecular Genetics* 23 (18), 4832-45

OSMAN, E.Y., YEN, P.-F. & LORSON, C.L. (2012) Bifunctional RNAs targeting the intronic splicing silencer N1 increase SMN levels and reduce disease severity in an animal model of spinal muscular atrophy. *Molecular therapy* 20 (1), 119–126.

PACHERNEGG, S., MÜNSTER, Y., MUTH-KÖHNE, E., FUHRMANN, G. & HOLLMANN, M. (2015) GluA2 is rapidly edited at the Q/R site during neural differentiation in vitro. *Frontiers in Cellular Neuroscience*. 9 (March), 1–14.

PANDEY, S.P., RAI, R., GAUR, P. & PRASAD, S. (2015) Development- and age-related alterations in the expression of AMPA receptor subunit GluR2 and its trafficking proteins in the hippocampus of male mouse brain. *Biogerontology*. 16 (3), 317–328

PARAKH, S. & ATKIN, J.D. (2016) Protein Folding Alterations in Amyotrophic Lateral Sclerosis. *Brain Research*. 16, 30203–30267.

PARDO, C.A., XU, Z., BORCHELT, D.R., PRICE, D.L., SISODIA, S.S. & CLEVELAND, D.W. (1995) Superoxide dismutase is an abundant component in cell bodies, dendrites, and axons of motor neurons and in a subset of other neurons. *PNAS* 92 (4), 954–958

PASSINI, M.A., BU, J., RICHARDS, A.M., KINNECOM, C., SARDI, S.P., STANEK, L.M., HUA, Y., RIGO, F., MATSON, J., HUNG, G., KAYE, E.M., SHIHABUDDIN, L.S., KRAINER, A.R., BENNETT, C.F. & CHENG, S.H. (2011) Antisense oligonucleotides delivered to the mouse CNS ameliorate symptoms of severe spinal muscular atrophy. *Science translational medicine*. 3 (72)

PATTERSON, J.B. & SAMUEL, C.E. (1995) Expression and regulation by interferon of a double-stranded-RNA-specific adenosine deaminase from human cells: evidence for two forms of the deaminase. *Molecular and cellular biology*. 15 (10), 5376–5388.

PAUPARD, M.C., O'CONNELL, M.A., GERBER, A.P. & ZUKIN, R.S. (2000) Patterns of developmental expression of the RNA editing enzyme rADAR2. *Neuroscience*. 95 (3), 869–879.

PAZ, J.T., BRYANT, A.S., PENG, K., FENNO, L., YIZHAR, O., FRANKEL, W.N., DEISSEROTH, K. & HUGUENARD, J.R. (2011) A new mode of corticothalamic transmission revealed in the Gria4(-/-) model of absence epilepsy. *Nature neuroscience.* 14 (9), 1167–1173.

PAZ, N., LEVANON, E.Y., AMARIGLIO, N., HEIMBERGER, A.B., RAM, Z., CONSTANTINI, S., BARBASH, Z.S., ADAMSKY, K., SAFRAN, M., HIRSCHBERG, A., KRUPSKY, M., BEN-DOV, I., CAZACU, S., MIKKELSEN, T., BRODIE, C., EISENBERG, E. & RECHAVI, G. (2007) Altered adenosine-to-inosine RNA editing in human cancer. *Genome research.* 17 (11), 1586–1595

PAZ-YAACOV, N., LEVANON, E.Y., NEVO, E., KINAR, Y., HARMELIN, A., JACOB-HIRSCH, J., AMARIGLIO, N., EISENBERG, E. & RECHAVI, G. (2010) Adenosine-to-inosine RNA editing shapes transcriptome diversity in primates. *PNAS*. 107 (27), 12174–12179.

PELUFFO, H., FOSTER, E., AHMED, S.G., LAGO, N., HUTSON, T.H., MOON, L., YIP, P., WANISCH, K., CARABALLO-MIRALLES, V., OLMOS, G., LLADÓ, J., MCMAHON, S.B. & YÁÑEZ-MUÑOZ, R.J. (2012) Efficient gene expression from integration-deficient lentiviral vectors in the spinal cord. *Gene Therapy*. (October 2012), 645–657.

PENG, P.L., ZHONG, X., TU, W., SOUNDARAPANDIAN, M.M., MOLNER, P., ZHU, D., LAU, L., LIU, S., LIU, F. & LU, Y. (2006) ADAR2-dependent RNA editing of AMPA receptor subunit GluR2 determines vulnerability of neurons in forebrain ischemia. *Neuron*. 49 (5), 719–733.

PENN, A.C., BALIK, A. & GREGER, I.H. (2012) Steric antisense inhibition of AMPA receptor Q/R editing reveals tight coupling to intronic editing sites and splicing. *Nucleic acids research*. 41 (2), 1113–1123.

PENN, A.C., BALIK, A. & GREGER, I.H. (2013) Reciprocal regulation of A-to-I RNA editing and the vertebrate nervous system. *Frontiers in neuroscience*. 7 (April), 61.

PEREIRA, A.C., GRAY, J.D., KOGAN, J.F., DAVIDSON, R.L., RUBIN, T.G., OKAMOTO, M., MORRISON, J.H. & MCEWEN, B.S. (2016) Age and Alzheimer's disease gene expression profiles reversed by the glutamate modulator riluzole. *Molecular psychiatry*. [Epub ahead of print]

PETRINI, E.M., LU, J., COGNET, L., LOUNIS, B., EHLERS, M.D. & CHOQUET, D. (2009) Endocytic trafficking and recycling maintain a pool of mobile surface AMPA receptors required for synaptic potentiation. *Neuron*. 63 (1), 92–105.

PHELPS, K.J., TRAN, K., EIFLER, T., ERICKSON, A.I., FISHER, A.J. & BEAL, P. A (2015) Recognition of duplex RNA by the deaminase domain of the RNA editing enzyme ADAR2. *Nucleic acids research*. 1–10.

PHILIPS, T. & ROTHSTEIN, J.D. (2015) Rodent models of amyotrophic lateral sclerosis. *Current Protocols in Pharmacology*. 2015 (9), 5.67.1–5.67.21

PICARDI, E., MANZARI, C., MASTROPASQUA, F., AIELLO, I., ERCHIA, A.M.D. & PESOLE, G. (2015) Profiling RNA editing in human tissues : towards the inosinome Atlas. *Science Reports* 5, 14941

PINTO, Y., COHEN, H.Y. & LEVANON, E.Y. (2014) Mammalian conserved ADAR targets comprise only a small fragment of the human editosome. *Genome biology.* 15 (1), R5.

PIRHAN, D., YÜKSEL, N., EMRE, E., CENGIZ, A. & KÜRŞAT YILDIZ, D. (2016) Riluzole- and Resveratrol-Induced Delay of Retinal Ganglion Cell Death in an Experimental Model of Glaucoma. *Current eye research*. 41 (1), 59–69.

PLAITAKIS, A., CONSTANTAKAKIS, E. & SMITH, J. (1988) The neuroexcitotoxic amino acids glutamate and aspartate are altered in the spinal cord and brain in amyotrophic lateral sclerosis*. Annals of Neurology*. 24 (3), 446–449.

PLANT, K., PELKEY, K. A, BORTOLOTTO, Z. A, MORITA, D., TERASHIMA, A., MCBAIN, C.J., COLLINGRIDGE, G.L. & ISAAC, J.T.R. (2006) Transient incorporation of native GluR2-lacking AMPA receptors during hippocampal long-term potentiation. *Nature neuroscience*. 9 (5), 602–604.

POKRISHEVSKY, E., GRAD, L.I. & CASHMAN, N.R. (2016) TDP-43 or FUS-induced misfolded human wild-type SOD1 can propagate intercellularly in a prion-like fashion. *Scientific reports*. 622155.

POLSON, A.G. & BASS, B.L. (1994) Preferential selection of adenosines for modification by double-stranded RNA adenosine deaminase. *The EMBO journal*. 13 (23), 5701–5711.

POLYMENIDOU, M., LAGIER-TOURENNE, C., HUTT, K.R., HUELGA, S.C., MORAN, J., LIANG, T.Y., LING, S.-C., SUN, E., WANCEWICZ, E., MAZUR, C., KORDASIEWICZ, H., SEDAGHAT, Y., DONOHUE, J.P., SHIUE, L., BENNETT, C.F., YEO, G.W. & CLEVELAND, D.W. (2011) Long pre-mRNA depletion and RNA missplicing contribute to neuronal vulnerability from loss of TDP-43. *Nature neuroscience*. 14 (4), 459–468.

POPPLEWELL, L.J., TROLLET, C., DICKSON, G. & GRAHAM, I.R. (2009) Design of phosphorodiamidate morpholino oligomers (PMOs) for the induction of exon skipping of the human DMD gene. *Molecular therapy* 17 (3), 554–561

POPPLEWELL, L.J., ABU-DAYYA, A., KHANA, T., FLINTERMAN, M., ABDUL KHALIQUE, N., RAJU, L., ØPSTAD, C.L., SLIWKA, H.-R., PARTALI, V., DICKSON, G. & PUNGENTE, M.D. (2012) Novel cationic carotenoid lipids as delivery vectors of antisense oligonucleotides for exon skipping in Duchenne muscular dystrophy. *Molecules* 17 (2), 1138–1148.

PORATH, H.T., CARMI, S. & LEVANON, E.Y. (2014) A genome-wide map of hyper-edited RNA reveals numerous new sites. *Nature communications*. 5, 4726.

PORENSKY, P.N., MITRPANT, C., MCGOVERN, V.L., BEVAN, A.K., FOUST, K.D., KASPAR, B.K., WILTON, S.D. & BURGHES, A.H.M. (2012) A single administration of morpholino antisense oligomer rescues spinal muscular atrophy in mouse. *Human Molecular Genetics*. 21 (7), 1625–1638.

PRAMONO, Z.A.D., WEE, K.B., WANG, J.L., CHEN, Y.J., XIONG, Q. BIN, LAI, P.S. & YEE, W.C. (2012) A prospective study in the rational design of efficient antisense oligonucleotides for exon skipping in the DMD gene. *Human gene therapy*. 23 (7), 781–790.

RAAL, F.J., SANTOS, R.D., BLOM, D.J., MARAIS, A.D., CHARNG, M.-J., CROMWELL, W.C., LACHMANN, R.H., GAUDET, D., TAN, J.L., CHASAN-TABER, S., TRIBBLE, D.L., FLAIM, J.D. & CROOKE, S.T. (2010) Mipomersen, an apolipoprotein B synthesis inhibitor, for lowering of LDL cholesterol concentrations in patients with homozygous familial hypercholesterolaemia: a randomised, double-blind, placebo-controlled trial. *Lancet* 375 (9719), 998–1006.

RAITSKIN, O., CHO, D.S., SPERLING, J., NISHIKURA, K. & SPERLING, R. (2001) RNA editing activity is associated with splicing factors in lnRNP particles: The nuclear pre-mRNA processing machinery. *PNAS* 98 (12), 6571–6576.

RAITSKIN, O., ANGENITZKI, M., SPERLING, J. & SPERLING, R. (2002) Large nuclear RNP particles - The nuclear pre-mRNA processing machine. *Journal of Structural Biology.* 140 (1-3), 123–130.

RAJEWSKY, N. (2006) microRNA target predictions in animals. *Nature Genetics* 38, Suppl S8-13

RAM, O. & AST, G. (2007) SR proteins: a foot on the exon before the transition from intron to exon definition. *Trends in Genetics*. 23 (1), 5–7.

RAMASWAMI, G., ZHANG, R., PISKOL, R., KEEGAN, L.P., DENG, P., O'CONNELL, M.A. & LI, J.B. (2013) Identifying RNA editing sites using RNA sequencing data alone. *Nature Methods*. 10 (2), 128–132

RAMASWAMI, G. & LI, J.B. (2014) RADAR: a rigorously annotated database of A-to-I RNA editing. *Nucleic acids research*. 42 (1), D109–D113

RATTRAY, M. & BENDOTTI, C. (2006) Does excitotoxic cell death of motor neurons in ALS arise from glutamate transporter and glutamate receptor abnormalities? *Experimental neurology*. 201 (1), 15–23.

RAVITS, J., APPEL, S., BALOH, R.H., BAROHN, R., BROOKS, B.R., ELMAN, L., FLOETER, M.K., HENDERSON, C., LOMEN-HOERTH, C., MACKLIS, J.D., MCCLUSKEY, L., MITSUMOTO, H., PRZEDBORSKI, S., ROTHSTEIN, J., TROJANOWSKI, J.Q., VAN DEN BERG, L.H. & RINGEL, S. (2013) Deciphering amyotrophic lateral sclerosis: what phenotype, neuropathology and genetics are telling us about pathogenesis. *Amyotrophic lateral sclerosis & frontotemporal degeneration.* 14 Suppl 15–18.

REAUME, A.G., ELLIOTT, J.L., HOFFMAN, E.K., KOWALL, N.W., FERRANTE, R.J., SIWEK, D.F., WILCOX, H.M., FLOOD, D.G., BEAL, M.F., BROWN, R.H., SCOTT, R.W. & SNIDER, W.D. (1996) Motor neurons in Cu/Zn superoxide dismutase-deficient mice develop normally but exhibit enhanced cell death after axonal injury. *Nature genetics*. 13 (1), 43–47.

RÉGAL, L., VANOPDENBOSCH, L., TILKIN, P., VAN DEN BOSCH, L., THIJS, V., SCIOT, R. & ROBBERECHT, W. (2006) The G93C mutation in superoxide dismutase 1: clinicopathologic phenotype and prognosis. *Archives of neurology.* 63 (2), 262–267.

REIMERS, J.M., MILOVANOVIC, M. & WOLF, M.E. (2011) Quantitative analysis of AMPA receptor subunit composition in addiction-related brain regions. *Brain Research.* 1367223–233.

REISEL, D., BANNERMAN, D.M., SCHMITT, W.B., DEACON, R.M.J., FLINT, J., BORCHARDT, T., SEEBURG, P.H. & RAWLINS, J.N.P. (2002) Spatial memory dissociations in mice lacking GluR1. *Nature neuroscience*. 5 (9), 868–873.

RENTON, A.E., MAJOUNIE, E., WAITE, A., SIMÓN-SÁNCHEZ, J., ROLLINSON, S., GIBBS, J.R., SCHYMICK, J.C., LAAKSOVIRTA, H., SWIETEN, J.C. VAN, KAGANOVICH, A., SCHOLZ, S.W., DUCKWORTH, J., DING, J., TRABZUNI, D., GUERREIRO, R.J., ORRELL, R.W., NEAL, J., MURRAY, A., HALLIWELL, N., ET AL. (2011) A hexanucleotide repeat expansion in C9ORF72 is the cause of chromosome 9p21-linked ALS-FTD. *Neuron*. 72 (2), 257–268.

RENTON, A.E., CHIÒ, A. & TRAYNOR, B.J. (2014) State of play in amyotrophic lateral sclerosis genetics. *Nature neuroscience*. 17 (1), 17–23.

REUTER, J.S. & MATHEWS, D.H. (2010) RNAstructure: software for RNA secondary structure prediction and analysis. *BMC bioinformatics.* 11, 129.

RIEDER, L.E. & REENAN, R. A (2012) The intricate relationship between RNA structure, editing, and splicing. *Seminars in cell & developmental biology*. 23 (3), 281–288.

RIEDMANN, E.M., SCHOPOFF, S., HARTNER, J.C., RIEDMANN, E.V.A.M. & JANTSCH, M.F. (2008) Specificity of ADAR-mediated RNA editing in newly identified targets. *RNA*. 14, 1110–1118

RIGO, F., HUA, Y., CHUN, S.J., PRAKASH, T.P., KRAINER, A.R. & BENNETT, C.F. (2012) Synthetic oligonucleotides recruit ILF2/3 to RNA transcripts to modulate splicing. *Nature chemical biology*. 8 (6), 555–561.

RIGO, F., CHUN, S.J., NORRIS, D. A, HUNG, G., LEE, S., MATSON, J., FEY, R. A, GAUS, H., HUA, Y., GRUNDY, J.S., KRAINER, A.R., HENRY, S.P. & BENNETT, C.F. (2014) Pharmacology of a central nervous system delivered 2'-O-methoxyethyl-modified survival of motor neuron splicing oligonucleotide in mice and non-human primates. *The Journal of pharmacology and experimental therapeutics*. 350 (1), 46-55

RINGHOLZ, G.M., APPEL, S.H., BRADSHAW, M., COOKE, N.A., MOSNIK, D.M. & SCHULZ, P.E. (2005) Prevalence and patterns of cognitive impairment in sporadic ALS. *Neurology*. 65 (4), 586–590.

RIZZU, P., BLAUWENDRAAT, C., HEETVELD, S., LYNES, E.M., CASTILLO-LIZARDO, M., DHINGRA, A., PYZ, E., HOBERT, M., SYNOFZIK, M., SIMÓN-SÁNCHEZ, J., FRANCESCATTO, M. & HEUTINK, P. (2016) C9orf72 is differentially expressed in the central nervous system and myeloid cells and consistently reduced in C9orf72, MAPT and GRN mutation carriers. *Acta Neuropathologica Communications.* 4 (1), 37.

ROBBERECHT, W. & PHILIPS, T. (2013) The changing scene of amyotrophic lateral sclerosis. *Nature reviews. Neuroscience*. 14 (4), 248–264.

ROBBERSON, B.L., COTE, G.J. & BERGET, S.M. (1990) Exon definition may facilitate splice site selection in RNAs with multiple exons. *Molecular and cellular biology.* 10 (1), 84–94.

ROCA, X., SACHIDANANDAM, R. & KRAINER, A.R. (2005) Determinants of the inherent strength of human 5′ splice sites. *RNA*. 11, 683–698.

ROELZ, R., PILZ, I.H., MUTSCHLER, M. & PAHL, H.L. (2010) Of mice and men: human RNA polymerase III promoter U6 is more efficient than its murine homologue for shRNA expression from a lentiviral vector in both human and murine progenitor cells. *Experimental hematology*. 38 (9), 792–797.

ROHRER, J.D., GUERREIRO, R., VANDROVCOVA, J., UPHILL, J., REIMAN, D., BECK, J., ISAACS, A.M., AUTHIER, A., FERRARI, R., FOX, N.C., MACKENZIE, I.R.A., WARREN, J.D., DE SILVA, R., HOLTON, J., REVESZ, T., HARDY, J., MEAD, S. & ROSSOR, M.N. (2009) The heritability and genetics of frontotemporal lobar degeneration. *Neurology*. 73 (18), 1451–1456.

ROSEN, D.R., SIDDIQUE, T., PATTERSON, D., FIGLEWICZ, D.A., SAPP, P., HENTATI, A., DONALDSON, D., GOTO, J., O'REGAN, J.P., DENG, H.-X., RAHMANI, Z., KRIZUS, A., MCKENNA-YASEK, D., CAYABYAB, A., GASTON, S.M., BERGER, R., TANZI, R.E., HALPERIN, J.J., HERZFELDT, B., ET AL. (1993) Mutations in Cu/Zn superoxide dismutase gene are associated with familial amyotrophic later sclerosis. *Nature*. 362 (March), 59–62.

ROSEN, H.J., GORNO-TEMPINI, M.L., GOLDMAN, W.P., PERRY, R.J., SCHUFF, N., WEINER, M., FEIWELL, R., KRAMER, J.H. & MILLER, B.L. (2002) Patterns of brain atrophy in frontotemporal dementia and semantic dementia. *Neurology*. 58 (2), 198–208.

ROSENBERG, B.R., HAMILTON, C.E., MWANGI, M.M., DEWELL, S. & PAPAVASILIOU, F.N. (2011) Transcriptome-wide sequencing reveals numerous APOBEC1 mRNA-editing targets in transcript 3′ UTRs. *Nature Structural & Molecular Biology*. 18 (2), 230–236.

ROTHSTEIN, J.D., JIN, L., DYKES-HOBERG, M. & KUNCL, R.W. (1993) Chronic inhibition of glutamate uptake produces a model of slow neurotoxicity. *PNAS*. 90 (14), 6591–6595.

ROTHSTEIN, J.D. (2009) Current hypotheses for the underlying biology of amyotrophic lateral sclerosis. *Annals of neurology*. 65 Suppl 1S3–S9.

RUETER, S.M., DAWSON, T.R. & EMESON, R.B. (1999) Regulation of alternative splicing by RNA editing. *Nature*. 399 (May), 75–80.

RULA, E.Y., LAGRANGE, A.H., JACOBS, M.M., HU, N., ROBERT, L. & EMESON, R.B. (2008) Developmental Modulation of GABAA Receptor Function by RNA Editing. *Journal of Neuroscience*. 28 (24), 6196–6201.

SAAB, A.S., NEUMEYER, A., JAHN, H.M., CUPIDO, A., SIMEK, A.A.M., BOELE, H.-J., SCHELLER, A., LE MEUR, K., GOTZ, M., MONYER, H., SPRENGEL, R., RUBIO, M.E., DEITMER, J.W., DE ZEEUW, C.I. & KIRCHOFF, F. (2012) Bergmann Glial AMPA Receptors Are Required for Fine Motor Coordination. *Science*. 337, 749–753.

SALARDINI, E., ZEINODDINI, A., MOHAMMADINEJAD, P., KHODAIE-ARDAKANI, M.-R., ZAHRAEI, N., ZEINODDINI, A. & AKHONDZADEH, S. (2016) Riluzole combination therapy for moderate-to-severe major depressive disorder: A randomized, double-blind, placebo-controlled trial. *Journal of psychiatric research*. 75, 24–30.

SALTER, J.D., BENNETT, R.P. & SMITH, H.C. (2016) The APOBEC Protein Family: United by Structure, Divergent in Function. *Trends in Biochemical Sciences*. 41 (7), 578–594.

SAMUEL, C.E. (2012) ADARs: viruses and innate immunity. *Current topics in microbiology and immunology*. 353, 163–195.

SANJANA, N.E., LEVANON, E.Y., HUESKE, E. A, AMBROSE, J.M. & LI, J.B. (2012) Activity-dependent A-to-I RNA editing in rat cortical neurons. *Genetics*. 192 (1), 281–287.

SANJANA, N.E., SHALEM, O. & ZHANG, F. (2014) Improved vectors and genome-wide libraries for CRISPR screening. *Nature Methods*. 11 (8), 783–784.

SANSAM, C.L., WELLS, K.S. & EMESON, R.B. (2003) Modulation of RNA editing by functional nucleolar sequestration of ADAR2. *PNAS*. 100 (24), 14018–14023.

SAREEN, D., O'ROURKE, J.G., MEERA, P., MUHAMMAD, A.K.M.G., GRANT, S., SIMPKINSON, M., BELL, S., CARMONA, S., ORNELAS, L., SAHABIAN, A., GENDRON, T., PETRUCELLI, L., BAUGHN, M., RAVITS, J., HARMS, M.B., RIGO, F., BENNETT, C.F., OTIS, T.S., SVENDSEN, C.N., ET AL. (2013) Targeting RNA foci in iPSC-derived motor neurons from ALS patients with a C9ORF72 repeat expansion. *Science translational medicine.* 5 (208), 208ra149.

Sarepta (2015) Dose-Ranging Study of AVI-4658 to Induce Dystrophin Expression in Selected Duchenne Muscular Dystrophy (DMD) Patients. p.clinicaltrials.gov.

SASAKI, S., YAMASHITA, T., HIDEYAMA, T. & KWAK, S. (2014) Unique nuclear vacuoles in the motor neurons of conditional ADAR2-knockout mice. *Brain Research.* 1550, 36–46.

SASAKI, S., YAMASHITA, T. & SHIN, K. (2015) Autophagy in spinal motor neurons of conditional ADAR2-knockout mice: An implication for a role of calcium in increased autophagy flux in ALS. *Neuroscience Letters*. 598, 79–84.

SAVVA, Y.A., RIEDER, L.E. & REENAN, R.A. (2012) The ADAR protein family. *Genome biology.* 13 (12), 252

SAWADA, J., YAMASHITA, T., AIZAWA, H., ABURAKAWA, Y., HASEBE, N. & KWAK, S. (2009) Effects of antidepressants on GluR2 Q/R site-RNA editing in modified HeLa cell line. *Neuroscience research*. 64 (3), 251–258.

SCHIMMER, J. & BREAZZANO, S. (2016) Investor Outlook: Rising from the Ashes; GSK's European Approval of Strimvelis for ADA-SCID. *Human Gene Therapy Clinical Development.* 27 (2), 57–61.

SCHNEIDER, C.A., RASBAND, W.S. & ELICEIRI, K.W. (2012) NIH Image to ImageJ: 25 years of image analysis. *Nature Methods*. 9 (7), 671–675.

SCHOFT, V.K., SCHOPOFF, S. & JANTSCH, M.F. (2007) Regulation of glutamate receptor B pre-mRNA splicing by RNA editing. *Nucleic acids research*. 35 (11), 3723–3732.

SCHWARZ, L.A., HALL, B.J. & PATRICK, G.N. (2010) Activity-dependent ubiquitination of GluA1 mediates a distinct AMPA receptor endocytosis and sorting pathway. *The Journal of neuroscience* 30 (49), 16718–16729.

SEBBAG-SZNAJDER, N., RAITSKIN, O., ANGENITZKI, M., SATO, T.-A., SPERLING, J. & SPERLING, R. (2012) Regulation of alternative splicing within the supraspliceosome. *Journal of structural biology*. 177 (1), 152–159.

SHARMA, S., PATNAIK, S.K., TAGGART, R.T., KANNISTO, E.D., ENRIQUEZ, S.M., GOLLNICK, P. & BAYSAL, B.E. (2015) APOBEC3A cytidine deaminase induces RNA editing in monocytes and macrophages. *Nature communications*. 66881.

SHAW, P.J., FORREST, V., INCE, P.G., RICHARDSON, J.P. & WASTELL, H.J. (1995) CSF and Plasma Amino Acid Levels in Motor Neuron Disease: Elevation of CSF Glutamate in a Subset of Patients. *Neurodegeneration*. 4 (2), 209–216.

SHI, S.-H., HAYASHI, Y., ESTEBAN, J. A. & MALINOW, R. (2001) Subunit-Specific Rules Governing AMPA Receptor Trafficking to Synapses in Hippocampal Pyramidal Neurons. *Cell*. 105, 331–343.

SHIMO, T., TACHIBANA, K., SAITO, K., YOSHIDA, T., TOMITA, E., WAKI, R., YAMAMOTO, T., DOI, T., INOUE, T., KAWAKAMI, J. & OBIKA, S. (2014) Design and evaluation of locked nucleic acid-based splice-switching oligonucleotides in vitro. *Nucleic acids research*. 1–14.

SHOSHAN, E., MOBLEY, A.K., BRAEUER, R.R., KAMIYA, T., HUANG, L., VASQUEZ, M.E., SALAMEH, A., LEE, H.J., KIM, S.J., IVAN, C., VELAZQUEZ-TORRES, G., NIP, K.M., ZHU, K., BROOKS, D., JONES, S.J.M., BIROL, I., MOSQUEDA, M., WEN, Y., ETEROVIC, A.K., ET AL. (2015) Reduced adenosine-to-inosine miR-455-5p editing promotes melanoma growth and metastasis. *Nature Cell Biology*. 17, 311-321

SINGH, S.K. & WENGEL, J. (1998) *Universality of LNA-mediated high-affinity nucleic acid recognition*. 1247–1248

SIVA, K., COVELLO, G. & DENTI, M. a (2014) Exon-skipping antisense oligonucleotides to correct missplicing in neurogenetic diseases. *Nucleic acid therapeutics*. 24 (1), 69–86.

SLAVOV, D., CLARK, M. & GARDINER, K. (2000) Comparative analysis of the RED1 and RED2 A-to-I RNA editing genes from mammals, pufferfish and zebrafish. *Gene*. 250 (1-2), 41–51.

SLAVOV, D. & GARDINER, K. (2002) Phylogenetic comparison of the pre-mRNA adenosine deaminase ADAR2 genes and transcripts: conservation and diversity in editing site sequence and alternative splicing patterns. *Gene*. 299 (1-2), 83–94.

SMITH, R.A., MILLER, T.M., YAMANAKA, K., MONIA, B.P., CONDON, T.P., HUNG, G., LOBSIGER, C.S., WARD, C.M., MCALONIS-DOWNES, M., WEI, H., WANCEWICZ, E. V, BENNETT, C.F. & CLEVELAND, D.W. (2006) Antisense oligonucleotide therapy for neurodegenerative disease. *Journal of Clinical Investigation.* 116 (8), 2290–2296.

SOBOLEVSKY, A.I. (2015) Structure and gating of tetrameric glutamate receptors. The *Journal of physiology*. 593 (1), 29–38.

SODHI, M.S., BURNET, P.W.J., MAKOFF, A.J., KERWIN, R.W. & HARRISON, P.J. (2001) RNA editing of the 5-HT 2C receptor is reduced in schizophrenia. *Molecular psychiatry*. 6, 373–379.

SOLOMON, O., BAZAK, L., LEVANON, E., AMARIGLIO, N., UNGER, R., RECHAVI, G. & EYAL, E. (2014) Characterizing of functional human coding RNA editing from evolutionary, structural and dynamic perspectives. *Proteins*. 82 (11), 3117–3131.

SOMMER, B., KEINÄNEN, K., VERDOORN, T., WISDEN, W., BURNASHEV, N., HERB, A, KÖHLER, M., TAKAGI, T., SAKMANN, B. & SEEBURG, P.H. (1990) Flip and flop: a cell-specific functional switch in glutamate-operated channels of the CNS. *Science*. 249 (4976), 1580–1585.

SOMMER, B., KOHLER, M., SPRENGEL, F. & SEEBURG, P.H. (1991) RNA Editing in Brain Controls of Ion Flow in Glutamate-Gated a Determinant Channels. *Cell*. 67, 11–19.

SOO, K.Y., HALLORAN, M., SUNDARAMOORTHY, V., PARAKH, S., TOTH, R.P., SOUTHAM, K.A., MCLEAN, C.A., LOCK, P., KING, A., FARG, M.A. & ATKIN, J.D. (2015) Rab1-dependent ER-Golgi transport dysfunction is a common pathogenic mechanism in SOD1, TDP-43 and FUS-associated ALS. *Acta neuropathologica.* 130 (5), 679–697.

STALLINGS, N.R., PUTTAPARTHI, K., LUTHER, C.M., BURNS, D.K. & ELLIOTT, J.L. (2010) Progressive motor weakness in transgenic mice expressing human TDP-43. *Neurobiology of Disease*. 40 (2), 404–414.

STALMANS, S., BRACKE, N., WYNENDAELE, E., GEVAERT, B., PEREMANS, K., BURVENICH, C., POLIS, I. & DE SPIEGELEER, B. (2015) Cell-penetrating peptides selectively cross the blood-brain barrier in vivo. *PLoS ONE*. 10 (10), 1–22.

STEENLAND, H.W., KIM, S.S. & ZHUO, M. (2008) GluR3 subunit regulates sleep, breathing and seizure generation. *European Journal of Neuroscience*. 27 (5), 1166–1173.

STEPHENS, B., GUILOFF, R.J., NAVARRETE, R., NEWMAN, P., NIKHAR, N. & LEWIS, P. (2006) Widespread loss of neuronal populations in the spinal ventral horn in sporadic motor neuron disease. A morphometric study. *Journal of the neurological sciences*. 244 (1-2), 41–58

STEPHENS, O.M., YI-BRUNOZZI, H.Y. & BEAL, P.A. (2000) Analysis of the RNA-editing reaction of ADAR2 with structural and fluorescent analogues of the GluR-B R/G editing site. *Biochemistry*. 39 (40), 12243–12251.

STEPHENS, O.M., HAUDENSCHILD, B.L. & BEAL, P.A. (2004) The Binding Selectivity of ADAR2's dsRBMs Contributes to RNA-Editing Selectivity. *Chemistry & Biology.* 11, 1239–1250.

STEPHENSON, M.L. & ZAMECNIK, P.C. (1978) Inhibition of Rous sarcoma viral RNA translation by a specific oligodeoxyribonucleotide. *PNAS* 75 (1), 285–288.

STRONG, M.J., VOLKENING, K., HAMMOND, R., YANG, W., STRONG, W., LEYSTRA-LANTZ, C. & SHOESMITH, C. (2007) TDP43 is a human low molecular weight neurofilament (hNFL) mRNA-binding protein. *Molecular and cellular neurosciences.* 35 (2), 320–327.

SUMMERTON, J.E. (2005) Endo-Porter: a novel reagent for safe, effective delivery of substances into cells. *Annals of the New York Academy of Sciences*. 1058, 62–75.

SUN, H., KAWAHARA, Y., ITO, K., KANAZAWA, I. & KWAK, S. (2006) Slow and selective death of spinal motor neurons in vivo by intrathecal infusion of kainic acid: implications for AMPA receptor-mediated excitotoxicity in ALS. *Journal of neurochemistry*. 98 (3), 782–791

SUN, Y., OLSON, R., HORNING, M., ARMSTRONG, N., MAYER, M. & GOUAUX, E. (2002) Mechanism of glutamate receptor desensitization. *Nature*. 417 (6886), 245–253

SUN, Y., LI, X., WU, D., PAN, Q., JI, Y., REN, H. & DING, K. (2016) RED: A Java-MySQL Software for Identifying and Visualizing RNA Editing Sites Using Rule-Based and Statistical Filters. *Plos One*. 11 (3), e0150465.

SUN, Z.-W., ZHANG, L., ZHU, S.-J., CHEN, W.-C. & MEI, B. (2010) Excitotoxicity effects of glutamate on human neuroblastoma SH-SY5Y cells via oxidative damage. *Neuroscience bulletin.* 26 (1), 8–16

SWANSON, G.T., FELDMEYER, D., KANEDA, M. & CULL-CANDY, S.G. (1996) Effect of RNA editing and subunit co-assembly single-channel properties of recombinant kainate receptors. *The Journal of Physiology.* 492 (1), 129–142.

SWANSON, G.T., KAMBOJ, S.K. & CULL-CANDY, S.G. (1997) Single-channel properties of recombinant AMPA receptors depend on RNA editing, splice variation, and subunit composition. *Journal of Neuroscience*. 17 (1), 58–69.

TAKUMA, H., KWAK, S., YOSHIZAWA, T. & KANAZAWA, I. (1999) Reduction of GluR2 RNA editing, a molecular change that increases calcium influx through AMPA receptors, selective in the spinal ventral gray of patients with amyotrophic lateral sclerosis. *Annals of neurology*. 46 (6), 806–815.

TALBOT, K. (2014) Amyotrophic lateral sclerosis: cell vulnerability or system vulnerability? *Journal of anatomy.* 224 (1), 45–51.

TARIQ, A. & JANTSCH, M.F. (2012) Transcript diversification in the nervous system: A to I RNA editing in CNS function and disease development. *Frontiers in neuroscience.* 6 (July), 99

TER BRAKE, O., 'T HOOFT, K., LIU, Y.P., CENTLIVRE, M., VON EIJE, K.J. & BERKHOUT, B. (2008) Lentiviral vector design for multiple shRNA expression and durable HIV-1 inhibition. *Molecular therapy*. 16 (3), 557–564.

TICOZZI, N., TILOCA, C., MORELLI, C., COLOMBRITA, C., POLETTI, B., DORETTI, A., MADERNA, L., MESSINA, S., RATTI, A. & SILANI, V. (2011) Genetics of familial Amyotrophic lateral sclerosis. *Archives italiennes de biologie*. 149 (1), 65–82

TOOZE, J., HOLLINSHEAD, M., FULLER, S.D., TOOZE, S.A. & HUTTNER, W.B. (1989) Morphological and biochemical evidence showing neuronal properties in AtT-20 cells and their growth cones. *European journal of cell biology*. 49 (2), 259–273.

TOTH, P.P. (2013) Emerging LDL therapies: Mipomersen-antisense oligonucleotide therapy in the management of hypercholesterolemia. *Journal of clinical lipidology*. 7 (3 Suppl), S6–S10

TRAYNELIS, S.F., WOLLMUTH, L.P., MCBAIN, C.J., MENNITI, F.S., VANCE, K.M., OGDEN, K.K., HANSEN, K.B., YUAN, H., MYERS, S.J. & DINGLEDINE, R. (2010) Glutamate Receptor Ion Channels : Structure , Regulation , and Function. *Pharmacological Reviews.* 62 (3), 405–496

TREMBLAY, R.G., SIKORSKA, M., SANDHU, J.K., LANTHIER, P., RIBECCO-LUTKIEWICZ, M. & BANI-YAGHOUB, M. (2010) Differentiation of mouse Neuro 2A cells into dopamine neurons. *Journal of neuroscience methods*. 186 (1), 60–67.

TSUIJI, H., IGUCHI, Y., FURUYA, A., KATAOKA, A., HATSUTA, H., ATSUTA, N., TANAKA, F., HASHIZUME, Y., AKATSU, H., MURAYAMA, S., SOBUE, G. & YAMANAKA, K. (2013) Spliceosome integrity is defective in the motor neuron diseases ALS and SMA. *EMBO molecular medicine*. 5 (2), 221–234

UDAN-JOHNS, M., BENGOECHEA, R., BELL, S., SHAO, J., DIAMOND, M.I., TRUE, H.L., WEIHL, C.C. & BALOH, R.H. (2014) Prion-like nuclear aggregation of TDP-43 during heat shock is regulated by HSP40/70 chaperones. *Human molecular genetics*. 23 (1), 157–170

VAN DAMME, P., VAN DEN BOSCH, L., VAN HOUTTE, E., CALLEWAERT, G. & ROBBERECHT, W. (2002) GluR2-dependent properties of AMPA receptors determine the selective vulnerability of motor neurons to excitotoxicity. *Journal of Neurophysiology*. 88 (3), 1279–1287.

VAN DEN BOSCH, L., VANDENBERGHE, W., KLAASSEN, H., VAN HOUTTE, E. & ROBBERECHT, W. (2000) Ca(2+)-permeable AMPA receptors and selective vulnerability of motor neurons. *Journal of the neurological sciences*. 180 (1-2), 29–34.

VAN DEN HAUTE, C., EGGERMONT, K., NUTTIN, B., DEBYSER, Z. & BAEKELANDT, V. (2003) Lentiviral Vector-Mediated Delivery of Short Hairpin RNA Results in Persistent Knockdown of Gene Expression in Mouse Brain. *Human Gene Therapy.* 14 (18), 1799–1807.

VAN DEVENTER, S.J.H., TAMI, J.A. & WEDEL, M.K. (2004) A randomised, controlled, double blind, escalating dose study of alicaforsen enema in active ulcerative colitis. *Gut*. 53 (11), 1646–1651.

VASCONCELOS, N.L., GOMES, E.D., OLIVEIRA, E.P., SILVA, C.J., LIMA, R., SOUSA, N., SALGADO, A.J. & SILVA, N.A. (2016) Combining neuroprotective agents: effect of riluzole and magnesium in a rat model of thoracic spinal cord injury. *The spine journal* [Epub ahead of print]

VELDINK, J.H., KALMIJN, S., GROENEVELD, G.J., TITULAER, M.J., WOKKE, J.H.J. & VAN DEN BERG, L.H. (2005) Physical activity and the association with sporadic ALS. *Neurology*. 64 (2), 241–245

VELTROP, M. & AARTSMA-RUS, A. (2014) Antisense-mediated exon skipping: Taking advantage of a trick from Mother Nature to treat rare genetic diseases. *Experimental cell research.* 325 (1), 50–55.

VENØ, M.T., BRAMSEN, J.B., BENDIXEN, C., PANITZ, F., HOLM, I.E., ÖHMAN, M. & KJEMS, J. (2012) Spatio-temporal regulation of ADAR editing during development in porcine neural tissues. *RNA biology.* 9 (8), 1054–1065.

VERBEECK, C., DENG, Q., DEJESUS-HERNANDEZ, M., TAYLOR, G., CEBALLOS-DIAZ, C., KOCERHA, J., GOLDE, T., DAS, P., RADEMAKERS, R., DICKSON, D.W. & KUKAR, T. (2012) Expression of Fused in sarcoma mutations in mice recapitulates the neuropathology of FUS proteinopathies and provides insight into disease pathogenesis. *Molecular neurodegeneration*. 7, 53

VERHAART, I.E.C., VAN VLIET-VAN DEN DOOL, L., SIPKENS, J. A, DE KIMPE, S.J., KOLFSCHOTEN, I.G.M., VAN DEUTEKOM, J.C.T., LIEFAARD, L., RIDINGS, J.E., HOOD, S.R. & AARTSMA-RUS, A. (2014) The Dynamics of Compound, Transcript, and Protein Effects After Treatment With 2OMePS Antisense Oligonucleotides in mdx Mice. *Molecular therapy. Nucleic acids*. 3 (October 2013), e148.

VIDIGAL, J.A. & VENTURA, A. (2015) Rapid and efficient one-step generation of paired gRNA CRISPR-Cas9 libraries. *Nature communications*. 6, 8083.

VITALI, P., BASYUK, E., LE MEUR, E., BERTRAND, E., MUSCATELLI, F., CAVAILLÉ, J. & HUTTENHOFER, A. (2005) ADAR2-mediated editing of RNA substrates in the nucleolus is inhibited by C/D small nucleolar RNAs. *The Journal of cell biology*. 169 (5), 745–753

VOSS, O.P., MILNE, S., SHARKEY, J., O'NEILL, M.J. & MCCULLOCH, J. (2007) Molecular mechanisms of neurite growth with AMPA receptor potentiation. *Neuropharmacology*. 52 (2), 590–597.

WAHLESTEDT, C., SALMI, P., GOOD, L., KELA, J., JOHNSSON, T., HO, T., BROBERGER, C., PORRECA, F., LAI, J., REN, K., OSSIPOV, M., KOSHKIN, A., JAKOBSEN, N., SKOUV, J., OERUM, H., JACOBSEN, M.H. & WENGEL, J. (2000) Potent and nontoxic antisense oligonucleotides containing locked nucleic acids. *PNAS*. 97 (10), 5633–5638

WAHLSTEDT, H., DANIEL, C., ENSTERO, M. & MARIE, O. (2009) Large-scale mRNA sequencing determines global regulation of RNA editing during brain development. *Genome Research.* 19, 978–986.

WAINGER, B.J., KISKINIS, E., MELLIN, C., WISKOW, O., HAN, S.S.W., SANDOE, J., PEREZ, N.P., WILLIAMS, L.A., LEE, S., BOULTING, G., BERRY, J.D., BROWN, R.H., CUDKOWICZ, M.E., BEAN, B.P., EGGAN, K. & WOOLF, C.J. (2014) Intrinsic membrane hyperexcitability of amyotrophic lateral sclerosis patient-derived motor neurons. *Cell reports*. 7 (1), 1–11

WAITE, A.J., BÄUMER, D., EAST, S., NEAL, J., MORRIS, H.R., ANSORGE, O. & BLAKE, D.J. (2014) Reduced C9orf72 protein levels in frontal cortex of amyotrophic lateral sclerosis and frontotemporal degeneration brain with the C9ORF72 hexanucleotide repeat expansion. *Neurobiology of aging.* 35 (7), 1779.e5–e1779.e13.

WAN, Y., KERTESZ, M., SPITALE, R.C., SEGAL, E. & CHANG, H. (2013) Understanding the transcriptome through RNA structure. *Nature Reviews Genetics.* 29 (9), 997–1003.

WANG, A.L., CARROLL, R.C. & NAWY, S. (2014) Down-Regulation of the RNA Editing Enzyme ADAR2 Contributes to RGC Death in a Mouse Model of Glaucoma *PLoS ONE*. 9 (3), e91288.

WANG, E.T., SANDBERG, R., LUO, S., KHREBTUKOVA, I. & ZHANG, L. (2008) Alternative Isoform Regulation in Human Tissue Transcriptomes. *Nature*. 456 (7221), 470–476.

WANG, H., LIU, H. & ZHANG, Z. (2011) Elimination of redundant synaptic inputs in the absence of synaptic strengthening. *The Journal of neuroscience* 31 (46), 16675–16684.

WANG, R., PALAVICINI, J.P., WANG, H., MAITI, P., BIANCHI, E., XU, S., LLOYD, B.N., DAWSON-SCULLY, K., KANG, D.E. & LAKSHMANA, M.K. (2014a) RanBP9 overexpression accelerates loss of dendritic spines in a mouse model of Alzheimer's disease. *Neurobiology of disease.* 69, 169–179.

WANG, X., YING, W., DUNLAP, K.A., LIN, G., SATTERFIELD, M.C., BURGHARDT, R.C., WU, G. & BAZER, F.W. (2014b) Arginine decarboxylase and agmatinase: an alternative pathway for de novo biosynthesis of polyamines for development of mammalian conceptuses. *Biology of reproduction*. 90 (4), 84.

WANG, Y., MA, M., XIAO, X. & WANG, Z. (2012) Intronic splicing enhancers, cognate splicing factors and context-dependent regulation rules. *Nature Structural & Molecular Biology.* 19 (10), 1044–1052

WANG, Z., GERSTEIN, M. & SNYDER, M. (2009) RNA-Seq: a revolutionary tool for transcriptomics. *Nature reviews. Genetics.* 10 (1), 57–63.

WANG, Z., XIAO, X., VAN NOSTRAND, E. & BURGE, C.B. (2006) General and Specific Functions of Exonic Splicing Silencers in Splicing Control. *Mol Cell.* 23 (1), 61–70.

WARITA, H., MANABE, Y., MURAKAMI, T., SHIOTE, M., SHIRO, Y., HAYASHI, T., NAGANO, I., SHOJI, M. & ABE, K. (2002) Tardive decrease of astrocytic glutamate transporter protein in transgenic mice with ALS-linked mutant SOD1. *Neurological research.* 24 (6), 577–581

WATANABE, S.Y., ALBSOUL-YOUNES, A.M., KAWANO, T., ITOH, H., KAZIRO, Y., NAKAJIMA, S. & NAKAJIMA, Y. (1999) Calcium phosphate-mediated transfection of primary cultured brain neurons using GFP expression as a marker: application for single neuron electrophysiology. *Neuroscience research*. 33 (1), 71–78.

WATERSTON, R.H., LINDBLAD-TOH, K., BIRNEY, E., ROGERS, J., ABRIL, J.F., AGARWAL, P., AGARWALA, R., AINSCOUGH, R., ALEXANDERSSON, M., AN, P., ANTONARAKIS, S.E., ATTWOOD, J., BAERTSCH, R., BAILEY, J., BARLOW, K., BECK, S., BERRY, E., BIRREN, B., BLOOM, T., ET AL. (2002) Initial sequencing and comparative analysis of the mouse genome. *Nature*. 420 (6915), 520–562

WHEELER, T.M., LEGER, A.J., PANDEY, S.K., MACLEOD, A R., NAKAMORI, M., CHENG, S.H., WENTWORTH, B.M., BENNETT, C.F. & THORNTON, C. A (2012) Targeting nuclear RNA for in vivo correction of myotonic dystrophy. *Nature*. 488 (7409), 111–115.

WHITNEY, N.P., PENG, H., ERDMANN, N.B., TIAN, C., MONAGHAN, D.T. & ZHENG, J.C. (2008) Calcium-permeable AMPA receptors containing Q/R-unedited GluR2 direct human neural progenitor cell differentiation to neurons. *FASEB journal*. 22 (8), 2888–2900.

WICKS, P., ABRAHAMS, S., PAPPS, B., AL-CHALABI, A., SHAW, C.E., LEIGH, P.N. & GOLDSTEIN, L.H. (2009) SOD1 and cognitive dysfunction in familial amyotrophic lateral sclerosis. *Journal of neurology*. 256 (2), 234–241

WIEDHOLZ, L.M., OWENS, W.A., HORTON, R.E., FEYDER, M., KARLSSON, R.-M., HEFNER, K., SPRENGEL, R., CELIKEL, T., DAWS, L.C. & HOLMES, A. (2008) Mice lacking the AMPA GluR1 receptor exhibit striatal hyperdopaminergia and 'schizophrenia-related' behaviors. *Molecular psychiatry.* 13 (6), 631–640.

WILLARD, S.S. & KOOCHEKPOUR, S. (2013) Glutamate, glutamate receptors, and downstream signaling pathways. *International journal of biological sciences*. 9 (9), 948–959.

WONG, K., LYDDON, R. & DRACHEVA, S. (2009) TaqMan-based, real-time quantitative polymerase chain reaction method for RNA editing analysis. Analytical biochemistry. 390 (2), 173–180.

WONG, S.K., SATO, S. & LAZINSKI, D.W. (2001) Substrate recognition by ADAR1 and ADAR2. *RNA*. 7 (6), 846–858.

WRIGHT, A. & VISSEL, B. (2012) The essential role of AMPA receptor GluR2 subunit RNA editing in the normal and diseased brain. *Frontiers in molecular neuroscience*. 5 (April), 34..

WU, B., CLOER, C., LU, P., MILAZI, S., SHABAN, M., SHAH, S.N., MARSTON-POE, L., MOULTON, H.M. & LU, Q.L. (2014) Exon skipping restores dystrophin expression, but fails to prevent disease progression in later stage dystrophic dko mice. *Gene therapy.* (April), 1–9.

WUOLIKAINEN, A., MORITZ, T., MARKLUND, S.L., ANTTI, H. & ANDERSEN, P.M. (2011) Disease-related changes in the cerebrospinal fluid metabolome in amyotrophic lateral sclerosis detected by GC/TOFMS. *PloS one.* 6 (4), e17947.

XIAO, S., SANELLI, T., DIB, S., SHEPS, D., FINDLATER, J., BILBAO, J., KEITH, J., ZINMAN, L., ROGAEVA, E. & ROBERTSON, J. (2011) RNA targets of TDP-43 identified by UV-CLIP are deregulated in ALS. *Molecular and Cellular Neuroscience.* 47 (3), 167–180.

XU, M., WELLS, K.S. & EMESON, R.B. (2006) Substrate-dependent Contribution of Double-stranded RNA-binding Motifs to ADAR2 Function. *Molecular Biology of the Cell.* 17 (July), 3211–3220.

XU, Z., POIDEVIN, M., LI, X., LI, Y., SHU, L., NELSON, D.L., LI, H., HALES, C.M., GEARING, M., WINGO, T.S. & JIN, P. (2013) Expanded GGGGCC repeat RNA associated with amyotrophic lateral sclerosis and frontotemporal dementia causes neurodegeneration *PNAS*. 110 (19), 7778–7783.

YAMASHITA, T., HIDEYAMA, T., HACHIGA, K., TERAMOTO, S., TAKANO, J., IWATA, N., SAIDO, T.C. & KWAK, S. (2012a) A role for calpain-dependent cleavage of TDP-43 in amyotrophic lateral sclerosis pathology. *Nature communications.* 3, 1307.

YAMASHITA, T., HIDEYAMA, T., TERAMOTO, S. & KWAK, S. (2012b) The abnormal processing of TDP-43 is not an upstream event of reduced ADAR2 activity in ALS motor neurons. *Neuroscience research*. 73 (2), 153–160.

YAMASHITA, T., TADAMI, C., NISHIMOTO, Y., HIDEYAMA, T., KIMURA, D., SUZUKI, T. & KWAK, S. (2012c) RNA editing of the Q/R site of GluA2 in different cultured cell lines that constitutively express different levels of RNA editing enzyme ADAR2. *Neuroscience research*. 73 (1), 42–48.

YAMASHITA, T., CHAI, H.L., TERAMOTO, S., TSUJI, S., SHIMAZAKI, K., MURAMATSU, S. & KWAK, S. (2013) Rescue of amyotrophic lateral sclerosis phenotype in a mouse model by intravenous AAV9-ADAR2 delivery to motor neurons. *EMBO molecular medicine*. 5 (11), 1710–1719.

YAMASHITA, T. & KWAK, S. (2014) The molecular link between inefficient GluA2 Q/R site-RNA editing and TDP-43 pathology in motor neurons of sporadic amyotrophic lateral sclerosis patients. *Brain research*. 1584, 28–38

YÁÑEZ-MUÑOZ, R.J., BALAGGAN, K.S., MACNEIL, A., HOWE, S.J., SCHMIDT, M., SMITH, A.J., BUCH, P., MACLAREN, R.E., ANDERSON, P.N., BARKER, S.E., DURAN, Y., BARTHOLOMAE, C., VON KALLE, C., HECKENLIVELY, J.R., KINNON, C., ALI, R.R. & THRASHER, A.J. (2006) Effective gene therapy with nonintegrating lentiviral vectors. *Nature medicine*. 12 (3), 348–353

YANG, L., NIU, H., GAO, X., WANG, Q., HAN, G., CAO, L., CAI, C., WEILER, J. & YIN, H. (2013) Effective Exon Skipping and Dystrophin Restoration by 2'-O-Methoxyethyl Antisense Oligonucleotide in Dystrophin-Deficient Mice. *PLoS ONE*. 8 (4).

YASUI, M., SUENAGA, E., KOYAMA, N., MASUTANI, C., HANAOKA, F., GRUZ, P., SHIBUTANI, S., NOHMI, T., HAYASHI, M. & HONMA, M. (2008) Miscoding Properties of 2′-Deoxyinosine, a Nitric Oxide-Derived DNA Adduct, during Translesion Synthesis Catalyzed by Human DNA Polymerases. *Journal of Molecular Biology.* 377 (4), 1015–1023

YE, Z., CHEN, Z., LAN, X., HARA, S., SUNKEL, B., HUANG, T.H.-M., ELNITSKI, L., WANG, Q. & JIN, V.X. (2014) Computational analysis reveals a correlation of exon-skipping events with splicing, transcription and epigenetic factors*. Nucleic acids research.* 42 (5), 2856–2869.

YEO, G. & BURGE, C.B. (2004) Maximum Entropy Modeling of Short Sequence Motifs with Applications to RNA Splicing Signals. *Journal of Computational Biology*. 11 (2-3), 377–394.

YI-BRUNOZZI, H.Y., STEPHENS, O.M. & BEAL, P. A (2001) Conformational changes that occur during an RNA-editing adenosine deamination reaction. *The Journal of biological chemistry*. 276 (41), 37827–37833.

YIN, H.Z. & WEISS, J.H. (2012) Marked synergism between mutant SOD1 and glutamate transport inhibition in the induction of motor neuronal degeneration in spinal cord slice cultures. *Brain research*. 1448, 153–162.

YLÄ-HERTTUALA, S. (2012) Endgame: Glybera Finally Recommended for Approval as the First Gene Therapy Drug in the European Union. *Molecular Therapy.* 20 (10), 1831–1832

YU, Y., SU, F.-C., CALLAGHAN, B.C., GOUTMAN, S.A., BATTERMAN, S.A. & FELDMAN, E.L. (2014) Environmental Risk Factors and Amyotrophic Lateral Sclerosis (ALS): A Case-Control Study of ALS in Michigan*. PloS one*. 9 (6), e101186.

ZAMECNIK, P.C. & STEPHENSON, M.L. (1978) Inhibition of Rous sarcoma virus replication and cell transformation by a specific oligodeoxynucleotide *Biochemistry* 75 (1), 280–284.

ZANETTE, G., TAMBURIN, S., MANGANOTTI, P., REFATTI, N., FORGIONE, A. & RIZZUTO, N. (2002) Different mechanisms contribute to motor cortex hyperexcitability in amyotrophic lateral sclerosis*. Clinical Neurophysiology*. 113 (11), 1688–1697.

ZEITELHOFER, M., VESSEY, J.P., XIE, Y., TÜBING, F., THOMAS, S., KIEBLER, M. & DAHM, R. (2007) High-efficiency transfection of mammalian neurons via nucleofection. *Nature protocols.* 2 (7), 1692–1704.

ZHANG, K., DONNELLY, C.J., HAEUSLER, A.R., GRIMA, J.C., MACHAMER, J.B., STEINWALD, P., DALEY, E.L., MILLER, S.J., CUNNINGHAM, K.M., VIDENSKY, S., GUPTA, S., THOMAS, M. A., HONG, I., CHIU, S.-L., HUGANIR, R.L., OSTROW, L.W., MATUNIS, M.J., WANG, J., SATTLER, R., ET AL. (2015) The C9orf72 repeat expansion disrupts nucleocytoplasmic transport. *Nature*. 525, 56-61

ZHANG, L., YANG, C.-S., VARELAS, X. & MONTI, S. (2016) Altered RNA editing in 3′ UTR perturbs microRNA-mediated regulation of oncogenes and tumor-suppressors. *Scientific Reports*. 6 (November 2015), 23226.

ZHANG, X.H.F. & CHASIN, L.A. (2004) Computational definition of sequence motifs governing constitutive exon splicing. *Genes and Development*. 18 (11), 1241–1250.

ZHANG, Y., WANG, H., PAN, H., BAO, X., LI, M., JIN, J. & WU, X. (2006) Gene delivery into primary cerebral cortical neurons by lentiviral vector. *Cell Biology International.* 30 (10), 777–783

ZHOU, H., JANGHRA, N., MITRPANT, C., DICKINSON, R.L., ANTHONY, K., PRICE, L., EPERON, I.C., WILTON, S.D., MORGAN, J. & MUNTONI, F. (2013) A novel morpholino oligomer targeting ISS-N1 improves rescue of severe spinal muscular atrophy transgenic mice. *Human gene therapy.* 24 (3), 331–342.

ZHOU, R., HOLMES, A., DU, J., MALKESMAN, O., YUAN, P., WANG, Y., DAMSCHRODER-WILLIAMS, P., CHEN, G., GUITART, X. & MANJI, H.K. (2009) Genome-wide gene expression profiling in GluR1 knockout mice: Key role of the calcium signaling pathway in glutamatergically mediated hippocampal transmission. *European Journal of Neuroscience*. 30 (12), 2318–2326.

ZOU, L.-L., MA, J.-L., WANG, T., YANG, T.-B. & LIU, C.-B. (2013) Cell-penetrating Peptide-mediated therapeutic molecule delivery into the central nervous system. *Current neuropharmacology*. 11 (2), 197–208.

ZUKER, M. (2003) Mfold web server for nucleic acid folding and hybridization prediction. *Nucleic Acids Research.* 31 (13), 3406–3415.

9 APPENDIX 1

Multiple sequence alignment by MUSCLE 3.8 (Clustal) between human, rat and mouse. Exon 11 of *Gria2* is highlighted in grey, followed by intron 11. The edited adenosine is highlighted in red. Stars beneath bases indicate perfect alignment across species. Dashes indicate a gap in sequence before the alignment continues.

```
human           AAAGCTGATATTGCAATTGCTCCATTAACTATTACCCTTGTGAGAGAAGAGGTGATTGAC
rat             AAAGCTGACATTGCAATTGCTCCATTAACTATCACTCTCGTGAGAGAAGAGGTGATTGAC
mouse           AAAGCTGATATTGCCATTGCTCCATTAACTATCACTCTCGTGAGAGAAGAGGTGATTGAC
                ******** ***** ********************** ** ** **********************

human           TTCTCAAAGCCCTTCATGAGCCTCGGGATATCTATCATGATCAAGAAGCCTCAGAAGTCC
rat             TTCTCCAAGCCCTTCATGAGTCTTGGAATCTCTATCATGATCAAGAAGCCTCAGAAGTCC
mouse           TTCTCGAAGCCATTCATGAGCCTTGGAATCTCTATCATGATCAAGAAGCCTCAGAAGTCC
                ***** ***** ******** ** ** ** ******************************

human           AAACCAGGAGTGTTTTCCTTTCTTGATCCTTTAGCCTATGAGATCTGGATGTGCATTGTT
rat             AAACCAGGAGTGTTTTCCTTTCTTGATCCTTTAGCCTATGAGATCTGGATGTGCATTGTG
mouse           AAACCAGGAGTGTTTTCCTTTCTTGATCCTTTAGCCTATGAGATCTGGATGTGCATTGTG
                ************************************************************

human           TTTGCCTACATTGGGGTCAGTGTAGTTTTATTCCTGGTCAGCAGATTTAGCCCCTACGAG
rat             TTTGCCTACATTGGGGTCAGTGTAGTTTTATTCCTGGTCAGCAGATTTAGCCCCTACGAG
mouse           TTTGCCTACATTGGGGTCAGTGTAGTTTTATTCCTGGTCAGCAGATTTAGCCCCTACGAG
                ************************************************************

human           TGGCACACTGAGGAGTTTGAAGATGGAAGAGAAACACAAAGTAGTGAATCAACTAATGAA
rat             TGGCACACTGAGGAATTTGAAGATGGAAGAGAAACACAAAGTAGTGAATCAACTAATGAA
mouse           TGGCACACTGAGGAATTTGAAGATGGAAGAGAAACACAAAGTAGTGAATCAACTAATGAA
                ************** ********************************************

human           TTTGGGATTTTTAATAGTCTCTGGTTTTCCTTGGGTGCCTTTATGCAGCAAGGATGCGAT
rat             TTTGGGATTTTTAATAGTCTCTGGTTTTCCTTGGGTGCCTTTATGCAGCAAGGATGCGAT
mouse           TTTGGGATTTTTAATAGTCTCTGGTTTTCCTTGGGTGCCTTTATGCAGCAAGGATGCGAT
                ************************************************************

human           ATTTCGCCAAGGTTGGTTACTCACCTGCTTCAACTTTGTGCATTTCAGGTCTCAAGTGGA
rat             ATTTCGCCAAGGTTGGTCACTCACCTGCTTCAACTTTGTGCATTTTAGGTCTCAAGTGAA
mouse           ATTTCGCCAAGGTTGGTCACTCACCTGCTTCAACTTTGTGCATTTTAGGTCTCAAGTGGA
                ****************** *************************** ************ *

human           CATTCATGGTGTTTATGGATTCACCCTAAAGAAGTTACCAGCTGCCGACTTCCTGTCCAA
rat             TATTCATGGTGTTTATGAATTCACCATAAAGATGTCACCAGCTGCCAACCATTTGTCCAA
mouse           TATTCATGGTGTCTATGAATTCACTATAAAGATGTCAGCAGCTGCCGACCATTTGTCCAA
                 *********** **** ******  ****** ** * ******** **    *******

human           GC-AGTTTAAGACTCTTGAAGGACATCCTCTTAGCTTCGGCATAAGTCTGTGAAATATTT
rat             GC-AATTTAAGATGCTTAGAGGGCAAATTTTTACCATCGGCATAAGCCTGTGAATTACCT
mouse           GCAAATTTAAGATGCTTAGAAGGCAAATTTTTACCGTCGGCGTAAGCCTGTGAAATACCT
                ** * *******  ***  * * **   * *** * ***** **** ******* **  *

human           GAACAATGTTCTTTGAATGTTGCTCATCTATTTCTCTGGTGAAATTATACACACCATGAA
rat             GAACAATGTTCCTGGAATGTTGATCAGGTGTTTCCCTGGTGAAATTATAAACACCATGGA
mouse           GAACAATGTTCCTTGAATGTTGATCATGTGTTTCCCTGGTGAAATCATATACACCATGGA
                *********** * ******** ***  * **** ********** *** ******** *

human           GAGGCTATAAAATGCATAAGGTTCCTATCATTCCATGCCTTCTTGGAGGGGTACCGTGTT
rat             GAGGCTATAAAATGCATAAGGTTCCTATCATTCCATGCCTGCTTGGAGGGGTACCGTGTT
mouse           GAGGCTATAAAATGCAGAAGGTTCCTATCATTCCATGCCTGCTTGGAGGGGTACCGTGTT
                *************** ********************** ******************

human           TTTGCTGCATATTCTCATTTTACAGTCATCTGTGTGTTGATCCACAGACCTGTATATGGG
rat             TTTGCTGCATATTCTCATTTTACAGTTATCTGTGTGTTCATCCACAGACCTGTATATGGG
```

```
mouse           TTTGCTGCATATTCTCATTTTACAGTTATCTGTGTGTTCATCCACAGACCTGTATATGGG
                ************************** *********** *********************

human           AAAATGGGCAACATTATTTATTAACTGCAAAGT-AACACCTTGTTAGATAAAACTTCGTT
rat             AAAATGGGCGATTTTAGCTTTTTCCTACAGAGTCAACAACTTGTGAGACAACACTTCATT
mouse           AAAATGGGCGAGGTTAGATTTTTCCTACAGGGTCAACAACTTGTTAGACAACACTTCATT
                ********* *  ***  * **  ** **  ** **** ***** *** ** ***** **

human           GGCACACATCTCATCTCTTTTATTTTCCCATCATTAGTTCATGGAAATGGTATGGGAGAG
rat             T-CACATACCTCATCTT-TTTATTTCCCTAACATCAACTCATGGAAATGGTGTGTGAGCG
mouse           TGCACATACCTCATCTC-TTTATTTCTCTAACATCAATTCATGGAAATGGTGTGTTTGTG
                  **** * *******  *******  * * *** *  ************* **   * *

human           ATATTATAAAATTTATTTTTTTTCTAGGTGAGGTTGCTGGATTAATA---TAATAGCATA
rat             AGATTATTCAA------CTTTTTAAATGTTAGGGTTCTGGATTAAAATGTTGATTATACA
mouse           AGGTTATTAAA------AGTTTTAAATGTTAGGCTCCTGGAGTAAAAAGTTGATCACACA
                *  ****  **        ****  * ** *** * ***** *** *   * **   * *

human           TTTTCAACTACCCACAAATGCCTGGAAGGGACTA-ATCATTCATTAAAAA-ACCTGT-CC
rat             GTTTCAAGTATCTAGAAATACAGACAGAAAAAAAGATGGCTTGCTGAAAATTCCTATGCC
mouse           --------TATCTAGAAATGCAGACAGAAAAAGA-ATAGCTTGCTGAAAATTCCTGTGCC
                        ** * * **** *    *    *  * **   *   * ****  *** * **

human           ATATCGAATGGTAATACACACACACATGGAATAAACTCACCTACCTTTAATCTCATTATG
rat             ACCTTGAATAGT------------------ACATACTCACACACCTCTCTTCCCATCAGG
mouse           ACGTTGAAGGAT------------------ACATACTCACACACCTCGATTCACATCAGG
                *  * ***   *                  * * ******  ****    ** *** * *

human           ATATGTTAAATCCCTGCACTAGAATACCTAATTATAATGAATCTACCACAAAGTACCCAT
rat             TTATAAT-TATCTCAGGCTTAAAGTACCTAATTATCA-ATATCTGTTGCAAATCACCAAT
mouse           TTATAAT-TATCTCAGGCTTCAAGTACTTAATTATCA-GTATTTGTCACAAATCACCAAT
                 ***  *  *** * *   *  * *** ******* *   ** *    ****  *** **

human           TGATTTTATTCATGTTGCACGTATGAATAAGAATGATAGCCATGTTTGGCTCTTCAGAGG
rat             TGCTTTTGTTTATGTTAC-------AACATGAATCATAACTATTTGCATCTCTTCAGATA
mouse           TGCTATTGTTTATGTTAC-------AACATGAATGATAATTACCTGTATCTCTTCGGATA
                ** * ** ** ***** *       ** * **** ***   *  *    ****** **

human           AATAAATCATGATTTTTCTAGTGTG-----ATTAACATTTTAAGTCAAAATGATTATCAC
rat             AATGAATCCCACTTTTACTAGTCTATTATCATTAACATTT-AATCCAAGGTG-TTATTTG
mouse           AATAAATCCCACTTTTGCTAGTGTGTTATCATTAACATTTATAGCCAAGATG-TTATGTG
                *** ****    **** ***** *      **********  *  ***  ** ****

human           TCTACTGGCACATTTTAATTTGGGCTCTATTACCCTTCTTCGATTTTACAGGATATCTTA
rat             TCTCTTGGGA-AGTTCAATTTGAGCTCAAATAGCTTCTTTCCATTCCAATAATAATCT--
mouse           TCTCTTGGGGAAGTTCAATTTGATCTGGAATAAACACTTTTGATTCCAATAATAATCT--
                ***  ***   * ** ******  **  * **      **  ***  *      ****

human           ATAACTAGTGGAGCGGGTGCCTTTCATGATACAATTTTATTATATTGTAAATTTTTAAAA
rat             -TTGCTAGTTAAGGGAGTGACTTTT-TAATGATAAGTCAATGAAACATTAGTTTTTGGGT
mouse           -TTACTAGTTAAGGGAGTTAGTTTT-TGATGATAATTCATTGAAATGTTAGTTTTTGTGT
                 *  *****  ** * **   ***  * **   *  * * *  *   * * *****

human           TCACTTTTGAGAATAACAAGTGATTAATTTAAGAAAACTGTATGAGAAGCTCAAAGATTT
rat             TC---TTGGAAAATTATAAGCAATTAATTTCTTAATGA-ATATAAGCATCTCAAAAGTGC
mouse           TC---TTGGAAAATTATAAGCAATTAATTTCATAATGA-ATATAAGCATTTCA-------
                **   ** ** *** * ***  ********   **     *** ** *  ***

human           GCATCTTTTGCAATCTTTTTAGTATATTTCACTGAGTAAGATAAAGGAAATACATCATGT
rat             ATAGCTTTC-TAAGTGTCTTAATATCCTTTACTGGCTGAGGATAGGGAAATATATTTTTT
mouse           --AGCTTTC-TAAGTGTTTTAATATCTTCCACTGGCTGAGAAGAGGGAAATATATCATTT
                  * ****   **   * *** ***  *  ****  * **   * ******* **  * *

human           AGCCAGAAATTATCAGTAGCTTACTTCTCTGATAGTAGGTAATTATAGTGGGAATGATAA
rat             AGGCAGAAATTAGTAAACACTTA--TTTCTGATAGCCAGTTGGTATTATGATAATGCATT
mouse           AGGCAGAGATTATTATATGCTTA--TTTCTGAGAGCCAGTTGCTGTTATGGTACTGCATT
                ** **** ****  *    ****  * ***** **   **   * *  **  * **

human           AAAAAAATTACAT-----------TTTTATGAATTATACAGATTTT--------AAAAAT
rat             ATAAAAATCACATAAAAAGAAAAAATAACAGAACTATGTAGCTCCT-AAAAAAGAAAAAT
```

```
mouse           ACAAAAATCACATATAAAGAAAAATTAACTGAACTATGTAGATCTTTTAAAAAGAAAAAT
                * ****** ****           *    *** ***  ** *  *        ******

human           TTCAGTTCCACCAGATTCCCTGTGACTTCCCTGTGGGACTTCAGTGAATTAG--AAATAT
rat             CTTAGCTCCAT---ATTTACAGTGGAGTCTCTTTATGCCTTGCCTGAATTAG--AAATAT
mouse           CTTAACTTCAT---ATTCACAGTGGATTCTCTTTATGGCATCCCTGAATTAGAAAAAGAA
                 * *  * **    ***  * ***   ** ** *  * * *   ********  *** *

human           GCCAATGGAATTTGCACAGCATGACATATGTGTGTATATATATGTGTATATATATATATA
rat             TCTACATACATTTGTATGACATGA-------ATGAAGGAGTATGTGGTCCTTTATATACA
mouse           TCTAGTTATATTTGCATGACATGA-------GTGAAGGAGCGTATGGTCCTAAGTAAACA
                 * *     ***** *   *****        ** *      * **    *   ** * *

human           TATATATATATATATATATATATATACACACACATTTTTTTTATCTCTGACAA-AATA
rat             ----------------------------------------ATTAACCACTAACAA-CATG
mouse           ----------------------------------------GTTAACCACTGACAACAATG
                                                         ** * * ** ****  **

human           TATAAGATTCATAGTTTTATCATCTCTGTATTTAGTTTATTTGATCTAAGTTAAAGATAT
rat             TAGAAGGATCT---GCCTCTCATCTCT---CATAG-TTATCTGAATTAGGTTAAATATAT
mouse           GGGAAGGGTCA---GCCTCTCATCTCT---CATAG-TTACCTTGTTTAGATTAAATATAT
                   ***  **       * ********     *** ***  *    **  ***** ****

human           ACAGAGAAGTTTCTAATAATTTGGAGGCAAATACTAACCAAATTGGGGTCTCGGAG----
rat             GAAGATTAGTTTCTAACAATGAGAAAGAGAAAAGTAGCAAAATTGAGGA-TCAGAG----
mouse           GAAGATCAGTTTCTAACAATGAGGAAGAGAAAAATAACAAGATTTGGGG-TCAGAGAGCA
                  ***  ********* ***  * * *  ** * ** * * ***  **  ** ***

human           AACATTCTGACCCATAAAATGATAAAGAAGTGGTTCTCCCTTTGGTAAGAAGAACAATGA
rat             AACATCCTATTCCATA-ACTATTAGATTAATAGT--TTACTATGGT---AAGACCTTTGA
mouse           AACATTCTCTTCCATAGAACACTAAATTGATAGTT-TAGCTTTGGA---AAGACCTCTGA
                ***** **   ***** *    ** *    * **  *  ** ***    **** *  ***

human           AGTATGTTACCCTAGTTCTGAAATGTAA-------------GGCAATAATATCCTGTGCT
rat             ATCAGG--------GTTCT-AAGTAAAAGGGAGTTGAGTTTGGCCAGCATACATTACACT
mouse           GTCAGG--------GTTCT-AAGTAAAA------TGTGCCTGGTCA---------GCACT
                   * *        ***** ** *  **             **  *           **

human           ATGTCTTTTGGAT-------------------------------------------------
rat             CTGTCCTTTGGATTGGATAAGAAGTTCTCTCTCTCTCTCTCTCTCTCTCTCTCTCTCTCT
mouse           CTATCTTTTCTCTC----------TCCTCTCTCTCTCTCTCTCTCTCTCTCTCTCTCTCT
                 * ** ***   *

human           ----------------------AGTAGGGAGAAGTGTATGTGGGTTCATTATGAAGTAG
rat             CTCTCTCTCTCTCTGTGTGTGTGTGTGTGTGTGTGTGTGTGTGTGTTGGGGTGTAT
mouse           CTCTCTCTCTCTCTCTCCATATATATATATATATATATATAT----------------
                                *         * * * *

human           GATG-TGTCAGCCCAGTCTGGCCTGGGTTCCAGTAGATGCCTGCGCCT------------
rat             AATGATGTACACACTGTCCTGCGTTCCTTAGACAAGATCTGGAAGCTTTCCTACATTCTA
mouse           ------------------------------------------------------------


human           -GGGCATGATGGCACTGCAGGTAGTTGTTTAGGTATCCAGTGTTTGTCAGGGAGTGGGAA
rat             CTTACAACACAGCACTGAAGTTACCT-------TAACAAGTGTTTGCTAAGAACTAGATA
mouse           ------------------------------------------------------------


human           ACCTATTTGCACACAGGGACTGGAGCACAAGGCATATCAGCAATCTGTATTATCCCAGAG
rat             ATCTTTTG--CTTTTGTGGCTGTAGTACAAGGCAACTTAT---TCTAGAACATCCTAGAA
mouse           ------------------------------------------------------------


human           TCCACCATGACATATAGATGACTTCTCCTTTTCATCAAGGCTGCATCTAAATTAAGATGT
rat             T-CACTATGGTATTCAGATAATTTCTCATTTT-ATCAAGCTTGCTTCTTACATAGGATAG
mouse           ---------ATATTCAGACAATTTTTCATTTTTATCAAGCTTGTTTCTTAAGAAGAATAT
                           **  ***  * ** ** **** ******  **  *** *   *  **

human           TTT-TTCTGTGCTTTTGATTTCATTCATGAGTCATGAC--ACTACAATTTCACATGTAGT
rat             TTTGTTCTGTGC------TTTCATTCTTGAACCAAGACTAGCTAC-AGTTCACATACAAG
```

```
mouse           TTTCTTCTGTGC------TTTCATTCTTGAGACAAGGCTTGCTAC-ATTGCACATACAAT
                *** ********      ******** ***  ** * *   **** * * *****  *


human           AACTTTTATTTCCTGGTAGGATAAACAGATTTTTAGATAGCATATTTTTCCTTGTTATTG
rat             AACATTTAATTCCTAGTAAGAAACACAGGTTTTTAGTTAATGTA-CTTCCCTT--TATTG
mouse           AACACTTATTTCTTAGAAAGAAACACAGGTTTTTAGTTAAGGTA-TTTTCCTTAATATTG
                ***  *** *** * * * ** * **** ******* **   **  ** ****  *****


human           ATTGGTATTTTTTCATTCAGAATGTATTTGATACAAATTTATTTTATTAAAACATTTGAG
rat             ------ATTTT----ATGGACATGTA---AATAT-AGTACATAACATTAAAA-ATAAAAT
mouse           ------ATTTTTTTAATTAACATGTA---AATAT-AGTATATACCATTAAAA-ATAAAAT
                      *****     *    *****    ***  * *  **   ******* **   *


human           GTACATATCTTTC-ACTTATGCTATATATGAATTTTAAAATTCAACATAATACAT----T
rat             GTATTTTTCTTTCTGCTTATGCTCCATGTGTATTTAAGAACTGTAACTAAAGCATAACAT
mouse           GTATTTTTCTTTCTGCTTATGCACCATATATATTTAAAAATTATAACTAAAACATGATAT
                ***  * ******  *******   ** *  **** * ** *  *  ***  ***    *


human           GGAAAAGTTAATGATTTTT----------AATGAACAAAACTATCATTTTTTAAGAATGC
rat             TGCCAGTTTAATGACCATTTTATGCAAAGAATGAACACAACTATCATGTTT--GGAAGGC
mouse           TGCCAGTTTAATGACCATTTTAAGAAAAGAATGAACACAACTATCATATTTT-GGAATGC
                 *  *  *******   **          ******** ********* ***   *** **


human           AATGATGGTTACCCTAGTTGAGAAGAATACAGTAGCTTATTATCATTTTTAAAAAGCATG
rat             AGTGATGACCATTGCAGATCAGAGTGGTAGAGTGGGCTACTCTC---TAAAACGAGGTAA
mouse           AGTAATGACCACTGCAGATCAGAACAGTAGAGTGGGTTAGTCTCTTTTTAAAAGAGCTAA
                * * ***   *    ** * ***    ** *** *  ** * **   *  **  **


human           ACATCCACAGATCACTTTAGAAATGTCTTTAAATATTAAAAAAATT------ATGAT-TC
rat             AAATTAACAGACCACTTAGAAATTCCTTTTAAATATTTTTGAAAATATATCCATCATGCT
mouse           AAATTAACAGACCACTTAGAAACTCCTTTTAATTATTTTTGAAAGTGCAGCAATCAT-CC
                * **  ***** *****   ** *   ***** ****    *** *      ** **


human           TTTTCCAAGTAAAATATGATATGAAACTATATTATTAATGTTAATAGGACACATTTAAGT
rat             TTTTTCAAGTAAAATCTACTATGGAACTCCATTAAGAATGTGGAAAGGACATATTTGAAT
mouse           CTTTTCAAGTAAAGTCTACTATGGACCTCCATTAAGGATGTTGAAAGAACATATTTGAAT
                 *** ******** * *  **** * **  ****   ****  * ** *** **** * *


human           TGTAATCTAGAGTTATTTATTAAATTAAGTGATTTCTCATTTTTCTGAAATTA-------
rat             TATAGTCTCAGATCATTTACTGGATTCATTGA-CTATAACTTGTCCAAAATTACAAAAGA
mouse           TACAGTCTAGGATGATTTAATGAATTCAGTGA-CTATAACTTGTCCAAAATTACAAAAGA
                *  * ***    * ***** *  *** * ***  * * * ** **  ******


human           ------------------------------------------------------------
rat             AGAAAAGAAGAAGAAGAAGAAGAAGAAGAAGAAGAAGAAGAAGAAGAAGAAGAAGAA
mouse           AG--AAGGAGAAGAAGAAGAAAGAAAGAAGAAAGAAGGAGAAGAAGAAGAAGAAGAA


human           ------------------------------------------------------------
rat             GAAGAAGAAGAAGAAGAAGAAGAAGGAAGAGGAGGAGGAGGAGGAGGAGGAGAATGT
mouse           GAAGAAGAAGAAGAAGAAGAAGAAG--------------------------------


human           ------------------------------------------------------------
rat             GGAAAGGACATATTTGAATTATAGTCTCAGATCATTTACTGGATTCATTGACTATAACTT
mouse           ------------------------------------------------------------


human           ------------------------------------------------------------
rat             GTCCAAAATTACAAAAGAAGAAAAGAAGAAGAAGAAGAAGAAGAAGAAGAAGAAGAA
mouse           ----------------------AAGAAGAAGAAGAAGAAGAAGAAGAAGAAGAAGAA


human           ------------------------------------------------------------
rat             GAAGAAGAAGAAGAAGAAGAAGAAGAAGAAGAAGAAGAAGAAGGAAGAGGAGGAGGA
mouse           AAAGAAGAGGAGGAGGAGGAGGAGGAGGAGGAGGAAGAAGAAGAAA------------


human           ------------------------AGTTTAGAATATCTTATCTATAAGACATGGTCTCAT
```

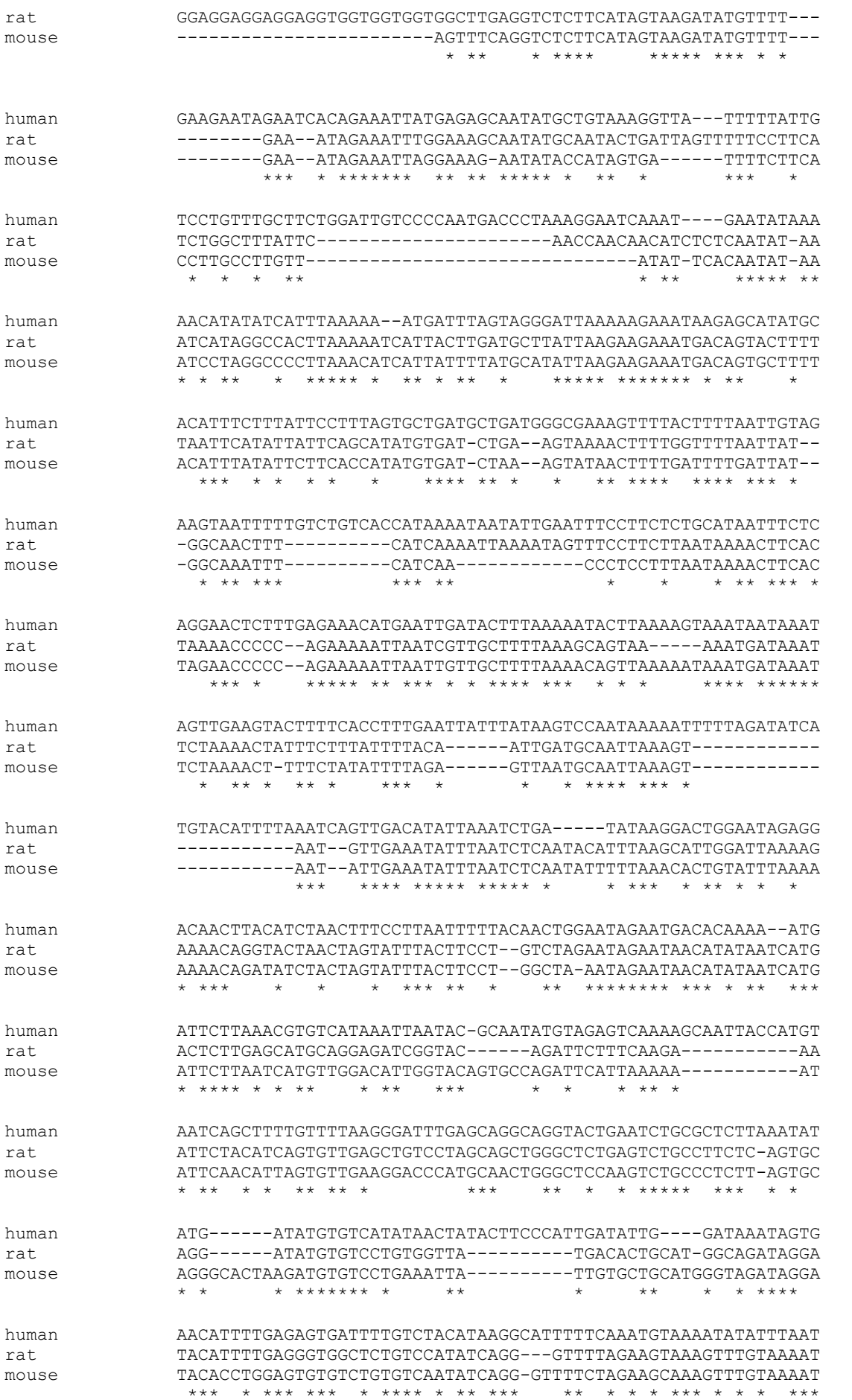
rat GGAGGAGGAGGAGGTGGTGGTGGTGGCTTGAGGTCTCTTCATAGTAAGATATGTTTT---
mouse ----------AGTTTCAGGTCTCTTCATAGTAAGATATGTTTT---
human GAAGAATAGAATCACAGAAATTATGAGAGCAATATGCTGTAAAGGTTA---TTTTTATTG
rat --------GAA--ATAGAAATTTGGAAAGCAATATGCAATACTGATTAGTTTTTCCTTCA
mouse --------GAA--ATAGAAATTAGGAAAG-AATATACCATAGTGA------TTTTCTTCA
human TCCTGTTTGCTTCTGGATTGTCCCCAATGACCCTAAAGGAATCAAAT----GAATATAAA
rat TCTGGCTTTATTC----------AACCAACAACATCTCTCAATAT-AA
mouse CCTTGCCTTGTT----------ATAT-TCACAATAT-AA
human AACATATATCATTTAAAAA--ATGATTTAGTAGGGATTAAAAAGAAATAAGAGCATATGC
rat ATCATAGGCCACTTAAAAATCATTACTTGATGCTTATTAAGAAGAAATGACAGTACTTTT
mouse ATCCTAGGCCCCTTAAACATCATTATTTTATGCATATTAAGAAGAAATGACAGTGCTTTT
human ACATTTCTTTATTCCTTTAGTGCTGATGCTGATGGGCGAAAGTTTTACTTTTAATTGTAG
rat TAATTCATATTATTCAGCATATGTGAT-CTGA--AGTAAAACTTTTGGTTTTAATTAT--
mouse ACATTTATATTCTTCACCATATGTGAT-CTAA--AGTATAACTTTTGATTTTGATTAT--
human AAGTAATTTTTGTCTGTCACCATAAAATAATATTGAATTTCCTTCTCTGCATAATTTCTC
rat -GGCAACTTT----------CATCAAAATTAAAATAGTTTCCTTCTTAATAAAACTTCAC
mouse -GGCAAATTT----------CATCAA----------CCCTCCTTTAATAAAACTTCAC
human AGGAACTCTTTGAGAAACATGAATTGATACTTTAAAAATACTTAAAAGTAAATAATAAAT
rat TAAAACCCCC--AGAAAAATTAATCGTTGCTTTTAAAGCAGTAA-----AAATGATAAAT
mouse TAGAACCCCC--AGAAAAATTAATTGTTGCTTTTAAAACAGTTAAAAATAAATGATAAAT
human AGTTGAAGTACTTTTCACCTTTGAATTATTTATAAGTCCAATAAAAATTTTTAGATATCA
rat TCTAAAACTATTTCTTTATTTTACA------ATTGATGCAATTAAAGT----------
mouse TCTAAAACT-TTTCTATATTTTAGA------GTTAATGCAATTAAAGT----------
human TGTACATTTTAAATCAGTTGACATATTAAATCTGA-----TATAAGGACTGGAATAGAGG
rat ----------AAT--GTTGAAATATTTAATCTCAATACATTTAAGCATTGGATTAAAAG
mouse ----------AAT--ATTGAAATATTTAATCTCAATATTTTTAAACACTGTATTTAAAA
human ACAACTTACATCTAACTTTCCTTAATTTTTACAACTGGAATAGAATGACACAAAA--ATG
rat AAAACAGGTACTAACTAGTATTTACTTCCT--GTCTAGAATAGAATAACATATAATCATG
mouse AAAACAGATATCTACTAGTATTTACTTCCT--GGCTA-AATAGAATAACATATAATCATG
human ATTCTTAAACGTGTCATAAATTAATAC-GCAATATGTAGAGTCAAAAGCAATTACCATGT
rat ACTCTTGAGCATGCAGGAGATCGGTAC------AGATTCTTTCAAGA----------AA
mouse ATTCTTAATCATGTTGGACATTGGTACAGTGCCAGATTCATTAAAAA----------AT
human AATCAGCTTTTGTTTTAAGGGATTTGAGCAGGCAGGTACTGAATCTGCGCTCTTAAATAT
rat ATTCTACATCAGTGTTGAGCTGTCCTAGCAGCTGGGCTCTGAGTCTGCCTTCTC-AGTGC
mouse ATTCAACATTAGTGTTGAAGGACCCATGCAACTGGGCTCCAAGTCTGCCCTCTT-AGTGC
human ATG------ATATGTGTCATATAACTATACTTCCCATTGATATTG----GATAAATAGTG
rat AGG------ATATGTGTCCTGTGGTTA----------TGACACTGCAT-GGCAGATAGGA
mouse AGGGCACTAAGATGTGTCCTGAAATTA----------TTGTGCTGCATGGGTAGATAGGA
human AACATTTTGAGAGTGATTTTGTCTACATAAGGCATTTTTCAAATGTAAAATATATTTAAT
rat TACATTTTGAGGGTGGCTCTGTCCATATCAGG---GTTTTAGAAGTAAAGTTTGTAAAAT
mouse TACACCTGGAGTGTGTCTGTGTCAATATCAGG-GTTTTCTAGAAGCAAAGTTTGTAAAAT

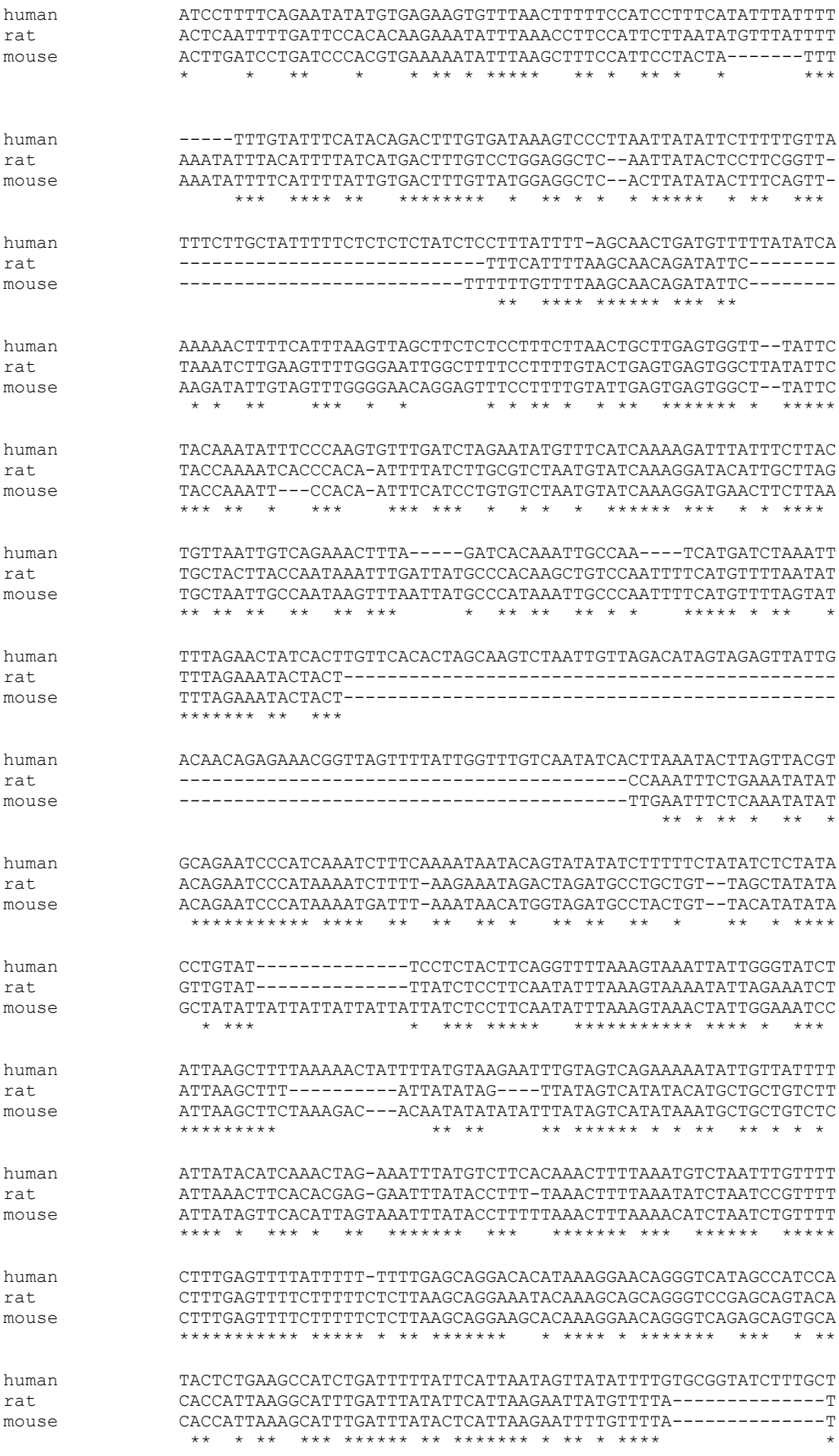
human ATCCTTTTCAGAATATATGTGAGAAGTGTTTAACTTTTTCCATCCTTTCATATTTATTTT
rat ACTCAATTTTGATTCCACACAAGAAATATTTAAACCTTCCATTCTTAATATGTTTATTTT
mouse ACTTGATCCTGATCCCACGTGAAAAATATTTAAGCTTTCCATTCCTACTA-------TTT
human -----TTTGTATTTCATACAGACTTTGTGATAAAGTCCCTTAATTATATTCTTTTTGTTA
rat AAATATTTACATTTTATCATGACTTTGTCCTGGAGGCTC--AATTATACTCCTTCGGTT-
mouse AAATATTTTCATTTTATTGTGACTTTGTTATGGAGGCTC--ACTTATATACTTTCAGTT-
human TTTCTTGCTATTTTTCTCTCTCTATCTCCTTTATTTT-AGCAACTGATGTTTTTATATCA
rat ----------TTTCATTTTAAGCAACAGATATTC--------
mouse ----------TTTTTTGTTTTAAGCAACAGATATTC--------
human AAAAACTTTTCATTTAAGTTAGCTTCTCTCCTTTCTTAACTGCTTGAGTGGTT--TATTC
rat TAAATCTTGAAGTTTTGGGAATTGGCTTTTCCTTTTGTACTGAGTGAGTGGCTTATATTC
mouse AAGATATTGTAGTTTGGGGAACAGGAGTTTCCTTTTGTATTGAGTGAGTGGCT--TATTC
human TACAAATATTTCCCAAGTGTTTGATCTAGAATATGTTTCATCAAAAGATTTATTTCTTAC
rat TACCAAAATCACCCACA-ATTTTATCTTGCGTCTAATGTATCAAAGGATACATTGCTTAG
mouse TACCAAATT---CCACA-ATTTCATCCTGTGTCTAATGTATCAAAGGATGAACTTCTTAA
human TGTTAATTGTCAGAAACTTTA-----GATCACAAATTGCCAA----TCATGATCTAAATT
rat TGCTACTTACCAATAAATTTGATTATGCCCACAAGCTGTCCAATTTTCATGTTTTAATAT
mouse TGCTAATTGCCAATAAGTTTAATTATGCCCATAAATTGCCCAATTTTCATGTTTTAGTAT
human TTTAGAACTATCACTTGTTCACACTAGCAAGTCTAATTGTTAGACATAGTAGAGTTATTG
rat TTTAGAAATACTACT----------
mouse TTTAGAAATACTACT----------
human ACAACAGAGAAACGGTTAGTTTTATTGGTTTGTCAATATCACTTAAATACTTAGTTACGT
rat ----------CCAAATTTCTGAAATATAT
mouse ----------TTGAATTTCTCAAATATAT
human GCAGAATCCCATCAAATCTTTCAAAATAATACAGTATATATCTTTTTCTATATCTCTATA
rat ACAGAATCCCATAAAATCTTTT-AAGAAATAGACTAGATGCCTGCTGT--TAGCTATATA
mouse ACAGAATCCCATAAAATGATTT-AAATAACATGGTAGATGCCTACTGT--TACATATATA
human CCTGTAT----------TCCTCTACTTCAGGTTTTAAAGTAAATTATTGGGTATCT
rat GTTGTAT----------TTATCTCCTTCAATATTTAAAGTAAAATATTAGAAATCT
mouse GCTATATTATTATTATTATTATCTCCTTCAATATTTAAAGTAAACTATTGGAAATCC
human ATTAAGCTTTTAAAAACTATTTTATGTAAGAATTTGTAGTCAGAAAAATATTGTTATTTT
rat ATTAAGCTTT----------ATTATATAG----TTATAGTCATATACATGCTGCTGTCTT
mouse ATTAAGCTTCTAAAGAC---ACAATATATATATTTATAGTCATATAAATGCTGCTGTCTC
human ATTATACATCAAACTAG-AAATTTATGTCTTCACAAACTTTTAAATGTCTAATTTGTTTT
rat ATTAAACTTCACACGAG-GAATTTATACCTTT-TAAACTTTTAAATATCTAATCCGTTTT
mouse ATTATAGTTCACATTAGTAAATTTATACCTTTTTAAACTTTAAAACATCTAATCTGTTTT
human CTTTGAGTTTTATTTTT-TTTTGAGCAGGACACATAAAGGAACAGGGTCATAGCCATCCA
rat CTTTGAGTTTTCTTTTTCTCTTAAGCAGGAAATACAAAGCAGCAGGGTCCGAGCAGTACA
mouse CTTTGAGTTTTCTTTTTCTCTTAAGCAGGAAGCACAAAGGAACAGGGTCAGAGCAGTGCA
human TACTCTGAAGCCATCTGATTTTTATTCATTAATAGTTATATTTTGTGCGGTATCTTTGCT
rat CACCATTAAGGCATTTGATTTATATTCATTAAGAATTATGTTTTA----------T
mouse CACCATTAAAGCATTTGATTTATACTCATTAAGAATTTTGTTTTA----------T

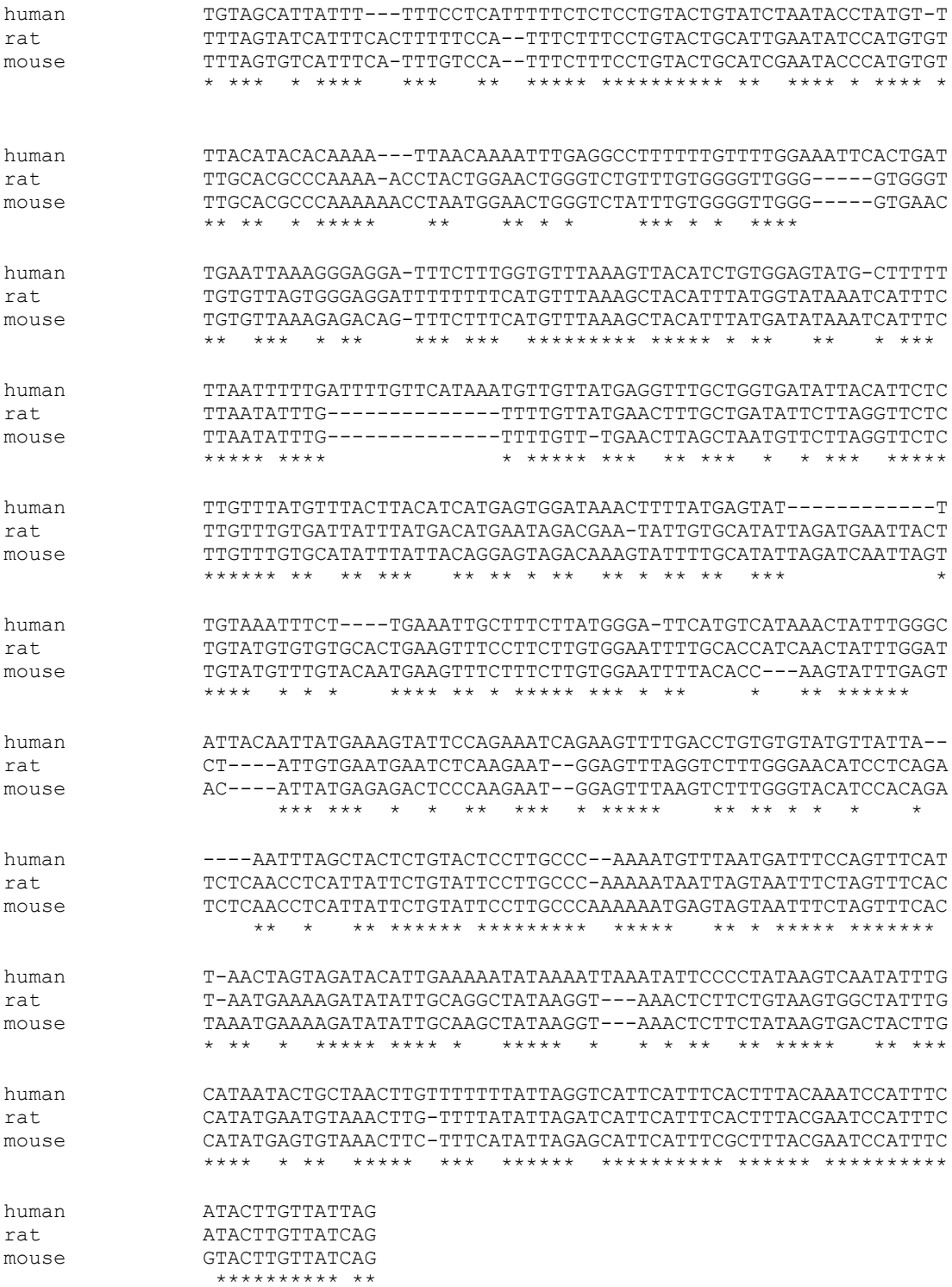
human TGTAGCATTATTT---TTTCCTCATTTTTCTCTCCTGTACTGTATCTAATACCTATGT-T
rat TTTAGTATCATTTCACTTTTTCCA--TTTCTTTCCTGTACTGCATTGAATATCCATGTGT
mouse TTTAGTGTCATTTCA-TTTGTCCA--TTTCTTTCCTGTACTGCATCGAATACCCATGTGT
human TTACATACACAAAA---TTAACAAAATTTGAGGCCTTTTTTGTTTTGGAAATTCACTGAT
rat TTGCACGCCCAAAA-ACCTACTGGAACTGGGTCTGTTTGTGGGGTTGGG-----GTGGGT
mouse TTGCACGCCCAAAAAACCTAATGGAACTGGGTCTATTTGTGGGGTTGGG-----GTGAAC
human TGAATTAAAGGGAGGA-TTTCTTTGGTGTTTAAAGTTACATCTGTGGAGTATG-CTTTTT
rat TGTGTTAGTGGGAGGATTTTTTTTCATGTTTAAAGCTACATTTATGGTATAAATCATTTC
mouse TGTGTTAAAGAGACAG-TTTCTTTCATGTTTAAAGCTACATTTATGATATAAATCATTTC
human TTAATTTTTGATTTTGTTCATAAATGTTGTTATGAGGTTTGCTGGTGATATTACATTCTC
rat TTAATATTTG---------------TTTTGTTATGAACTTTGCTGATATTCTTAGGTTCTC
mouse TTAATATTTG---------------TTTTGTT-TGAACTTAGCTAATGTTCTTAGGTTCTC
human TTGTTTATGTTTACTTACATCATGAGTGGATAAACTTTTATGAGTAT------------T
rat TTGTTTGTGATTATTTATGACATGAATAGACGAA-TATTGTGCATATTAGATGAATTACT
mouse TTGTTTGTGCATATTTATTACAGGAGTAGACAAAGTATTTTGCATATTAGATCAATTAGT
human TGTAAATTTCT----TGAAATTGCTTTCTTATGGGA-TTCATGTCATAAACTATTTGGGC
rat TGTATGTGTGTGCACTGAAGTTTCCTTCTTGTGGAATTTTGCACCATCAACTATTTGGAT
mouse TGTATGTTTGTACAATGAAGTTTCTTTCTTGTGGAATTTTACACC---AAGTATTTGAGT
human ATTACAATTATGAAAGTATTCCAGAAATCAGAAGTTTTGACCTGTGTGTATGTTATTA--
rat CT----ATTGTGAATGAATCTCAAGAAT--GGAGTTTAGGTCTTTGGGAACATCCTCAGA
mouse AC----ATTATGAGAGACTCCCAAGAAT--GGAGTTTAAGTCTTTGGGTACATCCACAGA
human ----AATTTAGCTACTCTGTACTCCTTGCCC--AAAATGTTTAATGATTTCCAGTTTCAT
rat TCTCAACCTCATTATTCTGTATTCCTTGCCC-AAAAATAATTAGTAATTTCTAGTTTCAC
mouse TCTCAACCTCATTATTCTGTATTCCTTGCCCAAAAAATGAGTAGTAATTTCTAGTTTCAC
human T-AACTAGTAGATACATTGAAAAATATAAAATTAAATATTCCCCTATAAGTCAATATTTG
rat T-AATGAAAAGATATATTGCAGGCTATAAGGT---AAACTCTTCTGTAAGTGGCTATTTG
mouse TAAATGAAAAGATATATTGCAAGCTATAAGGT---AAACTCTTCTATAAGTGACTACTTG
human CATAATACTGCTAACTTGTTTTTTTATTAGGTCATTCATTTCACTTTACAAATCCATTTC
rat CATATGAATGTAAACTTG-TTTTATATTAGATCATTCATTTCACTTTACGAATCCATTTC
mouse CATATGAGTGTAAACTTC-TTTCATATTAGAGCATTCATTTCGCTTTACGAATCCATTTC
human ATACTTGTTATTAG
rat ATACTTGTTATCAG
mouse GTACTTGTTATCAG

10 APPENDIX 2 – SECONDARY STRUCTURE MODELS: MFOLD

Models shown in increasing order of free energy (Model 1 = MFE structure). Full structure shown in bottom left corner of each structure. Area surrounding the Q/R site is enlarged, with the Q/R site highlighted by the red arrow.

10.1 HUMAN SECONDARY STRUCTURE MODELS

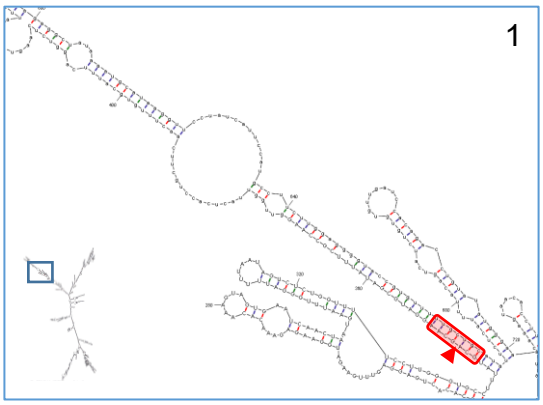

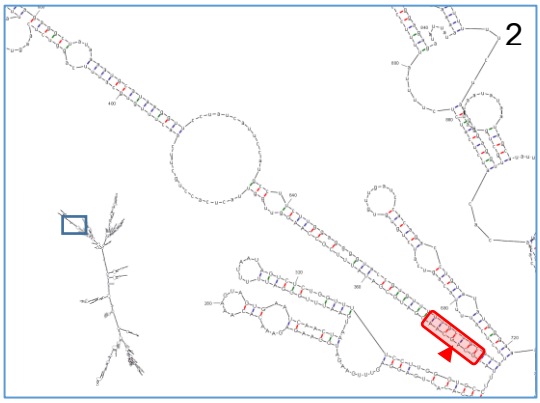

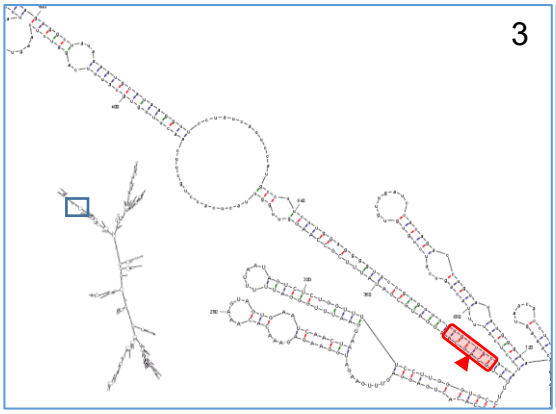

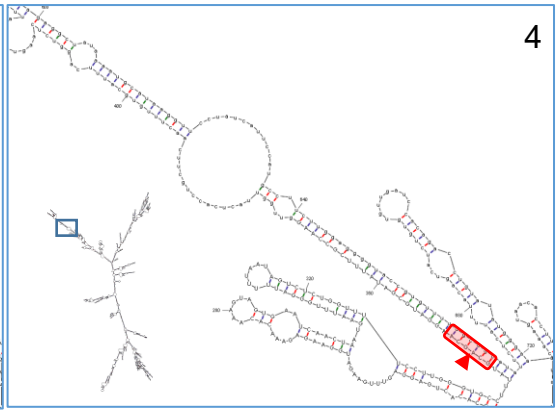

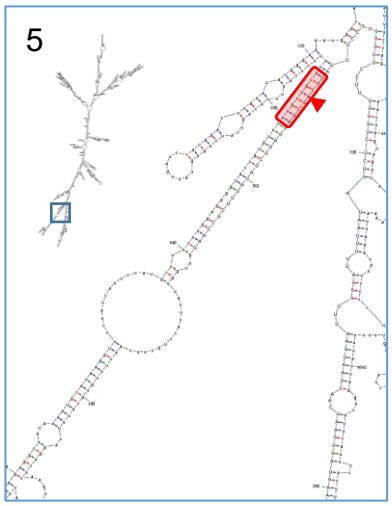

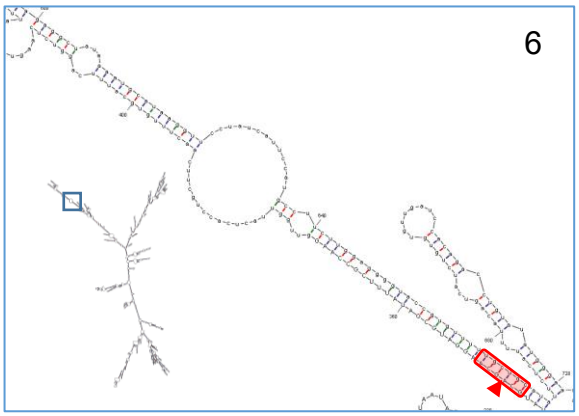

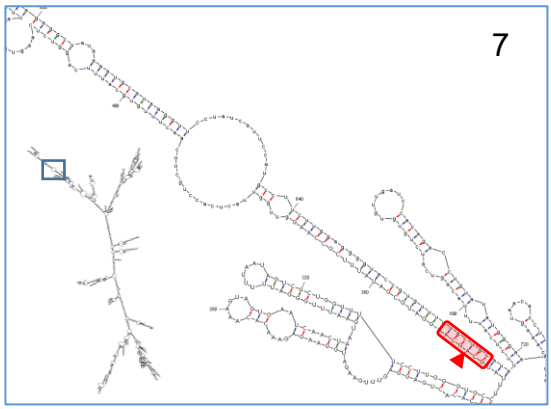
7

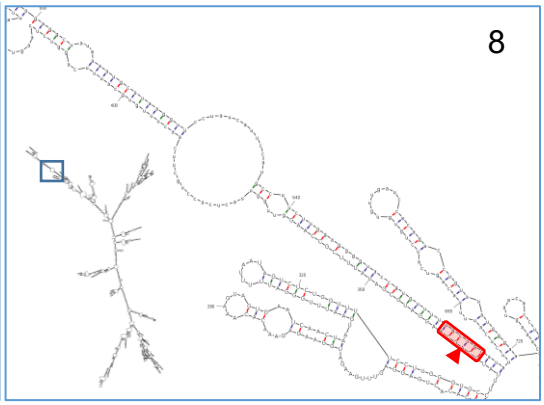
8

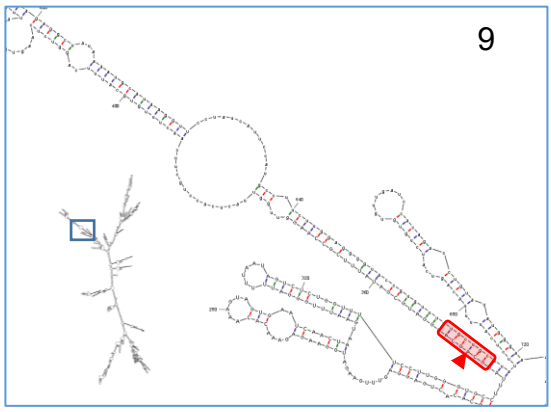
9

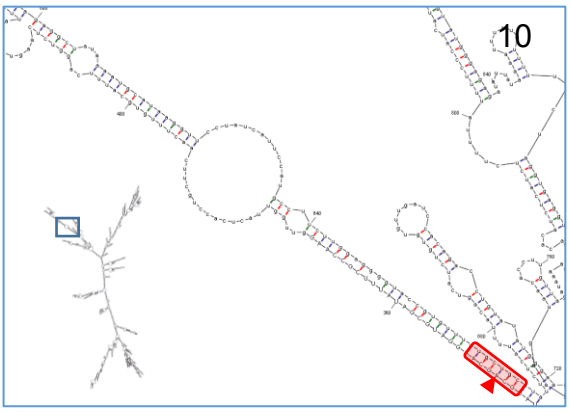
10

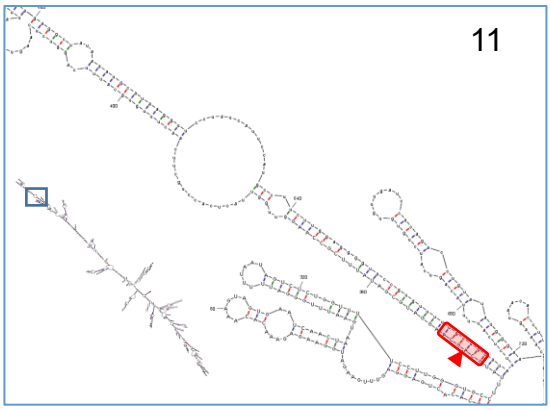
11

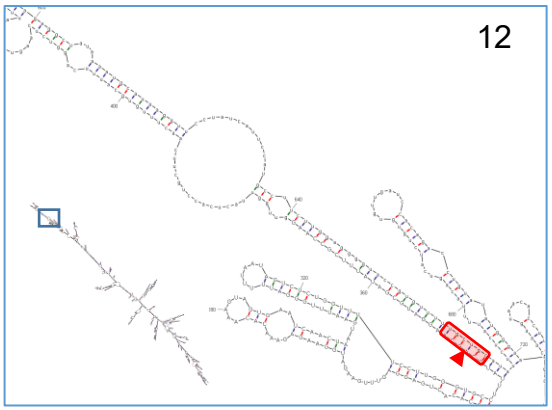
12

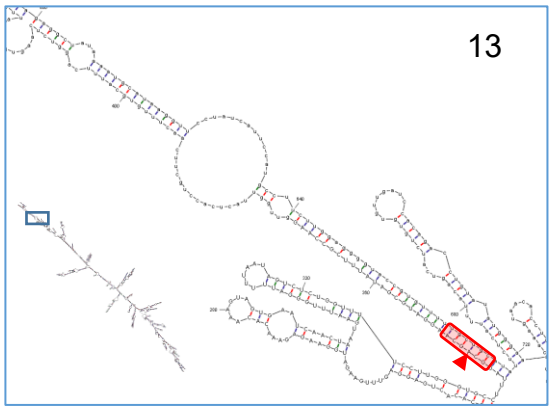
13

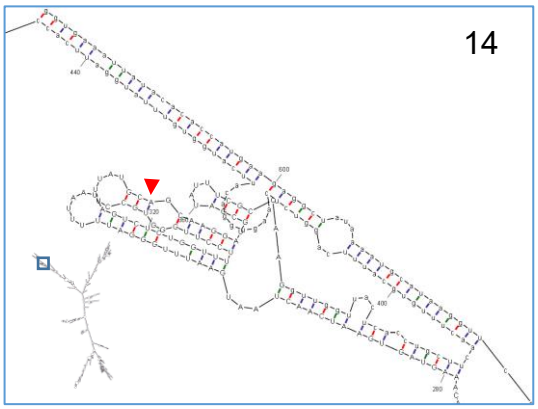
14

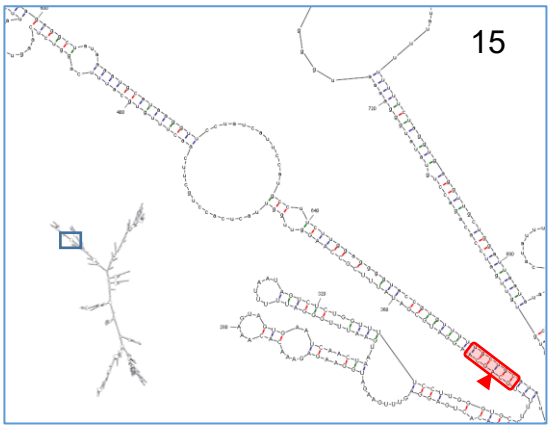
15

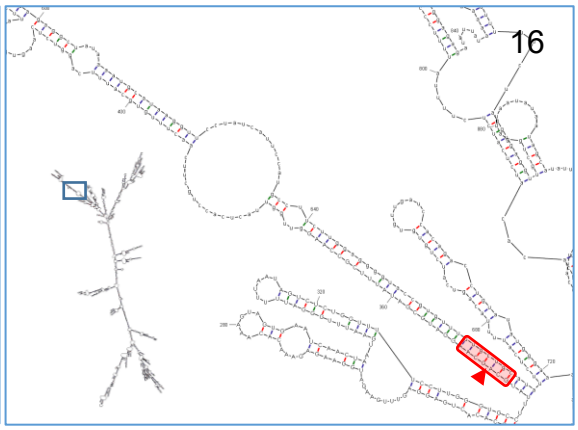
16

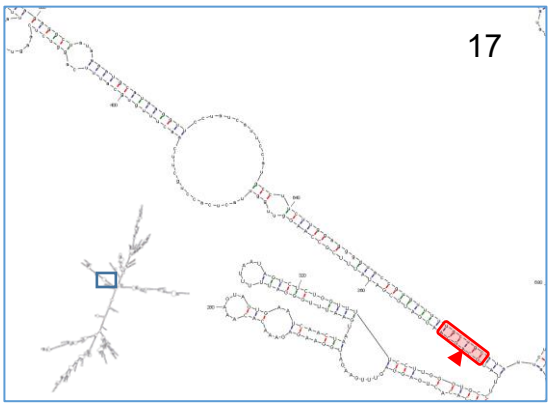
17

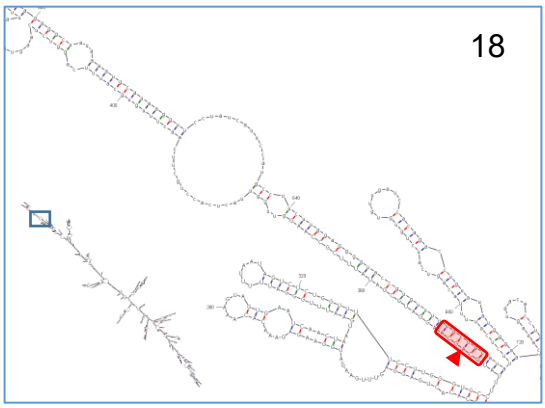
18

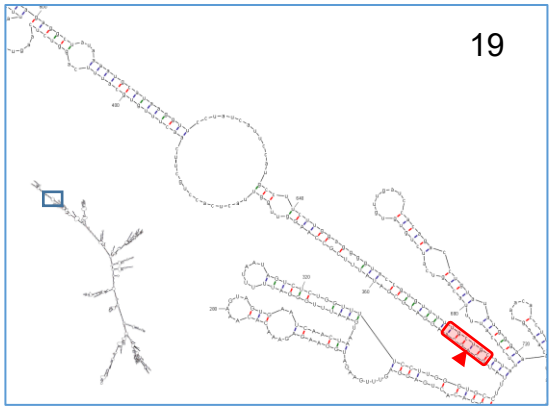
19

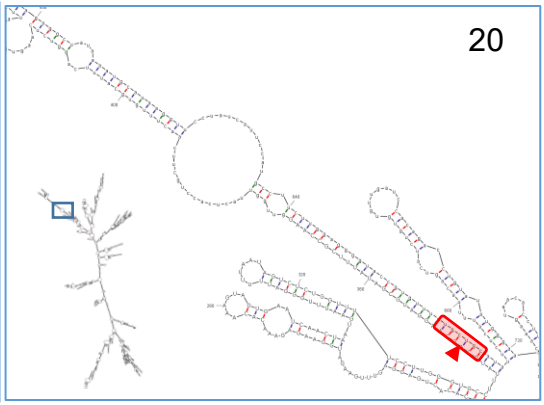
20

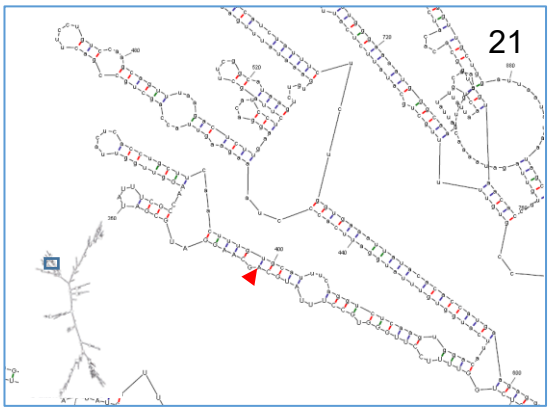
21

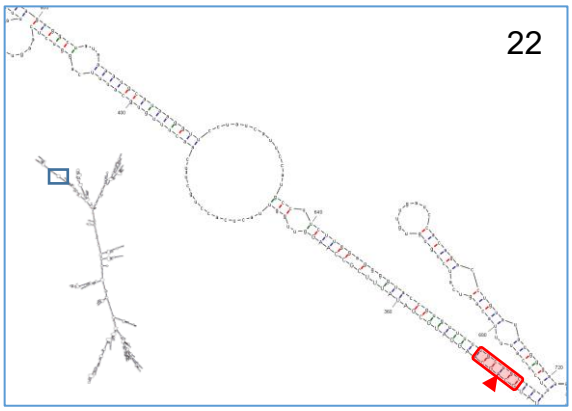
22

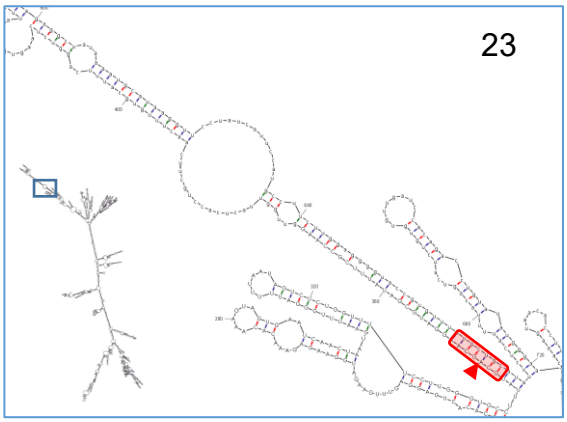
23

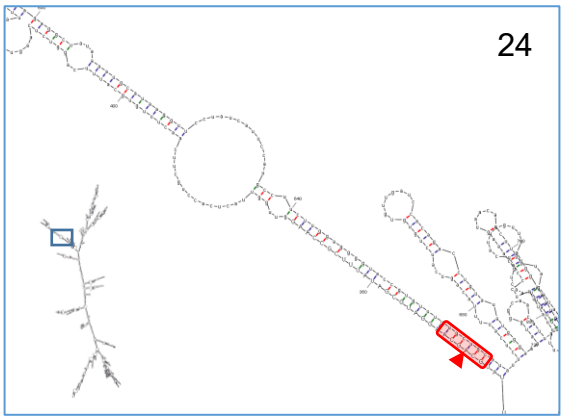
24

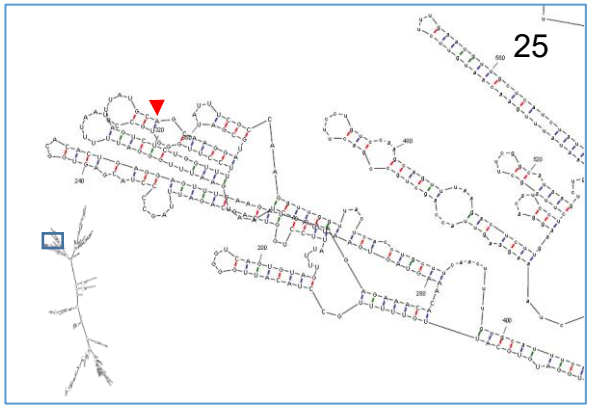
25

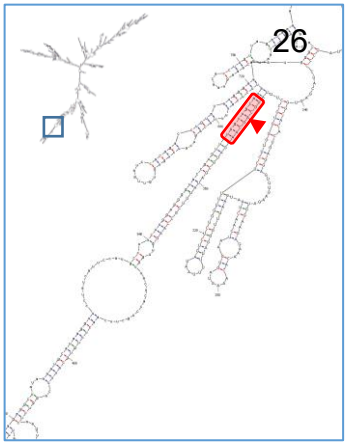
26

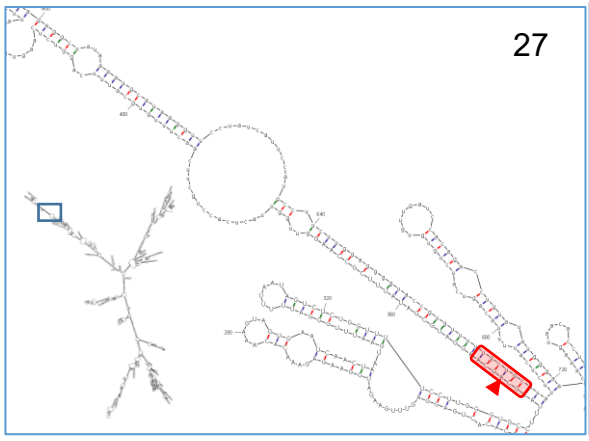
27

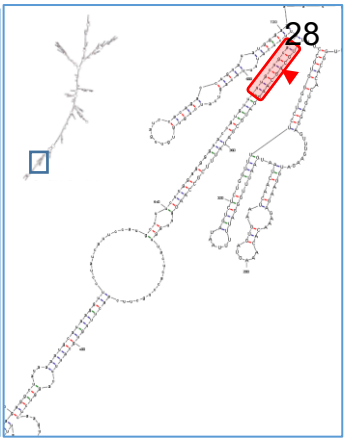
28

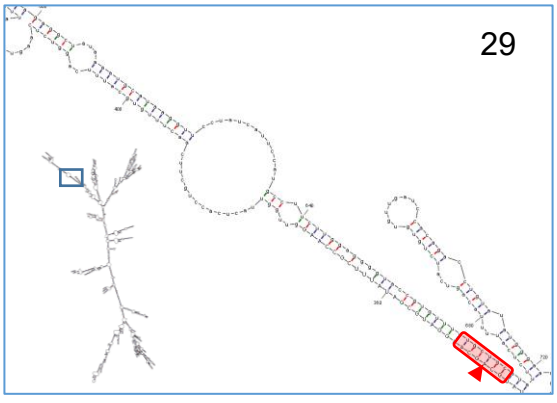
29

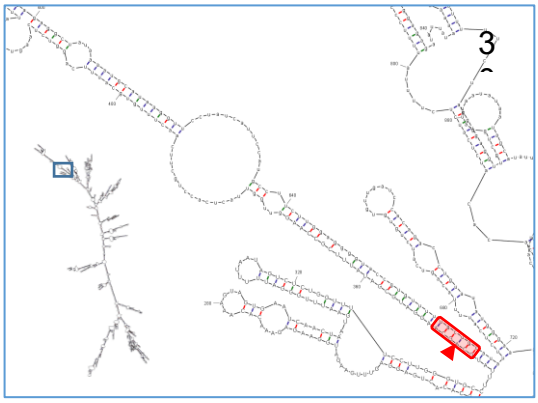
3

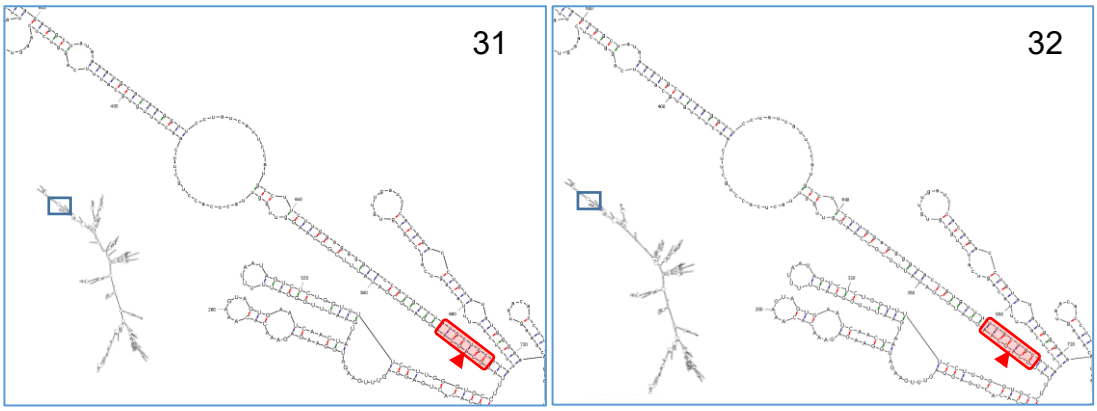
31
32

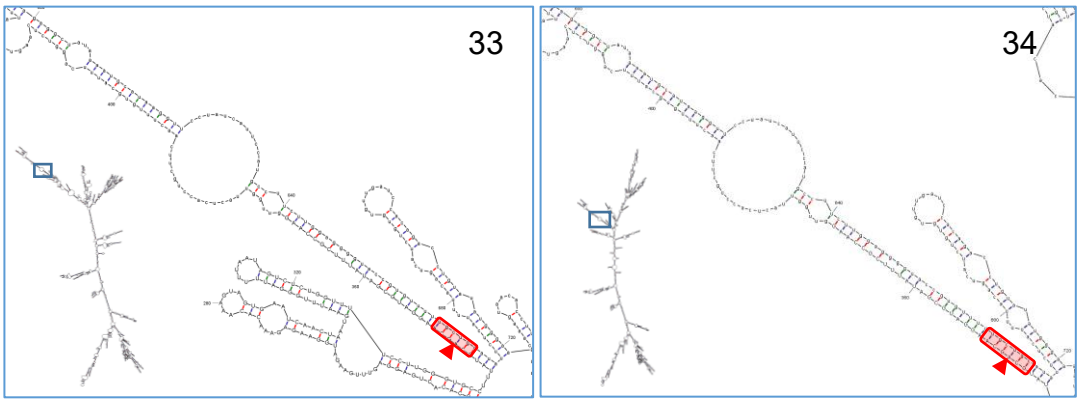
33
34

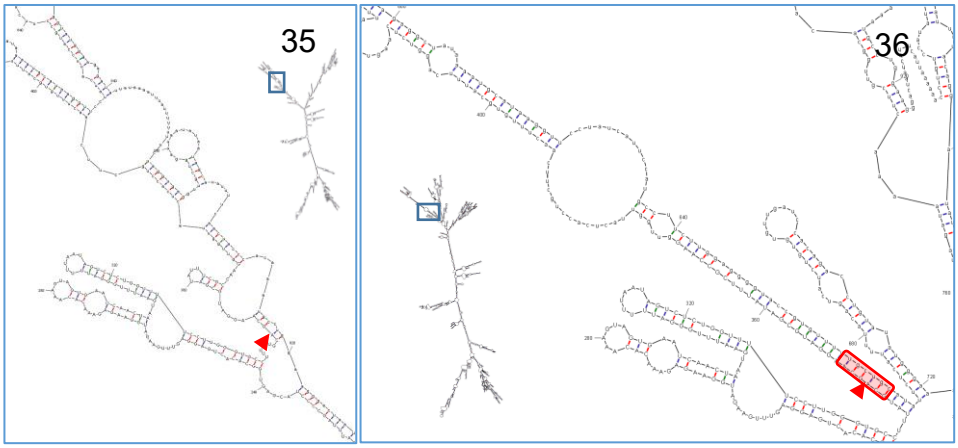
35
36

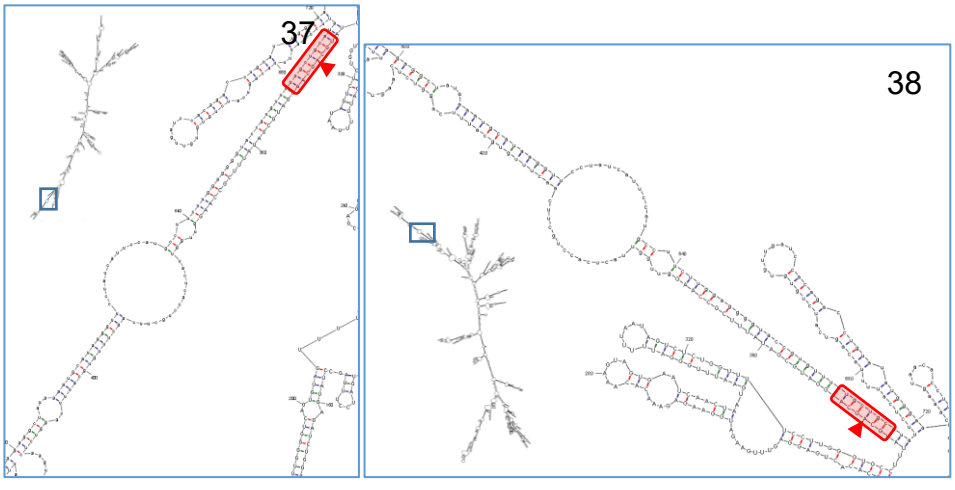
37
38

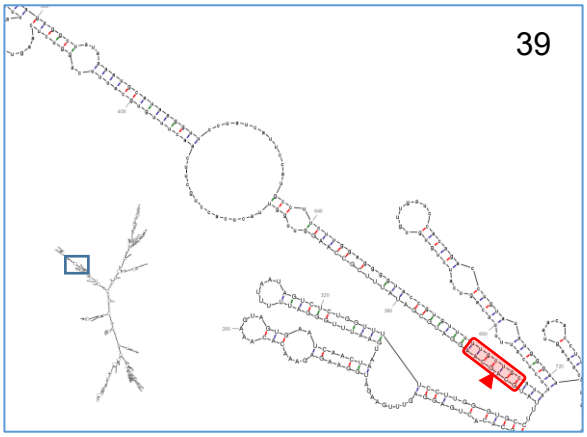
39

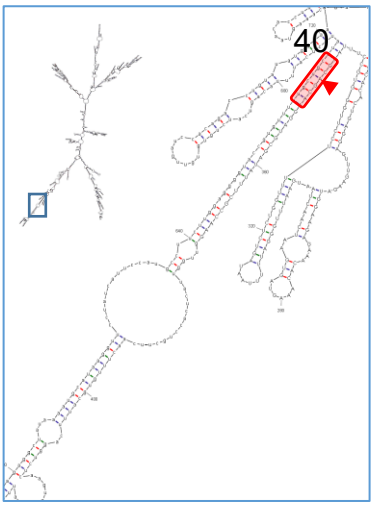
40

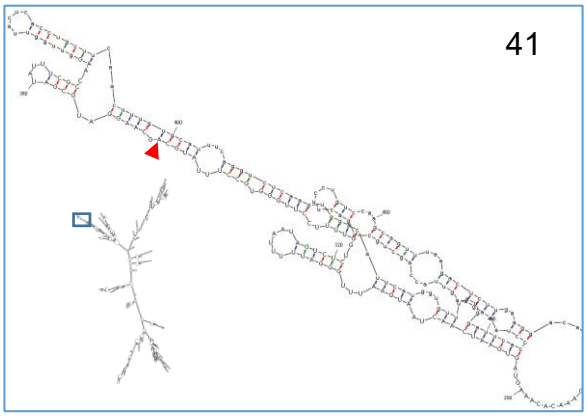
41

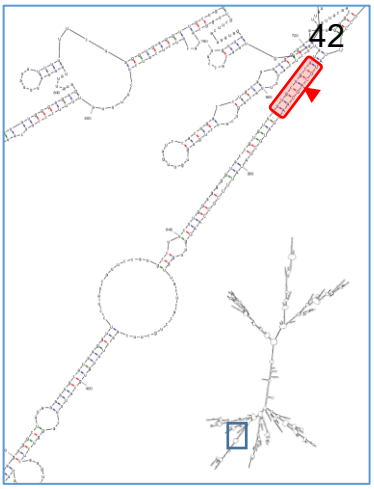
42

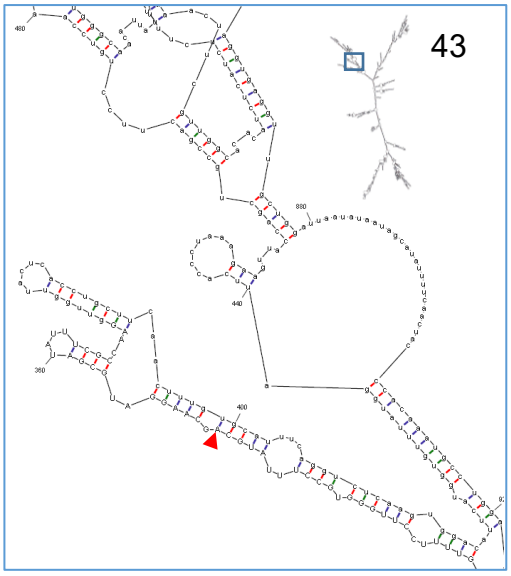
43

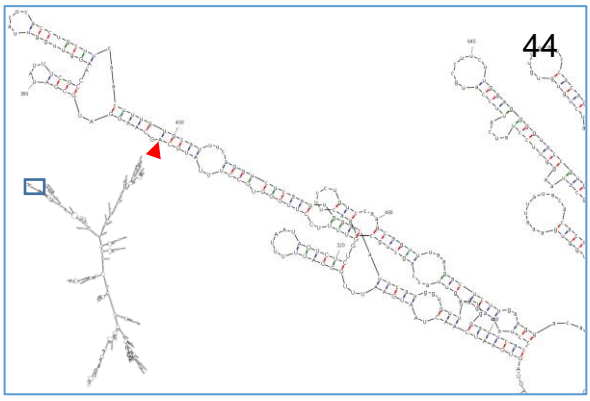
44

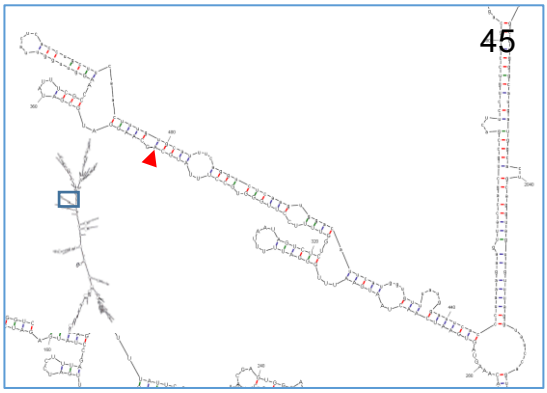
45

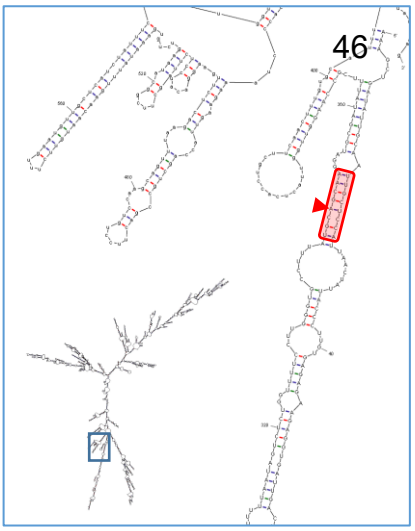
46

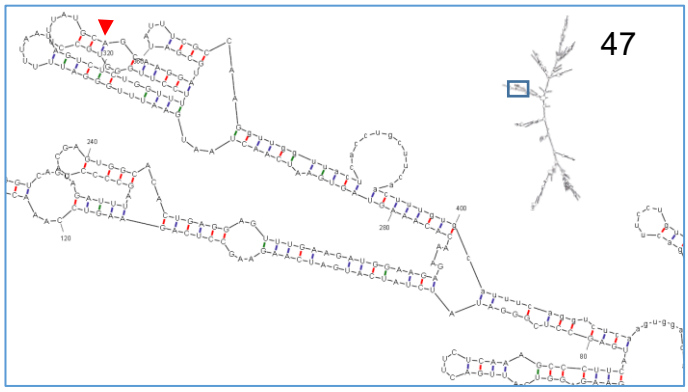
47

10.2 Rat Secondary Structure Models

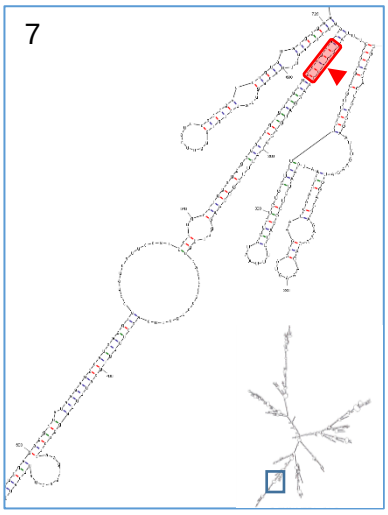
7

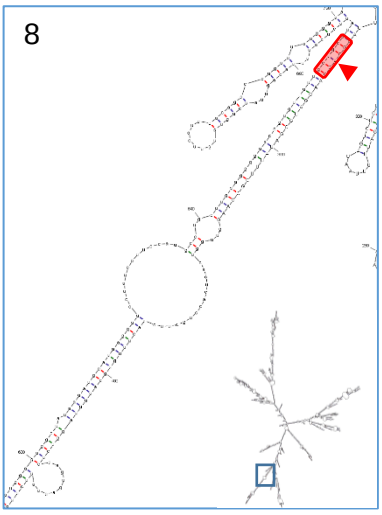
8

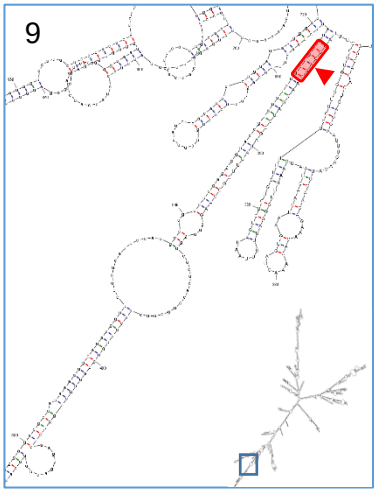
9

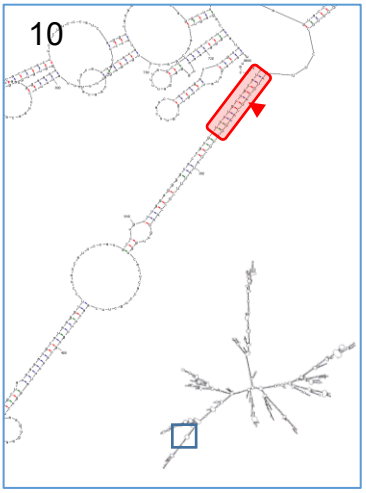
10

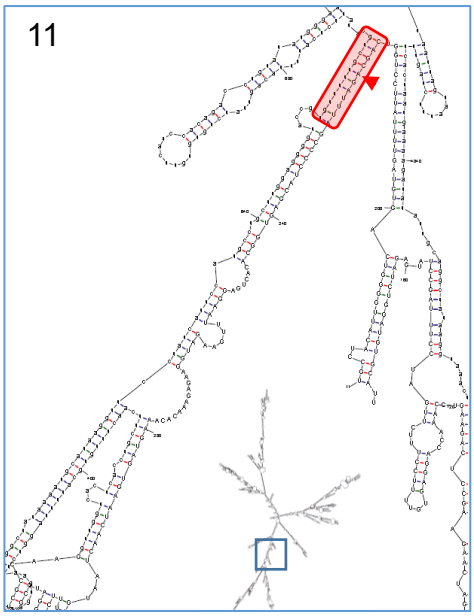
11

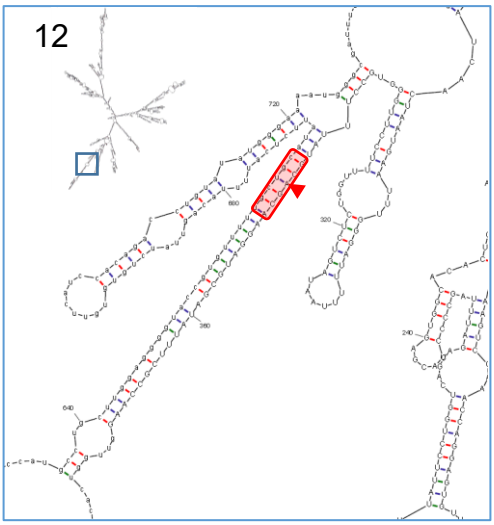
12

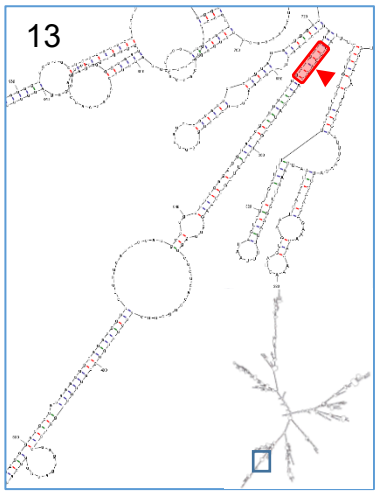
13

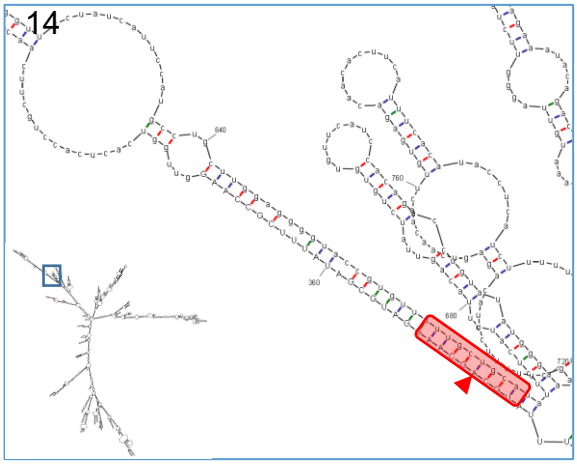
14

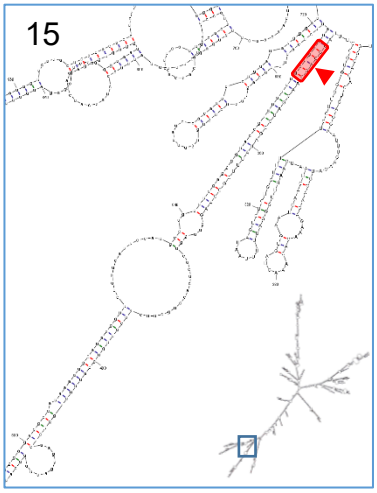
15

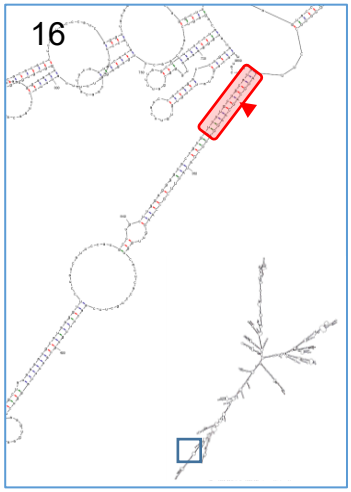
16

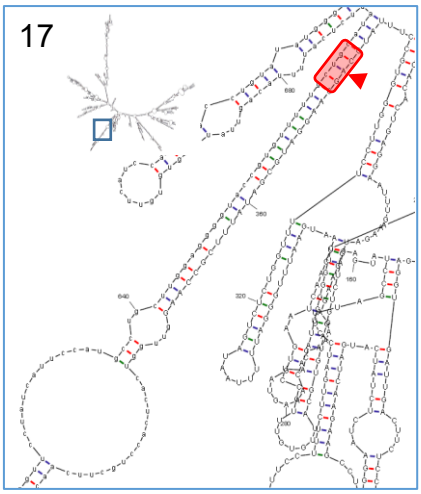
17

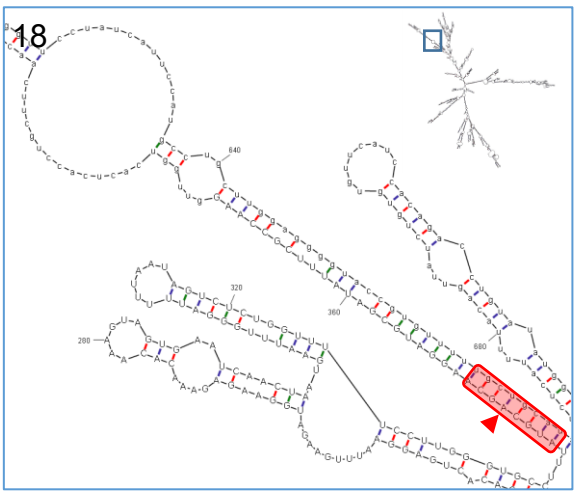
18

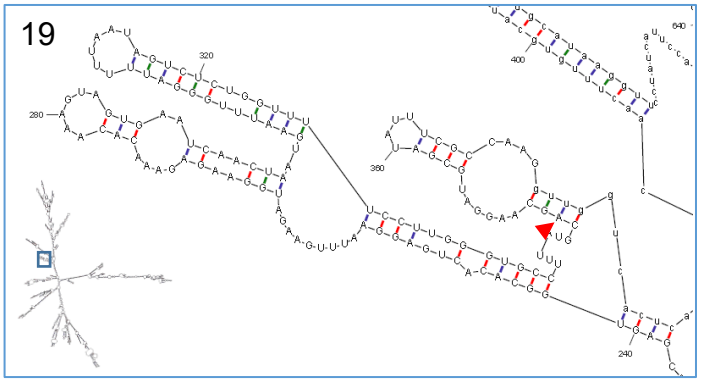
19

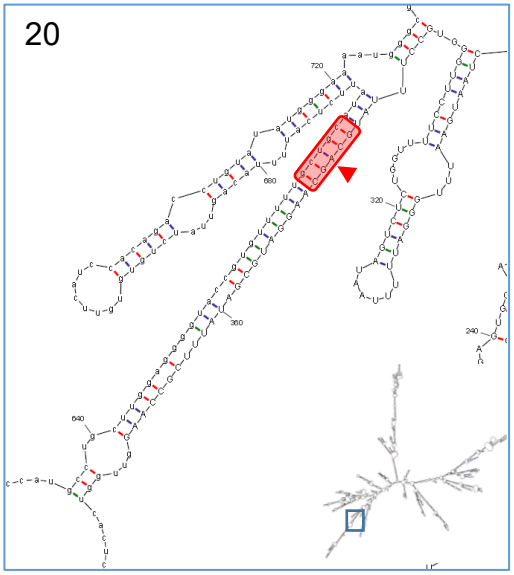
20

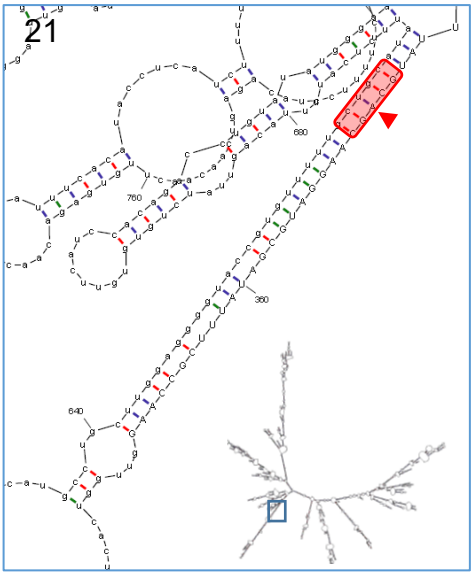
21

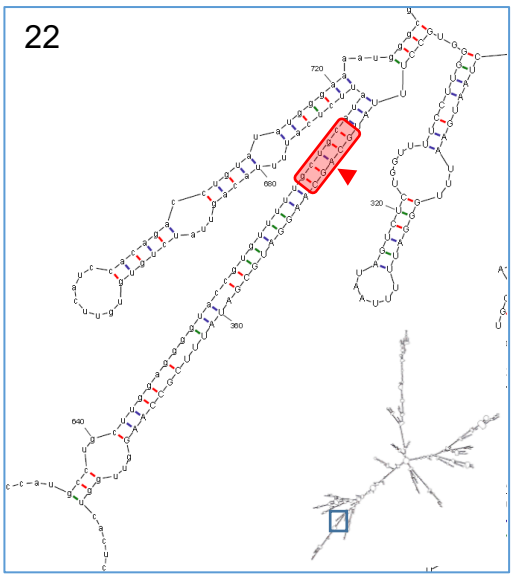
22

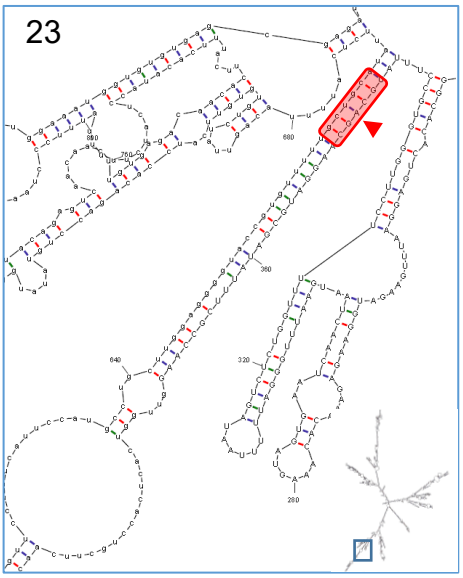
23

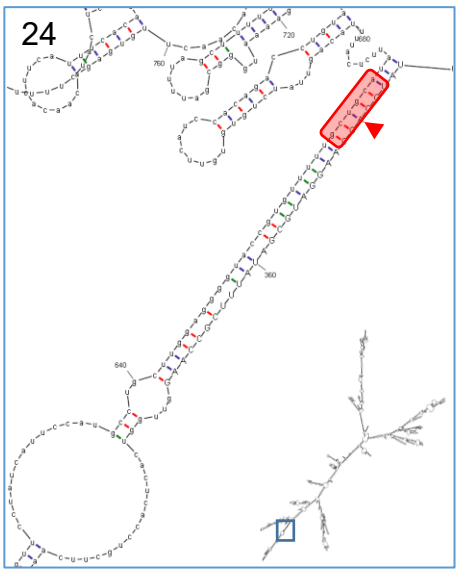
24

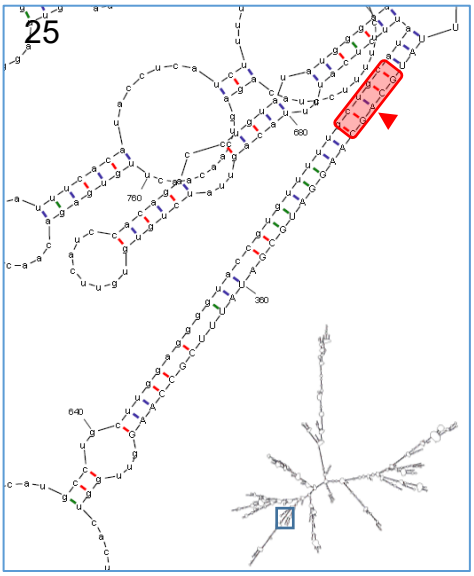
25

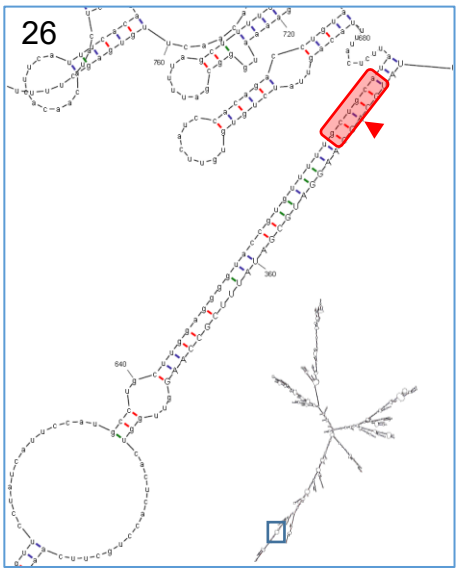
26

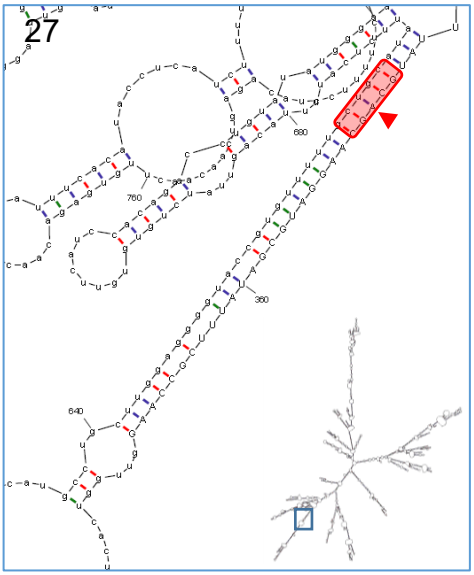
27

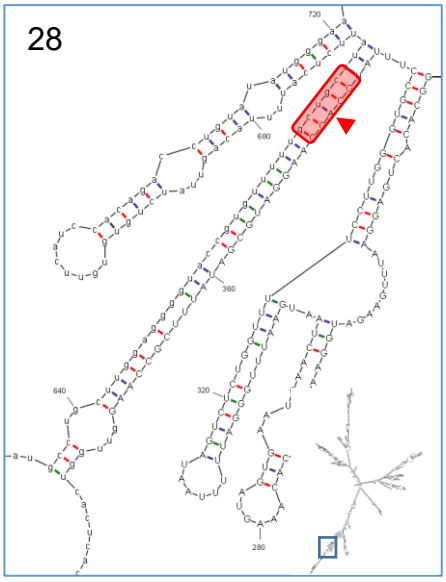
28

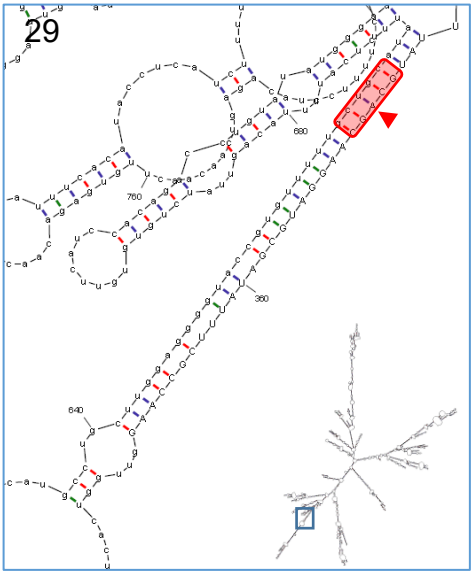
29

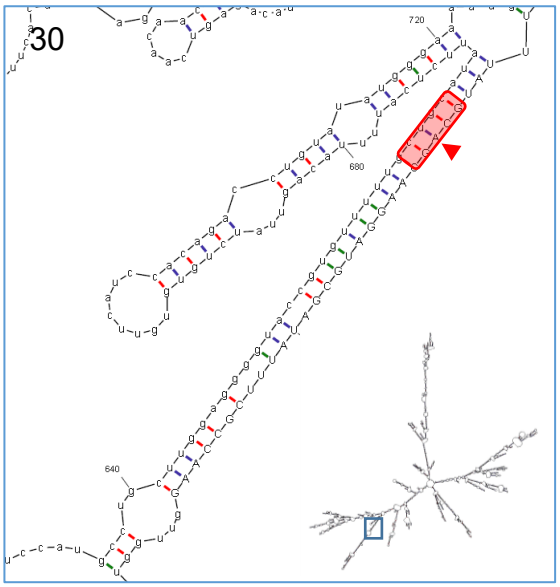
30

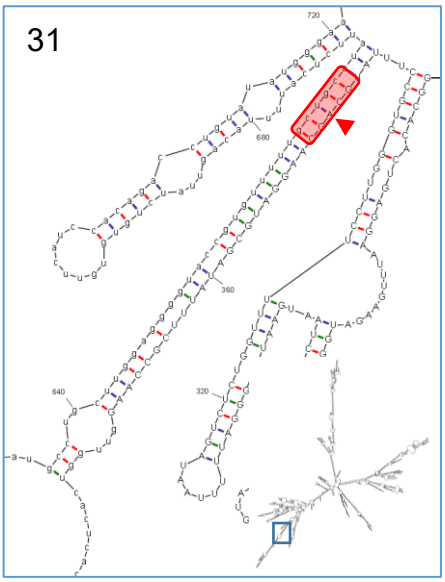
31

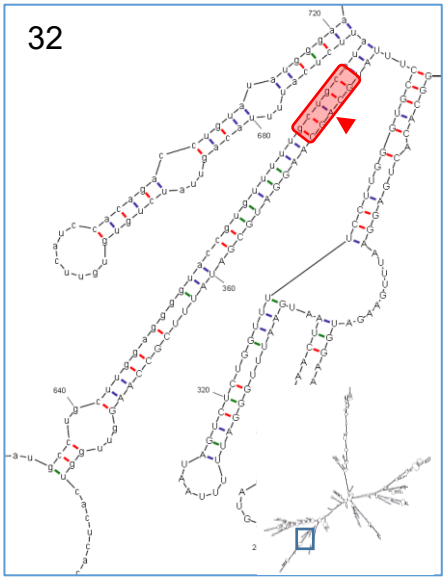
32

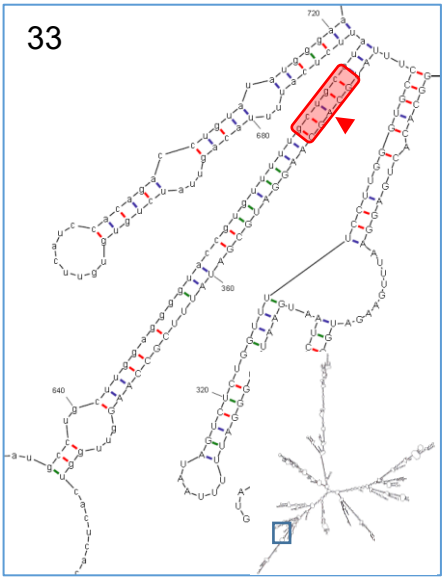
33

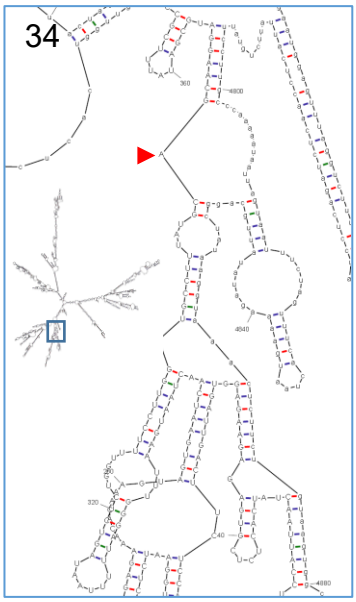
34

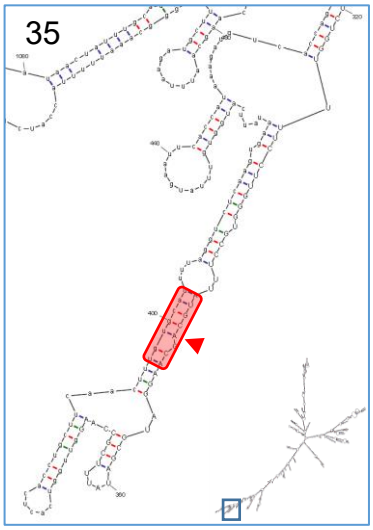
35

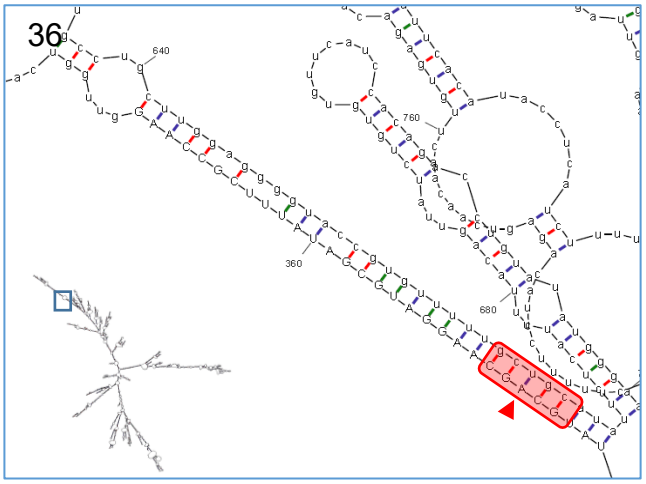

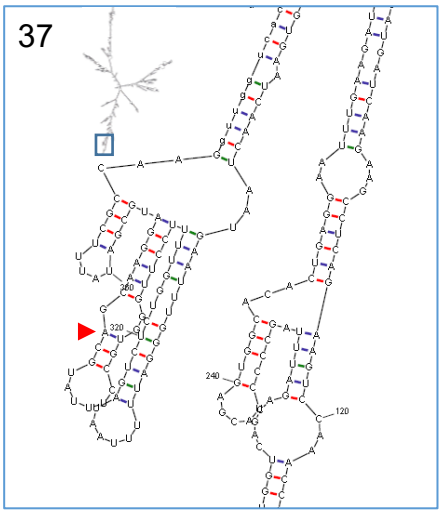

10.3 MOUSE SECONDARY STRUCTURE MODELS

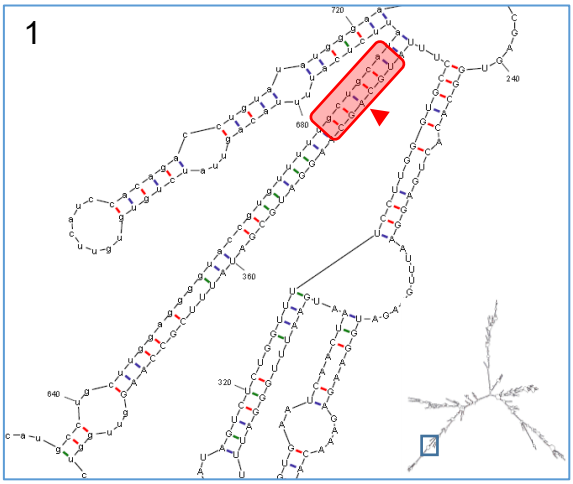

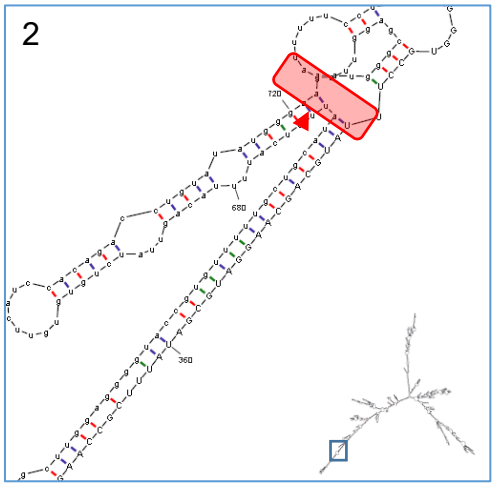

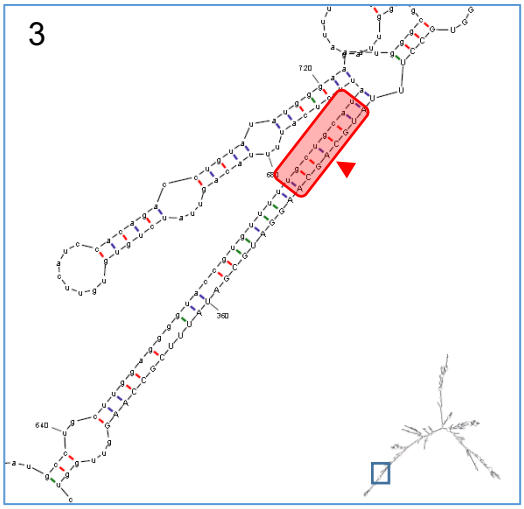

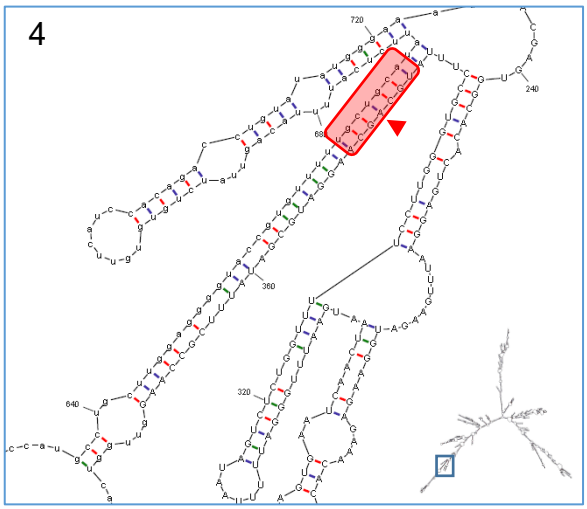

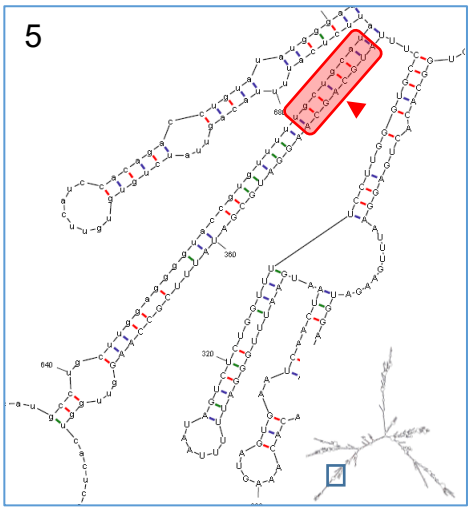
5

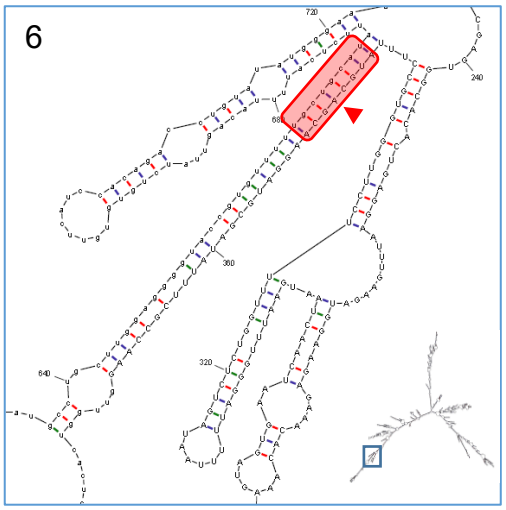
6

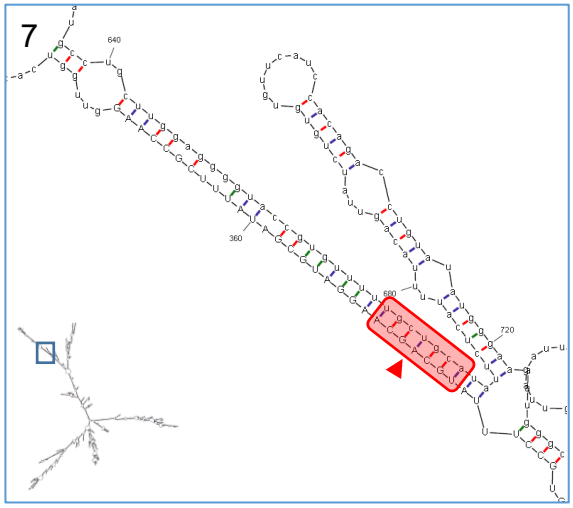
7

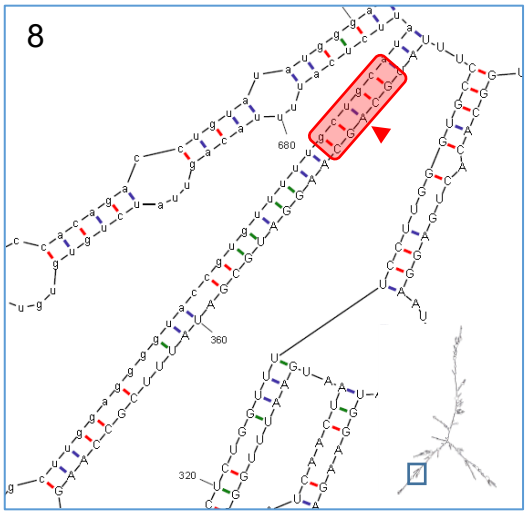
8

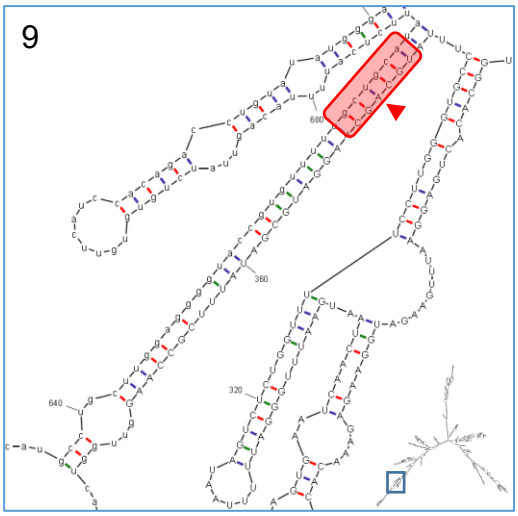
9

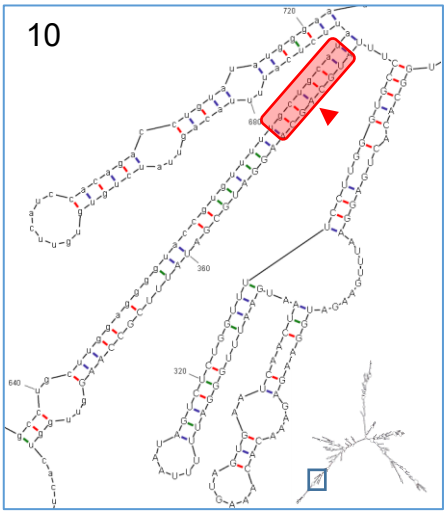
10

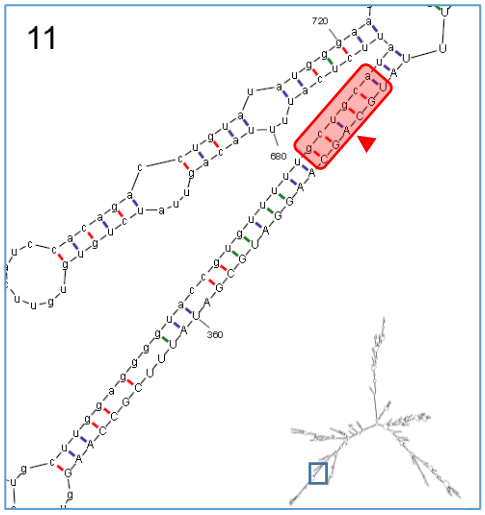
11
720
680
360

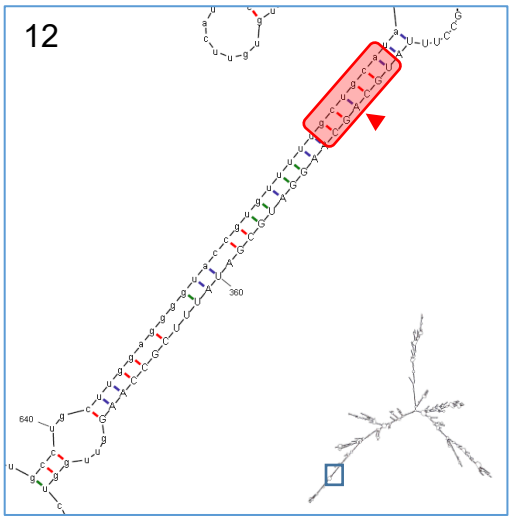
12
360
640

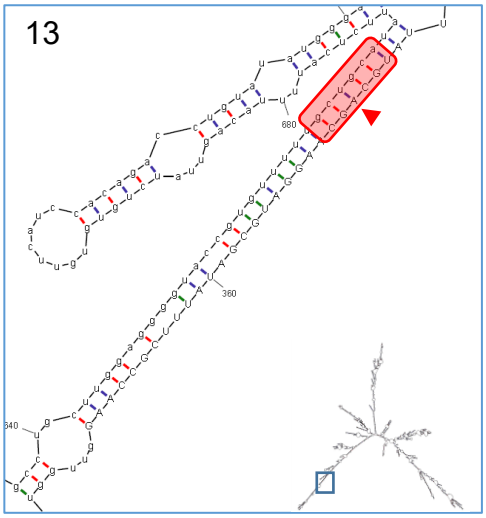
13
680
360
640

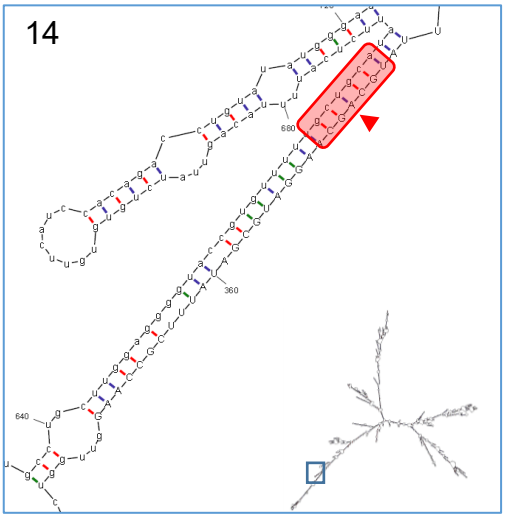
14
680
360
640

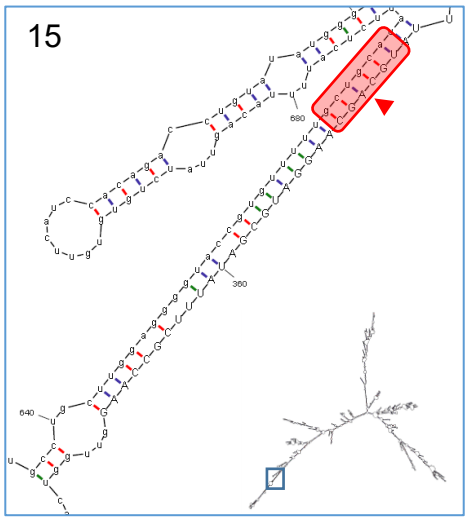
15
680
360
640

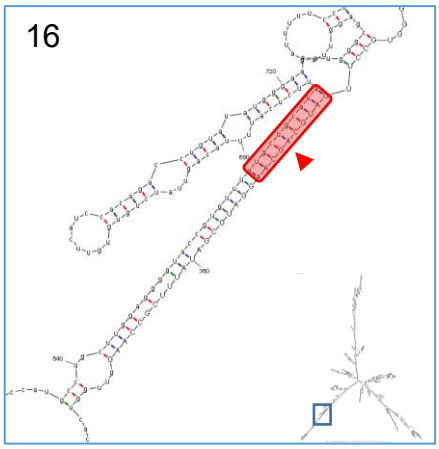
16
720
680
360
640

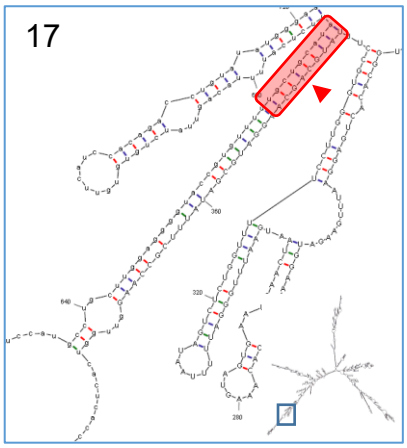
17

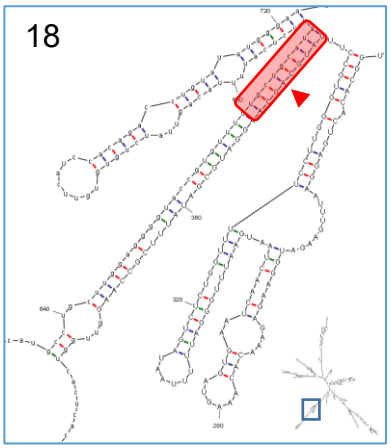
18

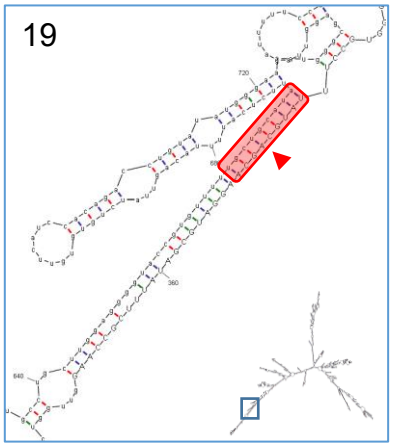
19

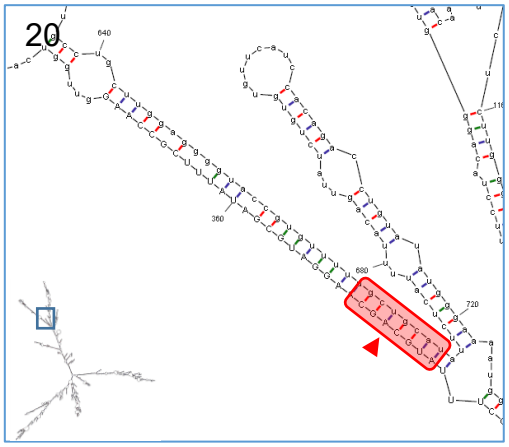
20

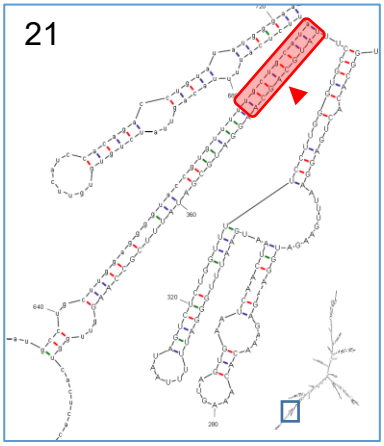
21

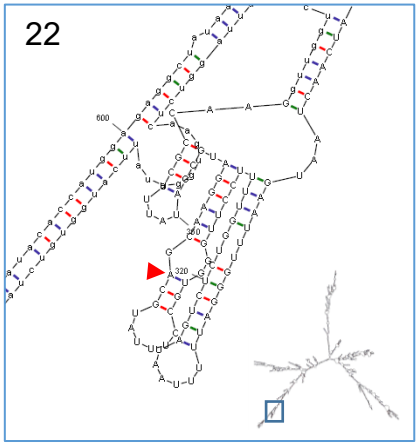
22

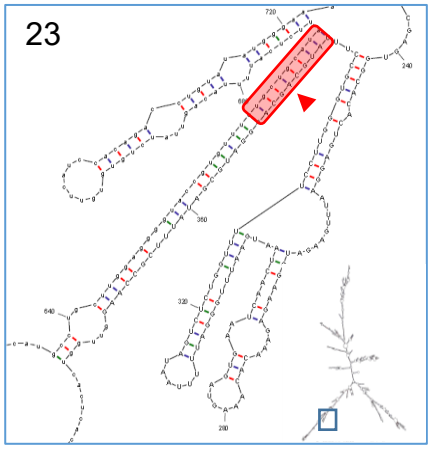
23

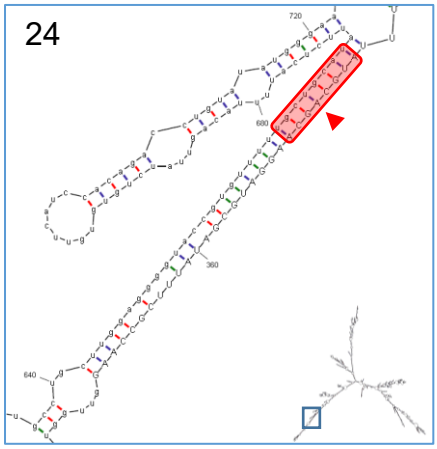
24

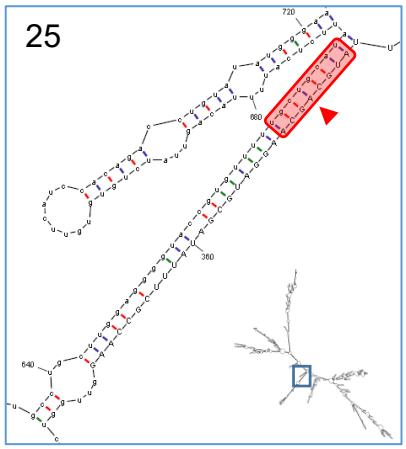
25

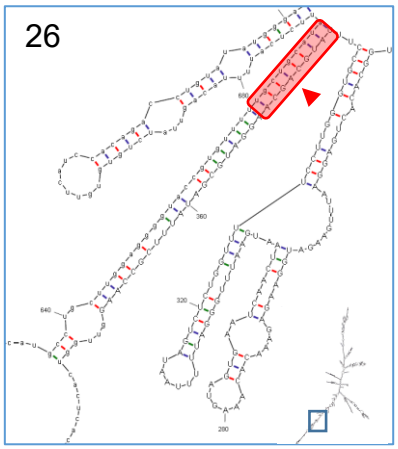
26

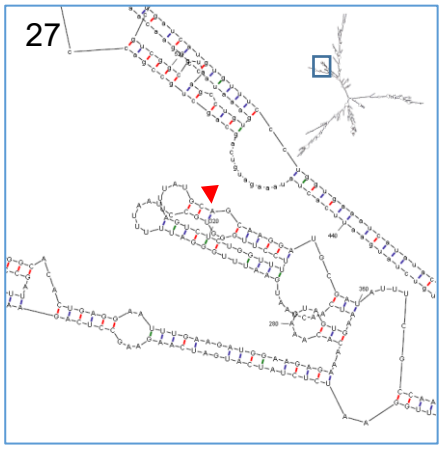
27

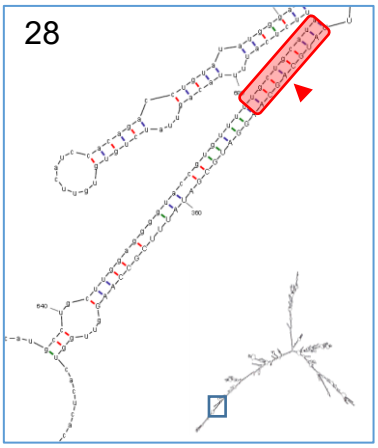
28

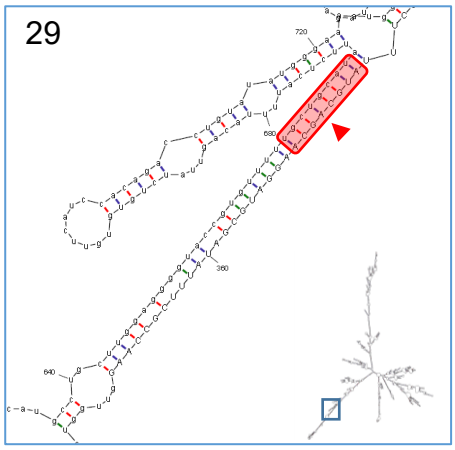
29

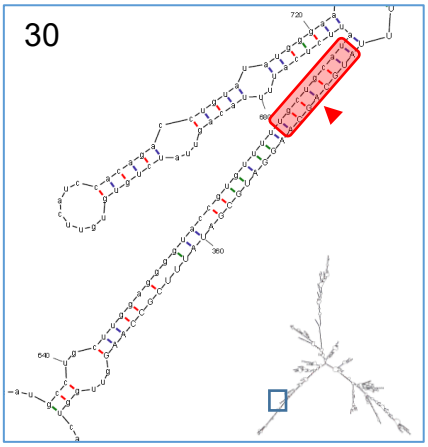
30

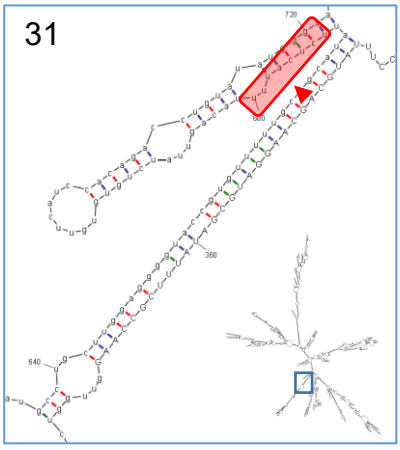
31

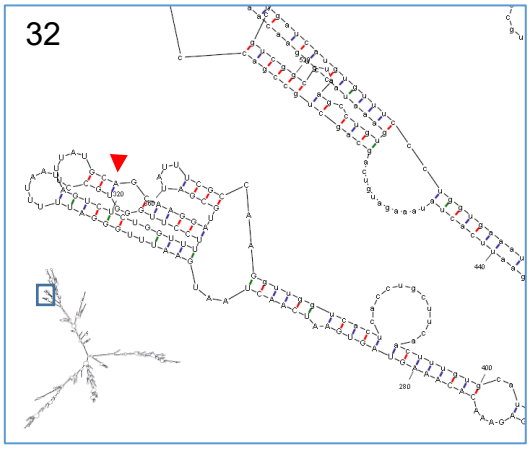
32

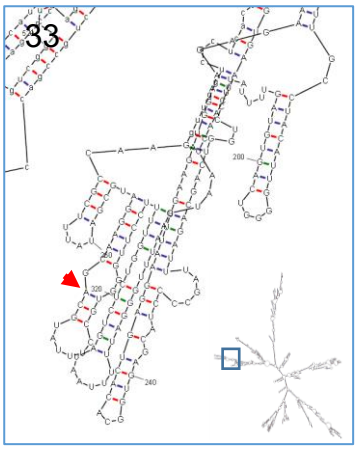
33

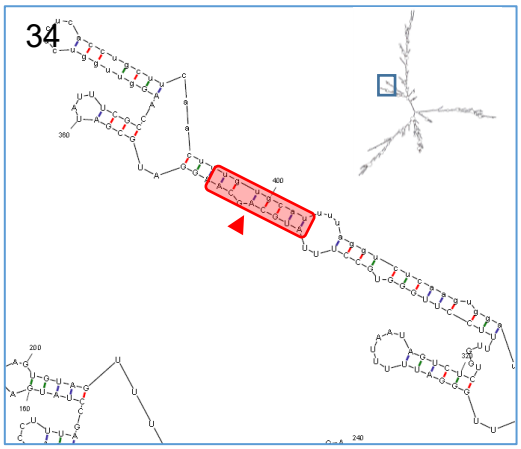
34

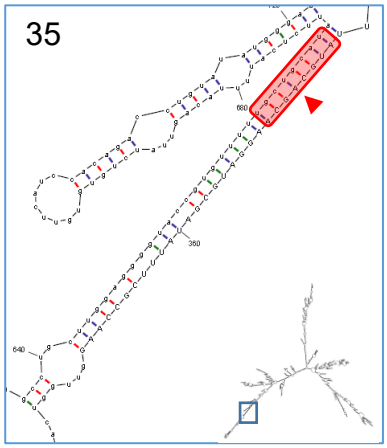
35

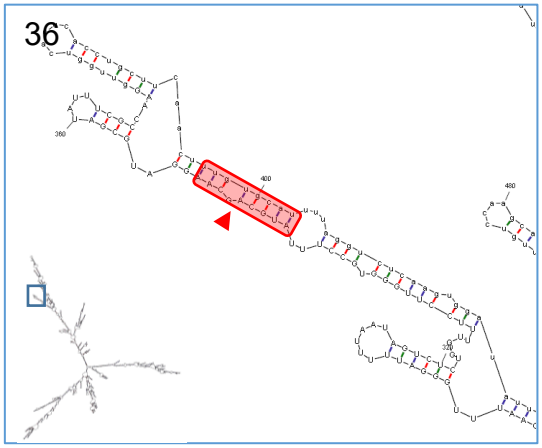
36

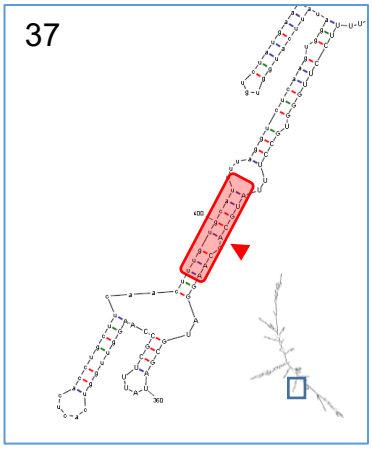
37

10.4 Free Energies of Exon 11 – Intron 11 Secondary Structures (ΔG; kcal/mol)

	Human	Rat	Mouse
1	-1180.20	-1211.36	-1133.00
2	-1177.80	-1211.26	-1132.90
3	-1177.30	-1210.06	-1132.40
4	-1176.30	-1209.86	-1131.70
5	-1175.80	-1209.86	-1131.60
6	-1175.40	-1208.46	-1131.50
7	-1175.30	-1207.96	-1131.00
8	-1175.10	-1207.86	-1129.90
9	-1173.90	-1207.46	-1129.70
10	-1173.90	-1206.96	-1129.50
11	-1173.70	-1206.76	-1129.40
12	-1173.00	-1206.36	-1129.30
13	-1172.80	-1206.26	-1128.80
14	-1172.60	-1206.26	-1128.50
15	-1172.50	-1205.46	-1128.50
16	-1171.10	-1205.36	-1128.10
17	-1170.40	-1205.26	-1128.00
18	-1170.00	-1204.86	-1127.80
19	-1169.50	-1204.06	-1127.50
20	-1169.50	-1203.56	-1127.20
21	-1169.40	-1203.46	-1127.20
22	-1168.70	-1203.36	-1127.10
23	-1168.70	-1203.26	-1126.90
24	-1168.70	-1202.36	-1126.00
25	-1167.70	-1202.36	-1125.50
26	-1137.60	-1201.66	-1125.10
27	-1167.10	-1201.56	-1125.10
28	-1166.80	-1201.46	-1124.00
29	-1166.50	-1200.96	-1122.20
30	-1165.40	-1200.96	-1120.80
31	-1164.70	-1200.96	-1118.90
32	-1164.40	-1196.26	-1118.50
33	-1164.20	-1194.46	-1117.00
34	-1164.00	-1194.06	-1114.60
35	-1163.80	-1191.76	-1110.90
36	-1163.20	-1191.26	-1107.90
37	-1161.90	-1185.56	-1104.20
38	-1161.90		
39	-1161.30		
40	-1159.80		
41	-1159.60		
42	-1157.50		
43	-1154.90		
44	-1154.40		
45	-1149.90		
46	-1147.60		
47	-1139.00		

11 APPENDIX 3 – SECONDARY STRUCTURE OF THE B13 MINIGENE

11.1 MFOLD PREDICTIONS

15 predicted models of secondary structure of the B13 minigene from the MFold output. Complete minigene is shown, with the area surrounding the Q/R editing site enlarged and the edited adenosine highlighted in red. 11 out of the 15 models show the same double-stranded pattern followed by internal loops found in the exon 11 – intron 11 models. Free energy (ΔG) shown in the top left hand corner of each model (kcal/mol).

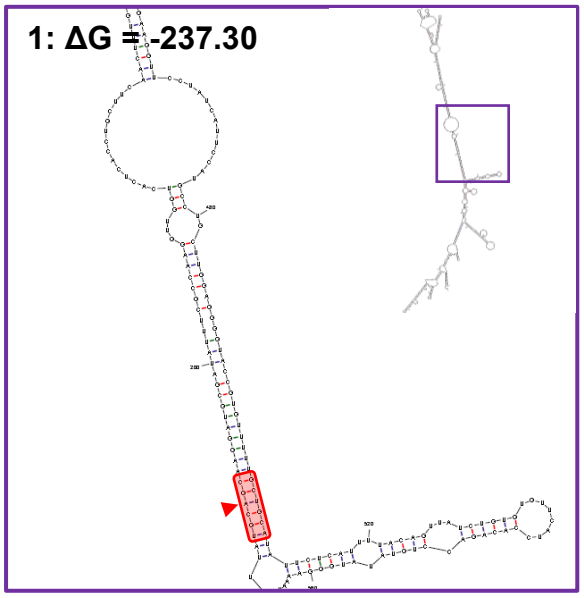

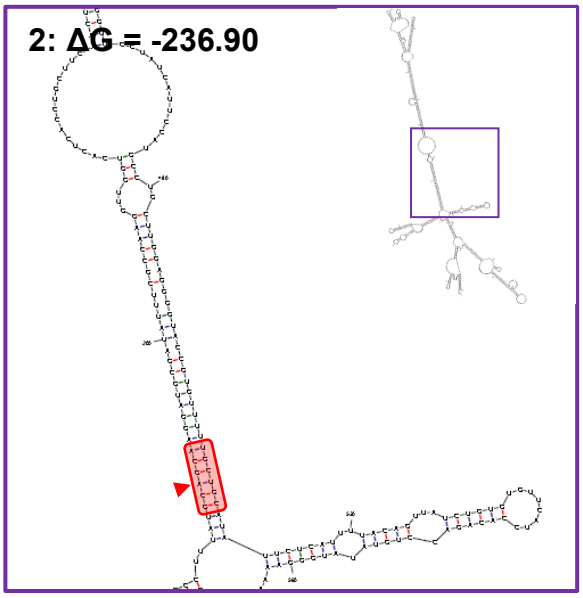

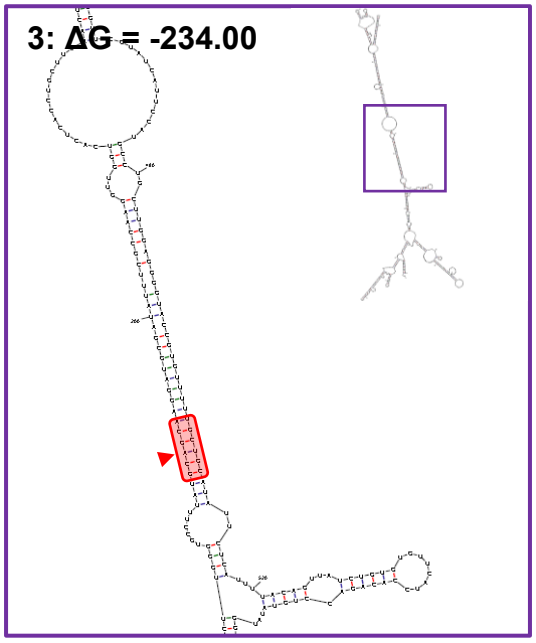

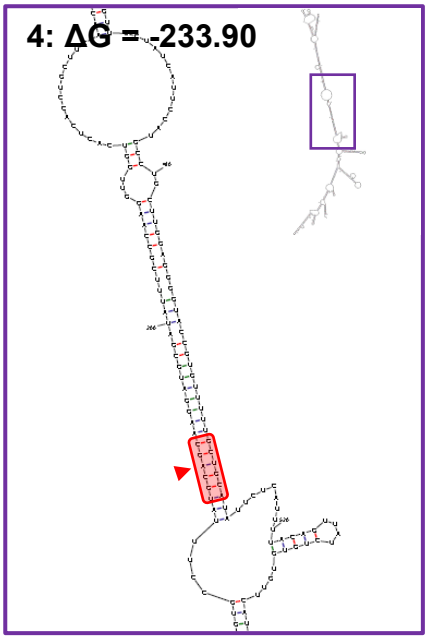

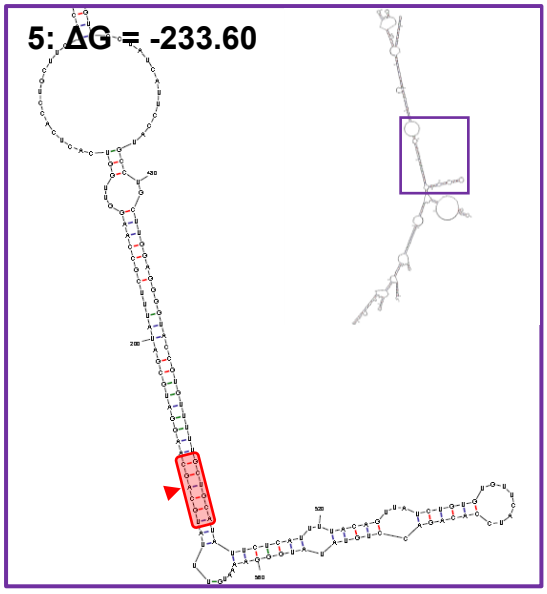
5: ΔG = -233.60

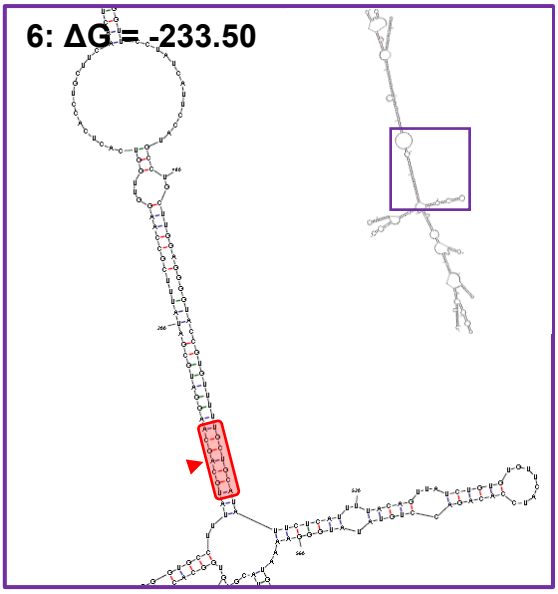
6: ΔG = -233.50

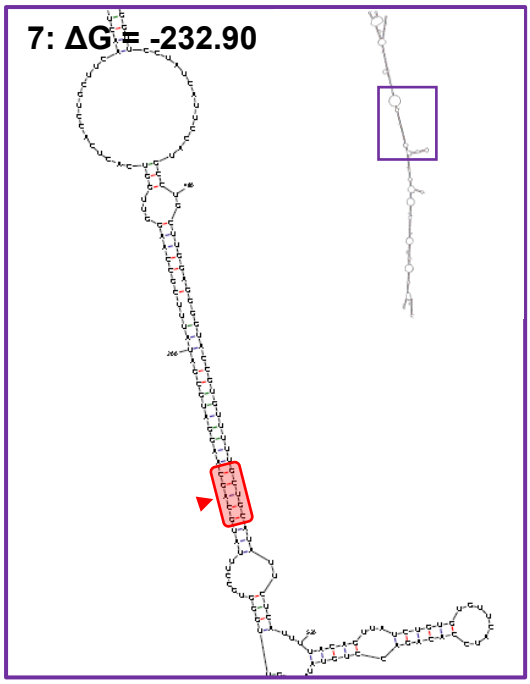
7: ΔG = -232.90

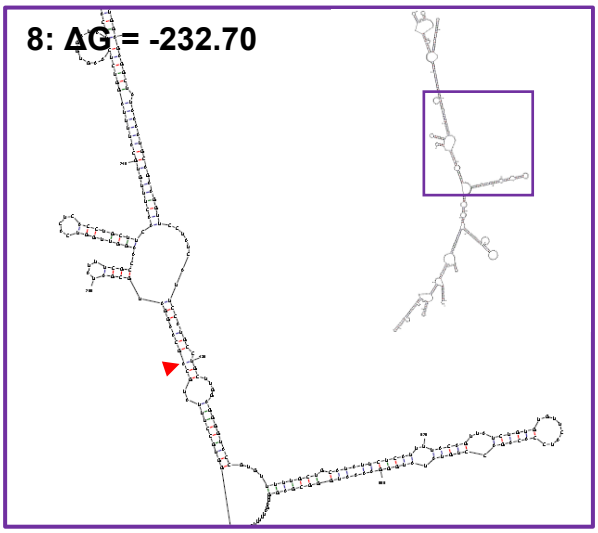
8: ΔG = -232.70

9: ΔG = -232.20

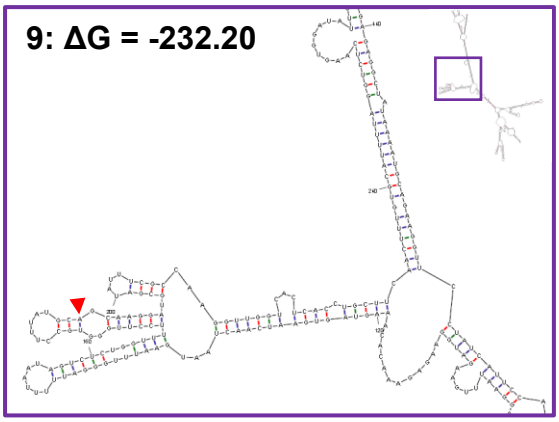

10: ΔG = -231.30

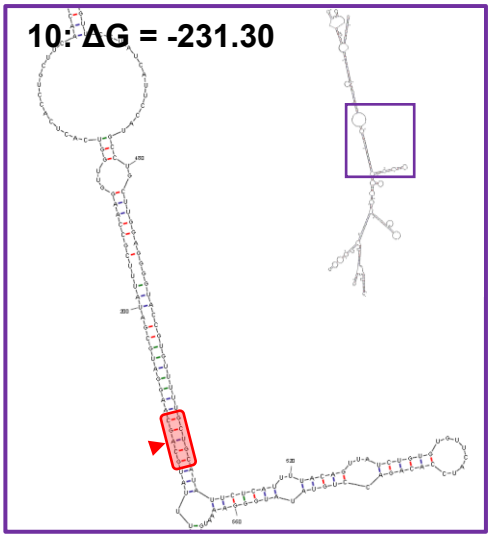

11: ΔG = -230.90

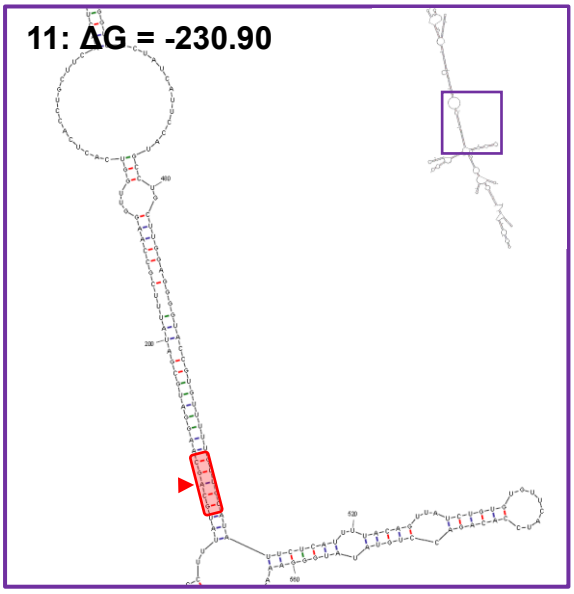

12: ΔG = -230.00

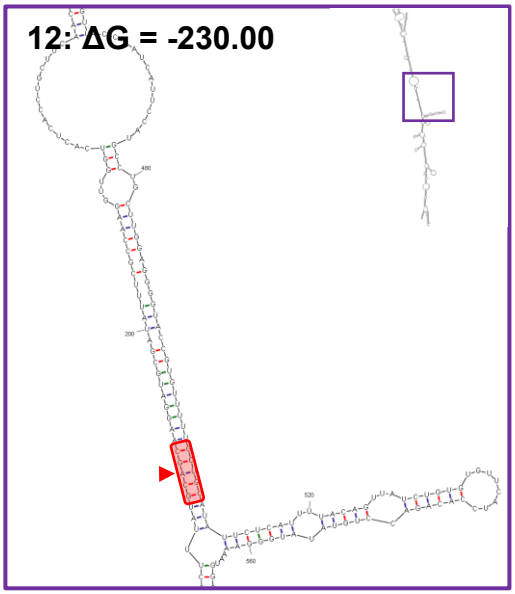

13: ΔG = -229.60

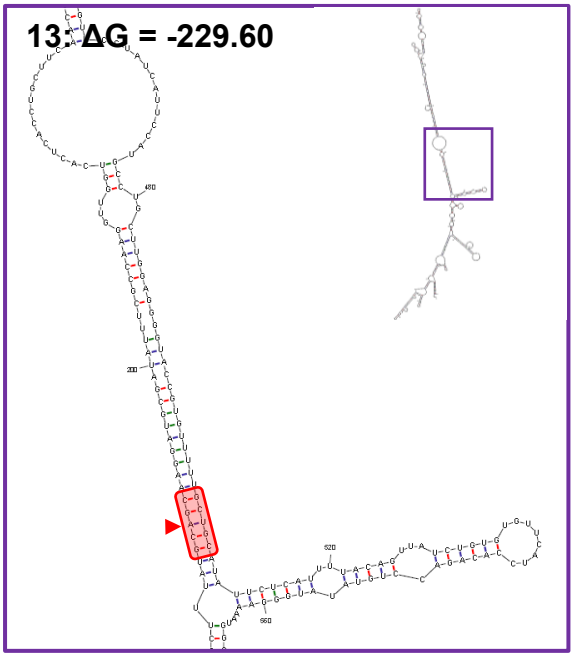

14: ΔG = -227.80

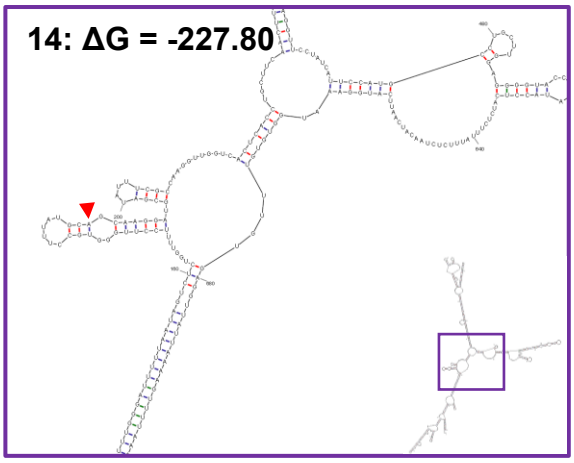

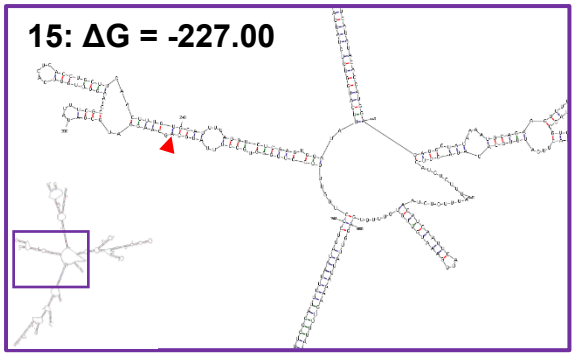
15: ΔG = -227.00